EXPERIMENTAL STUDY ON CONSOLIDATION BEHAVIOUR AND SHEAR STRENGTH GAIN FOR SATURATED/UNSATURATED TREATED FLUID FINE TAILINGS

by

BEREKET TSEGAI FISSEHA

A thesis submitted in partial fulfillment of the requirements for the degree of

DOCTOR OF PHILOSOPHY

in

GEOENVIRONMENTAL ENGINEERING

Department of Civil and Environmental Engineering
University of Alberta

Abstract

Mining industries face enormous challenges during handling and managing hydraulically placed soft tailings such as fluid fine tailings (FFT) throughout the operations and closure period. These soft deposits require sufficient bearing capacity along the profile that can support machinery and cover materials (i.e., sand capping) for the specified period. The presence of unsaturated zones, and its influence towards an increase in effective stress for the soft FFT has been theoretically defined and established as integral part of soil mechanics principles.

A new meso-scale column apparatus was designed, constructed, and assembled to carry out the consolidation behaviours of deposited FFT using increments of applied suction method. The column apparatus was designed to mimic field condition by allowing process of desaturation of deposited FFT due to dewatering process using applied suction method. The column apparatus was designed to incorporate variations of moisture flux that frequents near the ground surface due to either rainfall or evaporation using the desaturation or wetting processes. The process of consolidation and desaturation due to applied suction were aligned with shear strength measurements for the FFT materials under investigation. The presence of negative pore-water pressure (suction) contributed towards an increase in effective stress distribution calculation.

Experimental tests were carried out to investigate consolidation and shear strength behaviours of treated fluid fine tailings (FFT) using newly developed column apparatus and vane shear measuring equipment. The column apparatus used increments of applied suction through its bottom boundary to characterize the consolidation behaviours of FFTs. The FFTs constitutive relationships during the consolidation process were defined using independent stress state variables such as effective stress, suction and void ratio. Shear strength of the FFTs were characterized using vane shear measuring device simultaneously while the consolidation process

progressed. The results provided a basis to establish the constitutive relationships of FFTs in terms of stress–strain states. In addition, the column apparatus attempted investigating formation of interlayer or transitional zone under controlled environment as the process of saturation/desaturation developed to simulate effects of evaporation during field trials.

Two treated FFTs were used to conduct the experimental work, namely flocculated FFT and flocculated centrifuged tailings cake (FCTC).

Results of settlement, change in void ratio, rate of excess pore pressure dissipation, suction distribution within the deposited FFT profile and developed shear strength during the experimental investigation were monitored, and analysed. Plausible agreements were found between characterization for the FFTs between standard laboratory and meso-scale test apparatuses.

During the self-weight consolidation results of FFTs both from the experimental work were agreed with results predicted using numerical modelling exercises. In addition, the experimental results were in good agreement with results reported in literature for FFTs. The results of consolidation using applied suction (isotropic method) provides 30% higher strain rates compared to the consolidation using step load method (k_0-loading). The numerical modelling process for the consolidation using applied suction stage show further refinement to achieve credible agreement. Undrained shear strength measurement for the FFTs show linear correlation with the corresponding effective stress providing an average slope of 0.27 to 0.37 for both flocculated FFT and centrifuged FFT. The linear correlation shows FFTs behaviour to natural soils such as clays. Higher undrained shear strength can be obtained due to drying and desiccation process of tailings, by initiating the development of higher negative pore pressure on the surface of the tailings. In addition, effects of scaling were compared between standard laboratory testing and

meso-scale testing. The results were evaluated, consistent and agreeable results were observed between the standard and meso-scale testing.

In conclusion, the research study provides significant contributions in designing, assembling and developing the column apparatus, which can be used to characterize FFTs and soft tailings to mimic effects of moisture fluxes being observed near the surface during field condition. These research findings can be further studies by applying field scale experiments. Furthermore, the findings from the experimental research investigation can be integrated in versatile numerical modelling software to analyze and refine the saturated/unsaturated behaviours of deposited FFTs which are central during the design of mine waste structures.

Acknowledgments

First and foremost, I would like to sincerely thank my supervisor Dr. G. Ward Wilson for his immense kindness and support while undertaking my Ph.D. study, and for his generous financial support by creating research-related project work at the Geotechnical Centre. Dr. Wilson created a platform, which allowed me to shine and show my commitment to my work and problem-solving skills. I am indebted to him for believing in me and facilitated to pursue and achieve my dream. Equally, I would like to thank my co-supervisor, Dr. Delwyn G. Fredlund for his kindness and continuous hands-on support and guidance during the research work program. Dr. Fredlund provided prompt responses, feedbacks on the experimental work and encouragements. I am grateful for the opportunity and for the mentorship over the course of my research study. Without the generous support of my two supervisors' with their time, expertise and feedback, this thesis would not have been possible.

I would like to thank and recognize my fellow graduate student at the time Dr. Nicolas Olmedo for his extraordinary design, assembly and calibration work for the vane shear testing device (VSTD) and shear strength measuring equipment (SSME) and Dr. Michael Lipsett for supporting and collaborating during the development of the equipment. Without this newly developed equipment, the research work would not have been completed.

I would like to thank the staff at the Geotechnical Centre Laboratory, Civil and Environmental Engineering at the University of Alberta. Dr. Louis Kabwe, Mrs Christine Hereygers, and graduate students at the time for their continuous support, assistance, and technical advice during my Ph.D. research work.

I would like to thank Sally Petaske, Vivian Giang, Jennifer Stogowski for their continuous support, care and accessibility and creating a friendly, comfortable environment for the graduate students. Without your support, the research study could not have been completed.

I would like to thank fellow graduate students who have provided with their support and friendship, which was much needed during the extended research study period. To name the list of graduate students at the time of my study, Dr. Ahlam Abdulneebi, Dr. Neeltje Slingerland, Mr. Sebastian Fernandez, Mr. David Barsi, Ms Janeen Ogloza, Mr. Prempeh Owusu and many more.

I would like to thank SoilVision Systems Ltd. and NSERC (natural science and engineering research council) for sponsoring my research studies by providing financial support through the partnership program specified as the postgraduate scholarship program (PSII). In addition, I would like to thank the industry sponsors under COSIA for the financial and in-kind support during the research work.

I would like to thank to my friend Audrey Murray and Yodit Alem for proofreading the draft version of my thesis, without your feedback and comments the writing part of thesis would not be completed.

Last but not least, I would like to thank all my siblings, family and friend who believed in me and support me tirelessly while I was going through my research study at the University of Alberta. Most importantly, I would like to thank my parents for inspiring me from young age to dream and pursue my dreams against all odds.

Table of Content

List of Tables

List of Figures

List of symbols

10^{ξ} = Soil suction transformed into arithmetic scale

c' = effective cohesion, which is the shear strength intercept when the effective normal stress is equal to zero.

α = an empirical constant

ξ, ζ, η = Eulerian coordinates

X, Y, Z = Lagrangian coordinates

ξ_i = X-coordinate at the inflection point on the transformed scale (transformed soil suction)

e_0 = initial fines void ratio

e = void ratio

e_r = void ratio as a reference point at which the permeability is known

e^y = natural number raised to the dummy variable power

ϕ' = effective angle of internal friction

ϕ^b = angle indicating the rate of increase in shear strength relative to the matric suction

ϕ_s = volumetric solid content, or volume fraction

γ_s = unit weight of solid

γ_w = unit weight of water

m_2^w = water storage modulus

ψ = matric suction

ψ_{aev} = true air-entry value

ψ_{rs} = suction near residual conditions of the soil

$C(\psi)$ = correction factor directing the *w*-SWCC towards a suction of 10^6 kPa at zero water content

e(w) = void ratio as a function of gravimetric water content

$e(\psi)$ = void ratio written as a function of soil suction

$S_r(\psi)$ = degree of saturation at given suction

$w(\psi)$ = gravimetric water content written as a function of soil suction

k = hydraulic conductivity

k_{sd} (e) = dimensionless saturated permeability function at reference void ratio

k_{sw} = saturated coefficient of permeability at another selected void ratio

k_{unsat} = unsaturated hydraulic conductivity

k_{sat} = saturated hydraulic conductivity

k_y = hydraulic conductivity in the y direction

k_{wx} and k_{wy} = major and minor permeability functions in the x and y directions, respectively

k_x, k_y, k_z = hydraulic conductivity in the corresponding Lagrangian coordinate *X*, *Y*, and *Z* direction

K = constant, depending on dimensions on shape of the vane

$k_{ref}(\psi)$ = reference saturated coefficient of permeability as a function of soil suction

$k_w(\psi)$ = coefficient of permeability as a function of soil suction

$k_{rw}(\psi)$ = relative coefficient of permeability for changes in the degree of saturation

$k_{sw}(e)$ = saturated coefficient of permeability as a function of void ratio

k_{sr} = saturated coefficient of permeability at the reference state (i.e., a reference void ratio).

k_ξ, k_ζ, k_η = hydraulic conductivity in corresponding Eulerian $\xi, \zeta, \text{and } \eta$ direction

τ = shear strength of soil

τ_{ff} = shear stress on the failure plane at failure

$(\sigma_f - u_w)_f$ = effective normal stress on the failure plane at failure

σ' = effective stress

σ_{ff} = total normal stress on the failure plane at failure

$(\sigma_f - u_w)_f$ = net normal stress on the failure plane at failure

u_{wf} = pore-water pressure at failure

u_{af} = pore-air pressure on the failure plane at failure

$(u_a - u_w)_f$ = matric suction on the failure plane at failure

ρ_0 = initial density of mixture

ρ = density

ρ_w = water density

μ = fluid viscosity

u_e = excess pore pressure

θ_w = volumetric content of water

θ_a = volumetric content of gas

θ_s = volumetric content of solids

θ-SWCC = volumetric soil-water characteristic curves

w-SWCC = gravimetric soil-water characteristic curve

S-SWCC = Degree of saturation – soil-water characteristic curve

SS(ξ) = degree of saturation as a function of the transformed suction

SS(ξ_i) = degree of saturation at the inflection point

SS'(ξ_i) = first derivative of the transformed equation at the inflection point

S' = first derivative of the soil-water characteristic curve equation

$v_{\xi}^{f}, v_{\zeta}^{f}, v_{\eta}^{f}$ = velocity of fluids in $\xi, \zeta, and\ \eta$ direction

$v_{\xi}^{s}, v_{\zeta}^{s}, v_{\eta}^{s}$ = velocity of solids in $\xi, \zeta, and\ \eta$ direction

φ = one of the fitting parameters for the void ratio versus coefficient of permeability measurements

$\circ$ = second exponential fitting parameter for the void ratio versus coefficient of permeability measurements

$\mathring{a}$, ḅ, ć, ḍ, ḟ, ḡ = empirical material parameters for the void ratio constitutive relationships

Å, Ḃ, Ç, Ḍ, Ḟ, Ḡ = empirical material parameters *for the* water content constitutive relationships

ǫ = upper limit of integration (i.e., ln (100000))

$\mathring{A}$, *Ḃ, Ć, Ḋ, Ȅ, Ḟ* = experimental parameters

a_{sh} = minimum void ratio

a_{sh}/b_{sh} = slope of the line of tangency

c_{sh} = curvature of the shrinkage curve

a_f = fitting parameter near the inflection point on the *w*-SWCC

a_{fs} = fitting parameter near the inflection point on the *S*-SWCC

C_g = the gravity term

C_{wv} = coefficient of consolidation for the unsaturated soils

C = constant representing all factors (other than void ratio) affecting the calculation of the saturated coefficient of permeability

Dia = measured diameter of the vane

d = Stokes diameter of particle

dx, *dy*, *dz* = change in dimensions in the *x*-, *y*-, and *z*-directions

f(n) = a relation as the function of n

FR = the solid filling rate

g = gravitational acceleration

G_s = specific gravity of solid

H = measured height of vane

h_0 = initial water head

h_w = hydraulic head in the water phase

ḿ and ṅ are two material parameters accounting for the effect of suction on the hydraulic conductivity,

m_f = fitting parameter related to the curvature

m_{fs} = fitting parameter related to the curvature near residual degree of saturation conditions

n = porosity

n_f = fitting parameter related to the maximum rate of gravimetric water content change

n_{fs} = fitting parameter related to the maximum rate of degree of saturation change

s = shear strength of the clay

S_0 = initial degree of saturation and initial degree of saturation at the start of the S-SWCC test

S = Kynch's particle flux density function

SC_0 = solids content by weight

S_r = degree of saturation

T = torque

t_0= initial time

t = time

t_f = final time

u_a = air pressure

u_w = water pressure

$u_a - u_w$ = *air pressure minus water pressure,* matric suction

$\dot{u}, \dot{v}, \dot{w}$ = displacement of soil solids, and

$\dot{u}_0, \dot{v}_0, \dot{w}_0$ = initial displacement of soil solids.

V_o = initial overall volume of the element

V_w = volume of water in the element

v_s = solid hindering settling velocity

v_{st} = Stokes particle settling velocity

w = gravimetric water content

y = dummy variable of integration representing the natural logarithm of suction

Z_c = minimum effective stress

List of abbreviations

1D = one-dimensional

2D = two-dimensional

3D = three-dimensional

AEV = air-entry values

AER = Alberta energy board

ASTM = American standard testing of materials

COF = cyclone overflow

CT = composite tailings

CU = Cambridge University

CUF = cyclone underflow

DC = direct current

DL6 = datalogger type for negative pore pressure measuring sensor

DS = direct shear

DSS = direct simple shear

EM50 = datalogger type for volumetric water content measuring sensor

e-SWCC = void ratio soil-water characteristic curve

FCTC = flocculated centrifuged tailings cake

FFT = fluid fine tailings

FMFT = flocculated mature fine tailings

GUI = graphical user interface

ILFT = inline flocculated tailings

ILTT = inline thickened tailings

LL = liquid limit

LSC = large-strain consolidation

LVDT = linear vertical displacement tensiometer

MBI = methylene blue index

MFT= mature fine tailings

NGI = Norwegian Geotechnical Institute

NST = non-segregated tailings

OCR = over-consolidated ratio

PID = Proportional-Integral-Derivative

PL = plastic limit

PVC = polyvinyl chloride

PWP = pore-water pressure

SC = shrinkage curve

SWCC = soil-water characteristic curve

SSME = shear strength measuring equipment

S-SWCC = degree of saturation soil-water characteristic curve

TT = thickened tailings

T5 = negative pore pressure measuring sensor

T5E = volumetric water content measuring sensor from decagon

USPF = unsaturated soil property functions

U of S = University of Saskatchewan

VSTD = vane shear testing device

θ-SWCC = volumetric water content soil-water characteristic curve

w-SWCC = gravimetric water content soil-water characteristic curve

Chapter One: Introduction

1.1 Introduction

The objective of this research program is to understand consolidation and shear strength gain properties for the oil sands tailings upon deposition within a containment and to advance the knowledge of the governing engineering properties and influence on the process.

Large volumes of fluid tailings are produced by oil sands mining operations in Northern Alberta using bitumen extraction processes. The oil sands tailings are composed of sand, silt, clay, and a small amount of bitumen. Upon deposition, sand-size particles get segregated and settle out quickly, forming a tailings-dedicated area beach. In addition, the sand-size particles can be used for the construction of dykes. The fine particles and unrecovered bitumen flow into the tailings pond as a slurry known as fluid fine tailings (FFT). The high fines content increases in significance during the extraction processes due to the addition of dispersing agents (Beier, Alostaz, & Sego, 2009). The FFTs consists of about 8% solids upon storage. Settlement of the deposited tailings occurs in the tailings pond area. Within 2-3 years the solids content of the FFT reaches approximately 30% – 35% (OSTC, 2012). At a solids content of 35%, sedimentation ceases and the process of self-weight compression governs. Field measurements show that the tailings compress slowly in the tailings pond because of the low hydraulic conductivity and high thixotropic strength of the material (Jeeravipoolvarn, Scott, & Chalaturnyk, 2009). Mine operators are currently using containments, such as dams, tailings storage facilities (TSF) above grade or in a pit, to store FFTs. The containments create large surface footprints and, to date, have proven to present an engineering challenge to reclaim.

A number of operators are exploring a wide range of technologies in an effort to improve the dewatering properties of FFT. These technologies enhance consolidation and accelerate the build-up of shear strength and the trafficability of materials that can be used in reclamation. Some of the technologies under consideration are composite tailings (i.e., combining fine tailings with sands and flocculent, coagulants), centrifugation, conventional thickening, inline flocculation and thickening or the combination of these techniques with thin-lift deposition or rim-ditching and deep deposits. The new technologies improve post-deposition dewatering through desiccation (i.e., evaporation, drainage and/or freeze-thaw) and consolidation (Morgenstern & Scott, 1995). A number of sites have been established and conducted field trials with the objective of applying different dewatering technologies on large-scale operations, should the field trials be successful.

For instance, deposition of In-line flocculated fluid fine tailings at some distance from the deposition point, has been used on a commercial scale (Matthews, Dhadli, House, & Simms, 2011; Wells, 2011). Firstly, the in-line flocculation technique was used in combination with thin-lift deposition, and the use of flocculants was believed to facilitate the dewatering process considerably (flocculation and sedimentation/consolidation over one or two days) and subsequently the process of evaporation takeover to further the dewatering process over weeks and months. Therefore, the use of flocculated FFT in deeper deposits has increased to facilitate the potential consolidation behaviour due to the flocculation processes. Numerous academic research and field trials (Dunmola et al., 2014; Jeeravipoolvarn, Scott, & Chalaturnyk, 2010; Qi, Simms & Vanapalli, 2017a; Qi, Simms, Vanapalli, & Soleimani, 2017b; Rozina, Mizani, Malek, Sanchez-Sardon, & Simms, 2015; Soleimani, Simms, Dunmola, Freeman, & Wilson, 2014) have shown the advantages of flocculated FFTs consolidation behaviour compared to that of raw FFT up to some critical stress levels. Lately, the use of flocculated and dewatered tailings cakes (using centrifuged technique) has been used in larger quantities in deeper deposits as an alternative to previously applied techniques.

It is well-known that geotechnical and geoenvironmental engineering problems, such as stability of earth-fill structures, consolidation of tailings deposits (high volume change in the case of FFTs), and reclamation of tailings impoundments, can best be analyzed using fundamental principles of soil mechanics for both saturated and unsaturated conditions. For example, unsaturated flow behaviour has been used to predict the dewaterability of thin and/or multilayer tailings deposits of high-density hard rock tailings, evaporation and drainage processes (Fisseha, Bryan, & Simms, 2010; Qi, Simms, Vanapalli, & Daliri, 2016; Qi et al., 2017a, 2017b; Salfate, Wilson, Wijiewickreme, & Simms, 2010; Simms et al., 2007; 2010; 2017).

An understanding of the consolidation, shear strength development and desiccation processes assist towards improving design considerations. Understanding these physical processes is important for the development and improvement of long-term solutions. The Investigation of the stress path and stress-strain-strength relationships of deposited slurry tailings treated using various technologies is necessary to further understand the governing properties of the FFTs. It is expected that the findings will improve understanding of consolidation and shear strength processes of oil sands tailings. These findings can be applied during designing for different ground condition deposition scenarios. The improvement, modification, and/or development of a versatile numerical model that can analyze and accurately predict the saturated and unsaturated flow properties of deposited FFT is critical to implementation on a commercial scale.

1.2 Objective of the research program

The objective of this research is to further understand and characterize the fluid fine tailings while consolidating, in relation to saturated/unsaturated zones, under a controlled stress environment

using a column apparatus. In the field, the process of desaturation, drying, and desiccation from the surface of fully saturated tailings occurs due to atmospheric flux boundary conditions such as evaporation and evapotranspiration between the ground surface and the surrounding atmosphere. A transition/interlayer zone forms due to the changing of the water table within the soil profile as the saturation and desaturation processes alternate on the deposited tailings due to rainfall or evaporation, respectively. The formation of dried and desiccated transition zone near the surface of tailings furthers possibility and application of cover and sand capping engineering designs over the tailings. These engineering designs are required for the earth fill structures and key elements to maintain the performance, integrity, and functionality of the earth fill structure design.

Figure 1.1 presents a generic transition/interlayer zone between the unsaturated and saturated conditions. Fully saturated tailings were deposited in the column and water was withdrawn from the tailings regularly using an incremental applied suction method at the bottom boundary. The column apparatus enables the investigation and characterization of materials on the transition/interlayer zone using controlled suction increments through the base compared to the actual process of evaporation and rainfall. The column mimics existing field condition drying and desiccating process of a transition/interlayer zone. The drying/desiccation process that occurred during conceptual field trial and column testing in the lab showed comparable development of the transition zone, except for the change in the direction of flux. While the process of consolidation, drying/desiccation progressed irrespective of the flux direction either using applied suction at the bottom boundary or through evaporation and rainfall on the surface for actual field condition. The column apparatus is embedded within Figure 1.1 to illustrate and visualise the formation of transition zone.

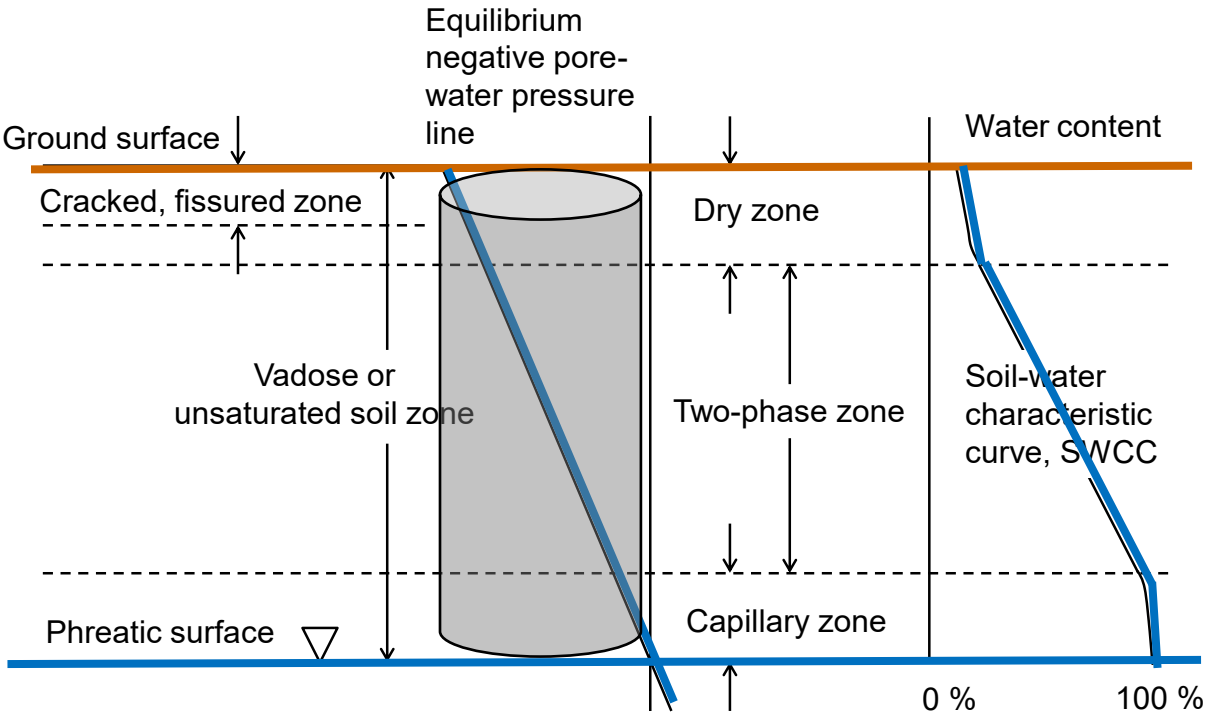

Figure 1. 1 Representation of interlayer or transitional zone between the saturated and unsaturated soil condition (adapted from Fredlund, 2016).

A necessary secondary objective is to characterize the undrained shear strength developed in deposited FFTs in relation to the total and effective stress as the consolidation process advanced. The characterization of undrained shear strength is carried out through laboratory experimental testing and the findings will assist in the validation of the use of soil mechanic principles during the handling, analysis, and designing phases of engineering structures, such as containment for the FFT.

Details of the research objectives are presented as follows:

I. To replicate the development of transition/interlayer zone near the surface of deposited material similar to actual field condition using the column apparatus testing under a controlled environment in order to investigate the progression of consolidation and desaturation of a fully saturated tailings.

II. To describe the design and development of meso scale column apparatus and vane shear measuring equipment, characterize a transition/interlayer zone of materials and obtain engineering properties in relation to tailings consolidation under its own self-weight and increments of applied suction.

III. To compare engineering properties obtained using standard laboratory characterization testing and meso-scale column test. Determine the effect of scaling during the engineering properties of tailings.

IV. To analyse and interpret the measured results in relation to the fundamental principles of saturated-unsaturated soil mechanics.

1.3 The Application of the research program

Familiarity with the development of shear strength for FFTs and slurry tailings in relation to their consolidation behaviour is essential to gain insight into how the transition zone is formed, as well as continuing to contribute to an increase in the strength that can support the loads of cover material and machineries near the ground surface which are vital during the anticipated reclamation work (Mckenna, 2012, 2016; Ansah-Sam, 2016).

A conceptual figure is used to illustrate an industrial application of the transition zone characterization from the present study. Schematic figures for the placed tailings within a containment for theoretically an existing mine are presented in Figure 1.2 and Figure 1.3. For instance, if a decision can be made to cap or cover the dried/desiccated surface crust of tailings using coarser materials, either an upstream or centerline method of dam/dyke construction can

be used to carry out remediation and reclamation work as presented in Figure 1.2 The strength of the desiccated layer, its bearing capacity, type of machinery considered and the load that can be supported by the dried/desiccated layer need to be evaluated and assessed prior considering essential engineering decisions. Figure 1.3 presents schematics of the machinery while pushing sand capping of coarser material over the desiccated layer and the orientation of undrained shear strength under consideration.

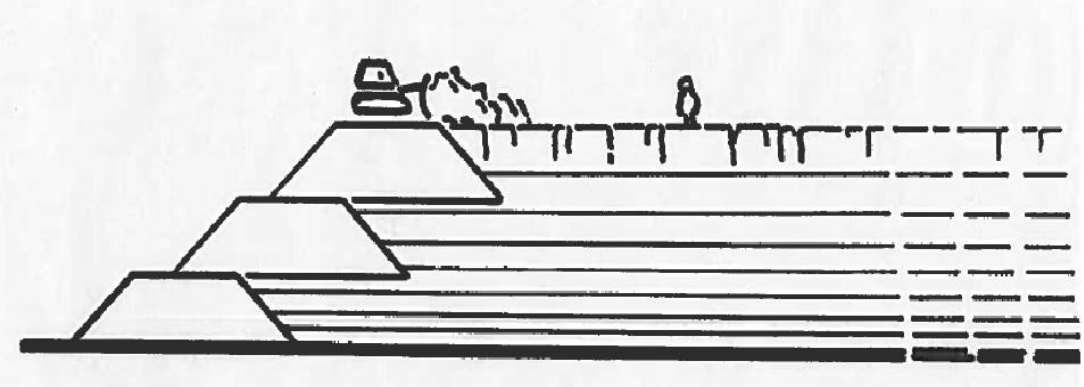

Figure 1. 2 Illustration of tailings impoundment and dried and desiccated tailings near the surface.

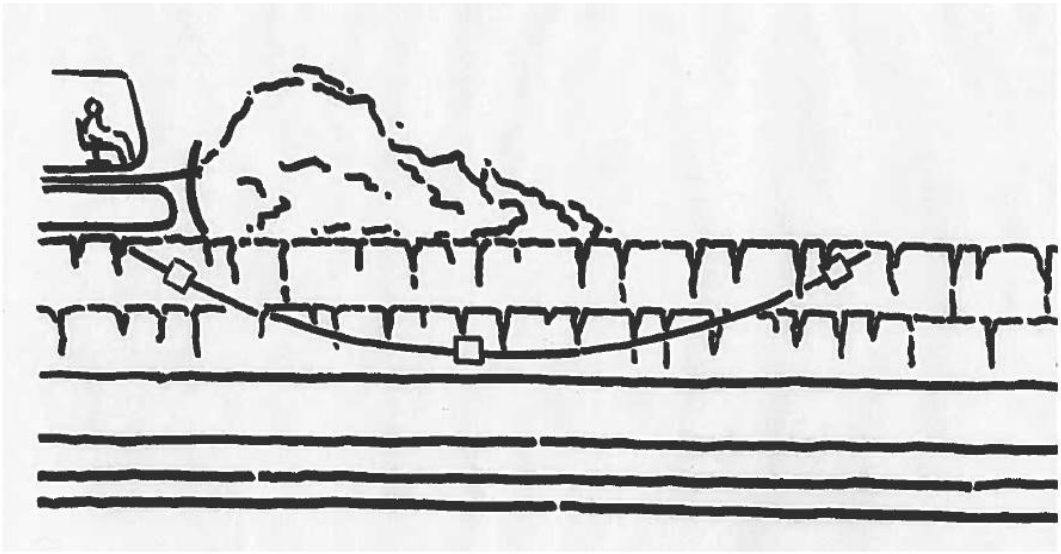

Figure 1. 3 Illustration of construction work to facilitate the next stage of tailings storage facility, remediation, and reclamation work.

1.4 Novelty

Although there exists extensive work on the consolidation behaviour of FFTs (Pollock, 1988; Jeeravipoolvarn, 2010), none of the studies were carried out using an applied negative water pressure technique and/or at meso-scale level to characterize the transition zone under controlled environment (Fisseha et al., 2017b). The formation of transition zone has been established in previous research work (Fredlund et al., 2012). In addition, a limited number of studies on shear strength for FFT are present to date. This research combined both the consolidation properties and undrained shear strength characterization of FFT.

1.5 Scope of the research program

The scope of the research study include;

I. To carry out laboratory tests to characterize the tailings and obtain geotechnical index and engineering properties under saturated-unsaturated conditions, which are vital during the numerical analysis stage. The material characterization program includes:
    a. Geotechnical index properties for the materials used
    b. Settling properties of materials
    c. Unsaturated soil properties of materials which includes soil-water characteristic curve and shrinkage curve
    d. Consolidation properties of materials which includes large strain consolidation and hydraulic conductivity curves of the materials.

II. To carry out meso-scale laboratory tests using newly designed and assembled column apparatus and vane shear measuring equipment. The Meso-scale column testing of materials will be used to characterize and compare engineering properties obtained using standard

laboratory characterization testing specified in section (i). The meso-scale column testing method and the properties analyzed were:

a. Self-weight consolidation method: The following properties were analyzed during the self-weight consolidation test: vertical strain, excess pore water pressure dissipation, effective stress calculations, undrained shear strength with depth and undrained shear strength in relation to confining effective stress.

b. Consolidation using applied suction method: The following properties were analyzed during the consolidation using applied suction test: vertical strain, isotropic and k_0 loading comparison, suction distribution with depth and time, undrained shear strength with depth and time, and undrained shear strength in relation to effective stress.

III. To carry out undrained shear strength of tailings using vane shear measuring device while the consolidation process progressed using the meso-scale column apparatus.

IV. To carry out numerical analysis using commercially available software such as finite element and difference methods to validate the results using initial and boundary conditions.

V. To assess the overall effective stress and undrained shear strength of the material under investigation.

1.6 Organization of the thesis

The outline of the thesis is presented as follows

Chapter 2: This chapter consists of literature reviews.

i) on the various types of oil sands tailings, which were developed as a result of the composition tailings and the technologies adapted by the operators in an effort to manage the generated waste during the bitumen extraction process.

ii) of the physical processes involved from the deposition stage of fluid fine tailings such as sedimentation, the transition from sedimentation to consolidation, self-weight consolidation, large-strain consolidation, drying and desiccation and shear strength gain of the tailings while going from the slurry state to desaturation, and

iii) on the properties of unsaturated soils for high volume change tailings, which includes different forms of soil-water characteristic curve (SWCC), shrinkage curve, and unsaturated soil property functions (USPF) such as water storage function and the unsaturated hydraulic permeability functions.

Chapter 3: This chapter provides theories on the process of consolidation for high volume change materials such as slurry tailings. The objectives of this chapter are to: i) define the functionality of the column apparatus used, ii) present the formulae for sedimentation and self-weight consolidation theories, iii) define the formulae for large-strain consolidation and transient water flow in saturated-unsaturated conditions, v) present the constitutive relationships, vi) outline necessary considerations for the consolidation process using incremental applied suction, and vii) briefly explain theories of undrained shear strength.

Chapter 4: This chapter provides the laboratory test program conducted during the present research study. The chapter contains i) a description of the materials used and characterized to determine the geotechnical index and engineering properties, ii) a description of developed equipment used to characterize the tailings using meso-scale column, and iii) an illustration and calibration of the instruments used during the experimental test.

Chapter 5: This chapter provides the laboratory measured results. The results are presented in two main sections:

i) presentation of results. The results are organized into the following three subsections: a) material characterization stage, b) self-weight consolidation stage for the column test, and c) consolidation using increments applied suction for the column test.

ii) challenges encountered during the experimental work.

Chapter 6: This chapter provides analysis and interpretation of results presented in chapter five. This chapter is organized into two main sections: i) analysis and interpretation of results. This section is subdivided into the following: a) material characterization stage, b) self-weight consolidation stage of the column test, and c) consolidation using applied suction stage for the column test, and ii) a modelling exercise carried out to validate the measured results using the available software/tools.

Chapter 7: This chapter discusses the main results obtained from the research program and provides procedure on how to evaluate characterization of transition zone.

Chapter 8: This chapter summarizes presented chapters, conclusion and recommendations for future work.

1.7 Related publications

The following section presents a summary of publications that have been submitted to various journals and conferences related to the research carried out for this thesis.

Fisseha, B.T., Wilson, G.W., and Fredlund, D.G. (2017a). "Assessment of large-strain consolidation and shear strength for saturated/unsaturated fluid fine tailings." 70th Canadian geotechnical conference, Ottawa, Canada.

Fisseha, B.T., Wilson, G.W., and Fredlund, D.G. (2017b). “Large-strain consolidation column with applied negative water pressures.” Proceedings of the Second Pan-Am Conference on Unsaturated Soils, Dallas, TX, USA.

Fisseha, B.T., Wilson, G.W., and Simms, P.H. (2018). "Assessment of self-weight consolidation of flocculated fluid fine tailings under various environmental conditions.” 21st international seminar of paste and thickened tailings, Perth, WA, AUS.

Olmedo, N., **Fisseha, B.T**., Wilson, G.W., Barczyk, M., Zhang, H. and Lipsett, M. (2020). “An Automated Vane Shear Test Tool for Environmental Monitoring with Unmanned Ground Vehicles.” Journal of Terramechanics 91:53-63. June 2020. DOI: 10.1016/j.jterra.2020.05.003.

Chapter Two: Literature Review

2.1 Introduction

This chapter begins with a brief review of Alberta's oil sands and bitumen extraction processes, followed by the various types of Oil Sands Tailings. The physical processes displayed during tailings deposition such as sedimentation, self-weight consolidation, and large-strain consolidation are presented. The transition from saturated to unsaturated soils and a literature review of unsaturated soils and desiccation processes are presented, as well as the subsequent process once the slurry tailings are deposited. A literature review of theory of shear strength, laboratory shear testing techniques, and the factors affecting measurement are briefly summarized.

2.2 Alberta's Oil Sands Tailings, bitumen extraction and properties

The Northern Alberta's Oil Sands mining production was introduced due to higher global demand for energy, crude oil and fossil fuel. Northern Alberta's Oil Sands reserves are located in three major areas, namely Athabasca, Cold Lake and Peace River, covering approximately 142,200 km^2 with area of 4,800 km^2 possibly minable from surface (Mizani, S. 2016). The reserves have been estimated to contain 1.7 trillion barrels of bitumen and the existing technologies are sufficient for the recovery of an estimated 170 billion barrels.

2.2.1 Bitumen extraction and basic properties of oil sands tailings

The Athabasca deposit is the largest of the three oil sands deposits in Alberta and is composed of muskeg and glacial till. The overburden thickness is less than 75 m from the surface, which

makes it appropriate for surface mining (EUB, 2004; ERCB, 2011). Chalaturnyk, Scott, & Ozum, 2002) described the composition of the Athabasca formation as a combination of bitumen (12% average), water (3-6%) and silts and clays minerals (84-86%). The clay minerals are a mixture of kaolinite and illite with small amounts of smectite, vermiculite, chlorite, and mixed layer clay mineral, as detailed in Kaminsky, 2008; Kotlyar, Sparks, & Kodama, 1984; Ignasiak et al., 1985).

Researchers attributed the presence of mixed clay layers (kaolinite-smectite and illite-smectite) with < 50% swelling characteristics in the oil sands composition to poor settling behaviours once the tailings were formed (Bayliss and Levinson, 1976; Ignasiak et al. 1983; Dusseault et al. 1989; Smith and Ng, 1993). Nadeau et al., (1984) described the reasons for the swelling characteristics are not well understood, either due to the presence of smectite layers or surface charge distribution alternation of kaolinite and illite particles.

The major companies extracting Alberta oil sands (Syncrude, Suncor, Canadian Natural Resources Ltd and Imperial oil) implement the Clark Hot Water Extraction (CHWE) process to extract the bitumen from the oil sands. Oil sands tailings are produced through the extraction process, and later transported to dedicated storage area within the mine facility.

2.3 Types of oil sands tailings

This section presents a description of various types of oil sands tailings which are produced following the bitumen extraction process in Northern Alberta, Canada using numerous dewatering technologies (Sobkowicz and Morgenstern, 2009; OSRIN, 2010; OSTC, 2012; CTMC, 2014; Fair, 2014; Read, 2014;Hyndman et al., 2018).

2.3.1 Fluid fine tailings (FFT)

Oil sands tailings are a by-product of surface mining activity for the extraction of bitumen. The FFT tailings are composed of coarse sized particles (sand), fines content, residual bitumen, and water. The coarser particles settle quickly during deposition, and the fine particles remain in suspension at the tailings pond. Sedimentation also takes place in the tailings pond. Sedimentation of fine tailings generally takes about 2-3 years to achieve a solids contents of 20% for the deposited fine tailings. Once the fine tailings reach a specified solids content, a matrix starts to form and the process of self-weight consolidation initiates. This leads to an increase in the density of the deposits (J. D. Scott & Dusseault, 1982). Scott and Dusseault (1982) stated that the term “fluid fine tailings” (FFT) should be used when the fines content is about 90% and the settle-to-solids content is 30% and the materials compression behaviour is exceedingly slow. FFT are a major problem for the oil sands industry due to their slow settling behaviour and low hydraulic conductivity. FFT contain roughly 84%(v/v) water, which is not released quickly through a natural process. Therefore, FFT deposits require large containment ponds for storage, which creates a large environmental, engineering, and economical concern (OSTC, 2012; CTMC, 2012; Beier et al., 2013; Fair, 2014; Read, 2014, Hyndman et al., 2018).

2.3.2 Cyclone underflow/overflow tailings

The oil sands industry uses hydrocyclones to separate the coarse and fine particles (OSRIN, 2010). The sand sized particles, or coarse tailings, are referred to as cyclone underflow (CUF) and fine size tailings are referred to as cyclone overflow (COF). The quantity of coarse and fine particles generated in the overflow and underflow can be adjusted by the cyclone. CUF are mixture of stripped fines and water and are similar in composition than composite tailings (CT) (Sobkowicz and Morgenstern, 2009). The coarse materials produced by the CUF can be used as

construction material leading towards CT production. On the other hand, the COF is a source of new fines and contributes to the FFT. COF is either directly deposited into a tailings pond or further processed to improve settling behaviour by a thickener or other methods.

2.3.3 Composite tailings (CT) and non-segregating tailings (NST)

Composite tailings (CT) and non-segregating tailings (NST) are a mixture of coarse and fine mine waste products such as sand, fine tailings, and flocculant/coagulant to enhance the process of consolidation and non-segregating deposits. CT and NST are designed to combine both legacy fines and new fine to create reclaimable surface land. CT has sand to fine ratio greater than 3:1 (to facilitate consolidation) and less than 5:1 (to permit fines capture) (Caughill, Morgenstren, & Scott, 1993; Matthews et al., 2002; Pollock et al., 2000; OSRIN, 2010).

Bromwell and Oxford (1977) described the combination of sand and pre-thickened phosphatic clay mixture using inline flocculated method. The authors reported that a 13% solids content was required for the pre-thickened clay slurry to produce a sand-clay mixture for production of a non-segregating tailings.

Caughill (1922) attempted to apply CT technology to the FFT through the use of flocculants and coagulants. According to Caughill (1992) the process of sedimentation is rapid after the FFT are treated with flocculants or coagulant due to the phenomenon known as hindered settling, which is dependent on the additives.

Matthews et al. (2002) summarized the development of CT technology at Syncrude Ltd. and presented schematic flow charts showing major processes related to CT production. They found that the CT was not significantly different from that produced through the conventional method

(i.e., a blend of sand and fine tailings with chemical additives). The final products were non-segregated tailings with a high permeability, allowing them to settle faster.

Luo (2004) described a pilot-scale test carried out at Syncrude in 1995 to study the effect of CT underneath FFT deposits to improve the water release and densification rate. The CT process was characterized as having an average of 20% fines (4:1 sand to fines ratio) and produced a slurry density of approximately 60% solids (OSRIN, 2010).

Shell conducted a NST field scale testing program by mixing thickener underflow products with coarse tailings with a high sand content (Shell Canada Ltd., 2009a, b; OSRIN, 2010). Laboratory test results showed high undrained shear strength and hydraulic conductivity properties of CT and in-line thickened tailings (ILTT) (Jeeravipoolvarn, 2010).

Suncor applied CT technology at the commercial scale and continued to this date (Suncor 2009), Syncrude's conducted field demonstration using NST, in 1995, and CT prototype in 1997-1998. Syncrude Mildred Lake has been operating using CT since 2000. Canadian Natural Resources Limited (2009) conducted a feasibility study of desiccation and mixing of overburden soils with fluid fine tailings. The technology was described as "minor or less capable" and was not considered for a primary role in the fine tailings' solution for the Mildred Lake Site (Syncrude Canada Ltd., 2008; OSRIN, 2010; OSTC, 2012; Hyndman et al., 2018).

Field scale trials for CT tailings can be found in literature (Hyndman et al., 2018; COSIA, 2018). Some of field scale CT deposits are presented herein. Hyndman et al. (2018) summarized the subaerially deposits of in the area known as the East Pit at the Mildred Lake site, subaqueous deposits in the Syncrude Base Mine (West Pit) and planned at Aurora North mine using CT beaching.

Hyndman et al., (2018) discussed the field testing on the variations in using thickener underflow instead of FFT and use of different coagulants by Shell at the Muskeg River Mine and at Horizon mien operated by CNRL.

Hyndman et al., (2018), and COSIA (2018) stated the limitations of CT with a recipe of 4:1 SFR, the higher demand for sand, required large pit-volume as containment and the cost for re-handling.

2.3.4 Thickened tailings (TT)

The term thickened tailings (TT) refers to processed tailings or COF, which have been thickened with the addition of a flocculant using thickeners in order to increase the tailings concentration by increasing the solids content during the deposition process.

TT technology consists of numerous engineering systems system variables include: the preparation of the feed for the thickener, type of thickening process, selection and development of the chemical additives for thickening (i.e., flocculants, coagulants), the process of transportation and deposition of tailings, and the method of reusing overflow from the thickening process (OSRIN, 2010).

Generally, thickened tailings produce a discharge with a solids content that reaches up to 50% with a typical sand to fines ratio (SFR) ≤ 1. A higher solids content can be achieved using a high rate thickener if there is a sand to fines ratio of 0.8 to 1 (Sobkowicz and Morgenstern, 2009; OSRIN, 2010). However, the solids content of CUF varies since the thickeners can be used as

heat recovery and water clarifier. Basic properties of TT are summarized in Jeeravipoolvarn (2010).

Xu and Cymerman (1999) reported on the influence of thickeners with assistance from different coagulants and flocculants. Various dosages generated suitable thickened tailings products for deposition.

Rudman et al. (2008) designed a thickener with a rake mechanism to facilitate their dewatering, and transport underflow materials from the base. The released water will be recycled to account for other mining operations since it is relatively uncontaminated by solids (i.e. < 1%). The thickened tailings are transported to the tailings deposition area through pumping or other transportation methods.

Hyndman et al., (2018) stated the use of thickeners were tested in early 2000's by industry and government partners at the Syncrude Aurora Mine with numerous successful test deposits. Similarly, thickeners were used at the Muskeg River Mine and later at the JackPine Mine of Shell Canada using the warm water recovered from the extraction process. The overall observation shows segregation of underflow material using thickener because of shearing during transportation in the pipeline. as of this date, thickeners have not delivered the desired effect according to many researchers, and nor generated reclaimable deposits (Hyndman et al., 2018).

2.3.5 Inline-flocculated tailings

The inline flocculation process involves mixing of the flocculant/coagulant with high fines content tailings from COF (OSRIN, 2010). The flocculation process was designed to improve the particle size by aggregating the particles and increasing the hydraulic conductivity, consolidation, and strength behaviour of COF (Jeeravipoolvarn et al., 2008). Hyndman et al., (2018) described the inline-flocculated process as the process of thickening without a thickener.

Bromwell and Oxford (1977) concurrently combined the waste clay stream using inline discharge to improve settling behaviours for tailings disposal. Bromwell and Oxford (1977) added chemicals into the process to improve the technology's efficiency. The addition of chemicals include in the injection of flocculants into the tailings stream prior to mixing the coarse (sand) and fine tailings (clay). The sedimentation and dewatering process was significantly improved. The inline flocculation process, however, was dependent on the chemistry of the clay, sand, and the reagents used. Since the parameters can differ significantly in the field, the process requires onsite optimization.

A method employing inline-thickening using a common-line disposal was evaluated in experimental studies at Syncrude in 2004 using the cyclone underflow tailings and chemical additives. An inline-thickening objective to rapidly increase solids content of the tailings and reduce the shortage of water during short- and long-term periods by recycling released water from the fine tailings composition (Shaw & Wang, 2005). The experimental study considered numerous objectives including obtaining: a solids contents over 35%, a yield strength of 0.2 kPa, and a slope angle on the deposit of ~1%. In addition, the deposit had to be able to sustain a hydraulically placed sand cap for reclamation (Shaw and Wang, 2005).

Yuan and Shaw (2007) introduced a three stages process of chemical addition (i.e., flocculation, coagulation and aggregation) for FFT tailings with sand to fines ratio (SFR) between 0 to 0.4 following the dilution of high fines/low solids COF at Syncrude. The process produced coarser aggregates from Syncrude tailings (OSTC, 2012).

Beier et al. (2013) described options of flocculated tailings deposition to facilitate its dewatering in the field either using sequences of thin layers through settlement, drainage and evaporation or in thicker deposits (>10m) through the self-weight consolidation process.

Hyndman et al., (2018) described the process of inline-flocculated tailings technology applied as having two different deposits. One method is thin-lift dewatering of flocculated tailings discharged from a shallow slope to densify using atmospheric drying or freeze-thaw process, the released water will be collected at the tailings pond. Another method is, to accelerate dewatering process using a deep deposit or in-pit deposit of inline flocculated tailings (Lahaie et al., 2010).

Suncor used a flocculated thin-lift procedure at its tailings reduction operation (TRO) (Wells & Riley, 2007). Although field scale trials were conducted at other sites, commercial operations continue at both the Suncor and Shell MRM (now operated by CNRL) site sand are known as Atmospheric Fines Drying (AFD) (CTMC, 2012, Hyndman et al., 2018).

2.3.6 Flocculated centrifuged tailings cake (FCTC)

The flocculated centrifuged tailings cake (FCTC) is composed of FFT tailings dredged from the tailings pond and treated with polyacrylamide flocculants followed by water separation using mechanical and gravity forces. The centrifuge dewatering process consists of two steps. First the flocculated FFT are dewatered using the horizontal solid bowl scroll technology (Lahaie, 2008).

Next, two streams will be formed: solid free water and cake. The water released was then transferred to the tailings pond for further recycling. The concentrated solids (i.e., cake) can be trucked to the disposal site at a dedicated storage area for further land reclamation (Hurtado, 2018). The centrifuged tailings cake reached as high as 60% of solids content (Devenny, 2010). The advantage of dewatering using centrifuge technique is an instant release of water. The level of densification can be controlled using rotating the angle and speed of centrifuge (Read, 2014). The centrifuge technology was developed at bench scale at CANMET (Mikula, Munoz, & Omotoso, 2009) for FFT. Implementation of centrifuge technology at a commercial scale was commissioned in 2015 at Syncrude and CNRL (formerly know as Shell) (Fair, 2008; Read, 2014). An increase in the undrained shear strength of the centrifuged tailings can be achieved due to exposure to the atmosphere, and the freeze-thaw cycle (Rima & Beier, 2018).

2.4 Physical process involved during deposition of fluid fine tailings

This section presents a brief literature review on numerous physical processes exhibited during the deposition of fluid fine tailings or slurry tailings.

2.4.1 Introduction

Extensive research has presented on the deformation of soils in the field of soil mechanics. The research shows there are various forms of deformation such as plastic flow, elastic deformation, shear deformation, undrained creep, primary compression, secondary compression, and liquefaction. The different forms of deformation are stress dependent and some are time dependent.

Early studies of compressibility of soils mainly focused on naturally deposited cohesive soils. A time-dependent linear elastic model was proposed by Terzaghi (1925) to predict the compression

behaviour for a thin layer soil with a low permeability. The proposed model assumed small strains, constant hydraulic conductivity, and constant coefficient of volume change. Taylor and Mechant (1940) illustrated the deformation of soils past the primary stage by using an elastoviscous model. Therefore, deformation of the soil could be quantified in both primary and secondary stages using Terzaghi's proposed model and the Taylor and Mechant model, respectively. However, the compression and consolidation behaviour of the slurry sediments and soft soils are considerably different from naturally deposited soils (i.e., normally consolidated and overconsolidated). Myint (2008) argued that the prediction of compressibility behaviour using Terzaghi's consolidation theory underestimated the magnitude and overestimated the degree of compression (consolidation).

2.4.2 Historical developments for compressibility of soft and slurry soils

Historically, the major theories of sedimentation and consolidation were developed independently in different disciplines (O'Neil, 2002; Toorman, 1996). A number of researchers in the field of chemical engineering were Coe and Clevenger, (1916), Kynch (1952), Fitch (1966a,1966b), and Concha and Bustos (1987). In the field of soil mechanics, the consolidation theory was developed by Terzaghi (1925, 1942), and Biot (1941). Once the theory of sedimentation was developed by Kynch (1952) in the field of chemistry, it was applied to the sedimentation of soils and a unified theory was developed for sedimentation and consolidation (Gibson, England & Hussey, 1967; Been & Sills, 1981; McRoberts & Nixon, 1976; Tan, 1995).

A number of researchers investigated and reported the process of self-weight consolidation (Been & Sills, 1981; Lee & Sills, 1981; Toorman, 1996). Been (1980) was the first to show the similarity between Kynch's theory and traditional consolidation. Been showed that both Kynch's

sedimentation theory and Gibson's large-strain consolidation theory (Gibson, England & Hussey, 1967) can be derived from a two-phase flow model.

Been (1980, 1981) observed and reported that there was no effective stress during the sedimentation process of the soft soils. The transition from sedimentation to consolidation has been investigated by Pane and Schiffman (1985) and Tan et al. (1988). An interaction coefficient was introduced by Pane and Schiffman (1985) to describe the initiating of effective stress during the transition process from sedimentation to consolidation. Somogyi (1980) proposed a large-strain consolidation formulation that had the excess pore pressure variable included in the governing equation. A nonlinear equation was proposed by Tan et al. (1988) to predict the hydraulic conductivity and effective stress from void ratio for stress levels up to 50 kPa.

Jeeravipoolvarn et al. (2009, 2010) used an equation developed by Somogyi (1980) and the coefficient of interaction introduced by Pane and Schiffman (1985) to model sedimentation and consolidation of mine waste tailings. A number of research studies have been carried out to advance an understanding of the slurry type of soil consolidation (Carrier & Keshian, 1979; Carrier III, Bromwell, & Somogyi, 1983; Carrier & Beckman, 1984; Toorman, 1996, 1999).

2.4.3 Sedimentation

Soil formation, in the case of hydraulically placed slurry soils and mine waste tailings, typically goes through various stages depending on the initial state of the material and the physical process involved. Myint (2008) provided a literature review on the sedimentation process of ultra-soft soils. Most of the literature identified the process of sedimentation as the initial stage of soil formation, which involved the conversion of solid particles in suspension into loose deposits of sediments. Jeeravipoolvarn (2010) paraphrased the term "hindered sedimentation" in reference to the

process of clustered particle settling en masse, which creates a clear interface between the supernatant water accumulated on top and the slurry soil mass.

Numerous research studies have been conducted on sedimentation and Myint (2008) summarized and presented a literature review on the process of sedimentation of ultra-soft soils. Russel, Saville, and Schowalter (1989) specified that the velocity of clay and clay-size particles during the sedimentation process is a statistical average of the solid particles governed by the collective action of gravitational forces, Brownian force, interparticle electrical force, van der Waals forces, and Stokesian viscous forces.

Research on the sedimentation of soil particles has been conducted since the early 1900s. Mishler (1912) and Coe and Clevenger (1916) investigated soil particle sedimentation and the findings were implemented during the design of thickeners in the field of chemical and process engineering.

During the process of sedimentation, it was perceived that the solid-water interface moved linearly downward with time. Holdich and Butt (1997) identified the settling velocity of particles as a function of solids concentration after observing a constant settling rate. Been and Sills (1981) presented the nonexistence of effective stress during the sedimentation process. Tan et al. (1990) reported that as the soil particles continue to settle and increase in solids content, a zone is developed in which the settled particles change from a suspension to a soil. Studies suggest there is a transition zone between sedimentation and consolidation, where effective stress is partially developed (Been, 1980; Been & Sills, 1981; Tan et al., 1990).

Kynch (1952) developed a theory of sedimentation of soil particles due to gravitational forces. Kynch's theory was based on kinematics theory and described the settlement of soil particles through a fluid suspension as a wave propagation phenomenon. Kynch assumed that the velocity

of the solid particles in a fluid only depended on the local concentration, while the solids particles had the same shape and size and the motion was one-dimensional. McRoberts and Nixon (1976) applied Kynch's sedimentation theory to soils.

Kynch's (1952) assumption is considered to be inaccurate since experimental observations show the presence of a "compression zone" near the bottom boundary. The "compression zone" negates the assumption of uniform sedimentation throughout the column. A number of researchers have pointed out that the settling rate is not only dependent on concentration alone but also on stress gradient (Fitch, 1966, 1979; Michaels & Bolger, 1962; Shirato et al., 1970). Talmage and Fitch (1955) further modified the sedimentation theory. Scott (1966) and Fitch (1966, 1979) provide a discussion on the modified sedimentation theory. According to Fitch's modification, three separate zones of sedimentation were identified: i) clarification zone, where the separation and settlement of independent flocculants occur; ii) settling zone**,** where the zone in which the solid structure of flocculants is formed and continues to settle at the same rate; iii) compression zone, where the solid structure exhibits compression.

Kynch's (1952) theory of sedimentation has been modified numerous times in order to account for the observed compaction zone and an upward movement of compaction boundary (Concha and Bustos, 1987; Fitch, 1966, 1979: Tiller, 1981).

2.4.4 Transition from sedimentation to consolidation

For a given slurry, there appears to be no sharp boundary during the transition from sedimentation to consolidation. Both the sedimentation and consolidation processes occur concurrently at the top and bottom of the column, respectively. During this time, the boundary between the suspension and the sediments is formed.

Myint (2008) presented a literature review on the transition from sedimentation to consolidation. Been and Sills (1981) and Imai (1981) reported that no sharp boundary exists between the sedimentation and consolidation zones. Rather, both processes occur in respective segments. According to Li and Williams (1995), there are different densities between the upper and lower portions of the column indicating a sharp boundary line. The determination of a transition from slurry to soil has been attempted by Been and Sills (1981), and also by Bowden (1988) who used effective stress computations. Jardine and Hight (1987) used a conceptual representation of the transition point. On the other hand, Tan (1995) challenged the idea of a partial existence of effective stress and argued it should not only be present but also fully control the deformation process. As such, the transition point is the point where effective stress becomes valid. Pane and Schiffman (1985) proposed that there was a transition stage in which a partial effective stress was present. The transition point from sedimentation to consolidation has been studied and reported (Abu-Hejleh, Znidarcic, & Barnes, 1996; Been & Sills,1981; Jardine & Hight,1987; Liu & Znidarčić, 1991; Tan et al., 1988).

2.4.5 Self-weight consolidation

Self-weight consolidation is the process of consolidation due to collective effects of gravitational and Stokesian viscous forces applied on the clay or clay-size particles in suspension over an extended period of time. It is possible to observe the effective stress build-up during the process of self-weight consolidation. Effective stress become equivalent to the overburden pressure when the process is completed. McVay, Townsend, and Bloomquist (1986) and Huerta, Kriegsmann, and Krizek (1988) observed the effect of self-weight consolidation over a longer period post deposition and commented on the challenges it caused in engineering practice.

Myint (2008) summarised and presented a literature review on the self-weight consolidation processes. Imai (1981) observed the sedimentation and self-weight consolidation of slurry soils within a given settling column. Both processes occurred simultaneously in the upper and lower parts of the column. According to Been and Sills (1981), and Li and Williams (1995), slurry soils with low solids content exhibited the process of self-weight consolidation beginning at the bottom of the deposits. These statements imply the self-weight consolidation happens when the material has the highest overburden weight (i.e., at the bottom of the column). On the other hand, Scott, Dusseault, and Carrier (1986) noted a distinction between sedimentation and self-weight consolidation. They noted that there was no slurry density change along the column during the sedimentation process with the exception of the bottom of the column. Scott, Dusseault, and Carrier (1986) concluded that the process of self-weight consolidation occurred from top to bottom of the column, which is near the drainage surface of the deposits.

Li and Williams (1995) conducted column tests for sedimentation and self-weight consolidation by using pore pressure measurements within a column and stated that the development of effective stress occurred first at the base due to the formation of the sediment and proceeded upward. These results are confirmed in recent studies conducted at a slurry pond (i.e., Silt pond) in Changi East, Singapore, where self-weight consolidation begins at the base.

2.4.6 Large-strain consolidation

The deformation of soil is usually categorized as small strain and large strain. Terzaghi's theory of consolidation is applied for soils with small strain changes. It is generally not used to represent soils where the compressibility is greater than 20% (Schiffman, Pane, & Gibson, 1984. Large-strain consolidation is defined when a thick layer of soil exhibits substantial compressibility in its layers. Gibson, England, and Hussey (1967) proposed modelling the process of large-strain

consolidation for fine-grained or slurry soils using finite strain theory. Koppula (1970) and Somogyi (1980) modified Gibson's one-dimensional finite strain model. A number of researchers applied the theory of large-strain consolidation to very soft soils (Been & Sills, 1981; Cargill, 1982a; Cargill, 1982b; Lee & Sills, 1981). A similar theory was proposed by Mikasa (1961) where another method of analysis is used to solve the consolidation properties of soft clays and self-weight consolidation.

2.4.6.1 Compression under applied load

Numerous researchers used the characterization of soft and slurry soil consolidation properties by using external applied load tests. An applied load test is considered to represent the large-strain consolidation part assuming negligible self-weight consolidation. The characterization test provides an important relationship between effective stress and void ratio and hydraulic conductivity as the soft soils consolidate. The constitutive relationships between void ratio and effective stress and hydraulic conductivity and void ratio are used to solve the finite strain consolidation theory developed by Gibson, England, and Hussey (1967), Koppula (1970), and Somogyi (1980). A number of researchers attempt to formulate a relationship between the void ratio and effective stress and hydraulic conductivity and void ratio using experimental data (Bartholomeeusen et al., 2002; Cargill, 1982; Carrier, Bromwell, and Somogyi, 1983; Jeeravipoolvarn, 2010; Somogyi, 1980). Figure 2.1(a) and Figure 2.1(b) presents an illustration of the conceptual relationships of the constitutive equations as defined using compressibility and hydraulic conductivity curves.

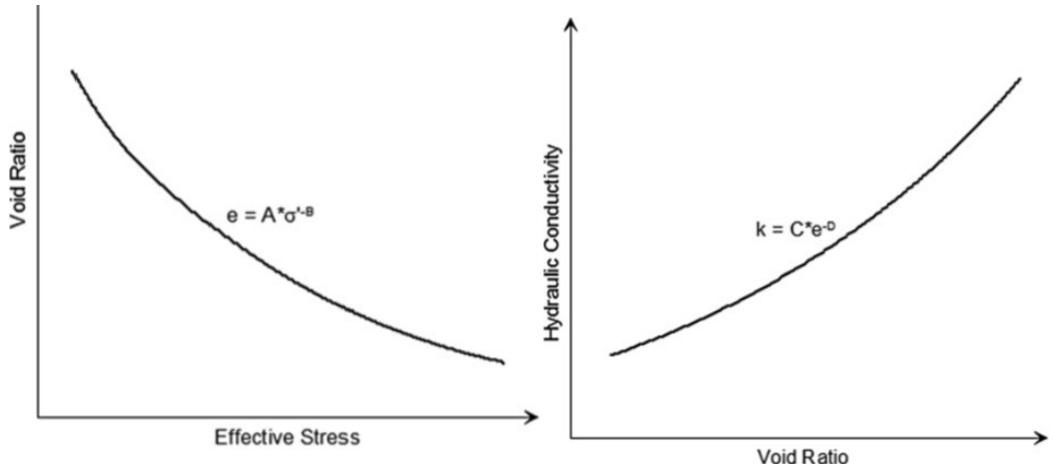

a) Compressibility curve b) Hydraulic conductivity curve

Figure 2. 1 A compressibility curve and a hydraulic conductivity curve of a slurry material.

2.4.7 Transition from saturated to unsaturated

Identification and representation of the saturation state of a given soil is important for the solution of practical geotechnical engineering problems. For instance, the mechanical response of soils varies depending on degree of saturation during the volumetric compression (Alonso, Olivella, Pinyol, 2005, 2011, 2013; Bolzon, Schrefler, & Zienkiewicz, 1996; Gens, 2010) and shear strength determination (Fredlund, Morgenstern, & Widger, 1978; Ng & Pang, 2000; Vanapalli, Fredlund, & Pufahl, 1996). The consistent representation of the transition between saturated and unsaturated soil condition is important when assessing a representative constitutive model to depict soil behaviour. Figure 2.2 presents the soil-water characteristic curve showing the transition from saturated to unsaturated state.

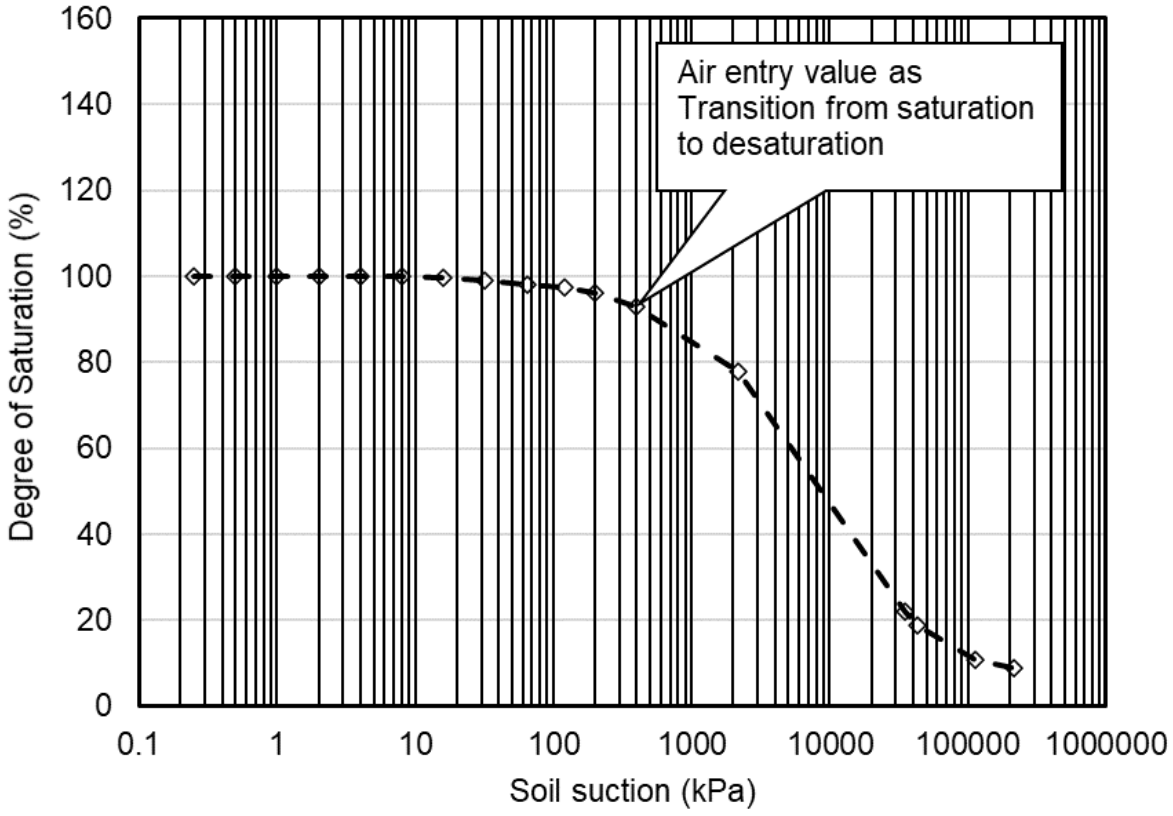

Figure 2. 2 The soil-water characteristic curve showing transition from saturation to desaturation using air-entry value (AEV) water being withdrawn with increase in suction.

Figure 2.2 presents the process of transition zone from fully saturation to desaturation condition. The air-entry values (AEV) is used to define start of desaturation of a soil sample and can be seen in SWCC curve plotted using degree of saturation and soil suction.

The transition from saturated to unsaturated condition can be identified by using the soil-water characteristic curve (SWCC) in terms of degree of saturation where the air-entry value is the starting point of the transition (Fredlund, Rahardjo, & Fredlund, 2012). Lloret-Cabot et al. (2018) presented an experimental test conducted on reconstituted samples of Barcelona clayey silt to examine the process of desaturation by using an air-drying process (Boso, 2005). Similarly, the transition point in the opposite direction (from unsaturated to saturated condition) is investigated

for a number of soils such as Barcelona clayey silt (Boso, 2005), Speswhite kaolin (Sivakumar, 1993), and London clay (Monroy, 2006). The process of saturation is studied during different types of loading by alternating and keeping the water content and suction constant.

The following parameters play a significant role in assessing the stress history in the transition zone and assist in the selection of a representative constitutive model. These factors include initial degree of saturation, air-entry value with its corresponding suction, and the dry density of soil. The representation of transition zone from saturation to desaturation and vice versa is important in the formulation of a unified constitutive model that represents the soil conditions. These constitutive models are important since field conditions are constantly changing in terms of degree of saturation due to environmental factors such as rainfall and evaporation. In the case of mine waste handling, the addition of subsequent lifts deposition on top of an already dried layer of desiccated tailings changes the degree of saturation. The underlying tailings undergo a transition from the unsaturated state to the saturated state as moisture from fresh deposits flows down within the tailings.

2.4.8 Principles of unsaturated soils mechanics

An unsaturated soil is defined as having three phases: i) solid particles of soil, ii) water, and iii) air. Fredlund and Morgenstern (1977) defined unsaturated as a fourth phase mixture with the addition of the contractile skin (i.e., air-water interface). In general, unsaturated soil is illustrated by the zone above the water table. Unsaturated soil is characterized by the presence of negative pore-water pressure relative to the internal and external air pressure. Fredlund, Rahardjo, and Fredlund (2012) described unsaturated soil principles and properties.

An introduction to the definition of the soil-water characteristic curve (SWCC) will first be described. Then a brief summary will follow, starting with early developments in the fields of soil physics and agronomy followed by their application to the geotechnical engineering field related to the soil-water characteristic curve. An overview of the different forms of SWCCs, their determination, and the estimation of various forms of unsaturated soil property function (USPF) will be illustrated.

The theory of the soil-water characteristic curve (SWCC) is defined as the central constitutive relationship to fully understand the unsaturated soil behaviour and interpret the responses observed once subjected to different field conditions. Fredlund and Morgenstern (1977) established theoretical formulations based on the stress state that provided solutions to problems related to unsaturated soil behaviour. These theoretical formulations were based on the principles of multiphase continuum mechanics. The SWCC was used as a connection between the theory, behaviour, and material properties measured in the laboratory. The formulation was instrumental in defining and solving unsaturated soil problems using a theoretical stress state basis.

The soil-water characteristic curve (SWCC) is an unsaturated soil property that shows the relationship between the amount of water in a soil and various applied soil suction values (Fredlund and Rahardjo, 1993). SWCC has been commonly used for the estimation of other unsaturated soil property functions such as the unsaturated coefficient of permeability function, the water storage function, and the shear strength function. It is important that the SWCC be accurately represented by the proposed mathematical equation.

2.4.8.1 Historical developments of SWCC theories

A brief summary of the development of the theory of SWCC from a historical perspective is presented herein. The theory of SWCC and its behavioural understanding has arisen out of research in agricultural-related disciplines (e.g., soil science, soil physics, and agronomy) (Fredlund, Rahardjo, & Fredlund, 2012). Numerous researchers made significant contributions to characterize and broaden the knowledge and understanding of the SWCC. Barbour (1998) revised the theory of SWCC development within the field of soil physics in the early days. He noted pioneers in the development of SWCC theories as follows. Baver (1940) presented the availability of moisture in soil and its development and application related to the field of soil physics. Slichter (1905) noted Schumacher and Wollny (1800s) from Europe and F.H. King and Slichter (1897-1899) from North America are regarded as the pioneers that undertook the availability of soil moisture works during the early 1800s. King (1899) studied the measurement of the ability of soil to store water. Slichter (1899) developed a conceptual model to visualize and calculate pore distribution geometry based on a series of spherical soil particles packing arrangements.

Briggs (1897) attempted to make distinctions between different classes of water based on the mechanism by which the water was held, such as hygroscopic, capillary, and gravitational water. Haines (1927) researched the air-water interface and furthered developed the hysteresis concept which was originally introduced by Briggs (1897). The concept of air-water interface or contractile skin was viewed as a thin film of water being wrapped around the solid particles of the solid grains of the soil that lead to an increase in applied stress between the particles. The concept of air-water interface led to the capillary model use consideration in order to describe the soil behaviour by using a series of glass tubes with different diameters. The capillary model was further expanded to include individual tubes with varying diameter, thereby providing an explanation of

hysteresis associated with wetting and drying processes. A mathematical relationship was developed from the capillary model between the radius of curvature, meniscus of the air-water interface, and the difference in pressure between water and air phases.

Richards (1928) developed mathematical equations for flow within unsaturated soils centered on the capillary conduction concept and storage as a function of capillary potential. One disadvantage of the capillary model was that it encouraged the view of capillary phenomena in soils to be envisaged as a series of capillary tubes of constant diameter. The air-entry value, for example, was the suction at which the largest diameter capillary tube began to drain. This model had to be modified to provide insight into the distribution of fluid-filled pores as the degree of saturation changes. Fredlund and Rahardjo (1993) noted the limitations in the general application of the capillary model to unsaturated soil mechanics. The capillary model was a micromechanics-type model that could not be directly incorporated into a macro-continuum mechanics framework for solving practical geotechnical engineering problems.

2.4.8.2 Soil-water characteristic curve (SWCC)

The soil-water characteristic curve (SWCC) describes the constitutive relationship between the amount of water content (i.e., either gravimetric or volumetric) in the soil or the degree of saturation of the soil and its corresponding soil suction (Fredlund & Rahardjo, 1993). SWCC provides different relationships for the drying and wetting processes for a given soil. The soil-water characteristic curve provides a theoretical basis for understanding the behaviour of unsaturated soils and is essential to the estimation of unsaturated soil property functions (USPF) such as the permeability function, the water storage function, and the shear strength function (Fredlund, Rahardjo, & Fredlund, 2012).

A number of mathematical equations have been proposed to characterize and represent the SWCC by a number of researchers which can be found in the literature (Assouline, Tessier, & Bruand, 1998, 2000; Brooks & Corey, 1964; Brutsaert, 1967; Bumb et al., 1992; Campbell, 1974; Farrell & Larson, 1972; Fredlund & Xing, 1994; Gardner, 1958; Groenevelt & Grant, 2004; Kosugi, 1994; Laliberte, 1969;McKee & Bumb, Murphy, & Everett, 1984, 1987; Pachepsky, Shcherbakov, & Korsunskaya, 1995; Parent, Cabral, & Zornberg, 2007; Pereira & Fredlund, 2000; Pham & Fredlund, 2008; Russo, 1988; van Genuchten, 1980). The developed mathematical equations attempt to provide representation of SWCC for the characteristics best exhibited from the natural soils.

Out of the multiple developed mathematical formulations, the Brooks and Corey's (1964) equation, the Gardner's (1974) equation, three different forms of the van Genuchten's (1980) equations, and the Fredlund and Xing's (1994) equation appear to be the six commonly used SWCC equations in the field of geotechnical engineering practices. The equation by Brooks and Corey (1964) uses a form of power-law function starting at the air-entry value point of the soil, which makes the equation simple in form. The disadvantage of using the Brooks and Corey (1964) equation is that it is discontinuous at the desaturation point (i.e., the air-entry value point). The Gardner (1974) mathematical equation is a continuous function originally proposed to form a coefficient of permeability function by fitting laboratory measured data of unsaturated soil permeability properties. (The Gardner permeability function was later used to define the SWCC.) van Genuchten (1980) developed a mathematical equation using three parameters with the flexibility to be suitable in fitting a wider range of soils. The van Genuchten (1980) equation was simplified through the suggestion of a fixed relationship between the two fitting variables known as *m* and *n*. The proposed simplifications made it possible to obtain a closed-form permeability function for an unsaturated soil when substituting the SWCC equation into the Burdine (1953) and the Mualem (1967) integral formulas for the unsaturated permeability function. The equation by

van Genuchten (1980) with two parameters become less flexible mathematically compared to the original equation with three parameters when attempting a best fit of the experimental SWCC data. Zhang (2010) noted that in using the van Genuchten (1980) equation, a reasonable fit can be achieved for laboratory data with high and medium water contents and not to the soils at high suction zone (i.e., pass residual water content). The Fredlund and Xing (1994) equation is a four-parameter mathematical equation that can serve in fitting the SWCC data over the complete range of soil suction values with better flexibility. Leong and Rahardjo (1997) stated the Fredlund-Xing (1994) equation performed best for fitting all soil types after evaluating several proposed sigmoidal SWCC equations.

Zhang and Chen (2005) recognized that the Fredlund and Xing (1994) sigmoidal SWCC equation was designed to best fit well-graded soils with one dominant pore size using unimodal SWCCs and bimodal SWCCs that are used when multiple pore sizes exist within the soils. It should be noted that gap-graded soil required modification to the fitting equations to properly represent the bimodal or multimodal SWCC's. Burger and Shackelford (2001a, 2001b) presented modification to the Brooks and Corey (1964), van Genuchten (1980), and Fredlund and Xing (1994) SWCC functions using piecewise continuous forms in order to account for the bimodal patterns of SWCCs from experimental tests. The proposed piecewise continuous forms of the above specified equations were tested on pelletized and sand diatomaceous earth mixtures with dual porosities. Zhang and Chen (2005) proposed a technique to estimate the bimodal or multimodal SWCCs for bimodal or multimodal soils using unimodal SWCCs for the characteristic components corresponding to respective pore series.

2.4.8.2.1Forms of soil-water characteristic curves

The SWCC is primarily used as the basis to estimate unsaturated soil property functions. Different designations for the amount of water in the soil generate different forms of SWCC, such as gravimetric water content SWCC, volumetric water content SWCC, instantaneous volumetric water content SWCC, and degree of saturation SWCC.

2.4.8.2.2Gravimetric water content versus suction relationship (w-SWCC)

The gravimetric-SWCC is one of the several forms that can describe the constitutive function of SWCC, which is defined as the relationship between gravimetric water content of the soil and its corresponding suction. The *w*-SWCC can be obtained for either the drying or wetting processes. The Fredlund and Xing (1994) equation (with the correction factor for zero water content at a 10^6 kPa), among existing best-fitting empirical formulas, can be used to fit the entire dataset. The regression analysis function, the Fredlund and Xing (1994) equation, yields four fitting parameters that provide a mathematical representation of the *w*-SWCC. The mathematical formula for the Fredlund and Xing (1994) equation is presented in Eq. [2.1],

$$w(\psi) = \frac{w_s\, C\,(\psi)}{\left(\ln\left(\exp(1) + \left({}^{\psi}/_{a_f}\right)^{n_f}\right)\right)^{m_f}} \qquad [2.1]$$

where:

$w(\psi)$ = water content at any suction, ψ,

a_f = fitting parameter near the inflection point on the *w*-SWCC,

n_f = fitting parameter related to the maximum rate of gravimetric water content change,

m_f = fitting parameter related to the curvature near residual conditions of the soil,

ψ_r = suction near residual conditions of the soil, and

C(ψ) = correction factor directing the *w*-SWCC towards a suction of 10^6 *kPa* at zero water content, written as

The Fredlund and Xing (1994) equation presented in Eq [2.2] is produced by inserting the correction factor, *C*(*ψ*), into Eq. [2.1].

$$w(\psi) = \frac{w_s\,(1-\ln(1+\psi/\psi_r)/\ln(1+10^6/\psi_r))}{\left(\ln\left(\exp(1)+\left(\psi/a_f\right)^{n_f}\right)\right)^{m_f}} \quad [2.2]$$

When there is considerable overall volume change in the low suction range, it might not be possible to obtain a close fit of the measured data points using the Fredlund and Xing (1994) equation or possibly any other commonly proposed fitting equation. It is important to have a close fit of the data on the *w*-SWCC when the data is combined with the shrinkage curve data for the calculation of other volume-mass SWCCs. Pham and Fredlund (2008) proposed a bimodal fitting equation and possibly used to fit data from *w*-SWCC.

Fredlund and Rahardjo (1993) described that the change in gravimetric water content with suction doesn't permit the separation of the two independent processes that occur during the drying process. The two independent processes are a) change in water content due to the change in volume and b) change in water content changes due to desaturation. The mathematical representation is completed by differentiating the basic volume-mass relationship equation as presented in Eq. [2.3] and [2.4].

$$Se = wG_s \quad [2.3]$$

$$\Delta w = \frac{S_f \Delta e + e_f \Delta S}{G_s} \quad [2.4]$$

where:

S = degree of saturation,

e = void ratio.

The subscript "*f*" refers to the "final" volume-mass states. The separation between effects due to volume change and due to desaturation can be completed by using the shrinkage curve.

2.4.8.2.3Shrinkage curve (SC)

The shrinkage curve (SC) establishes the relationship between gravimetric water content and void ratio of a given soil change in volume (i.e., void ratio) during its drying process. The shrinkage curve for a given soil can be presented by plotting the gravimetric water content of a given soil specimen on the abscissa (*x – axis*) and its corresponding void ratio on the ordinate (*y – axis*). The shrinkage curve plays an essential role in estimating unsaturated soil property functions for soils that undergo significant volume change with change in the soil suction. During the measurement of the shrinkage curve, soil specimens for the shrinkage curve test should have similar initial volume-mass properties (i.e., water content and void ratio) to those used for the *w*-SWCC laboratory test.

The properties of shrinkage of soils have been investigated since the early 1900s (Tempany, 1917). Several studies were carried out to define the process of shrinkage of soils (Bronswijk, 1991; Haines, 1923; Keen, 2018; Stirk, 1954). There are four shrinkage phases identified: namely, structural shrinkage, normal shrinkage, residual shrinkage, and zero shrinkage. An investigation into the residual and normal shrinkage concepts and their interpretation for a given soil shrinkage

curve was presented by Haines (1923). Terzaghi (1925) presented a comparison of soils shrinking behaviour to the soils' isotropic compression properties. Sridharan and Rao (1971) discussed the use of the modified effective stress concept as physical mechanism and related it with the shrinkage property of a given soil specimen. Kim et al. (1992) investigated the processes of shrinkage and the geometry of shrinkage volume with respect to the physical ripening which naturally occurs in a marine clay soil. Marinho (1994) studied and presented shrinkage curve functions.

M. Fredlund (2000) presented a hyperbolic function equation to generate the shrinkage curve of a soil and presented a theoretical procedure for estimating the shrinkage curve. The mathematical equation for the shrinkage curve accurately represents the behaviour of drying soil from a near-saturated state (M. Fredlund, 2000). Cornelis et al. (2006) proposed a simplified parametric model and assessed the magnitude and geometry of number of soil shrinkage behaviours.

The following hyperbolic equation proposed by M. Fredlund (2000) can be used to represent the shrinkage curve.

$$e(w) = a_{sh}\left[\left(\frac{\mathrm{w}}{b_{sh}}\right)^{c_{sh}} + 1\right]^{\frac{1}{\mathrm{c_{sh}}}} \qquad [2.5]$$

where:

e(w) = void ratio as a function of gravimetric water content,

a_{sh} = minimum void ratio, e-min,

a_{sh}/b_{sh} = slope of the line of tangency,

c_{sh} = curvature of the shrinkage curve, and

w = gravimetric water content.

The relationship between the fitting parameters from the equation by M. Fredlund (2000) and volume-mass properties of soil is presented in Eq. [2.6].

$$\frac{a_{sh}}{b_{sh}} = \frac{G_s}{S_0} \quad [2.6]$$

where:

S_0 = initial degree of saturation.

M. Fredlund (2000) showed the shrinkage curve as a one-piece smooth curve represented by $e(w) = (a_{sh}/b_{sh}) * w$ as its asymptotic line. The shrinkage curve yields a straight asymptotic line at a larger gravimetric water content value. Zhang (2016) utilized the equation proposed by M. Fredlund (2000) as a basis during the estimation of permeability function for high volume change soils.

2.4.8.2.4Void ratio versus suction relationship (e-SWCC)

Fredlund and Zhang (2013) demonstrated that the change in volume (i.e., change in void ratio) in relation to the change with suction can be computed using the combination of empirical equation for gravimetric water content (*w*-SWCC) and the shrinkage curve, SC. As it has been defined in the previous sections, the shrinkage curve relates the change in void ratio to the change in gravimetric water content as the soil dries out, and the *w*-SWCC presents the relationship between the gravimetric water content to soil suction. Substituting the equation for *w*-SWCC into the shrinkage curve equation yields an equation as presented in Eq. [2.7].

$$e(\psi) = a_{sh}\left(\left(\frac{w_s\left(1-\ln\left(1+{}^{\Psi}/_{\psi_r}\right)\right)/\ln\left(1+{}^{\Psi}/_{\psi_r}\right)}{b_{sh}\left(\ln\left(\exp(1)+\left({}^{\Psi}/_{a_f}\right)^{n_f}\right)\right)^{m_f}}\right)^{C_{sh}} + 1\right)^{{}^{1}/_{C_{sh}}} \quad [2.7]$$

2.4.8.2.5Volumetric water content versus suction relationship (θ-SWCC)

Fredlund (2017) and Zhang (2016) illustrated the determination of volumetric water content for soils which undergo high volume change during drying by defining the change in volumetric water content with respect to total volume and introducing the term “instantaneous,” which described the change in soil volume as change in soil suction occurred.

The instantaneous volumetric water content, θ_i, of the soil can be computed using Eq. [2.8] based on the *w*-SWCC and the shrinkage curve, SC.

$$\theta_i(\psi) = \frac{G_s w(\psi)}{1+e(\psi)} \quad [2.8]$$

where:

$w(\psi)$ = gravimetric water content written as a function of soil suction,

$e(\psi)$ = void ratio as a function of soil suction.

The Fredlund-Xing (1994) equation for *w*-SWCC and the M. Fredlund (2000) equation for shrinkage curve can be substituted into Eq. [2.8] and yield the following Eq. [2.9]:

$$\theta_i(\psi) = \frac{G_s w_s (1 - \ln(1 + \psi/\psi_r)/\ln(1 + 10^6/\psi_r))}{\left(\ln\left(\exp(1) + \left(\psi/a_f\right)^{n_f}\right)\right)^{m_f}\left(1 + a_{sh}\left(\left(\frac{w_s\left(1 - \ln\left(1 + \psi/\psi_r\right)\right)/\ln\left(1 + \psi/\psi_r\right)}{b_{sh}\left(\ln\left(\exp(1) + \left(\psi/a_f\right)^{n_f}\right)\right)^{m_f}}\right)^{C_{sh}} + 1\right)^{1/C_{sh}}\right)}$$

[2.9]

The θ_i-SWCC equation will be used for the determination of water storage function, m_2^w.

2.4.8.2.6 Saturation versus suction relationship based on w-SWCC and SC data (S-SWCC)

Fredlund (2017) summarized the association between the degree of saturation and soil suction using the volume-mass relationship using the *w*-SWCC for the gravimetric water content and the shrinkage curve for the corresponding void ratio for the given soil suction given in Eq. [2.10].

$$S(\psi) = \frac{G_s w(\psi)}{e(w(\psi))} \qquad [2.10]$$

where:

$S(\psi)$ = degree of saturation,

$w(\psi)$ = Fredlund-Xing (1994) equation for the *w*-SWCC or any other equation that fits the laboratory data,

$e(\psi)$ = void ratio written as a function of soil suction, ψ.

Eq. [2.11] is rewritten through the substitution *w*-SWCC equation and the SC equation and is presented below.

$$S(\psi) = \frac{G_s w_s (1 - \ln(1 + \psi/\psi_r)/\ln(1 + 10^6/\psi_r))}{a_{sh}\left(\ln\left(\exp(1) + \left(\psi/a_f\right)^{n_f}\right)\right)^{m_f}\left(\left(\frac{w_s\left(1 - \ln\left(1 + \psi/\psi_r\right)\right)/\ln\left(1 + \psi/\psi_r\right)}{b_{sh}\left(\ln\left(\exp(1) + \left(\psi/a_f\right)^{n_f}\right)\right)^{m_f}}\right)^{c_{sh}} + 1\right)^{1/c_{sh}}} \quad [2.11]$$

Fredlund (2017) and Zhang (2016) presented a modified equation, which was used to fit data points to generate a new set of fitting parameters for soils with high change in volume by using the Fredlund-Xing (1994) equation. Zhang (2016) noted a "true" air-entry value for the new desaturation point. The equation used to fit the degree of saturation is presented in Eq. [2.12].

$$S(\psi) = \frac{S_0(1 - \ln(1 + \psi/\psi_{rs})/\ln(1 + 10^6/\psi_{rs}))}{\left(\ln\left(\exp(1) + \left(\psi/a_{fs}\right)^{n_{fs}}\right)\right)^{m_{fs}}} \quad [2.12]$$

where:

$S(\psi)$ = degree of saturation at any soil suction,

S_0 = initial degree of saturation which is generally quite close to 100%,

a_{fs} = fitting parameter near the inflection point on the *S*-SWCC,

n_{fs} = fitting parameter related to the maximum rate of degree of saturation change,

m_{fs} = fitting parameter related to the curvature near residual degree of saturation conditions, and

ψ_{rs} = suction near residual conditions of the soil.

Zhang and Fredlund (2015) illustrated the procedure to compute the "true" air-entry value using an analytical procedure using conversion of the logarithmic scale to the arithmetic scale and also a transformation technique. Eq. [2.13] was used to transform the degree of saturation of SWCC.

$$SS(\psi) = \frac{S_0\left(1-ln\left(1+ {}^{10^{\xi}}/_{\psi_{rs}}\right)/ln(1+ 10^6/\psi_{rs})\right)}{\left(ln\left(exp(1)+\left({}^{10^{\xi}}/_{a_{fs}}\right)^{n_{fs}}\right)\right)^{m_{fs}}} \quad [2.13]$$

where:

$SS(\xi)$ = degree of saturation as a function of the transformed suction,

10^{ξ} = Soil suction transformed into arithmetic scale,

Eq. [2.14] is used to compute the "true" air-entry value of the soil using i) coordinates of the inflection point on the transformed suction scale plot, ii) line of tangency through the inflection point, and iii) degree of saturation at the start of the SWCC test, as detailed in Fredlund (2017) and Zhang (2016).

$$\psi_{aev} = 10^{\xi_i + \frac{S_0 - SS(\xi_i)}{SS'(\xi_i)}} \quad [2.14]$$

where:

Ψ_{aev} = true air-entry value,

ξ_i = X-coordinate at the inflection point on the transformed scale (transformed soil suction),

S_o = initial degree of saturation at the start of the S-SWCC test,

$SS(\xi_i)$ = degree of saturation at the inflection point,

$SS'(\xi_i)$ = first derivative of the transformed equation at the inflection point.

2.4.8.3 Unsaturated soils property functions (USPF)

Soil properties such as permeability, water storage, shear strength, etc. vary considerably with the degree of saturation as the soil becomes unsaturated, demonstrating the presence of nonlinear correlation compared to the saturated soil property functions, which are considered

constant and linear. M. Fredlund (2000) summarized unsaturated soil property functions and its role during geotechnical engineering practice. Different forms of SWCC are used for the estimation of the USPFs, which are imperative and central for solving saturated-unsaturated problems associated with seepage, deformation, etc.

Fredlund (2017) illustrated determination of USPFs using different forms of SWCC for solving saturated-unsaturated transient seepage problems through the following partial differential equations as presented in Eq. [2.15].

$$\frac{\partial}{\partial x}\left(k_{wx}\frac{\partial h_w}{\partial x}\right)+\frac{\partial}{\partial y}\left(k_{wy}\frac{\partial h_w}{\partial y}\right)=m_2^w\rho_w g\frac{\partial h_w}{\partial t} \quad [2.15]$$

where:

k_{wx} and k_{wy} = major and minor permeability functions,

m_2^w = water storage function,

h_w = hydraulic head in the water phase, (i.e., elevation head plus water pressure head),

g = acceleration due to gravity, and

t = time.

Assuming the k_{wx} and k_{wy} are equal (i.e., k_w), expanding the equation gives the following presented in Eq. [2.16]:

$$k_w\frac{\partial^2 h_w}{\partial x^2}+\frac{\partial k_w}{\partial x}\frac{\partial h_w}{\partial x}+\ k_w\frac{\partial^2 h_w}{\partial y^2}+\frac{\partial k_w}{\partial y}\frac{\partial h_w}{\partial y}=m_2^w\rho_w g\frac{\partial h_w}{\partial t} \quad [2.16]$$

Fredlund (2017) recommended determining USPFs such as permeability and storage functions as independent soil property functions as opposed to single “diffusivity” type variables. Fredlund

pointed out that two main mass-volume variables which influence estimation of the permeability function. These variables are void ratio, and degree of saturation.

Zhang (2016) identified the discrepancy during the estimation techniques for the unsaturated permeability function between soils with high volume change and the conventional assumption of rigid soil structure.

2.4.8.3.1The water storage function

The slope of the instantaneous volumetric water content versus soil suction from the θ_r-SWCC is defined as the water storage property, m_2^w. It is calculated by differentiating the θ_w-SWCC equation as presented in Eq. [2.17].

$$m_2^w = \frac{d\theta_w}{d\psi} \qquad [2.17]$$

where:

ψ = total suction in high suction range (i.e., suctions > 1500 kPa) and matric suction in low suction range (i.e., suctions < 1500 kPa),

θ_w = volumetric water content.

Fredlund and Rahardjo (1993) noted the water storage function, m_2^w, equal to the coefficient of volume change of saturated soils, m_v, at small suction close to zero. It has been stated that the inflection point of the θ_w-SWCC curve is where the maximum water storage value is achieved, and the minimum is at the residual suction value.

2.4.8.3.2The permeability function

Fredlund (2017) summarized estimation of the permeability function for soils which undergo high volume change and can be computed using Eq. [2.18].

$$k_{rw}(\psi) = \frac{k_w(\psi)}{k_{ref}(\psi)} \quad [2.18]$$

where:

$k_{ref}(\psi)$ = reference saturated coefficient of permeability as a function of soil suction. In other words, $k_{ref}(\psi)$ is the saturated coefficient of permeability corresponding to the void ratio at a designated soil suction,

$k_w(\psi)$ = coefficient of permeability as a function of soil suction,

$k_{rw}(\psi)$ = relative coefficient of permeability for changes in the degree of saturation.

Eq. [2.19] for the "dimensionless saturated permeability function," $k_{sd}(\psi)$, is given below

$$k_{sd}(e) = \frac{k_{sw}(e)}{k_{sr}} \quad [2.19]$$

where:

$k_{sw}(e)$ = saturated coefficient of permeability as a function of void ratio, and

k_{sr} = saturated coefficient of permeability at the reference state (i.e., a reference void ratio).

i) Estimation of coefficient of permeability function with respect to void ratio changes

Chapuis (2012) described that the estimation of saturated coefficient of permeability of porous materials, such as soils, is dependent on the size of the pores and the tortuosity of the flow path. Therefore, each factor can be treated separately as the effect of void ratio and the effect of degree of saturation.

Eq. [2.20] is developed by using Kozeny-Carmen's (1937) equation for saturated soils presented below:

$$k_{rw}(e) = \frac{C\, e^3}{1+e} \qquad [2.20]$$

where:

C = constant representing all factors (other than void ratio) affecting the calculation of the saturated coefficient of permeability.

Incorporating Eq. [2.19] and [2.20], coefficients of permeability affected due to change in void ratio can be estimated using Eq. [2.21] as a proportionality:

$$k_{sd}(e) = \frac{k_{sw}(e)}{k_{sr}} = \left(\frac{e^3}{1+e}\right) \Big/ \left(\frac{e_r^3}{1+e_r}\right) \qquad [2.21]$$

where:

k_{sr} = saturated coefficient of permeability at a known reference void ratio,

k_{sw} = saturated coefficient of permeability at another selected void ratio of *e*,

e_r = void ratio as a reference point at which the permeability is known, and

e = void ratio at which the permeability is to be calculated.

The "reference saturated coefficient of permeability" function for void ratio change can be written in terms of soil suction, $k_{ref}(\psi)$, as shown in Eq. [2.22].

$$k_{ws}(\psi) = \frac{C\left(a_{sh}\left(\left(\frac{w_s\left(1-ln\left(1+{}^{\psi}/_{\psi_r}\right)/ln\left(1+{}^{10^6}/_{\psi_r}\right)\right)}{b_{sh}\left(ln\left(exp(1)+\left({}^{\psi}/_{a_f}\right)^{n_f}\right)\right)^{m_f}}\right)^{c_{sh}}+1\right)^{\frac{1}{c_{sh}}}\right)^{x}}{1+a_{sh}\left(\left(\frac{w_s\left(1-ln\left(1+{}^{\psi}/_{\psi_r}\right)/ln\left(1+{}^{10^6}/_{\psi_r}\right)\right)}{b_{sh}\left(ln\left(exp(1)+\left({}^{\psi}/_{a_f}\right)^{n_f}\right)\right)^{m_f}}\right)^{c_{sh}}+1\right)^{\frac{1}{c_{sh}}}} \quad [2.22]$$

Somogyi's (1980) equation presented as Eq. [2.23] can be used to form the relationship between the change in void ratio and saturated permeability.

$$k_{sw}(e) = {}_{\varphi}e^{\circ} \quad [2.23]$$

where:

$k_{sw}(e)$ = saturated coefficient of permeability,

φ = one of the fitting parameters for the void ratio versus coefficient of permeability measurements, and

$\circ$ = second exponential fitting parameter for the void ratio versus coefficient of permeability measurements.

ii) Estimation of coefficient of permeability function with respect to change in degree of saturation

Childs and Collis-George (1950) proposed a model for estimating the coefficient of permeability based on a random variation in pore sizes assuming negligible change in volume as the soil dries. The model was later improved by Marshall (1958) and further modified by Kunze, Uehara, & Graham (1968). Fredlund, Xing, and Huang (1994b) used the Fredlund and Xing (1994a) soil-water characteristic curve equation along with the Childs and Collis-George (1950) physical model to compute a water permeability function. The Fredlund, Xing and Huang (1994b) relative permeability function took the following form when using the degree of saturation SWCC.

$$k_{rw}(\psi) = \frac{\int_{ln\,\psi}^{\varrho} \frac{S(e^{y}) - S(\psi)}{e^{y}} S'(e^{y}) dy}{\int_{ln(\psi_{aev})}^{\varrho} \frac{S(e^{y}) - S(\psi_{aev})}{e^{y}} S'(e^{y}) dy} \quad [2.24]$$

where:

ϱ = upper limit of integration (i.e., $\ln(1{,}000{,}000)$),

y = dummy variable of integration representing the natural logarithm of suction,

S' = first derivative of the soil-water characteristic curve equation, and

e^{y} = natural number raised to the dummy variable power.

The permeability function calculated using the Fredlund, Xing and Huang (1994b) integration procedure consists of a series of discrete data points that can be best fit using the Fredlund and Xing (1994a) SWCC equation or the Gardner (1958) equation. In so doing, the permeability function becomes a closed-form, continuous function.

The volumetric water content is the water content with the volume of water referenced to the original total volume of the soil specimen. The instantaneous volumetric water content is the water content with the volume of water referenced to the instantaneous total volume of the soil specimen. Each form of the SWCC provides similar information to the geotechnical engineer if the soil does not undergo volume change as soil suction is increased. When soil undergoes volume change, as is the case for soft clays and slurry soils, the gravimetric water content SWCC, instantaneous volumetric water content SWCC, and degree of saturation SWCC are distinctly different from one another. The volumetric water content SWCC is not of significance when the soil undergoes high volume change. Conventional permeability functions (e.g., the Fredlund, Xing, and Huang equation; van Genuchten–Burdine equation; van Genuchten–Mualem equation) produce reasonable estimations using the volumetric water content SWCC when there is no volume change during drying. The volumetric water content SWCC is no longer appropriate in the estimation of the relative permeability function when soil undergoes volume change. It is important to know that the relative coefficient of permeability function, as well as the AEV, must be estimated from the degree of saturation for the SWCC (M. Fredlund et al., 2011).

2.4.9 Desiccation

Desiccation is a process of drying and crack formation starting at the surface of the soil. Desiccation of soils mostly occurs in arid and dry areas where the rate of evaporation is exceedingly higher than precipitation. The occurrence of desiccation on the soil changes its stress path, drainage path, and degree of saturation.

Abu-Hejleh, Znidarčić, and Barnes (1996) proposed a model that combines the finite strain and desiccation for fine grained soils. The proposed model closely represents what happens in engineering practice. Four sequential segments were used during modelling the process of

consolidation and desiccation. These four segments represent one-dimensional (1D) consolidation, 1D shrinkage, vertical crack formation and propagation during desiccation and three-dimensional (3D) shrinkage.

Seneviratne et al. (1996) proposed a model for finite strain with evaporation. He reported that the model simulates desiccation by showing an increase in evaporative potential. The evaporation mechanism model produces a similar effect to desiccation by generating suction when the evaporative potential increases more than the water available within the soil. The results using the model are in qualitative agreement with reported observations. The model does not include sedimentation and quantitative verification is left for future work.

Qiu (2000) developed a model that can predict the sedimentation, consolidation, desiccation, crack formation and propagation, total volume of tailings, and water availability for recycling. According to Qui, the model performs for sandy and clayey tailings. The model also predicts the initial stage of desiccation on the surface of deposited tailings. From simulation results provided by Qiu and Sego (2007), they reported that the process of sedimentation has not been investigated in detail and additional work is required.

2.5 Shear strength of soils

Analyzing undrained shear strength of oil sands tailings is a primary objective of this research. The research findings are intended to lead towards an improvement in tailings deposit design. Oil sands industries have explored new possible technologies that can provide or facilitate improved values of undrained shear strength of deposited tailings (i.e., 5 kPa within a year as stated in Directive 074, which was suspended later by Alberta Energy Regulator (AER)) in contrast to the conventional approach. However, to date no studies have been conducted to characterize

consolidation and shearing behaviour of oil sands tailings, tailings treated through different treatments using column testing, and direct simple shear tests. For example, Gholami (2014) investigated the shear behaviour of amended oil sands tailings using simple shear device, and Jeeravipoolvarn (2010) conducted limited vane shear strength tests to characterize the shearing behaviour of oil sands tailings.

The strength of a soil is defined as the resistance to internal friction of a soil to shearing forces and can be computed through a well-defined equilibrium equation developed by Coulomb around 1776. Shear strength was modified by Mohr in 1900 after observations of stress-dependent and stress-independent components of soil strength. Total shear resistance of soils is computed through multiplication of a stress-dependent component, effective stress, with the angle of internal friction, ϕ, and the sum of a constant stress-independent component, namely cohesion, *c'*. The angle of internal friction is proportional to the normal stresses acting on the soil as depicted in the formula presented in Eq. [2.25].

$$\tau = c' + \sigma' \tan \phi \qquad [2.25]$$

where:

τ = shear strength of soil, *kPa,*

c' = cohesion, unitless,

σ' = effective stress, *kPa,*

ϕ = friction angle, *degrees*.

Figure 2.3 presents the shearing response of soils classified as type I, II, and II-A. These classifications are generic and widely used as part of soil mechanics fundamentals. Type I soils

are described as loose sand, normally consolidated, and lightly overconsolidated clays. Type II soils are soil types of dense sands and overconsolidated clays. Type II-A soils are overconsolidated clay soils, which have developed shear bands, and particles of a soil orientated parallel to the direction of the shear bands, causing the final shear stress of these clays to decrease below the critical state shear stress. Critical state is defined as the stress state reached by a soil when no further change in shear stress and volume occurs under continuous shearing at a constant normal effective stress.

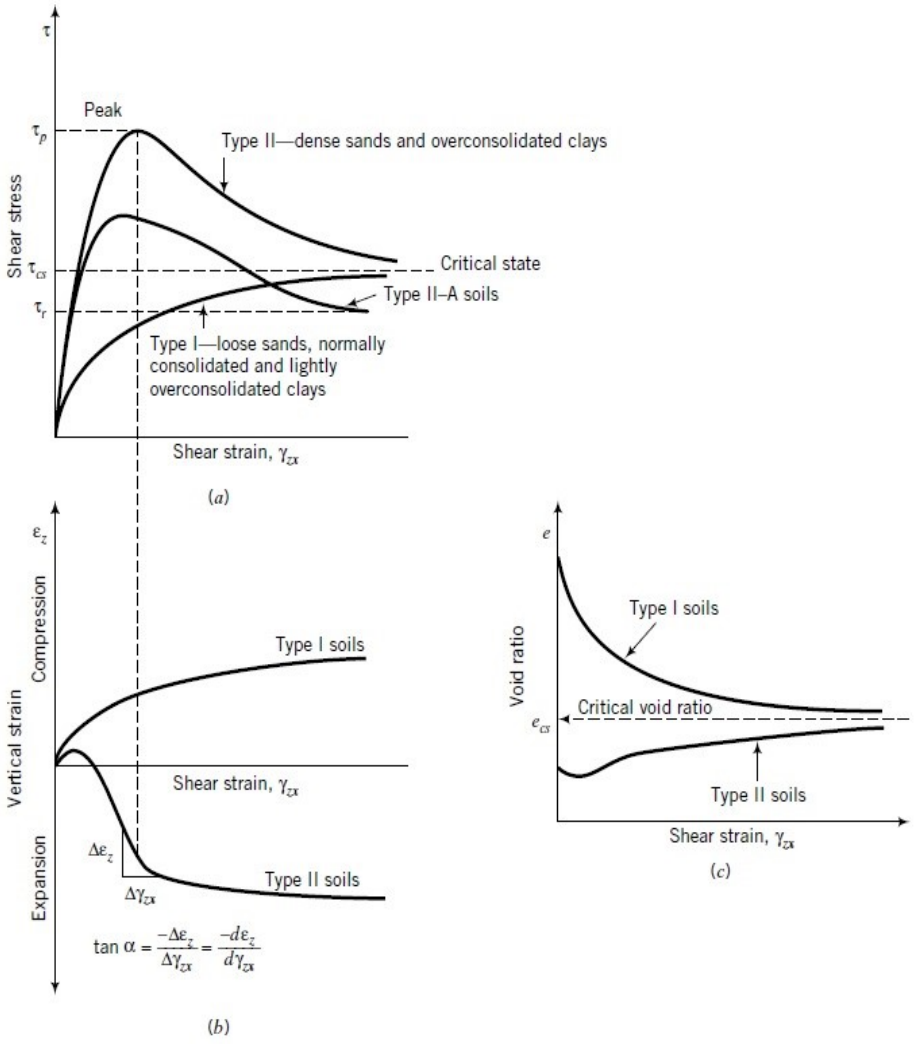

Figure 2. 3 Shearing response of soils (adapted from Budhu, 2011).

Figure 2.3(a) presents plots of shear stress versus shear strain of three soil types, Figure 2.3(b) presents plots of shear strain versus vertical strains of the soil types, and Figure 2.3(c) presents void ratio versus shear strain plots for the soil types.

2.5.1 Shear strength test

Over the years, a number of laboratory testing devices have been developed that are capable of measuring constitutive relations and shear strength parameters of soils and determining relationships between stress and strain. These devices are the triaxial test, the direct simple shear test (DSS), the direct shear test (DS), and the hollow cylinder test.

Direct shear (DS) testing is the easiest and fastest test among all techniques, also used by Terzaghi (1922-25), Hvorslev (1934-1937), Prevost and Hoeg (1975), and Dyvik et al. (1987). When accurate measurements of shear strength parameters and the stress-strain relationship are required, direct shear testing is not preferred. Direct shear tests cannot be an appropriate test to fully simulate field conditions due to the main limitations, which are that i) pore-water pressure is not measured, ii) drainage cannot be controlled, iii) the area where shear and vertical loads applied is not constant, and iv) non-uniform stress deformations result from stress concentrations at the edge.

To overcome limitations associated with the direct shear test, the Direct Simple Shear (DSS) device was developed by Bjerrum and Landva in 1960 (Bjerrum & Landva, 1966), which is capable of keeping the area of sliding constant and imposing more uniform stress distribution. In addition, double drainage paths improve the consolidation process. Simple shear (DSS) test is conducted on cohesive soils to determine stress-strain characteristics of the soil. During DSS testing, volume of soil specimen is held constant and the soil sheared under undrained condition.

The DSS test is capable of measuring homogenous states of stress, thereby avoiding stress concentrations that exist in other shear testing devices. This configuration is closer to in-situ conditions and the results of the first phase of the testing can be compared to one-dimensional k_0-consolidation.

Figure 2.4 illustrates a schematic of stress conditions and deformations using the DSS apparatus. As shown, a vertical load is applied perpendicular to the specimen while shearing force is applied horizontally. Major and minor principal stress during consolidation is vertical and horizontal, respectively. During shearing, major and minor principal stresses will rotate.

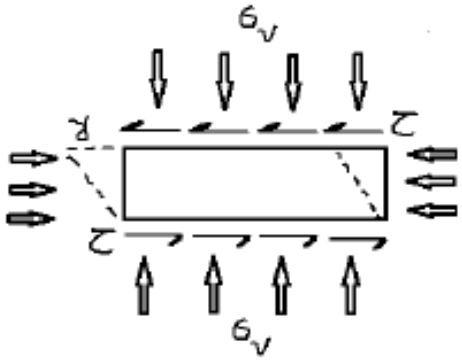

Figure 2. 4 Stress conditions and deformation using DSS apparatus.

Drained and undrained shear strength testing can be conducted using the DSS apparatus based on the material type and required engineering properties. In order to determine the drained shear strength, the vertical load should remain unchanged during the shearing phase. Undrained shear strength can be characterized by keeping the volume of the sample constant.

A general description of the DSS testing apparatus is that a cylindrical or cubical soil specimen is enclosed within a reinforced rubber membrane, as shown in Figure 2.5. The specimen is allowed to be deformed vertically not radially, since the reinforced rubber membrane will serve to prevent

radial deformation during shearing. Procedures have been developed to achieve the best quality for sample preparation and mounting of the specimen between porous stones for a variety of soils. (ASTM D6528; Bjerrum & Landva, 1966).

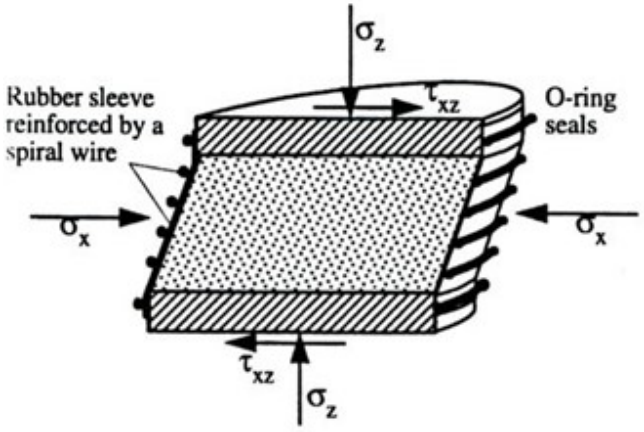

Figure 2. 5 Specimen confinement during DSS testing.

The DSS test applies k_0-consolidation stress in steps to the subjected soil sample. In the case of overconsolidated sample, samples are loaded to their past maximum vertical stress followed by unloaded prior shearing to obtain horizontal stress. Drained and undrained conditions can be performed using the DSS device. Bjerrum and Landva (1966) noted that a constant volume of sample is maintained during the undrained condition by continuously adjusting the vertical stress so that the specimen height is kept constant. The change in vertical stress is assumed to be equal to the change in pore-water pressure that would have occurred during a truly undrained test, as confirmed by Dyvik et al. (1987). Bjerrum noted that results completed using the DSS device exhibit lower shear strengths than tests conducted using triaxial testing equipment.

Dyvik et al. (1987) conducted experiments on normally consolidated clays to verify the hypothesis by using a constant volume shear test with pore-water pressure measurement. The authors described that pressurized cells were used to enclose samples to facilitate fully saturated condition. The results of the undrained test (associated with pore water pressure measurement) and the conventional constant volume test, including stress path and stress-strain relationship on similarly prepared samples, were found to be almost identical in saturated states.

Leroueil (1996) described the influence of various factors on the compressibility of natural clays. Strain rate, stress path, temperature, sample disturbance, and restructuring of sample are some of the listed factors. The hypothesis of the constant volume test is that any change in the vertical stress during shearing is equivalent to the change in pore-water pressure during undrained testing.

Out of the different versions of the DSS apparatus that are available, two versions are presented here to illustrate the differences. First, the one introduced by Kjellman (1951) and completed by Bjerrum and Landva (1966) of the Norwegian Geotechnical Institute (NGI), and second, a version from Cambridge University (CU) (Roscoe, 1953). A circular sample enclosed within a wire reinforced rubber membrane is used in the NGI apparatus. Lateral movement is controlled by a wire-reinforced rubber membrane. The rubber membrane is stiff enough to facilitate k_0-consolidation and keep a constant volume during shearing. On the other hand, the CU equipment uses a sample with a square cross-section area and the lateral deformation remains constant using rigid boundaries.

In a laboratory test setting, it is intended that the test sample should be representative of a point in the ground. This assumption is true if the stresses and strains are uniform, a requirement that no laboratory test can completely satisfy. Laboratory tests are always “a compromise between

the theoretically possible and the practically feasible" (Lacasse et al., 1981). One of the DSS apparatus' limitations is non-uniform distribution of stress, and therefore deformations are non-homogeneous. The lack of shear stresses at the edges causes non-homogenous deformation, while normal force is applied in all directions including edges. Figure 2.6 presents shear stress and normal stress distribution in a Simple Shear. Airey and Wood (1987) investigated stress distribution homogeneity during shearing using a conventional Simple Shear apparatus instrumented with load cells at the edges. Stress distributions are uniform at least in the middle third of the sample and are equal to the average measured stresses in the boundary.

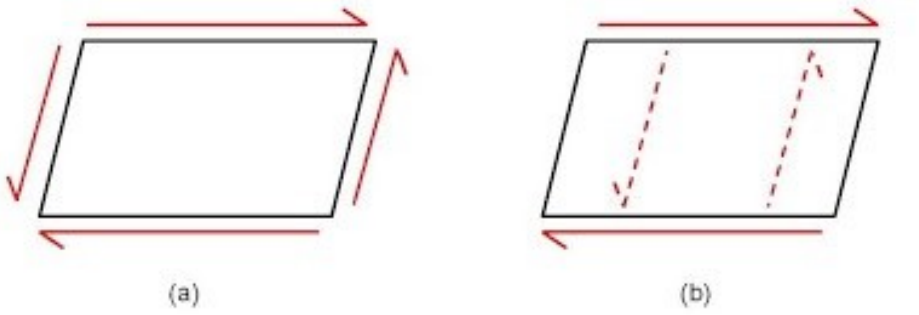

Figure 2. 6 Shear testing under a) pure shear and b) direct simple shear

The NGI and Cambridge DSS's were compared by Budhu (1984). The author attempted to characterize behaviours of similarly prepared sand specimens. Developments of non-uniformity were observed during monotonic loading and clearly visible during cyclic loading. However, some major differences in the results were observed. Budhu stated his observation as follows: "The rigid boundaries of the Cambridge apparatus force the sample to deform in a simple shear configuration, but the 'flexible' vertical boundary of the NGI type apparatus cannot do so except, perhaps, at small shear strains." (Budhu, 1984, pp. 134-135).

2.5.2 Measurement of shear strength using the vane shear device

Laboratory and in-situ shear strength of a soil can be measured using the vane shear apparatus as described in ASTM D4648M-16 and D2573-08. The vane shear technique was originally developed by British Army to measure clay sediments' cohesion (Skempton, 1949; Boyce, 1983). The vane shear apparatus is composed of two crossed blades fixed at a right angle to each other and attached to a rod. The vane blades have well-defined dimensions, height, and diameter, and used for soils with different shear strengths values as recommended in ASTM. Vane shear testing is conducted by pushing the vane fully to the desired depth into the prepared specimen in the case of laboratory testing and into the ground for in-situ testing. Torque will be applied to the vane through the attached and extended rod either through the torque-generating motor or another device. The rotation will cause the soil to shear along a cylindrical rapture surface of engaged vane dimensions. Estimation of shear strength will be computed using measured torque rotation (Cadling & Odenstad, 1950).

Chandler (1988) discussed the factors affecting the vane shear test such as type and geometry of vane, insertion method and type of blade, duration of rest period prior to test, rate of rotation, and complex deformation patterns from non-uniform stress distribution and progressive failure. Roy and Leblanc (1988) noted the influence of disturbance during vane insertion, time and shear velocity on measurement, and interpretation of vane shear test. The author noted the actual shear surface is larger than the cylindrical surface defined by the dimensions of the blades. Menzies and Merrifield (1980) investigated and measured shear stress distribution on the blades of an instrumented vane on laboratory sand and field clays. The authors compared measured shear stress distributions of the blade with analytical results obtained by Donald et al. (1977).

Perlow and Richards (1977) discussed the influence of vane size, rotation rate, and sample disturbance on vane shear strength measurement. Sharifounnasab and Ullrich (1985) discussed the influence of plasticity on the vane shear test by conducting a series of laboratory vane shear tests with different shear rates. The authors suggested that partial drainage occurred during the slow rate vane shear test on low plastic clays. The authors concluded that highly plastic clay demonstrates an undrained condition and an increase in vane shear strength with an increase in shear rate. The influence of anisotropy has been investigated by many researchers (Aas, 1965; Menzies & Mailey, 1976).

The shear strength of a soil can be obtained using an empirical correlation or theoretical formulas. The correlation is based on used torque and an assumed shear stress distribution on the sides of the vane blade. For instance, (Bjerrum, 1972, 1973) provided a correlation of the plasticity index of a soil to the ratio of vane shear strength for the preconsolidation stress. Bjerrum et al. (1975) suggested that vane strength can be uniquely related to a preconsolidation pressure and plasticity of young and aged clays. Lacassa, Ladd, and Baligh (1978) and Jamiolkowski et al. (1985) have suggested that field vane strength should be related to the in-situ effective stress and to the OCR using more general equation.

2.5.3 Shear strength characteristic of clays

The objective of the present research study is to investigate the shear strength behaviour of oil sand tailings using vane shear equipment. Therefore, this section will explore shear strength characteristics of clays since engineering properties of soft clays have similarity with fundamental properties of oil sand tailings. Figure 2.7 illustrates an example of monotonic shear response of a kaolinite specimen in a DSS apparatus.

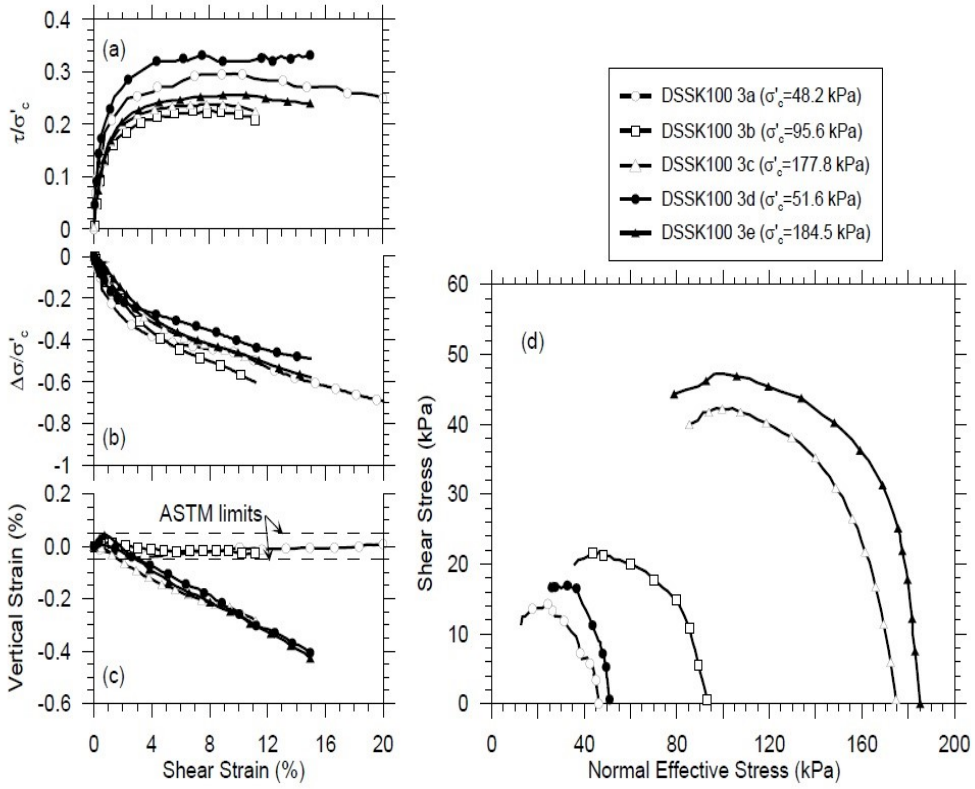

Figure 2. 7 Direct Simple Shear test results for Kaolinite specimens (Bro, Stewart, & Pradel, 2013).

Some of the main factors affecting monotonic shear response of clays when using a Direct Simple Shear apparatus are described below.

2.5.4 Anisotropy of specimens

An anisotropy property of a soil specimen can be caused through either inherent or stress-induced activities (Lofroth, 2018). Different soils structures can be formed during soil formation process which causes inherent anisotropy properties of the soil. On the other hand, stress-induced anisotropy is caused due to stress-induced consolidation process where the effective consolidation pressures are not equal in all directions. A model was proposed by Larsson (1977)

for soft clays. This model has the ability to estimate undrained shear strength parameters in planes at different orientations, and these parameters will examine the influence of anisotropy on the behaviour of clay specimens.

2.5.5 Stress history and stress state

The effect of stress history on a soil can be observed through graphs of normalized stress by the preconsolidation versus strain. Ladd and Foott (1974) reported that clay specimens with a similar overconsolidation ratio (OCR) but a different consolidation stress history show a similar stress-strain response when normalized by consolidation pressure. Figure 2.8 shows an example of a clay specimen consolidated at two different consolidation pressures in their studies. However, the shear response graphs are coincided once deviator stress is normalized by consolidation pressure. Similarly, Figure 2.8 shows the normalized shear stress behaviour in a DSS device. It should be noted that discrepancies of normalized graphs are unavoidable as a result of existing inherent anisotropy of specimens.

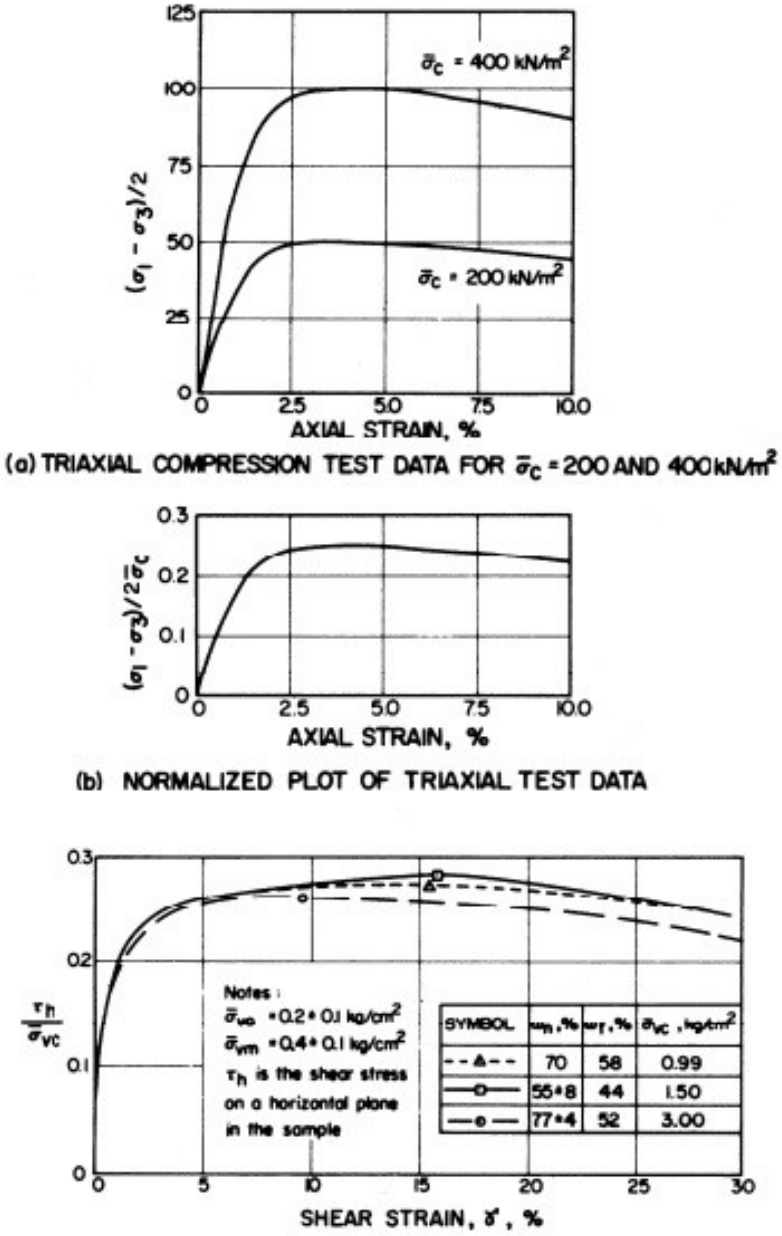

Figure 2. 8 Normalized behaviour using idealized triaxial compression test data for homogeneous clay and direct simple shear test data for normally consolidated Maine organic clay (Ladd and Foott, 1974).

2.5.6 Sample preparation

Hanzawa et al. (2007) investigated the effect of sample preparation by conducting shear strength tests using a DSS apparatus of undisturbed and remoulded samples of plastic Drammen clay, with different OCR's. Figure 2.9 shows sample results of the investigation. Results have shown the shearing response of both undisturbed and remoulded specimens to be equal, leading to the conclusion that the effect of sample disturbance can be overcome at high consolidation stress.

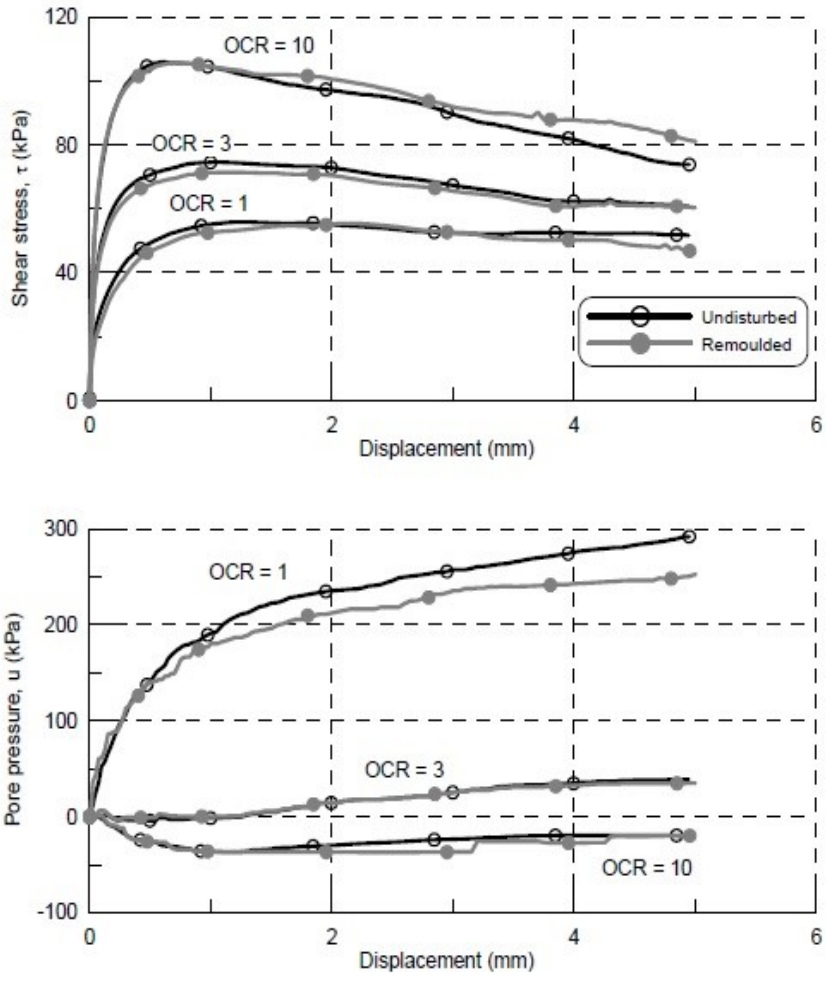

Figure 2. 9 Comparison of direct shear testing on remoulded and undisturbed specimens of plastic Drammen clay (Hanzawa et al., 2007).

2.5.7 Shearing rate and shearing mechanism

Hanzawa et al. (2007) published the results of two different clay samples from Norway and Japan in an investigation conducted using a conventional NGI apparatus and a custom-made DSS device. Results using the second apparatus give higher strength compared to NGI for all samples consolidated to the in-situ stress values. Different shearing mechanisms, various shear strain rates, and anisotropy of samples were found as the main reasons for the discrepancy in the collected results.

Bro, Stewart, and Pradel (2013) investigated undrained shear strength of different clay samples by conducting a different series of tests at different displacement rates. In the first series, a low displacement rate (i.e., 1%/hr) was considered to infer constant volume test as described by ASTM (D6528). In the following series, higher rates of displacements were used to enable partial drainage. Results showed that at high displacement rates, the undrained strength cannot be estimated accurately, since the change in height is relatively large compared to the maximum allowable height change recommended by ASTM (less than 0.05%). To maintain the desired constant volume was difficult due to change in sample height. The authors concluded that only a low displacement rate can meet the requirements of truly undrained shear strength in constant volume DSS testing.

2.5.8 Shear strength development in slurry

Watari (1984) presented marine clay's shear strength in relation to its water content using vane shear device, as shown in Figure 2.10(a). Estimation bearing capacity was conducted based on experimental results and concluded that reclaimed land will possess a shear strength of 1 kPa near the surface.

Inoue, Tan, and Lee (1990) presented a normalized plot of yield shear stress versus moisture content from different clays by using procedures developed by Matsui and Ito (1977). Inoue, Tan, and Lee (1990) concluded that the results showed unique behaviour when plotting yield shear stress against the parameter *w*/*wL* ratio as presented in Figure 2.10(b). The difference between Figure 2.10(a) and Figure 2.10(b) is notable since that there is no distinct relationship between shear strength and water content as presented in Figure 2.10(a). On the other hand, there are three distinct zones when the plot is made using shear strength and a ratio of *w*/*wL*, as presented in Figure 2.10(b). These regions show negligible shear strength at a higher moisture content, a transition zone where the shear strength developed noticeably, and a region where significant shear strength advanced. Ito and Matsui (1975) identified the change in water clay system at the microscopic mechanism when the value of *w*/*wL* within 1.4 to 2. According Watari (1984), there is a dramatic change in the yield shear strength at a *w*/*wL*, of 1.6 when the test conducted was used a vane type test. It is indicative that the yield shear strength of slurry is controlled by its clay content since *wL* is used to normalize the water content.

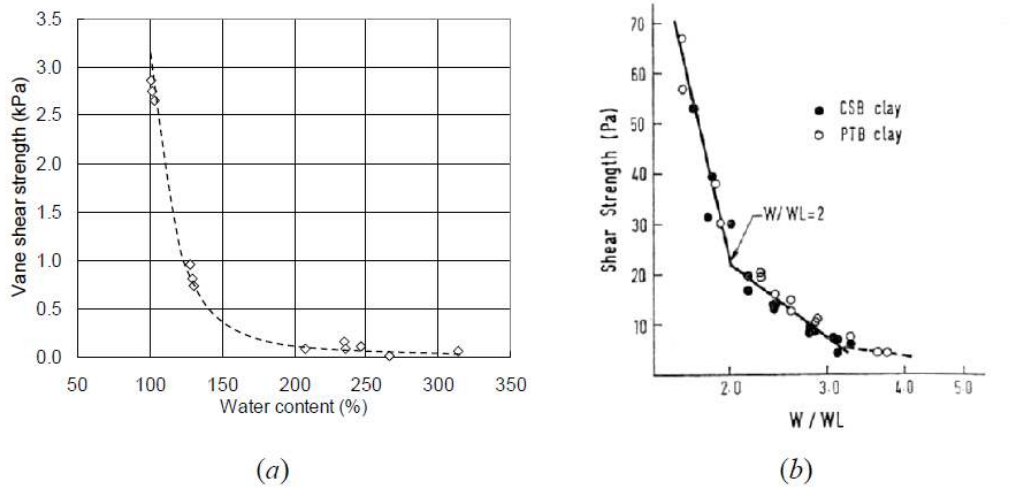

Figure 2. 10 Shear strength behaviour of soft clays: (a) vane shear strength vs. water content (modified from Watari, 1984) (b) shear strength vs. w/wL (modified from Inoue, Tan & Lee, 1990).

Seed, WoodWard, and Lundgren (1964a, 1964b) and Tan et al. (1994) investigated the relationship between liquid limit and shear strength of clay-sand mixtures using the thin plate penetration method. It was concluded that there was a linear relationship between liquid limit and clay content until the sand content becomes higher (i.e., greater than 60% in most cases). Tan et al. (1994) used silt fraction instead of clay fraction.

2.5.9 Shear behaviour of hard rock tailings

Mine waste tailings such as hard rock and oil sands tailings were given limited attention, despite the fact that the study of soils subjected to shearing has been investigated since 1970s. Lately, adopted environmental regulations and policies have forced operators and researchers to carry out research on shearing behaviours of hard rock and oil sands tailings. For instance, tailings "Directive 074" were given by Alberta Energy Regulator (AER) which enforces the capture of fines, total tailings volume reduction and reclamation of the landscape by the operators in less than 5 years. The sections below will explore how shear strength of tailings is affected by different initial state variables.

i) Void ratio

Al-Tarhouni, Simms, and Sivathayalan (2011) and Daliri et al. (2013) reported the influence of void ratio (density) of hard rock tailings on the mechanical response. The authors noted that the decrease in void ratio of reconstituted samples of gold tailings provides results changing the shear behaviour of the tailings from strain softening to hardening. The decrease in void ratio was observed at a fixed consolidation pressure. Figure 2.11 shows a typical example of monotonic response of gold tailings over a range of void ratios.

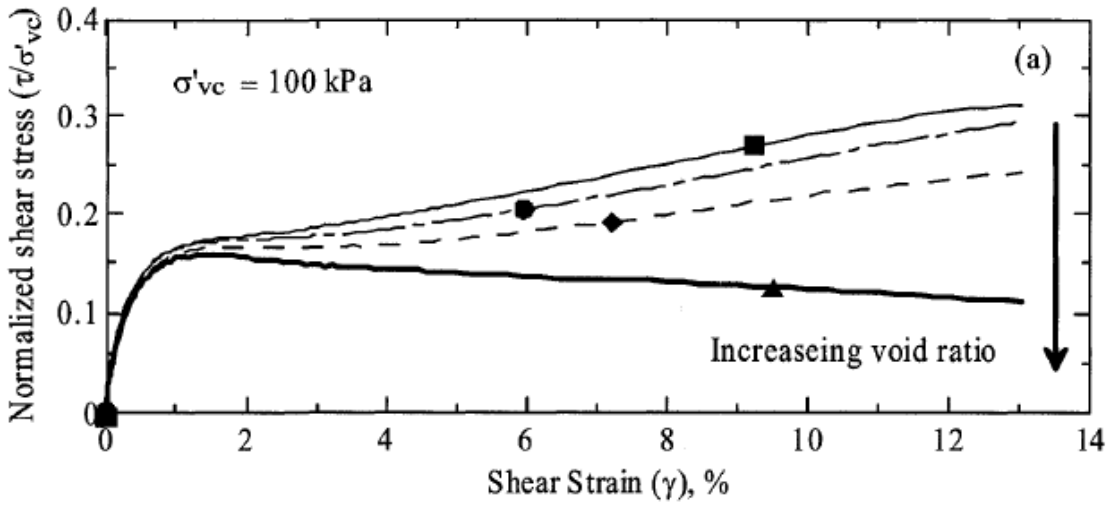

Figure 2. 11 Monotonic response of gold tailings over a range of void ratios (Al-Tarhouni, Simms, & Sivathayalan, 2011).

ii) Degree of saturation

Al-Tarhouni, Simms, and Sivathayalan (2011) examined the influence of degree of saturation on behaviour of mine tailings in a DSS test by varying the saturation of samples between 0.9 and 1.0 during the investigation. The results are presented in Figure 2.12, and the behaviour of the samples was found to be identical while having different degrees of saturation.

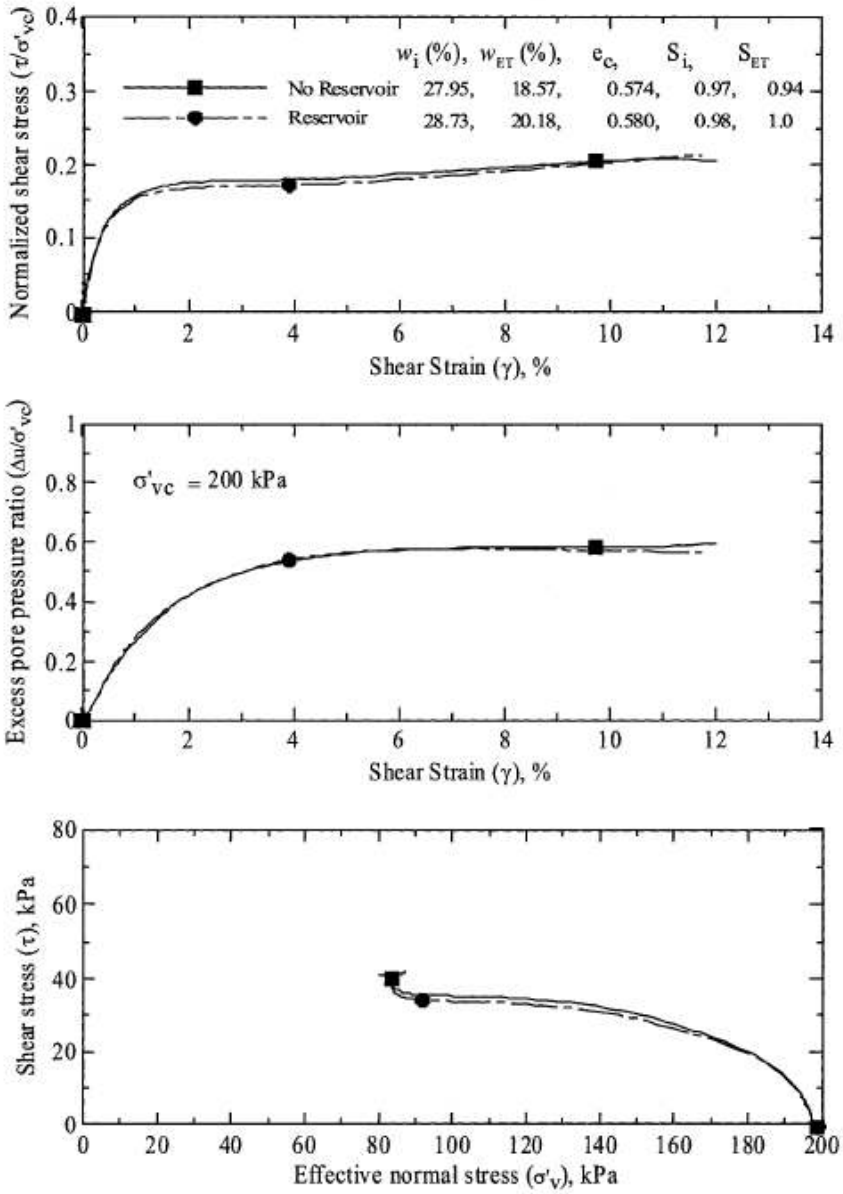

Figure 2. 12 Comparison of two samples with a similar postconsolidation void ratio, e_o, with one of the tests connected to a water reservoir to increase degree of saturation: (a) normalized shear stress versus shear strain, (b) excess pore pressure ratio versus shear strain, (c) stress path (Al-Tarhouni, Simms, & Sivathayalan, 2011).

Chapter Three: Theory

3.1 Introduction

The formulas derived from that of large strain consolidation theories coupled with unsaturated flow properties are central for a number of engineering applications including the evaporation of water to assist in the dewaterability of deposited tailings (Daliri et al., 2014; Fujiyasu & Fahey, 2000; Matthews et al., 2011; Qi et al., 2016; Simms et al., 2010; Soleimani et al., 2014; Wells, 2011).

The consolidation processes start with fully saturated tailings deposits, followed by sedimentation, self-weight consolidation, the transition from a fully saturated to desaturated state, and desiccation and crack formation. A literature review of the physical processes related to the slurry tailings deposition was presented in Chapter 2.

This chapter presents theory and formulas related to the physical processes relevant to the deposited slurry tailings in these experiments. The experiments were conducted in two stages differentiated by changes in the applied boundary conditions: (i) sedimentation and self-weight consolidation and (ii) consolidation process using an applied negative water pressure (suction) at the bottom boundary (i.e., the base of the column). The applied negative pressure at the bottom of the column simulated the effect of evaporation from the deposited tailings surface during field trial conditions. These experiments were conducted in stages on the same tailings.

3.2 Overview of column apparatus functionality

This section presents an overview of the functionality of the column apparatus, which was used to carry out the laboratory study. The column apparatus facilitates the use of controlled physical processes, such as incremental applied suction and the measurement and analysis of the changes observed in the freshly deposited tailings. The experiments were conducted in two stages defined by different boundary conditions.

3.2.1 Hypothesis of column apparatus functionality

The column apparatus is composed of two main components: an acrylic column and a polyvinyl (PVC) base plate. The base plate includes a high air-entry value ceramic disk. A drainage path was made within the base plate using grooves to facilitate movement of water during the consolidation process. The porous ceramic disk can withstand a pressure difference of up to 100 kPa and is suitable for the application of negative pore-water pressures (Fredlund, Rahardjo, & Fredlund, 2012). The negative pressure (i.e., suction relative to atmospheric air pressure) applied to the column apparatus was used as driving force for the consolidation of the tailings.

The column mimics field condition drying and desiccating process of a transition/interlayer zone. The drying/desiccation process that occurred during a field trial and column testing in the lab showed comparable development of the transition zone, except for the change in the direction of flux. While the process of consolidation, drying/desiccation progressed irrespective of the flux direction either using applied suction at the bottom boundary or through evaporation and rainfall on the surface for actual field condition. Figure 1.1 in Chapter 1 was used to illustrate and visualise the formation of transition zone using the column apparatus. Details of the column apparatus

design are presented in (Fisseha, Wilson, & Fredlund, 2017b) and are summarized in Chapter 4, section 4.2.3.

Experiments were conducted in two stages: (i) sedimentation and self-weight consolidation and (ii) consolidation using an applied negative water pressure (suction). During the consolidation-using suction stage, the water table line (i.e., zero pressure line) moves to a lower level along the deposited slurry tailings thickness. The continuous withdrawal of water may generate an unsaturated zone near the surface of the deposited tailings. A consolidated zone develops near the surface, and the unsaturated region is expected to continue to establish negative pore-water pressures. Subsequently, the desaturated tailings may start to pull away from the walls of the column boundary. Consequently, cracks may form and propagate downward from the surface of the deposited tailings. It is anticipated that the column testing will mimic the saturated-unsaturated behaviour of deposited tailings under field conditions.

3.2.2 Sedimentation/self-weight consolidation – Stage 1

The first stage of experiments investigated sedimentation/self-weight consolidation immediately after the tailings were deposited. The drainage boundary was at the top surface of the deposited tailings during this stage, which progressed until the excess pore pressure was fully dissipated and no vertical strain was registered. Figures 3.1 to 3.3 present schematic representations of the process of sedimentation and self-weight consolidation during Stage 1 with time.

Figure 3.1 shows the profile of the tailings immediately following deposition of the slurry. Figure 3.1 (a) provides a conceptual illustration of the tailings with a uniformly distributed solids content at the initial stage. The drainage flow during the self-weight consolidation process was in an upward direction as shown using the arrows. Figure 3.1 (b) presents the distribution of hydrostatic

pressure and the total and effective stress of the tailings and the top and bottom boundaries at its initial stage (i.e., time = t_0).

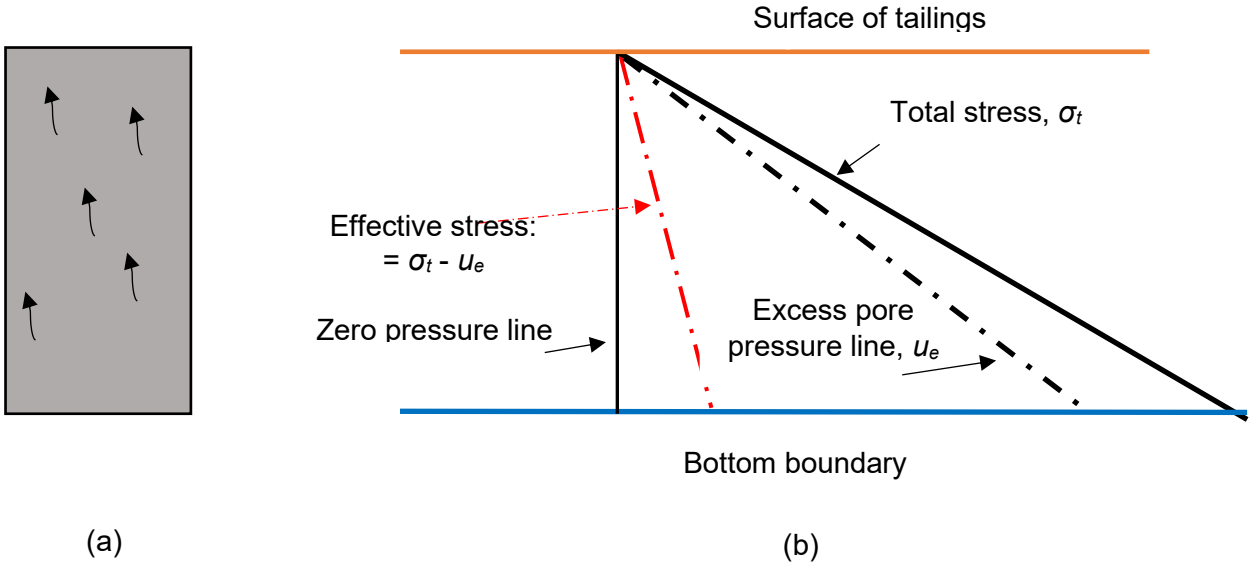

Figure 3. 1 The process of self-weight consolidation at the initial stage: (a) column apparatus showing self-weight consolidation, flow direction at time = t_0 and (b) conceptual plots on distribution of hydrostatic pressure, total and effective stress.

Figure 3.2 shows a schematic representation of the tailings while undergoing the sedimentation/self-weight consolidation process and the accumulation of supernatant water over the tailings surface. Figure 3.2(a) provides a conceptual illustration of the change in the total height of the tailings (i.e., vertical strain), the flow direction, and the accumulation of supernatant water as sedimentation/self-weight consolidation progressed. Figure 3.2(b) presents the distribution of excess pore pressure, total and effective stress of the tailings, and the top and bottom boundaries at some time during the process (i.e., time = t). The change in the total height of the tailings with time is denoted by the dotted line at the surface of tailings in Figure 3.2(b). The presence of supernatant water overlaying the surface of the deposited tailings was included to mimic the process of self-weight consolidation measured in the laboratory.

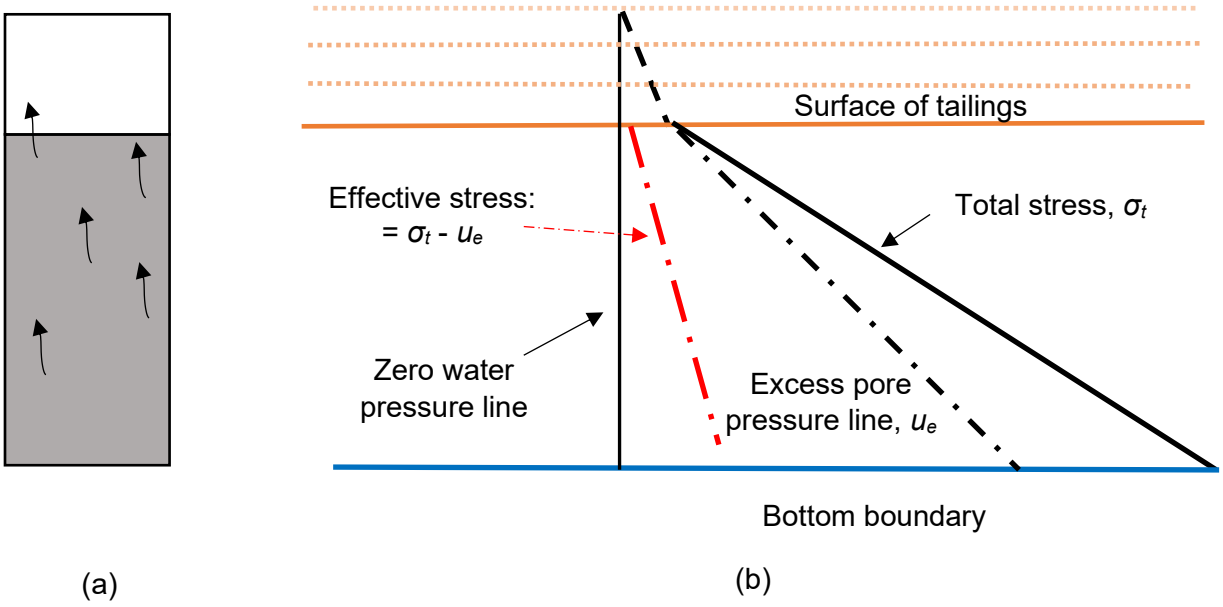

Figure 3. 2 The process of self-weight consolidation at the intermediate stage: (a) the column apparatus showing self-weight consolidation, flow direction during the time = t, (b) conceptual plots on distribution of excess pore pressure, total and effective stress.

Similar to Figure 3.1 and 3.2, Figure 3.3 illustrates the final stage of the self-weight consolidation process. Figure 3.3(a) and Figure 3.3(b) show the change in the total height of the tailings, the flow direction and the distribution of stress (effective and total stress), and hydrostatic water pressure as the sedimentation/ self-weight consolidation process concluded. The top and bottom boundaries of the tailings surface at the final time (i.e., time = t_f) is included in Figure 3.3 (b).

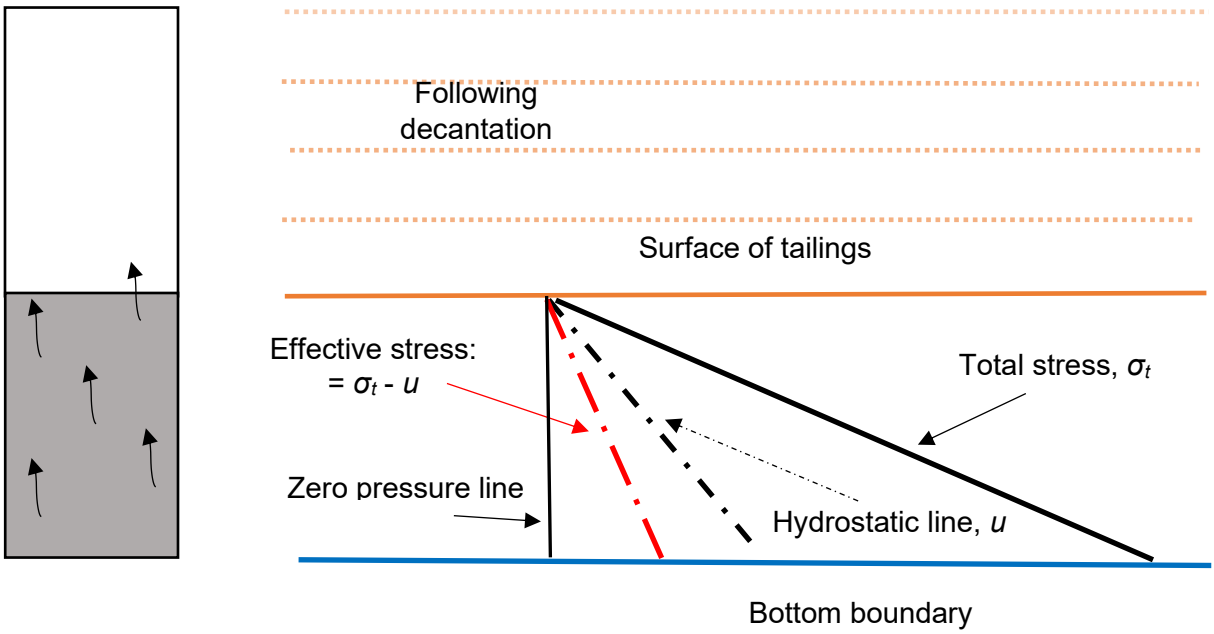

Figure 3. 3 The process of self-weight consolidation at the final stage: (a) column apparatus showing self-weight consolidation, flow direction during the time = t_f, (b) conceptual plots on distribution of hydrostatic pressure, total and effective stress.

3.2.2.1 Initial condition

The initial condition during the self-weight consolidation process can be specified using the initial void ratio, initial solids content, or initial bulk density. The formulae to calculate the initial void ratio, e_0, is presented in Eq. [3.1] in terms of solids content:

$$e_0 = G_s\left(\frac{100}{SC_0} - 1\right) \qquad [3.1]$$

where:

e_0 = initial fines void ratio,

G_s = specific gravity of solid, and

SC_0 = solids content by weight (%).

The initial void ratio, e_0, can be calculated based on initial bulk density, ρ_0, using Eq. [3.2]:

$$e_0 = \frac{\rho_w G_s - \rho_0}{\rho_0 - \rho_w} \quad [3.2]$$

where:

ρ_0 = initial density of mixture, kg/m^3,

G_s = specific gravity of solid, and

ρ_w = water density, kg/m^3.

3.2.2.2 Boundary condition

The boundary condition can be applied at the surface of the tailings, assuming that the excess pore-water pressure was zero, u_e = 0. The reason to ascribe the surface of the tailings as the boundary was due to the free drainage of water towards the direction of the upper boundary during the self-weight consolidation process. Eq. [3.3] presents the boundary condition in the Eulerian coordinate system (SoilVision manual, 2017).

$$u_{wstatic} = \gamma_w(h_0 - \eta) \quad [3.3]$$

where:

$u_{wstatic}$ = static pore water pressure, kPa,

γ_w = unit weight of water, kN/m^3,

h_0 = initial water head, m, and

η = Eulerian coordinate.

3.2.3 Consolidation using applied suction – Stage 2

The process of consolidation using an applied suction, also specified as Stage 2, following completion of the self-weight consolidation process (Stage 1) is described in this section. The process of consolidation using an applied suction was completed incrementally by applying incremental increases in suction to the bottom boundary. This process uses the bottom boundary as its drainage boundary, as the flow of water is directed in a downward direction due to the exerted suction at the bottom of the column. A schematic representation of the consolidation process using applied suction is given in Figures 3.4 to 3.6. Part (a) of each figure displays the change in total height and direction of water flow, and part (b) presents the conceptual change in hydrostatic water pressure or suction with respect to the total and effective stress on the deposited tailings. The change in water pressure distribution from hydrostatic at the end of self-weight consolidation, Figure 3.4, to an applied suction within the deposited tailings once the applied suction reached an equilibrium condition, is shown in Figures 3.5 and Figure 3.6. These schematic figures attempt to present selected applied suction conditions carried out during the laboratory testing. The change in total volume (or volumetric strain) is depicted using the dashed line, and the solid line represents the final measured volume during the incremental applied suction period.

Figure 3.4 parts (a) and (b) present the end of the self-weight consolidation process and prior to initiating the applied suction, illustrating the existing condition prior to the applied suction stage, as shown in Figures 3.5 and 3.6.

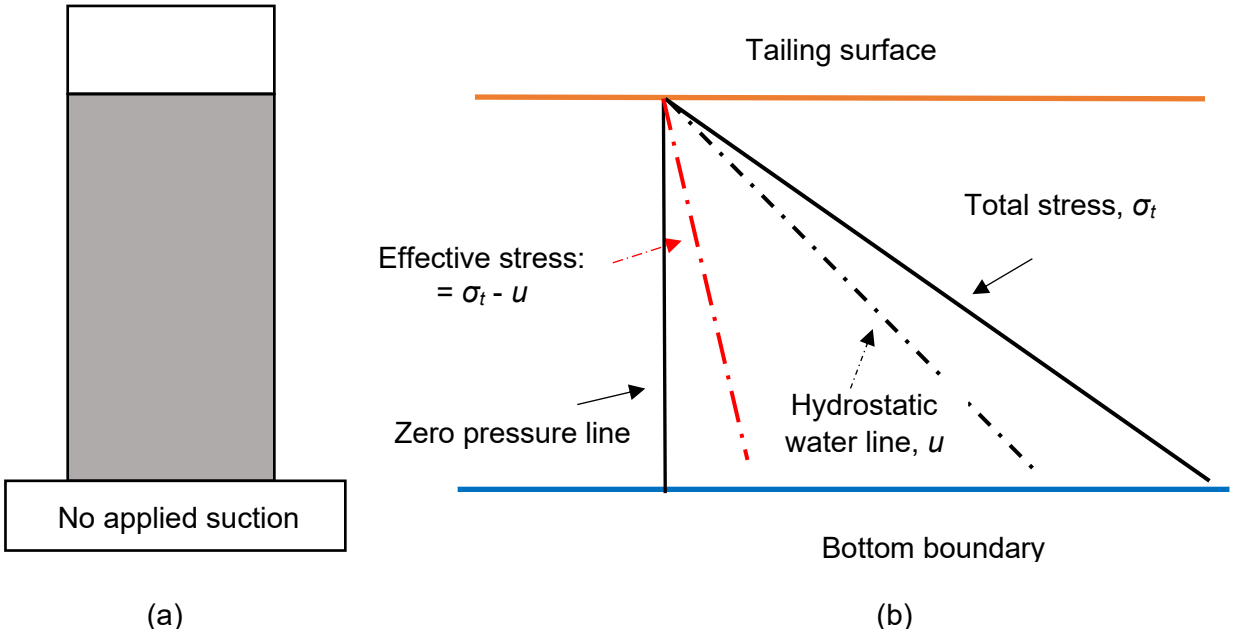

Figure 3. 4 End of self-weight consolidation: (a) column with no applied suction at the base, (b) conceptual plots for total and effective stress distributions condition.

Figure 3.5(a) and Figure 3.5(b) depict consolidation during an applied negative pore-water pressure of 10 kPa, following the end of the self-weight consolidation process. Figure 3.5 shows the change in total volume and flow direction. Further, both part (a) and part (b) of Figure 3.5 display the distribution of pore-water, as well as total and effective stress within the deposited tailing.

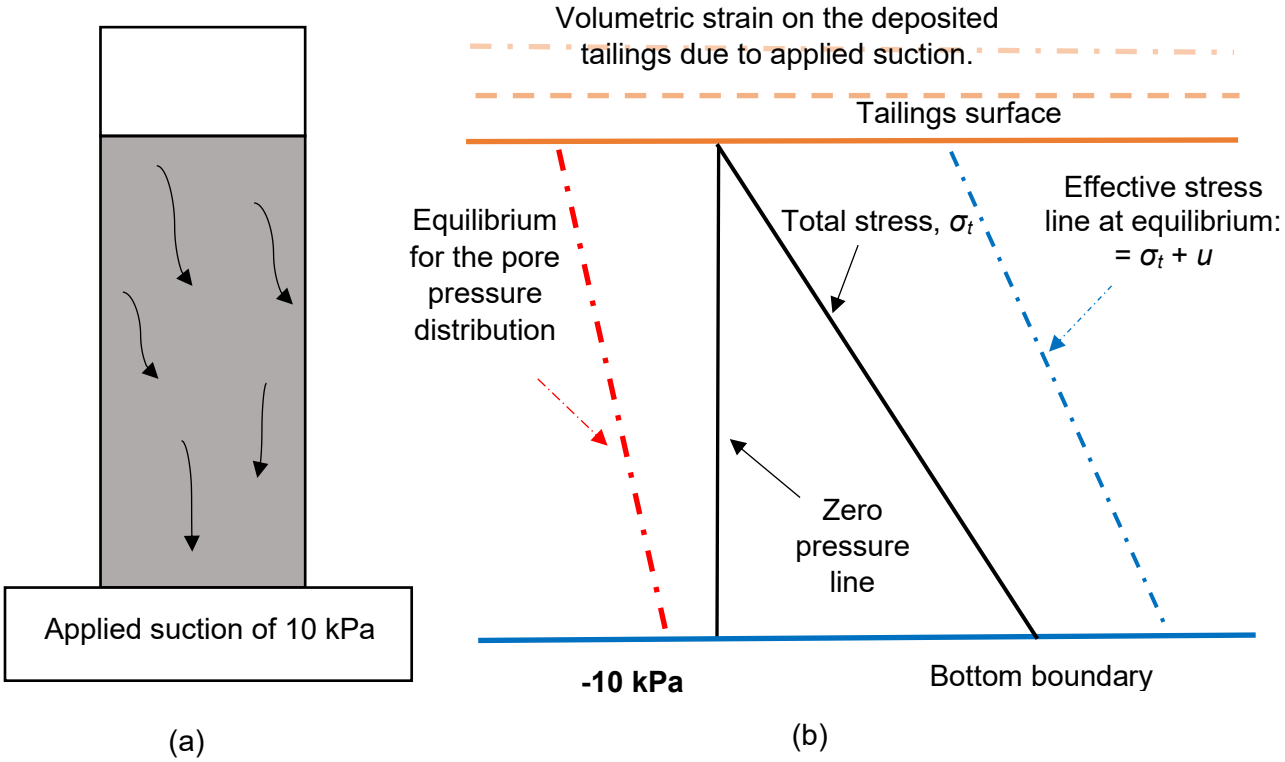

Figure 3. 5 The process of consolidation during applied suction of 10 kPa: (a) column with 10 kPa applied suction at the base, (b) conceptual plots for total and effective stress distribution, under applied suction conditions.

Similarly, Figure 3.6(a) and (b) present a conceptual representation of an applied suction of 30 kPa following the equilibrium being reached during the previous applied suction stage. Figure 3.6(a) shows the change in total volume and flow direction, and Figure 3.6(b) illustrates the distribution of suction and total and effective stress within the deposited tailings.

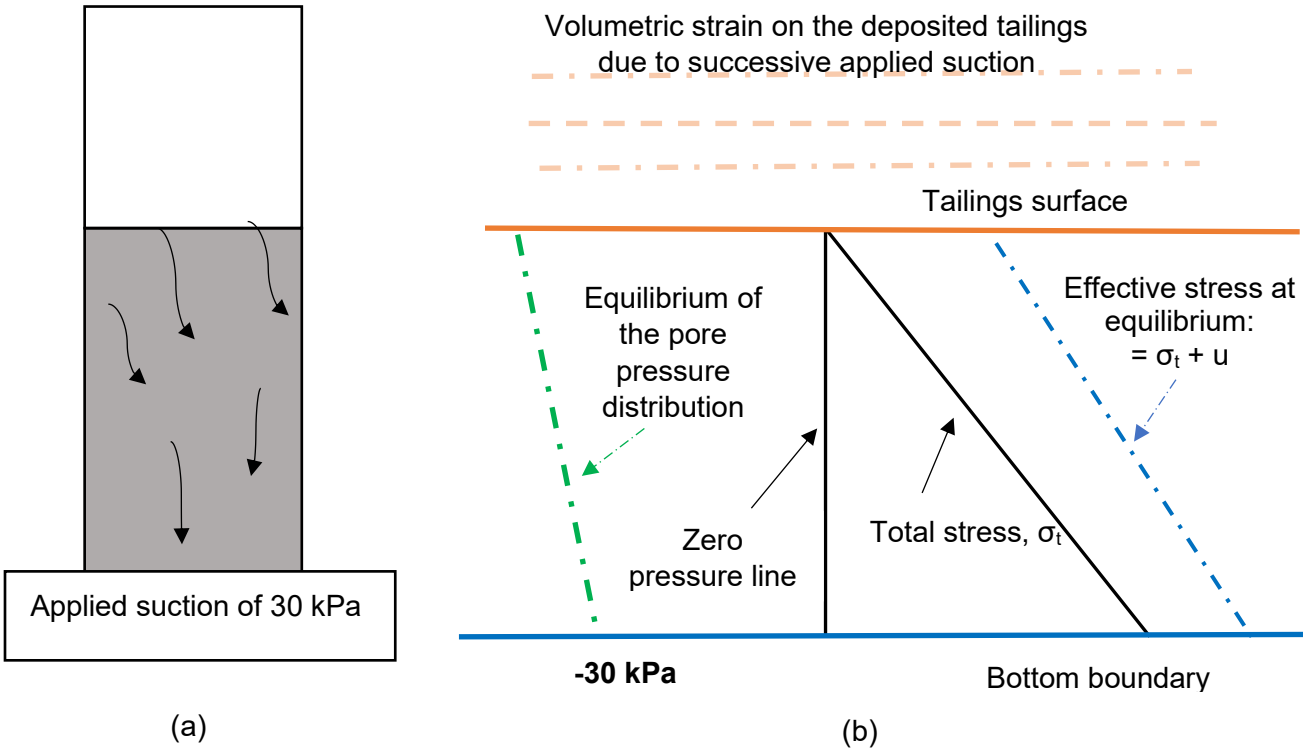

Figure 3. 6 The process of consolidation during applied suction of 30 kPa: (a) column with 30 kPa applied suction at the base, (b) conceptual plots for total and effective stress distributions, under applied suction conditions.

3.2.3.1 Initial condition

The initial conditions during consolidation using an applied suction can be specified in terms of the void ratio, solids content, or total hydraulic head of the deposited tailings when the self-weight consolidation process is completed.

3.2.3.2 Boundary condition

The boundary conditions during consolidation using applied suction can be specified as constant applied suction at the bottom of the column apparatus for each incremental applied suction.

3.3 Formulation of sedimentation and self-weight consolidation

The formulation for the sedimentation and self-weight consolidation process is presented in the following subsections.

3.3.1 Hindering settling sedimentation

Kynch (1952) proposed a theory of sedimentation by assuming that the velocity of a falling particle in suspension is governed by its local density. Therefore, the process of sedimentation can be determined using principles of mass conservation. The equation for sedimentation is given in Eq. [3.4]:

$$S = \rho v \qquad [3.4]$$

where:

S = Kynch's particle flux density function,

ρ = density, kg/m^3, and

v_s = solid hindering settling velocity, *m/sec*.

Defining the height as *y* above the bottom of the column of particles in suspension for a particle flux (i.e., *S*) which varies with height as the particles continue to settle with time, and considering the layers at *y* and (*y* + *dy)*:

$$\frac{\partial \rho}{\partial t} = \frac{\partial S}{\partial y} \qquad [3.5]$$

The governing equation can be rewritten as given in Eq. [3.6] by assuming a constant falling velocity of the particle:

$$\frac{\partial \rho}{\partial t} + V(\rho)\frac{\partial \rho}{\partial y} = 0 \qquad [3.6]$$

where:

$$V(\rho) = -\frac{dS}{d\rho}$$

Hindered sedimentation's governing equation is given by Eq. [3.6] and solved using the partial differential equation or with an alternative numerical method analysis.

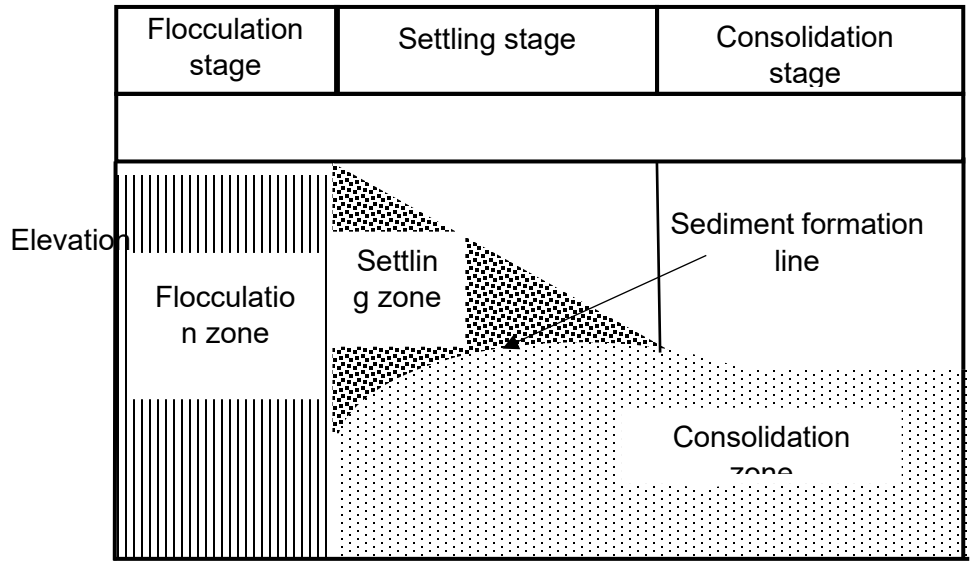

Figure 3. 7 The characteristics of sedimentation of clay-water mixtures (modified from Imai, 1981).

Equation [3.6] was used to analyze the sedimentation of soils by McRoberts & Nixon (1976). Figure 3.7 presents a schematic solution of the sedimentation process of slurry soil assuming the

particle velocity is constant. Discontinuous interfaces were observed during sedimentation at the interface between the supernatant water and particle suspension, and the interface between the sediment at the bottom and the particle suspension above it.

3.3.2 Hindering settling velocity

The settling velocity of solid particles under suspension in viscous fluid was defined by Stokes (1851), assuming no hindering between the solid particles. The settling velocity defined by Stokes is given as:

$$v_{st} = \frac{(\gamma_s - \gamma_w)d^2}{18\mu} \quad [3.7]$$

where:

v_{st} = Stokes particle settling velocity, *m/sec*,

d = Stokes diameter of particle, *m,*

γ_s = unit weight of solid, *kN/m^3,*

γ_w = unit weight of water, *kN/m^3*, and

μ = fluid viscosity, *kg/s-m.*

Schofield and Wroth (1968) indicated the validity of Stoke's settling velocity of particles is for small sizes by assuming the diameter of particles range between 0.05 mm and 1 μm. It is also known that there is a change in the hindering settling velocity with solids density or porosity.

$$v_s = v_{st} f(n) \quad [3.8]$$

where:

v_s = hindering settling velocity, *m/sec*,

v_{st} = Stokes velocity of a particle, *m/sec*,

n = porosity, and

f(n) = a relation as the function of n.

Richardson and Zaki (1954) proposed an empirical formula for the determination of particles' hindering velocity using Stoke's velocity. The equation has been referenced in literature (Been, 1980; Bürger & Hvistendahl, 2001; Masala, 1998; Toorman, 1999), and is presented as follows:

$$v_s = v_{st}(1 - \phi_s)^{\alpha} \quad [3.9]$$

where:

ϕ_s = volumetric solid content, or volume fraction, and

α = an empirical constant.

Moreover, Toorman (1996), Pane and Schiffman (1997) and Jeeravipoolvarn (2010) present the relationship between settling velocity and hydraulic conductivity at a given void ratio as shown in the Eq. [3.10].

$$v_s = -\left(\frac{\gamma_w}{\gamma_s} - 1\right)\frac{k}{1+e} \quad [3.10]$$

where:

k = hydraulic conductivity, *m/s*, and

e = void ratio.

3.4 Formulation of large-strain consolidation

Gibson, England, and Hussey (1967) proposed a model for the process of large-strain consolidation for fine-grained or slurry soils using finite strain theory. Koppula (1970) and Somogyi (1980) modified Gibson's one-dimensional finite strain model. A number of researchers applied the theory of large-strain consolidation to very soft soils (Cargill, 1984; Been & Sills, 1981).

3.4.1 Coordinate systems

The governing equation for sedimentation and large-strain consolidation can be formulated using either Eulerian or Langrangian coordinate systems. A fixed coordinate system was assumed when the Lagrangian coordinate system was used. On the other hand, Eulerian coordinate system assists in tracking continuously moving soil elements as soft tailings progress to consolidation. The governing equation formulated using the Lagrangian coordinate system can be transferred to an Eulerian coordinate system using the transformation equation presented herein.

The Eulerian and Lagrangian coordinate systems and their relationship is expressed in Eq. [3.11], [3.12] and [3.13].

$$\xi = X + \underset{\wedge}{u} + \underset{\wedge}{u}_0 \qquad [3.11]$$

$$\zeta = Y + \underset{\cdot}{v} + \underset{\cdot}{v}_0 \qquad [3.12]$$

$$\eta = Z + \acute{w} + \acute{w}_0 \qquad [3.13]$$

where:

ξ, ζ, η = Eulerian coordinates,

X, Y, Z = Lagrangian coordinates,

$\dot{u}, \dot{v}, \dot{w}$ = displacement of soil solids, and

$\dot{u}_0, \dot{v}_0, \dot{w}_0$ = initial displacement of soil solids.

A general coordinate transformation equation presented in Eq. [3.14] was used to transfer the formulated governing equation from one to the other coordinate systems.

$$\frac{\partial F(\xi,\zeta,\eta)}{\partial \eta} = \frac{1+ e_0}{1+e} \frac{\partial F(\xi,\zeta,\eta)}{\partial Z} \qquad [3.14]$$

The 1D, quasi-2D, and quasi-3D formulation was obtained by using the simplified coordinate transformation Eq. [3.14]. Derivation of the governing equation is presented in the following subsections.

3.4.2 Derivation of governing equation in Eulerian coordinate

The sedimentation and consolidation theory has been formulated using two-phase flows and the assumptions listed below (Bürger & Hvistendahl, 2001; Gibson et al., 1967; Gustavsson, 2003; Lee, 1979; Mcvay, Townsend, & Bloomquist, 1986; Tan, 1986; Zhang & Thode, 2012; *SoilVision*®, 2012):

- Fully saturated mixture of solid and fluid phase,
- The solid and fluid phase are considered incompressible,
- There was no transfer of mass between the fluid and solid phase,

- There was no surface tension developed between the fluid and solid phases,
- The relative velocity between the pore fluid and soil matrix is governed by the Darcy-Gersevanov equation, and
- Compressibility and hydraulic conductivity of the soil mixture are determined using state parameters of the mixture such as void ratio.

Assuming the volumetric content of water, gas, and solids phases are represented by the following parameters, θ_w, θ_a, and θ_s, respectively in Eq. [3.15].

$$\theta_w + \theta_a + \theta_s = 1 \quad [3.15]$$

The degree of saturation and porosity can be used to express the volumetric water content of the phases are presented in Eq. [3.16], [3.17] and [3.18].

$$\theta_a = n(1 - S_r) \quad [3.16]$$

$$\theta_w = nS_r \quad [3.17]$$

$$\theta_s = 1 - n \quad [3.18]$$

The following fluid and solid phases are given using principles of mass conservation, as described below in Eq. [3.19] and [3.20].

Fluid phase:

$$\frac{\partial(\theta_w v_\xi^f)}{\partial \xi} + \frac{\partial(\theta_w v_\zeta^f)}{\partial \zeta} + \frac{\partial(\theta_w v_\eta^f)}{\partial \eta} + \frac{\partial \theta_w}{\partial t} = 0 \quad [3.19]$$

Solid phase:

$$\frac{\partial(\theta_s v_\xi^s)}{\partial \xi} + \frac{\partial(\theta_s v_\zeta^s)}{\partial \zeta} + \frac{\partial(\theta_s v_\eta^s)}{\partial \eta} + \frac{\partial \theta_s}{\partial t} = 0 \quad [3.20]$$

where:

$v_\xi^f, v_\zeta^f, v_\eta^f$ = velocity of fluids in $\xi, \zeta, and\ \eta$ direction, *m/s*,

$v_\xi^s, v_\zeta^s, v_\eta^s$ = velocity of solids in $\xi, \zeta, and\ \eta$ direction, *m/s*,

$\theta_w, \theta_a, \theta_s$ = volumetric content of water, gas, and solid phases, m^3/m^3,

n = porosity, and

ξ, ζ, η = Eulerian coordinate system.

Equation [3.21] is obtained by rearranging and summing equations given in Eq. [3.19] and [3.20]:

$$\frac{\partial[v_\xi^s(1-\theta_a)]}{\partial \xi} + \frac{\partial[v_\zeta^s(1-\theta_a)]}{\partial \zeta} + \frac{\partial[v_\eta^s(1-\theta_a)]}{\partial \eta} + \frac{\partial[\theta_w(v_\xi^v - v_\xi^s)]}{\partial \xi} + \frac{\partial[\theta_w(v_\zeta^v - v_\zeta^s)]}{\partial \zeta} + \frac{\partial[\theta_w(v_\eta^v - v_\eta^s)]}{\partial \eta} + \frac{\partial(1-\theta_a)}{\partial t} = 0 \quad [3.21]$$

The velocity of the fluid in relation to the solids is obtained by applying the Darcy-Gersevanov law:

$$\theta_w(v_\xi^v - v_\xi^s) = -\frac{k_\xi}{\gamma_w}\frac{\partial u_e}{\partial \xi} \quad [3.22]$$

$$\theta_w(v_\zeta^v - v_\zeta^s) = -\frac{k_\zeta}{\gamma_w}\frac{\partial u_e}{\partial \zeta} \quad [3.23]$$

$$\theta_w\left(v_\eta^v - v_\eta^s\right) = -\frac{k_\eta}{\gamma_w}\frac{\partial u_e}{\partial \eta} \quad [3.24]$$

where:

k_ξ, k_ζ, k_η = hydraulic conductivity in $\xi, \zeta, \text{and } \eta$ direction, *m/sec*,

u_e = excess pore fluid pressure, *kPa*, and

γ_w = unit weight of fluid, *kN/m³*.

Combining Eq. [3.21], [3.22], [3.23] and [3.24] results in Eq. [3.25]:

$$\frac{\partial[v_\xi^s(1-\theta_a)]}{\partial \xi} + \frac{\partial[v_\zeta^s(1-\theta_a)]}{\partial \zeta} + \frac{\partial[v_\eta^s(1-\theta_a)]}{\partial \eta} - \frac{\partial}{\partial \xi}\left[-\frac{k_\xi}{\gamma_w}\frac{\partial u_e}{\partial \xi}\right] - \frac{\partial}{\partial \zeta}\left[\frac{k_\zeta}{\gamma_w}\frac{\partial u_e}{\partial \zeta}\right] - \frac{\partial}{\partial \eta}\left[\frac{k_\eta}{\gamma_w}\frac{\partial u_e}{\partial \eta}\right] - \frac{\partial(\theta_a)}{\partial t} = 0 \quad [3.25]$$

Equation [3.20] can be extended and rewritten in the following format:

$$\left[\frac{\partial v_\xi^s}{\partial \xi} + \frac{\partial v_\zeta^s}{\partial \zeta} + \frac{\partial v_\eta^s}{\partial \eta}\right] = \frac{1}{(1-n)}\left[\frac{\partial(n)}{\partial t} + v_\xi^s\frac{\partial(n)}{\partial \xi} + v_\zeta^s\frac{\partial(n)}{\partial \zeta} + v_\eta^s\frac{\partial(n)}{\partial \eta}\right] \quad [3.26]$$

After substituting Eq. [3.26] into Eq. [3.25], Eq. [3.27] is derived as follows:

$$\frac{\partial}{\partial \xi}\left[-\frac{k_\xi}{\gamma_w}\frac{\partial u_e}{\partial \xi}\right] - \frac{\partial}{\partial \zeta}\left[\frac{k_\zeta}{\gamma_w}\frac{\partial u_e}{\partial \zeta}\right] - \frac{\partial}{\partial \eta}\left[\frac{k_\eta}{\gamma_w}\frac{\partial u_e}{\partial \eta}\right] + Sink = \frac{1-\theta_a}{1-n}\left[\frac{\partial(n)}{\partial t} + v_\xi^s\frac{\partial(n)}{\partial \xi} + v_\zeta^s\frac{\partial(n)}{\partial \zeta} + v_\eta^s\frac{\partial(n)}{\partial \eta}\right] - \left[\frac{\partial(\theta_a)}{\partial t} + v_\xi^s\frac{\partial(\theta_a)}{\partial \xi} + v_\zeta^s\frac{\partial(\theta_a)}{\partial \zeta} + v_\eta^s\frac{\partial(\theta_a)}{\partial \eta} + v_\eta^s\right] \quad [3.27]$$

Equation [3.27] can be rewritten by substituting the following parameters:

n = e/(1+e) and $\theta_a = n(1 - S_r)$,

$$\frac{\partial}{\partial \xi}\left[-\frac{k_\xi}{\gamma_w}\frac{\partial u_e}{\partial \xi}\right]-\frac{\partial}{\partial \zeta}\left[\frac{k_\zeta}{\gamma_w}\frac{\partial u_e}{\partial \zeta}\right]-\frac{\partial}{\partial \eta}\left[\frac{k_\eta}{\gamma_w}\frac{\partial u_e}{\partial \eta}\right]+Sink=\frac{1}{1+e}\left[\frac{D[(S_r e)]}{Dt}\right] \quad [3.28]$$

$$\frac{De}{Dt}=\frac{\partial(S_r e)}{\partial t}+v_\xi^s\frac{\partial(S_r e)}{\partial \xi}+v_\zeta^s\frac{\partial(S_r e)}{\partial \zeta}+v_\eta^s\frac{\partial(S_r e)}{\partial \eta} \quad [3.29]$$

where:

S_r = degree of saturation, and

$D(S_r e)/Dt$ = differential of materials with respect to time (material derivative).

Using the volumetric water content, θ_w, on the right side of Eq. [3.28], the governing equation can be expressed as:

$$\frac{\partial}{\partial \xi}\left[-\frac{k_\xi}{\gamma_w}\frac{\partial u_e}{\partial \xi}\right]-\frac{\partial}{\partial \zeta}\left[\frac{k_\zeta}{\gamma_w}\frac{\partial u_e}{\partial \zeta}\right]-\frac{\partial}{\partial \eta}\left[\frac{k_\eta}{\gamma_w}\frac{\partial u_e}{\partial \eta}\right]+Sink=\frac{1}{1+e}\left[\frac{D[\theta_w(1+e)]}{Dt}\right] \quad [3.30]$$

$$\frac{D[\theta_w(1+e)]}{Dt}=\frac{\partial[\theta_w(1+e)]}{\partial t}+v_\xi^s\frac{\partial[\theta_w(1+e)]}{\partial \xi}+v_\zeta^s\frac{\partial[\theta_w(1+e)]}{\partial \zeta}+v_\eta^s\frac{\partial[\theta_w(1+e)]}{\partial \eta} \quad [3.31]$$

Equation [3.28] or [3.31] is the general unified formulation of sedimentation and large-strain consolidation for saturated or unsaturated conditions in the Eulerian coordinate system.

The Lagrangian formulation for 1D, quasi-2D, and quasi-3D large-strain consolidation and sedimentation are presented in the sections below.

3.4.3 One-dimensional (1D) large-strain consolidation and sedimentation

Somogyi (1984) developed a simplified version of the 1D sedimentation/consolidation model. Its extension, the 1D large-strain consolidation and sedimentation model, is presented in Eq. [3.32] below.

$$\frac{\partial}{\partial z}\left[-\frac{k_Y}{\gamma_w}\frac{1+e_0}{1+e}\frac{\partial u_e}{\partial Y}\right]+v_s\left[\frac{\theta_w}{a_v(1+e)}\left(\frac{(\gamma_s-\gamma_w)}{1+e_0}+\frac{\partial u_e}{\partial Y}\right)-\frac{\partial \theta_w}{\partial Y}\right]-\frac{\theta_w}{(1+e_0)a_v}\left[(\gamma_s-\gamma_w)FR+\frac{\partial q(t)}{\partial t}\right]=\frac{(1+e)}{1+e_0}\frac{\partial \theta_w}{\partial t}-\frac{\theta_w}{a_v(1+e_0)}\frac{\partial u_e}{\partial t} \quad [3.32]$$

$$FR=\frac{\partial(\Delta Z)}{\partial t}\Big/(1+e_0),\ a_v=\frac{\partial \sigma'}{\partial e} \quad [3.33]$$

where:

e = void ratio at a time, *unitless*,

e_0 = initial void ratio, *unitless*,

u_e = excess pore pressure, *kPa,*

k_y = hydraulic conductivity, *m/s*,

γ_w = unit weight of water, *kN/m*^{3},

γ_s = unit weight of solid, *kN/m*^{3},

θ_w = volumetric water content, *unitless*,

σ' = effective stress, *kPa*,

v_s = solid settling velocity, *m/s*,

FR = the solid filling rate, *m/s*,

$\frac{\partial(\Delta Z)}{\partial t}$ = mixture content filling rate, *m/s*,

$\frac{\partial(q(t))}{\partial t}$ = surcharge rate, *kPa/s*, and

Y = Lagrangian coordinate, *m.*

3.4.4 Quasi-2D and quasi-3D large-strain consolidation and the sedimentation model

Jeeravipoolvarn (2010) developed quasi-2D and quasi-3D models for large-strain consolidation. The quasi-2D model allows the flow of water into a true 2D space; however, the deformation of solids is restricted to exist vertically. The quasi-2D large-strain consolidation and sedimentation is expressed in Eq. [3.34] as follows:

$$\frac{1+e}{1+e_0}\frac{\partial}{\partial X}\left(\frac{k_X}{\gamma_w}\frac{\partial u_e}{\partial X}\right)+\frac{\partial}{\partial Y}\left[\frac{k_Y}{\gamma_w}\frac{1+e}{1+e_0}\frac{\partial u_e}{\partial Y}\right]+v_s\left[\frac{\theta_w}{a_v(1+e_0)}\left(\frac{(\gamma_s-\gamma_w)}{(1+e_0)}+\frac{\partial u_e}{\partial Y}\right)-\frac{\partial \theta_w}{\partial Y}\right]-\frac{\theta_w}{a_v(1+e)}\left[(\gamma_s-\gamma_w)FR+\frac{\partial q(t)}{\partial t}\right]=\frac{(1+e)}{1+e_0}\frac{\partial \theta_w}{\partial t}-\frac{\theta_w}{a_v(1+e_0)}\frac{\partial u_e}{\partial t} \quad [3.34]$$

where:

k_x, k_y = hydraulic conductivity in the Lagrangian coordinate *X*, and *Y* direction, *m/s*, and

X, *Y* = Lagrangian coordinate, *m*.

Similarly, the quasi-3D governing equation is expressed in Eq. [3.35].

$$\frac{1+e}{1+e_0}\left[\frac{\partial}{\partial X}\left(\frac{k_X}{\gamma_w}\frac{\partial u_e}{\partial X}\right)+\frac{\partial}{\partial Y}\left[\frac{k_Y}{\gamma_w}\frac{1+e}{1+e_0}\frac{\partial u_e}{\partial Y}\right]\right]+\frac{\partial}{\partial Z}\left[\frac{k_z}{\gamma_w}\frac{1+e_0}{1+e}\frac{\partial u_e}{\partial Z}\right]+v_s\left[\frac{\theta_w}{a_v(1+e)}\left(\frac{(\gamma_s-\gamma_w)}{(1+e_0)}+\frac{\partial u_e}{\partial Z}\right)-\frac{\partial \theta_w}{\partial Z}\right]-\frac{\theta_w}{a_v(1+e_0)}\left[(\gamma_s-\gamma_w)FR+\frac{\partial q(t)}{\partial t}\right]=\frac{(1+e)}{1+e_0}\frac{\partial \theta_w}{\partial t}-\frac{\theta_w}{a_v(1+e_0)}\frac{\partial u_e}{\partial t} \quad [3.35]$$

where:

k_x, k_y, k_z = hydraulic conductivity in the Lagrangian coordinate *X*, *Y*, and *Z* direction, *m/s*, and

X, Y, Z = Lagrangian coordinate, *m*.

3.5 Formulation of transient water flow in saturated-unsaturated soils

The theory of transient water flow in saturated-unsaturated soils can be derived by assuming the continuity of the water phase. The equation for two-dimensional seepage analysis for transient flow is given as follows (Fredlund, Rahardjo and Fredlund, 2012).

Equation [3.36] is formulated using the considerations of total stress change is zero with time. The net flux of water through an element of unsaturated soil is calculated by using the rate of volume of water entering and leaving the element with time.

$$\frac{\partial(\frac{V_w}{V_0})}{\partial t} = \frac{\partial v_{wx}}{\partial x} + \frac{\partial v_{wy}}{\partial y} \qquad [3.36]$$

where:

V_w = volume of water in the element, *unitless*,

V_o = initial overall volume of the element (i.e., *dx*, *dy*, *dz*),

dx, *dy*, *dz* = dimensions in the *x*-, *y*-, and *z*-directions, respectively, and

$\partial(\frac{v_w}{v_0})/\partial t$ = rate of change in the volume of water in the soil element with respect to the initial volume of the element.

Transient water flow differs from the steady-state condition due to the change in the net water balance within the soil element with time. The amount of water present in the soil with the applied suction can be expressed using volumetric soil-water characteristic curves (θ-SWCC), and the water storage can be calculated by differentiating the change in volumetric water content with respect to the soil suction [i.e., $d\theta/d(u_a - u_w)$]. The water storage modulus, m_2^w is obtained by

taking the slope of the differentiated volumetric water content versus suction plot on an arithmetic scale.

The continuity condition can be satisfied by equating the divergence of the water flow rates $(\frac{\partial v_x}{\partial x} + \frac{\partial v_y}{\partial y})$ with the time derivative of the constitutive equation for the water phase.

$$\frac{\partial}{\partial x}\left(k_{wxx}\frac{\partial h_w}{\partial x} + k_{wxy}\frac{\partial h_w}{\partial y}\right) + \frac{\partial}{\partial y}\left(k_{wyx}\frac{\partial h_w}{\partial x} + k_{wyy}\frac{\partial h_w}{\partial y}\right) = m_2^w \rho_w g \frac{\partial h_w}{\partial t} \quad [3.37]$$

Equation [3.37] is the governing equation for transient water flow in an isotropic soil. Here, the pore-air pressure is assumed to remain constant with time. The simplified governing equation can be presented by assuming that major and minor permeability coefficients coincide the *x* and *y* directions respectively, given by Eq. [3.38] below.

$$\frac{\partial}{\partial x}\left(k_{w1}\frac{\partial h_w}{\partial x}\right) + \frac{\partial}{\partial y}\left(k_{w2}\frac{\partial h_w}{\partial y}\right) = m_2^w \rho_w g \frac{\partial h_w}{\partial t} \quad [3.38]$$

Soils under the isotropic condition obtain an equal coefficient of permeability (i.e., $k_{w1} = k_{w2} = k_w(u_a - u_w)$), and rearranging yields the Eq. [3.39].

$$k_w \frac{\partial^2 h_w}{\partial x^2} + \frac{\partial k_w}{\partial x}\frac{\partial h_w}{\partial x} + k_w \frac{\partial^2 h_w}{\partial y^2} + \frac{\partial k_w}{\partial y}\frac{\partial h_w}{\partial y} = m_2^w \rho_w g \frac{\partial h_w}{\partial t} \quad [3.39]$$

where:

k_{wx} and k_{wy} = major and minor permeability functions, *m/s*,

m_2^w = water storage function, *unitless*,

h_w = hydraulic head in the water phase (i.e., elevation head plus water pressure head), *m*,

g = acceleration due to gravity, m/s^2, and

t = time, *sec*.

Equation [3.40] can be expressed by using pore-water pressure by substituting (y + $u_w/\rho_w g$) for the hydraulic head term (h_w) as follows:

$$c_v^w \frac{\partial^2 u_w}{\partial x^2} + \frac{c_v^w}{k_w}\frac{\partial k_w}{\partial x}\frac{\partial u_w}{\partial x} + c_v^w \frac{\partial^2 u_w}{\partial y^2} + \frac{c_v^w}{k_w}\frac{\partial k_w}{\partial y}\frac{\partial u_w}{\partial y} + c_g \frac{\partial k_w}{\partial y} = \frac{\partial u_w}{\partial t} \quad [3.40]$$

where:

C_{wv} = $k_w/(\rho_w g m_2^w)$, coefficient of consolidation for the unsaturated soils, and

$C_g = 1/m_2^w$, the gravity term.

In the case of the anisotropic soil condition, the obtained governing equation for isotropic soils can be used by assuming the major and minor axes coincide and by setting $k_{wx} = k_{wy}$ as equal.

3.6 Constitutive relationships

In finite strain consolidation modelling, the relationship between the compressibility of the material and the hydraulic conductivity is used to characterize material behaviours. Here, the compressibility curve is obtained from the relationship between the effective stress and void ratio. Further, the hydraulic conductivity curve is the relationship between the hydraulic conductivity of a given material and its respective void ratio. These two constitutive relationships are used to solve the finite strain consolidation governing equation presented in section 3.4.3.

3.6.1 Compressibility functions

The generic formula to represent the constitutive relationship of the material compressibility is specified by using the effective stress (σ') and the void ratio (e), as presented in Eq. [3.41].

$$e = f(\sigma') \quad [3.41]$$

3.6.2 Hydraulic conductivity function

Similarly, the generic constitutive relationship for the hydraulic conductivity (*k*) of the material is given from the void ratio (*e*) and the hydraulic conductivity relationship as described in Eq. [3.42].

$$k = f(e) \quad [3.42]$$

Table 3. 1 A summary of compressibility and hydraulic conductivity curves.

Functions	Compressibility equations	Conductivity equations	Parameters description
Power function	$e = A_{\circ}\sigma'^{\dot{B}}$	$k_{sat} = \acute{C}e^{\dot{D}}$	*e* = void ratio *σ'* = effective stress $A_{\circ}$, $\dot{B}$, $\acute{C}$, $\dot{D}$ = experimental parameters k_{sat} = saturated hydraulic conductivity
Extended power function	$e = A_{\circ}(\sigma' + Z_c)^{\dot{B}}$	$k_{sat} = (\ddot{E}e^{\dot{F}})/(1+e)$	*e* = void ratio *σ'* = effective stress Z_c = minimum effective stress $A_{\circ}$, $\dot{B}$, $\ddot{E}$, $\dot{F}$ = experimental parameters k_{sat} = saturated hydraulic conductivity
Log function	$e = A_{\circ}ln(\sigma') + \dot{B}$	$e = \acute{C}ln(k_{sat}) + \dot{D}$	*e* = void ratio *σ'* = effective stress $A_{\circ}$, $\dot{B}$, $\acute{C}$, $\dot{D}$ = experimental parameters k_{sat} = saturated hydraulic conductivity

Weibull Function	$e = A_{\circ} - \dot{B}exp(-\dot{E}\sigma'^{\dot{F}})$	$k_{sat} = \acute{C}e^{\dot{D}}$	e = void ratio σ' = effective stress $A_{\circ}, \dot{B}, \acute{C}, \dot{D}, \dot{E}, \dot{F}$ = experimental parameters k_{sat} = saturated hydraulic conductivity

3.7 Considerations for the consolidation using applied suction process

The process of consolidation using applied suction is a continuation of the self-weight consolidation process as described in the previous section. To reiterate and in reference to that section, it has been detailed that the direction of flow is downward during the Stage 2 consolidation process. There is a possibility of desaturation near the surface of the deposited tailings, which occurs as the incremental applied suction pulls out the water continuously. Part of the tailings will remain fully saturated, and other parts of the tailings transition from saturated to unsaturated. Therefore, a transitional zone is displayed at this stage.

The literature review section in Chapter 2 presented an overview of the effect of negative pore-water pressure (suction) on overall volume change as the soil starts to desaturate. It has been noted that there is difficulty with the principle of effective stress when applied to unsaturated soils (Bishop & Blight, 1963; Fredlund & Morgenstern, 1976). The constitutive relationship for unsaturated soils is described based on two independent stress state variables, namely net stress ($\sigma - u_a$) and matric suction ($u_a - u_w$), where u_a is the pore-air pressure (usually assumed to be zero in nature) and u_w is the pore-water pressure (Fredlund & Rahardjo, 1993). The behaviour of unsaturated soils can be characterized using a 3D constitutive surface and has been previously detailed in this paper's literature review section (see (Fredlund, Rahardjo and Fredlund, 2012).

The following two conditions may be encountered during the process of consolidation using an applied suction at the bottom boundary.

1. **Fully saturated:** A 2D constitutive relationship will be used to characterize the property of the tailings and compute the compressibility and hydraulic conductivity relationship as the consolidation process progresses. This is utilized to determine and hypothesize results of deposited tailings in terms of their final void ratio and settlement height, etc.

2. **Partly saturated-unsaturated (transitional):** The transition zone created during the consolidation process occurs as the state of deposited tailings changes from saturated to unsaturated. When the transition zone starts to form near the surface of tailings, the tailings can be best characterized utilizing 3D constitutive surfaces. However, the fully saturated tailings located near the bottom of the column are under a fully saturated condition and best characterized using 2D constitutive relationships. Therefore, 2D and 3D constitutive surfaces can define the deposited tailings based on the state of degree of saturation, respectively. As it has been described in Condition 1, the compressibility and hydraulic conductivity curves (2D) were used during the fully saturated stage. During the unsaturated condition, the following constitutive surfaces were employed to characterize the tailings: void ratio or water content – net normal stress – suction (e *or* w – $(\sigma - u_a)$ – $(u_a - u_w)$); degree of saturation – net normal stress – suction (S_r – $(\sigma - u_a)$ – $(u_a - u_w)$); and, unsaturated hydraulic conductivity – suction – void ratio (k_{unsat} – $(u_a - u_w)$ – e) for the desaturated tailing.

The 3D constitutive surface for void ratio – net normal stress – suction (e – $(\sigma - u_a)$ – $(u_a - u_w)$) can be computed using the measured soil-water characteristic curve (SWCC), presented in Eq. [3.43], and the Shrinkage Curve (SC), presented in Eq. [3.44], to generate the relationship between void ratio and suction as presented in Eq. [3.45].

$$w(\psi) = \frac{w_s\, C\,(\psi)}{\left(\ln\left(\exp(1) + \left({}^{\psi}/_{a_f}\right)^{n_f}\right)\right)^{m_f}} \quad [3.43]$$

where:

$w(\psi)$ = water content at any suction, ψ,

a_f = fitting parameter near the inflection point on the *w*-SWCC,

n_f = fitting parameter related to the maximum rate of gravimetric water content change,

m_f = fitting parameter related to the curvature near residual conditions of the soil,

ψ_r = suction near residual conditions of the soil, and

C(ψ) = correction factor directing the *w*-SWCC towards a suction of 10^6 kPa at zero water content, written as:

$$e(w) = a_{sh}\left[\left(\frac{\mathrm{w}}{b_{sh}}\right)^{c_{sh}} + 1\right]^{\frac{1}{\mathrm{c_{sh}}}} \quad [3.44]$$

where:

$e(w)$ = void ratio as a function of gravimetric water content,

a_{sh} = minimum void ratio, *e*-min,

a_{sh}/b_{sh} = slope of the line of tangency,

c_{sh} = curvature of the shrinkage curve, and

w = gravimetric water content.

$$e(\psi) = a_{sh}\left(\left(\frac{\mathrm{w_s}\left(1 - \ln\left(1 + {}^{\Psi}/_{\psi_r}\right)\right)/\ln\left(1 + {}^{\Psi}/_{\psi_r}\right)}{b_{sh}\left(\ln\left(\exp(1) + \left({}^{\Psi}/_{a_f}\right)^{n_f}\right)\right)^{m_f}}\right)^{C_{sh}} + 1\right)^{{}^{1}/_{C_{sh}}} \quad [3.45]$$

The relationship between the void ratio and the net normal stress is obtained from the measured compressibility curve, presented using Eq. [3.41]. The required 3D constitutive surface is obtained by combining the two relationships (i.e., void ratio versus suction and void ratio versus net normal stress).

Similarly, the 3D constitutive surface of degree of saturation – net normal stress – suction can be obtained using Eq. [3.45] and [3.46].

$$S_r(\psi) = \frac{G_s w(\psi)}{e(w(\psi))} \quad [3.46]$$

where:

$S_r(\psi)$ = degree of saturation,

$w(\psi)$ = Fredlund-Xing (1994) equation for the *w*-SWCC, or any other equation that fits the laboratory data,

$e(\psi)$ = void ratio written as a function of soil suction, ψ.

The mathematical functions proposed by Vu and Fredlund (2006) can also be used to fit the 3D constitutive surfaces of void ratio or gravimetric water content constitutive surface for the unsaturated tailings condition. The mathematical function with six parameters was initially developed for modelling expansive soils (Vu & Fredlund, 2006). Qi et al. (2016) produced the methodology on how to compute constitutive surfaces for the unsaturated soils, largely by adopting (Vu & Fredlund, 2006) mathematical functions. The hydraulic conductivity curve obtained from a large-strain compression test will be used to define the saturated hydraulic conductivity and void ratio relationship, as presented in Eq. [3.42]. The three constitutive surfaces

presented below are sufficient to develop a constitutive relationship during the unsaturated soils condition:

$$e = \mathring{a} + \dot{b} log \left[\frac{1+\acute{c}(\sigma-u_a)+\dot{d}(u_a-u_w)}{1+\dot{f}(\sigma-u_a)+\bar{g}(u_a-u_w)}\right] \quad [3.47]$$

$$w = \mathring{A} + \dot{B} log \left[\frac{1+\acute{C}(\sigma-u_a)+\dot{D}(u_a-u_w)}{1+\dot{F}(\sigma-u_a)+\bar{G}(u_a-u_w)}\right] \quad [3.48]$$

$$k = \frac{Ce^D}{1+\acute{m}[(u_a-u_w)/(\rho_w g)]^{\dot{n}}} \quad [3.49]$$

where:

w = gravimetric water content,

ρ_w = density of water, kg/m^3,

g = gravitational acceleration, m/sec^2,

$\acute{m}$ *and* $\dot{n}$ are two material parameters accounting for the effect of suction on the hydraulic conductivity,

$\mathring{a}$, $\dot{b}$, $\acute{c}$, $\dot{d}$, $\dot{f}$, $\bar{g}$ and $\mathring{A}$, $\dot{B}$, $\acute{C}$, $\dot{D}$, $\dot{F}$, $\bar{G}$ are empirical material parameters for the void ratio and water content constitutive relationships, respectively.

Qi et al. (2016) developed a finite difference method to compute the transient consolidation process by using a 2D and 3D constitutive relationship for the saturated and unsaturated soil conditions respectively, as presented in Figure 3.8.

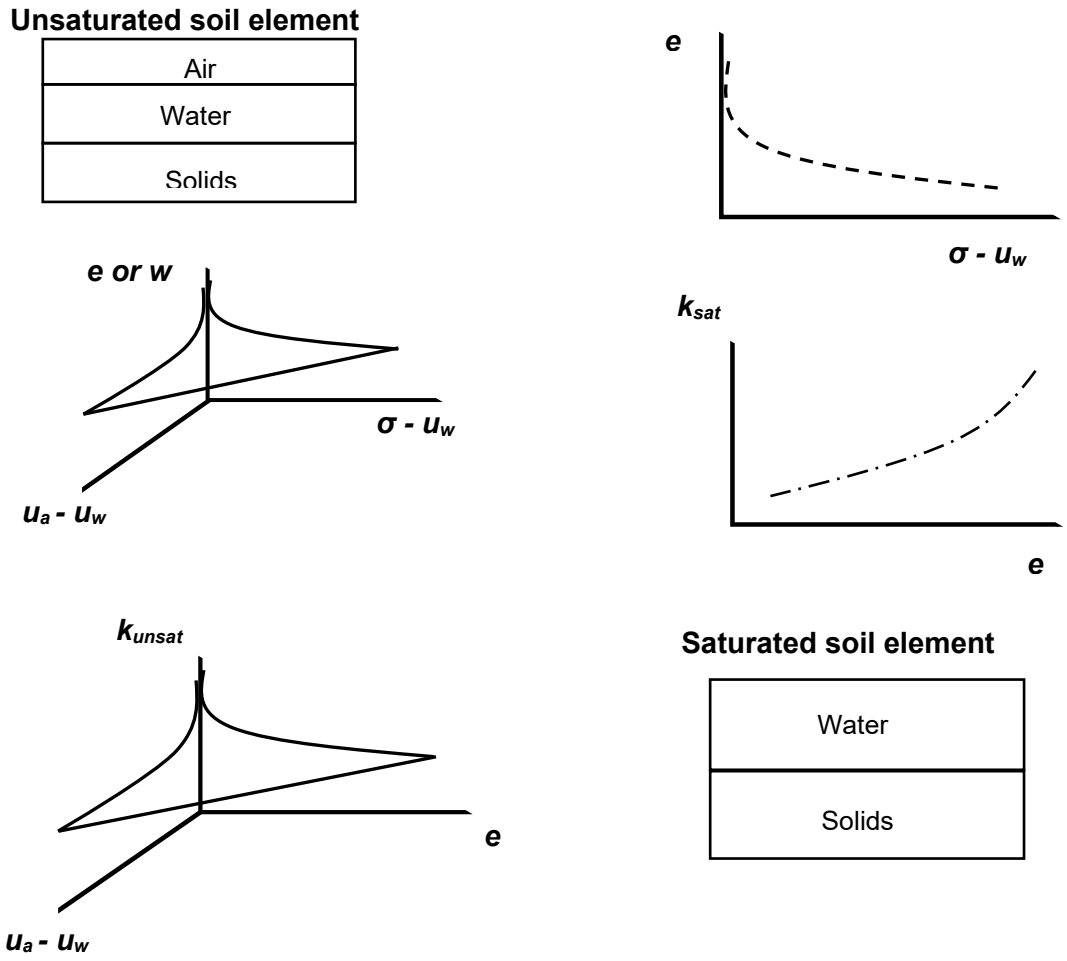

Figure 3. 8 Conceptual diagrams used to formulate 3D constitutive surfaces in the case of an unsaturated condition, and 2D constitutive relationships in the case of a fully saturated condition (adapted from Qi et al., 2016).

3.8 Shear strength of soils

The shear strength of soils is defined as the resistance of the soil to internal frictional forces. The Mohr-Coulomb formula is used to compute the shear strength of saturated soils.

3.8.1 Shear strength for saturated soils

The shear strength of a saturated soil is described using the principles of effective stress (Terzaghi, 1943) and Mohr-Coulomb failure criteria. Eq. [3.50] presents the formula to calculate the saturated soil's shear strength.

$$\tau_{ff} = c' + \left(\sigma_f - u_w\right)\left(\sigma_f - u_w\right)_f \tan\phi' \quad [3.50]$$

where:

τ_{ff} = shear stress on the failure plane at failure,

c' = effective cohesion, which is the shear strength intercept when the effective normal stress is equal to zero,

$\left(\sigma_f - u_w\right)_f$ = effective normal stress on the failure plane at failure,

σ_{ff} = total normal stress on the failure plane at failure,

u_{wf} = pore-water pressure at failure,

ϕ' = effective angle of internal friction.

3.8.2 Unsaturated shear strength equation

Fredlund, Morgenstern, and Widger (1978) presented the derivation of the formula for the shear strength of unsaturated soils using two independent stress state variables. The shear strength formula is presented in Eq. [3.51] (Fredlund and Rahardjo,1993).

$$\tau_{ff} = c' + \left(\sigma_f - u_w\right)\left(\sigma_f - u_w\right)_f \tan\phi' + (u_a - u_w)_f \tan\phi^b \quad [3.51]$$

where:

τ_{ff} = shear stress on the failure plane at failure,

c' = effective cohesion or intercept of the "extended" Mohr-Coulomb failure envelope on the shear stress axis where the net normal stress and the matric suction at failure are equal to zero,

$(\sigma_f - u_w)_f$ = net normal stress on the failure plane at failure,

σ_{ff} = total normal stress on the failure plane at failure,

u_{af} = pore-air pressure on the failure plane at failure,

ϕ' = angle of internal friction associated with the net normal stress state variable, $(\sigma_f - u_f)_f$,

$(u_a - u_w)_f$ = matric suction on the failure plane at failure,

ϕ^b = angle indicating the rate of increase in shear strength relative to the suction, $(u_a - u_w)_f$.

3.8.3 Nonlinearity of failure envelope

A number of researchers investigated the relationship between shear strength and matric suction and observed a nonlinear relationship (Gan, Fredlund, & Rahardjo, 1988; Escario & Jucâ, 1989; Vanapalli et al., 1996). Figure 3.9 illustrates a nonlinear relationship between matric suction and shear strength.

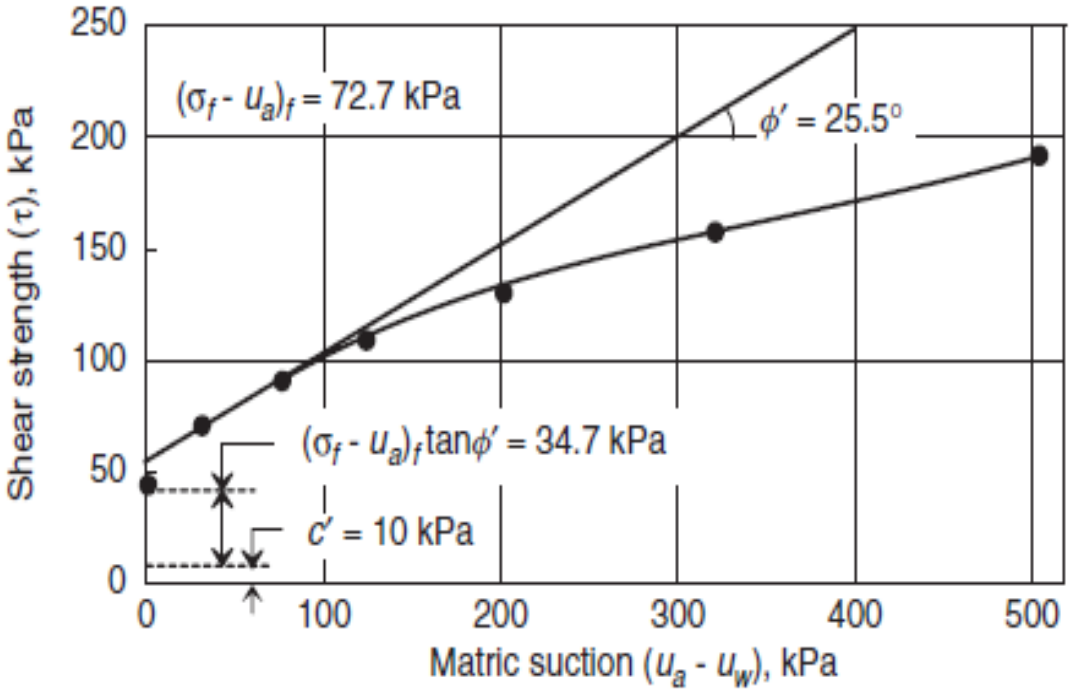

Figure 3. 9 Direct shear test results exhibiting nonlinear behaviour of failure envelope projected onto τ versus $u_a - u_w$ plane (adapted from Gan, 1986).

The friction angle ϕ^b is equal to ϕ' at low matric suction (i.e., fully saturated condition). The ϕ^b decreases as the suction increases. Therefore, the ϕ^b is a function of matric suction. A number of researchers predict the shear strength of unsaturated soils using the soil-water characteristic curve and saturated shear strength parameters (Vanapalli et al., 1996; Fredlund et al., 1996).

A number of laboratory techniques are available to measure and determine the shear strength of saturated and unsaturated soils. This section only presents the vane shear strength technique, which was used during the research study.

3.8.4 Vane shear strength of soils

The shear strength of soils can be measured using vane shear equipment as one of its strength-measuring apparatuses. The literature review section presents a detailed description of shear strength with associated factors and considerations. This section presents a brief summary of the formulae used to measure the shear strength of deposited tailings using vane shear equipment. Eq. [3.52] and [3.53] exhibit the formula to compute shear strength of soils using vane shear equipment, as described by ASTM 4648M-16 and D2573-08.

$$T = s \times K \quad [3.52]$$

where:

T = Torque, *N·m,*

s = shear strength of the clay, *kPa*, and

K = constant, depending on dimensions on shape of the vane, m^3.

The value of K is calculated as follows by assuming uniform shear strength distribution across the end of the cylinder and around the perimeter of the vane:

$$K = \left(\frac{\pi}{10^6}\right) \times \left(\frac{(Dia)^2 H}{2}\right) \times \left[1 + \left(\frac{(Dia)}{3H}\right)\right] \quad [3.53]$$

where:

Dia = measured diameter of the vane, *cm*, and

H = measured height of vane, *cm*.

3.8.5 Error estimation and factors affecting vane shear measurements

Measurement of vane shear strength were corrected for the possible error incorporated during the laboratory experiment test. Vane shear strength measurement values include the following errors. The measured vane shear values were corrected to exclude the extended rod resistance at different depths.

1. **Errors from extended rod attached to vane blade**: measured results using vane instrument show additional shear resistance due to the attached extended rod with the vane blade. Therefore, the additional shear strength from the extended rod were deducted from the measured data in order to correct it. The correlation between insertion depth of the extended rod and its measured shear resistance without vane blade were calibrated in the laboratory. Table 3.2 presents the correlation between the insertion depth and shear resistance for the extended rod.

Table 3. 2 A summary of vane blade extended rod resistance with tailings depth.

Depth from column base (m)	Extended rod resistance (kPa)
0.7	1.1
0.12	0.93
0.17	0.85
0.27	0.5

2. **Error correction factor**: the measured vane shear strength values were further corrected based on a correction factor developed in relation to plasticity index material as presented in Figure 3.10 (Bjerrum, 1973).

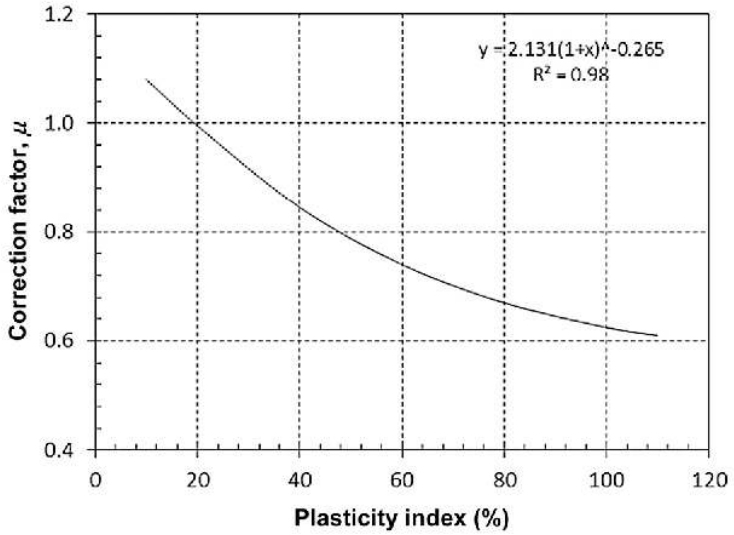

Figure 3. 10 Correlation used to correct measured vane shear strength (adapted from Bjerrum, 1973).

In addition, a number of factors could possibly affect the undrained shear strength measurement using vane equipment. The following listed factors are to mention some: vane blade geometry, type of blade, insertion method, duration of rest period prior test commenced, rate of rotation, deformation patterns from non-uniform stress distribution, progressive failures (Chandler, 1988). The influence of disturbance during vane insertion, time and shear velocity on measurement, and interpretation of vane shear test affect the shear strength results (Roy & Leblanc ,1988). In addition, the effect of vane insertion in generating dilatant behaviour within the deposited tailings, extended rod friction contributed error measurements of undrained shear strength of the tailings.

The research attempts the characterization of measured vane shear strength in relation to the increase in effective stress due to the incrementally applied suction process. The focus of the research was anchored in identifying exhibited vane shear strength of tailings as the process of consolidation progressed, particularly if the tailings behaved similar to the natural soft soils (i.e,

clay dominated soils). Additional controlled tests and implemented correction factors are imperative for the results of measured vane shear strength's prior stating further conclusion.

CHAPTER FOUR: LABORATORY TEST PROGRAM

This section presents the laboratory test program conducted during this research study. The chapter is divided into two subsections, namely i) materials used and the characterization test carried out during the research program, and ii) the equipment used and developed to conduct the research program.

4.1 Materials used and characterization

The materials used and the characterization tests are described in this section.

4.1.1 Material description

Two types of FFT were obtained from an oil sands mining site one untreated and one pretreated. The first material was treated in house using chemical additives to improve its sedimentation/self-weight consolidation process using a procedure designed to replicate one of the mine operators in the field. The second material was treated at the mine site in a chemical and mechanical dewatering process prior to delivery. Details of the two tailings and their corresponding material properties are described in the section below.

4.1.1.1 Flocculated fluid fine tailings (FFT)

Raw FFTs were flocculated to increase the sedimentation/self-weight consolidation rate of the tailings upon deposition. The FFTs were placed in a 20-L pail and were mixed to achieve a homogenous mixture. The desired solids content of FFTs was 38%, which was achieved through the addition of process water that was shipped from the mine site.

Prior to the flocculation of the FFTs, the flocculant solution was prepared by adding 4 grams of polymer to 996 grams of process water to achieve a concentration of 0.4% (w/w), using a commercially available anionic polymer, A3338. The fresh flocculant solution was prepared a minimum of 24 hours prior to being used. This ensured that the solid grain polymers completely mixed within the process water (Vedoy & Soares, 2015).

A combination of laboratory tests, such as the column settling test and yield strength test, were conducted to determine the flocculant dose required to achieve optimum dewaterability for the FFTs. The method on how to determine the optimum flocculant dosage for the FFTs both in the laboratory and field scale has been described, discussed, and presented in literature (Dunmola et al., 2014; Fisseha, Wilson, & Fredlund, 2017a; Fisseha, Wilson & Simms, 2018; Mizani, He & Simms, 2013). The procedures and calculation details followed in preparing the flocculant solution and flocculated FFT, and typical outputs are outlined in Mizani (2016). The optimum flocculant dosage is defined the dosage that provide speedy settling rate of the tailings (i.e., release of bleed water) as the increase in the strength of flocculated tailings. The optimum flocculant dosage was determined to be 1000 ppm for the given FFTs used during the research program.

4.1.1.2 Flocculated centrifuged tailings cake (FCTC)

The flocculated centrifuged tailings cake (FCTC) was received in a 200-L tote. Prior to delivery the tailings was treated with a flocculant and gypsum ($CaSO_4$) at the mine process plant and then mechanically dewatered in a centrifuge. The methods of production of the FCTC samples are beyond the scope of this research. The initial solids content and other index properties of FCTC tailings were determined upon delivery to the University of Alberta Geotechnical Centre. The initial solids content of the FCTC sample was 52.5% following the homogenization of the FCTC. The initial properties of the samples before delivery were not provided.

4.1.2 Material characterization test

A number of standard geotechnical laboratory tests were conducted to characterize the flocculated FFT and FCTC. A brief description of the laboratory test procedure is presented below.

4.1.2.1 Geotechnical index property

The geotechnical index properties were measured to characterize the tailings. The following tests were conducted for both the flocculated FFT and FCTC: particle size distribution (ASTM D422/D7928), Atterberg limits (i.e., liquid limit [LL], and plastic limit [PL]) (ASTM D4318), specific gravity (*Gs*) (ASTM D854), bitumen content, and Methylene Blue Index (MBI) content. The index property tests were conducted for all the samples with bitumen.

4.1.2.2 Column settling test

A standard settling test was conducted by placing the tailings into a 1,000 mL standard graduated cylinder with a height of ~34.5 cm. The change in volume (i.e., change in vertical strain) with time was monitored as settling progressed. The graduated cylinder was sealed using a rubber stopper to prevent evaporation. As the deposited material settled, bleed water collected on top of the settled tailings within the cylinder. Figure 4.1 presents column settling tests during the laboratory investigation process during the laboratory characterization of flocculated FFT.

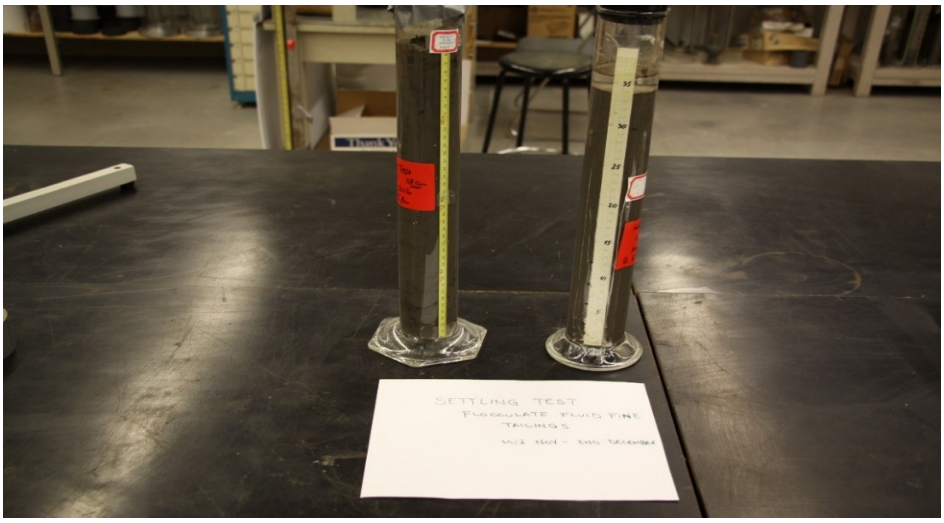

Figure 4. 1 Column settling test.

4.1.3 Unsaturated soils property test

Laboratory tests were carried out to obtain unsaturated properties for the flocculated FFT and FCTC. The shrinkage curve (SC) test and soil-water characteristic curve (SWCC) test were conducted. A brief description of the laboratory test procedure that was carried out is presented below.

4.1.3.1 Shrinkage curve (SC)

The shrinkage curve (SC) test was conducted by following the procedure outlined by Fredlund and Houston (2013). The tailings were prepared and placed into steel containers, which were sealed at the bottom with paraffin paper glued to the bottom of the container. The volume of the container was measured using a caliber. The change in volume and water content was measured using the caliber and by weighing the container as the sample dried. The relationship between the gravimetric water content and void ratio was generated using the measured data. Figure 4.2

shows the shrinkage curve test carried out during the unsaturated property testing for the flocculated FFT.

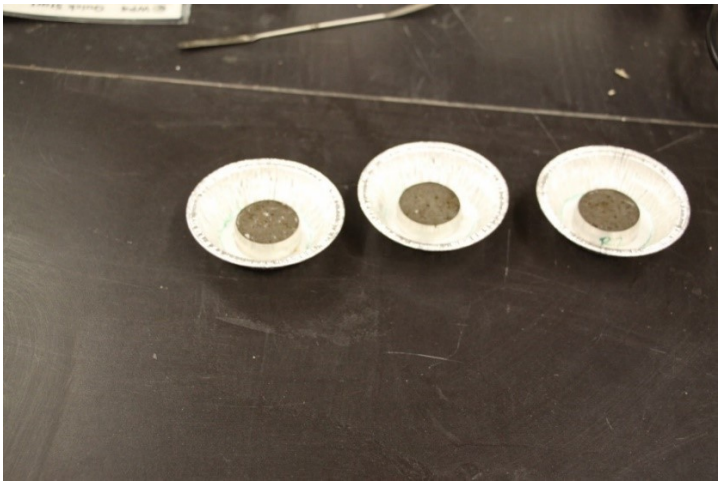

Figure 4. 2 Shrinkage curve test.

4.1.3.2 Soil–water characteristic curve (SWCC)

The SWCC was measured by applying air pressure to a saturated sample of tailings using the principles of the axis-translational technique. Three separate apparatuses were used to complete the entire range of SWCC. A University of Saskatchewan (U of S) Pressure Plate Cell was used to characterize the relationship between matric suction and gravimetric water content for the lower ranges of suction, between 0 to 400 kPa, and a Pressure Plate apparatus with a higher air-entry value was used for the range of suction between 500 to 1,500 kPa. Lastly, a WT4-P apparatus was used to measure the total suction from 2,000 to 10,000 kPa. Figures 4.3 to 4.5 show the apparatus used during the SWCC test conducted at the laboratory.

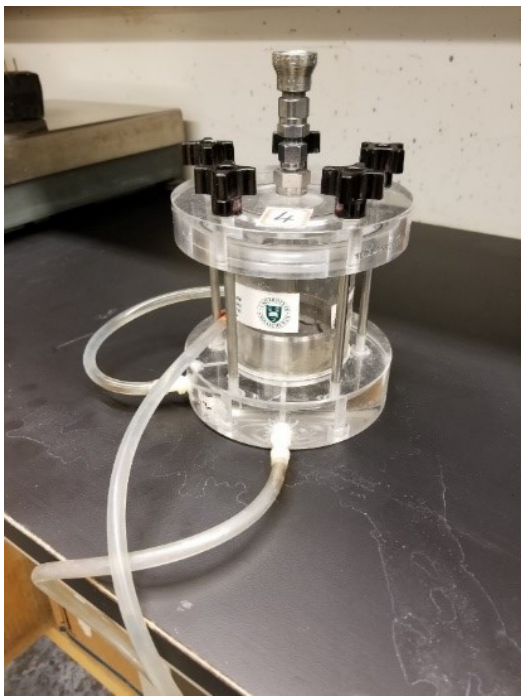

Figure 4. 3 U of S Pressure plate cell for SWCC test on suction ranges 0 to 400 kPa.

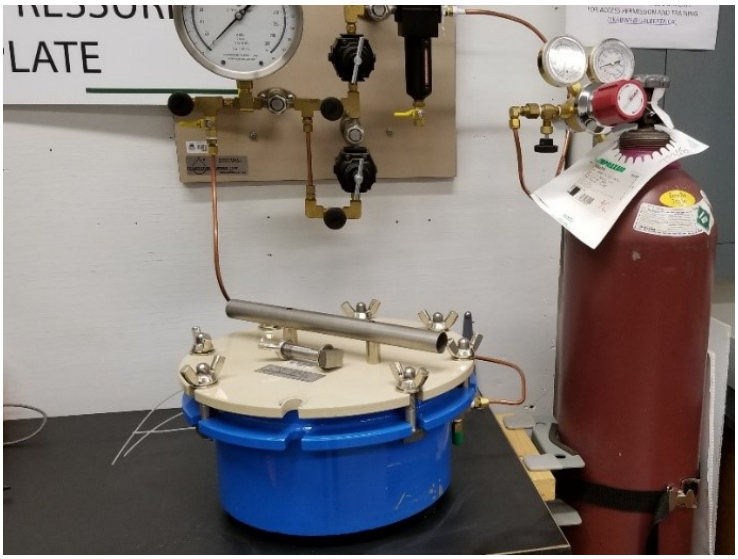

Figure 4. 4 Pressure plate for SWCC test on suction ranges 500 to 1,500 kPa.

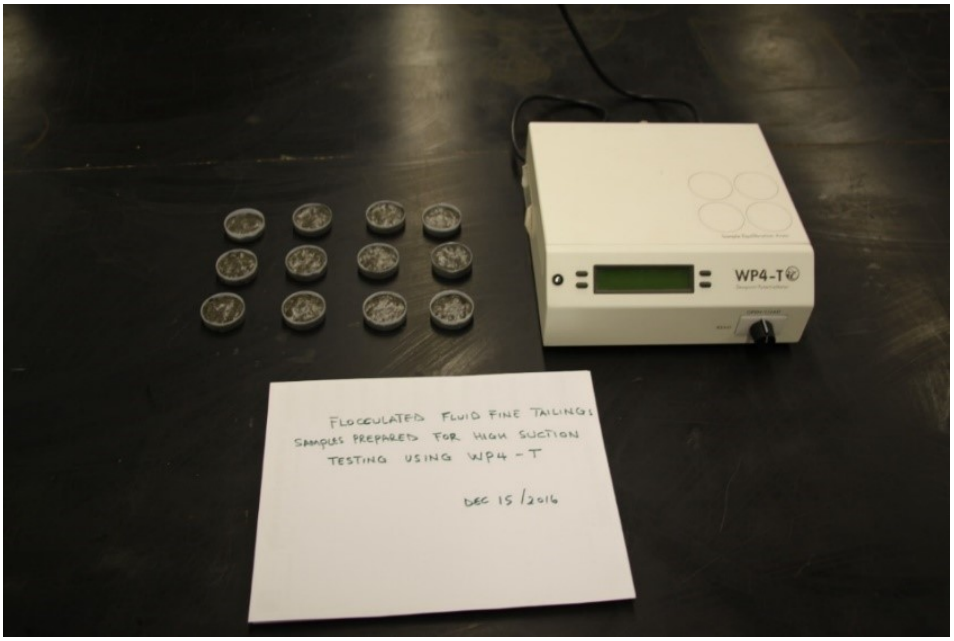

Figure 4. 5 WT4-P apparatus for SWCC test on suction above 2,000 kPa.

4.1.4 Large-strain consolidation properties

A large-strain consolidation (LSC) testing apparatus (multi-step loading) was used to determine the consolidation properties of the tailings under investigation during the research program. The LSC apparatus confined the materials within the consolidation cell. The consolidation characteristics provided the compressibility and hydraulic conductivity relationships of the tailings. Details of the multi-step loading consolidometer are explained by (Jeeravipoolvarn, 2010).

4.1.4.1 Compressibility curve

A multi-step loading apparatus 150 mm in diameter and 250 mm tall was used to characterize the compressibility of the tailings. In the case of the flocculated FFT, the tailings were poured into the LSC apparatus and left to complete their self-weight consolidation process for 85 to 90 days. In the case of the FCTC, incremental loads were applied once placed tailings became stable within

the apparatus, which took a few days after deposition. Subsequently, an incremental external surcharge load was applied to the tailings using a dead load (up to 10 kPa). A loading frame along with an air pressure belloframe were used for pressures greater than 10 kPa. The pressure transducer situated at the base of the LSC apparatus was used to monitor the change in excess pore pressure generated due to the applied loads. A linear vertical displacement transducer (LVDT) was attached to monitor the change in height of the placed materials.

Once each increment of load was applied, the consolidation process was evaluated by monitoring the change in height of the sample and the dissipation of excess pore pressure with time. Plots of height versus time and excess pore pressure versus time were plotted after consolidation was complete. Subsequently, plots of effective stress versus void ratio (i.e., compressibility curves) were then computed for the tailings tested. Figure 4.6 presents the apparatus for LSC test.

4.1.4.2 Hydraulic conductivity curve

The hydraulic conductivity of the tailings was measured once the process of consolidation for each applied load was completed. A constant head permeability test was then conducted using an upward flow gradient through the tailings specimen. Plots of hydraulic conductivity versus void ratio were computed for each applied incremental load. Figure 4.6 presents the apparatus for hydraulic conductivity testing during compression test using external loads.

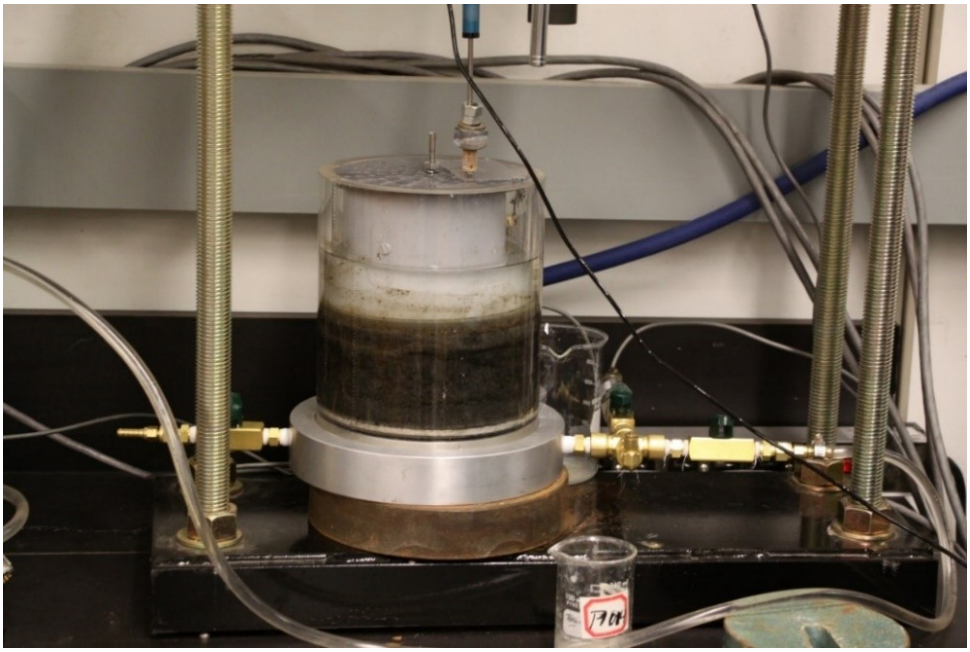

Figure 4. 6 Multi-step loading large-strain consolidometer testing.

4.1.5 Meso-scale test

A meso-scale column apparatus was designed, constructed, and used to characterize the consolidation properties of the tailings during the research program. The column apparatus used an negative water pressure applied at the base of the column to consolidate the tailings. The detailed design of the column apparatus is discussed in section 4.2.1.

A robotic vane shear testing equipment was designed and constructed to measure the undrained shear strength of the consolidating tailings. Details of the vane shear testing equipment are presented in section 4.2.2.

Laboratory investigations carried out using the column apparatus and vane shear testing equipment are presented below.

4.1.5.1 Self-weight consolidation

The column apparatus was used to carry out sedimentation/self-weight consolidation tests on the flocculated FFT. During the self-weight consolidation test, the total volume change, excess pore pressure dissipation, and developed undrained shear strength of the flocculated FFT were measured and monitored.

During the self-weight consolidation process, the flow of water was in an upward direction and the drainage boundary was at the interface between tailings and accumulated supernatant water. Once the self-weight consolidation process ceased (i.e., the change in height became infinitesimal), the accumulated bleed water due to settlement was decanted. It was deemed necessary to decant the accumulated surface bleed water prior to the start of the next stage. The removal of the surface water should not have altered the natural sedimentation process.

4.1.5.2 Consolidation using applied suction

Consolidation of the tailings continued using applied suction at the base of the column. Prior to starting the consolidation process, enough time was allowed for the tailings to come to equilibrium from the loading and unloading process. During the process of consolidation using applied suction, the total volume change (vertical) were monitored and measured using ruler attached to the column and (lateral) using visual observation and a ruler. The developed suction with the profile and developed undrained shear strength of the tailings were measured and monitored. The instruments used to carry out are described in the following section.

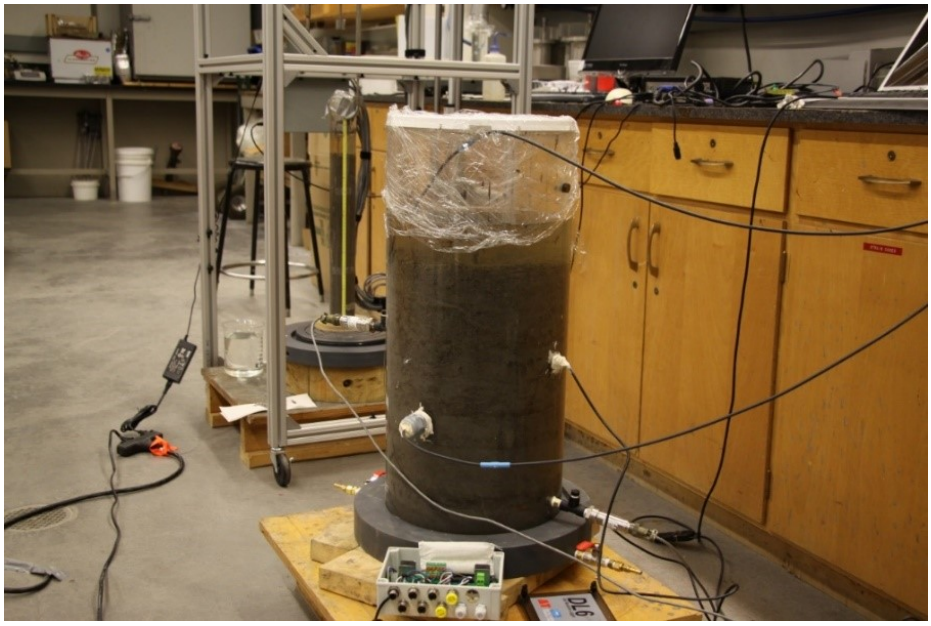

Figure 4. 7 Meso-scale column apparatus using applied suction.

Figure 4.7 presents the meso-scale column apparatus used to consolidate tailings using applied negative water pressure at the base boundary.

4.2 Equipment used during laboratory test program

The research program utilized various laboratory apparatuses and equipment to characterize and determine engineering properties for the flocculated FFT and FCTC. The equipment used during the laboratory testing are categorized as newly developed equipment i) meso-scale column apparatus and ii) shear strength measuring equipment. Each section describes the apparatus and equipment used.

4.2.1 Newly developed equipment

Newly designed equipment was used during the research program to characterize the engineering properties of tailings in a controlled environment. This section will detail equipment designed specifically for the research program including a meso-scale column and vane shear device used.

4.2.1.1 Meso-scale column apparatus

A meso-scale column apparatus was built to carry out the consolidation of high volume-changing slurry tailings. The column uses applied negative water pressure (i.e., matric suction) incrementally through the lower boundary to dewater slurry tailings. Fisseha, Wilson and Fredlund (2017a) presented the hypothesis, design considerations, and advantage and contributions of the column apparatus.

The column apparatus allowed to further the understanding and characterizing the FFTs while consolidating, in relation to saturated/unsaturated zones, under a controlled stress environment. In the field, the process of desaturation, drying, and desiccation occurred from the surface tailings as a result of atmospheric flux boundary such as evaporation and evapotranspiration between the ground surface and above (atmosphere). A transition/interlayer zone forms due to the changing of the water table within the soil profile as the saturation and desaturation processes alternate on the deposited tailings due to rainfall or evaporation, respectively. The meso-scale column mimics the field conditions as follows: Initially fully saturated tailings were deposited in the column and water was withdrawn from the tailings regularly using an incremental applied suction method at the bottom boundary. The column apparatus enables the investigation and characterization of the tailings on the transition/interlayer zone using applied controlled suction

increments through the base compared to the actual process of evaporation and rainfall, which happened through tailings surface. The drying and desiccation process between field condition and column displayed similar in the development of the transition zone with the exception in the direction of flux.

It had been established that the standard tests assisted the characterization of tailings compressibility and saturated-unsaturated flow properties using LSC, SWCC testings. However, the need for the development of meso-scale column apparatus was deemed necessary to assess effects of the following: (i) to combine the process of consolidation by dewatering towards unsaturation, (ii) to assess effects of coefficient of consolidation between k_0 loading and isotropic condition, (iii) assess the development of shear strength along the tailings profile as consolidation progressed using applied suction, (iv) to assess effect of scaling as the standard testing equipment only provide limited sample size.

4.2.1.1.1Design of the column apparatus

The column apparatus consists of an acrylic column, a polyvinyl (PVC) base plate, and a porous ceramic disc. A drainage path was made within the base plate to facilitate the movement of water during the consolidation process through applied negative water pressure. A high air-entry value porous ceramic disc was placed, overlaying the drainage path on the base plate, and used as a separator between the saturated slurry material and ambient air pressure. The porous ceramic disc can withstand a difference between air and water pressures of up to 100 kPa and is suitable for the application of negative pore-water pressures (Fredlund, Rahardjo & Fredlund, 2012). The drainage path grooves connect with the inlet and outlet ports of the base plate. The inlet and outlet ports are used to flush the drainage path either prior to the start of a laboratory test or during the

transition of loading to remove any possible air bubble developed within the drainage path. These ports are also used to apply negative pressure (i.e., suction relative to atmospheric air pressure) to the column apparatus to initiate a transient consolidation process (see Figure 4.8 to 4.12). The acrylic column was mounted into the base plate and provided a tight seal between the acrylic column and the base plate as shown in Figure 4.8 and Figure 4.10. A set of O-rings was used to ensure a tight seal between the acrylic column, porous ceramic disc, and base plate. Additionally, a donut-like ring with screws was used to provide a secure contact between the placed ceramic disc and the base plate. Details of the column apparatus design are presented in (Fisseha, Wilson & Fredlund 2017b).

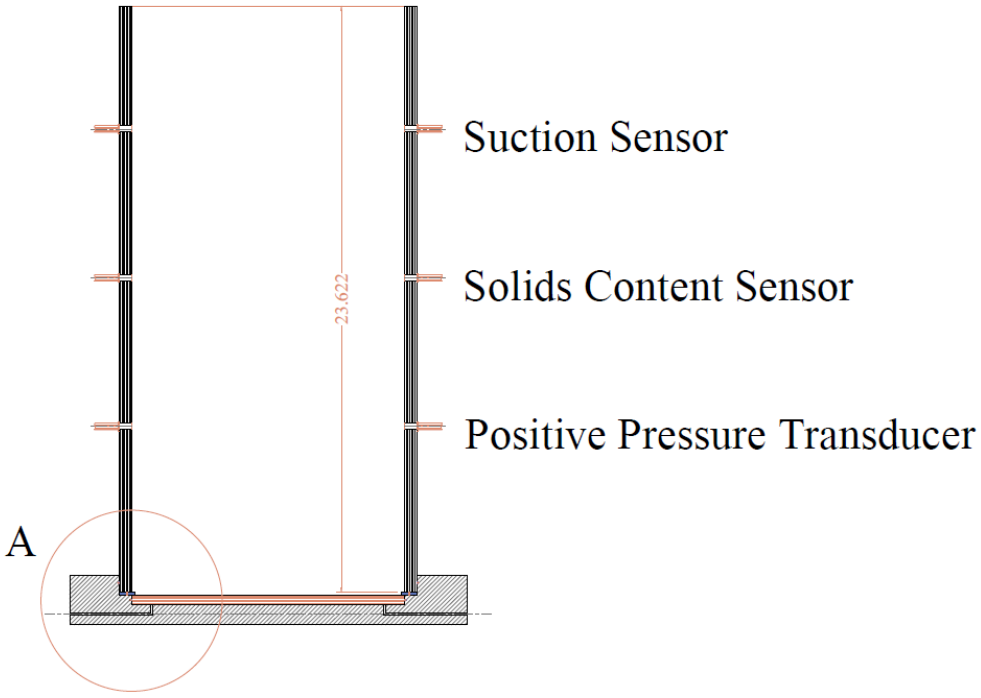

Figure 4. 8 Schematics of the new column apparatus (adapted from Fisseha, Wilson & Fredlund, 2017b).

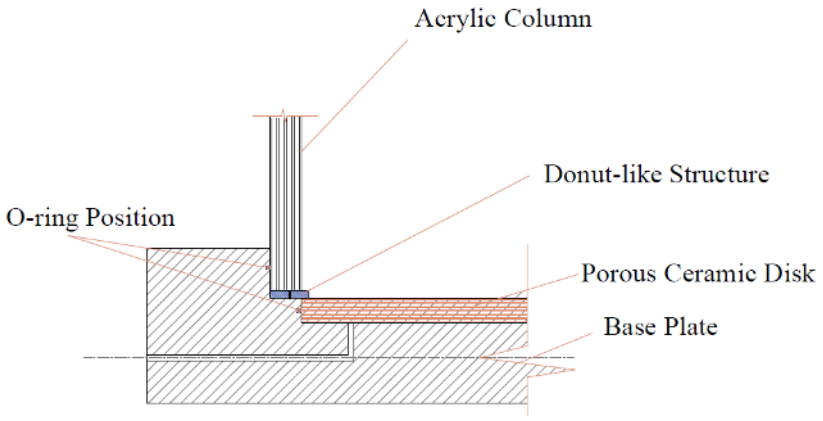

Figure 4. 9 Details of the new column apparatus (adapted from Fisseha, Wilson & Fredlund, 2017b).

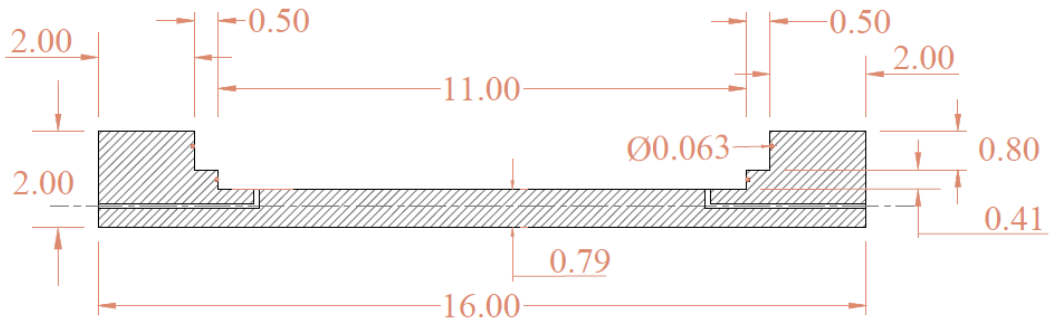

Figure 4. 10 Cross-section of the base plate (adapted from Fisseha, Wilson & Fredlund, 2017b).

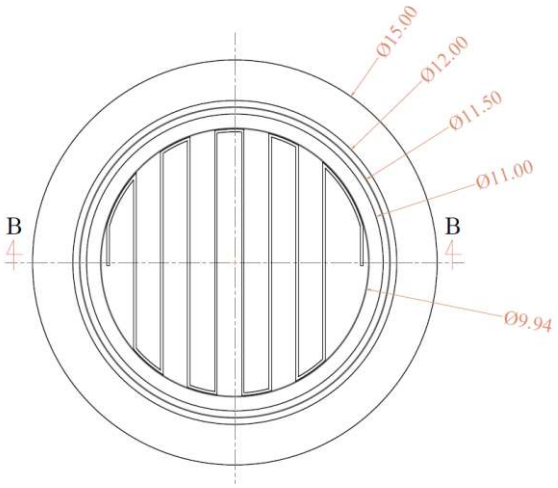

Figure 4. 11 Plan view of the base plate (adapted from Fisseha, Wilson & Fredlund, 2017b).

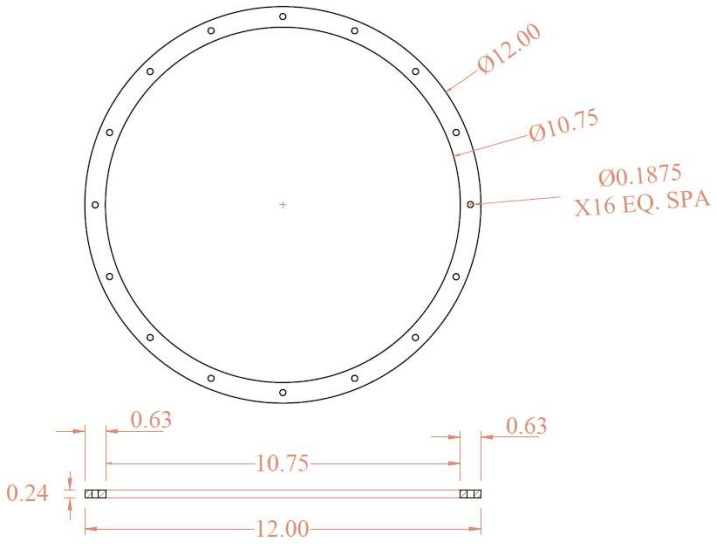

Figure 4. 12 Plan view and cross-section of the donut-like structure (adapted from Fisseha, Wilson & Fredlund, 2017b).

4.2.1.1.2 Hypothesis and overall arrangement of test setup

The laboratory LSC test for slurry tailings can be carried out using either incremental external surcharge loads (i.e., multi-step loading test) or applying negative water pressure at the bottom boundary and draining the moisture from the tailings. Both tests are conducted under stress-controlled conditions. The meso-scale column apparatus used during this research program was designed to use applied negative water pressure at the bottom of the column boundary.

During the consolidation test using the column apparatus, the water table line (i.e., zero pressure line) moved to a lower level along the thickness of the deposited slurry tailings. The continuous withdrawal of water caused the development of an unsaturated zone near the surface of the deposited tailings. A consolidated zone develops near the surface, and the unsaturated region is expected to continue to establish negative pore water pressure, and subsequently, the desaturated material may pull away from the walls of the column boundary. Consequently, cracks may form and propagate downward from the surface of the deposited tailings. Although change

in flux direction during the column apparatus test was different compared to change in flux direction from tailings surface during field trials (i.e., as a result of evaporation); the overall dewatering mechanism, and suction development on the tailings profile during field trials occurred in similar fashion. Therefore, it was anticipated that the column testing would mimic the saturated-unsaturated behavior of deposited tailings under field conditions.

Figure 4.13 presents schematics of the meso-scale column setup with applied suction using a vacuum pump (vacuum source), desiccator, and regulator. Vacuum is used to apply the negative water pressure (i.e., suction) to the base boundary of the column. The desiccator is used not only as a connection between the column and the vacuum pump (vacuum source) but also to collect the drained water from the column as the consolidation test progresses. A regulator is attached to control the applied negative water pressure incrementally.

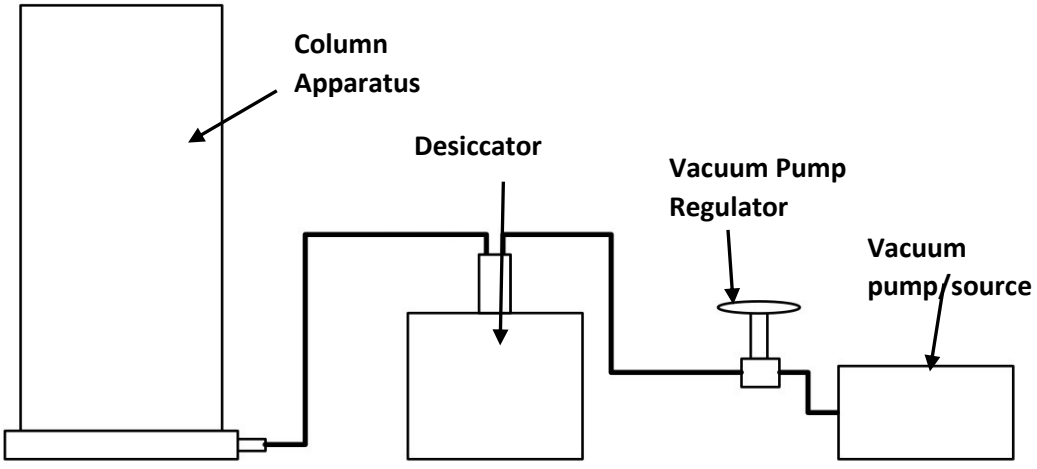

Figure 4. 13 Schematics of conceptual setup for the column apparatus with the applied negative water pressure (adapted from Fisseha, Wilson & Fredlund, 2017b).

The column apparatus remains open at the top, and additional testing equipment can be applied to collect data while the consolidation of tailings progresses. For example, in the present research, shear strength measuring equipment was installed at the open end of the column. The undrained shear strength test was carried out on the deposited tailings as consolidation progressed with an applied suction. Table 4.1 presents a summary of differences between multi-stage step loading consolidation apparatuses and the column using applied suction.

Table 4. 1 Comparison of consolidation apparatus between column using applied suction with multi-step loading.

Description	Multi-stage step loading	Applied suction loading
Loading condition	k_0	isotropic
Generated zones	only saturated condition	saturated and unsaturated
Additional equipment accessibility	Not applicable	An open end allows for additional instrument installation

4.2.1.2 Undrained shear strength measuring equipment

The undrained shear strength of the deposited tailings was measured using the newly designed and built vane shear testing device. Details of the device are presented below.

4.2.1.2.1Vane shear testing device (VSTD) and its design

The vane shear testing device was designed and assembled in the laboratory in an effort to measure the change in shear strength developed during the stages of self-weight consolidation and consolidation using applied suction. The parts and design of VSTD are presented below.

The vane shear testing device (VSTD) consists of a DC motor, a gearbox, three angular position sensors, and a torsional spring (Figure 4.14). A DC motor is used to provide continuous torque (rotation) to the attached vane blade while permitting precise speed control. A reconfigurable gearbox is designed to allow the rotational speed of the vane to meet ASTM lab or field criteria. Figure 4.14 presents the VSTD. Details of the VSTD configuration, mechanics, and calibration are outlined in (Olmedo, Fisseha, Wilson, Barczyk, Zhang, & Lipsett, 2019).

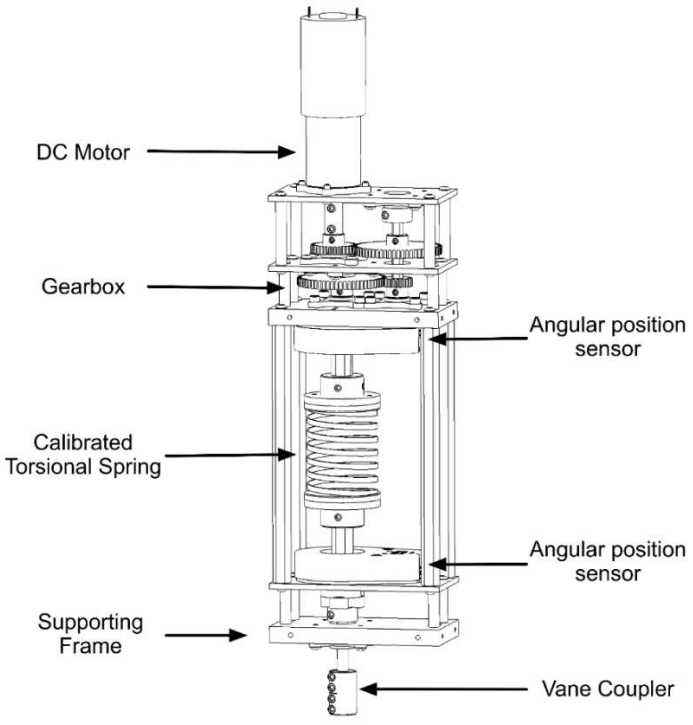

Figure 4. 14 Vane shear testing device (VSTD).

Three VSTDs were mounted on the 6-inch diameter carrier plate platform so that they were equally spaced. Each VSTD is configured with a different vane rod length, which allowed vane tests to be conducted at three different depths without the need to re-insert the vanes in the test specimen. Each VSTD was independently controlled using graphical user interface (GUI).

The spacing between each VSTD was designed within the limit of the column apparatus diameter (i.e., 30 cm) to have clear entrance into the column apparatus during the insertion process of the attached vane blade. Each vane blade is connected to its respective VSTD using an extended rod. An adapter is used to connect each VSTD with its corresponding extended rod. Each vane shear blade is designed to reach different depths within the column apparatus with an extendable rod to measure the undrained shear strength of the consolidating tailings along the column profile (Figure 4.15).

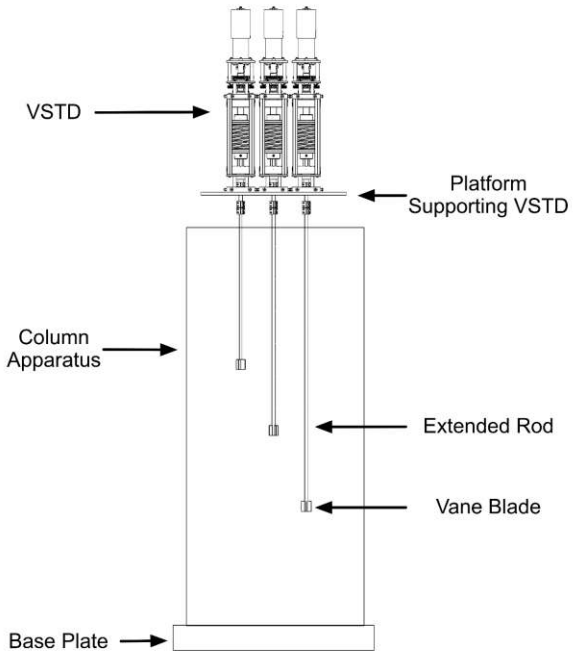

Figure 4. 15 Cross-section view of the VSTD setup mounted on a platform with the column apparatus.

4.2.2.2.2Shear strength measuring equipment (SSME)

The newly designed, assembled, and calibrated SSME was used to measure the undrained shear strength of deposited and consolidating slurry tailings in conjunction with the new column apparatus. The SSME was designed to have high precision measurements to characterize soft soils, slurry tailings, or materials in the laboratory. The SSME system consists of three subsystems: i) three vane shear testing devices (VSTD), ii) a structural frame, and iii) a mechanical traverse. The design was carried out in accordance with the ASTM standards specified in ASTM D4648/D4648M-16 and ASTM D2573/D2573M-15. The SSME and VSTD are controlled using a computer.

i. ***Structural frame and mechanical traverse***

The platform, supporting the three VSTDs, was mounted onto a framework to keep each positioned VSTD in place. Industry standard aluminum framing was used to build the primary supporting structure. A 1.5-inch 8020 t-slotted aluminum extrusions was fixed with standard brackets to produce a 6-ft-high, 2-ft-wide rectangular structure (Figure 4.16). The frame is supported by four caster wheels to make it easily movable. Each wheel has a locking brake to prevent undesired motion during testing.

The structural frame supports a custom mechanical traverse. The linear motion mechanism is designed to control the vertical movement of the platform (i.e., that holds the VSTDs) to introduce the extended vane into the deposited tailing sample to the desired depth with a controlled speed. The mechanical traverse consists of two linear guides, an equipment carrier plate, and an actuator (Figure 4.16). Figure 4.16(a) and Figure 4.16(b) show the SSME system and column apparatus front and side views, respectively. The two linear guides are rigidly attached to the structural frame. Four linear bearings were used to move the equipment carrier plate on the linear guides.

The VSTDs are connected to the carrier plate using aluminum extrusions, which allowed the vertical placement of the tools to be modified depending on the application requirements.

The platform operates using an electric linear actuator consisting of a lead-screw mechanism driven by a DC motor. The linear actuator has built-in limit switches and a linear potentiometer to provide automatic stops at the end of the range of motion and feedback of the extension of the actuator. A linear motion controller was built to control the speed and extension (distance) of the actuator. An MC33926 full H-bridge motor driver is used to drive the DC motor. A 72 MHz ARM Cortex-M4 microcontroller receives feedback from the linear actuator, and sends commands to the motor driver. A Proportional-Integral-Derivative (PID) controller in the microcontroller uses the feedback from the actuator and the desired velocity to drive the system to the desired extension. Figure 4.17 presents different positions of SSME system. Figure 4.17(a) and Figure 4.17(b) show the apparatus prior to and after insertion of the shear measuring equipment within the column. The microcontroller is interfaced with a computer to allow the user to provide the desired position and velocity commands using a GUI. A data logger is used to record measured data during testing.

ii. *Advantages of the SSME system*

The design and use of the SSME system led to numerous benefits for the test program. The equipment enables the measurement of the undrained shear strength gain of the deposited tailings during i) the self-weight consolidation process and ii) the continuous dewatering/consolidation process through loading using the negative water pressure with minimum disturbance. Additional advantages of the equipment are that it was customized to fit the meso-scale column apparatus compared to stationary devices that are difficult to match with

customized testing devices. The design of computerized systems for the SSME minimizes human error.

The SSME's notable advantages compared to the commercially available vane shear measuring devices are summarized as follows: i) Each VSTD is designed to function using computerized triggers to reset, zero, and execute vane shear tests; ii) Multiple points within the same deposited material profile can be measured at the same time with a minimal disturbance due to insertion; iii) The SSME system is designed to reduce operator error since the movement and speed of the system is controlled using the linear actuator; iv) Broader ranges of shear strength values (i.e., soft to denser) can be measured using SSME by changing the size of the vane blade compared to commercially available rheometers, which have specified range limits.

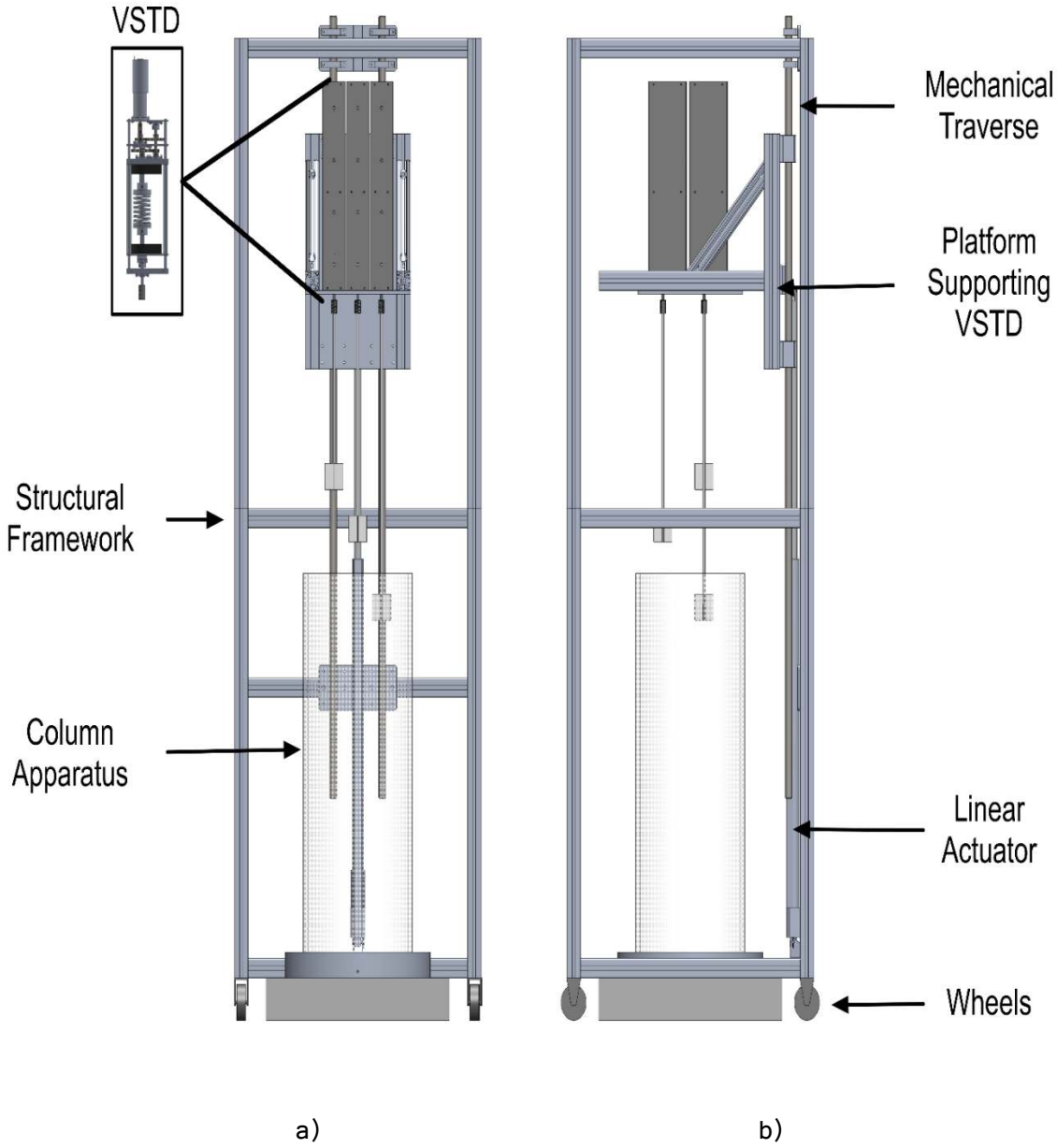

Figure 4. 16 The shear strength measuring equipment. Three main subsystems, three vane shear testing devices, a structural frame, and a mechanical traverse with a) front view and b) side view.

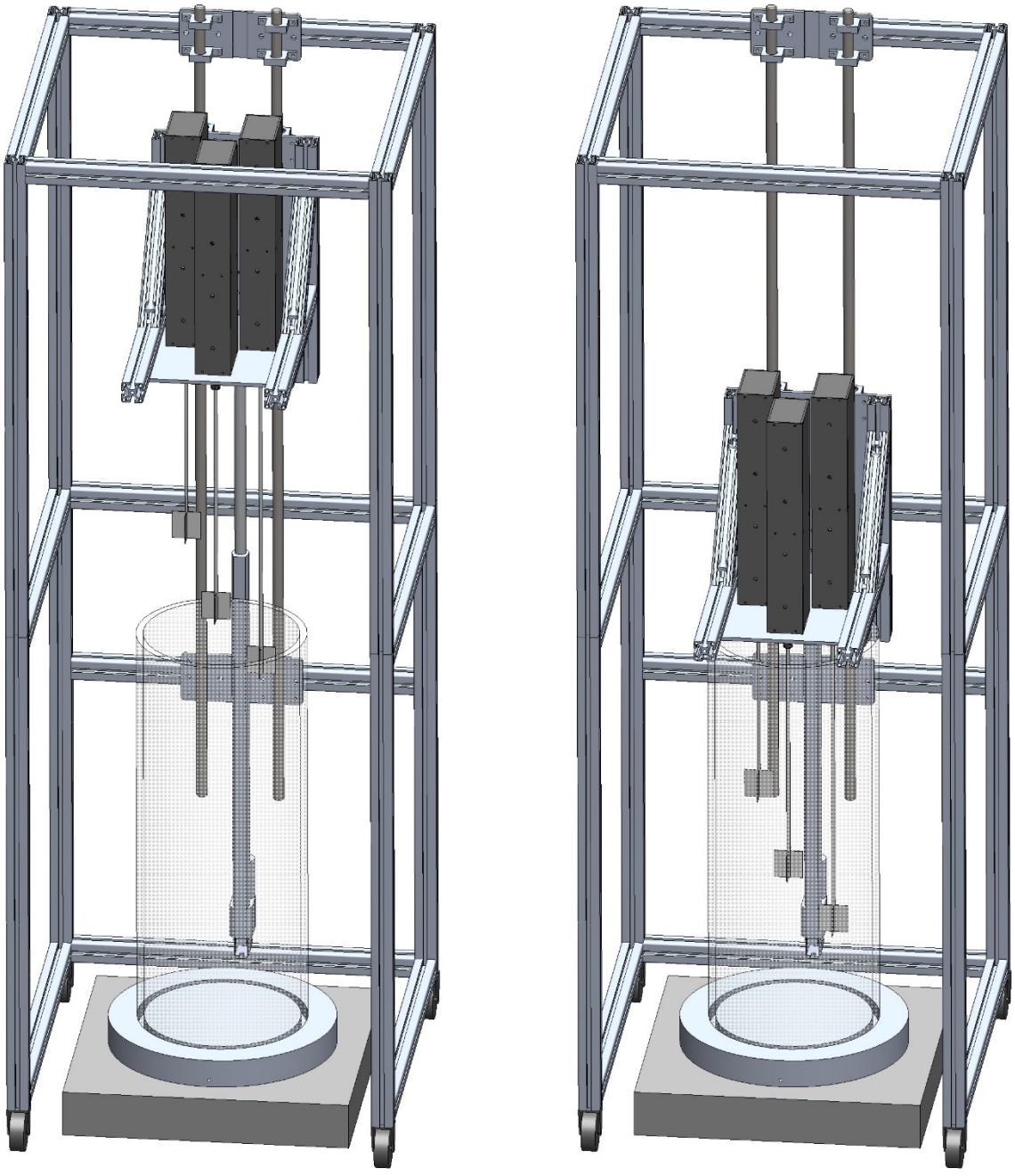

a) b)

Figure 4. 17 a) VSTD with the mechanical traverse in the upward position; b) VSTD with mechanical traverse in downward position.

4.3 Instrumentation on the column apparatus

Details of the column apparatus instrumentation during the laboratory test is presented herein.

4.3.1 Overview of instruments

The column apparatus was provided with a number of sensors which were able to monitor the change during stages of self-weight consolidation and consolidation using an applied suction of placed tailings. Details of the instrumentation are presented in the section below.

Sensors that can measure positive pore-water pressure, negative pore water pressure, and solids content were placed within the column apparatus. As the consolidation test progressed, the sensors measured the positive pore-water pressure, negative water pressure, and volumetric water content changes within the consolidating tailings. The different sensors were distributed throughout the height of the column. The reference datum was assumed to be at the base plate of the column (i.e., base=0 mm height). Total displacement changes in the height of the column of soil were monitored using a stationary camera that took pictures of the column at specified time intervals.

Table 4.2 presents a summary of sensor types and position used in relation to the expected state of saturation of the deposited tailings during the meso-scale experiment.

Table 4. 2. Summary of conceptual applied loading conditions with various generated saturated/unsaturated zones.

No.	Types of sensors	Column 1 Sensor depth from base plate (cm)	Column 2 Sensor depth from base plate (cm)
1	Controlled applied suction	Base of column	Base of column
		-	-
2	Positive pressure transducer	3	3
		28	29
3	Negative water pressure	14	15
		3 cm below surface	3 cm below surface
4	Volumetric water content	3	3
		25	26
5	Change in vertical and volumetric strain	Visual and tape measurement	Visual and tape measurement

4.3.2 Controlled applied suction at the base boundary

During the laboratory consolidation test using applied negative water pressure, vacuum pressure from a vacuum source was used to introduce the applied negative water pressure within the

deposited tailings. The vacuum pressure was applied incrementally at the base of the column. A regulator was used to monitor the applied suction at a given time and the available suction within the reservoir cylinder. A desiccator was attached between the vacuum source and the meso-scale column. The desiccator was used to accumulate dewatered water from the deposited tailings as the process of consolidation progressed. The maximum vacuum pressure applied was 60 kPa.

4.3.3 Positive pore pressure measuring transducer

A positive pore pressure measuring sensor from Omega was used to monitor the pore pressure distribution and dissipation during the sedimentation and consolidation process. The pore pressure measurement during sedimentation and the early stages of consolidation was positive. There were two transducers situated within each column apparatus. The first sensor was located close to the base of the base plate, and the second sensor was located at the mid-section of the column from the base. Details of sensor location in each column are summarized in Table 4.3. Figure 4.18 shows the positive pore pressure transducer measuring sensor used during the experimental work. Calibration data are presented in Appendix C.

Figure 4. 18 Positive pore pressure measuring sensor from Omega.

Table 4. 3 Summary of positive pressure transducers location within column 1 and 2 during the meso-scale laboratory test.

No.	Transducer id	Column id	Depth from base of the column (cm)
1	442827	1	3
2	442813	1	28
3	442842	2	3
4	417991	2	29

4.3.4 Negative water pressure measuring sensor

A negative water pressure sensor from meter© (Meter, 2018) was used to monitor the pore pressure distribution during the laboratory experimental work. Two T5 sensors with shaft lengths of 5 cm and 10 cm were placed in the middle and close to the surface of the tailings in the meso-scale columns. Details of the sensor locations for each column are summarized in Table 4.4. Figure 4.19 shows the T5 sensor used to measure negative pore pressure. The sensor placed near the surface of tailings were the only responsive sensors during the testing program.

Table 4. 4 Summary of negative pore pressure location within column 1 and 2 during the meso-scale laboratory test.

No.	Negative pore pressure measuring sensor	Column id	Depth from base of the column (cm)
1	T511	1	24
2	T512	1	35
3	T521	2	22
4	T522	2	27

Figure 4. 19 T5 - Negative pore pressure measuring sensor from meter©.

The data logger, DL6, (Delta-T, 2019) which is typically used to measure soil moisture, was used to record the measured negative pore pressure during the consolidation process while applied incremental suction progressed at the base boundary. Figure 4.20 shows the data logger.

Figure 4. 20 Data logger, DL6, used for recording negative water pressure.

4.3.5 Volumetric water content measuring sensor

A volumetric water content measuring sensor from Meter© (Meter, 2018) was used to monitor the change in volumetric water content during the experimental laboratory work. The sensors used were T5E decagon. Each column was provided with two decagon sensors; one sensor was placed near the base of the column and the second sensor was placed at the mid-section of the column apparatus. Details of the sensor positions are summarized in Table 4.5. The measurements were not used due to incorporated error.

Table 4. 5 Summary of volumetric water content measuring sensor location within column 1 and 2 during the meso-scale laboratory test.

No.	Volumetric water content sensor	Column id	Depth from base of the column (cm)
1	VW11	1	3
2	VW12	1	25
3	VW21	2	2
4	VW22	2	26

Figures 4.21 and 4.22 present used volumetric water content measuring sensor and data logger respectively.

Figure 4. 21 Volumetric water content measuring sensor from Meter©.

A data logger, EM50, from Meter© (Meter, 2018) was used to record measured volumetric water content data during the laboratory work.

Figure 4. 22 Data logger, EM50, used for recording volumetric water content from Meter©.

4.3.6 Vertical and volumetric strain measurement

The change in vertical strain and volumetric strain during the consolidation of deposited tailings was measured by using visual observation daily through the attached tape measurement at the outer shell of the meso-scale column. The volumetric strain was computed by taking the average height of tailings divided by the cross-sectional area. A detailed measurement of the change in vertical and volumetric strain is summarized in the results section.

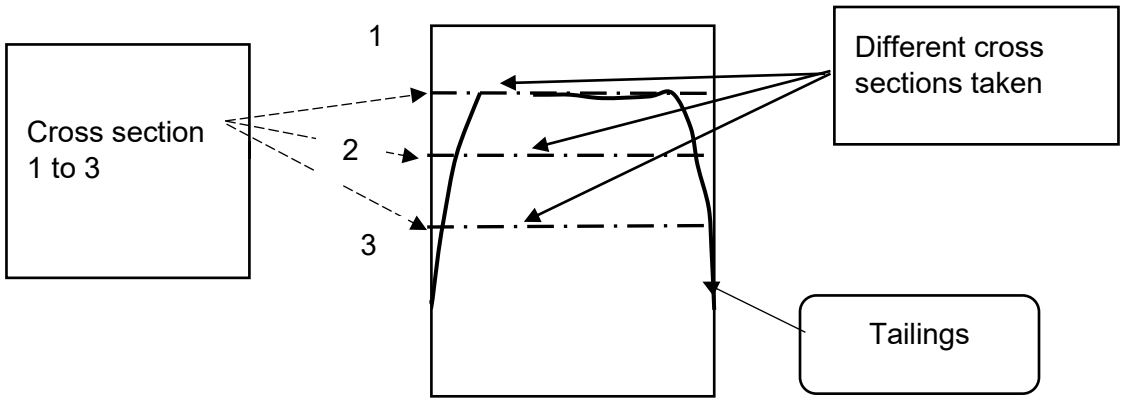

Figure 4. 23 Conceptual vertical and volumetric strain measurement cross sections used.

CHAPTER FIVE: PRESENTATION OF RESULTS

This section presents the measured results obtained during the laboratory test program for the present study. The chapter is divided into two major subtopics: i) presentation of results, and ii) an explanation of challenges encountered during testing.

5.1 Presentation of results

The measured raw data results from the experimental testing is presented in this section. The results are organized into three major sections and subsections. The major sections are i) material characterization, ii) self-weight consolidation, and iii) consolidation using applied suction.

5.1.1 Material characterization results

The results of material characterization obtained during the laboratory experimental work for the present study is presented in this section. Standard geotechnical index property testing techniques were used.

5.1.1.1 Geotechnical index properties

A summary of the geotechnical index properties for the flocculated FFT (material 1) and flocculated centrifuged tailings cake (FCTC) (material 2) is presented in Table 5.1. The summary of the index properties includes methylene blue index (MBI), percentage of bitumen content, particle grain size distribution (i.e., D_{50}, and D_{60}), specific gravity, Atterberg limits (i.e., liquid limit [LL] and plastic limit [PL]), and total fines content (i.e., < 44 micron) as per the oil sands tailings definition, percent of clay size particles and sand to fines ratio (SFR) are presented.

Table 5. 1 Summary of geotechnical index properties of the flocculated FFT and FCTC.

Properties	Flocculated FFT (Material 1)	FCTC (Material 2)
MBI (meq/100 g)	3.75	-
Bitumen Content (%)**	2.57	0.37
D_{50}, D_{60} (µm)	3.2, 6.3	1.4, 2.4
Specific Gravity, G_s	2.2	2.48
Liquid Limit (%)	42	57
Plastic Limit (%)	30	26
Fines content (< 44 µm) (%)	81	87
clay size particle (%)	40.5	53
SFR	0.24	0.15

** Bitumen content – calculated using total bitumen divided by dry tailings.
Major ions in pore fluid were not measured.

The particle size distribution for the flocculated FFT is presented in Figure 5.1, respectively. The results for the particle size distribution presented were carried using non-dispersed method.

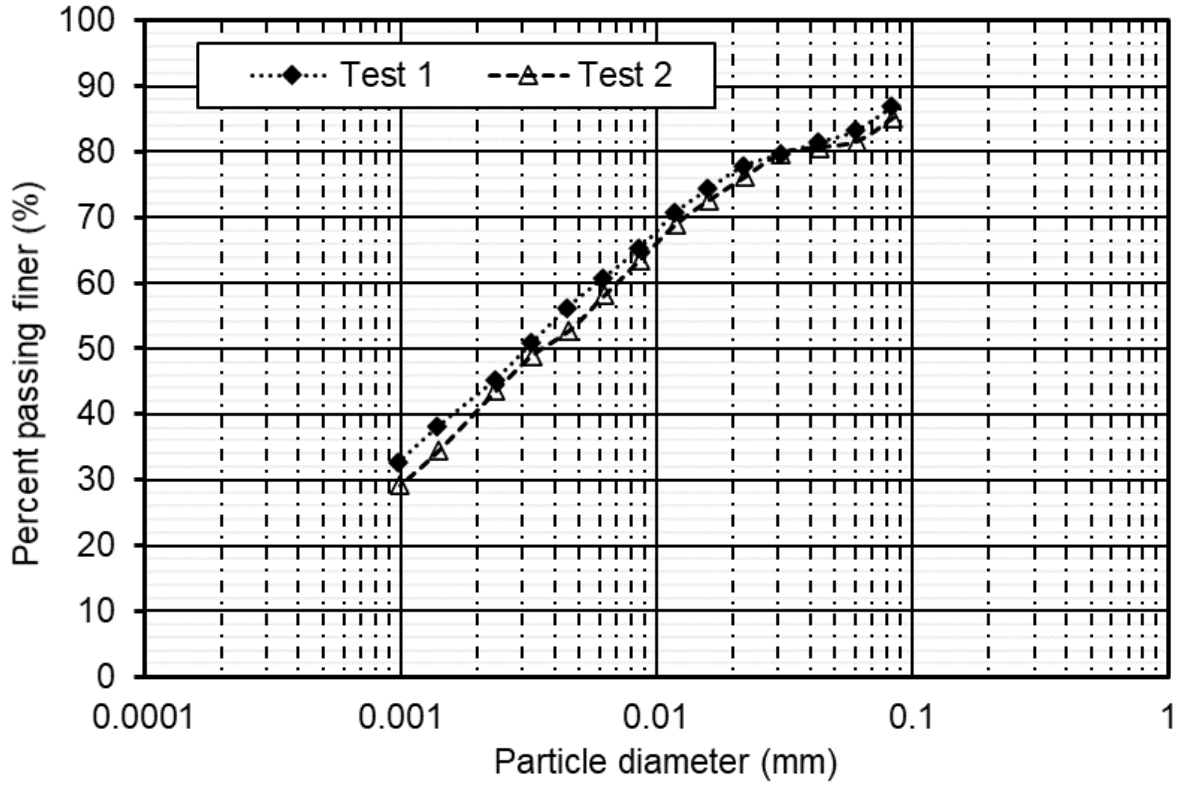

Figure 5. 1 Particle size distribution of the flocculated FFT.

5.1.1.2 Settling column properties

The settling column test results are presented in this section for both the flocculated FFT and FCTC.

Flocculated FFT

The column settling test was conducted for the characterization of the sedimentation/self-weight consolidation behaviour of the flocculated FFT. Results obtained from the column settling test are presented in Figure 5.3. The average initial void ratio was computed to be between 4.0 and 4.2 for the different trials. The average final void ratio was determined to be between 3.0 and 3.4 for a settling time of 75 and 91 days, respectively. The vertical strain (or average void ratio change) due to the self-weight consolidation process is substantial for the flocculated FFT, as illustrated in Figure 5.3. The four settling test trials were conducted since the tailings were from different batch, however each settling test was conducted using the same flocculant dosage.

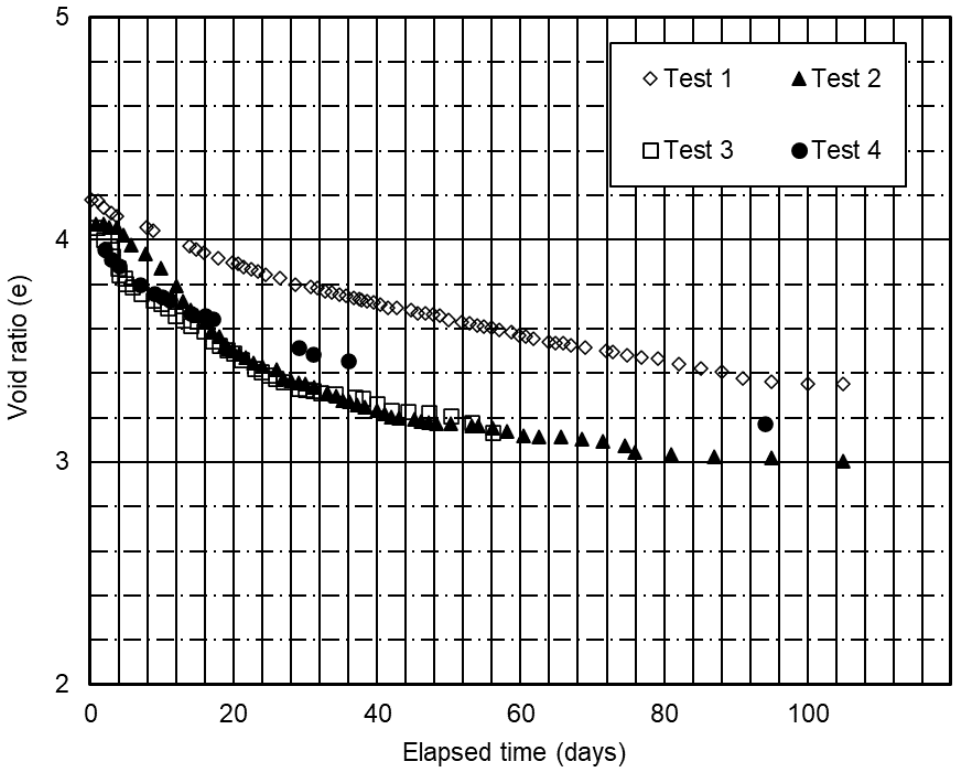

Figure 5. 2 Settlement of flocculated FFT from standard settling column test.

Flocculated centrifuged tailings cake (FCTC)

The column settling test was conducted to characterize the sedimentation/self-weight consolidation behaviour of the FCTC. Results obtained from the column settling test are presented in Figure 5.4. The average initial void ratio was computed to be between 2.01 to 2.03 for the two trial tests. The average final void ratio was determined to be between 1.8 for settling time of 250 days. There was no vertical strain (or average void ratio change) due to the self-weight consolidation process for the FCTC. The small change between initial and final void ratio is due to the removal of trapped air bubbles during the deposition process into the column or due to fabric adjustment as the material continued to stay in the column for longer period.

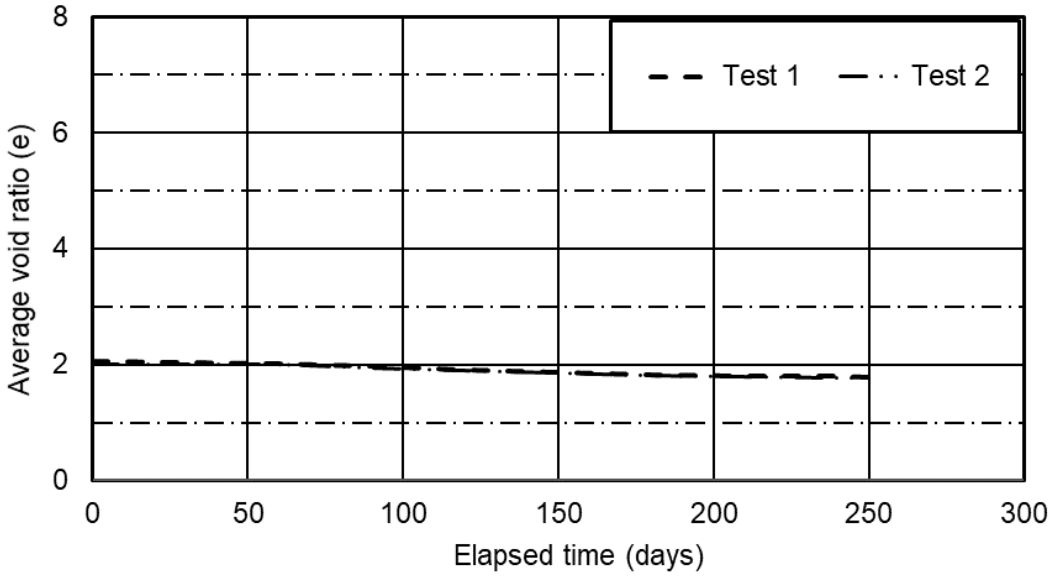

Figure 5. 3 Settlement of FCTC from column settling test.

5.1.1.3 Unsaturated soils properties

The unsaturated soils properties were determined for the flocculated FFT and FCTC tailings through laboratory testing by measuring for the soil-water characteristic curve (SWCC) and shrinkage curve (SC). Figure 5.5 and Figure 5.6 present the SWCC for the flocculated FFT and FCTC tailings, followed by the relationship for the shrinkage curve (SC) presented by Figure 5.7 and Figure 5.8 for the flocculated FFT and FCTC tailings, respectively.

5.1.1.3.1 Soil-water characteristic curve

The soil-water characteristic curve measured for the flocculated FFT and FCTC tailings is presented in Figure 5.5 and Figure 5.6, respectively.

Flocculated FFT

Figure 5.5 presents the measured SWCC for the flocculated FFT in terms of matric suction and gravimetric water content. The relationship between matric suction and degree of saturation was determined by using an empirical formula for tailings with high volume change (Zhang et al., 2015) based on the shrinkage curve data presented in Figure 5.7. Test 1 and 2 were tailings from the same batch and treatment. The SWCC plot (i.e., Figure 5.5) gives an air-entry value (AEV) of 200 to 250 kPa based on the degree of saturation plot for the flocculated tailings. This AEV is similar to the AEV obtained for oil sands tailings presented in the literature (Yao, 2016).

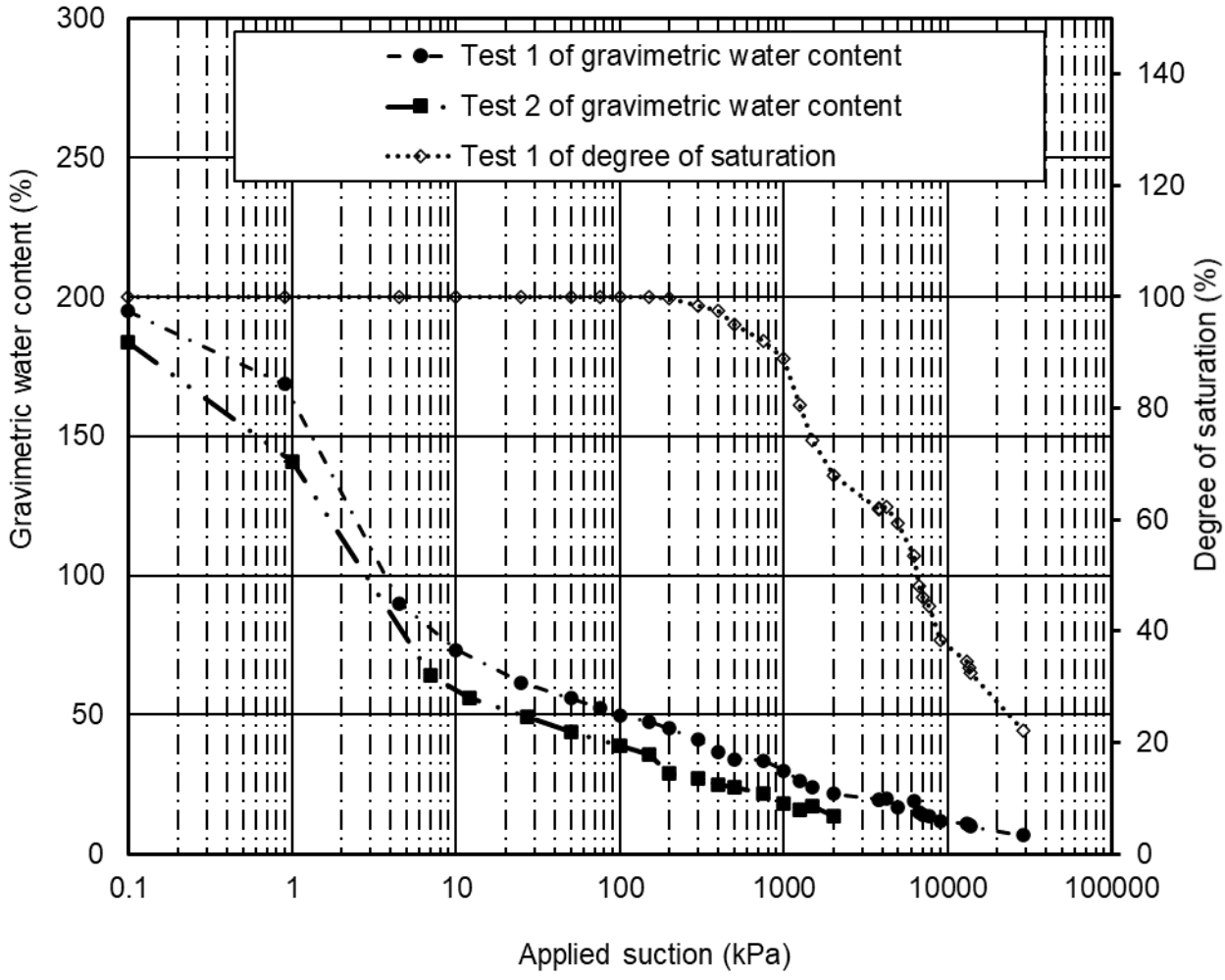

Figure 5. 4 Soil-water characteristic curve of the flocculated FFT.

Flocculated centrifuged tailing cake (FCTC)

Figure 5.6 presents the measured SWCC of the FCTC in terms of matric suction and gravimetric water content. The relationship between matric suction and degree of saturation was determined by using the SWCC and shrinkage curve presented in Figure 5.8. The SWCC plot (i.e., Figure 5.6) shows an average air-entry value (AEV) ranging between 550 to700 kPa for the FCTC. The FCTC SWCC results were used from research work used for the same material (Schafer, 2018).

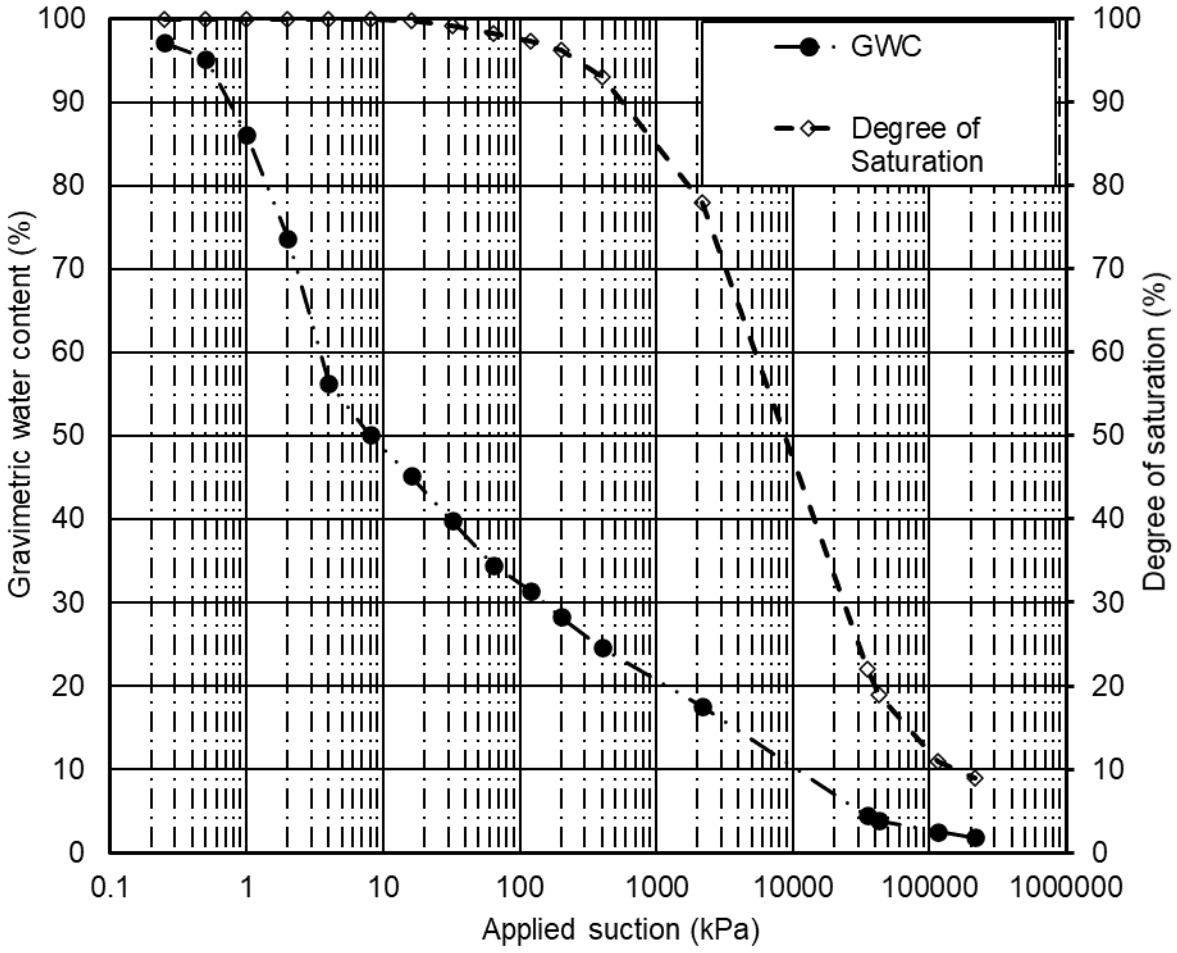

Figure 5. 5 Soil-water characteristic curve of the FCTC.

5.1.1.3.2Shrinkage curve

The measured results of shrinkage curve (SC) for the flocculated FFT and FCTC are presented in Figure 5.7 and Figure 5.8, respectively.

Flocculated FFT

Figure 5.7 presents the shrinkage curve of the flocculated FFT measured in the laboratory. The final void ratios of 0.71 and 0.63 were measured for Test 1 and Test 2, respectively. The measured results are consistent with the shrinkage curve obtained for similar tailings results reported by Yao (2016).

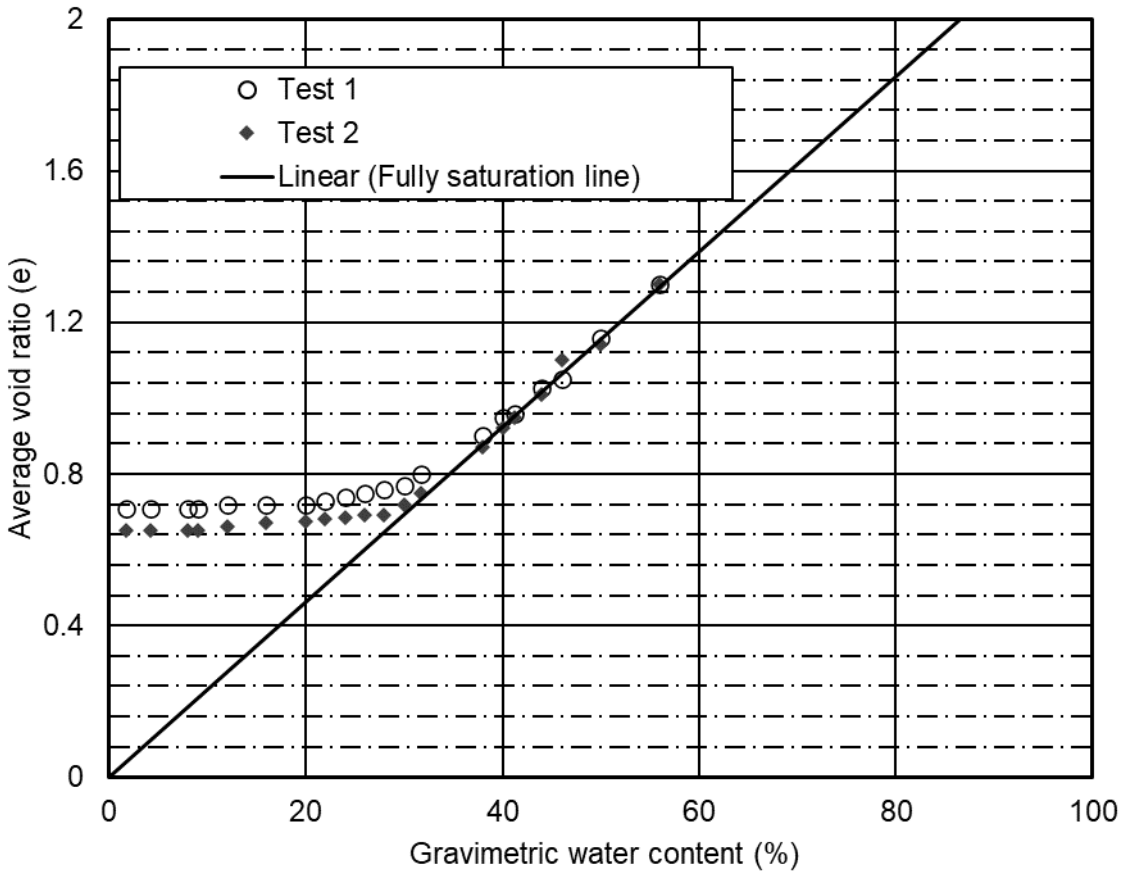

Figure 5. 6 Shrinkage curve of the flocculated FFT.

Flocculated centrifuged tailings cake (FCTC)

Figure 5.8 presents the shrinkage curve of the FCTC measured at the laboratory. The final void ratio was determined to be 0.49 and 0.5 for the sample Tests of 1 to 3 as presented in Figure 5.8. The FCTC Shrinkage curve results were used from research work used for the same material (Schafer, H. 2018).

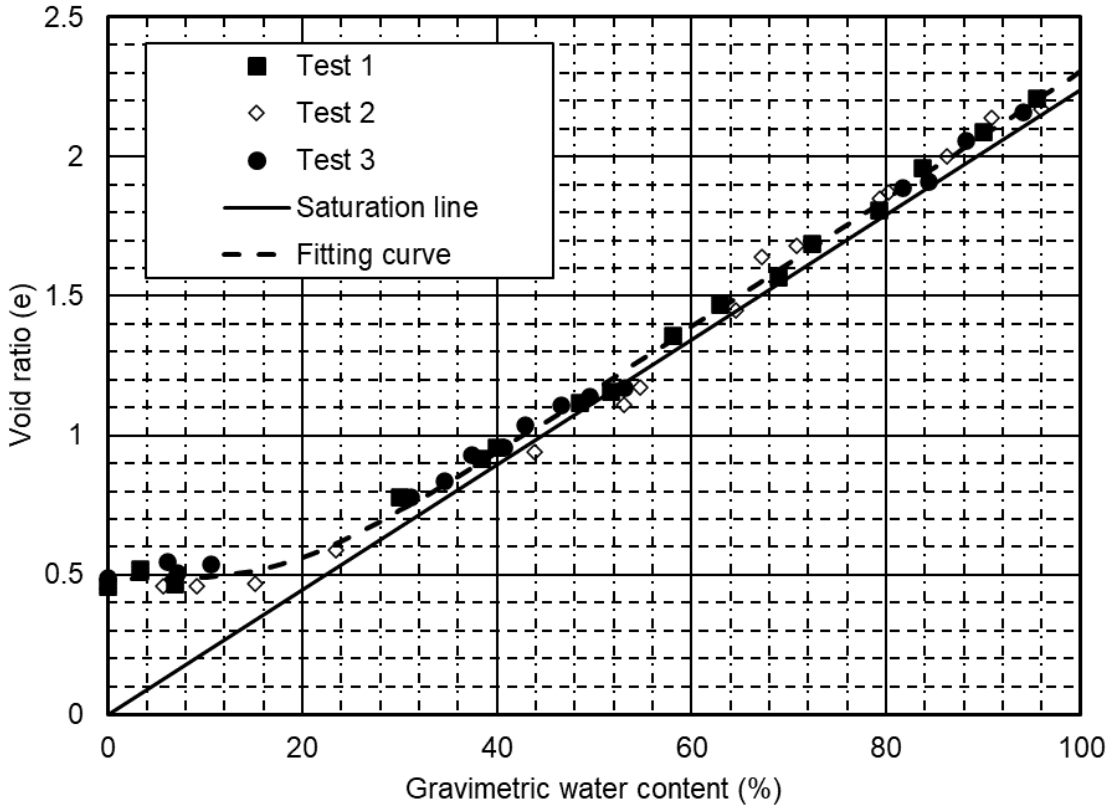

Figure 5. 7 Shrinkage curve of the FCTC.

5.1.1.4 Consolidation properties

The properties of consolidation are expressed using compressibility and hydraulic conductivity curve, which are presented in the section below.

5.1.1.4.1Compressibility curve

The measured relationship of the compressibility curve for the flocculated FFT and FCTC are presented herein.

Flocculated FFT

The compressibility curve for the flocculated FFT is presented in Figure 5.9. The average initial void ratio of the flocculated tailings was computed to be 3.2 once the self-weight consolidation process (or applied stress) was completed. The average final void ratio was determined to be 1.28 and corresponds to an applied effective stress of 200 kPa. The test were stopped at 200 kPa assuming good correlation was achieved. A power function was used to best fit the measured results of the compressibility curve as shown in Figure 5.9.

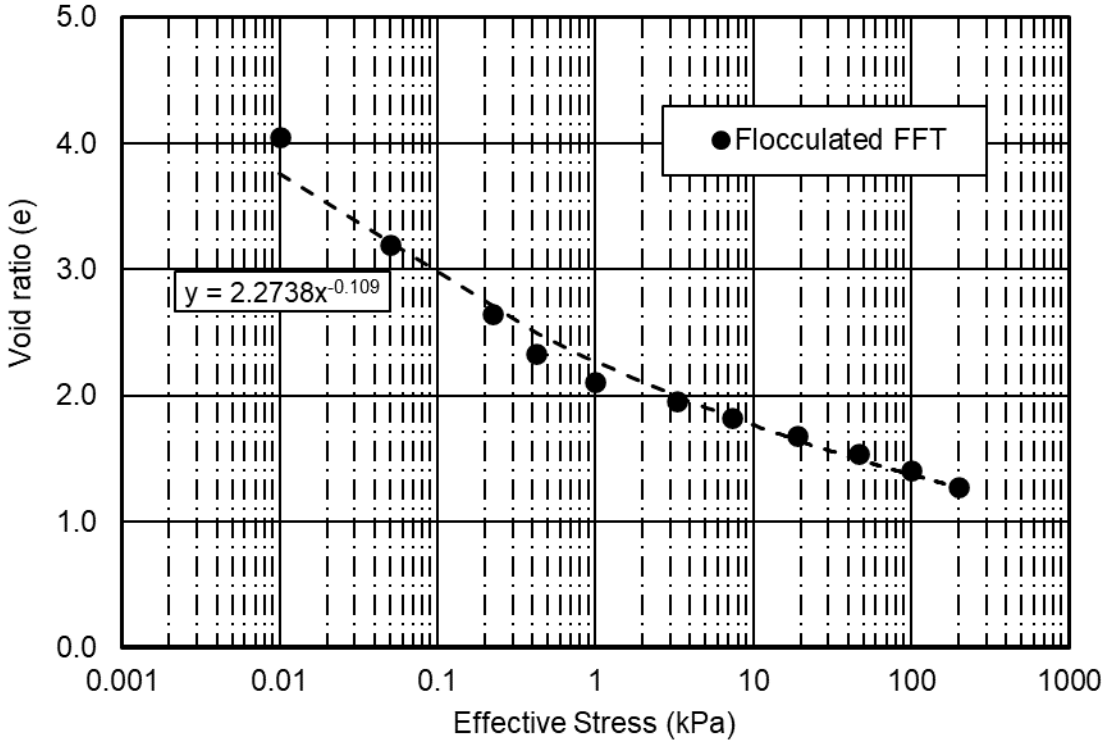

Figure 5. 8 Compressibility curve of the flocculated FFT using LSC apparatus.

Flocculated centrifuged tailings cake (FCTC)

The compressibility curve for the FCTC is presented in Figure 5.10. The average initial void ratio of FCTC was determined to be 2.01 under the initial self-weight consolidation stress. The average final void ratio was determined to be 0.64 and its value corresponds to an applied effective stress of 400 kPa. A power function was used to best fit the measured results of the compressibility curve, as shown in Figure 5.10.

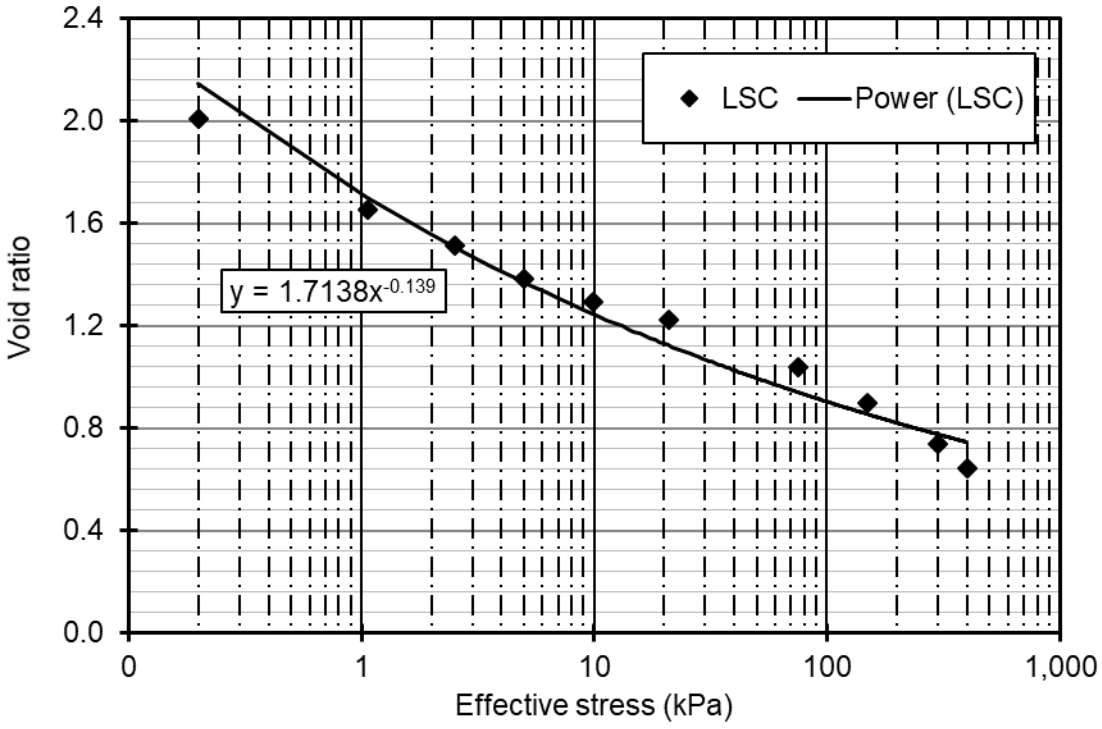

Figure 5. 9 Compressibility curve for the FCTC using LSC apparatus.

5.1.1.4.2Hydraulic conductivity curve

The measured relationship to define the hydraulic conductivity curve for the flocculated FFT and FCTC is presented herein.

Flocculated FFT

The hydraulic conductivity curve for the flocculated FFT is presented in Figure 5.11. The initial hydraulic conductivity was computed from settling test and determined to be 2.03E-05 m/sec at the average initial void ratio of 3.2. The final hydraulic conductivity was measured to be 4.13E-11

m/sec at average final void ratio of 1.41. The relationship between hydraulic conductivity and void ratio is best-fitted using a power function, as presented in Figure 5.11.

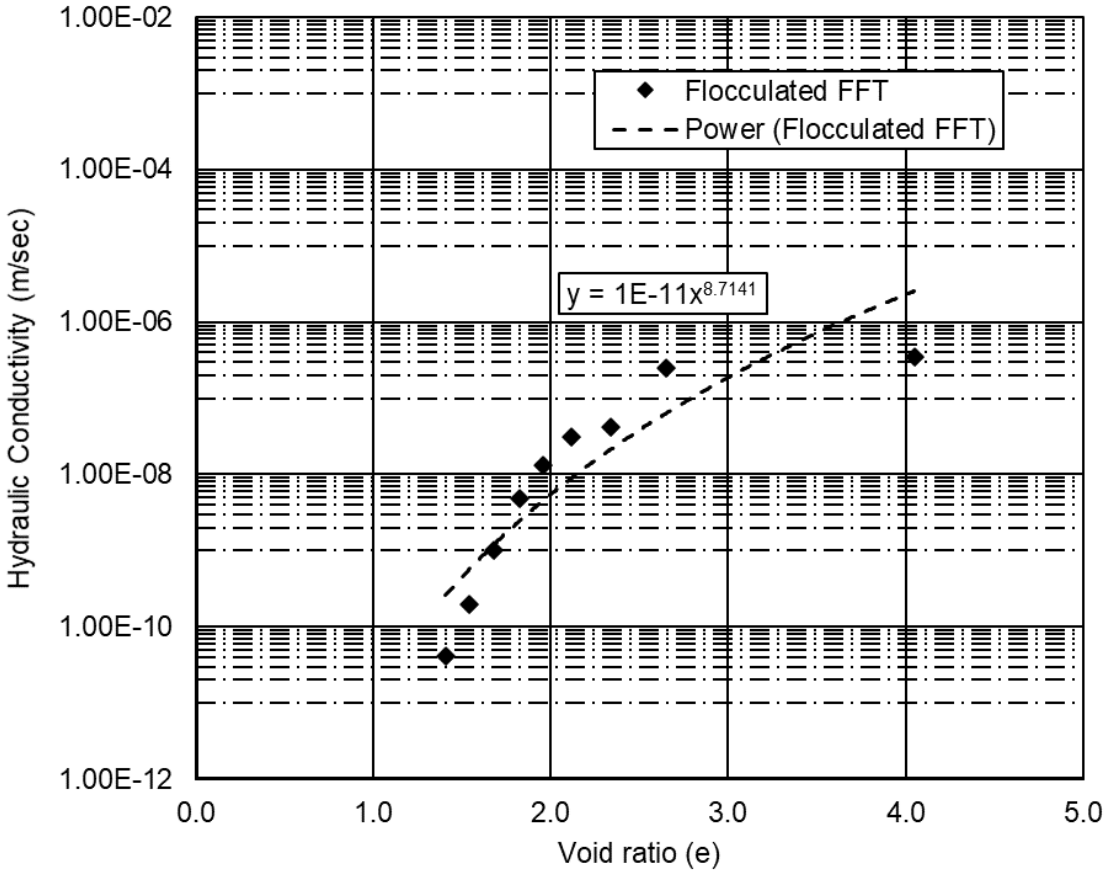

Figure 5. 10 Hydraulic conductivity curve of the flocculated FFT using LSC apparatus.

Flocculated centrifuged tailings cake (FCTC)

The hydraulic conductivity curve for the FCTC is presented in Figure 5.12. The initial hydraulic conductivity was determined to be 1.51E-08 m/sec at the average initial void ratio of 2.01. The final hydraulic conductivity was measured to be 9.89E-11 m/sec corresponding to average final void ratio of 0.64. The relationship between the hydraulic conductivity and void ratio is best-fitted using a power function.

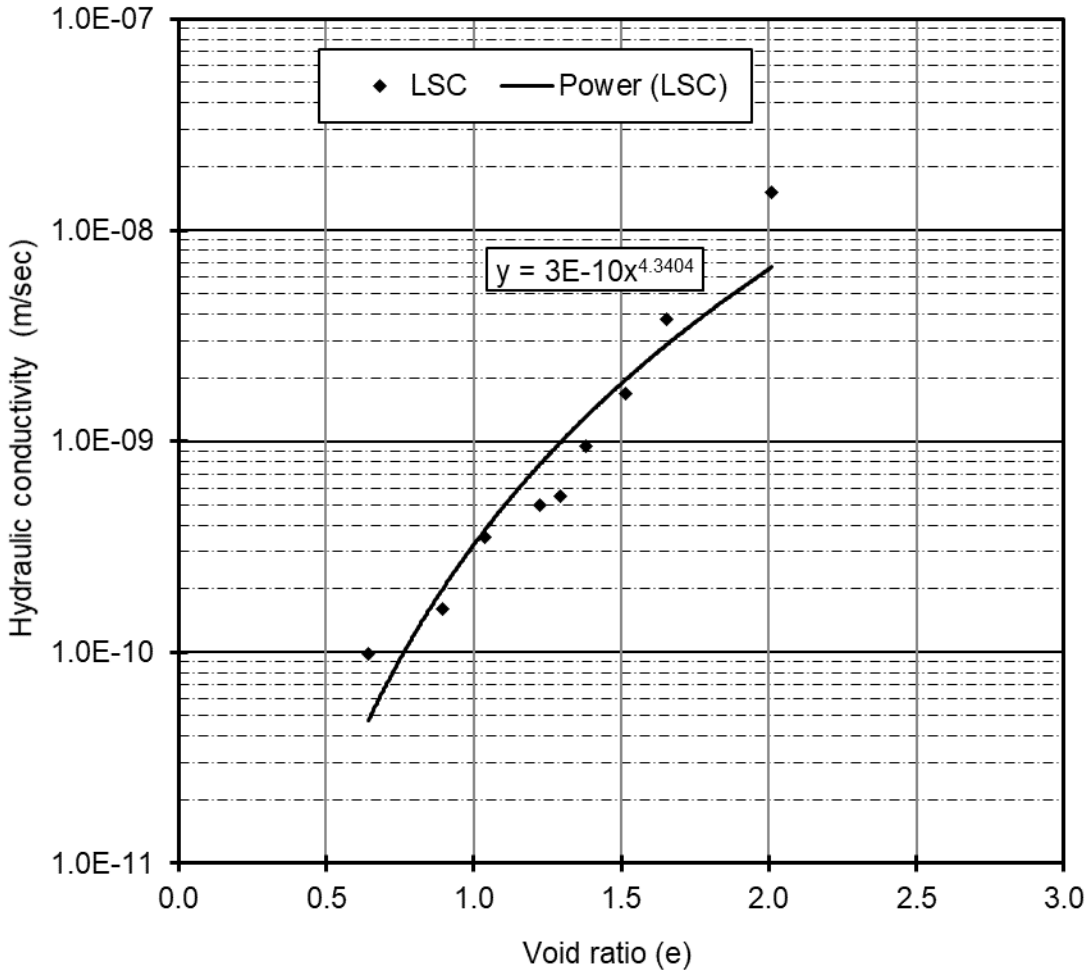

Figure 5. 11 Hydraulic conductivity curve of the FCTC using LSC apparatus.

5.1.2 Measured data from meso-scale test

This section presents results obtained during the sedimentation and self-weight consolidation process only using the meso-scale column testing apparatus.

5.1.2.1 Results of sedimentation and self-weight consolidation test

The process of sedimentation and self-weight consolidation was examined at the laboratory for the flocculated fluid fine tailings using the column apparatus during the present study. Details of the column apparatus is presented in Chapter 4.

The results obtained during the characterization testing for the flocculated FFT show a significant volume change (mainly vertical strain) during the deposition of the tailings. Therefore, sedimentation and self-weight consolidation tests were conducted at the start of the meso-scale testing. The sedimentation and self-weight consolidation process was conducted by placing the tailings into the column followed by observation. Further, measurements of change were made as the experimental testing was ongoing. The process of consolidation resulting from the applied suction (transient consolidation) following completion of the self-weight consolidation process for the tailings is presented in section 5.1.3.

Flocculated FFT

During the self-weight consolidation test, various data sets were measured from the meso-scale experimental test using the instrumented sensors and visual observation as described in Chapter 4. The measured data sets are the change in total vertical and volumetric strain, dissipation of excess pore pressure, and undrained shear strength. These measurements were made as the process of sedimentation progressed.

Settlement, vertical strain, and void ratio

The following schematic representation was exhibited during the self-weight consolidation process of deposited flocculated FFT. As the tailings progressed with the settling process, the

accumulated supernatant water was left at the top of the deposited tailings, as depicted in Figure 5.13.

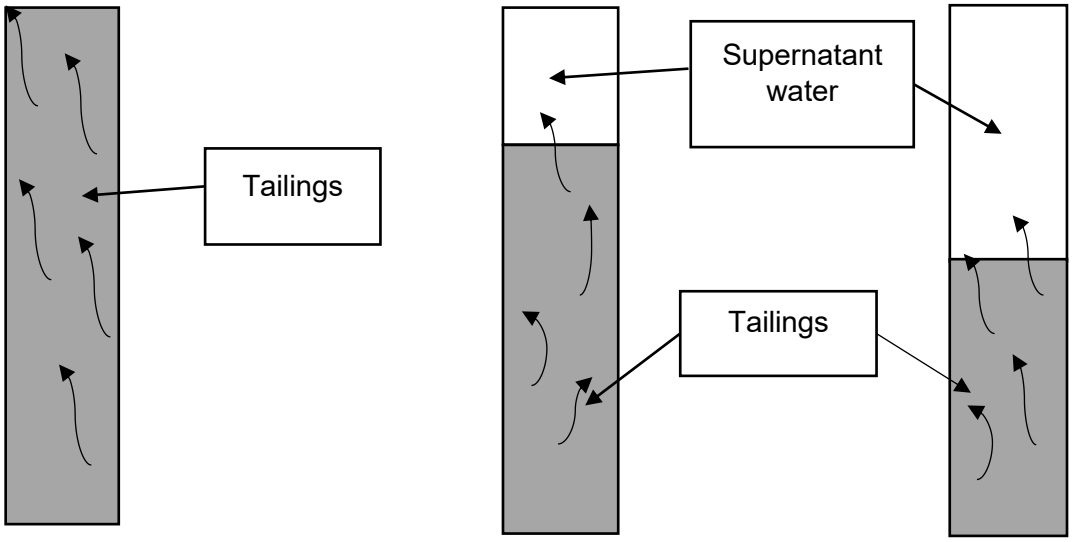

Figure 5. 12 Schematics of the self-weight consolidation over time for the flocculated FFT.

The measured change in vertical strain and void ratio during the self-weight consolidation test for the flocculated FFT is presented in Figure 5.14 and Figure 5.15. No change in lateral strain of deposited tailings was observed during the self-weight consolidation process. The change in volumetric strain was attributed to change in vertical strain only. Therefore, results of vertical strain and void ratio are presented under the self-weight consolidation testing section.

The initial deposited tailings thickness was 50.5 cm. Vertical strain (and void ratio) was observed immediately as the deposited tailings continued to settle. The vertical strain (and void ratio) plot shows a steep slope for the first 25 days after the start of the tailings placement. The slopes become gentler as the sedimentation and consolidation process progressed over roughly 60 days. The vertical strain (and void ratio) became infinitesimal by day 80 and beyond. The final tailings

thickness was determined to be 38.45 cm, and the vertical strain was 0.76 once the self-weight consolidation process completed. The results are presented in Figure 5.14.

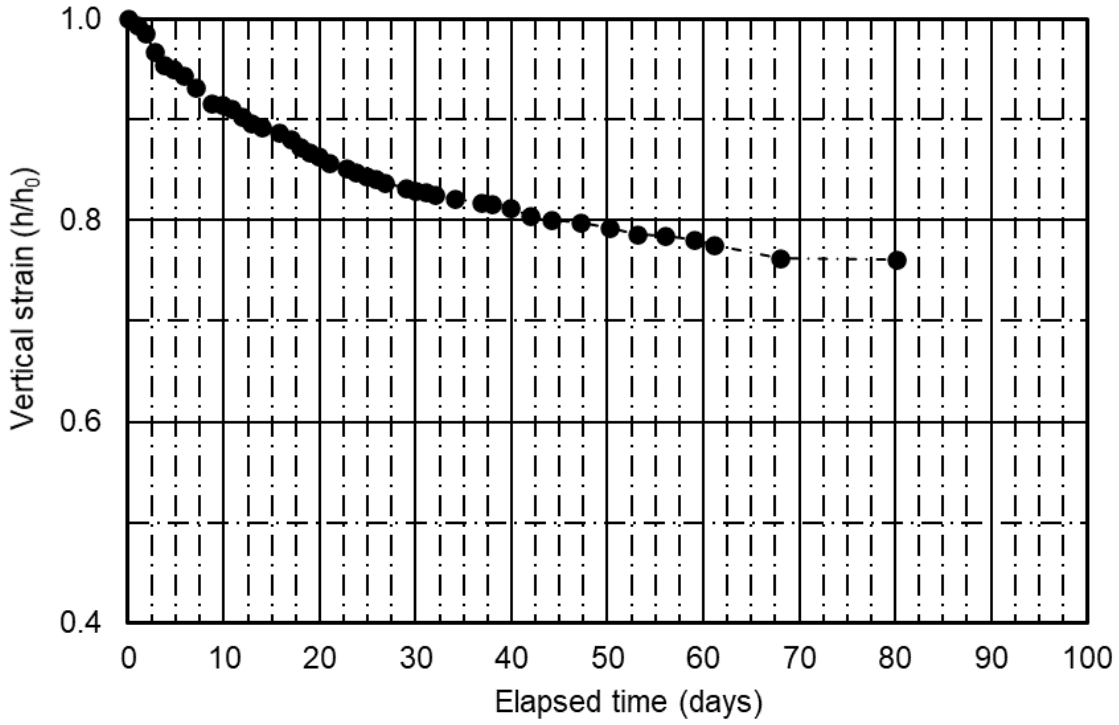

Figure 5. 13 Vertical strain during the self-weight consolidation for the flocculated FFT.

The initial void ratio was computed using initial solids content formula and was determined to be 4.09 for the initial deposited tailings thickness of 50.5 cm. The average final void ratio was determined to be 2.87 and the final tailings thickness was 38.45 cm by the end of the self-weight consolidation process on day 95.

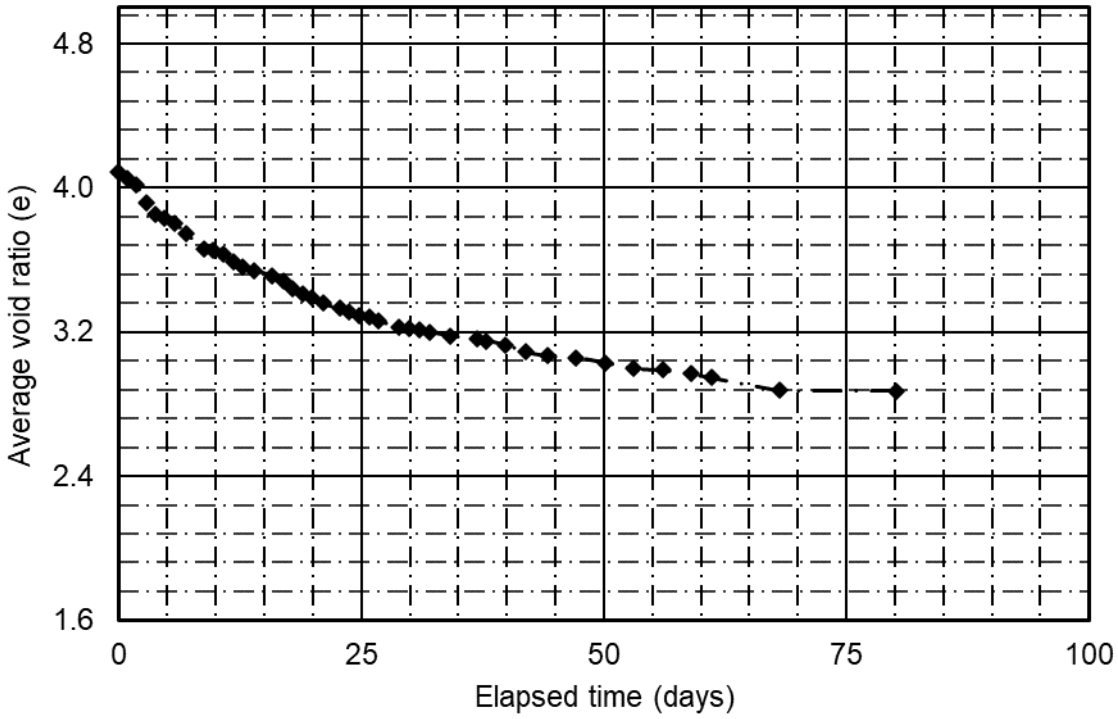

Figure 5. 14 Change in void ratio during the self-weight consolidation for the flocculated FFT.

In conclusion, the flocculated FFT exhibited vertical strain of 20% due to the sedimentation/self-weight consolidation process as presented in Figure 5.15.

Pore pressure dissipation

The measured pore water pressure dissipation during the self-weight consolidation process for the flocculated FFT is presented in Figure 5.16. Figure 5.16 presents measured excess pore pressure and expected hydrostatic pressure line for the tailings under experiment. Excess pore pressure was generated during the deposition of the tailings and dissipation of the excess pore pressure exhibited as the deposited flocculated tailings continued to settle with time.

During the self-weight consolidation process, the drainage boundary was at the tailings surface as depicted in Figure 5.13. Excess pore pressure was measured using the positive pressure transducers located at 28 cm and 3 cm from the base of column as presented in Figure 5.16. The measured excess pore pressure using the transducer located at 28 cm dissipated faster than the measured excess pore pressure using the transducer located at 3 cm from the base. The dissipation of excess pore pressure was monitored and compared to the expected hydrostatic pressure line as the tailings continued to settle. Figure 5.16 shows dissipation of excess pore pressure located at 28 cm on day 40 compared to the measured excess pore pressure located 3 cm from the base. Excess pore pressure measured by the sensor 3 cm from the base did not fully dissipate by day 60, as shown in Figure 5.16.

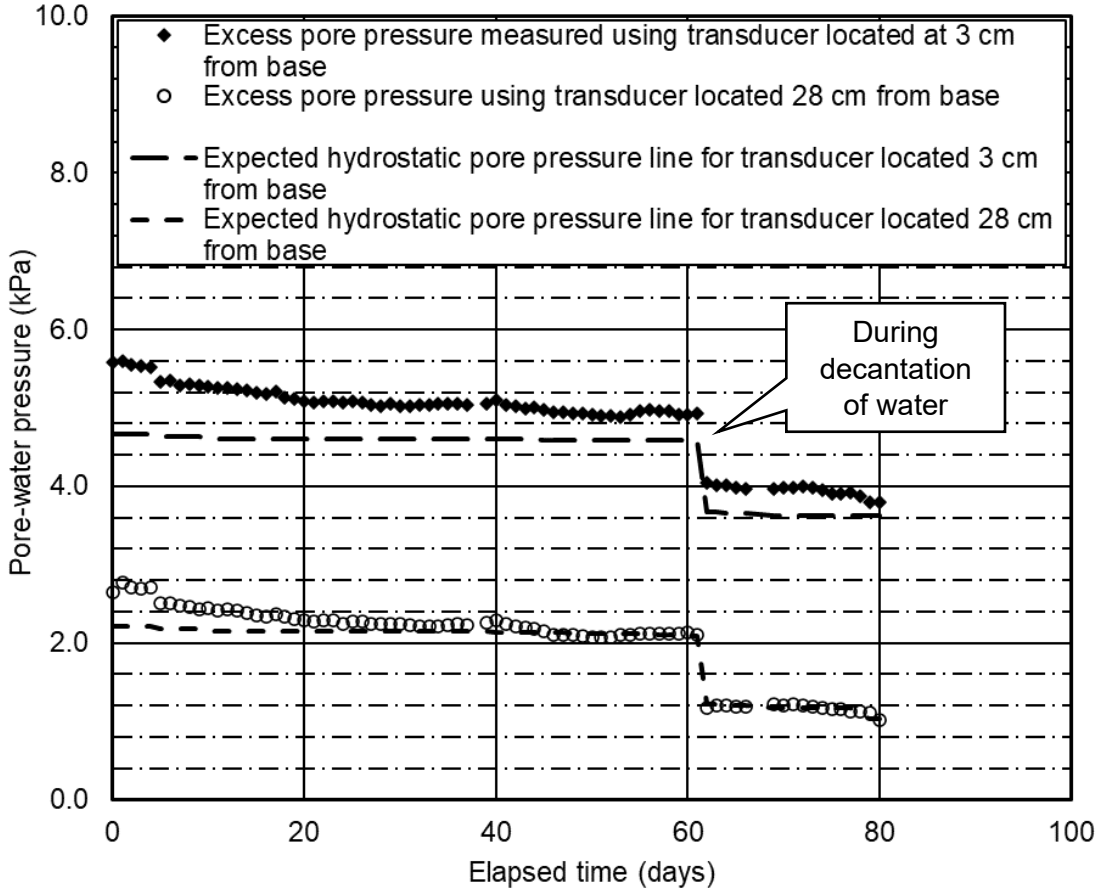

Figure 5. 15 Dissipation of excess pore pressure and expected hydrostatic line for the flocculated FFT pre- and post-decantation of supernatant water.

The total thickness of deposited tailings continued to change with the self-weight consolidation process. The bleed water was allowed to accumulate on top of the settled tailings until the change in the thickness of the tailings became small (i.e., infinitesimal) and full dissipation of generated excess pore pressure was displayed.

The excess pore pressure dissipation line depicts gradual dissipation of the pore pressure close to the bottom of the deposited tailings compared to the tailings at the surface. The change in tailings thickness is illustrated using the data marks in Figure 5.17. These data marks represent the surface of the tailings at a given time as the movement of the tailings mass continued during the sedimentation stage.

As shown in Figure 5.16, the measured excess pore pressure using the transducer located at 28 cm fully dissipated by day 60. However, a magnitude of 0.4 kPa of excess pore pressure was measured near the bottom of the column (i.e., transducer located 3 cm from the base). Since it required extended time to dissipate the observed excess pore pressure, a decision was made to proceed with the decantation of accumulated supernatant water from the surface of the tailings to simplify monitoring the dissipation of remaining excess pore pressure.

Figure 5.17 presents the measured pore water pressure of the deposited tailings for a selected time interval during the self-weight consolidation test. Figure 5.17 shows broken lines for the excess pore water pressure and a solid line for the expected hydrostatic pressure line as the consolidation progressed. The data points are measured values using the sensors instrumented as described in Chapter 4. During the consolidation process, the interface of the tailings and supernatant water accumulated continued to change. The change in the interface is presented in Figure 5.17 and Figure 5.18 using the data mark near the surface of the deposited tailings. The

expected hydrostatic water line remained unchanged since the bleed water was left to accumulate on the surface of the consolidating tailings for the first 60 days.

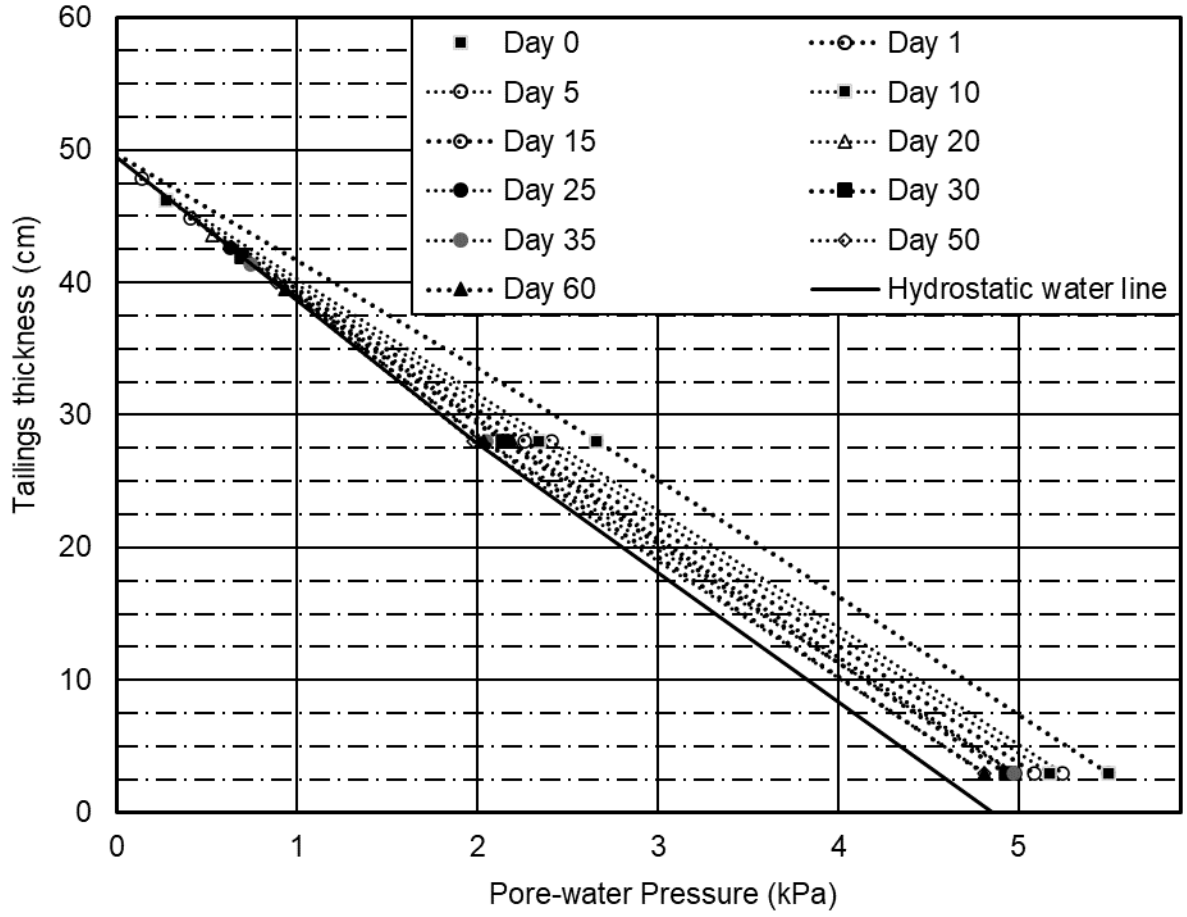

Figure 5. 16 Dissipation of excess pore pressure and expected hydrostatic line for the flocculated FFT.

The supernatant water was decanted when the excess pore pressure for the sensor located at 28 cm above the base of the column fully dissipated. The sensor located 3 cm above the base still showed excess pore water pressure of 0.4 kPa when the decantation was completed. The decision to decant the supernatant water was done in order to monitor the dissipation process of the remaining excess pore pressure near the base of the column as the progress of self-weight consolidation became significantly sluggish by day 60.

Once the decantation of the accumulated process was completed, the observed total tailings thickness was determined to be 39.5 cm, and the process of self-weight consolidation continued until the equilibrium condition was maintained. Figure 5.18 presents the dissipation of excess pore pressure once the supernatant water was removed from the surface of the tailings. Figure 5.18 presents the adjusted tailings thickness once the sedimentation process took effect.

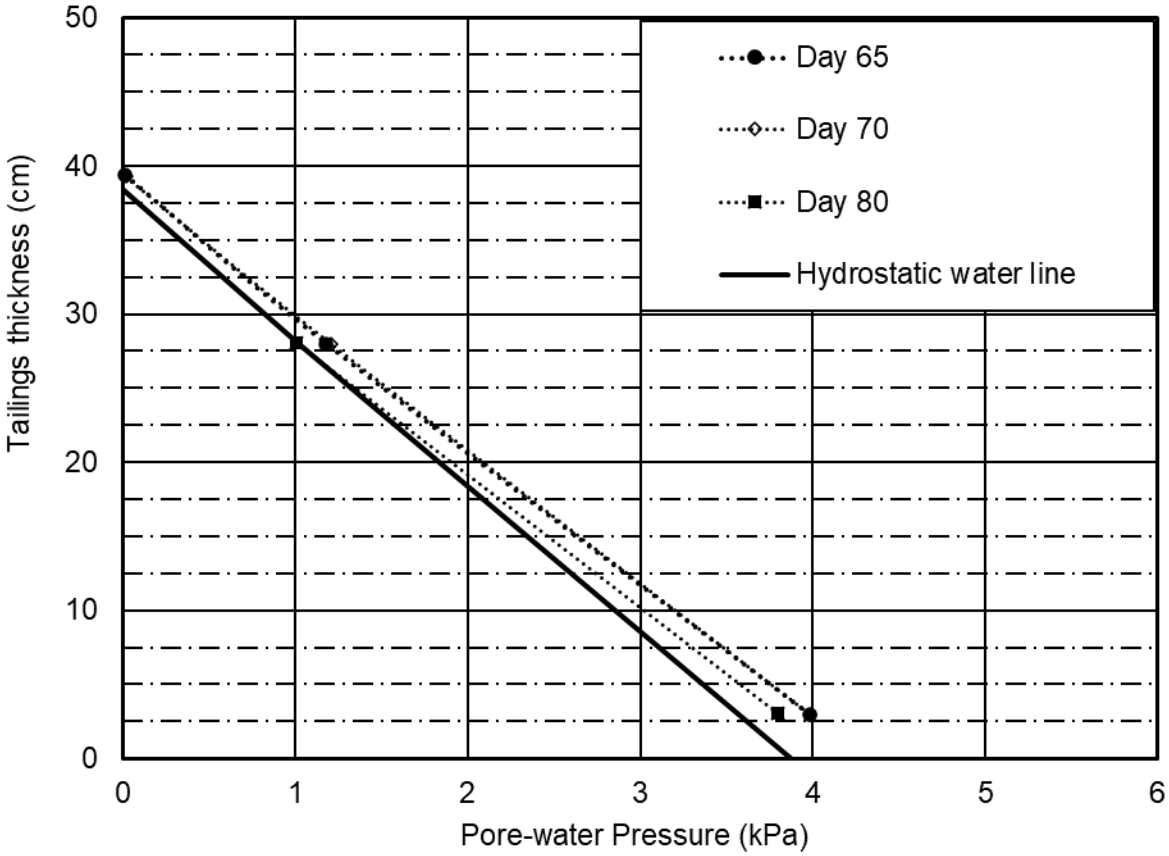

Figure 5. 17 Dissipation of excess pore pressure and expected hydrostatic line for the flocculated FFT post-decantation of supernatant water.

Similar to the dissipation process, the measured excess pore pressure using the situated two transducers were monitored and compared to the expected hydrostatic pressure line. The transducer located at 28 cm demonstrated measured and expected hydrostatic pressure in

agreement that by day 80 was showing complete dissipation of excess pore pressure through the surface boundary during the self-weight consolidation. However, the difference between measured excess pore pressure and the hydrostatic pressure line was determined to be about 0.4 kPa. This was shown on the transducer located 3 cm from the base of the column on day 80. Assuming the self-weight consolidation process was nearly completed, the process of consolidation using applied suction (i.e., transient consolidation) was initiated. The process of transient consolidation is presented in section 5.1.3.

Effective and total stress calculations

Equations related to the calculation of total and effective stresses are described below because of their importance in understanding the measured results.

The total stress of deposited flocculated tailings was computed using the formulae presented herein:

$$\sigma = \gamma_{sat}\, h_{tail} \qquad [5.1]$$

where:

σ = total stress at a given point within the deposited tailings, *kPa*,

γ_{sat} = saturated unit weight of flocculated tailings, kN/m^3,

h_{tail} = height of tailings at a given point, *m.*

$$\gamma_{sat} = \rho_{sat}\, g \qquad [5.2]$$

where:

ρ_{sat} = saturated density, *kg/m*^{3},

g = gravitational acceleration, *m/sec*^{2}.

$$\rho_{sat} = \frac{G_s+e}{1+e}\rho_w \quad [5.3]$$

G_s = specific gravity, *unitless*,

e = average void ratio, and

ρ_w = density of water, *kg/m*^{3}.

Effective stress was computed using the following formulae:

$$\sigma' = \sigma - (\gamma_w h_w + u_e) \quad [5.4]$$

where:

σ' = effective stress, *kPa*,

γ_w = unit weight of water, *kN/m*^{3},

h_w = height of water, *m*, and

u_e = excess pore pressure, *kPa*.

An average void ratio was first assumed for the entire column. As the tailings continued to settle, the assumed void ratio was computed using the original deposited thickness and the change in settlement. The average void ratio represents the change in tailings' density due to the process of sedimentation and self-weight consolidation. The saturated density of the placed tailings was computed using the assumed void ratio at a given time and with the Eq. [5.3] provided above. A

summary of used average void ratios and computed saturated densities are presented in Table 5.2. The tailings show changing void ratio over time, initially uniform void ratio was assumed for the entire column. Therefore, the computed saturated density changes with time as summarized in Table 5.2. Total stress was assumed to be linear within the tailings from top to bottom.

Table 5. 2 Summary of measured heights of tailings and computed average void ratio for the self-weight consolidation test.

Time (days) (rounded)	Total height of tailings (cm)	Average void ratio	Computed saturated density (kg/m^3)
1	50.5	4.07	1.246
10	46.2	3.65	1.269
20	43.6	3.39	1.285
30	41.9	3.22	1.289
40	41	3.13	1.303
50	40	3.03	1.31
61	39.2	2.95	1.32
80	38.45	2.87	1.4

The total and effective stress was computed using Eq. [5.1]. Selected plots are presented for numerous timelines from Figure 5.19(a) to Figure 5.19(h) to illustrate the change in total stress, effective stress, and pore pressure dissipation during the self-weight consolidation process.

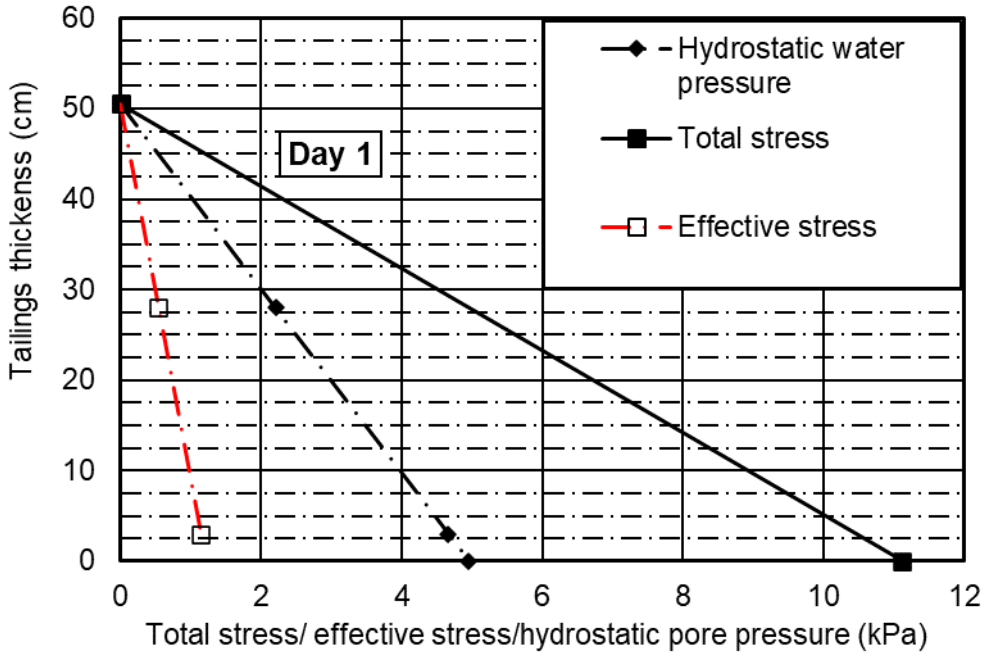

(a) Total and effective stresses after 1 day

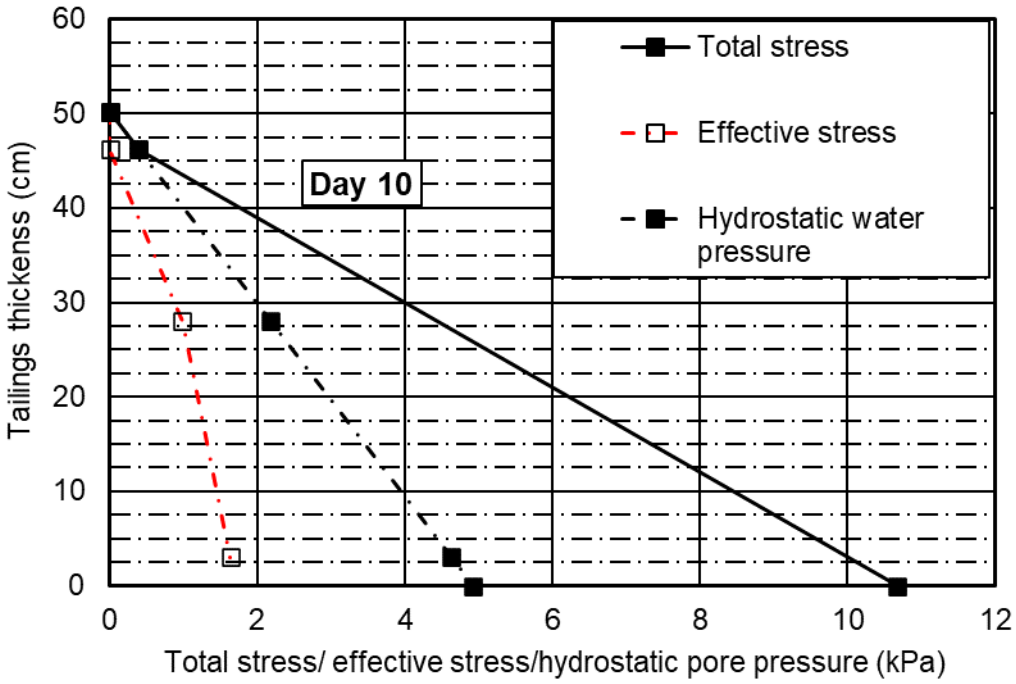

(b) *Total and effective stresses after 10 days*

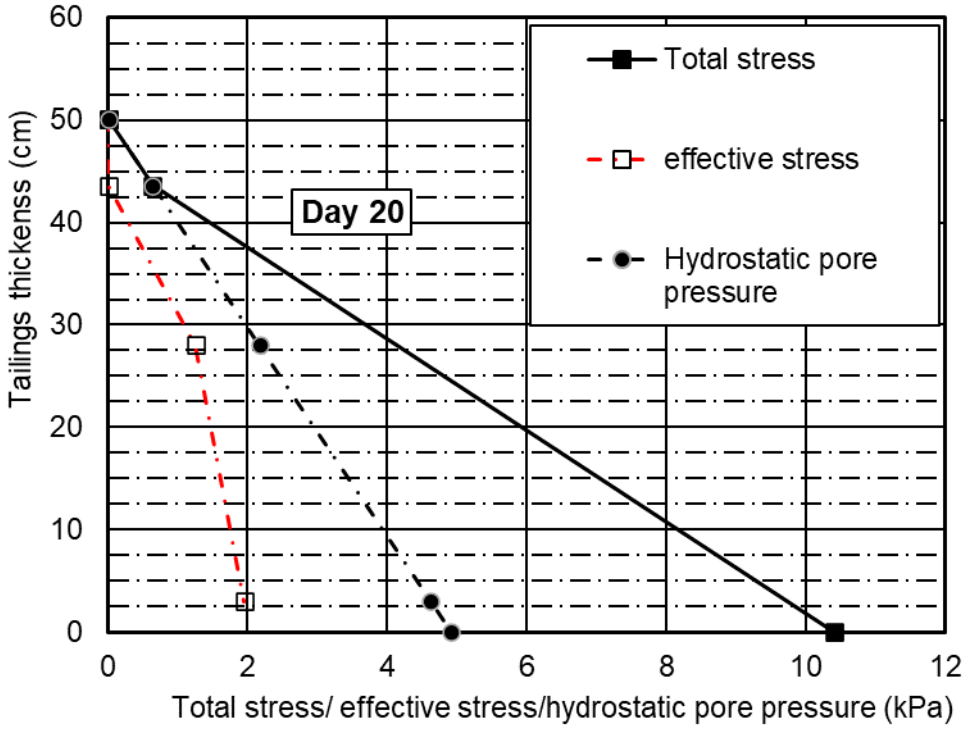

(c) *Total and effective stresses after 20 days*

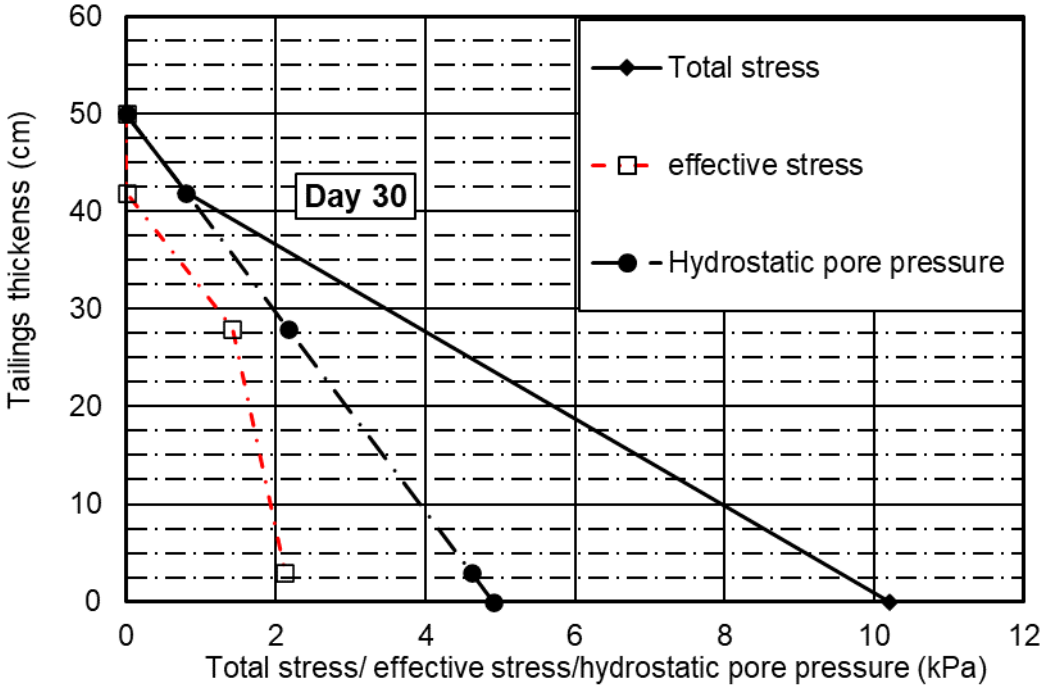

(d) *Total and effective stresses after 30 days*

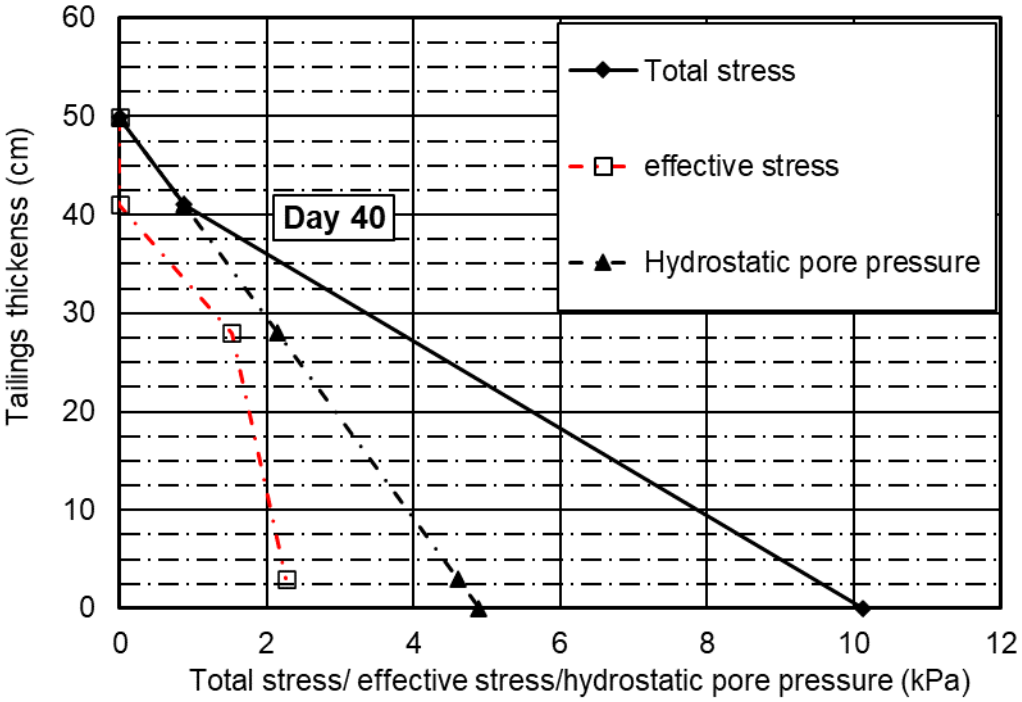

(e) ***Total and effective stresses after 40 days***

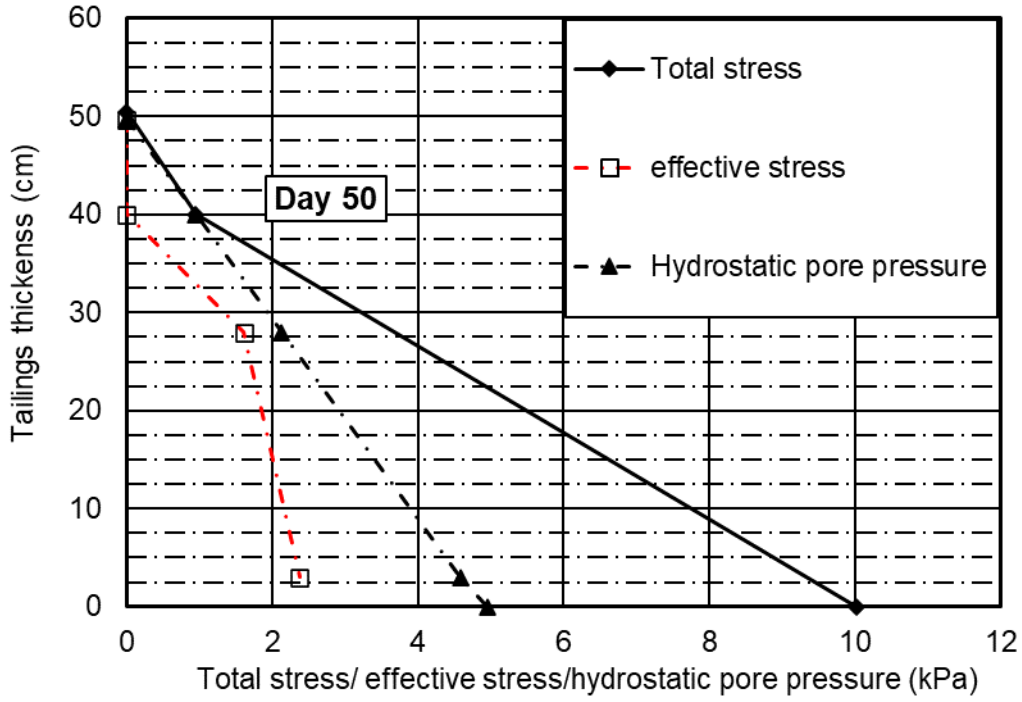

(f) ***Total and effective stresses after 50 days***

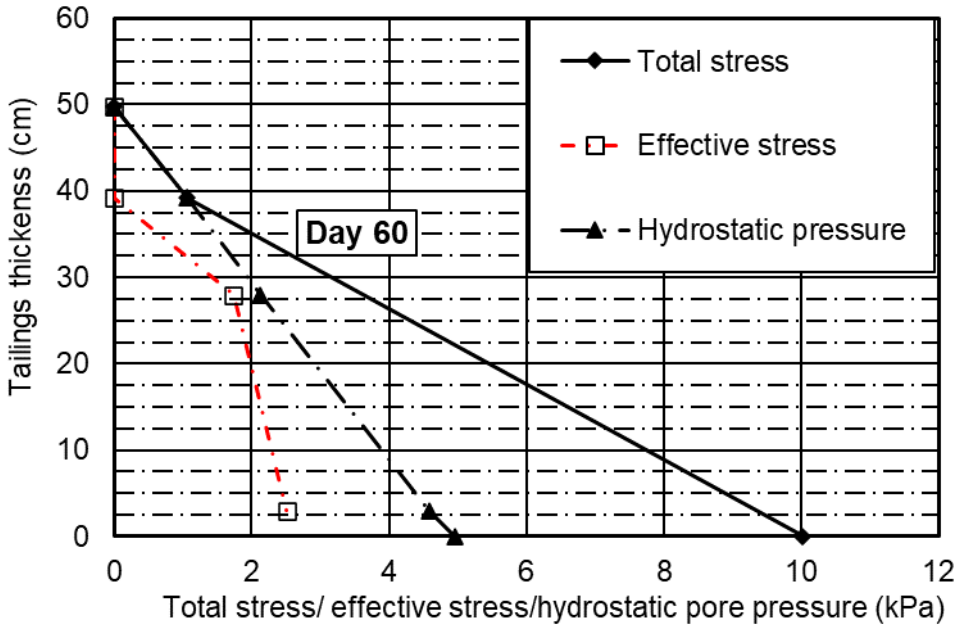

(g) *Total and effective stresses after 60 days*

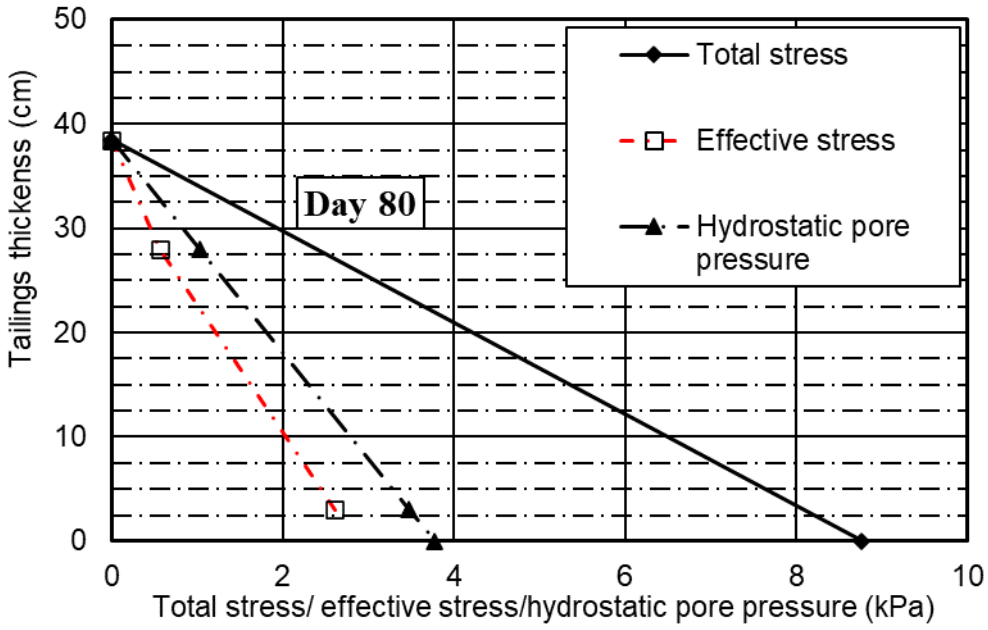

(h) *Total and effective stresses after 80 days*

Figure 5. 18 Plots of computed total stress, effective stress, and measured hydrostatic water pressure for different days during the self-weight consolidation tests: (a) after 1 day, (b) after 10 days, (c) after 20 days, (d) after 30 days, (e) after 40 days, (f) after 50 days, (g) after 60 days, and (h) after 80 days.

Undrained peak shear strength measurement with time and depth

The shear strength of deposited tailings was measured with depth and time as the sedimentation and self-weight consolidation process continued. The vane shear strength measuring equipment used to carry out the shear strength of deposited tailings was described in detail in Chapter 4, section 4.3. Selected results of measured vane shear strength of deposited flocculated FFT are presented in Figure 5.20(a) to Figure 5.20(f). These figures show the relationship between the measured vane shear strength and the angular deflection used by the vane shear testing equipment at different tailings depths and elapsed times. The angular deflection of the spring shows measured peak shear strength of the deposited tailings at a given depth and time. The peak vane shear strength indicates the strength of the placed tailings that can withstand prior shearing (or failure) of the deposited tailings. Figure 5.20(a) to Figure 5.20(f) show selected results of measured vane shear strength test with depth and time as the self-weight consolidation process continued.

The initial undrained shear strength of placed flocculated FFT was determined to be an average of 0.078 kPa. The initial vane shear strength was measured by using a number of batches which was prepared by thoroughly mixing the flocculants and the raw tailings using a procedure developed by one of the operators to carry out field trials. Details of the flocculation procedure have been presented in literature (Matthews, Dhadli, House, & Simms, 2011; Mizani, He, & Simms, 2013). Once the tailings were mixed with the flocculant, the flocculated tailings were placed into the meso-scale for further testing as described and outlined in Chapter 4. Table 5.3 presents a summary of the measured undrained shear strength of flocculated FFT immediately following its flocculation.

Table 5. 3 Summary of initial measured undrained shear strength of flocculated FFT.

Depth (cm)	Undrained shear strength (kPa)
16	0.0758
26	0.0812
36	0.0759
41	0.0755
46	0.076

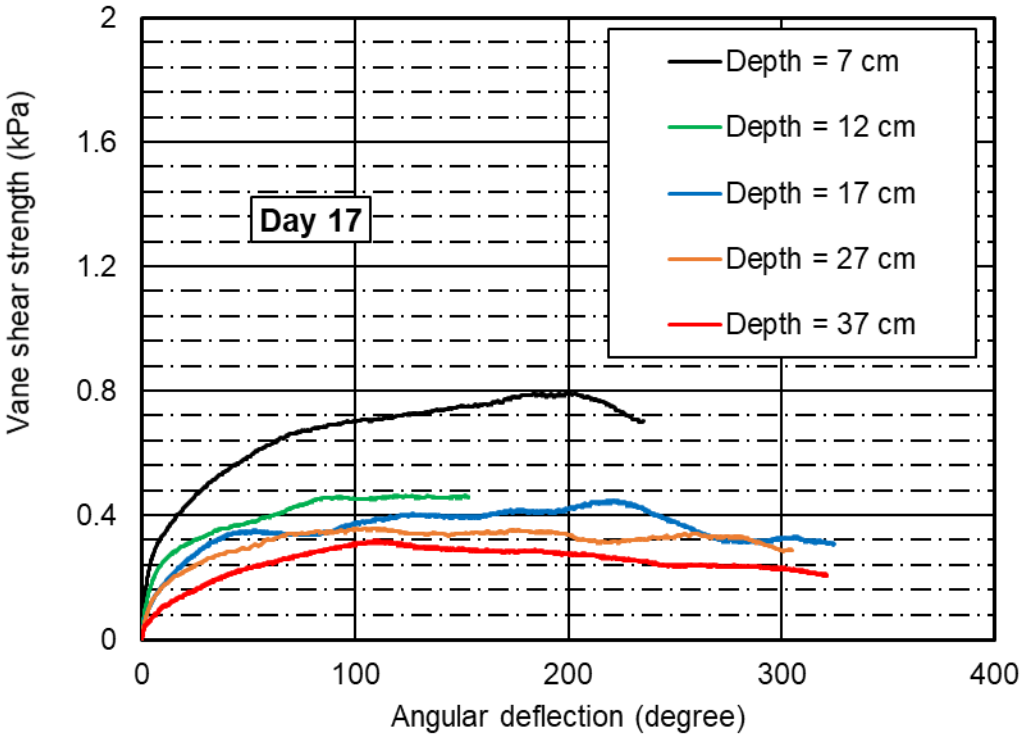

(a) Vane shear strength test after 17 days

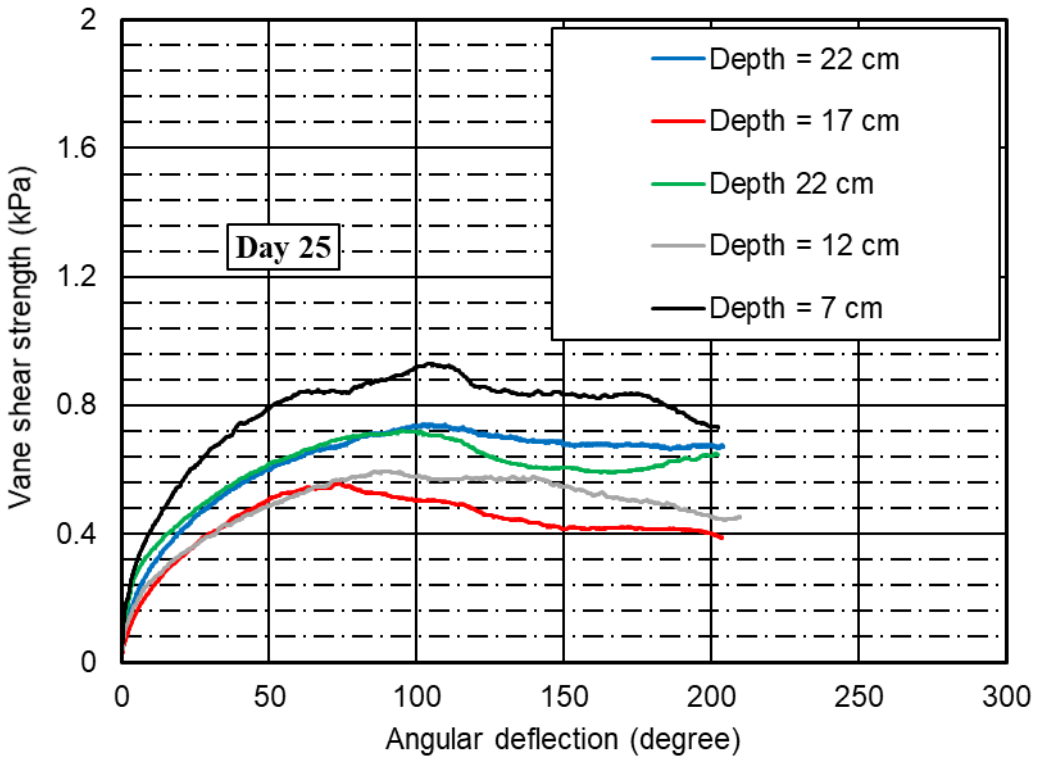

(b) Vane shear strength test after 25 days

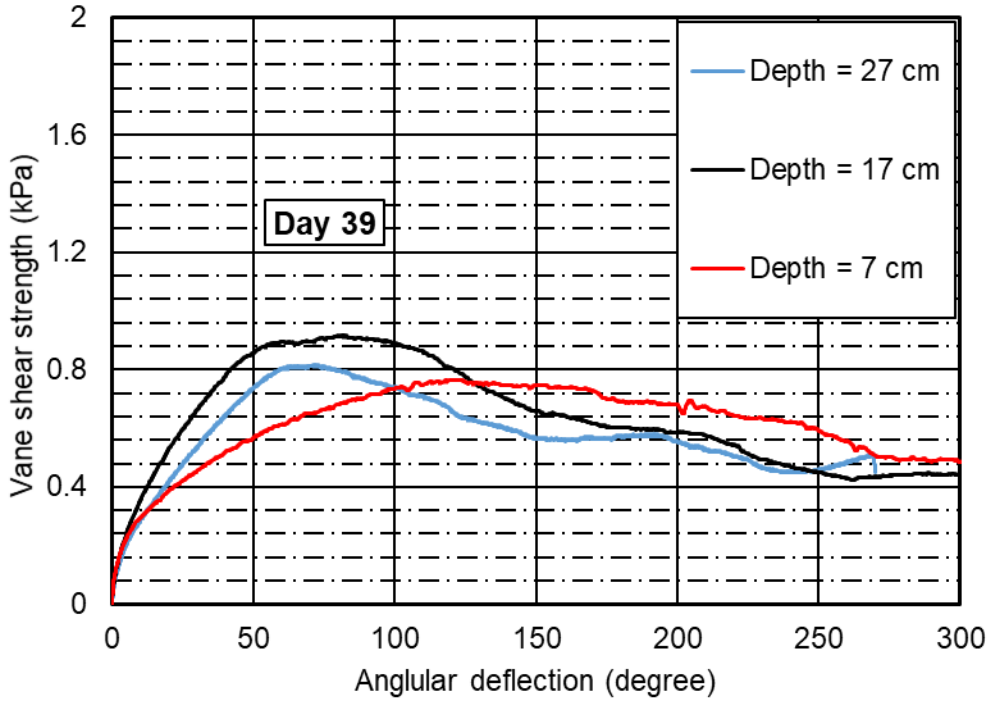

(c) Vane shear strength test after 39 days

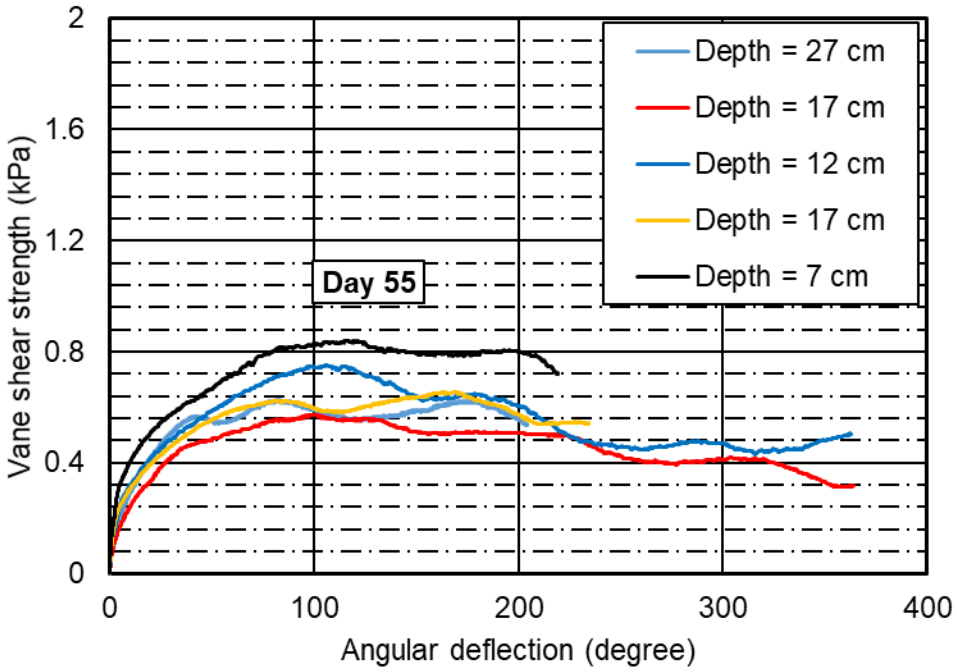

(d) Vane shear strength test after 55 days

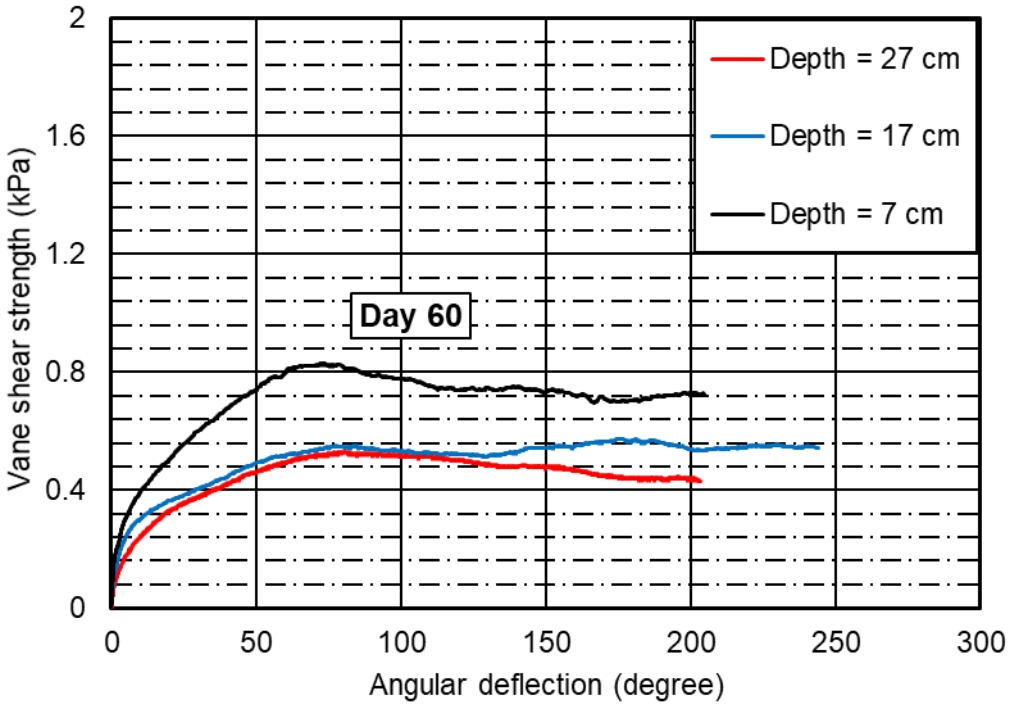

(e) Vane shear strength test after 60 days

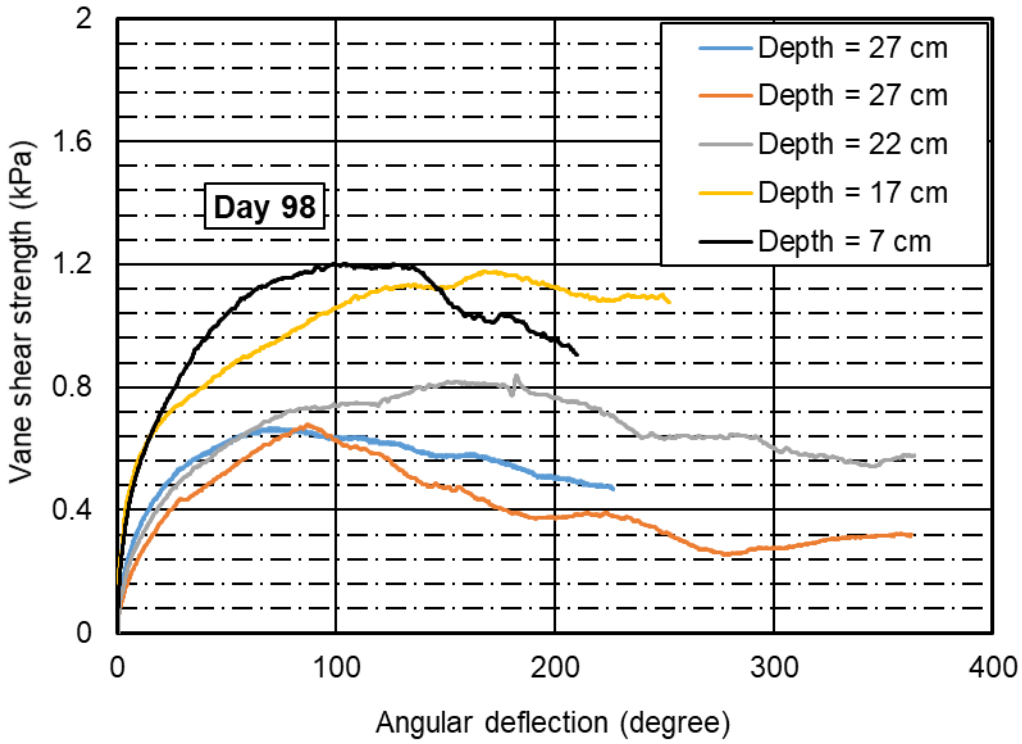

(f) *Vane shear strength test after 98 days*

Figure 5. 19 Vane shear strength test for the flocculated FFT during the self-weight consolidation process: (a) after 17 days, (b) after 25 days, (c) after 39 days, (d) after 55 days, (e) after 60 days, and (f) after 98 days.

Figure 5.21 presents measured peak vane shear strength with time and depth for the deposited flocculated FFT during the sedimentation/self-weight consolidation process. The general trend shows an increase in shear strength with depth and time as consolidation of deposited tailings progressed. The difference between the peak shear strength within the profile depth of tailings at a given time are smaller (i.e., in the order of a few pascal) and can possibly be attributed to friction associated with the insertion of the vane rod. Details of the interpretation and analysis will be presented in Chapter 6.

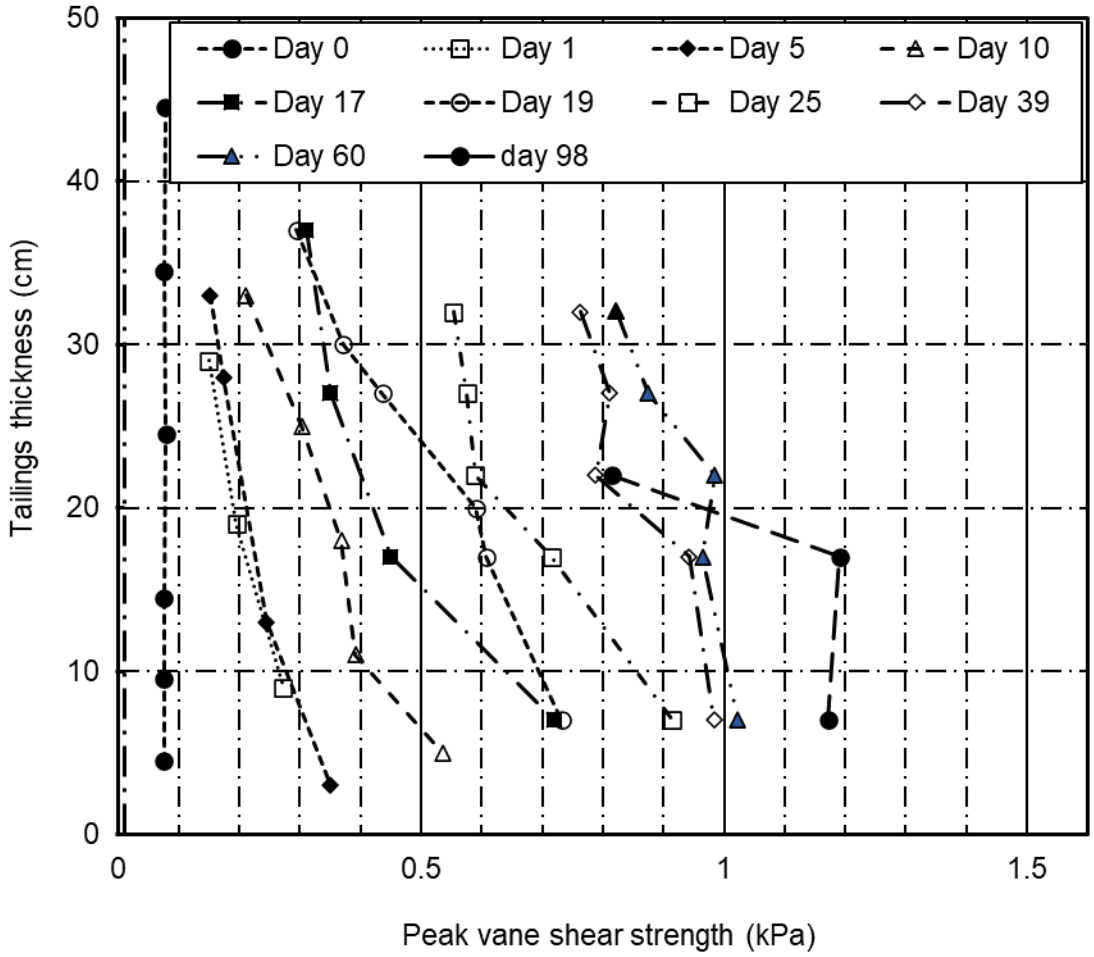

Figure 5. 20 Peak vane shear strength versus depth and time for the flocculated FFT during the self-weight consolidation process.

Flocculated centrifuged tailings cake (FCTC)

Measuring the possible self-weight consolidation process of the FCTC was attempted once the tailings had been placed within the meso-scale column. The section for the characterization test shows that there was no vertical strain (or change in void ratio) during the settling column test carried out for the FCTC. Similar results were obtained during the meso-scale column test and are presented herein.

Settlement, vertical strain, and void ratio

The vertical strain (i.e., void ratio change) measured during the sedimentation and self-weight consolidation test for the FCTC is presented in Figure 5.22 and Figure 5.23, respectively. There was no lateral strain observed during the self-weight consolidation test process. The change in volumetric strain was attributed only to the vertical strain at this stage of the test. Therefore, results of vertical strain and void ratio are presented for the self-weight consolidation testing section.

Generally, the deposited FCTC were monitored for a month in order to attain the equilibrium condition once the tailings had been placed in the column apparatus and to check if there was possible settlement of the placed tailings. The column settling test from the material characterization test indicates there was no expected change in settlement due to the self-weight consolidation process for the FCTC.

The initial deposited tailings thickness was 38 cm and the average initial void ratio was determined to be 2.21. There was no settlement for the deposited tailings during the time of the self-weight consolidation process. The final tailings thickness was measured to be 37.2 cm and the corresponding average void ratio was determined to be 2.14. The difference measured in total tailings thickness was 0.8 cm; this result was possibly due to adjustment of the deposited FCTC, which was scooped and placed in the meso-scale column. The deposited tailings underwent the process of meshing and became a continuous element with time. Figure 5.22 and Figure 5.23 present the vertical strain and average void ratio plots for the FCTC during the self-weight consolidation process, respectively.

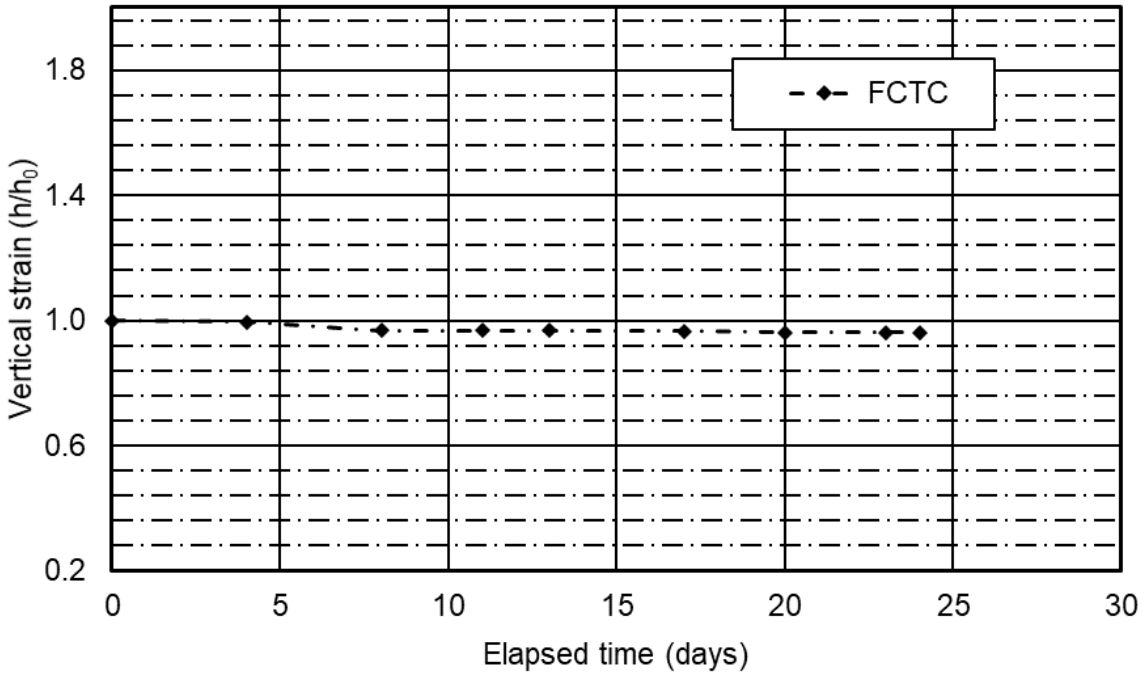

Figure 5. 21 Vertical strain during the self-weight consolidation process for the FCTC.

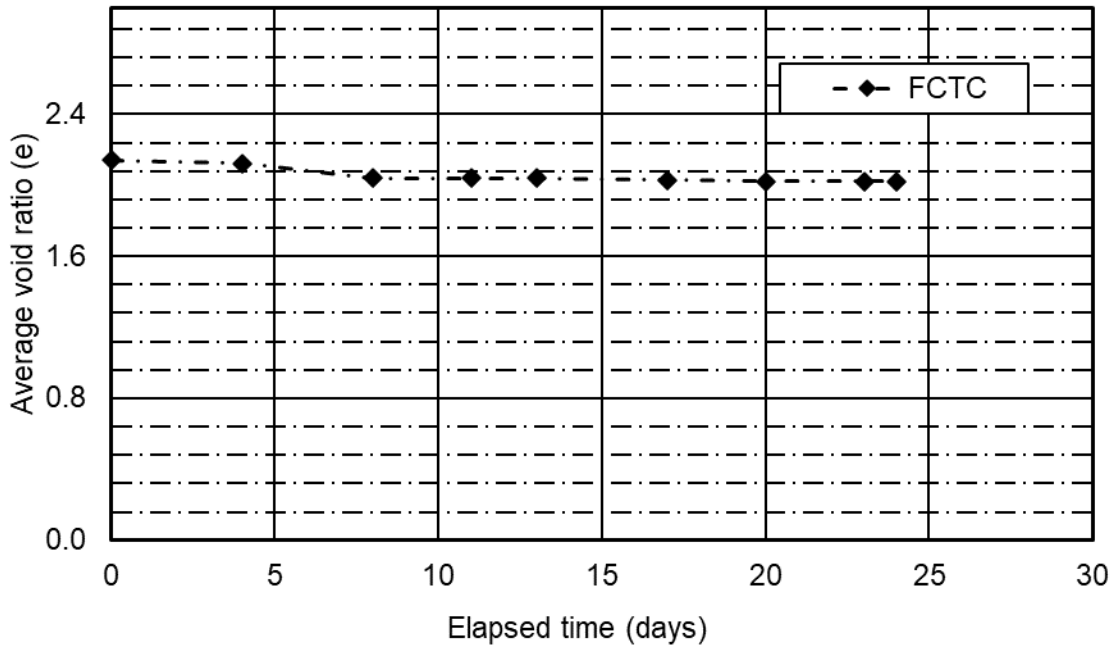

Figure 5. 22 Change in void ratio due to change in vertical strain during the self-weight consolidation process for the FCTC.

Pore pressure dissipation

The dissipation of excess pore-water pressure while depositing the FCTC into the meso-scale column was monitored using the positive pressure measuring sensor placed within the column apparatus. The sensor located 3 cm above the column base measured excess pore-water pressure at rough average of 0.45 kPa. Measured excess pore pressure took extensive time to dissipate due to the low hydraulic conductivity of the deposited tailings.

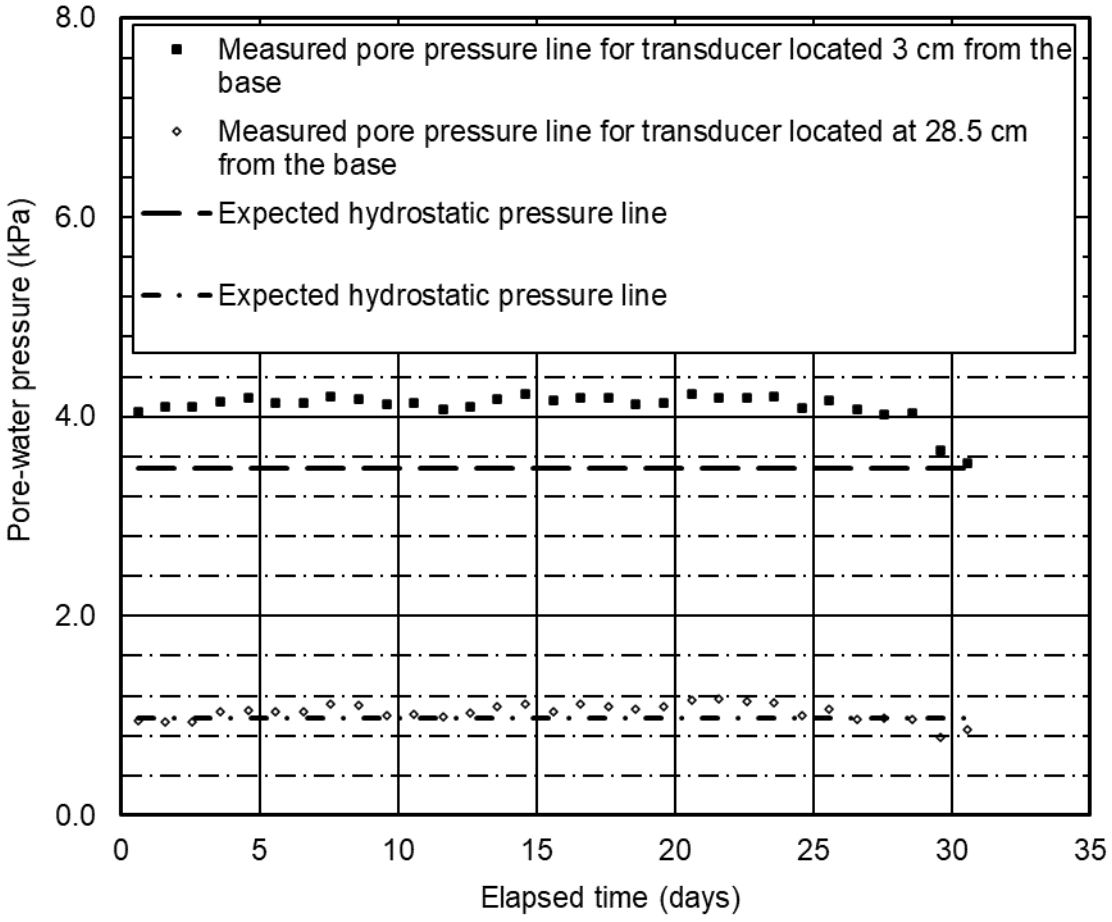

Figure 5. 23 Measured pore water pressure and expected hydrostatic pressure for the FCTC pre- and post-decantation of supernatant water from the tailings surface.

The sensor located at 28.5 cm from the base of the column measured more or less the same as the expected hydrostatic pressure. Therefore, it was decided to proceed to the next experimental stage considering the time it took to dissipate the measured excess pore pressure. The accumulated supernatant water was removed on day 28 and the decrease in excess pore pressure is depicted in Figure 5.24. The figure presents measured excess pore pressure and expected hydrostatic water line for the deposited FCTC during the self-weight consolidation experimental test.

Effective and total stress calculations

An average void ratio was first assumed for the entire column. Since there was no settlement during self-weight consolidation for the FCTC, the assumed void ratio and saturated density were used to compute the total stress of the deposited FCTC. Figure 5.25(a) and 5.25(b) presents the total and effective stress of the FCTC during the deposition state.

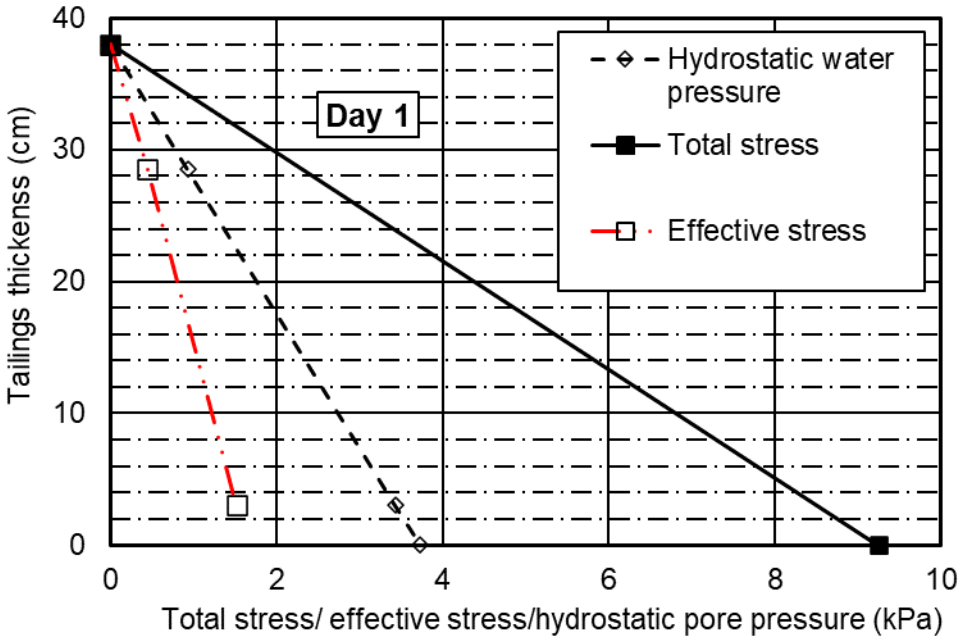

(a) Total and effective stresses after 1 day

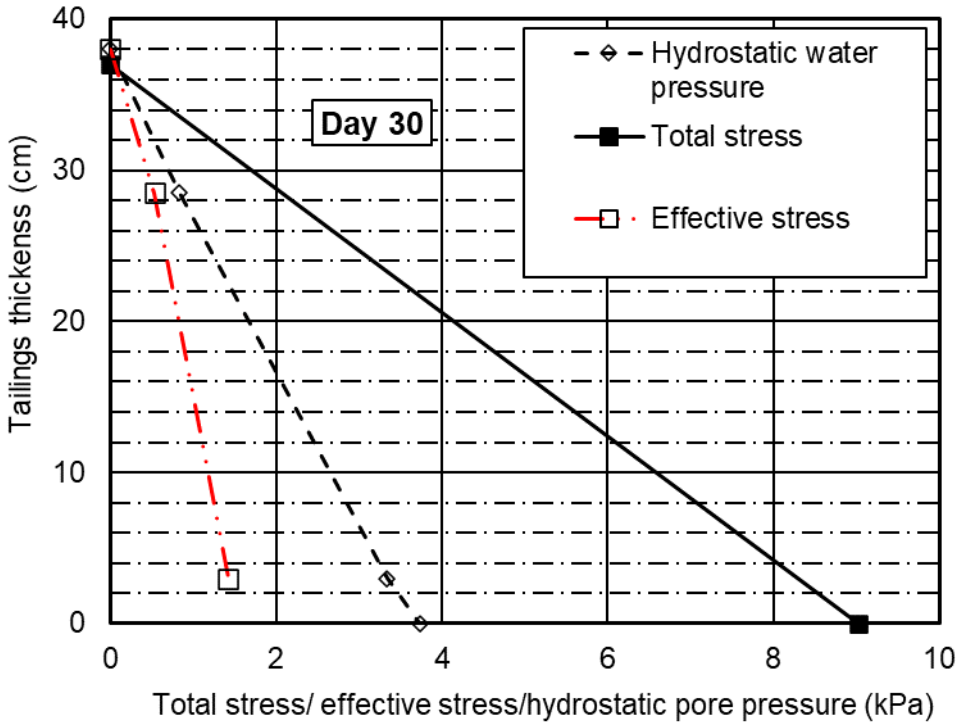

(b) ***Total and effective stresses after 30 days***

Figure 5. 24 Plots of computed total stress, effective stress, and measured hydrostatic water pressure for the deposited FCTC during the self-weight consolidation tests: a) after 1 day and b) after 30 days.

Undrained peak shear strength measurement with time and depth

The undrained shear strength of the deposited FCTC was measured with depth and time to obtain the initial values prior to the start of consolidation due to increments of suction process. Selected results of measured vane shear strength of deposited FCTC are presented in Figure 5.26. Figure 5.26 shows the relationship between the measured vane shear strength and the angular deflection used by the vane shear testing equipment at different tailings depths at specified times. The angular deflection of the spring shows measured peak shear strength of the deposited tailings

at a given depth and time. The peak vane shear strength indicates the strength of the placed tailings that can withstand prior shearing (or failure) of the deposited tailings.

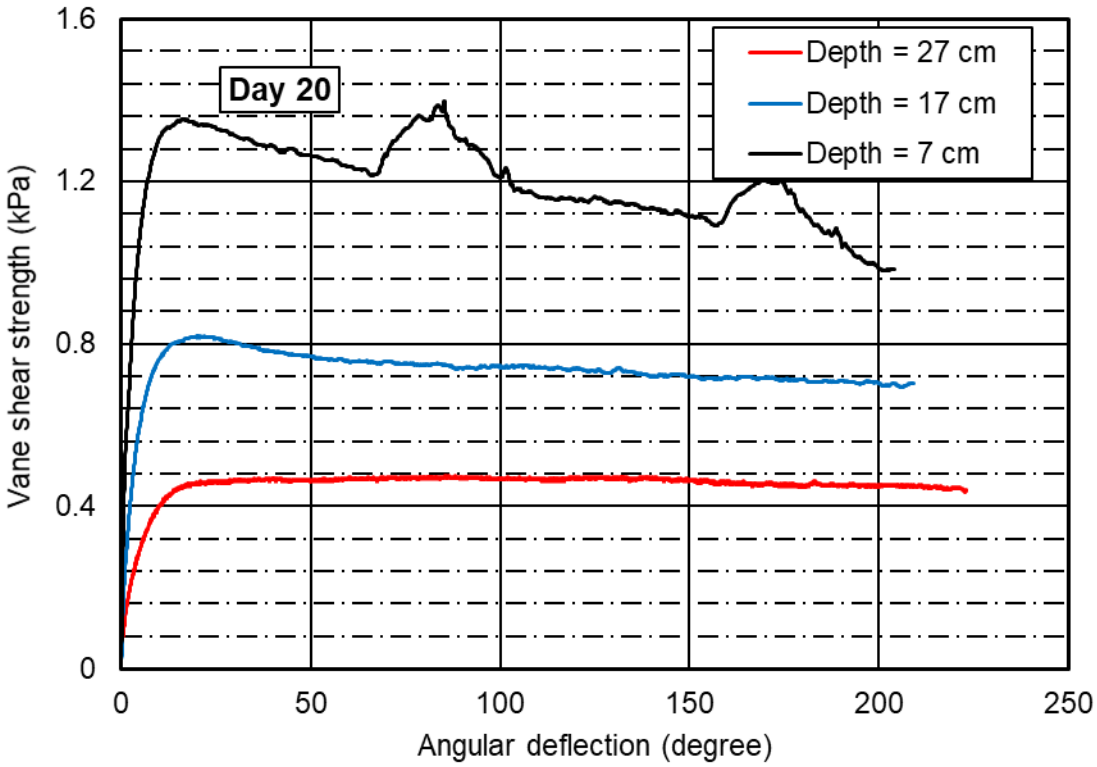

Figure 5. 25 Vane shear strength test for the FCTC during the self-weight consolidation process after 20 days.

The relationship between peak vane shear strength, deposited tailings thickness, and time interval after being subjected to the consolidation process is presented in Figure 5.27. The general trend observed for the undrained shear strength during the self-weight consolidation process for the FCTC was a slight increase in shear strength of 0.28 kPa near the base of the column. The increase in shear strength is expected due to a possible increase in solids content near the base with time although no significant self-weight change was observed. The undrained shear strength measured near the deposited tailings surface exhibit a slight decrease of 0.2 kPa with time. However, the change in measured undrained shear strength was not due to settlement, since there was no change in volume observed. The measured undrained shear strength values were

close and the differences are small enough to be considered within the factors that can contribute error to the measurement. The relationship between measured peak vane shear strength versus tailings thickness can be described using a power function.

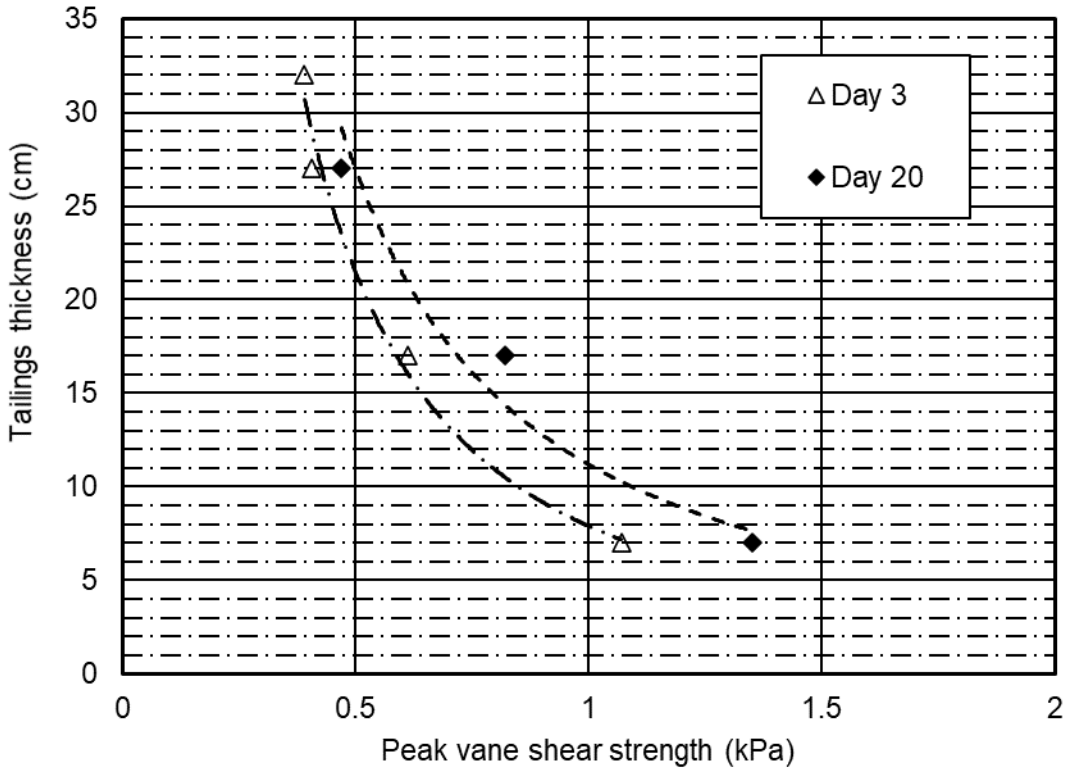

Figure 5. 26 Peak vane shear strength versus depth and time for the FCTC during the self-weight consolidation test.

5.1.3 Consolidation using applied suction

The second phase of the meso-scale column experiment investigated consolidation of deposited tailings using an applied suction technique. The first phase measured self-weight consolidation, and results are presented in section 5.1.2. The equilibrium condition was monitored using a pore pressure sensor for the tailings prior to using the applied suction technique to consolidate the tailings. A detailed description of the experimental setup and testing procedure is presented in Chapter 4.

The second phase of experiments measured consolidation in response to incremental applied suction at the base of the column. Selected results are presented in this section along with a detailed analysis. Additional test results for increments of suction are presented in Appendix A and Appendix B for the flocculated FFT and FCTC, respectively.

A schematic representation of the processes during consolidation using increments of applied suction is presented in Figure 5.28. The direction of flow was downward during this process since the suction pull was applied through the base of the column. Once each increment of suction had been applied, the consolidation process was allowed to reach equilibrium before additional suction was added.

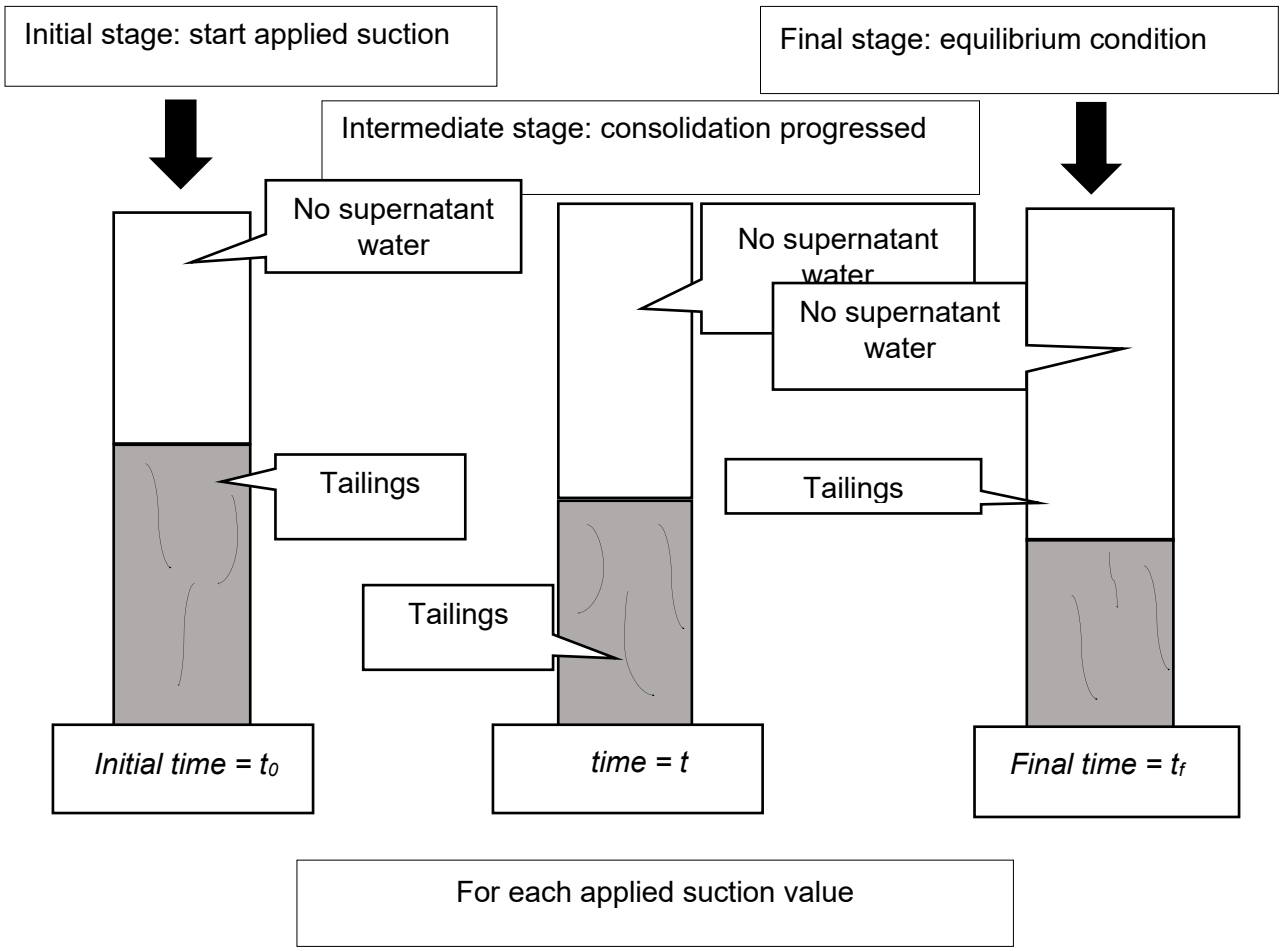

Figure 5. 27 Schematic representation of the process of consolidation using increments of applied suction using the meso-scale column.

The consolidation experiment required numerous stages of incrementally applied suction to characterize the tailings. The vertical strain (or void ratio change), pore pressure change, undrained shear strength, and peak shear strength with depth and time were measured for each increment of applied suction. These results are presented in the subsections below.

Measuring each increment of applied suction at equilibrium was time-consuming but important. The tailings used for these experiments required a long time to reach equilibrium due to the low hydraulic conductivity of fluid fine tailings. Also, a single vacuum suction reservoir, regulator, and

desiccator was used for two meso-scale columns with different material properties, which meant that the experiment was time limited by the material with the lower hydraulic conductivity. For these reasons, it took a long time for the columns to reach equilibrium following each increments of applied suction. However, ensuring equilibrium was essential in order to compute the stress-strain relationship for the column.

The experimental test during consolidation using increments of applied suction was conducted for the following two tailings:

i) *Flocculated FFT*: The flocculated FFT was described in detail in section 5.1.2 under the self-weight consolidation process.

ii) *Flocculated Centrifuged Tailings Cake (FCTC)*: No settlement was measured for the FCTC during the material characterization test; therefore, it was placed and observed for a limited time during the self-weight consolidation process prior to the applied suction testing phase.

The results for the applied suction for 20 kPa and 50 kPa are presented for the two tailings in the following section. The results are organized by the type of tailing and by applied suction. The results for each tailing are organized for each increment of suction as follows: i) settlement, vertical strain, and void ratio; ii) negative pore pressure distribution; iii) effective and total stress calculation; and iv) undrained shear strength measurement.

5.1.3.1 Applied suction of 20 kPa for the flocculated FFT

The results of consolidation for the flocculated FFT during the suction increments of 20 kPa are presented in this section.

Settlement, vertical strain, and void ratio

The vertical strain and change in average void ratio for the flocculated FFT are presented in Figure 5.29 and Figure 5.30, respectively. Smaller lateral deformation was measured and observed for the flocculated FFT. The measured vertical strain was 23.3% compared to the initial deposited tailings thickness as shown in Figure 5.29. The average initial and final void ratios were 2.86 and 1.66, respectively, by day 94 as shown in Figure 5.30.

The applied suction of 20 kPa was allowed a longer time to ensure the equilibrium condition had been reached since the pore pressure sensors placed were not responding at this stage. As the change in vertical strain or average void ratio became minimal, equilibrium was considered to have been reached, and subsequent suction increments were applied.

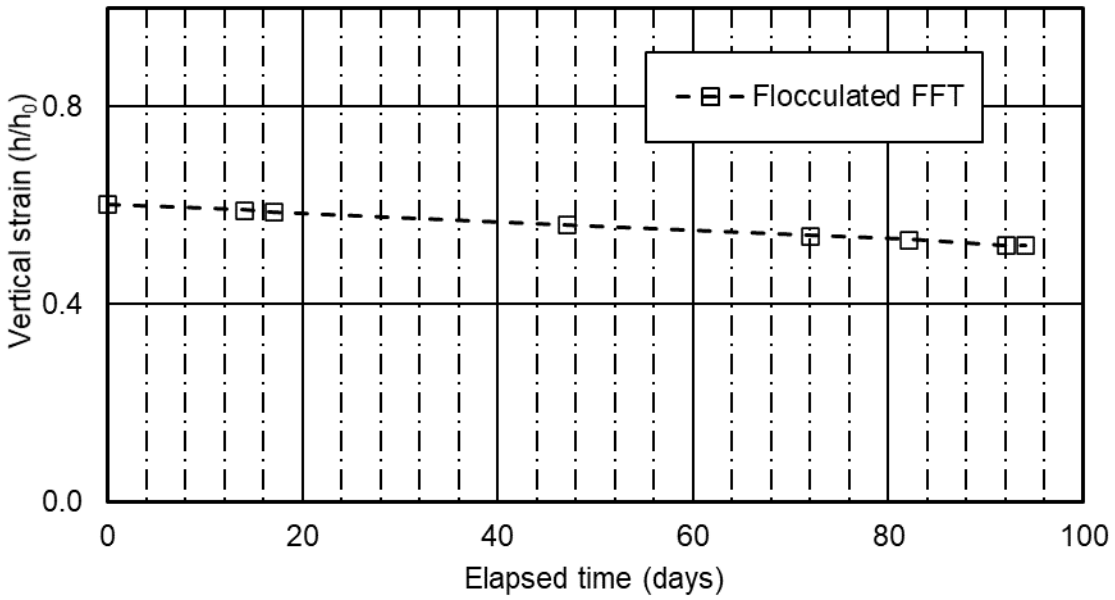

Figure 5. 28 Vertical strain due to incremental applied suction of 20 kPa for the flocculated FFT.

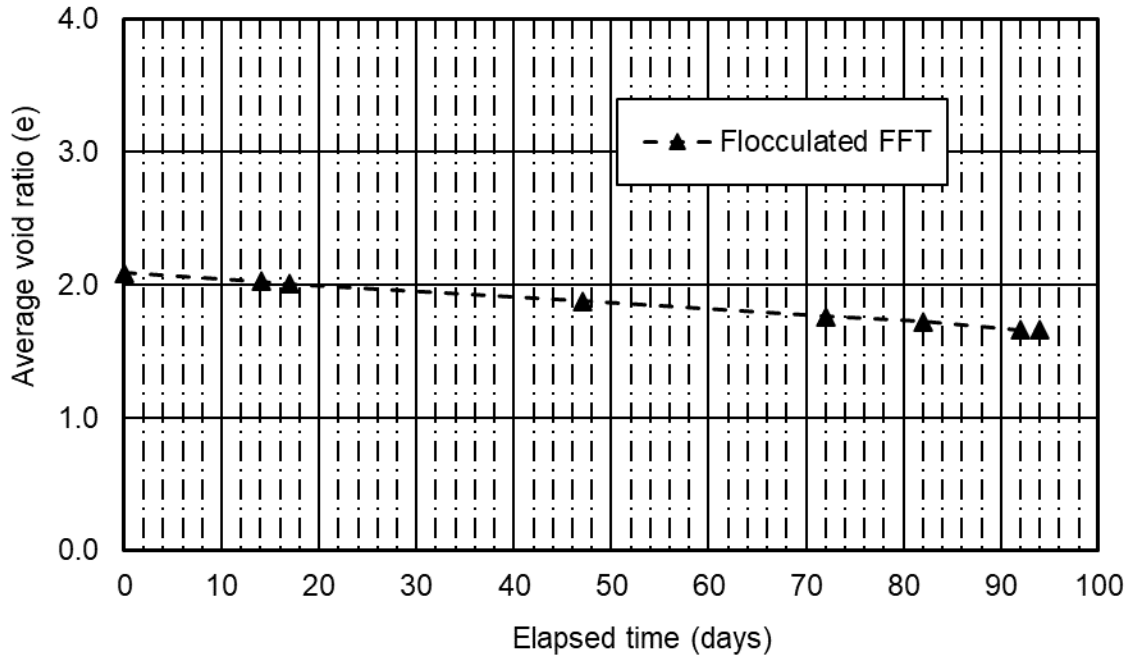

Figure 5. 29 Change in average void ratio due to increments of applied suction of 20 kPa for the flocculated FFT.

Pore pressure distribution

The pore pressure distribution was not determined during this suction stage. The sensors placed to measure negative pore-water pressure did not respond properly. However, the positive pore pressure measuring transducer situated on the side of the column did record some measurements in response to the applied suction at the base of the column. These results are presented in Figure 5.31 and Figure 5.32. The positive pore pressure sensors show an overall decrease in pore pressure once the suction was applied. The positive pressure transducer sensor located 3 cm above the base of the column measured a negative pore pressure following the applied suction. The measured readings are only considered to be an indicator in the absence of actual pore pressure measurements required to carry out the effective stress calculations.

For example, the hydrostatic pressure at 3 cm above the base was 3.5 kPa and an immediate decline in the pore pressure followed an applied suction of 10 kPa compared to the sensor located 28 cm above the base (i.e., near the tailings surface). Figure 5.31 shows the sensor located near the column base sensed the applied suction instantly as shown from the change in measured pore pressures. The change in pore pressure measured by the sensor near the surface showed a flatter slope compared to the sensor near the base, indicating the transitioning of the pore pressure distribution along the profile of the flocculated FFT.

Figure 5.32 shows pore pressure measurements for an applied suction of 20 kPa and a similar pattern was displayed; however, as stated above, these measurements were included to show the change in pore pressure distribution in the absence of negative pore pressure readings. The sensor near the surface didn't respond well once the measurement reached a zero value.

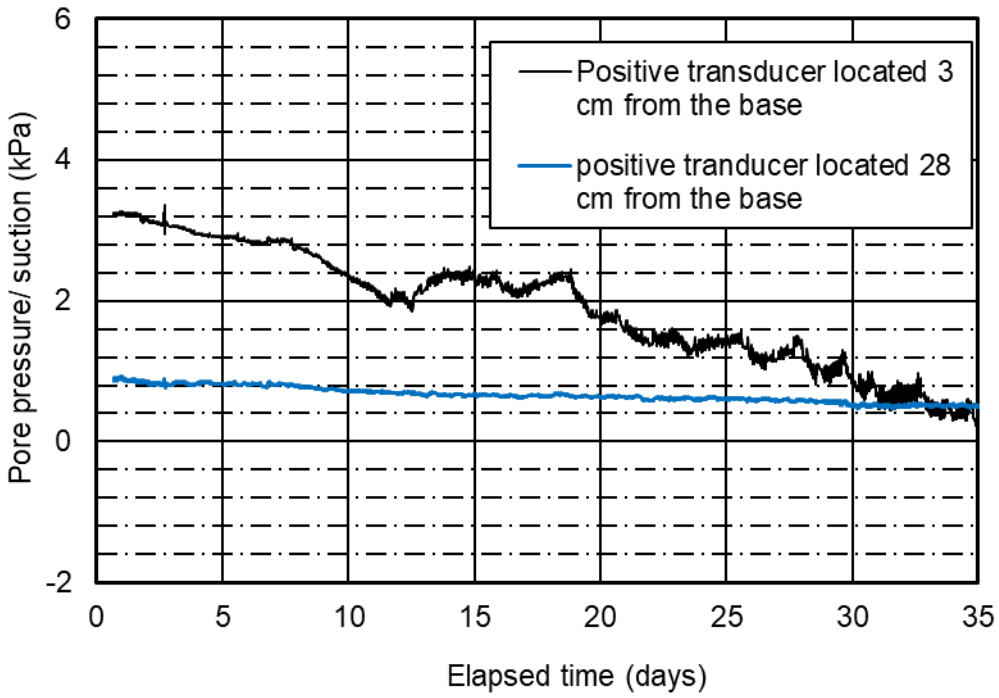

Figure 5. 30 Suction measured using the positive pressure transducer for the flocculated FFT during applied suction of 10 kPa.

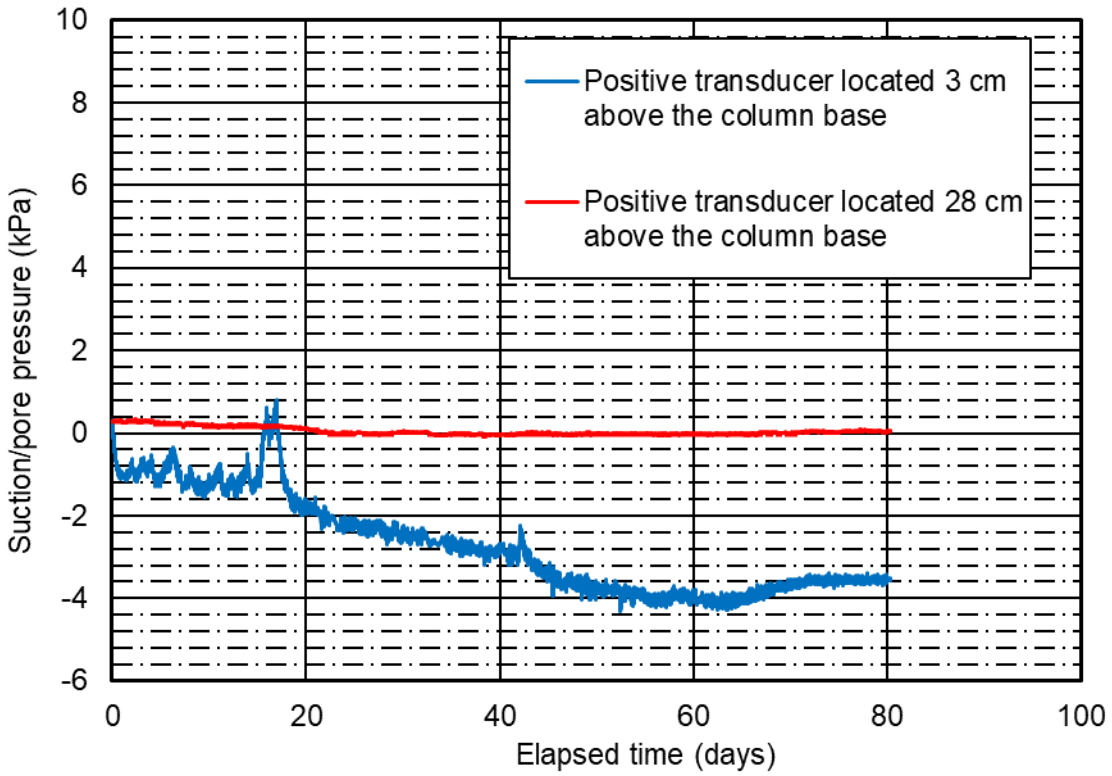

Figure 5. 31 Suction measured using the positive pressure transducer for the flocculated FFT during increments of suction of 20 kPa.

Effective stress calculations

The change in effective stress within the deposited tailings are calculated using the total stress and suction measured with time. The formula presented in Eq. [5.50] is used to calculate the effective stress.

$$\sigma' = \sigma - u \qquad [5.50]$$

where:

σ' = effective stress, *kPa*,

σ = total stress, *kPa*, and

u = pore pressure, *kPa.*

Assuming an equilibrium condition was reached by the end of the applied suction time, the progression of suction with time along the tailings thickness is estimated and the effective stress for the profile computed. Table 5.4 presents the distribution of suction for the tailings profile with time.

The calculated effective stress increased near the base of the column with additions in applied suction, which were sensed immediately near the base of the column. Over time, the applied suction increased in an upward direction, as did the effective stress. The rate of suction increase in an upward direction is controlled by the hydraulic conductivity of the tailings used. A summary of the suction distribution and calculated effective stress values results is presented in Table 5.4. Figure 5.33 presents the calculated effective stress with the tailings thickness for the increments of suction of 20 kPa.

Table 5. 4 Effective stress computed due to 20 kPa applied suction for the flocculated FFT.

Position within the column	Thickness (cm)	Time (days)					
		Day 15	Day 30	Day 45	Day 60	Day 75	Day 90
Bottom Suction (kPa)	0	20	20	20	20	20	20
Effective stress (kPa)		21.2	21.2	21.2	21.2	21.2	21.2
Near bottom suction (kPa)	5	3	8	12	15	17	18
Effective stress (kPa)		4.2	9.2	13.2	16.2	18.2	19.2
Middle section suction (kPa)	15	3	7	10	12	15	17
Effective stress (kPa)		3.5	7.5	10.5	12.5	15.5	17.5
Top suction (kPa)	28-30	2	4	7	11	14	16

Effective stress (kPa)		2	4	7	11	14	16

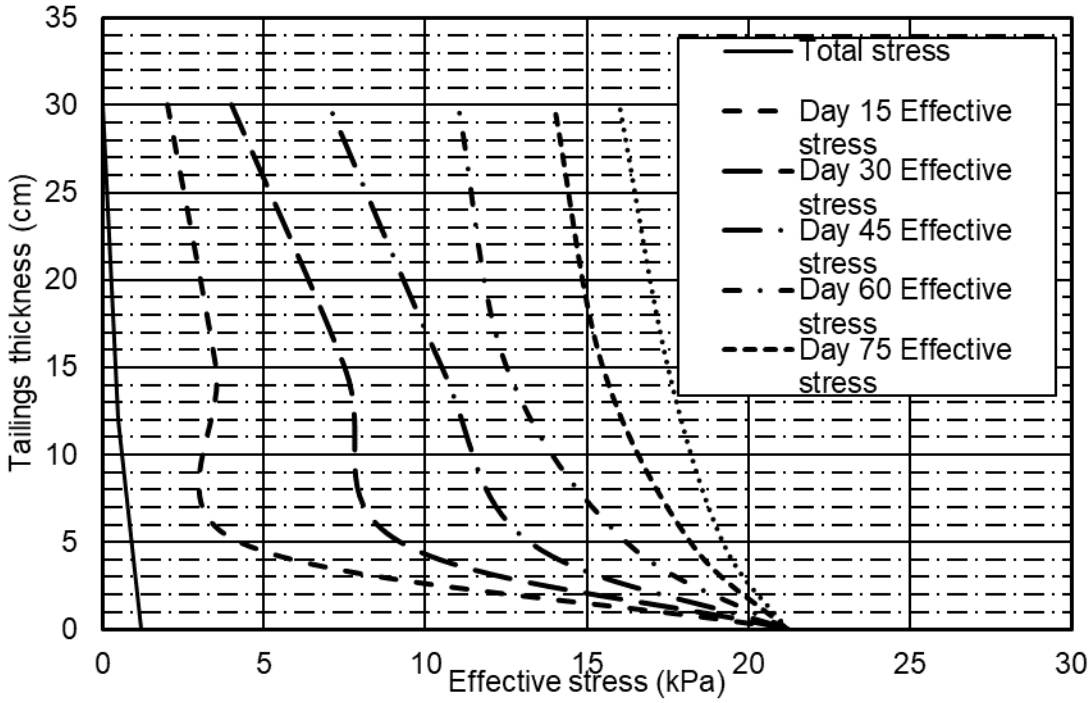

Figure 5. 32 Computed effective and total stress during increments of suction of 20 kPa for flocculated FFT.

Undrained peak shear strength measurement with time and depth

The results for the measured peak vane shear strength for the flocculated FFT with time are presented in Figure 5.34. Plots of peak vane shear strength versus angular deflection during an applied suction of tailings thickness are presented in Figure 5.34(a) to Figure 5.34(e). An increase in peak strength was measured near the base compared to the shear strength measurements near the surface of the tailings. The results of vane shear strength are in agreement with pore pressure measurement displayed near the bottom boundary. Peak shear strength of 3.1 kPa was determined at 7 cm above the base by day 5 and 9.65 kPa by day 87. The peak shear strength measured at 17 cm above the base increased with time at a slower rate and reached 3.57 kPa

by day 87. Shear strength measured near the surface (i.e., 27 cm from the base) displayed less than 1 kPa at all times. This was attributed to minimum total stress near the tailings surface and lower hydraulic conductivity of the FFT to increase the suction near tailings surface.

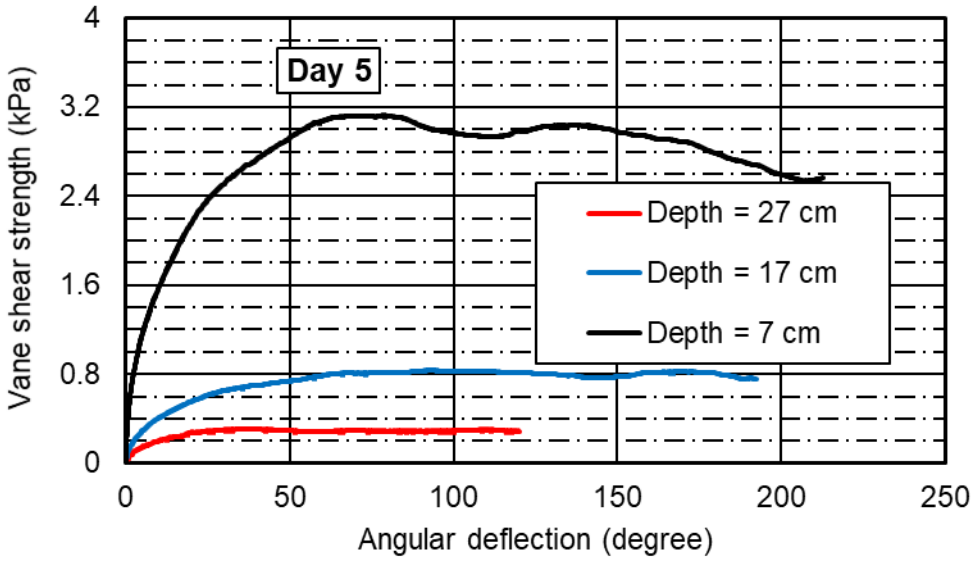

(a) Vane shear strength test after day 5

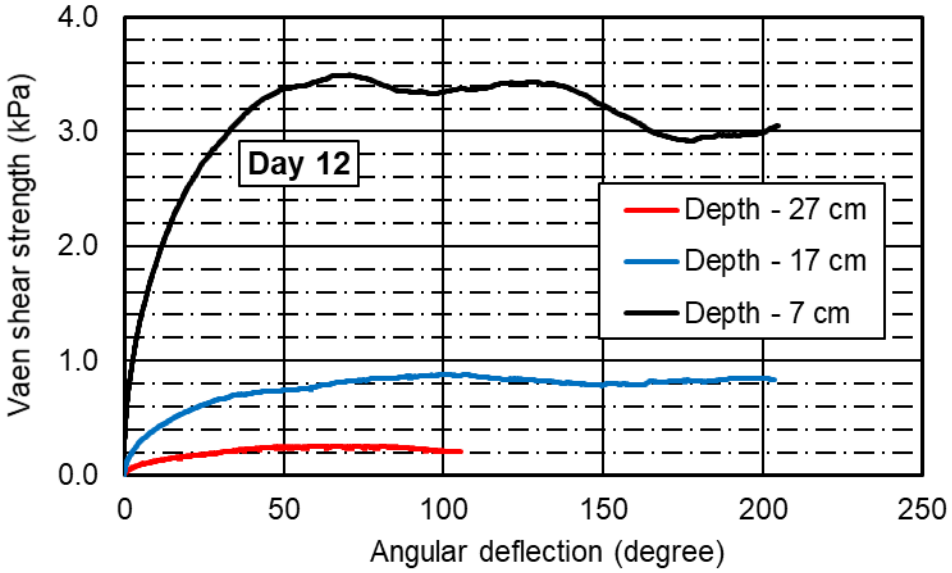

(b) *Vane shear strength test by day 12*

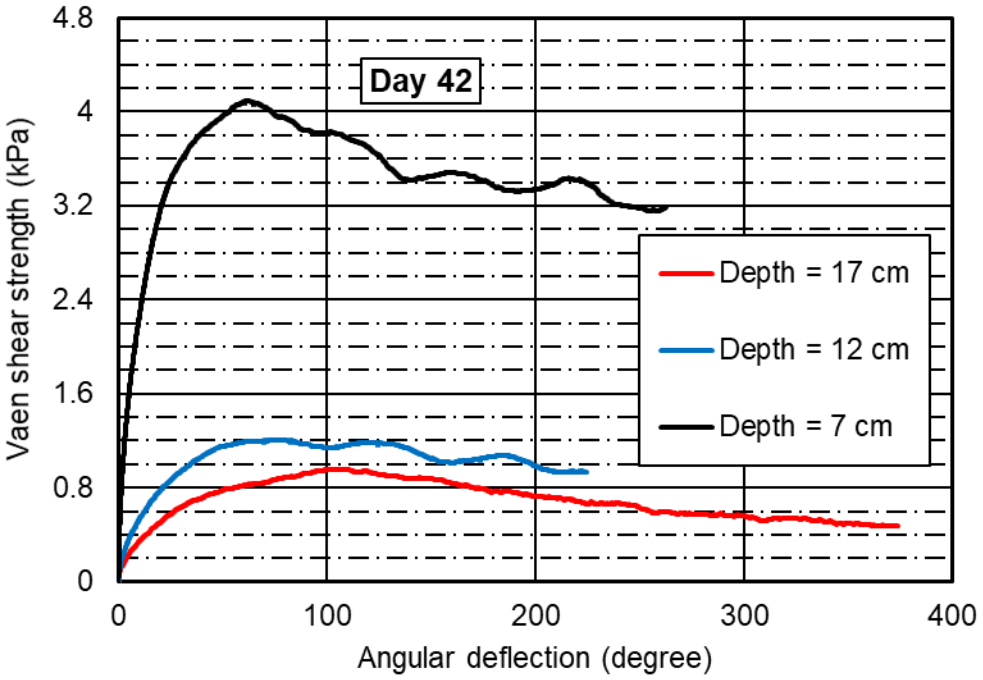

c) Vane shear strength test by day 42

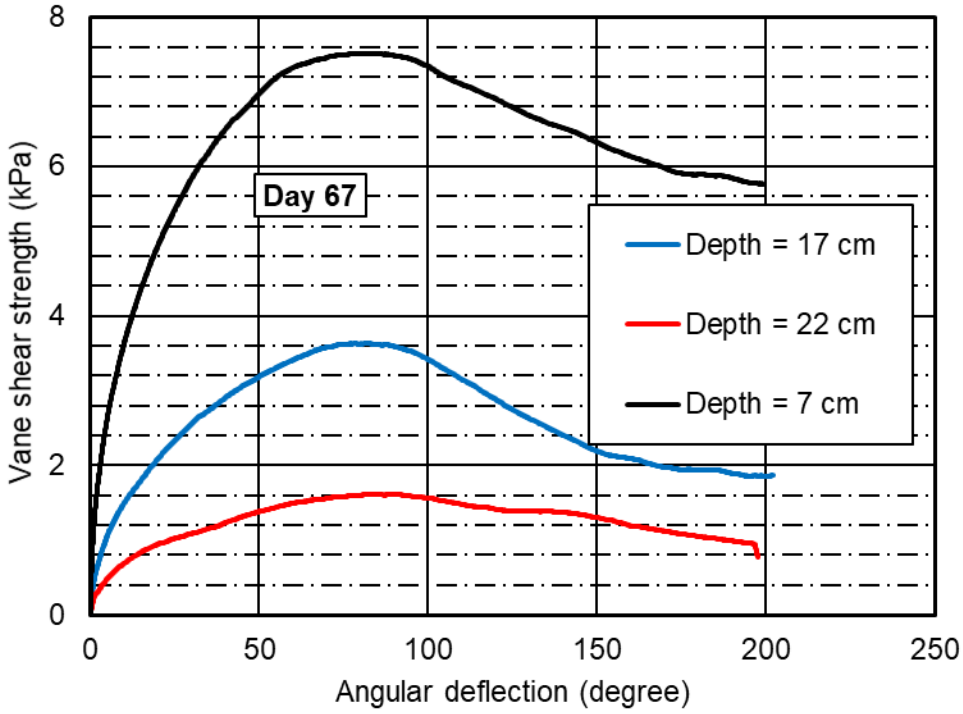

(d) *Vane shear strength test after day 67*

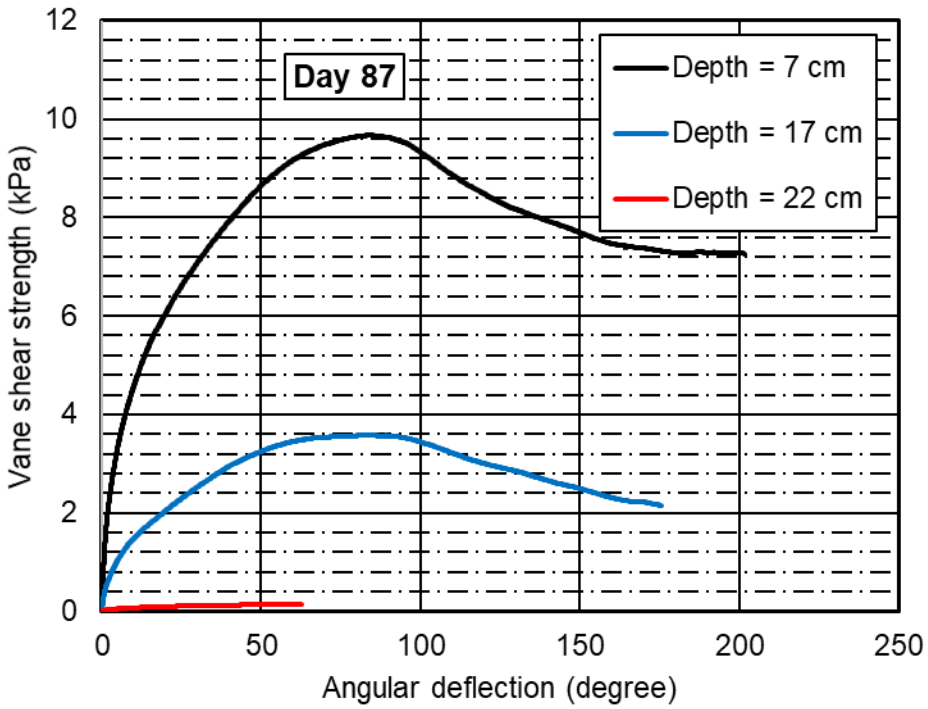

(e) *Vane shear strength test after day 87*

Figure 5. 33 Vane shear strength test using increments of suction of 20 kPa for flocculated FFT: (a) Day 5, (b) Day 12, (c) Day 42, (d) Day 67, and (e) Day 87.

The relationship between peak vane shear strength, tailings thickness, and the time of the incremental applied suction is presented in Figure 5.35. The general trend shows a large increase in undrained shear strength near the column base with time. The relationship between measured peak vane shear strength versus tailings thickness was best-fitted using the power function. The measured peak shear strength at the mid-section showed a moderate increase with time compared to near the tailings surface. The tailings near the surface exhibited a much lower rate of increase in undrained shear strength compared to near the base. The increase is generally attributed to the influence of an increase in suction to the tailings around the base.

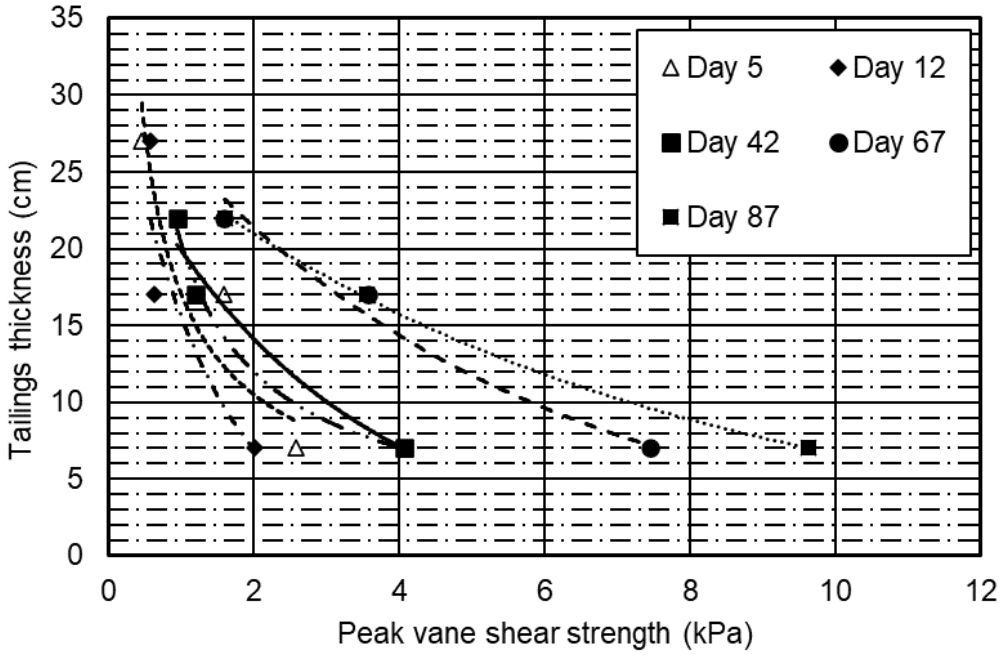

Figure 5. 34 Peak shear strength with depth and time using increments suction of 20 kPa for the flocculated FFT.

5.1.3.2 Applied suction of 50 kPa for the flocculated FFT

The results for an applied suction of 50 kPa are presented in this section for the flocculated FFT. A comparable process was carried out for 20 kPa of applied suction, above, and the results for the additional applied suction are presented to highlight changes in pore pressure, especially the negative pore pressure measured near the surface of the tailings (i.e., 3 to 5 cm below the surface).

Settlement, vertical strain, and void ratio

The change in both vertical and later strain was measured for the 50 kPa of incremental suction, and results are presented in Figure 5.36. The total strain was 1.4% for the incremental applied

suction and a cumulative total strain of 30% compared to its initial deposited volume. Figure 5.37 presents the change in average void ratio. The average initial and final void ratios were 1.18 and 1.11, respectively, as shown in Figure 5.37.

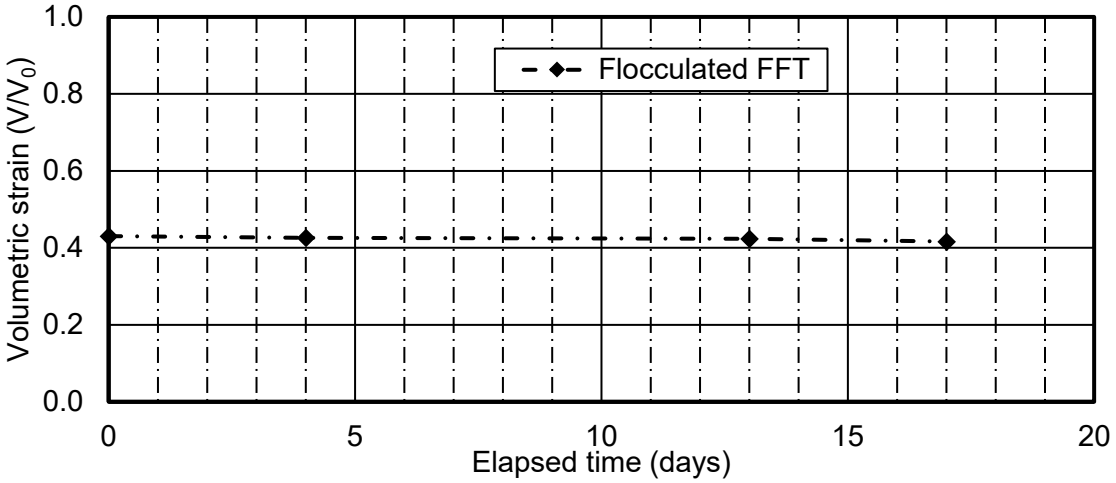

Figure 5. 35 Volumetric strain due to incremental applied suction of 50 kPa for the flocculated FFT.

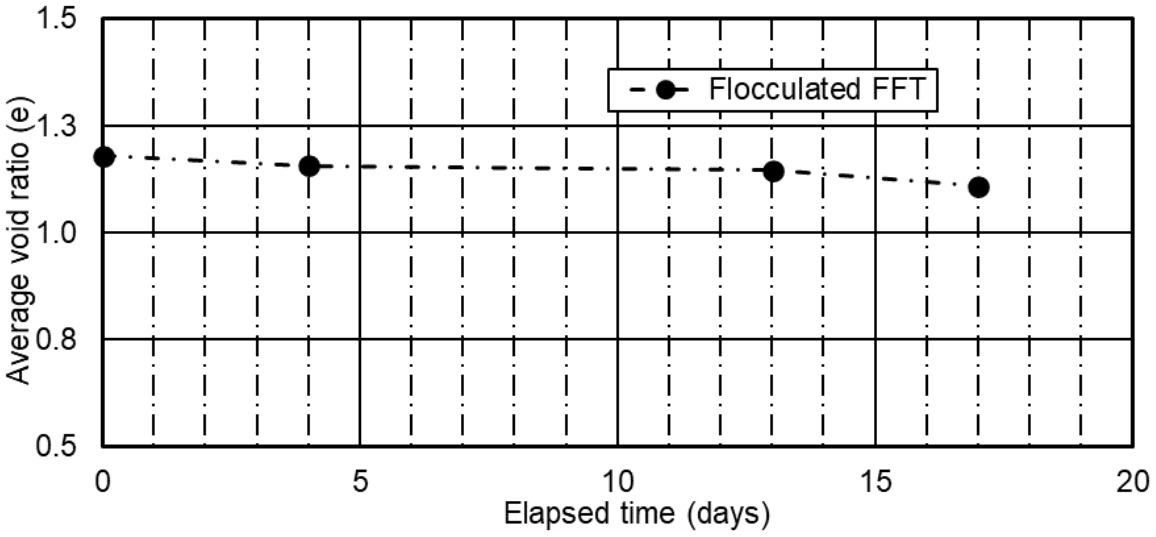

Figure 5. 36 Change in average void ratio due to increments of applied suction of 50 kPa for the flocculated FFT.

Pore pressure distribution

Figure 5.38 presents the negative pore pressure with time 3 to 5 cm below the tailings surface. The sensor was located 19 to 22cm from base of the column. The suction applied at the base was anchored at 50 kPa, and the suction that measured 3 to 5 cm below the surface reached 61 kPa by the time equilibrium was reached. Although the top of the column was covered with a lid, it is possible evaporation around the surface might have contributed to an increase in the suction near the surface.

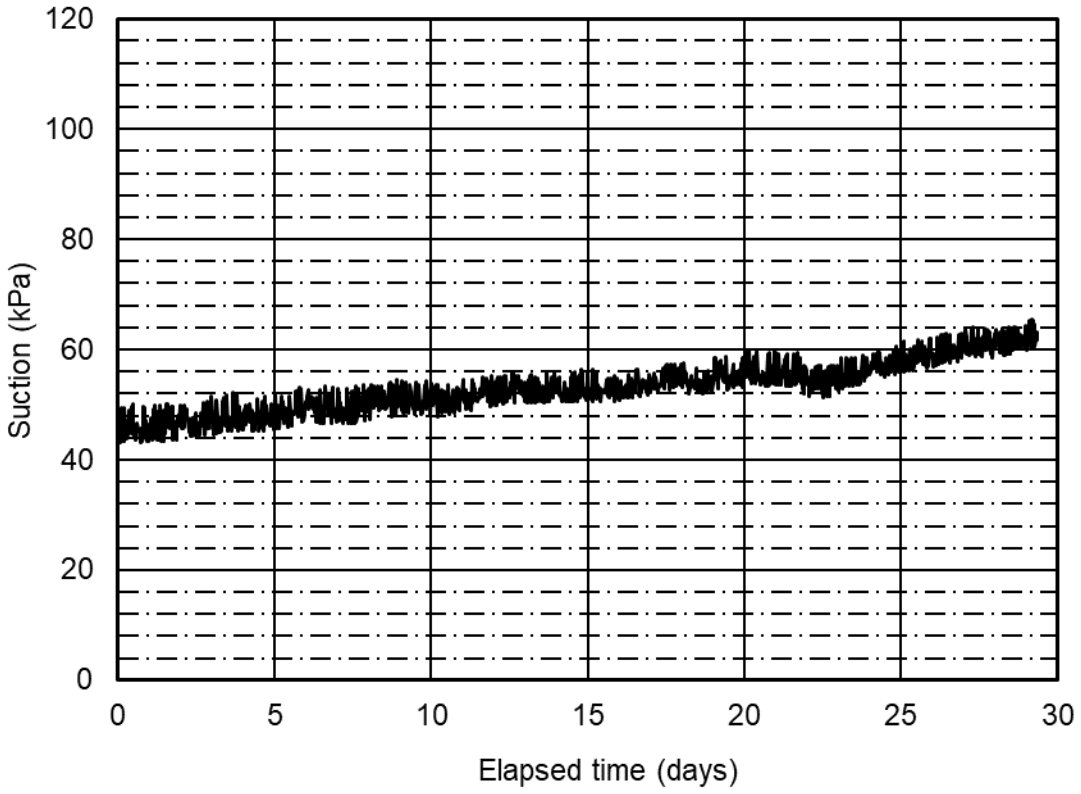

Figure 5. 37 Suction measured using the negative pore pressure sensor during increments of applied suction of 50 kPa for the flocculated FFT.

Effective stress calculations

The change in effective stress within the deposited tailings was calculated using the total stress and suction measured with time. The formula presented in Eq. [5.50] was used to calculate the effective stress.

Assuming equilibrium was reached by the end duration of the test for each increment of applied suction, the progression of suction with time along the tailings thickness was estimated and the effective stress for the profile was computed. Table 5.5 presents the distribution of suction and calculated effective stress for the flocculated FFT profile over time. Figure 5.39 presents the calculated effective stress for the tailings thickness.

Table 5. 5 Effective stress computed due to 50 kPa suction for the flocculated FFT.

Position within the column	Thickness (cm)	Time (days)					
		Day 5	Day 10	Day 14	Day 18	Day 21	Day 25
Bottom Suction (kPa)	0	50	50	50	50	50	50
Effective stress (kPa)		51.4	51.4	51.4	51.4	51.4	51.4
Near bottom suction (kPa)	5	40	42	44	45	47	49
Effective stress (kPa)		41.4	43.4	45.4	46.4	48.4	50.4
Middle section suction (kPa)	15	28	32	35	38	42	45
Effective stress (kPa)		28.7	32.7	35.7	38.7	42.7	45.7
Top suction (kPa)	20	35	40	43	48	55	61
Effective stress (kPa)		36.4	41.4	44.4	49.4	56.4	62.4

Similar to the applied suction of 20 kPa, the calculated effective stress increased near the base of the column and the increase was immediately sensed near the bottom of the column as shown in Figure 5.39. Over time the applied suction increased in an upward direction, as did the effective stress. The rate of suction increased from an equilibrium condition of 40 kPa to 50 kPa, which was faster than compared to the increase in suction from the hydrostatic pressure to applied suction of 20 kPa.

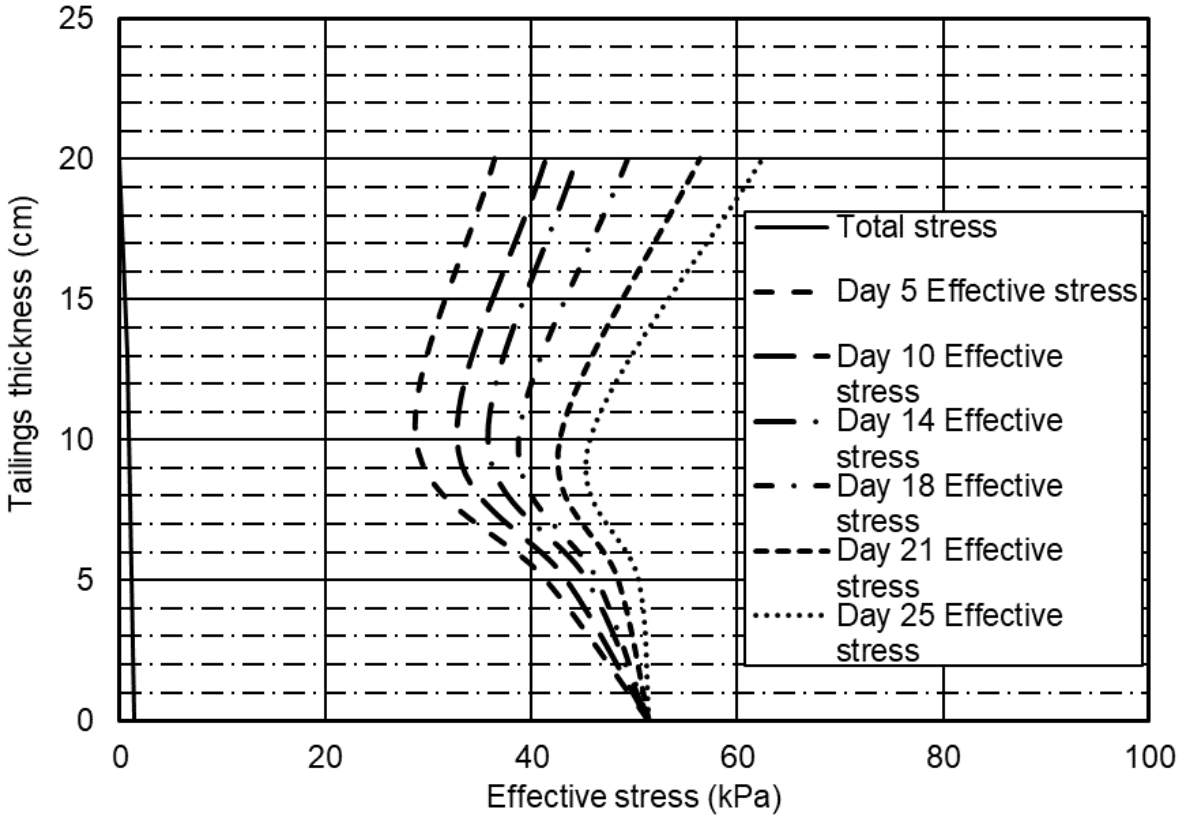

Figure 5. 38 Computed effective and total stress during increments of suction of 50 kPa for flocculated FFT.

Effective stress curves with time estimation

The development and progression of effective stress with time along the tailings profile due to incremental applied suction has been formed for the flocculated FFT. Figure 5.33 and 5.39

presents the effect stress curves for the applied suction of 20 kPa and 50 kPa, respectively. The bases for the conceptual effective stress curves and progression were completed using the following assumptions:

1. Constant applied suction at the bottom of the column for the given specific time

2. Measured suction near the surface of the tailings (~2-3 cm below the surface)

3. Total tailings settlement with time

Initially, effective stress curves for applied suction of 20 kPa was developed as shown in Figure 5.33. During the initial stage, the progression of the applied suction show gradual trend as the tailings were fully saturated, and suction were not developed within the profile yet. The applied suction was assumed to reach the applied value instantly near the column base. However, the development of suction within the tailings profile assumed to require longer time due to low hydraulic conductivity properties of the tailings. The curves show more gradual progression with time and depth to reach the equilibrium point as shown in Figure 5.33.

Figure 5.39 presents conceptual effective stress curves formed during 50 kPa applied suction process. As suction continued in increments from 20 to 50 kPa, the possible effect of evaporation were observed near the surface of tailings. Figure 5.39 shows higher suction and higher effective stress measurements near the surface compared to the mid section of the column with time. However, the applied suction at the column base were fixed for a specified time. Therefore, Figure 5.39 shows higher effective stress calculation due to higher suction and total stress near the base; followed by lower effective stress near the mid-section as suction gradually progressed within the tailings, and higher effective stress calculation near the surface due to evaporation.

These curves were constructed with limited available sensor within the column. The figures were only useful to show the development of suction and effective stress trends within the tailings column as consolidation progressed.

Undrained peak shear strength measurement with time and depth

The changes in peak vane shear strength for an applied suction of 50 kPa are presented in Figure 5.40. Plots of peak vane shear strength versus angular deflection with tailings thickness and time are presented in Figure 5.40(a) to Figure 5.40(d). An increase in peak shear strength was measured near the column base (i.e., 7 cm from the base) compared to tailings closer to the surface. The peak vane shear strength measurements are in agreement with the negative pore pressure measured immediately near the bottom of the column in response to an increase in suction. However, as the measured suction near the surface became larger, the shear strength measured mid-section the tailings (i.e., 17 cm from base) should have showed an equal or increased shear strength measurement. This affirms the assumption that evaporation might have contributed to the larger suction measurement displayed near the surface, while the mid-section showed lower suction than the base and near surface, before the equilibrium condition was achieved.

The difference between measured vane shear strength values at 7 cm and 17 cm decreased with time, which indicates an increase in suction with profile from the base towards the tailings surface with time. An additional consideration is that repeated vane shear tests start leaving disturbed marks on the tailings deposits, as these disturbed marks did not heal quickly in comparison to the tests conducted at the earlier stage. At the later stage, the continuous disturbance of tailings sample possibly might cause short circuiting of the applied suction, however it was not investigated at during the present study.

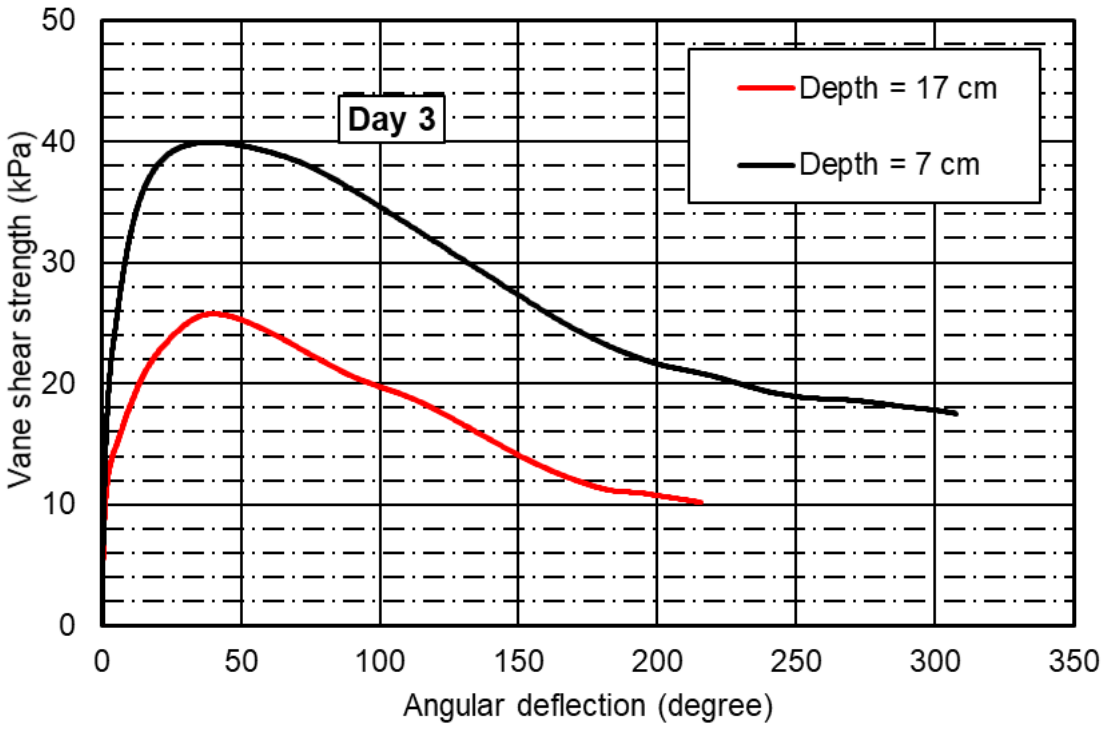

(a) Vane shear strength test after day 3

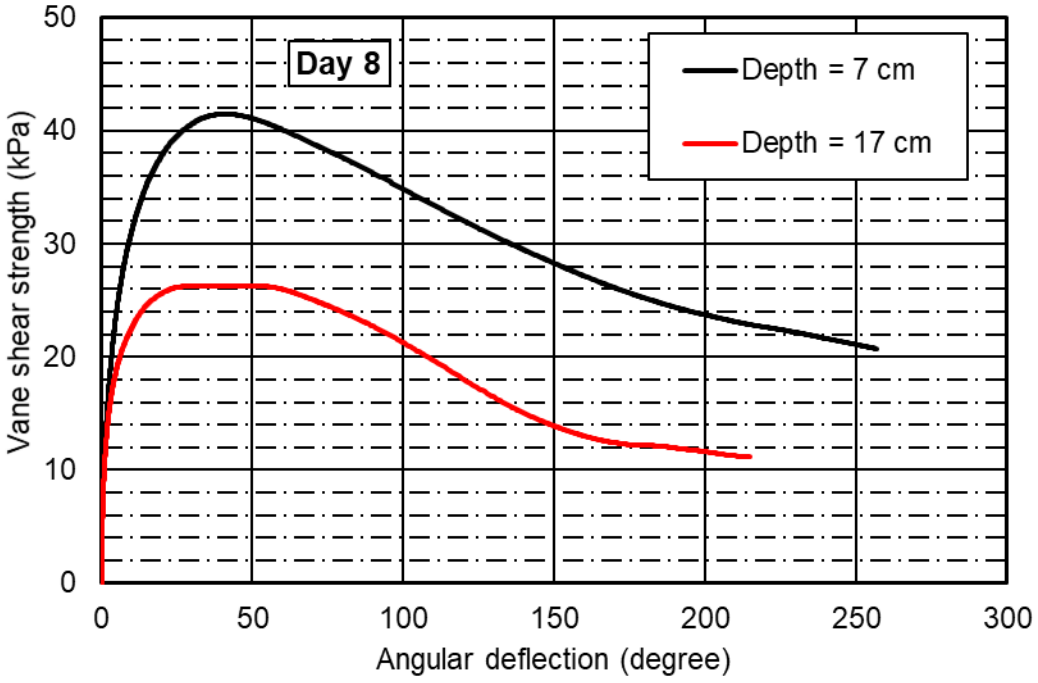

(b) Vane shear strength test after day 8

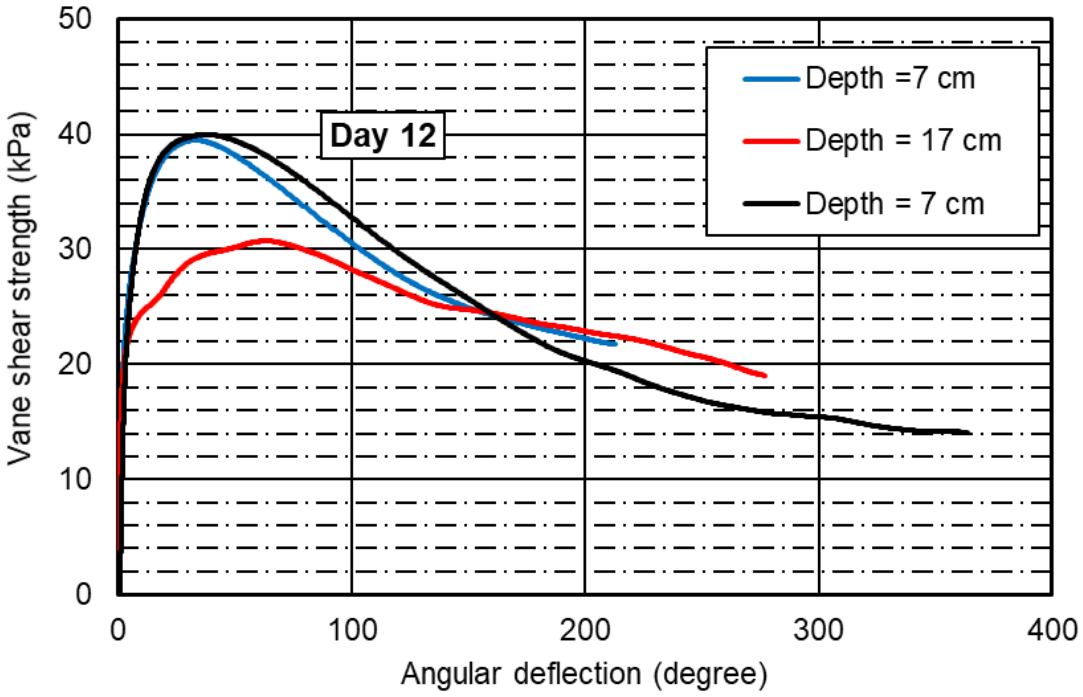

(c) shear strength test after day 12

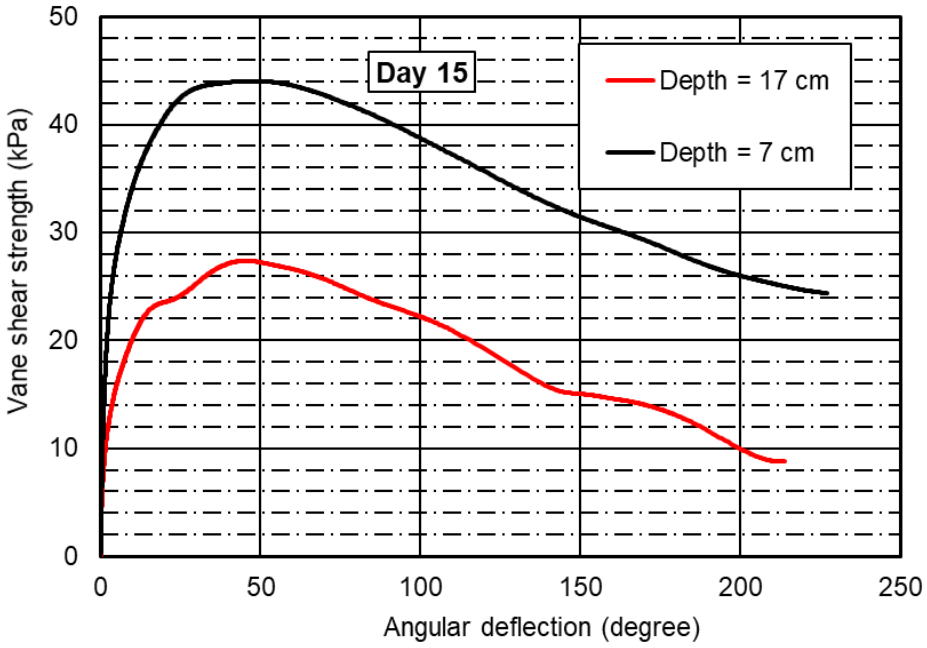

(d) Vane shear strength test after day 15

Figure 5. 39 Vane shear strength test for the flocculated FFT for the consolidation process using increments of suction 50 kPa: (a) Day 3, (b) Day 8, (c) Day 12, and (d) Day 15.

The relationship between peak vane shear strength, tailings thickness, and time for increments of applied suction is presented in Figure 5.41. The general trend shows a substantial increase in undrained shear strength near the column base with time. The vane shear strength measured near the mid to upper section shows a moderate increase with time compared to the peak strength near the column base. The increase was due to the decrease in hydraulic conductivity of the material with consolidation as the decrease in void ratio with the deformation process during the different stages of incremental suctions. If the hydraulic conductivity of the material was higher, slight differences between shear strength measurements would had been observed near the column base and mid-section. These differences contributed to the effective stress distribution between the base, mid-section, and near the surface of tailings.

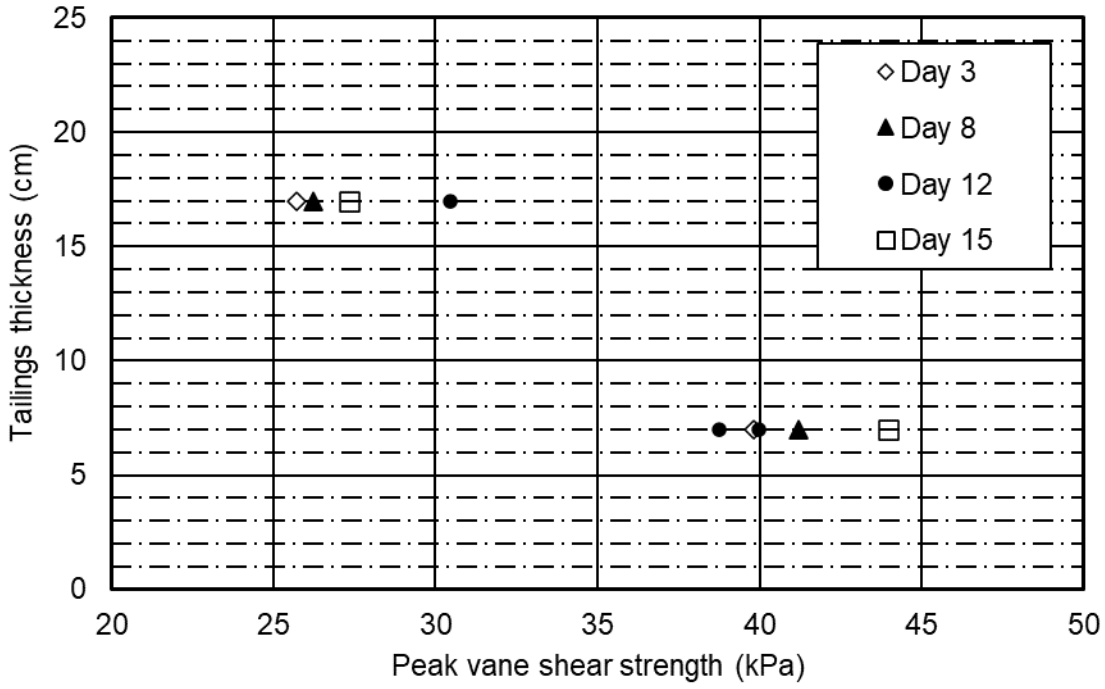

Figure 5. 40 Peak shear strength with depth and time using increments suction of 50 kPa for the flocculated FFT.

5.1.3.3 Applied suction of 20 kPa for the FCTC

The results of consolidation for the FCTC during increments of applied suction is presented herein. The results of increments of suction of 20 kPa for the FCTC is presented as follows: i) settlement, ii) pore pressure distribution, iii) effective stress calculations, and iv) undrained shear strength.

Settlement, vertical strain, and void ratio

The vertical strain and change in average void ratio for the FCTC are presented in Figure 5.42 and Figure 5.43, respectively. No later deformation was measured during the applied suction of 20 kPa. The measured vertical strain was 6.7% compared to the initial deposited tailings thickness as shown in Figure 5.41. The average initial and final void ratios were 2.02 and 1.76, respectively, by day 90 as shown in Figure 5.42.

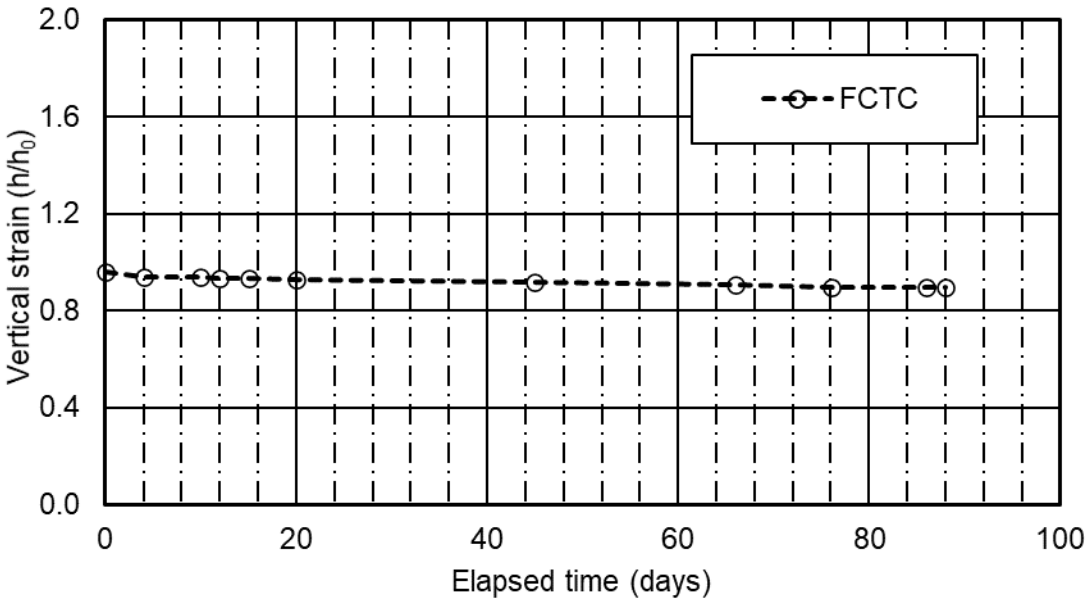

Figure 5. 41 Vertical strain due to incremental applied suction of 20 kPa for the FCTC.

A longer time was allowed to ensure equilibrium had been reached for an applied suction of 20 kPa because the pore pressure sensors were not responding. When the change in vertical strain or average void ratio became minimal, it was assumed that equilibrium had been reached, and subsequent incremental suction was applied.

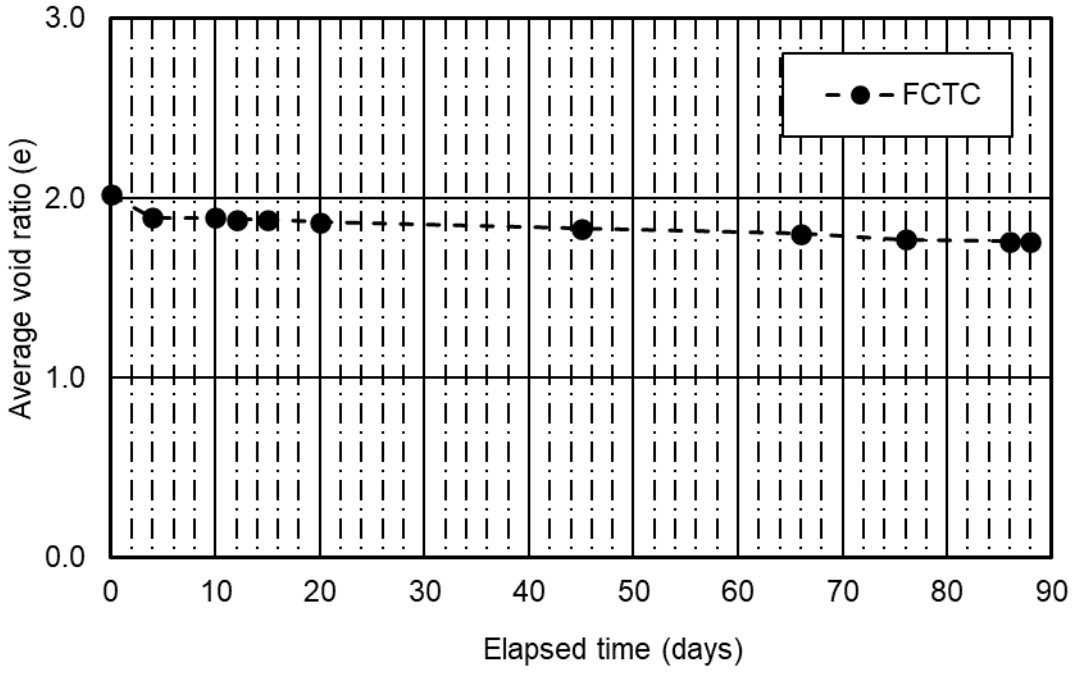

Figure 5. 42 Change in void ratio due to applied suction of 20 kPa for the FCTC.

Pore pressure distribution

There was no response from sensors placed in the column to measure negative pore pressure. The positive transducer sensor did not respond during the negative pressure application. Therefore, the determination of the equilibrium time for the pore pressure distribution was inferred from the vertical strain measurement.

Effective stress calculations

The change in effective stress within the deposited tailings was calculated using the total stress and estimated suction with time for the ranges of applied suction below 30 kPa. The effective stress was calculated using Eq. [5.50]. Assuming equilibrium was reached by the end of the applied suction time, the progression of suction with time along the tailings thickness was estimated and effective stress for the profile was computed. Table 5.6 presents summary of suction distribution and computed effective stress for the FCTC tailings thickness with time. Figure 5.44 presents computed effective stress for the tailings thickness for the FCTC.

Table 5. 6 Summary of suction and computed effective stress for the FCTC.

Position within the column	**Thickness (cm)**	**Time (days)**					
		Day 15	Day 30	Day 45	Day 60	Day 75	Day 90
Bottom suction (kPa)	0	20	20	20	20	20	20
Effective stress (kPa)		22.2	22.2	22.2	22.2	22.2	22.2
Near bottom suction (kPa)	5	4	6	8	11	14	18
Effective stress (kPa)		6.2	8.2	10.2	13.2	16.2	20.2
Middle section suction (kPa)	15	2	4	7	10	13	17
Effective stress (kPa)		3.1	5.1	8.1	11.1	14.1	18.1
Top suction (kPa)	37	1	3	5	8	13	16
Effective stress (kPa)		1	3	5	8	13	16

It is possible the measured suction was much lower than the anticipated equilibrium condition if the column was not in fact reached. The accuracy of the determination of whether or not equilibrium had been reached was impeded by the lack of pore pressure measurements. Figure 5.44 presents the effective stress calculation with time. A similar pattern was displayed for the

FCTC with an increase in effective stress near the base of the column, followed by the stress increase to an upward direction due to distribution of suction from the bottom up.

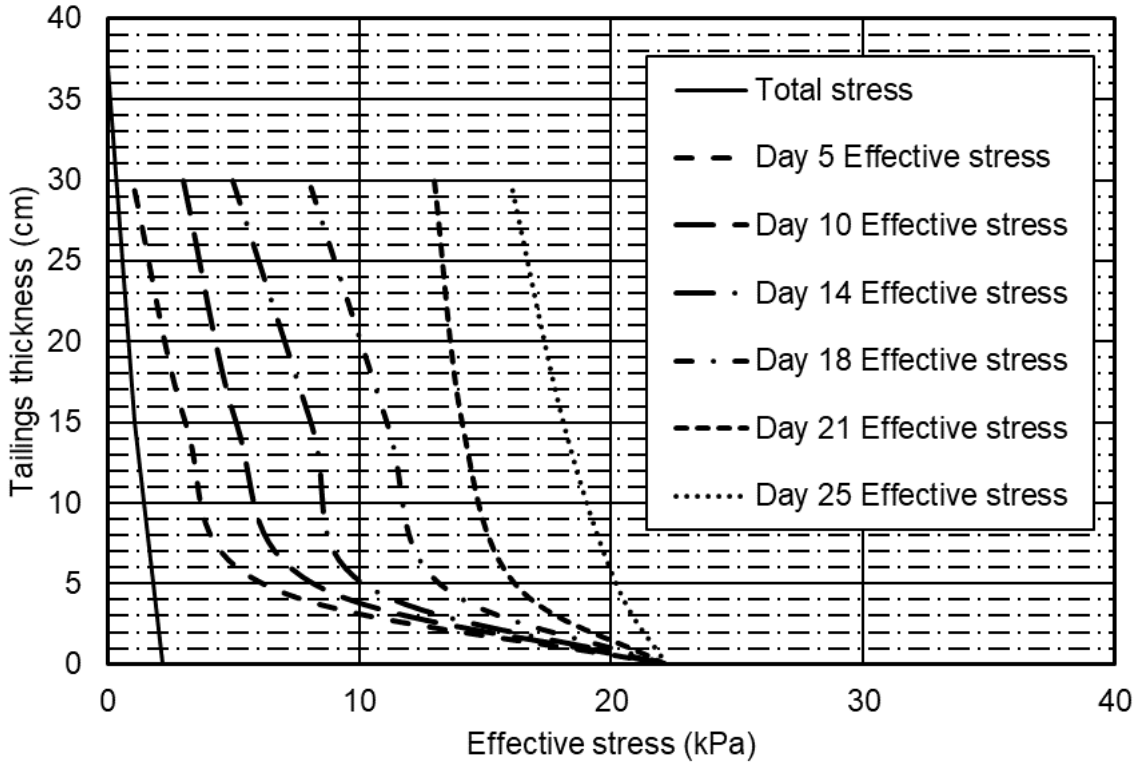

Figure 5. 43 Computed effective and total stress during increments of suction of 20 kPa for the FCTC.

Undrained peak shear strength measurement with time and depth

The results of the peak undrained strength for the FCTC under an applied suction of 20 kPa with time are presented in Figure 5.45. The relationship between the peak shear strength and angular deflection with time is presented in Figure 5.45(a) to Figure 5.45(e). An overall increase in peak shear strength was displayed near the column base compared to the mid-section and tailings surface of the column. The increase in the peak strength was influenced by the hydraulic

conductivity of the tailings, and the applied suction increased in an upwards direction with time, as observed for the flocculated FFT results.

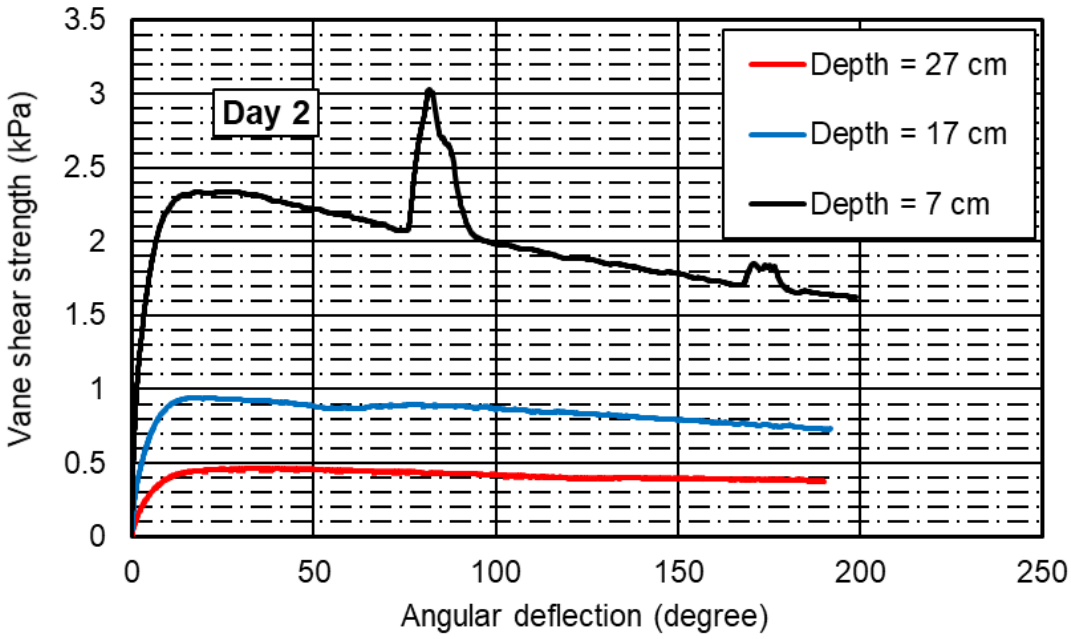

(a) Vane shear strength test after day 2

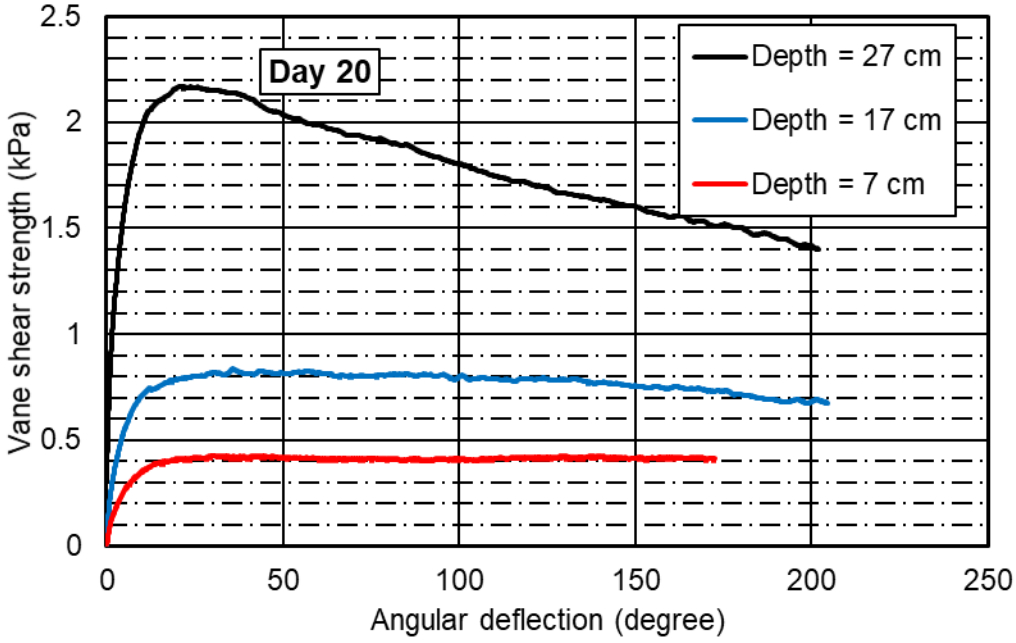

(b) *Vane shear strength test after day 20*

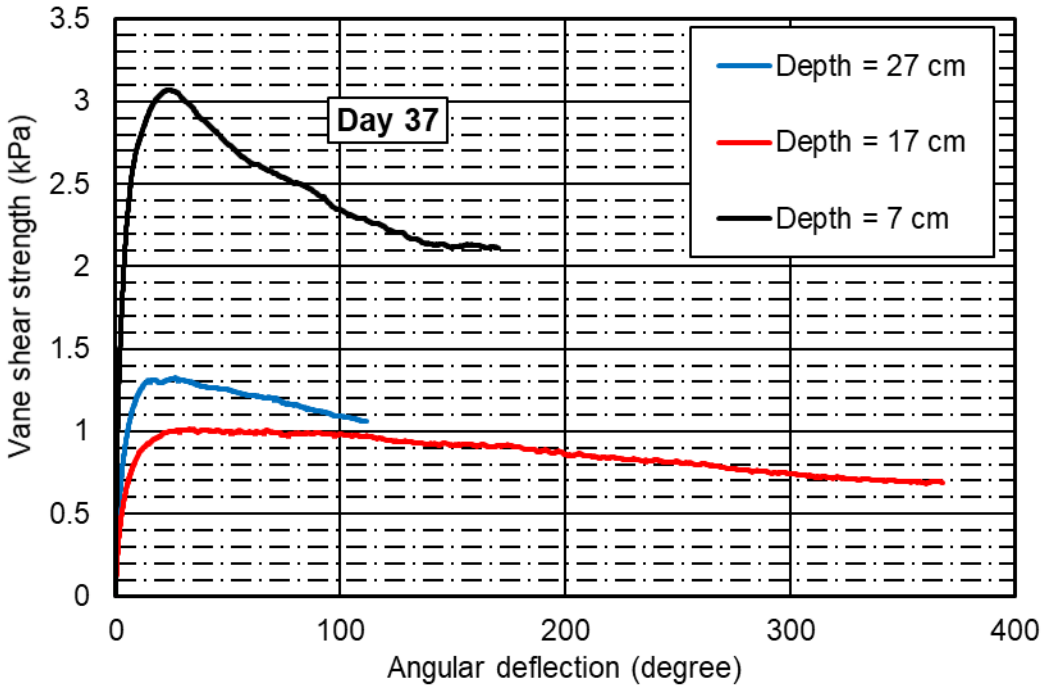

(c) ***Vane shear strength test after day 37***

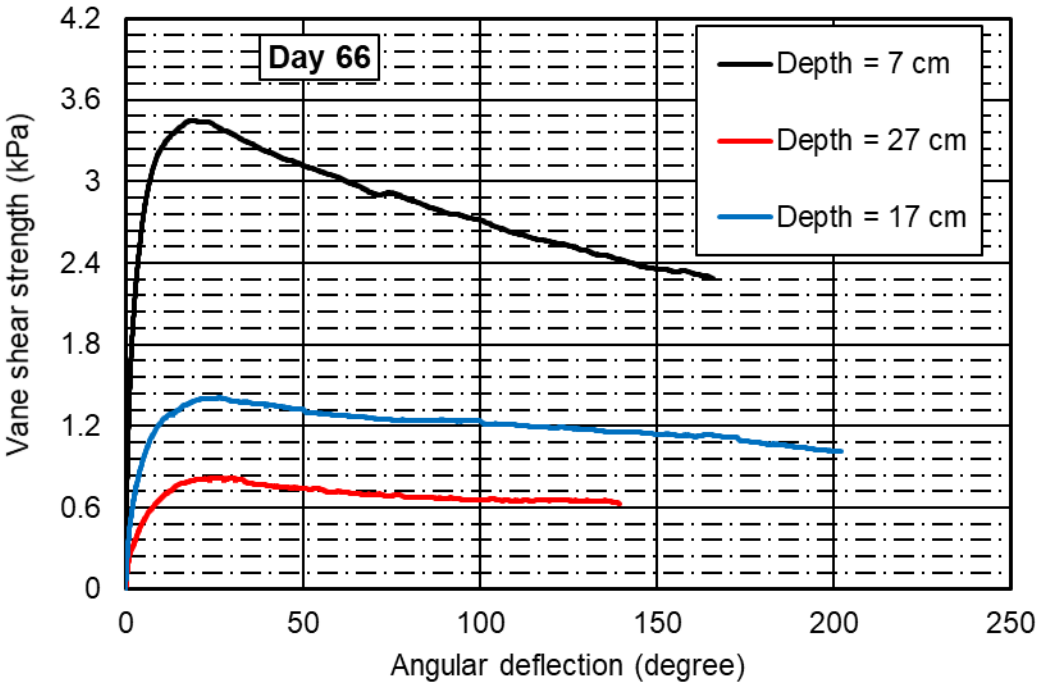

(d) Vane shear strength test after day 66

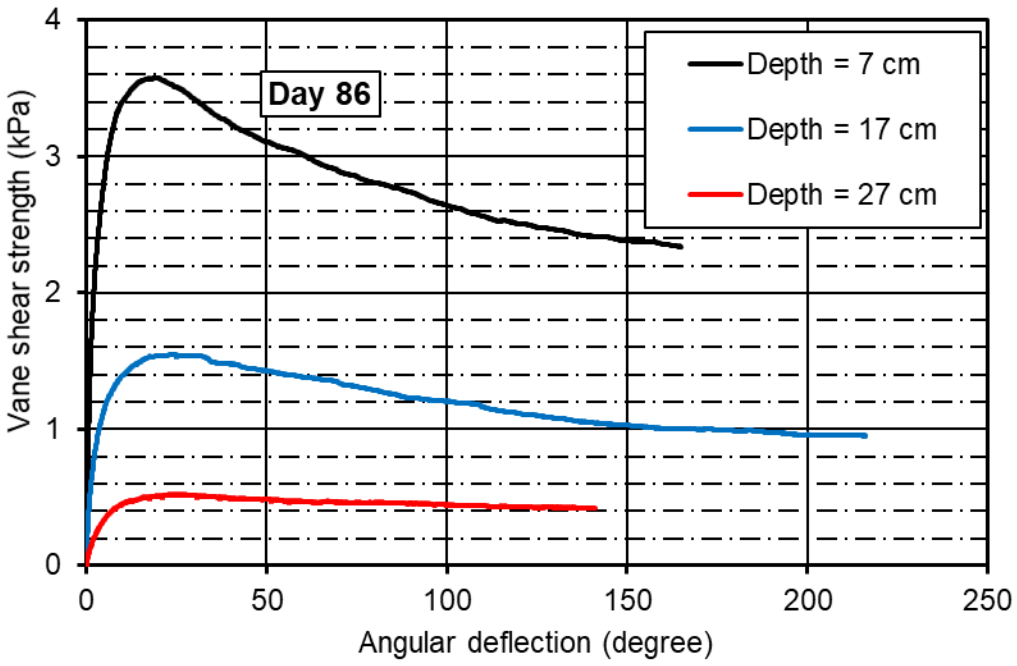

(e) Vane shear strength test after day 86

Figure 5. 44 Vane shear strength test for the FCTC using applied suction of 20 kPa process: (a) Day 2, (b) Day 20, (c) Day 37, (d) Day 66, and (e) Day 86.

The relationship between peak vane shear strength, corresponding tailings thickness, and duration for the applied incremental suction of FCTC is presented in Figure 5.46. The general trend displays an increase in the vane shear strength near the column base. The relationship can be described using a power function. There is an increase in undrained shear strength in the upward direction due to the increase in the suction distribution, which is dependent on the hydraulic conductivity of placed tailings. The increase in the final magnitude of the suction in an upward direction can be attributed to the applied suction and effect of evaporation.

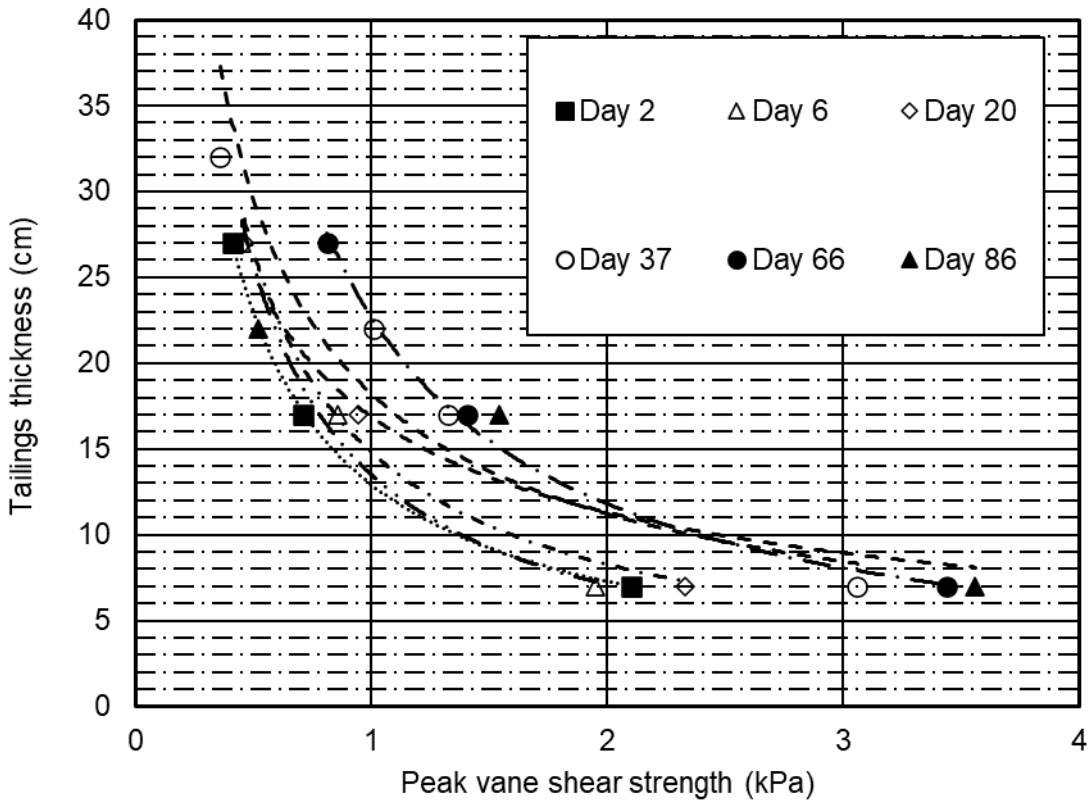

Figure 5. 45 Peak vane shear strength for the FCTC with depth and time during the applied suction of 20 kPa.

5.1.3.4 Applied suction of 50 kPa for the FCTC

The results of consolidation for the FCTC using increments suction of 50 kPa is presented herein.

Settlement, vertical strain, and void ratio

The total strain measured due to an applied suction of 50 kPa is presented in Figure 5.47. The total strain for the FCTC was 1.0% as presented in Figure 5.47. Figure 5.48 presents the change in average void ratio. The average initial and final void ratios were 1.39 and 1.36, respectively, on day 17 as shown in Figure 5.48.

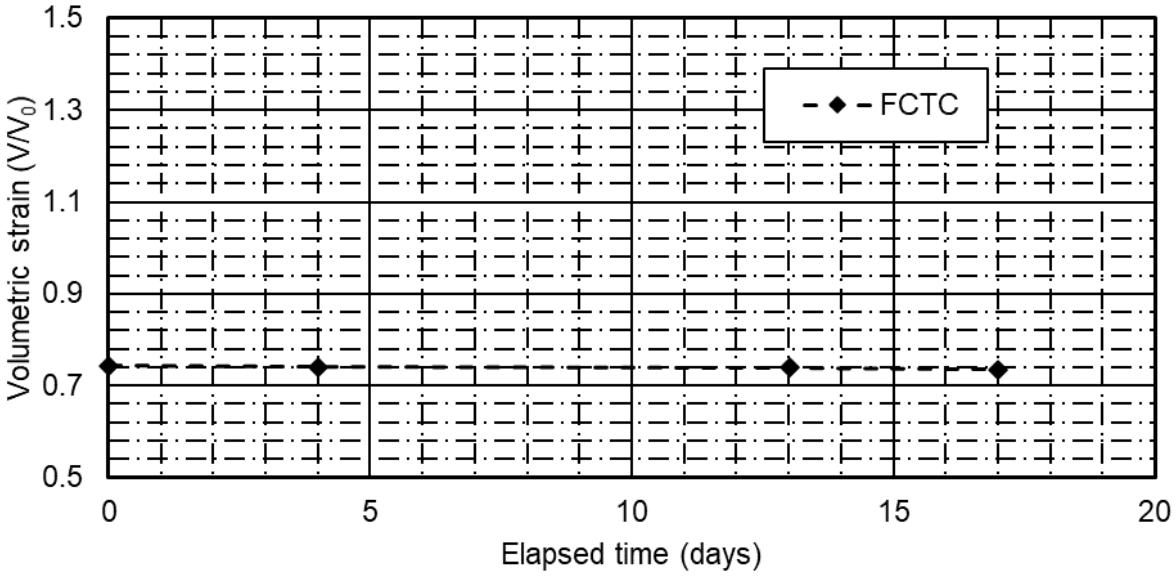

Figure 5. 46 Volumetric strain due to incremental applied suction of 50 kPa for the FCTC.

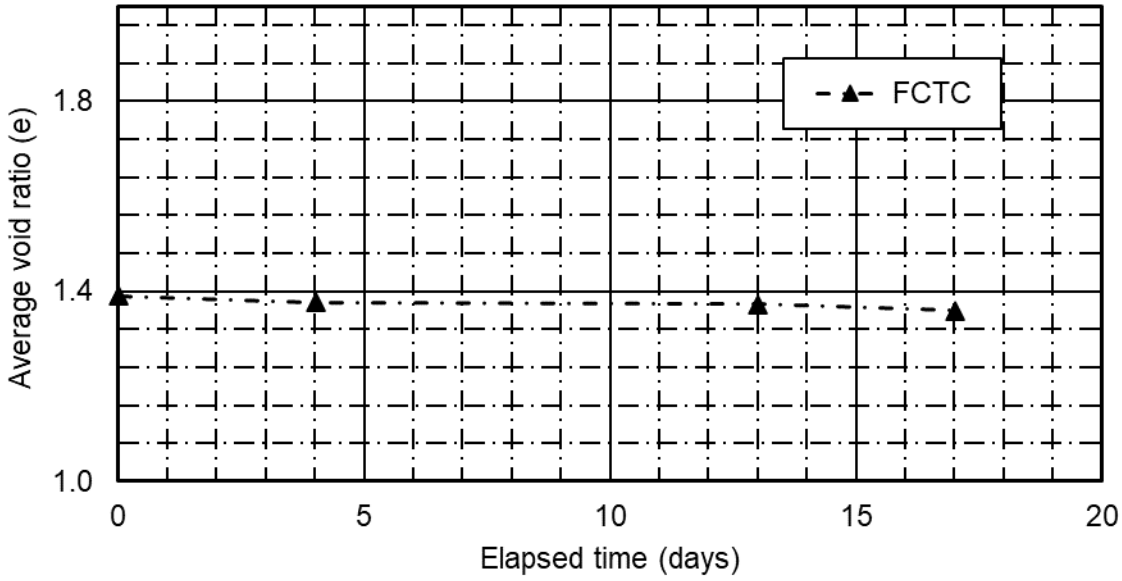

Figure 5. 47 Change in average void ratio due to increments of applied suction of 50 kPa for the FCTC.

Pore pressure distribution

Figure 5.49 presents the measured negative pore pressure with time during the process of consolidation using an applied suction of 50 kPa. The pore pressure sensor was located 26 cm from the column base. The applied suction at the bottom of the column was anchored at 50 kPa. The measured suction when the deposited tailings reached equilibrium was 56.7 kPa near the surface of the tailings.

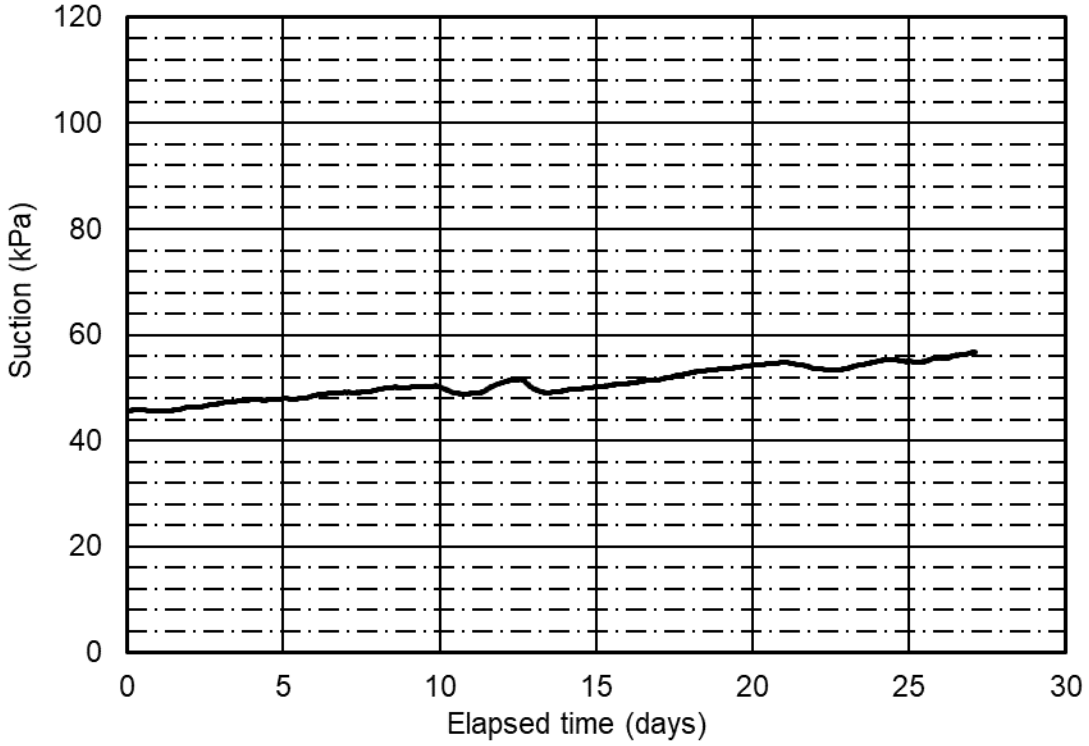

Figure 5. 48 Suction measured using the negative pore pressure sensor during increments of applied suction of 50 kPa for the FCTC.

Effective stress calculations

The change in effective stress within the tailings was calculated using the total stress and suction measured over time. Eq. [5.50] was used to calculate the effective stress.

Equilibrium condition was assumed by the end of the test period for the deposited tailings. The changes in the suction distribution within the profile over time were estimated using the anchored applied suction at the bottom boundary and measured suction near the surface. The effective stress was calculated based on the assumed distribution of suction and measured values for the tailings profile. Table 5.7 presents summary of suction distribution and computed effective stress for the FCTC tailings thickness with time during the 50 kPa applied suction. Figure 5.50 presents computed effective stress for the tailings thickness for the FCTC.

Table 5. 7 Summary of suction distribution and computed effective stress for the FCTC during 50 kPa applied suction.

Position within the column	Thickness (cm)	Time (days)					
		Day 5	Day 10	Day 14	Day 18	Day 21	Day 25
Bottom suction (kPa)	0	50	50	50	50	50	50
Effective stress (kPa)		51.4	51.4	51.4	51.4	51.4	51.4
Near bottom suction (kPa)	5	35	38	42	44	46	47
Effective stress (kPa)		36.4	39.4	43.4	45.4	47.4	48.4
Middle section suction (kPa)	15	25	27	30	33	36	39
Effective stress (kPa)		25.7	27.7	30.7	33.7	36.7	39.7
Top suction (kPa)	28	47.9	49	52	55	57	60
Effective stress (kPa)		48.6	49.7	52.7	55.7	57.7	60.7

It is assumed the effect of evaporation played a role in the increase of suction measured near the surface of tailings. This assumption is supported by the measured shear strength values, which were higher near the column base compared to the mid-section. It is possible, based on this suction distribution, that the column had not reached equilibrium.

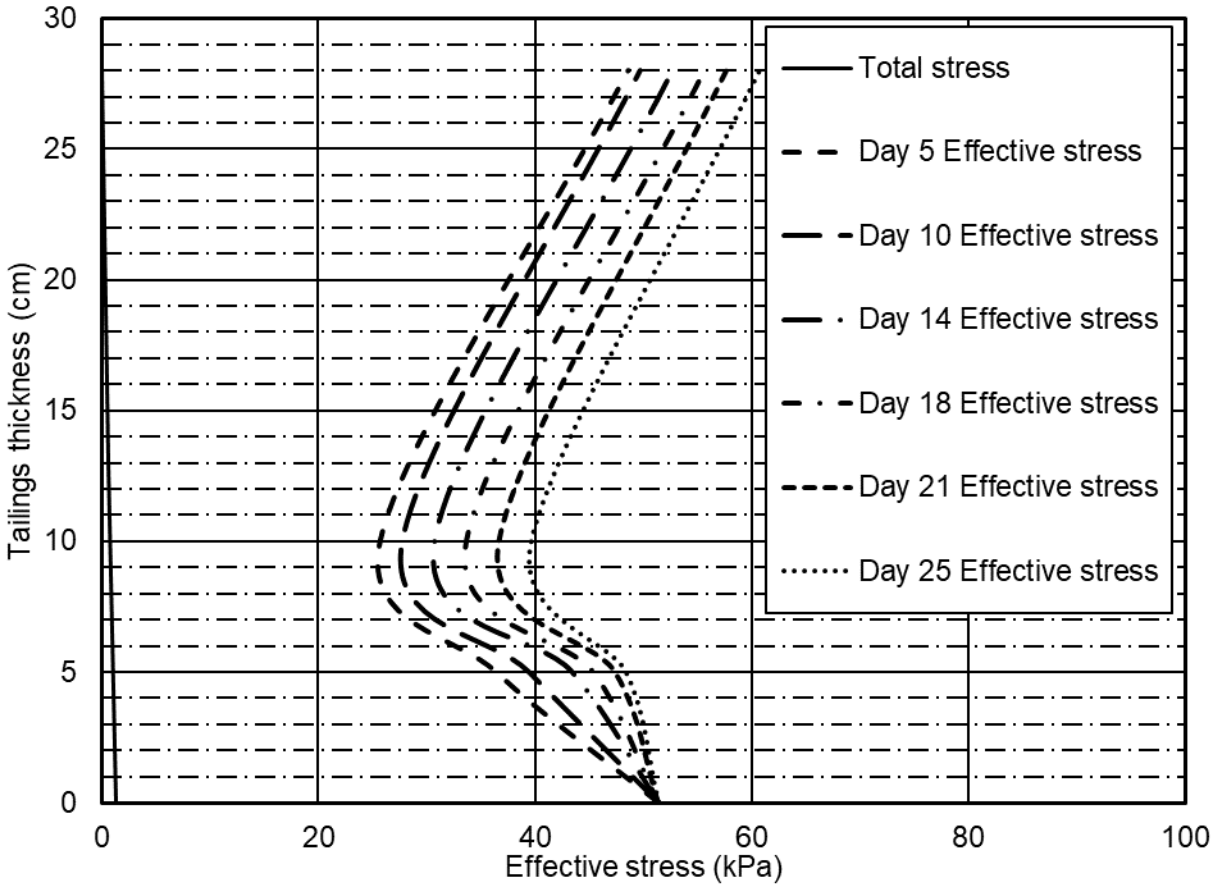

Figure 5. 49 Computed effective and total stress during increments of suction of 50 kPa for the FCTC.

Similar to the development and progression of effective stress curves described for the flocculated FFTs, the assumptions and considerations were applied for the FCTC during the construction of effective stress curves over time. Figure 5.44 and 5.50 presents the effect stress curves for the applied suction of 20 kPa and 50 kPa, respectively.

These curves were constructed with limited available sensor within the column. The figures were only useful to show the development of suction and effective stress trends within the tailings column as consolidation progressed.

Undrained peak shear strength measurement with time and depth

The undrained peak shear strength measured with time for the FCTC for an applied suction of 50 kPa is presented in Figure 5.51(a) and Figure 5.51(b). The peak shear strength with depth and time is presented in Figure 5.51. The peak undrained strength with time is presented in Figure 5.51. The relationship between the peak shear strength and angular deflection are presented in Figure 5.51(a) to Figure 5.51(e). An overall increase in peak shear strength was displayed near the column base compared to the middle and surface of the column.

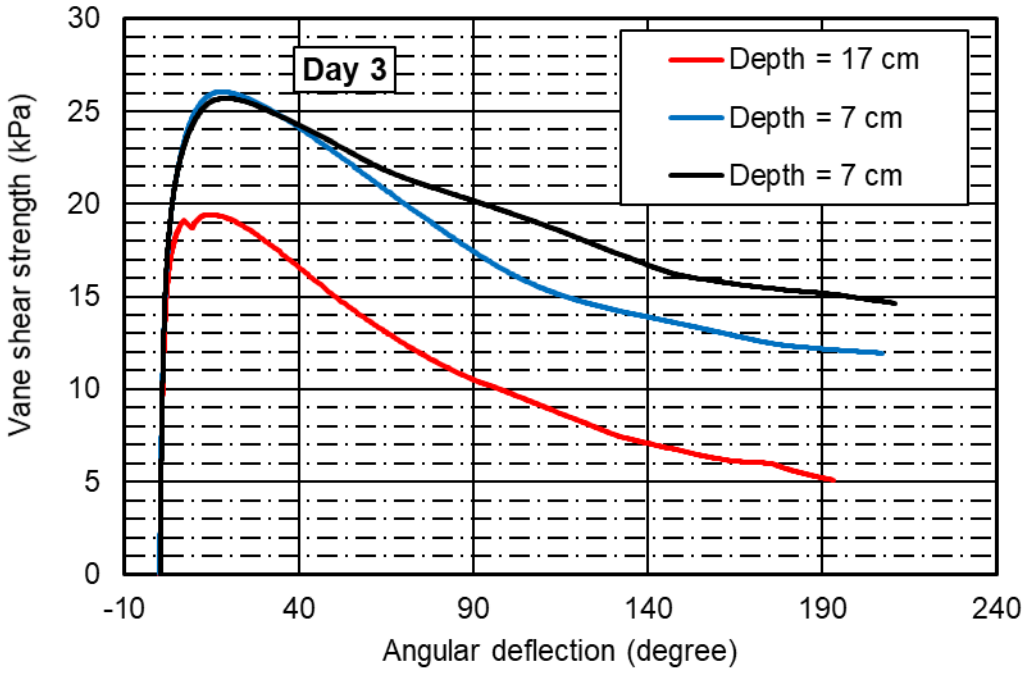

(a) Vane shear strength test after day 3

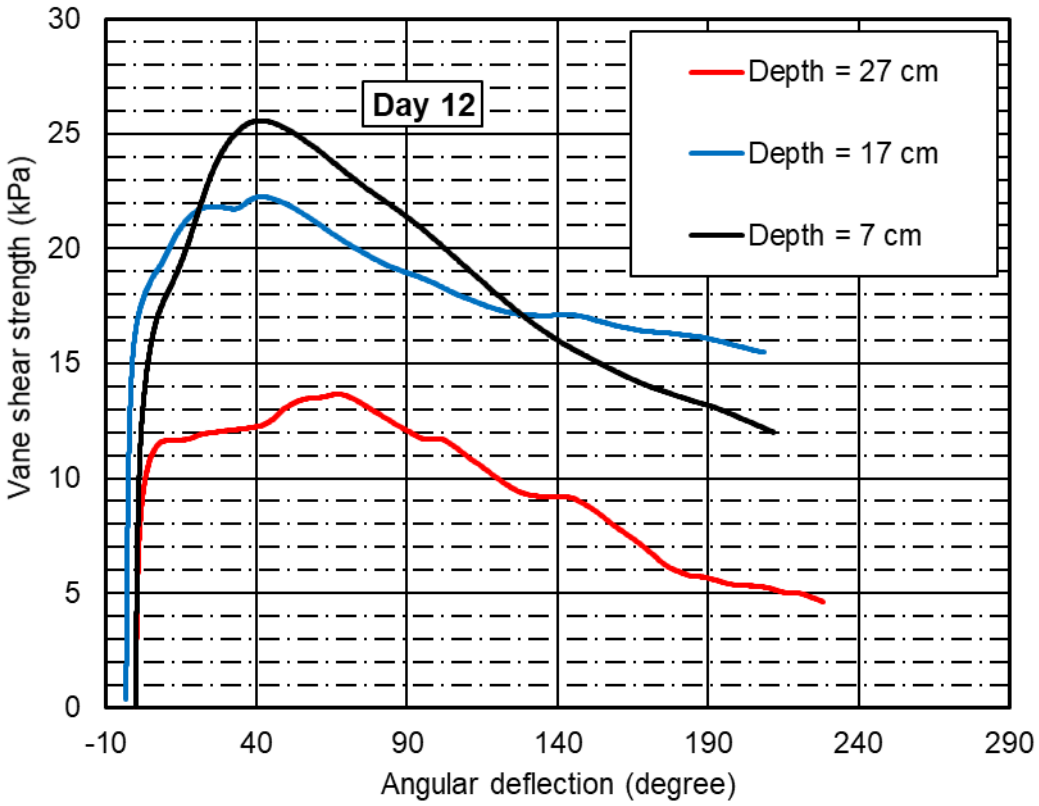

(b) Vane shear strength test after day 12

Figure 5. 50 Vane shear strength test for the FCTC during consolidation using applied suction of 50 kPa process: (a) Day 3 and (b) Day 12.

The relationship between peak vane shear strength and corresponding tailings thickness with time for the additional incremental suction of 10 kPa (i.e., from 40 kPa to 50 kPa) is presented in Figure 5.52. The general trend displays an increase in the vane shear strength near the column base. There is an increase with the undrained shear strength in the upward direction due to the increase in the suction distribution, which is dependent on the hydraulic conductivity of the tailings.

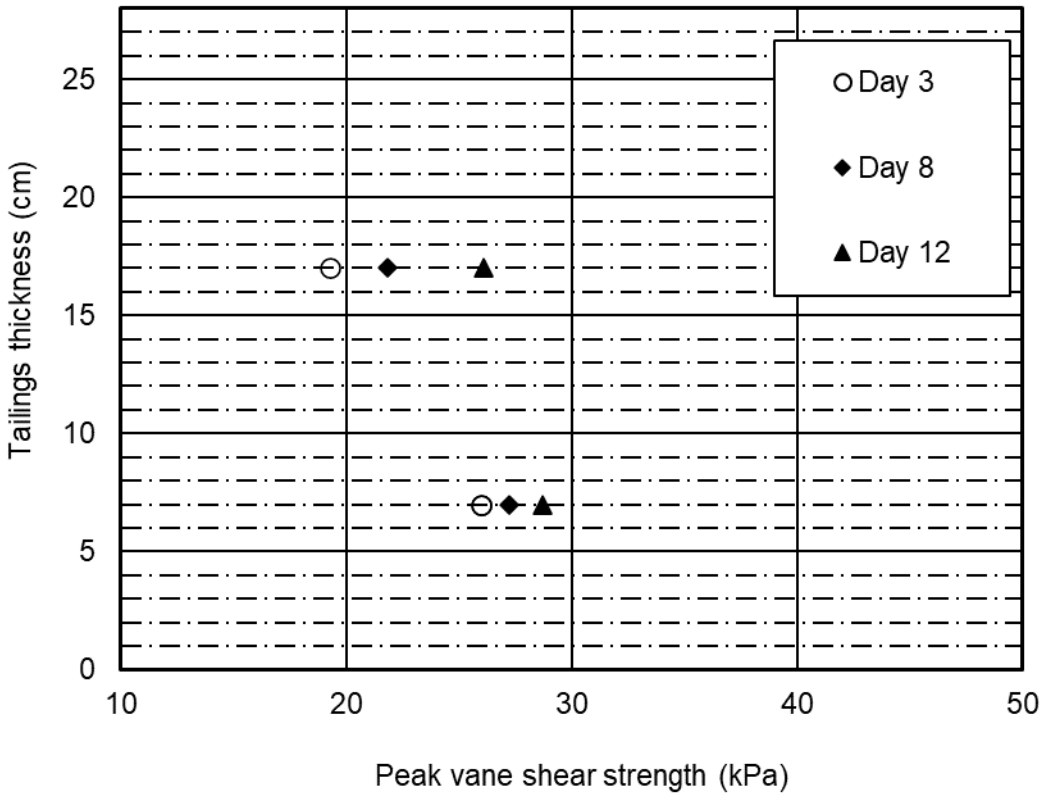

Figure 5. 51 Peak vane shear strength for the FCTC with depth and time during applied suction of 50 kPa.

5.2 Challenges encountered during laboratory testing

A number of challenges were encountered during the laboratory testing for the present study including challenges with the sensors and shear strength measuring equipment.

5.2.1 Challenges encountered during measurement from the placed sensors

A number of sensors were placed for the experimental work. Challenges encountered during the measurement for a given type of sensor are presented in this section.

5.2.1.1 Regulator to control the applied suction at the column base

The regulator used to control the applied suction to the column apparatus during the initial stage of the consolidation process (i.e., 10 kPa) was not properly functioning. The applied suction did not maintain a constantly set value (i.e., 10 kPa) for the duration of the test. The set values were dropped repeatedly until the malfunctioning regulator was replaced and tests were completed with a regulator capable of finer control. Measured suction values with time in arithmetic scale are presented in the results section.

5.2.1.2 Sensor for positive pore pressure measurement

The positive pore pressure measuring transducer responded well during the self-weight consolidation, but only for a limited time during the applied suction tests.

The positive transducer sensor did respond during the consolidation tests with applied suction and was used as an indicator to track the change in pore pressure within the tailings profile. The measurements from the positive pressure transducers were used to follow the change in pore pressure in the absence of suction measurements from the negative pore pressure sensors. It was essential to apply caution during the use of measured positive pore pressure values to understand the ongoing pore pressure process during the second phase of the consolidation process.

5.2.1.3 Negative pore pressure sensor

The negative pore pressure sensors did not respond during the early stage of the consolidation using applied suction. Additional negative pore pressure sensors were placed to track the change in negative pore pressure (suction) as it developed within the tailings profile.

In general, three negative pore pressure sensors were placed in each column apparatus. One sensor from each column was responding during the latter stage of the test. Using the controlled applied suction at the base as an anchor and the suction measured near the surface of the tailings, the developed suction along the profile was constructed.

Estimation for the column's mid-section suction were based on the fixed applied suction at the base, and measured suction near the surface of tailings.

5.2.1.4 Volumetric water content measuring sensor

Each column was supplied with two volumetric water content sensors. The volumetric water content measuring sensor responded from each column and provided the volumetric water content for the deposited tailings profile. However, the data measured were adjusted using raw data and back checking with numerical modelling results. The volumetric water content data were not used during the analysis.

5.2.1.5 Change in vertical and volumetric strain using measurement and visual observation

The vertical and volumetric strain determination was conducted using an average estimation of the change in vertical and lateral deformation which was guided using the height scale attached on the outside wall of the column apparatus. It is possible that minor errors were incorporated during the estimation of lateral deformation from the surface and along the depth. The estimation of volumetric strain was completed through measurements and visual assessment of the change in volume of the deposited tailings, both from the surface and along the perimeter depth of the column.

The profile of effective stress was formed based on change in total density from the settlement and change in applied suction from increments and evaporation. Estimation of total density within the profile were calibrated and back-checked using numerical model as a tool to compare the output for total stress with the measured total stress values and +/- 2% error was observed. Assumed values of suction was given for the mid-section of the column with time that ranges between the fixed applied suction at the base and measured suction values near the tailings surface; a +/- 10% error was assumed for the suction values. Effective stress values were calculated based on the total stress and assumed ranges of suction over time; roughly an overall +/-12% error is expected for the effective stress calculation.

5.2.2 Challenges encountered during measuring vane shear strength

This section presents the challenges encountered during the shear strength of tailings measurement using the vane shear measuring equipment.

5.2.2.1 Encounter minor obstructions placed within the deposits

Limited malfunctions were encountered during the vane shear measurement showing an abnormal value that did not follow the normal pattern. A possible explanation for the irregular records is that the inserted vane instruments became entangled with other wires and sensors. This led to the reporting of unpredicted values. These tests were repeated to resolve the observed issues on a case-by-case basis using judgment.

5.2.2.2 Encounter with disturbed tailings as experimental testing progressed

The positioning of the vane shear strength instrument frequently aligned within limited grid spaces while testing the undrained shear strength of the tailings given the diameter of the column and

vane instruments used (i.e., three vane blades). As testing progressed, the tailings continued to show signs of disturbance on the surface on the specified grid localities, particularly for the higher applied suction values. It is important to note that some of the vane shear strength measurements were conducted on disturbed elements of tailings (unhealed from previously disturbed shear tests). Some unreliable results were observed during the testing on the aforementioned grid spaces. Therefore, the observation led to a need to repeat some of the tests deemed as essential through checking the obtained values in comparison to the results obtained from previous tests with respect to tailings thickness (depth) and time for a given material. The unreliable values were witnessed at the later stage of the consolidation process using suction, particularly during the applied suction between the ranges of 40 kPa to 60 kPa.

CHAPTER SIX: ANALYSIS AND INTERPRETATION OF TEST RESULTS

6.1 Introduction

This chapter presents the analysis and interpretation of the results presented in Chapter 5. The chapter is organized as follows: i) material characterization analysis, ii) sedimentation/self-weight consolidation analysis, iii) analysis of consolidation using applied suction, and iv) modelling of flocculated FFT and flocculated centrifuged tailings cake (FCTC).

In each subsection the measured index properties and engineering properties for the given tailings are described. The results are then compared with results from the literature.

Modelling was done to assess if numerical tools can replicate measured results. This section includes a brief description of the model and material properties used, the initial and boundary conditions, modelling outputs, analysis and interpretation of the outputs in relation to measured results, and a discussion and recommendations.

6.2 Material characterization

Geotechnical index properties, geotechnical behaviour, settling column test results, unsaturated soil properties, and consolidation properties for both flocculated FFT and FCTC were compared with those reported in the literature. This is described below.

6.2.1 Geotechnical index properties

A summary of the geotechnical index properties for flocculated FFT and FCTC were presented in Table 5.1. Those from the literature are summarized and compared to the results in Chapter 5 in Table 6.1 and Table 6.2.

Flocculated FFT

Figure 5.1 shows the flocculated FFT consists of 15% fine sand, 45% silt, and 40% clay particles. The index properties of flocculated FFT were compared with the index properties of fluid fine tailings reported in the literature. Table 6.1 summarizes the geotechnical index properties for flocculated FFT from the present study and values reported in the literature.

Table 6. 1 Comparison of geotechnical index properties between flocculated FFT used in the present study and fluid fine tailings reported in the literature (modified after Yao, 2016).

Property Index	Flocculated FFT (present study)	MFT: Yao (2016)	Jeeravipoolvarn (2005)	Gholami (2014)	Suthaker (1995)	Rima (2013)
Solids content (%)	38	32	30	36	30	29
Bitumen content (%)	2.57	1.3	3	-	6	-
Specific gravity, G_s	2.2	2.3	2.28	2.2	2.1	2.36
Total density (kg/m^3)	-	1210	1280	-	-	-
Liquid limit (%)	42	55	44-53	45	47	55
Plastic limit (%)	30	28	21	19	20	25
Plasticity index (%)	12	27	23-32	26	27	30
Fines content (%)	80	91	93	93	92	92
Clay content (%)	40	48	48	46	55	53

The flocculated FFT from the present study had a solids content similar to tailings reported by Gholami (2014). The specific gravity summarized in Table 6.1 gives comparable values between all materials listed in the table and the flocculated FFT. The fines content for the flocculated FFT used in this study was 10% lower than the values reported in the literature. The liquid limit (LL) of flocculated FFT in this study was comparable to that reported by Gholami (2014), Suthaker (1995), and Jeeravipoolvarn (2005). The flocculated FFT and tailings from Yao (2016) had similar plastic limit values, and both were higher compared to the literature summarized in Table 6.1.

Flocculated centrifuged tailings cake (FCTC)

The FCTC consisted of 52% clay particles and 35% silt particles as shown in Figure 5.2. The total fines content for the FCTC was 87%. The index properties of FCTC were compared with the index properties of thickened tailings reported in literature and results are summarized in Table 6.2.

The solids content, specific gravity, and bitumen content for the FCTC were comparable with the tailings identified as “TT” reported by Innocent-Bernard (2013). The FCTC consisted of greater total fines and clay content than values reported in the literature. A 30% difference in total fines content was observed between the FCTC and the values from the literature. Note that while the FCTC and TT had similar properties, they were created differently (see Chapter 2, section 2.1).

Table 6. 2 Comparison of geotechnical index properties between the FCTC used in the present study and thickened tailings (TT) or inline thickened tailings (ILTT) reported in the literature (after Yao, 2016).

Property Index	FCTC (Schafer, 2018, Rima, 2018, present study)	TT: Yao (2016)	TT: Innocent-Bernard (2013)	TT: Jeeravipoolvarn (2008)	ILTT: Jeeravipoolvarn (2010)
Solids content (%)	55	35	52	39	-
Bitumen content (%)	0.37	2	0.33	1.8	-
Specific gravity, G_s	2.48	2.3	2.55	2.44(2.28)*	2.46
Void ratio, e	2.01	5	2.2	-	-
Liquid limit (%)	57	50	31	35(57)	66
Plastic limit (%)	26	22	11	16(27)	23
Plasticity index (%)	31	22	20	19(30)	43
Fines content (%)	87	28	52	54(100)	55
Clay content (%)	40	14	14-25	22(39)	4
SFR_{44}	-	0.44	0.9	0.85	0.82

*Parameters presented within bracket are measured on the fines portion of tailings (i.e., < 44 micron) (Yao, 2016).
** SFR_{44} – sand to fines ratio, < 44 micron is fines content.

6.2.2 Geotechnical behaviour of tailings

The geotechnical properties of oil sands tailings are commonly characterized using the ternary diagram developed by Scott and Cymerman (1984). The typical and alternate ternary diagram layouts are presented in Figure 6.1(a) and Figure 6.1(b). The ternary diagram consists of three apexes, namely vertical, left, and right corners representing 100% water, 100% sand, and 100% fines, respectively. The ternary diagram was used to provide the baseline properties of tailings used during the present study.

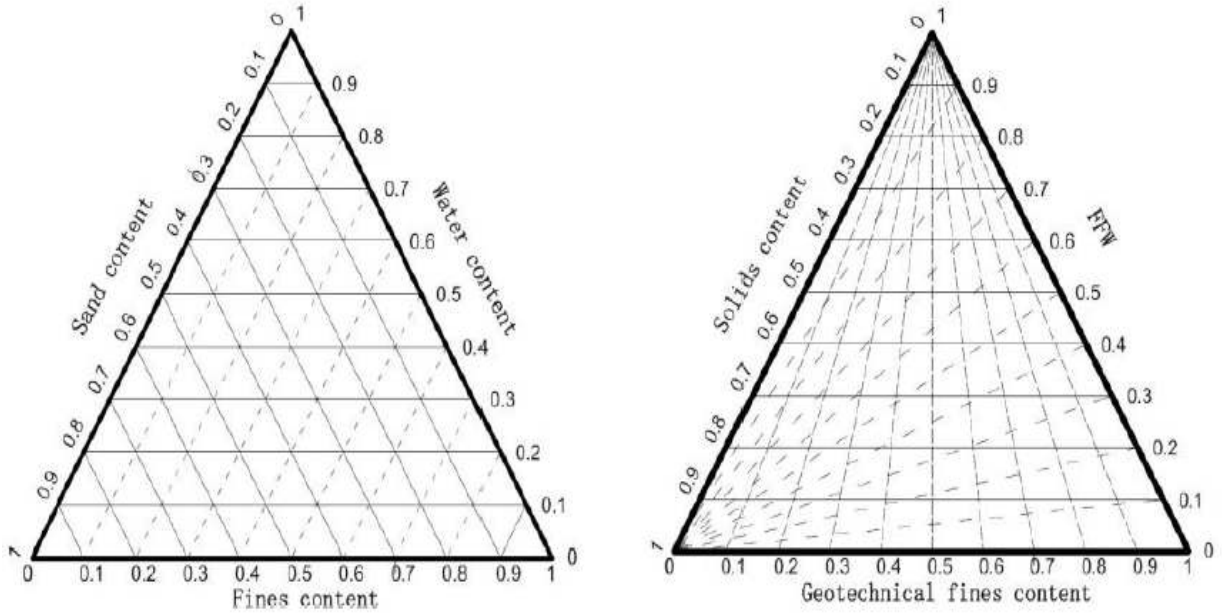

(a) (b)

Figure 6. 1(a) Typical layout of ternary diagram; (b) ternary diagram with alternate axes (after Sobkowicz & Morgenstern, 2009).

To improve tailings settlement, the raw FFT was treated with commercially available flocculants prior to deposition in the columns. The flocculation process was completed based on procedures developed by the industry for field trial cases. Numerous characterization tests have been conducted and presented in the literature detailing different aspects of the inline flocculation process for tailings (Dunmola et al., 2014; Fisseha, Wilson, & Fredlund, 2017a, 2018; Mizani, He, & Simms, 2013). This study used the flocculated tailings to study consolidation through applied suction at the meso-scale (Chapter 4).

Sobkowicz and Morgenstern (2009) used the ternary diagram to illustrate different types of oil sands tailings and tailings products available in the oil sands industry (Figure 6.2). Properties of the flocculated FFT and FCTC used in this study are included in Figure 6.2 to compare their composition with other existing oil sands tailings.

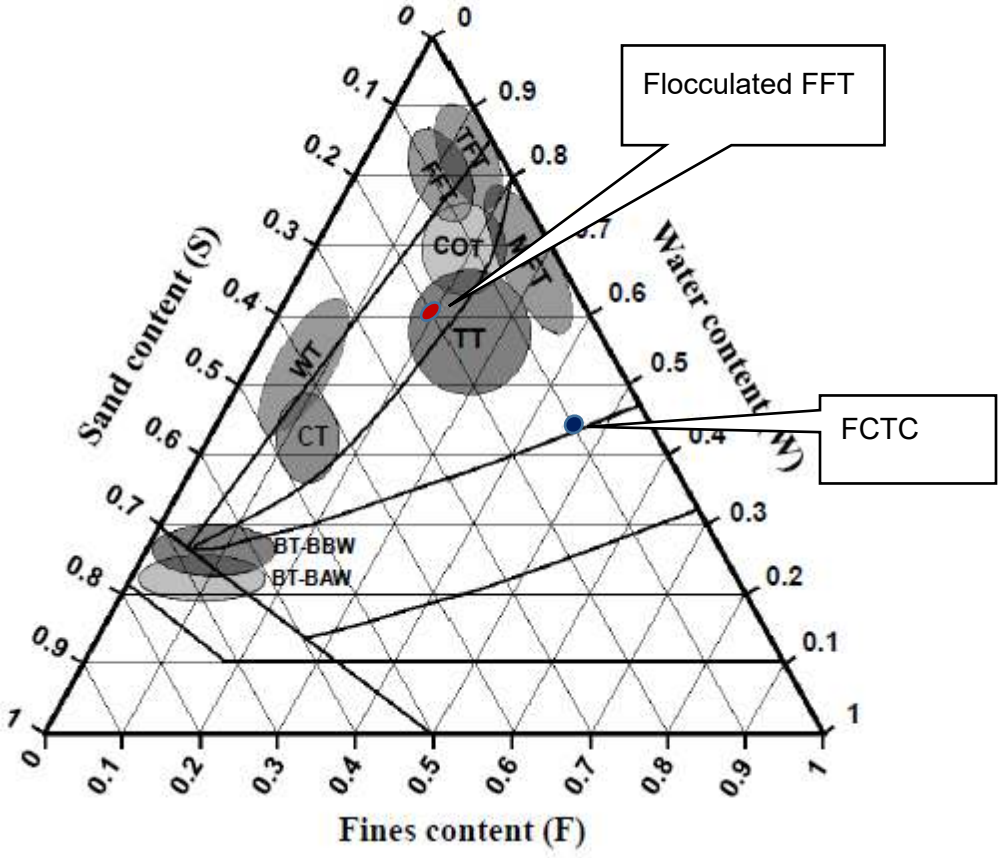

Figure 6. 2 Ternary diagram showing the composition of various oil sands tailings and tailings products (Sobkowicz & Morgenstern, 2009).

Azam and Scott (2005) plotted geotechnical boundary conditions on the ternary diagram to differentiate the tailings based on their solids and fines content. Figure 6.3 presents the ternary diagram for oil sands tailings, including the flocculated FFT and FCTC. Flocculated FFT are positioned near the non-segregating boundary close to the fluid fine tailings (FFT), while FCTC are on the non-pumpable boundary and in agreement with the observed behaviour.

The raw FFT used for the flocculated FFT were within the non-segregating boundary, as were the fluid fine tailings in the pond reported in the literature, as shown in Figure 6.3. Once the flocculated

FFT were produced through mixing the raw FFT with the flocculant solution, they exhibited non-segregating behaviour similar to the properties observed for the fluid fine tailings.

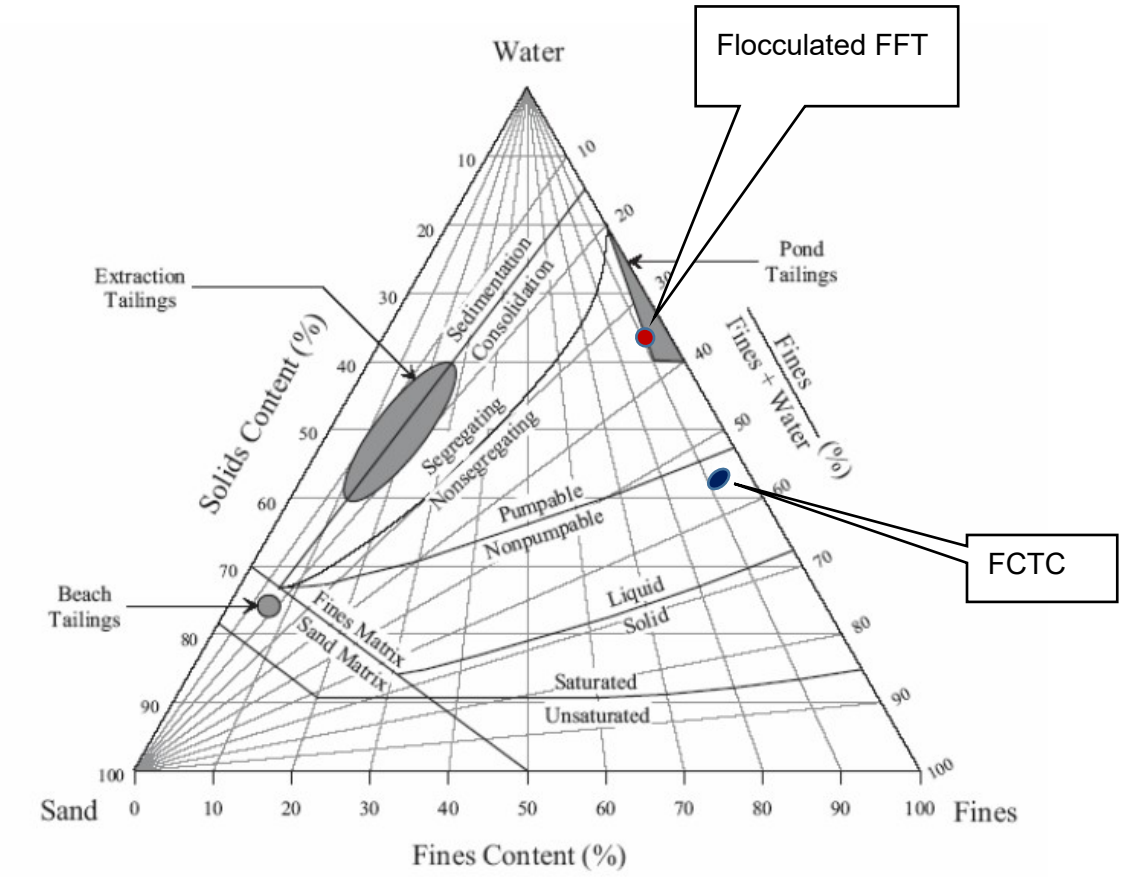

Figure 6. 3 Tailings properties diagram of oil sands tailings (modified from Azam & Scott, 2005; Jeeravipoolvarn, 2010).

The FCTC were different from the other types of tailings presented by Sobkowicz and Morgenstern (2009) (Figure 6.2). The FCTC had a higher solids content and higher fines content due to flocculation and centrifugation (Table 6.2). The FCTC can be plotted along the pumpable/non-pumpable boundary (Figure 6.3), which is in agreement with the non-pumpable behaviour observed at the laboratory.

Figure 6.4 illustrates the correlation between increased solids content and the observed geotechnical behaviours for different types of tailings. The flocculated FFT and the FCTC are shown in Figure 6.4, which illustrates their relative position based on solid content by weight with respect to the liquid limit, plastic limit, and shrinkage limit.

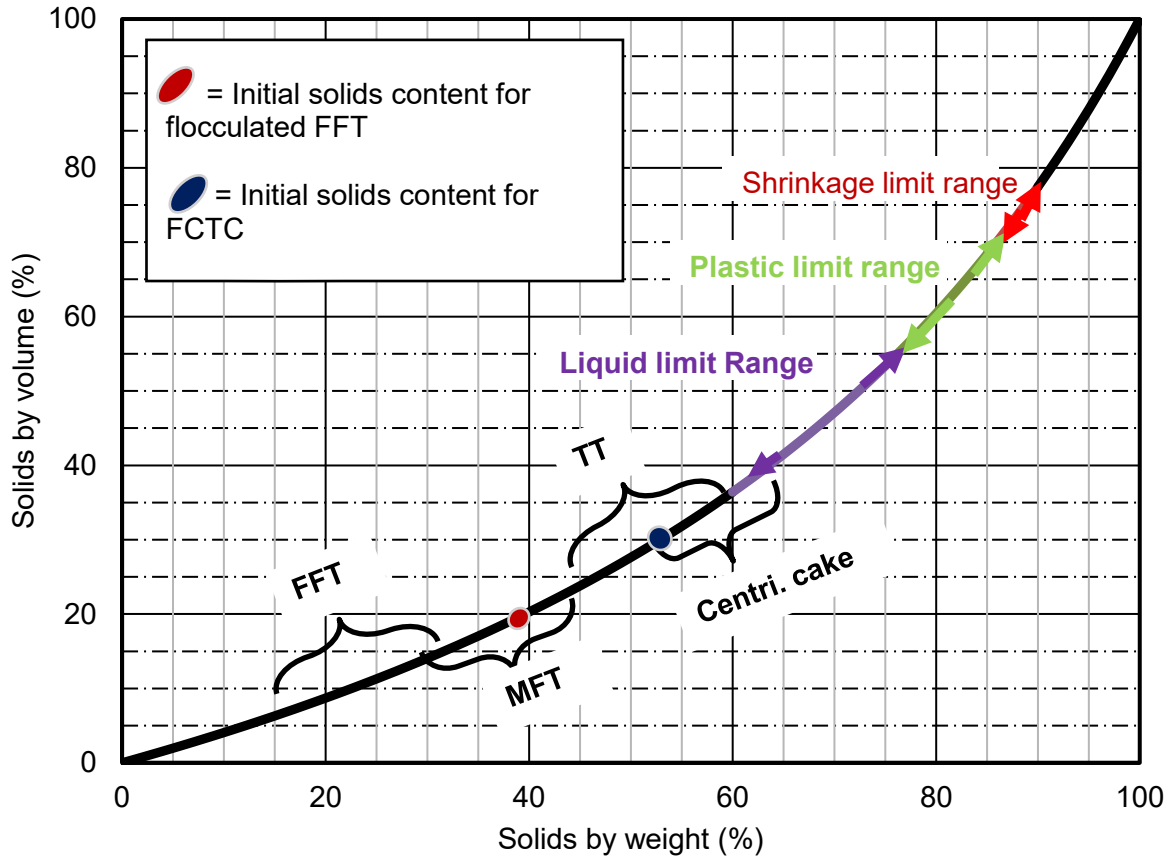

Figure 6. 4 Percentage of solids by mass versus percentage of solids by volume (modified from Fair & Beier, 2012).

The raw tailings mixture, 38% initial solids content by mass, was within the zone described by MFT as shown in Figure 6.4. Figure 6.4 describes the tailings used in relation to other available tailings technologies on the basis of resultant solids content.

The characteristics of the tailings cake (i.e., FCTC) were in agreement with the non-pumpable behaviour observed at the laboratory. The initial solids content (by mass) for the FCTC was 55%, which is below the liquid limit range defined by a shear strength of 1 to 2 kPa (Figure 6.4).

6.2.3 Settling column properties

The settling column results presented in Figure 5.3 for the flocculated FFT and in Figure 5.4 for the FCTC are discussed below. These results were compared with those of tailings with similar geotechnical properties as reported in the literature.

Flocculated FFT

The results presented in Figure 5.3 come from four separate tests prepared at different stage of the research program. A significant volume change occurred instantaneously following deposition of the tailings due to sedimentation and self-weight consolidation. Overall, slight variations in the measured settling rates were observed between the four tests. The variation in the results might possibly attributed from the composition of separate tailings batch.

Test 1 settled at a slower rate than Tests 2, 3, and 4. Tests 2, 3, and 4 demonstrated consistent settling rates with minor deviations either at the beginning or completion of the test. Variation in settling rates may be attributed to slight variations in composition from batch to batch, since each batch was prepared separately. Although effort was made to achieve a homogenous mixture, occasional variation was observed here as well as in the literature as summarized in Yao (2016). The final void ratios for Tests 2, 3, and 4 were 3.04, 3.01 (extrapolated), and 3.17. These results show consistency and repeatability between the settling column tests for the flocculated FFT.

Similar average settling rates were displayed between Tests 2 and 4, with slight variations near the start of the settling tests. The initial settling stage was slower for Test 2 than Test 4. The settling rates for Test 3 and Test 4 were the same for the initial stage lasting 17 days, followed by a slightly slower rate of settlement for Test 4 on day 29. No measurements were taken between days 17 and 29 for Test 4. The settling behaviour is assumed to show a slight curve as the tailings settled, as opposed to the straight line shown due to interpolation. Therefore, the minor differences between Test 3 and Test 4 can be partly attributed to lack of data and partly to variation in the initial batch composition. Settling column tests are used to calculate the initial hydraulic conductivity of the flocculated tailings in their initial state.

The settling column results were used to determine the duration of the self-weight consolidation test, as proposed by Imai (1981). Figure 6.5 shows the self-weight consolidation time for the flocculated FFT. The results from the settling column test were extrapolated to complete the curve after day 95 towards infinitesimal settlement. Therefore, the self-weight consolidation process was finalized by day 102 and the next stage of testing had commenced. The average hydraulic conductivity from the settling column test was determined to be $k = 3.42E\text{-}07$ *m/sec.*

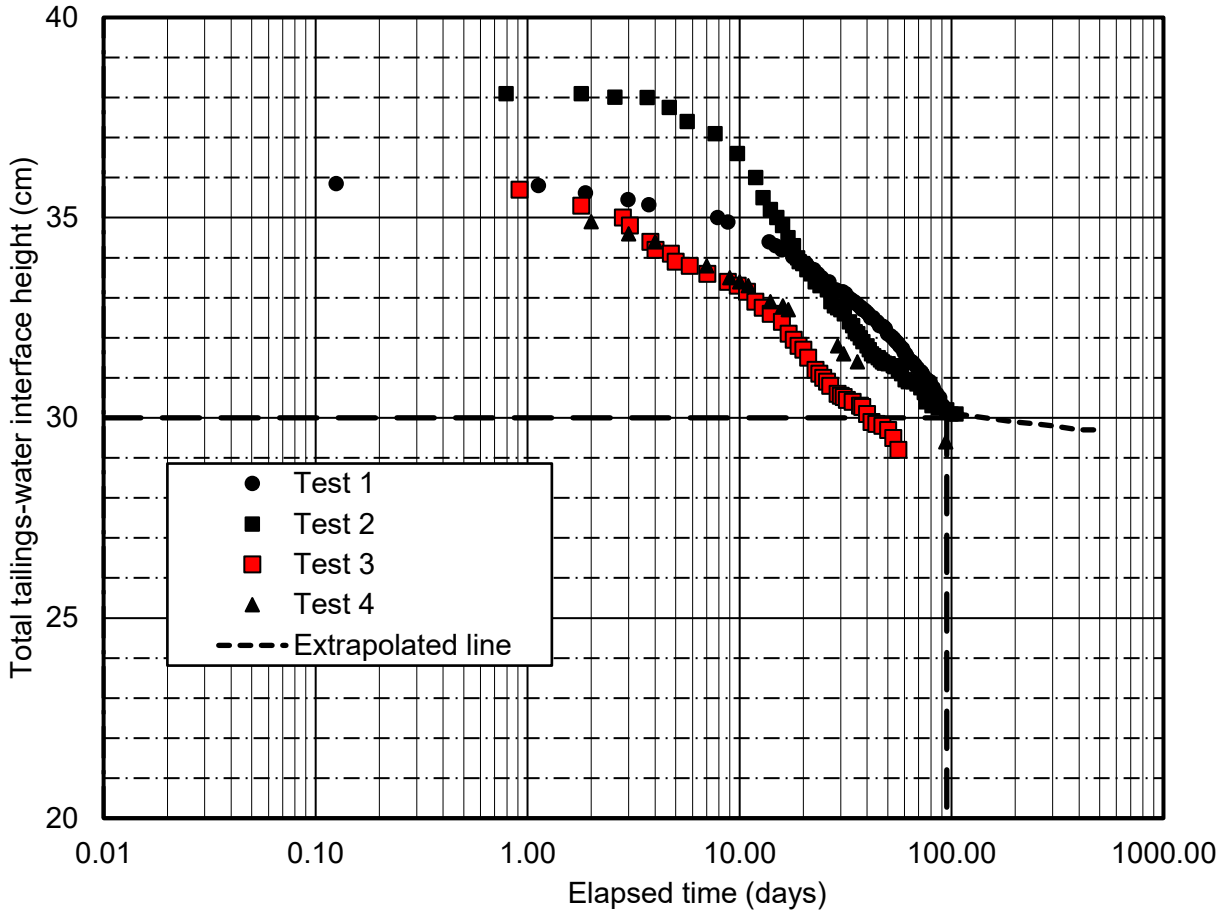

Figure 6. 5 Determination of self-weight completion using the method proposed by Imai (1981).

Flocculated centrifuged tailings cake (FCTC)

The settling column test results for the FCTC are presented in Figure 5.4, showing no significant settlement. The total height change of tailings (i.e., change in void ratio) shown in Figure 5.4 is assumed to be due to the fabric meshing of the tailings over a longer time. The FCTC was deposited by manually scooping the tailings into the meso-scale column apparatus. It is assumed the individual scoops required some time for the soil fabric to mesh together. It is believed that

the longer the tailings were left within the column, the more the tailings became a continuous fabric. In general, no settlement was observed for Test 1 and Test 2 for the FCTC.

The centrifugation process which produced the FCTC plays a significant role in modifying the engineering properties compared to the properties of fluid fine tailings. For instance, it is well documented that fluid fine tailings take longer to settle and consolidate. On the other hand, the FCTC exhibited no self-weight consolidation or settlement behaviour.

6.2.4 Unsaturated soils properties

The characterization tests included the determination of unsaturated soil properties for the flocculated FFT and FCTC. The results of the soil-water characteristic curve (SWCC) and shrinkage curve (SC) are discussed below and compared with values reported in the literature for various types of tailings.

6.2.4.1 Soil-water characteristic curve (SWCC)

The SWCC and shrinkage curve results were presented in Figure 5.5, 5.6, 5.7, and 5.8 for the flocculated FFT and FCTC tailings below. The measured results are discussed and compared with SWCC results for fluid fine tailings reported in the literature.

Flocculated FFT

Figure 5.5 presents the measured results of gravimetric water content and matric suction of SWCC for flocculated tailing of two test samples, namely Test 1 and Test 2. The degree of saturation with matric suction was computed and is presented in Figure 5.5. The degree of saturation was the same for Test 1 and Test 2, therefore only one data set is presented.

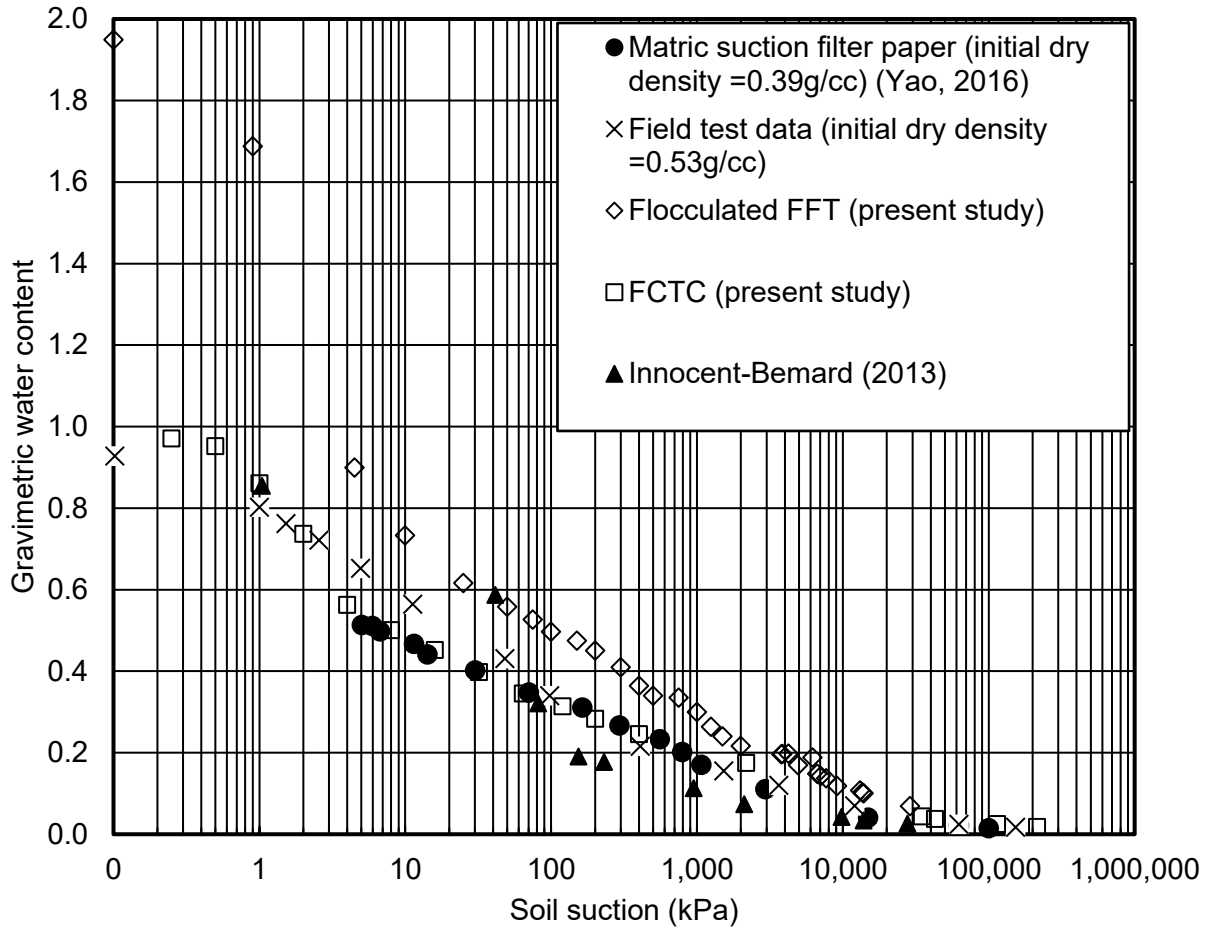

Figure 6. 6 Comparison of SWCC between FFT from the literature and the present study. (Modified from Yao, 2016).

The results from the SWCC were compared with results published in the literature for similar flocculated FFT (Yao, 2016; Owolagba & Azam, 2014). The measured air-entry value (AEV) was 200 to 250 kPa compared to 300 kPa reported by Yao (2016). It essential to note that determination of the AEV in the present study used consideration and corrections depicted by the principles shown for high volume change materials (Zhang, 2016). The minor variation between the measured and literature-reported AEV can be possibly explained by the inclusion of principles of high volume change materials for the present study from Zhang (2016) described as the “true AEV,” which were not considered by Yao (2016).

The SWCC for flocculated FFT was in agreement with the FFT SWCC results from the literature in the residual suction range. However, there was a notable difference in initial water content between the flocculated FFT and the flocculated tailings from the literature (Yao, 2016; Owolagba & Azam, 2014). The flocculated FFT had an initial water content of 190% compared to 95% reported in the literature by Yao (2016). The flocculated FFT undergoes a large volume change, which needs to be incorporated into the SWCC characterization. The effect of this volume change and the "true AEV" concept has been previously discussed by (Zhang, 2016) (see Chapter 2). Figure 6.7 compares the SWCC for flocculated FFT with that reported in the literature for FFT mixed with sand Yao (2016). The literature results reported in Yao (2016) had a SFR (sand to fine ratio) of up to 0.1. Similarly, larger changes were observed for the small suction range and the suction higher than 1000 kPa showed agreement. The flocculated FFT and FFT mixed with sand exhibited a similar trend for residual suction.

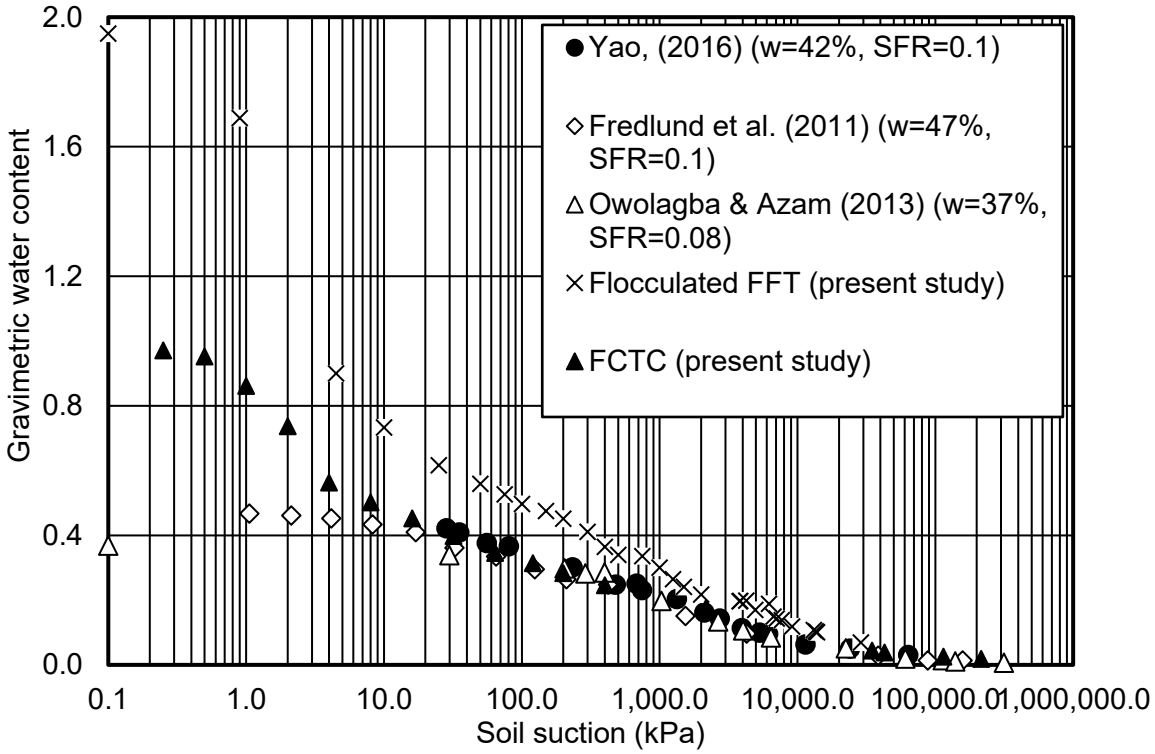

Figure 6. 7 Comparison of SWCC between TT from the literature (Innocent-Bernard, 2013; Yao, 2016) and FCTC (present study).

Flocculated centrifuged tailings cake (FCTC)

The SWCC results are presented using both gravimetric moisture content and degree of saturation in relation to the applied matric suction in Figure 5.6. The AEV was 200 kPa. The AEV provides the initial desaturation point for a material. The FCTC had a lower hydraulic conductivity compared to flocculated FFT due to a greater fines content. The FCTC were expected to have a higher AEV than the flocculated tailings; however, the characterization test results depicted the opposite result. In addition, the higher fines content of the FCTC generated a higher AEV than the AEV for the flocculated FFT. The correction factor to include the “true AEV” was not applied to the plot of degree of saturation and suction for the FCTC. As such, there was no high-volume change observed for the FCTC.

Figure 6.6 presents a comparison between the SWCC results for the FCTC and other flocculated fluid fine tailings reported in the literature. The FCTC data show strong agreement with reported field test data. The SWCC results for FCTC were also compared with SWCC results for FFT mixed with SFR up to 0.1, as presented in Figure 6.7. The FCTC had a higher gravimetric water content over the smaller suction range compared to results from the literature (Innocent-Bernard, 2013; Yao, 2016). The FCTC SWCC results above 20 kPa are in agreement with those of the FFT mixed with SFR of 0.1.

6.2.4.2 Shrinkage curve (SC)

The shrinkage curve results were presented in Figure 5.7 and Figure 5.8 for both flocculated FFT and FCTC, respectively.

Fredlund et al. (2002) noted that the composition of a material (i.e., grain size distribution) and its stress history defines the properties and pattern of its shrinkage curves (such as minimum void ratio, slope of the curve, and air entry point).

Flocculated FFT

The shrinkage curve for the flocculated FFT and results reported by Yao (2016) are presented in Figure 6.9. The final void ratios presented as a shrinkage limit for the flocculated FFT were 0.71 and 0.65 for Test 1 and Test 2, respectively, and the final void ratios reported by Yao (2016) were 0.54 to 0.7 (Figure 6.8).

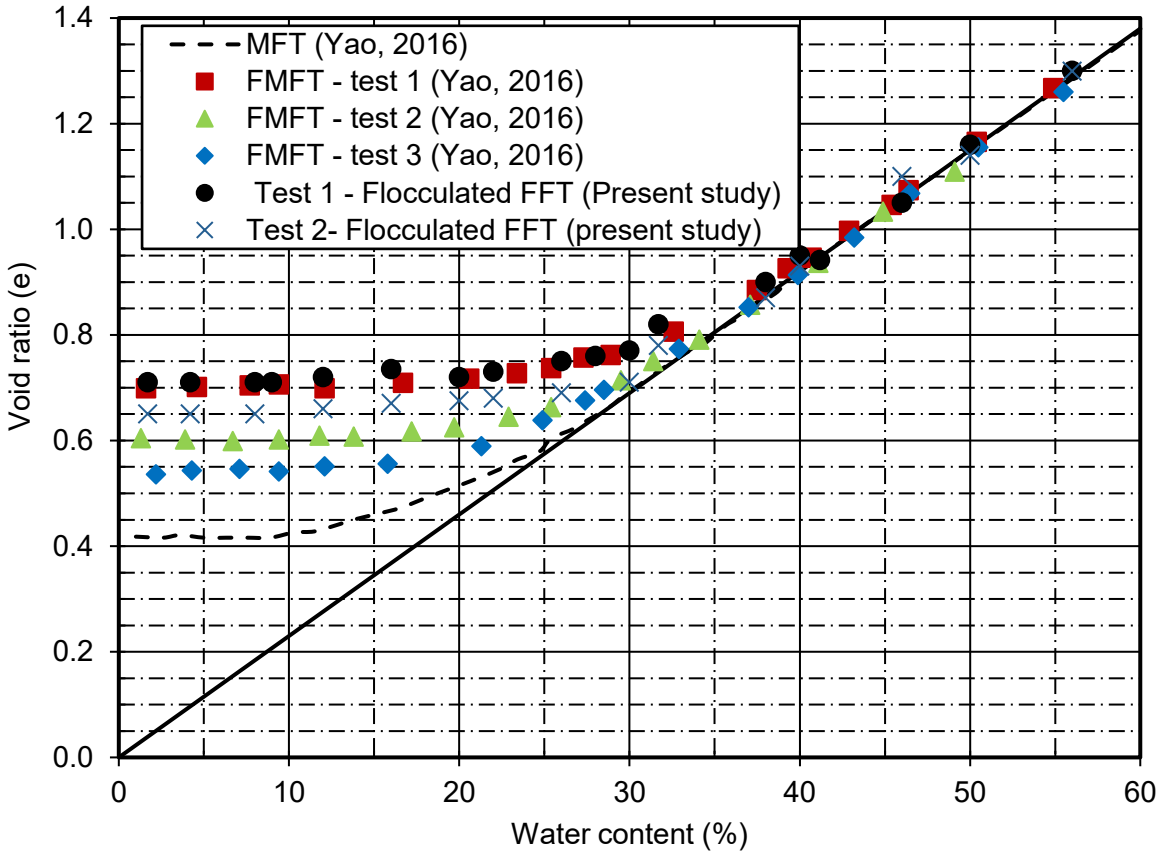

Figure 6. 8 Comparison of shrinkage curves for flocculated FFT reported in the literature (modified from Yao, 2016).

The shrinkage of non-treated fluid fine tailing is also presented in Figure 6.8 as indicated by the dark dashed line. The untreated tailings displayed a lower void ratio upon drying compared to the flocculated tailings. The change in the shrinkage curve that resulted between the non-treated and flocculated tailings was attributed to the flocculation of fines. The chemical properties of the flocculent used can be found in the literature and are not within the scope of this research.

Flocculated centrifuged tailings cake (FCTC)

The shrinkage curve for the FCTC (present study, Schafer, 2018) displayed consistent and repeatable void ratios between 0.48 and 0.51. A comparison for the FCTC and the flocculated FFT shows lower void ratio for the FCTC. The SC results for FCTC were in agreement with those reported by Owolagba and Azam (2014) and Yao (2016) as presented in Figure 6.9.

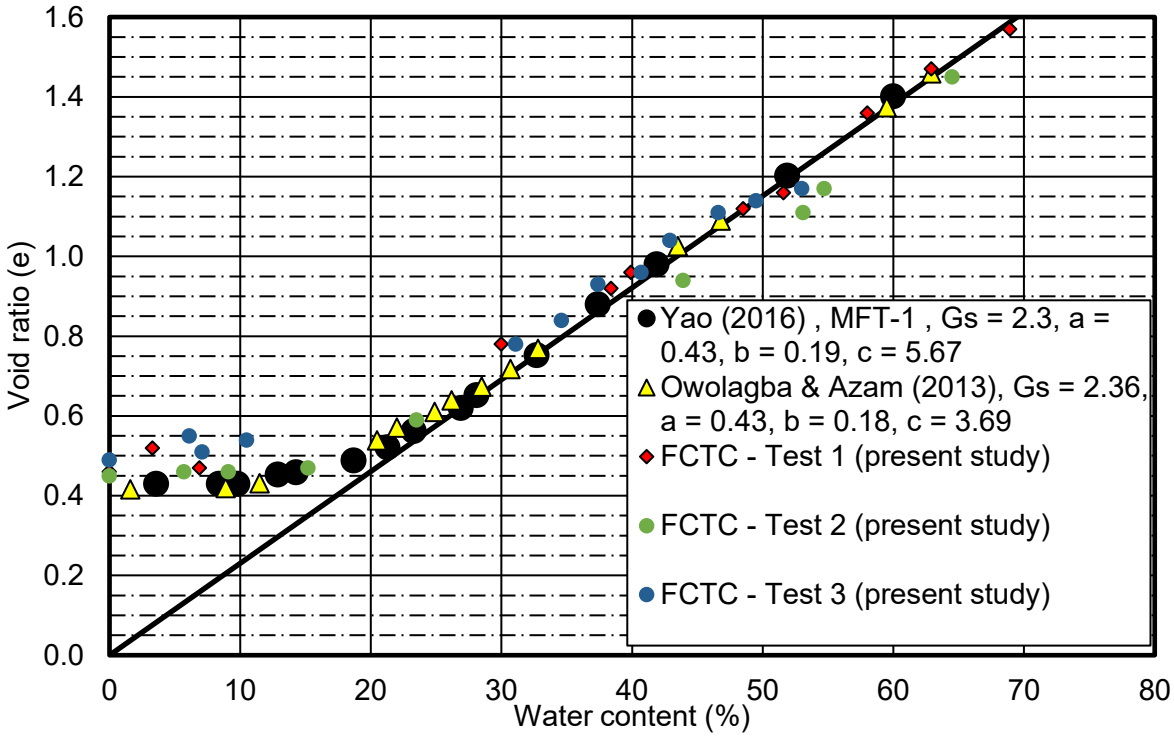

Figure 6. 9 Comparison of shrinkage curves between FCTC and those reported in the literature (modified from Yao, 2016).

The shrinkage curve results of the flocculated FFT and FCTC are presented in Figure 6.10. The results of flocculated FFT displayed greater volume change compared to FCTC. The final average void ratio shows 0.42 and 0.5 for the flocculated FFT and FCTC respectively as presented in Figure 6.10.

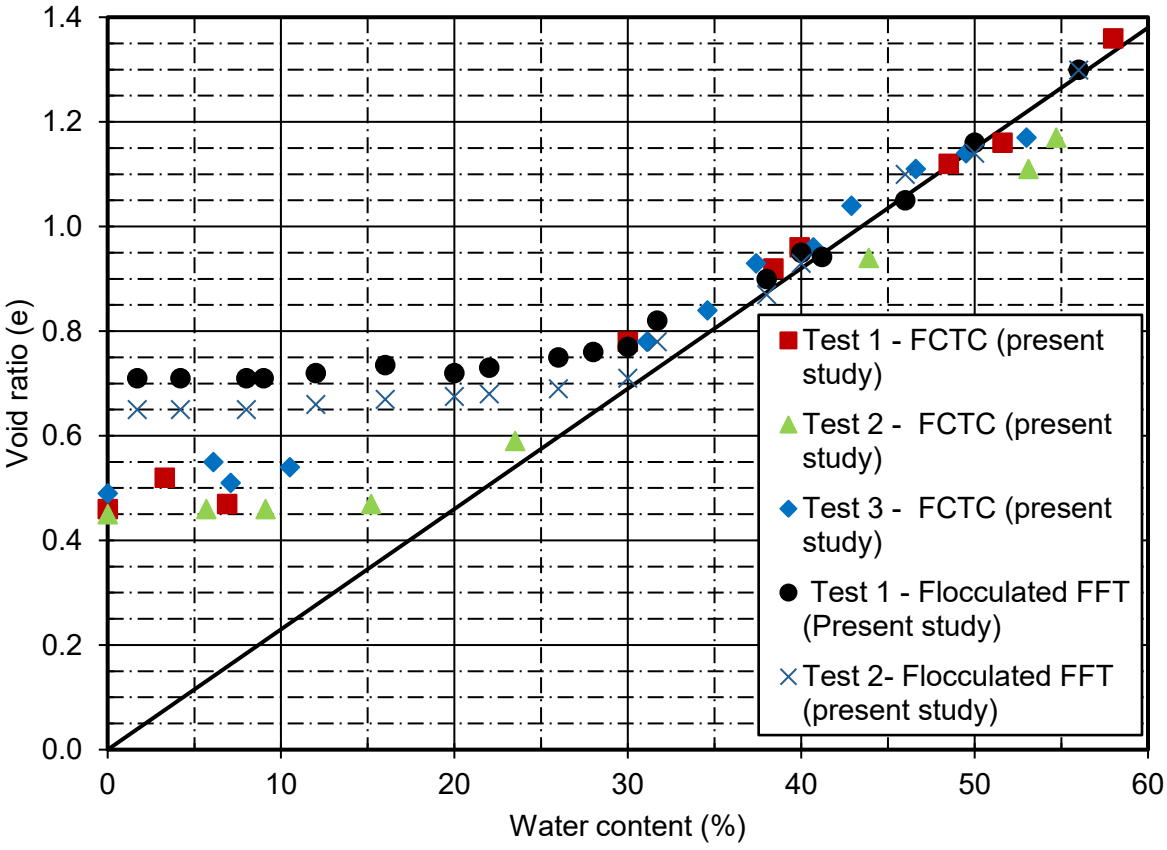

Figure 6. 10 Comparison of shrinkage curves between Flocculated FFT and FCTC used for the research program.

6.2.5 Consolidation properties

The consolidation properties of the tailings were expressed using the compressibility and hydraulic conductivity curves. These compressibility curves define the relationship between the applied effective stress and the void ratio. The hydraulic conductivity curve is defined using a relationship between hydraulic conductivity and void ratio.

6.2.5.1 Compressibility curves

The compressibility results for the flocculated FFT and FCTC obtained using multi-step loading with a large-strain consolidation (LSC) testing apparatus are presented in Figure 5.9 and Figure 5.10, respectively. The compressibility results are discussed and compared with results reported in the literature (Jeeravipoolvarn, 2010; Fisseha, Wilson & Simms, 2018).

Flocculated FFT

The compressibility curve results showed an initial void ratio of 4.1 and final void ratio of 1.28 at a corresponding effective stress of 200 kPa for the flocculated FFT. The initial void ratio for the flocculated FFT prior to the process of self-weight consolidation was 4.1, and this changed to 3.2 following consolidation. The compressibility curve was fit using the power function in Eq. [6.1] and summarized in Table 6.3.

$$e = 2.278\ x\ \sigma'^{-0.11} \qquad \text{Eq. [6.1]}$$

where

e = void ratio and,

σ' = effective stress, *kPa*.

The compressibility curve from the present study and from Fisseha, Wilson and Simms (2018) are presented in Figure 6.11. The differences in the initial void ratio between the present study and the flocculated FFT using different flocculent dosages (Fisseha, Wilson & Simms, 2018) possibly attributable to the composition of the tailings. The tailings in the present study were

composed of 40% clay, 45% silt and 15% fine sand, while those studied by Fisseha, Wilson and Simms (2018) had 40% clay, 50% silt and 10% fine sand.

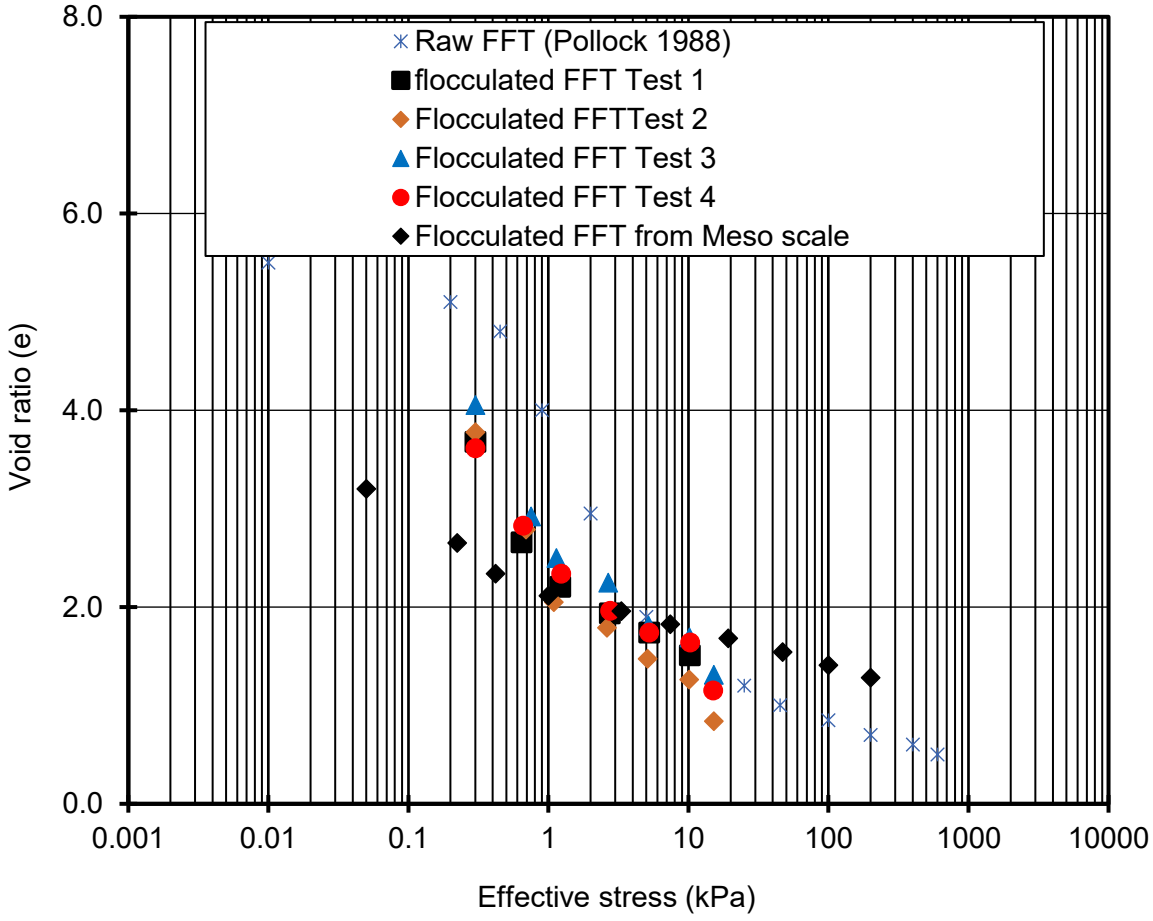

Figure 6. 11 Measured compressibility results from multi-step loading of LSC testing apparatus for the flocculated FFT (tailings flocculated with different dosages and raw tailings).

The LSC test using the flocculated FFT with various flocculent dosages was completed to a surcharge load of 15 kPa, and a surcharge load of 200 kPa for the flocculated FFT was applied during the present study. The results obtained from the present study and the flocculated FFT using various flocculent dosages provide compressibility data values for the first 15 kPa. The data points between applied surcharge loads of 15 kPa to 200 kPa displayed a roughly parallel slope

with the data points for raw FFT (Pollock, 1988). The difference is possibly due to the effect of flocculation used to facilitate the aggregation of fines.

Table 6. 3 Summary of compressibility curve reported in the literature (after Yao, 2016).

Author (year)	e_0	Equipment used for measurement	Fitting function
Pollock (1988)	5.1	Slurry consolidometer	$e = 3.38 \times \sigma'^{-0.309}$
Proskin (1998)	5.4	Slurry consolidometer	$e = 2.71 \times \sigma'^{-0.278}$
Znidarcic (2011)	4.6	Seepage induced test	$e = 3.27 \times (\sigma'+0.074)^{-0.279}$
Gan (2011)	4.9	Slurry consolidometer	$e = 3.12 \times \sigma'^{-0.208}$
Estepho (2014)	5.2	Seepage induced test	$e = 3.00 \times (\sigma' + 0.035)^{-0.177}$
Fisseha (2018) (Flocculated FFT)	4.1	Step-loading LSC	$e = 2.278 \times \sigma'^{-0.11}$
Fisseha (2018) (FCTC)	2.01	Step-loading LSC	$e = 1.714 \times \sigma'^{-0.139}$

Table 6.3 summarizes selected compressibility values reported in the literature (Yao, 2016). The fluid fine tailings measured by Pollock (1988), Proskin (1998) and Estepho (2014) show a higher initial void ratio compared to the flocculated FFT. The results presented by (Znidarcic, Miller, van Zyl, Fredlund, & Wells, 2011) and Estepho (2014) used different testing equipment than the slurry consolidometer or multi-stage loading large-strain consolidometer used in the present study.

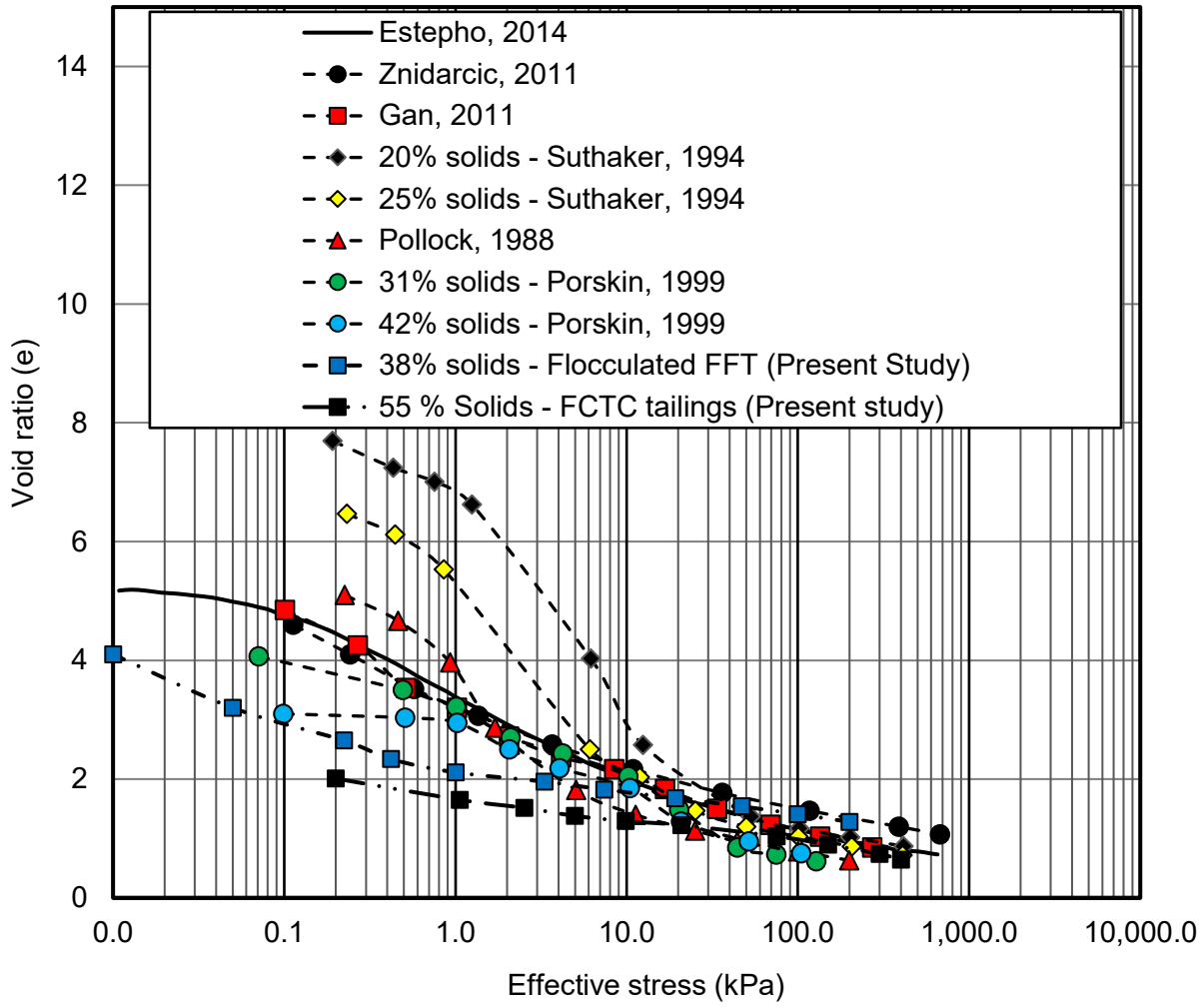

Figure 6. 12 Compressibility curves for different samples of fluid fine tailings reported in the literature compared with the flocculated FFT and FCTC of the present study (after Yao, 2016).

Figure 6.12 presents a summary of compressibility curves from the literature and the present study. The flocculated FFT (solids content, 38%) results are closer to the results reported by Proskin (1998), with solids content of 42%. The two curves fall closely on the plot as presented in Figure 6.12.

Figure 6.13 compares the compressibility curve for the flocculated FFT with that of different mine tailings. Coal, gold, and copper tailings show a flatter and more linear relationship between the effective stress and void ratio compared to the fluid fine tailings from oil sands industries.

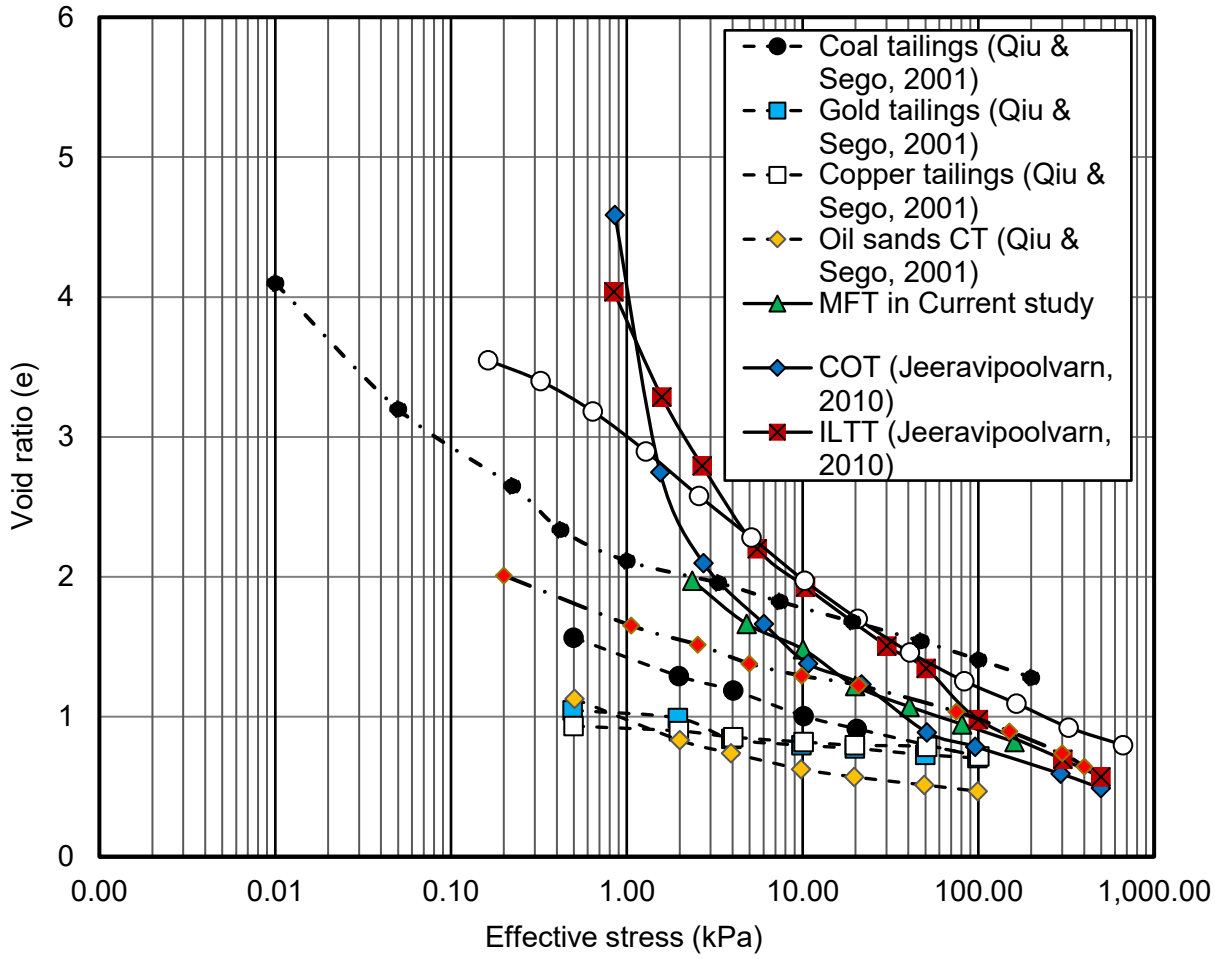

Figure 6. 13 Comparison of compressibility curves of different mine tailings reported from the literature (after Jeeravipoolvarn, 2010; Yao, 2016).

Flocculated centrifuged tailings cake (FCTC)

The compressibility curves show an initial void ratio of 2.01 and final void ratio of 0.64 at a corresponding effective stress of 400 kPa for the FCTC. The compressibility curve is best fit using the power function presented in Eq. [6.2] and summarized in Table 6.3.

$$e = 1.714\ x\ \sigma'^{-0.139}$$ Eq. [6.2]

where *e* = void ratio and,

σ' = effective stress, *kPa*.

Table 6.3 summarizes selected compressibility values reported in the literature (Yao, 2016). The initial void ratio for the FCTC is smaller than the initial void ratios reported in the literature by Pollock (1988), Proskin (1998), and Estepho (2014). This provides a context on the engineering property of the FCTC compared to the fluid fine tailings.

6.2.5.2 Hydraulic conductivity curves

The measured hydraulic conductivity results are discussed and compared in this section for both the flocculated FFT and FCTC.

Flocculated FFT

In the present study, hydraulic conductivity values of flocculated fluid fine tailings at their initial void ratio were obtained from a settling column test. The hydraulic conductivity during consolidation can be determined using the hindered sedimentation technique; however, that method is not valid for this physical process. The hydraulic conductivity of slurry tailings and soft soils is best determined using specialized tests for slurry-type soils, such as a large-strain consolidation apparatus, slurry consolidometer, and seepage-induced test, etc.

Large-strain consolidation equipment was used for the current research and compared below with results reported in the literature. The comparison of measured results with literature values

provides a reference in terms of magnitude for the fluid fine tailings. There was a slight difference at the initial stage of the flocculated tailings' permeability test which lies within a similar trend line as the tailings compressed with applied load, as presented in Figure 6.14 and Figure 6.15.

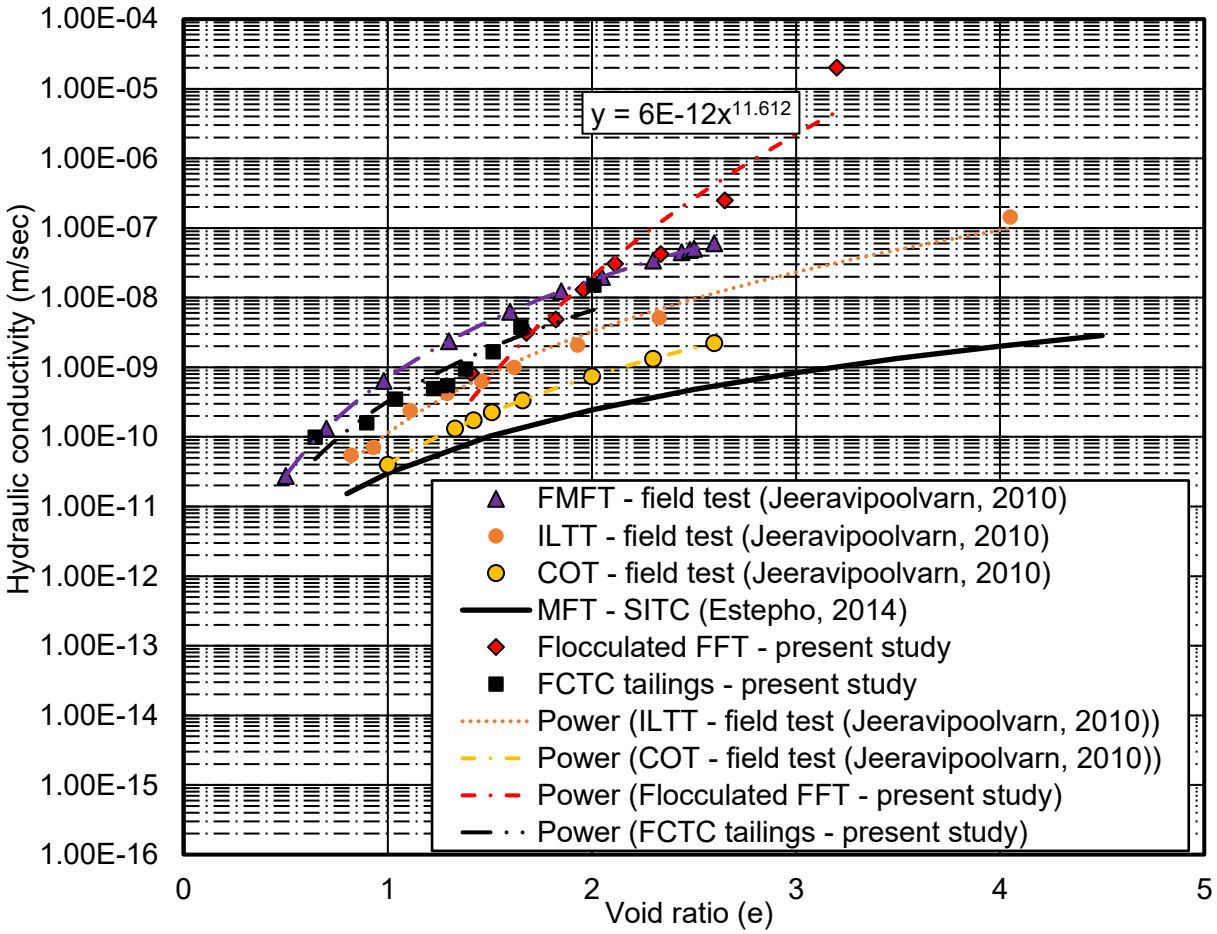

Figure 6. 14 Comparison of hydraulic conductivity between MFT, FMFT, ILTT, COT, flocculated FFT, and FCTC (after Jeeravipoolvarn, 2010; Yao, 2016).

There was a strong agreement at the lower void ratio and difference in results at its slurry stage (i.e., initial higher void ratio). The measured hydraulic conductivity in relation to the void ratio can be fit using a power or exponential function. The hydraulic conductivity result for the flocculated

FFT was fit using a power function. The relationship is expressed using the void ratio to calculate the hydraulic conductivity: k = 6E-12$(e)^{11.612}$ m/sec.

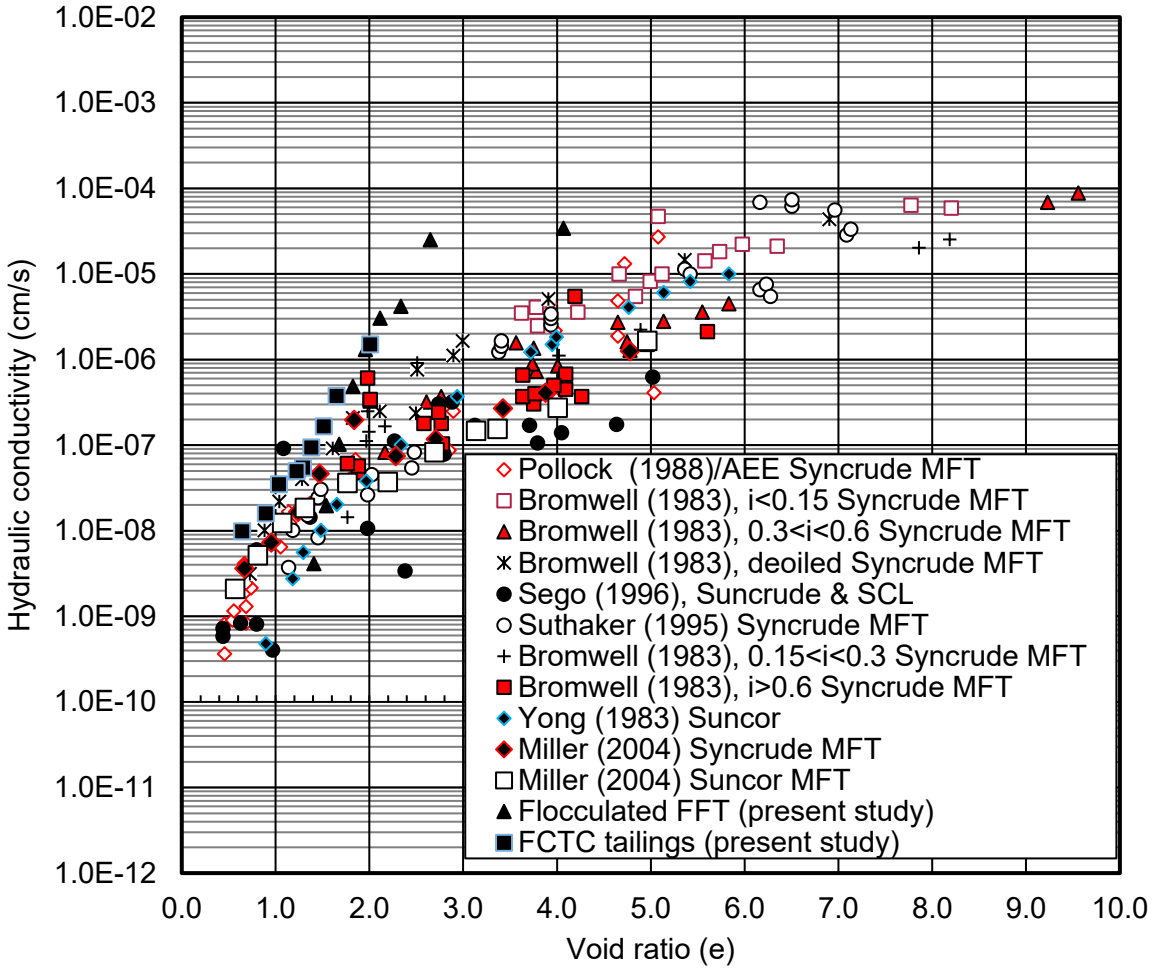

Figure 6. 15 Hydraulic conductivity of fluid fine tailings reported in the literature (after Jeeravipoolvarn, 2005; Yao, 2016).

Flocculated centrifuged tailings cake (FCTC)

The hydraulic conductivity results for the FCTC were compared with results of fluid fine tailings reported in the literature and summarized in Figure 6.14 and Figure 6.15. The FCTC had a hydraulic conductivity of 1.5E-8 *m/sec* at a void ratio of 2.01 during the initial stage, which

decreased to 1.0E-10 *m/sec* at a void ratio of 0.64 during the final test. The hydraulic conductivity results obtained for the FCTC were in agreement with results from the literature as shown in Figure 6.14 and Figure 6.15. Tailings with a high void ratio showed higher variation; however, as the void ratio decreased with compression and increased in solids content, the difference between the measured results was determined to be minor. The relationship was fit using the power function and presented in Eq. 6.3:

$$k = 3E^{-10}(e)^{4.34} \qquad \text{Eq. [6.3]}$$

k = hydraulic conductivity, *m/sec*,

e = void ratio.

6.3 Self-weight consolidation stage

The analysis and interpretation of results for the sedimentation/self-weight consolidation process from the meso-scale experimental test is presented in this section. The results are discussed and compared with results from the literature.

Flocculated FFT

The flocculated FFT tailings exhibited self-weight consolidation following placement of the tailings within the column apparatus.

The presentation of results categorized the measured results as follows: i) vertical strain or settlement, ii) excess pore pressure dissipation, iii) effective and total stress calculation, and iv) undrained shear strength.

Settlement, vertical strain, and void ratio

The vertical strain (settlement) results are presented in Figure 5.14 and Figure 5.15 in terms of vertical strain and void ratio, respectively. During the self-weight consolidation process, the measured change in volume was attributed to the change in vertical strain. The total tailings height change shows steeper slope at the early stage (i.e., for the first 30 days) in Figure 5.14 and Figure 5.15. The vertical strain continued from day 30 to day 80 with a gentle to flat slope. The total settlement is expressed in terms of the void ratio as presented in Figure 5.15. The evolution of the void ratio during self-weight consolidation began at an initial void ratio, e_0, of 4.1 and reached a void ratio of 3.2 by day 30 before arriving at the final void ratio, e_f, of 2.88 by day 80. An extended period was allowed for the self-weight consolidation process to ensure full dissipation of excess pore pressure within the deposits.

A comparison between the observed settlement from the column settling test (using a 1000 ml graduated cylinder) and the self-weight consolidation from the meso-scale test indicates the final void ratio of 3.0 (Test 2 and Test 4) for the settling test and 2.9 for the meso-scale test as shown in Figure 5.3 and Figure 5.15, respectively. In general, the results obtained from the material characterization test and meso-scale test were in agreement. The measured hydraulic conductivity from the meso-scale self-weight consolidation was 6.64E-07 m/sec compared to the hydraulic conductivity of 3.42E-07 m/sec from the settling column test. The hydraulic conductivity results show results appear within the same order of magnitude as results from a small scale (i.e., the settling column of a 1000 ml graduated cylinder) and meso-scale apparatus (i.e., 30 cm diameter and height of 0.6 m) for the flocculated FFT. The repeatable results show that the scale of the testing apparatus did not have a significant effect on the results.

Fisseha et al. (2018) reported self-weight consolidation results from experimental laboratory work for inline flocculated fluid fine tailings using various flocculent dosages. The flocculated FFT from the present study and reported in literature by Fisseha, Wilson and Simms (2018) used the same flocculation technique and recipe developed by the operators. The index properties of FFT used for both the present study and reported in Fisseha, Wilson and Simms (2018) were similar. Therefore, the results from the self-weight consolidation settlement for the present study were compared and discussed with results reported in (Fisseha, Wilson & Simms, 2018).

The self-weight consolidation settling test results for the present study were compared with results from the “Column 1- with no evaporation condition” described in Fisseha, Wilson and Simms (2018). The tests were similar with the exception of the height of the tailings. The tailings height in the present study was 0.505 m compared to 1.76 m deposited in Fisseha, Wilson and Simms (2018). The measured vertical strain for the flocculated FFT was 0.76 compared to a vertical strain of 0.7 reported by Fisseha, Wilson and Simms (2018). The vertical strain result measured by Fisseha, Wilson and Simms (2018) was measured at the point where the infinitesimal settlement begins (i.e., start of the flatter slope).

Dissipation of excess pore pressure

The results measured during the dissipation of excess pore pressure during the self-weight consolidation stage are presented in Figure 5.16, Figure 5.17, and Figure 5.18. The results obtained from the present study are discussed and compared with results reported in the literature.

Figure 5.16 shows results for the dissipation of excess pore pressure and expected hydrostatic pressure with time. Dissipation of excess pore pressure was observed immediately following the

deposition of flocculated FFT. The expected hydrostatic pressure and measured excess pore pressure during the start of the test showed a larger difference near the base of the column (i.e., 3 cm from the base) compared to near the tailings' interface (i.e., 28 cm from the column base) as expected. The excess pore pressure was fully dissipated near the tailings interface (i.e., from a sensor located at 28 cm) by day 40, but the dissipation of excess pore pressure took longer near the column base (i.e., from a sensor located at 3 cm). The difference between the expected hydrostatic pressure and excess pore pressure near the column base was 0.4 kPa. Since it required a longer time for the excess pore pressure to fully dissipate, the process of supernatant water decantation continued until day 60. Figure 5.16 shows the change in measured excess pore pressure and expected hydrostatic pressure after the removal of the accumulated supernatant water. The change in the hydrostatic pressure due to the removal of accumulated water was calculated and adjusted in Figure 5.16. The bleed water was removed by day 75 and 78 while monitoring for the dissipation of remaining excess pore pressure near the base.

Figure 5.17 shows the dissipation of excess pore pressure with time in relation to the tailings thickness until the decantation of supernatant water. The height of supernatant water, tailings and water interface, and locations of the two sensors (i.e., 28 cm and 3 cm from the base) were used to construct the isochrones (excess pore pressure and hydrostatic pressure lines). Selected isochrone lines are presented in Figure 5.17 to show the dissipation of excess pore pressure with time. As the self-weight consolidation process continued, the changes at the tailings-water interface can be traced using the data points presented for different time periods. These data points are closely aligned near the surface of tailings as shown in Figure 5.17. Figure 5.18 presents the excess pore pressure measured between the decantation of the supernatant water and completion of self-weight consolidation. The hydrostatic pressure line was computed using the difference between the tailings thickness and locations of the sensors.

Although the excess pore pressure measured with time became very small, the results and expected hydrostatic water line provided plausible and consistent results in depicting the dissipation process of excess pore pressure during the self-weight consolidation process for the flocculated FFT.

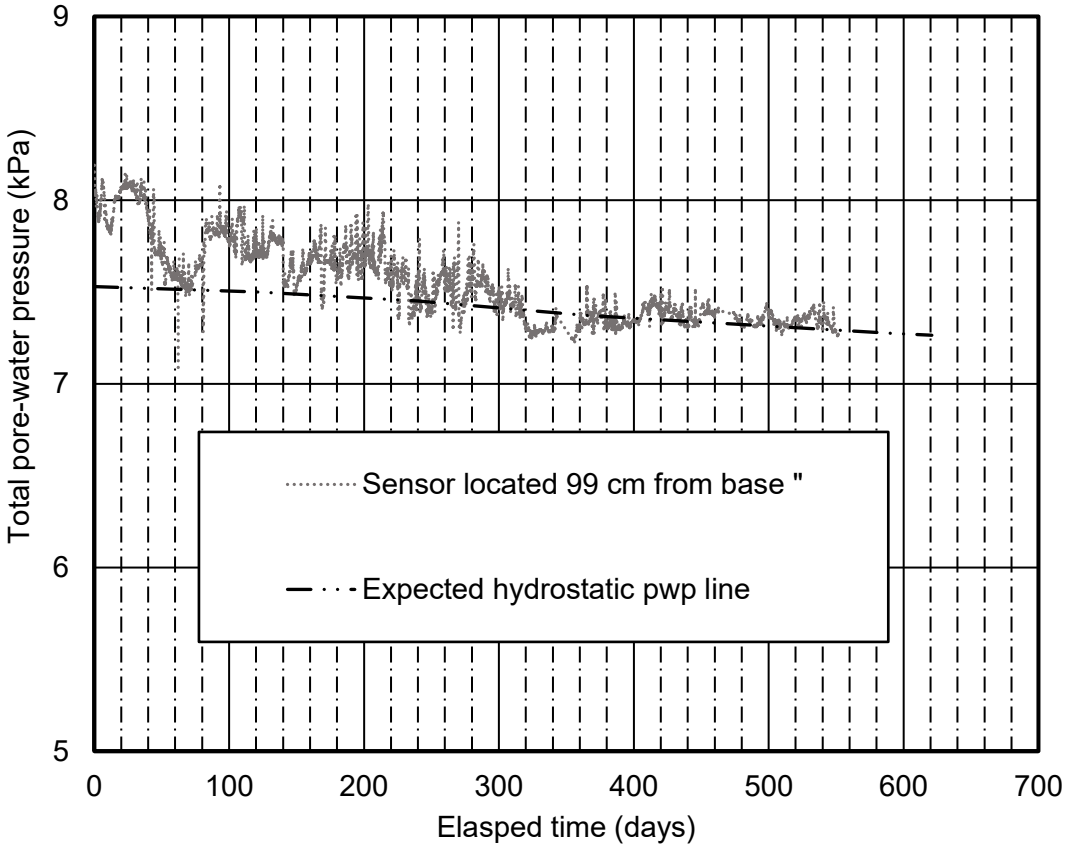

Figure 6. 16 Total pore-water pressure and expected hydrostatic pressure from meso-scale self-weight consolidation of inline flocculated FFT (modified from Fisseha, Wilson & Simms, 2018).

Fisseha, Wilson and Simms (2018) reported the dissipation of excess pore pressure for inline flocculated FFT deposited in a column. The thickness for the deposited tailings was 3.5 times that of the tailings in the present study. Fisseha, Wilson and Simms (2018) showed it took between 280 to 300 days for the excess pore pressure to dissipate from the column identified as “Column

1 – no evaporation condition." The time to dissipate the excess pore pressure was nearly 3.5 times that of the present study. The ratio of the tailings' thicknesses between the two studies is equal to that of the time to dissipate excess pore pressure. Figure 6.16 presents dissipation of excess pore pressure reported by Fisseha, Wilson and Simms (2018).

Effective and total stress calculations

The total stress at the start of the deposition was calculated assuming a uniform initial saturated density for the entire thickness of the tailings. As the self-weight consolidation progressed, it was assumed that the change in tailings density occurred with an increase in saturated density near the column base. The evolution of total density with time was computed for the self-weight consolidation period using the assumed saturated density as stated, the change in tailings thickness, and accumulated supernatant water. Table 5.3 summarizes all considerations (the assumed saturated density, total thickness, and average void ratio) for the flocculated FFT.

The effective stress for the flocculated FFT was calculated by subtracting the measured excess pore pressure from the calculated total stress for each day during the self-weight consolidation process, as summarized in Table 5.3. Figure 5.19 presents the change in total, effective stress and hydrostatic pressure line for the flocculated FFT during the self-weight consolidation process.

Figure 5.19(a) presents the measured total stress, hydrostatic pressure line, and calculated effective stress during the early stage of the flocculated FFT. The initial thickness of the tailings was 0.505 m. The calculated effective stress during the initial deposition stage was 0.5 kPa and 1.14 kPa for the tailings located 28 cm and 3 cm above the column base, respectively. The effective stress near the base of the column (i.e., 3 cm) increased to 2.5 kPa by day 60 just before the decantation of the supernatant water. Figure 5.19(a) to Figure 5.19(f) included the supernatant

water accumulated at the top of tailings surface and the change between tailings-water interface until day 60. After the supernatant water was decanted on day 60, the calculated effective stress near the base became 2.6 kPa by day 80. The effective stress that built up once supernatant water was decanted was insignificant, considering the time it took. Therefore, this affirms the slow process of excess pore pressure dissipation discussed above. Reported effective stress values from the literature are presented in Table 6.

Undrained peak shear strength measurement with time and depth

The undrained shear strength results measured for the flocculated FFT during the process of self-weight consolidation are presented and discussed in this section.

The vane shear strength in relation to the angular deflection of the spring during the failure stage of the self-weight consolidation process for the flocculated FFT is presented in Figure 5.20(a) to Figure 5.20(f). Following the deposition of the tailings, the undrained shear strength along the profile of the tailings was measured at specified depths. The results are presented in Figure 5.20(a) to Figure 5.20(f) and Figure 5.21. Measurement of shear strength was conducted at specified locations in relation to the column base as datum (i.e., minimum of three distinct locations within the depths using three vane blades). The measurements were completed at 7 cm, 17 cm, and 27 cm. Additional measurements are carried out and included by moving the vane shear equipment along the vertical axis as described in detail in Chapter 4, section 4.2.2. Figure 5.20(a) to Figure 5.20(f) provide results at specified times during the self-weight consolidation process. The plots show the relationship of angular deflection on the abscissa and vane shear strength on the ordinate.

The peak shear strength was determined at a desired depth on the tailings profile. The measurement was completed by applying torque at a constant revolution rate of 60 *degrees/min* as per the ASTM D2573-94 “Standard Test Method for Laboratory Vane Shear Test in Cohesive Soil.” Details on the vane shear equipment are presented in (Olmedo et al., 2019). During the shear test, the strength of the tailings increased until failure occurred when the tailings were not able to withstand the applied pressure (i.e., torque divided the contact area of the vane blades). Failure during the vane shear measurement was indicated using the measured angular deflection as shown in Figure 5.20(a) to Figure 5.20(f). The shear strength of the tailings increased with an increase in angular deflection until the maximum strength of the tailings was reached. Once failure occurred, the vane shear values showed lower values than the maximum (peak) shear values.

Figure 5.20(a) to Figure 5.20(f) present the change in peak undrained shear strength as the process of self-weight consolidation progressed with time. The initial undrained shear strengths measured for the flocculated tailings prior to deposition are summarized in Table 5.4. These initial shear strength measurements were conducted for each prepared batch of flocculated tailings. The results are within the range of initial shear strength values (i.e., 75 to 95 Pa) during field conditions for the flocculated FFT (Personal communication, 2016).

Selected vane shear strength measurements for different time intervals (days) for the self-weight consolidation process are presented in Figure 5.20(a) to Figure 5.20(f). Overall, an increase in shear strength was observed as the consolidation progressed. The initial undrained shear strength was 0.07 kPa near the base of the column, and near the end of the self-weight consolidation process on day 98, the undrained shear strength was 1.2 kPa.

Figure 5.20(a) to Figure 5.20(f) show the peak shear strength at a given time corresponding to the deposited tailings thickness. For instance, Figure 5.20(a) presents the measurements on day

17 during the self-weight consolidation test for the flocculated FFT. The vane shear strength at 7 cm, 12 cm, 17 cm, 27 cm, and 37 cm are presented. The peak shear strength was 0.8 kPa at 7 cm followed by 0.46 kPa at 12 cm and 0.31 kPa at 37 cm. Overall, the shear strength decreased between the column base and tailings interface. Figure 5.20(f) presents the vane shear strength versus angular deflection by day 80, which was near the end of self-weight consolidation testing. Figure 5.20(f) presents the peak vane shear strength of 1.2 kPa at 7 cm and 0.67 kPa at 27 cm. The total thickness of the tailings was determined to be 38.5 cm by day 80.

Figure 5.21 presents the vane shear strength with depth and time. Although the vane shear strength was measured in pascals, an increasing shear strength trend was observed with depth and time. The change in shear strength was smaller in values compared to the change in shear strength between the surface and the middle section of the deposits. However, the shear strength was larger near the column base. This occurred due to an increase in tailings density (i.e., solids content) near the column base compared to the tailings near the surface and in the middle section. Although the drainage boundary for the self-weight consolidation process was at the surface boundary, the shear strength showed larger values near the column base for the flocculated FFT.

Relationship between confining effective stress and undrained shear strength

The relationship between undrained shear strength and calculated effective stress of the flocculated tailings during the self-weight consolidation process is presented in Figure 6.17. A linear relationship was obtained to correlate the undrained shear strength and effective stress. The slope of the correlation was 0.42 by setting the intercept at 0.0. The undrained shear strength was not corrected for potential errors. For instance, additional excess pore pressure could have been generated while the insertion of the extended rod. Strength values could have ben included

due to resistance at to the extended rod. The extended vane rod was inserted periodically into the tailings during the test program.

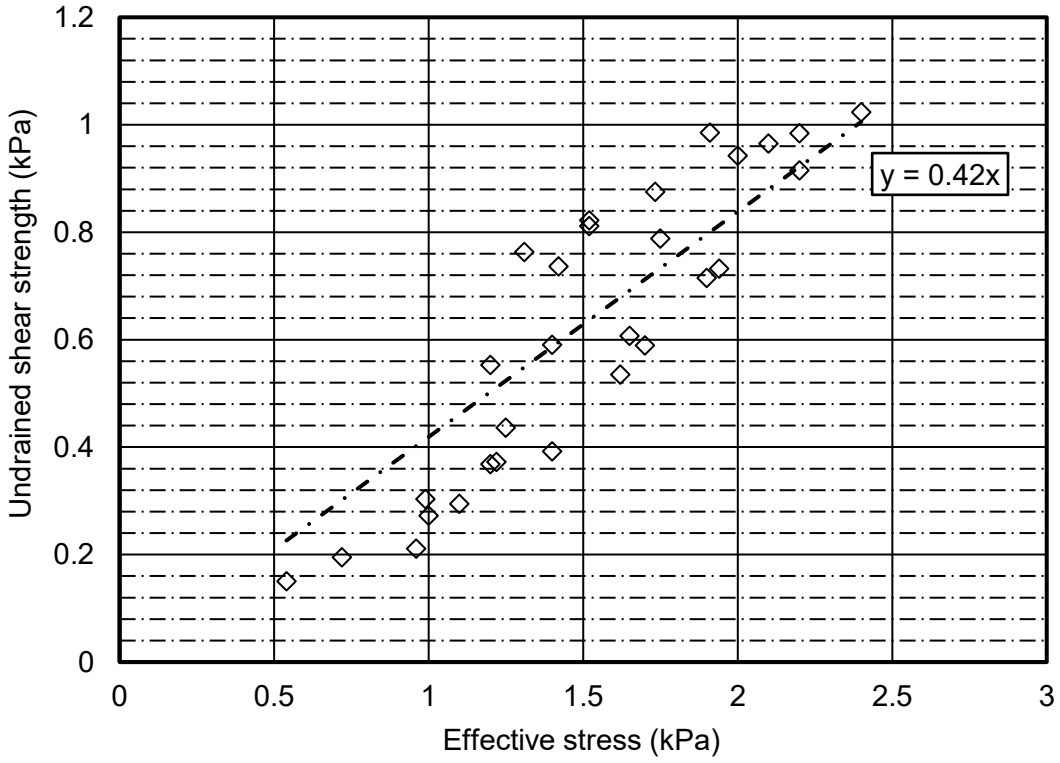

Figure 6. 17 The relationship between effective stress and measured peak undrained shear strength for the flocculated FFT during the self-weight consolidation process.

The slope between effective stress and undrained shear strength for natural clays reported in literature proved the following Boston blue clay was 0.2 (Ladd, 1973), Kaolinte clay was 0.24 - 0.25 (Ohara and Matsuda, 1978), and Manglerud quick clay was 0.16 – 0.22 (Bjerrum and Ladva, 1966) compared to 0.42 for the flocculated FFT during the sedimentation and self-weight consolidation stage. Summary of the literature results and measured from laboratory are presented in Table 6.4. The test for the natural soils shows that measurement was conducted on normally consolidated soils using simple shear testing device.

Table 6. 4 Summary of undrained shear strength values from literature and vane shear tests from laboratory.

Devices used	Literature reported by author name	State of the material tested	State of the sample preparation	Material type	Pore water pressure (kPa)	(τ/σ') max	Remarks
Simple shear test	Ladd (1973, 1979)	Natural soils	Normally consolidated clay	Boston blue clay	-	0.2	
	Ohara and Matsuda (1978)	Natural soils	Normally consolidated clay	Kaolin clay	10.78	0.24	
					22.54	0.25	
					32.34	0.25	
					41.16	0.24	
	Bjerrum and Ladva (1966)	Natural soils	Normally consolidated clay	Mangleru d quick clay	22.34	0.18	
					18.23	0.16	
					21.17	0.19	
					20.68	0.21	
					29.3	0.17	
					32.14	0.16	
					28.42	0.22	
					29.4	0.2	
					36.65	0.19	
Vane shear measuring test	The present study	flocculated fluid fine tailings consolidated self-weight and applied suction	Self-weight consolidation	flocculated FFT	Excess pore pressure	0.42	Collective slope
			Consolidation using applied suction method	flocculated FFT	10 to 30 (L)	0.44	Group slope
					10 to 30 (U)	0.37	Group slope
					30 to 40	0.44	Group slope
					50 to 60	0.66	
				FCTC	20 to 30 (L)	0.21	
					20 to 30 (U)	0.19	
					30 to 40	0.33	
					50 to 60	0.41	

L = Lower bound suction values used and
U = Upper bound suction values used.

Additional detailed analysis and interpretation of the correlation between effective stress and undrained shear strength are presented in the section 6.4 and part 5. Assuming the vane shear

strength results incorporated error measurement due to the extended rod's friction values and other factors listed in the literature review section (Chapter 2). The corrected undrained shear strength show reduced values than the presented results.

Flocculated centrifuged tailings cake (FCTC)

The results of the investigation to determine the self-weight consolidation for the FCTC are presented from Figure 5.22 to Figure 5.25. The results are discussed and analyzed in this section.

There was no self-weight consolidation observed for the FCTC following the deposition of the FCTC into the meso-scale column apparatus as depicted by Figure 5.22 and 5.23 for the vertical strain and change in void ratio, respectively.

The presentation of measured results for the FCTC during the self-weight consolidation stage are categorized as follows: i) vertical strain or void ratio with time, ii) excess pore pressure dissipation, iii) total and calculated effective stress, and iv) measured undrained shear strength.

Settlement, vertical strain, and void ratio

Figure 5.22 and Figure 5.23 present the measured vertical strain (settlement) and the change in void ratio for the FCTC, respectively. There was no change in settlement determined during the self-weight consolidation process for the FCTC. The negligible vertical strain measured and presented in Figure 5.22 is possibly from the FCTC adjustment in the tailings skeleton and fabric due to meshing of the tailings while the tailings sat within the column during the self-weight consolidation process. It should be noted that the placement of the FCTC was carried out using

a hand scoop in individual and separate chunks. Figure 5.23 presents the measured settlement in terms of void ratio change.

The results obtained from the settling column test (using a 1000 ml graduated cylinder) and results from the self-weight consolidation from the meso-scale test agreed by displaying that there was no vertical strain or settlement measured for the deposited FCTC. The average final void ratio was 2.02 for the tailings from the meso scale test by day 25, compared to the average final void ratio of 2.01 from the settling column test by day 50. The longer duration (i.e., 220 days) settling column test resulted in an average final void ratio of 1.76. A smaller remaining settlement was measured from the settling column test over an extended time (i.e., 3 cm for 250 days). This minor change in settlement has been ignored since it was negligible with time. These results are assumed to depict the infinitesimal settling of the FCTC.

Excess pore pressure dissipation

Figure 5.24 presents the dissipation of excess pore pressure and the expected computed hydrostatic pressure line during the self-weight consolidation process for the FCTC. Figure 5.24 displays the slow-moving dissipation process measured over the longer duration of the test (i.e., 28 days) for the tailings near the column base (i.e., sensor located 3 cm from the base). The excess pore pressure between day 28 and day 30 was due to removal of minor accumulated supernatant water from the surface. The excess pore pressure near the surface of the tailings (i.e., sensor located 29 cm from the base) was determined to be insignificant. The thickness of tailings above the sensor located at 29 cm was measured to be between 7 to 8 cm and the calculated pore pressure was 0.7 to 0.9 kPa. The measurement displayed from the sensor was within the margin of (+/-) error limits and it was difficult to interpret the results using the sensor situated near the surface of the tailings.

The column for the FCTC was left for observation for the process of self-weight consolidation for about 30 days. The reasons for the limited time for the self-weight consolidation process of the FCTC are listed below:

1. Overall, no vertical settlement was measured from the settling column test during the characterization test for the FCTC. The settlement that did occur was defined as infinitesimal and occurred following an extended time (i.e., 250 days).

2. There was little to no dissipation of excess pore pressure for the FCTC during the self-weight consolidation test conducted for 30 days. Therefore, it was assumed that dissipation of the excess pore pressure would take an extended period of time.

Therefore, the decision was made to conclude the self-weight consolidation for the FCTC and proceed with the following stage of tests.

Effective and total stress calculations

The measurement of total stress and calculation of effective stress following the deposition of the FCTC was completed using an assumed uniform initial saturated density for the entire thickness of tailings. Since there was no self-weight consolidation, minor adjustments were incorporated to reflect the possible change in saturated density near the base of the column during the initial stage and with time.

Figure 5.25(a) and Figure 5.25(b) present the measured total and calculated effective stress during the initial deposition and final self-weight consolidation tests (i.e., prior to proceeding to the

applied suction stage of the test). The initial thickness of the tailings was 0.37 m. Results for calculations of the effective stress during the initial deposition stage were 0.44 kPa and 1.52 kPa for the tailings located at 29 cm and 3 cm above the column base. There was no significant change in settlement; therefore, the calculated effective stress remained constant for the FCTC for the 30 days.

Undrained peak shear strength measurement with time and depth

The measured undrained shear strength results for the FCTC are presented in Figure 5.25 and Figure 5.26. The vane strength for the FCTC was limited at the start of the self-weight consolidation process to characterize its initial shear strength value with depth and was used as a baseline for the anticipated tests using the next experimental stage.

Figure 5.25 shows the initial vane shear strength in relation to the angular deflection for day 20. The undrained shear strength was higher near the column base compared to the tailings surface and middle section. The trend is similar with the results observed for the flocculated tailings. The vane shear strength was 1.07 kPa at 7 cm, 0.612 at 17 cm, and 0.405 kPa at 27 cm by day 3 compared to shear strengths of 1.35 kPa at 7 cm, 0.82 kPa at 17 cm, and 0.47 kPa at 27 cm by day 20. There was no significance change between day 3 and day 20, and all changes were within the range of error for the instrument.

6.4 Consolidation using the applied suction

The analysis and interpretation of results obtained during the consolidation process using an applied negative water pressure (suction) are presented herein. These results are presented in Chapter 5, section 5.1.3.

The analysis and interpretation of meso-scale results for both the flocculated FFT and FCTC were carried out in the following section and are organized as follows: i) stress and strain relationship, ii) pore pressure distribution, iii) effective stress calculations, iv) solids content determination, and v) undrained shear strength with depth.

Stress and strain relationship

The results of total strain due to incremental applied suction are expressed in terms of volumetric strain and the change in void ratio as shown in Figures 5.29, 5.30, 5.36, 5.37, 5.41, 5.42, 5.46, and 5.47 for both the flocculated FFT and FCTC. Additional plots of volumetric strain and change in void ratio are presented in Appendix A and B.

The combined results of all incremental applied suction in relation to the volumetric strain and void ratio are presented in Figure 6.18 and Figure 6.19, respectively, for both the flocculated FFT and FCTC. Figure 6.18 shows that the flocculated FFT achieved a 60% change in total volumetric strain due to an applied suction of 60 kPa, compared to 29% for the FCTC.

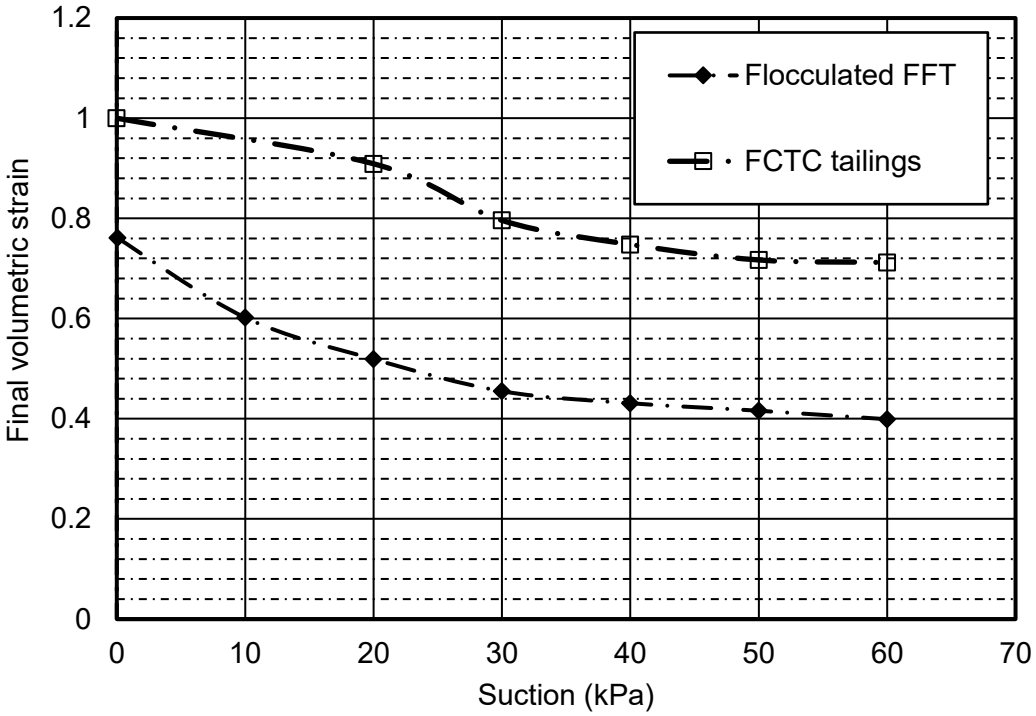

Figure 6. 18 Final volumetric strain measured during the meso-scale test in relation to the applied suction for the flocculated FFT and FCTC.

The self-weight consolidation process provided 0.76 of total strain and resulted in a 24% reduction in the thickness of the tailings. Large volumetric changes were observed during an applied suction of 30 kPa compared to the subsequent incremental loads. The large volume changes for flocculated FFT were observed during both the material characterization and meso-scale test periods. The FCTC exhibited less volumetric strain compared to flocculated FFT; however, similar changes were observed for the applied suction up to 30 kPa compared to the higher incremental suction values.

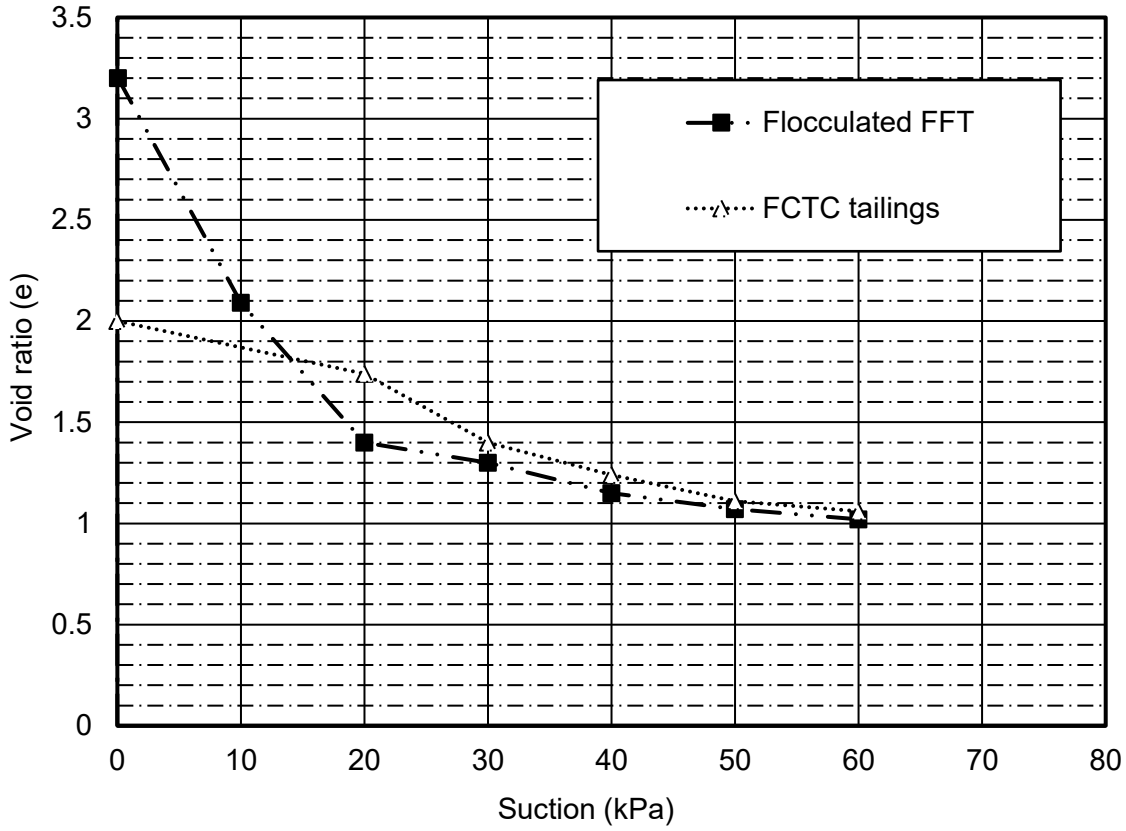

Figure 6. 19 Final void ratio measured during the meso-scale test in relation to the applied suction for the flocculated FFT and FCTC.

Figure 6.19 shows the final void ratios and applied incremental suction for both flocculated FFT and FCTC. The flocculated FFT shows larger volume changes compared to the FCTC in the initial stage and smaller volume changes as consolidation progressed. The volume change results presented in Figure 6.18 and Figure 6.19 are the same yet are expressed differently.

The plots of void ratio and applied suction are compared with values predicted using unsaturated soils properties (i.e., SWCC and SC) for both flocculated FFT and FCTC.

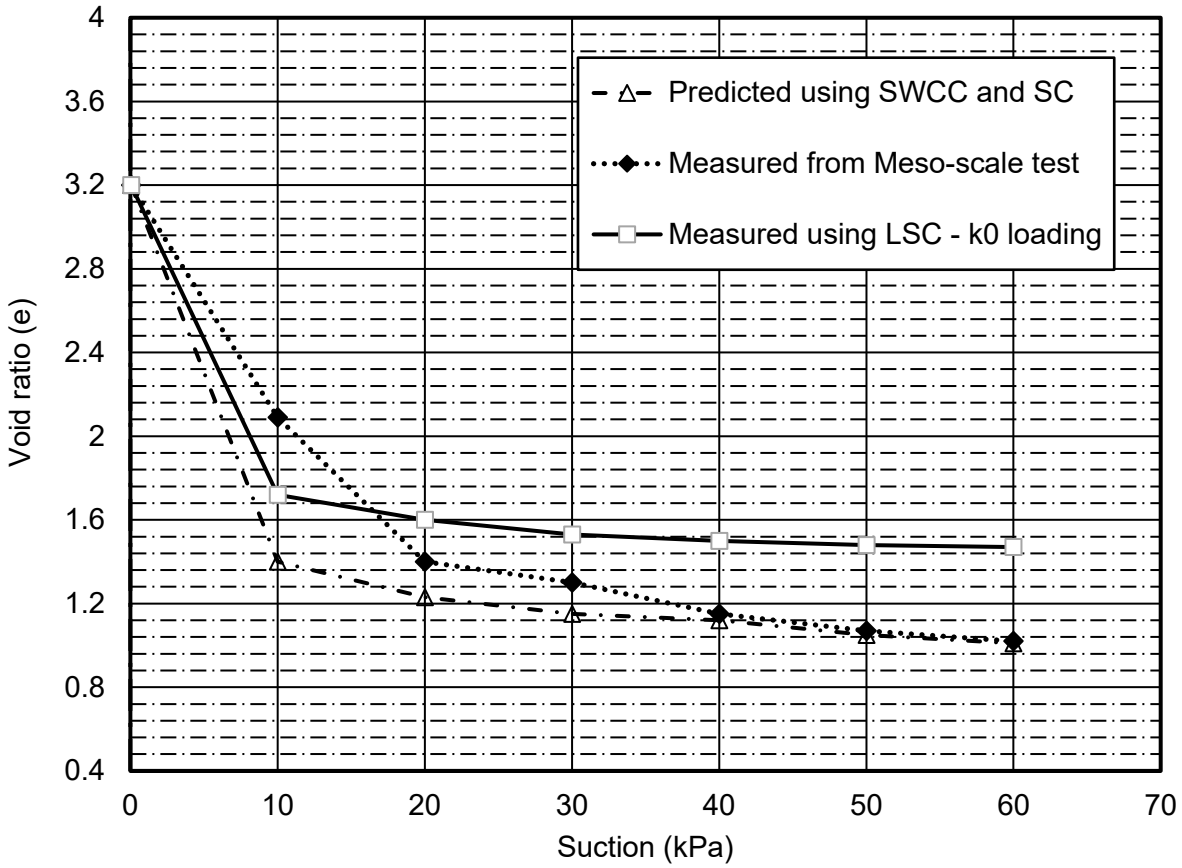

Figure 6. 20 Comparison of measured and predicted values of void ratio in relation to the applied suction for the flocculated FFT.

Figure 6.20 presents the measured and predicted results for the increments of suction of the flocculated FFT. Overall, bigger differences were observed between the measured and predicted results during the initial stage (i.e., from 10 to 30 kPa). The differences decreased with additional increments as expected. The results give reasonable agreement for the increments of suction of 40 to 60 kPa. The discrepancy at the initial stage was possibly due to not reaching equilibrium before the incremental suction was increased (i.e., 10 to 30 kPa). The pore pressure values were not available for those specified increments to confirm when equilibrium was reached. However, the measured and predicted results agreed for the later consolidation stage (i.e., 40 to 60 kPa

suction), when pore pressure measurements were available to confirm that equilibrium had been reached.

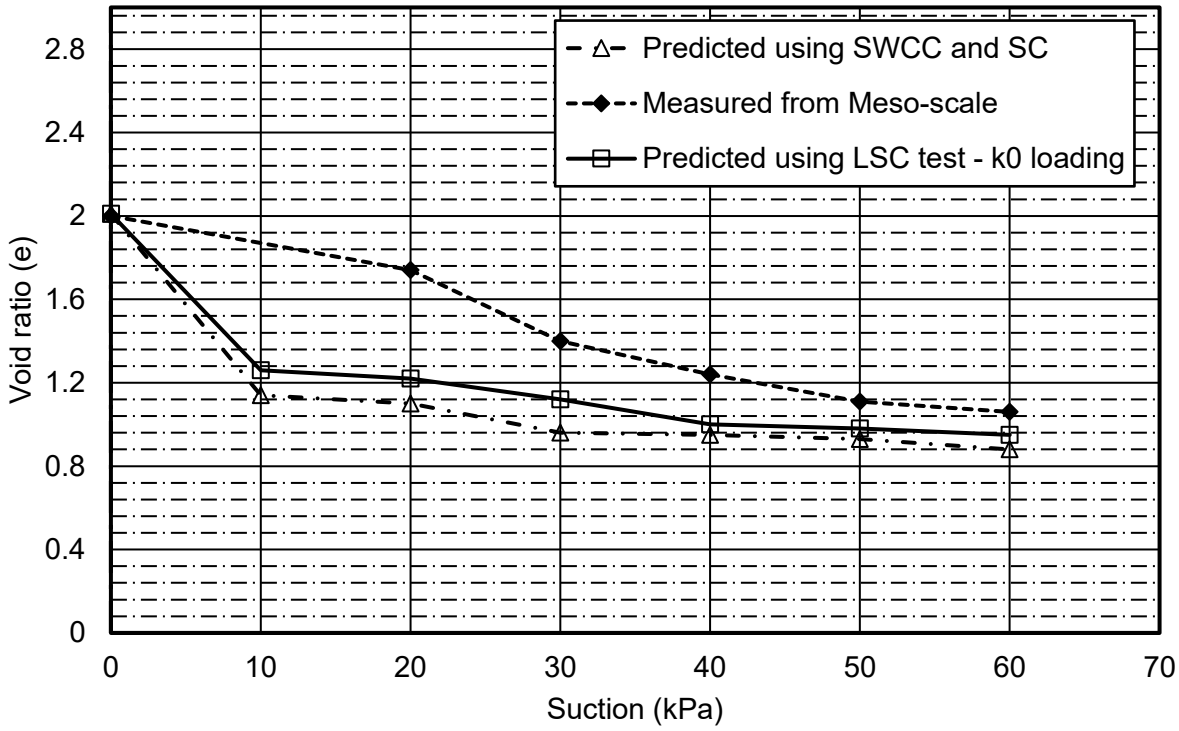

Figure 6. 21 Comparison of measured and predicted values of void ratio in relation to the applied suction for the FCTC.

Similarly, Figure 6.21 presents the measured and predicted results for the FCTC. Similar to the results observed in flocculated FFT, a larger difference was observed between the predicted and measured void ratio for the initial stage (i.e., 20 to 30 kPa). The possible reason for the discrepancy was that the tailings may not have been at equilibrium at the time when the test concluded. In addition, the lower hydraulic conductivity for FCTC required longer to reach equilibrium compared to the flocculated FFT. The higher increments showed better agreement for both prediction methods (unsaturated soil properties and LSC testing). However, there were still minor differences between the two values. These differences were probably due to difficulties estimating the volumetric strain for the meso-scale testing since the measurements were carried

out using a rough estimation technique. Overall, the predicted values were acceptable within the margins of error.

In general, acceptable results were achieved from the meso-scale testing, which asserts the use of the unsaturated soil property functions to predict expected volumetric strain and change in void ratio due to applied suction conditions either for laboratory or field conditions.

Table 6. 5 Comparison of equations used to predict the void ratio of meso-scale test using the unsaturated soils property relations and LSC tests.

Materials used	Fitting function	From unsaturated soil property results	R^2	LSC results	R^2
Flocculated FFT	power function	$e = 2.0949(\psi)^{-0.176}$	0.973	$e = 2.0031(\sigma')^{-0.077}$	0.967
FCTC	power function	$e = 2.8424(\psi)^{-0.312}$	0.949	$e = 2.6798(\sigma')^{-0.259}$	0.945

The relationships used to predict the void ratio are best represented using a power function for both methods (i.e., using unsaturated soil property and LSC test). The equations representing the correlation are summarized in Table 6.5. These equations can be used to predict the material properties from available data. Generic formulae can be developed by conducting significant characterization tests for fluid fine tailings.

Isotropic and k_0–loading conditions comparison

The compressibility results obtained under k_0 – loading conditions were compared to the meso-scale results, which were conducted under isotropic loading conditions and ideal in representing

the field trails. Theoretical formulations for both isotropic and k_0–loading conditions are summarized below to assist the analysis process.

The constitutive equation to determine the volumetric strain during an isotropic loading can be expressed as follows:

$$d\varepsilon_v = 3\left(\frac{1-2\mu}{E}\right) d(\sigma_3 - u_a) + \frac{3}{H}\, d(u_a - u_w) \quad [6.1]$$

where:

$d\varepsilon_v$ = decrease in volumetric strain due to incremental load

μ = Poisson's ratio

E = modulus of elasticity or Young's modulus for the soil structure

H = modulus of elasticity for the soil structure with respect to a change in matric suction, u_a - u_w

$d\sigma_3$ = incremental isotropic stress in three dimensions

The experimental test considered applied suction only; therefore, Eq. [6.1] was simplified to:

$$d\varepsilon_v = \frac{3}{H}\, d(u_a - u_w) \quad [6.2]$$

Assuming the Poisson's ratio in the range of 0.3 to 0.49 and using the measured modulus of elasticity with respect to change in suction (i.e., H) from the meso-scale test.

The expected change in volumetric strain from the k_0-loading test can be corrected using the constitutive equations presented in Eq. [6.3] and [6.4] for the determination of volumetric strain during the k_0–loading (i.e., compressibility curve from LSC test).

$$d\varepsilon_v = \frac{(1+\mu)(1+2\mu)}{E\,(1-\mu)} d(\sigma_y - u_a) + \frac{1+\mu}{H(1-\mu)}\, d(u_a - u_w) \quad [6.3]$$

where:

$d\varepsilon_v$ = decrease in volumetric strain due to incremental load

μ = Poisson's ratio

E = modulus of elasticity or Young's modulus for the soil structure

H = modulus of elasticity for the soil structure with respect to a change in matric suction, u_a - u_w

$d\sigma_y$ = stress increase in the y direction

Equation [6.3] can be simplified further as presented in Eq. [6.4], due to the absence of the suction component during the k_0–loading test.

$$d\varepsilon_v = \frac{(1+\mu)(1+2\mu)}{E\,(1-\mu)} d(\sigma_y - u_a) \quad [6.4]$$

Assuming the Poisson's ratio was in the range of 0.3 to 0.49, equating the modulus of elasticity with Young's modulus, the change in volumetric strain can be determined. The values obtained from the isotropic and k_0–loading test are presented in Table 6.6 in terms of measured final void ratio.

Table 6. 6 Comparison of measured and calculated volumetric strain results using isotropic and k_0–loading conditions.

Tailings type	Change in final void ratio	
	Isotropic loading	k_0-loading
	Measured	Measured
Flocculated FFT	1.02	1.47
FCTC	1.06	0.95

The modulus of elasticity determined from meso-scale testing for both flocculated FFT and FCTC were 0.121 and 0.159 MPa, respectively and agreed with values reported in the literature. These values fall within the range of very soft to soft soils and with high plasticity (http://www.geotechdata.info/parameter/soil-young's-modulus.html ; Obrzud & Truty, 2012; compiled from Kezdi, 1974; Prat et al., 1995). Appropriate correction factors are essential to be applied in order to determined reasonable agreements.

The results for isotropic and k_0–loading is presented in Table 6.6. The results measured using the LSC apparatus underestimated the final void ratio as shown in the case of flocculated FFT, however results of good agreement between isotropic and LSC test for the FCTC. The discrepancy for the flocculated FFT was due to high volume changing behaviours. Therefore, a correction factor was necessary to represent and assess the actual field conditions with better accuracy. The correction factor can be implemented during the design assumptions, settlement calculations, and empirical correlations used for the numerical modelling exercises.

Further tests are essential to show repeatability of the results. These results are vital to developing the correlation between the isotropic and k_0-loading. It is important to assume in the absence of one of the characterization results that the development of the empirical formula determines the required values for the modelling and preliminary design stages.

Pore pressure distribution

The applied negative pore pressure at the bottom boundary was specified and suction values were measured 2-3 cm below the tailings surface. These suction values are presented in Chapter 5, in Figure 5.38 and Figure 5.48 for flocculated FFT and FCTC, respectively. Figure 6.22 presents

the schematic for the applied negative pore pressure and position of measured suction are presented to illustrate how the pore pressure distribution formed and progressed with time.

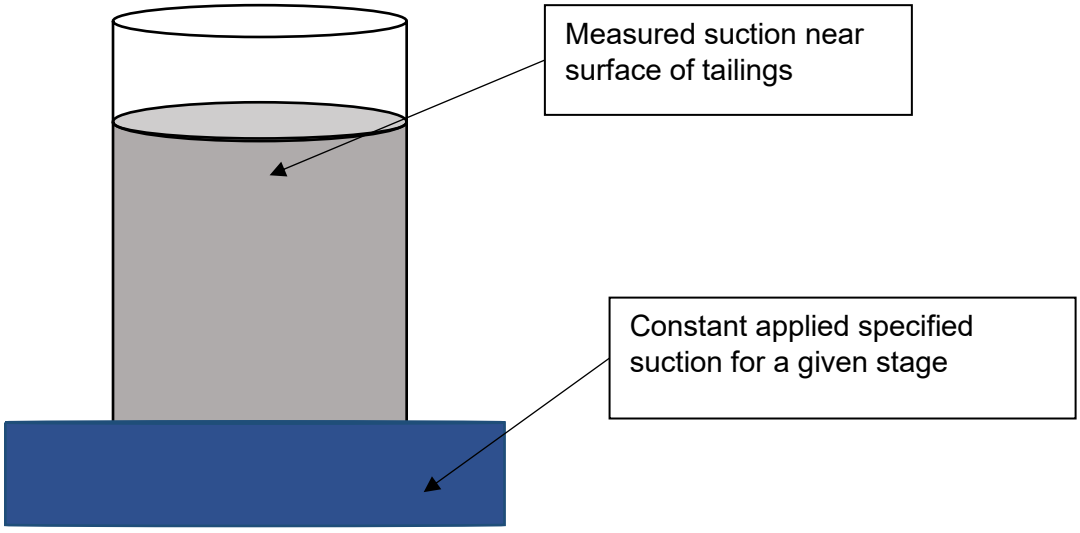

Figure 6. 22 Schematic presentation of specified and measured negative pore pressure during the meso-scale experimental testing.

Selected pore pressure results are presented in Figure 6.23 to demonstrate the progress of the pore pressure distribution. Since the process was similar for flocculated FFT and FCTC, selected results from the flocculated FFT test are presented.

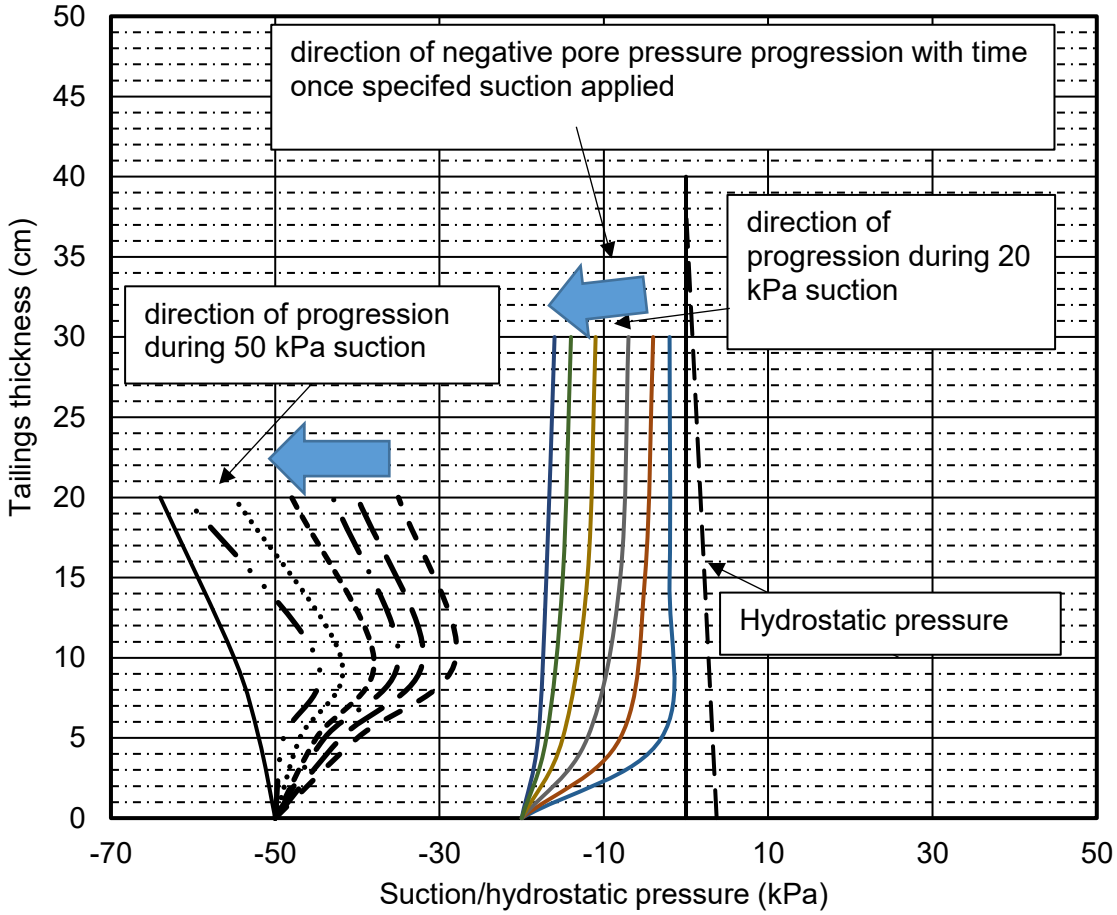

Figure 6. 23 Selected progress of pore pressure distribution with time for the flocculated FFT during the meso-scale experimental testing.

Figure 6.23 presents the unified pore pressure distribution results measured and estimated for the flocculated FFT. The results show the initial stage of hydrostatic pore pressure with depth prior to application of applied suction for consolidation. Once a suction of 20 kPa has been applied at the bottom boundary, the pore pressure progressed with time as shown in Figure 6.23. The bottom boundary rapidly transitioned its pore pressure values from the hydrostatic stage to the constant value of the applied suction. The distribution progressed with time from bottom to top and from zero pore pressure towards suction values higher than the constant value applied at the base.

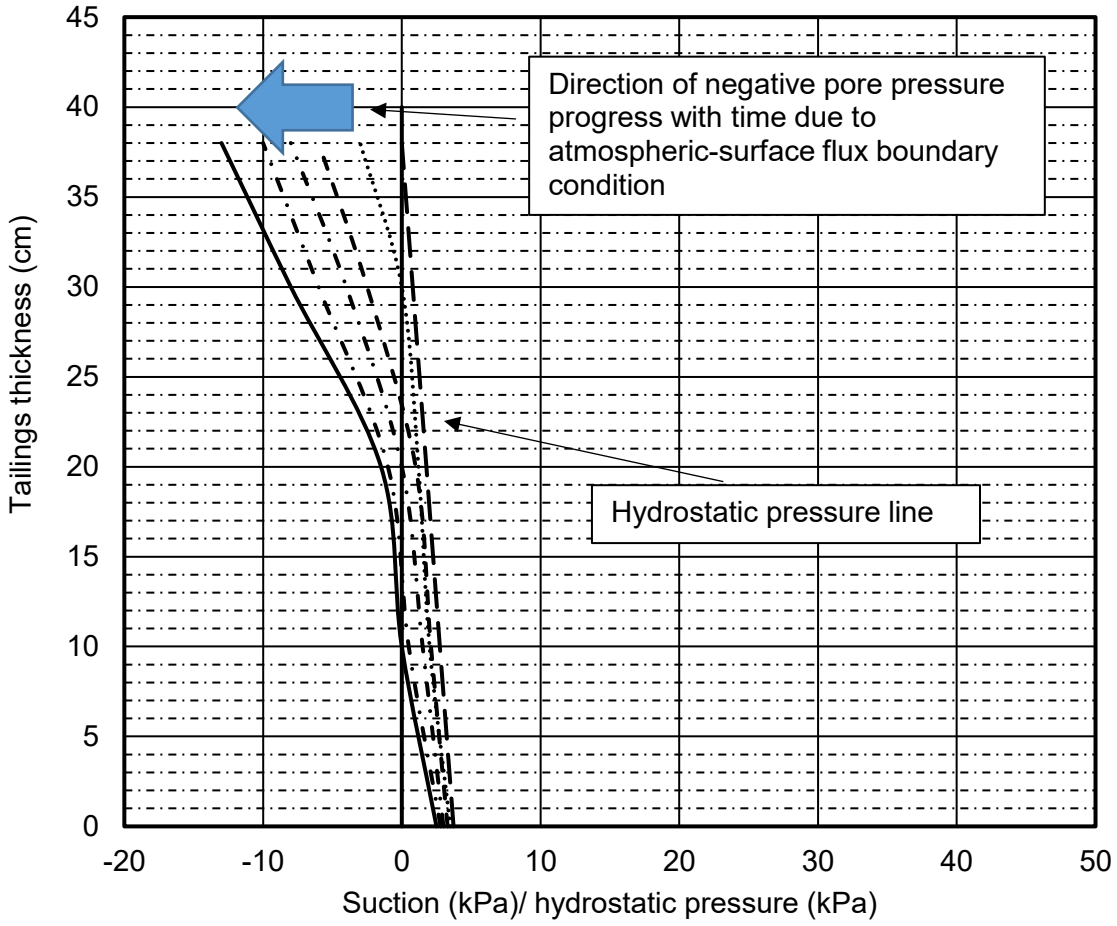

Figure 6. 24 Conceptual progression of pore pressure distribution with time due to atmospheric-surface flux boundary condition from field condition.

The rate of change was dependent on the hydraulic conductivity of the material under investigation. In general, the negative pore pressure progressed slowly for the tailings. However, the flocculated FFT showed rapid negative pore pressure within the profile compared to the FCTC due to lower hydraulic conductivity of the FCTC. The suction values near the surface of the tailings may have been affected by evaporation and were slightly higher than the middle section of the tailings. A similar process occurred during each incremental increase in applied suction. Pore pressure results for an applied suction of 50 kPa are presented in Figure 6.23 and show a similar pattern.

The results measured using the column apparatus were compared with the results observed from field condition tests conducted by other researchers. Figure 6.24 presents the progression of the pore pressure distribution from the materials exposed due to atmospheric-surface flux (Fredlund, Rahardjo & Fredlund, 2012) The pattern of pore pressure progression was the same for laboratory and field conditions. The agreement between the experimental results measured and the field conditions affirms the use of stress-controlled laboratory conditions to characterize and understand the transitional zone. These results affirm the proper functionality of the column apparatus as designed (see Chapter 3).

Effective stress calculations

Determination of effective stress distribution was completed by assuming an equilibrium condition had been reached at the end of each test period and before additional suction was applied. As it has been mentioned, the equilibrium condition might not have reached during the early stage of the experimental tests (i.e., 10 to 30 kPa suction increments). In addition, in the absence of pore pressure measurements from the midsection of the tailings, it was not possible to determine the effect of evaporation.

A rough estimate of the pore pressure can be completed by assuming suction values taken near the tailings surface, mid-section and known value of applied constant suction at the bottom. Assuming no effect from evaporation, higher suction was expected at the bottom with a decreasing trend towards the surface of tailing (top of column) during the initial stage. As dewatering progressed, the suction distribution became uniform along the profile. Subsequently, the suction near the surface became larger than the bottom. The calculation for the effective stress distribution required some adjustment to reflect assumed pore pressure distribution values

for both flocculated FFT and FCTC. Overall, the increase in effective stress distribution with an increase in suction measurement was exhibited as expected.

Solids content with profile

The measured and predicted solids content changes along the profile of the consolidating tailings are presented in Figure 6.25 for both flocculated FFT and FCTC. The solids contents were measured a few months after the completion of the consolidation test. The columns were covered at the top surface as they had been during the testing stage. The results were used to check if evaporation was occurring near the surface of the deposited tailings.

The solids content for the flocculated FFT showed a slight increase near the base of the column but was within the margin of error. The predicted solids content through the profile shows was uniform with an increase in the solids content near the surface due to higher suction. However, a 10% increase in solids content was observed compared to the predicted results using unsaturated soils property functions. Further assessment is required to verify the measured and predicted results. It is evident that an increase in solids content in the measured results could be attributed to an additional loss of moisture from the effect of evaporation over time.

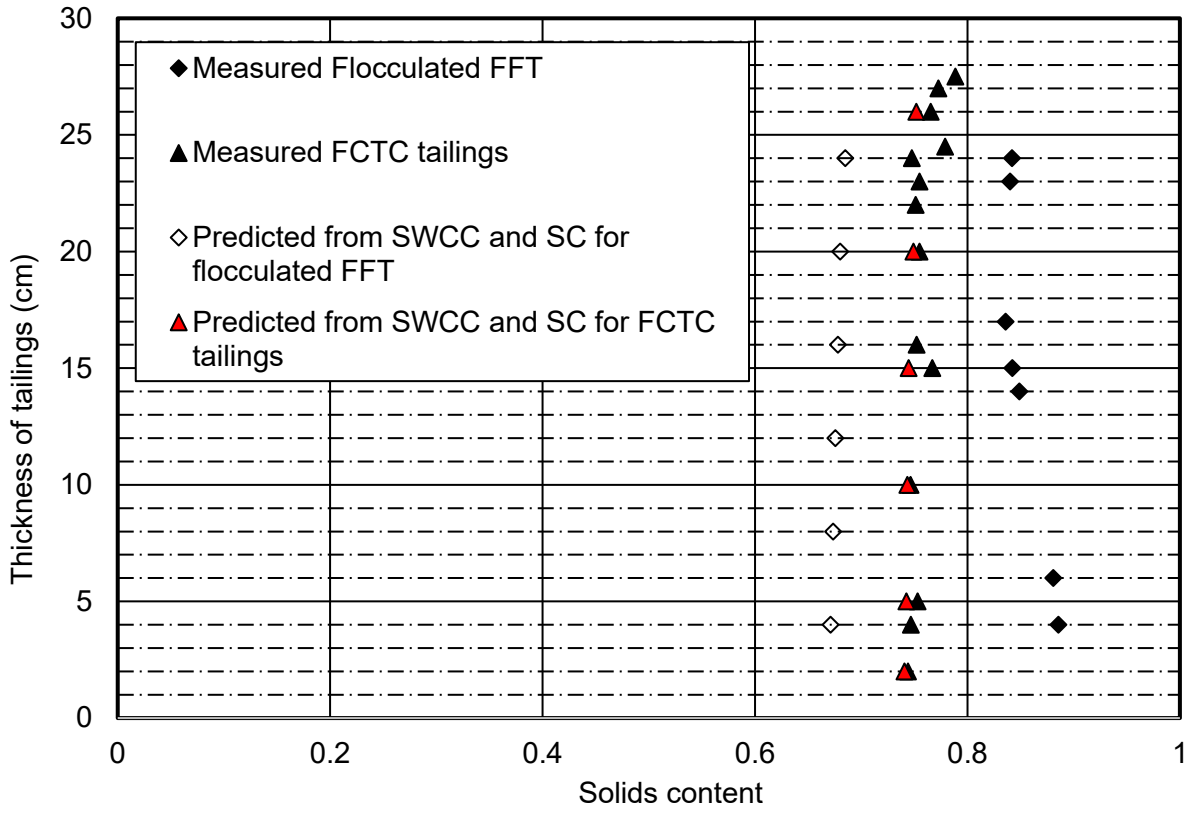

Figure 6. 25 Measured and predicted solids content profile with depth for the meso-scale column test at the end of the test period.

The FCTC show good correlation between measured and predicted solids content through the tailings profile. The effect of evaporation for the FCTC was limited near the surface, possibly due to the low hydraulic conductivity of the tailings. The differences between the measured and predicted solids contents can possibly be attributed to the higher hydraulic conductivity for the flocculated FFT compared to the FCTC.

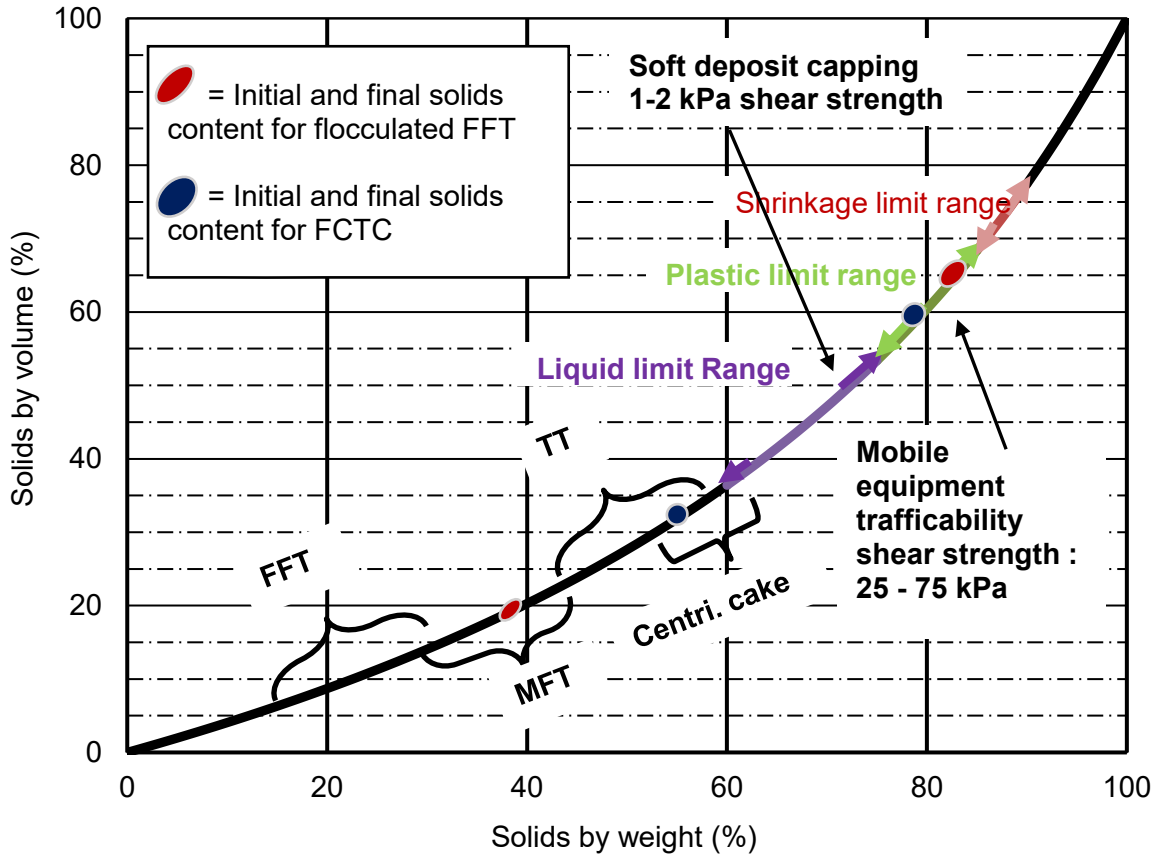

Figure 6. 26 Comparison of the initial and final solids content for both flocculated FFT and FCTC following completion of the experimental test (modified from Fair & Beier, 2012).

In general, an increase in solids content was observed between initial deposition and completion of dewatering using consolidation due to applied suction. The average final solid content for the profile was between 38% to 85% (with evaporation) for the flocculated FFT and from 52% to 75% for the FCTC. The final measured solids content for the flocculated FFT and FCTC falls within the range of plastic limit, which has values of undrained shear strength of ranging 25 - 75 kPa which are suitable for mobile equipment trafficability as indicated in Figure 6.26.

For instance, the final measured solids content for the flocculated FFT and FCTC falls within the range of plastic limit as shown in Figure 6.26 compared to its initial condition. The plastic limit

range has expected values of undrained shear strength ranging between 25 - 75 kPa, that is suitable for mobile equipment trafficability (Fair & Beier, 2012). The undrained shear strength values were verified with measured vane shear strength values as presented in the results section.

Degree of saturation with profile

The calculated degree of saturation along the profile of the consolidating tailings are presented in Figure 6.27 for both flocculated FFT and FCTC. Both Flocculated FFT and FCTC show fully saturated condition along the profile by the end of experimental test. The Flocculated FFTs show 100% saturation and the FCTC shows average of 95% saturation.

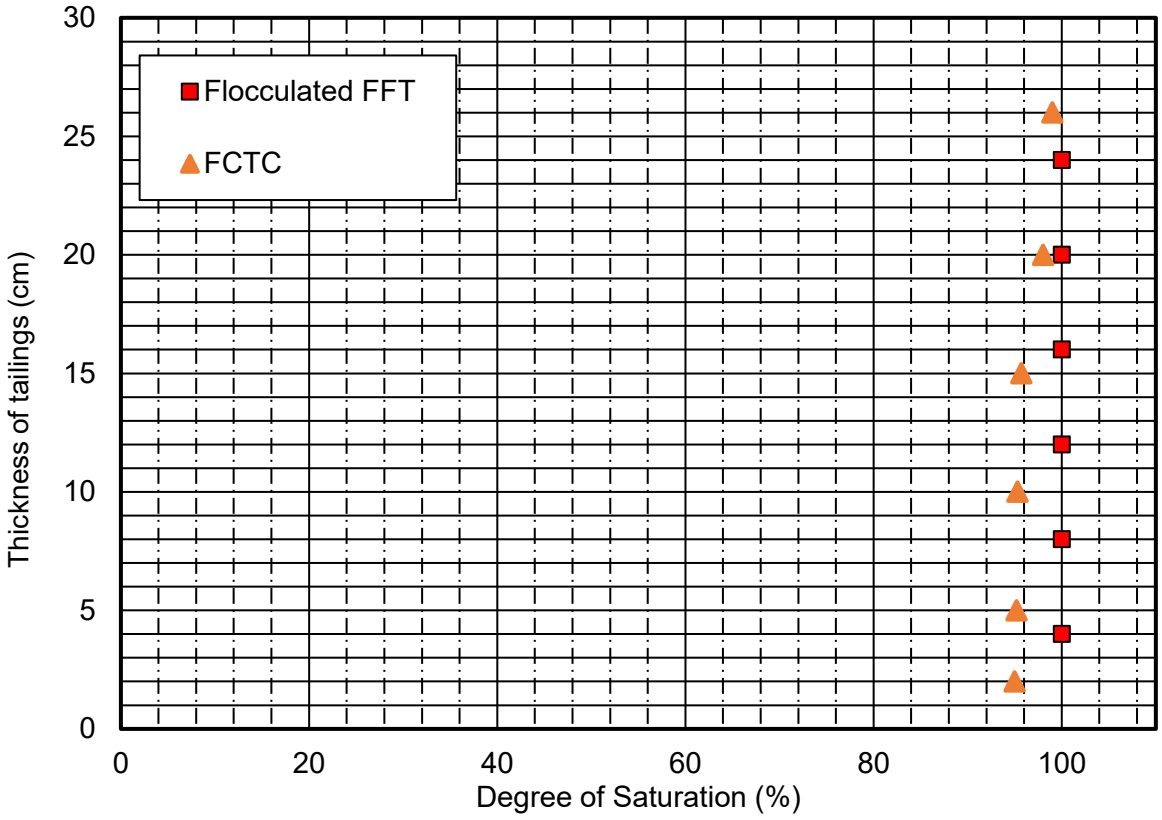

Figure 6. 27 Calculated degree of saturation profile with depth for the meso-scale column test at the end of the test period.

Undrained shear strength measurements

The undrained shear strength results are presented in Figure 5.44 and Figure 5.45 for the flocculated FFT and Figure 5.50 and Figure 5.51 for the FCTC with respect to angular deflection, depth, and time. Figure 6.28, Figure 6.29, and Figure 6.30 present the relationship between the undrained shear strength and corresponding effective stress values using assumed suction ranges for the flocculated FFT. Similarly, Figure 6.31, Figure 6.32 and Figure 6.33 present the relationship between the undrained shear strength and corresponding effective stress values using assumed suction ranges for the FCTC. Summary of undrained shear strength results from literature and the present study are presented in Table 6.4.

The effective stress values were calculated using an assumed suction value for the tailings by assuming that equilibrium had not been reached for the initial experimental testing stage. The effective stress was calculated assuming lower and upper bound suction values for that period there was no suction measurement (i.e., 10 – 30 *kPa*). The undrained shear strength values were adjusted to correct the error from the extended rod inclusion. Correction factor ranges between 0.5 to 2.2 *kPa* were applied to reflect various depth effects.

A linear relationship was obtained between the effective stress and undrained shear strength for the flocculated FFT. The corresponding slopes were 0.44, 0.37, 0.44, and 0.33 for the assumed suction values of 10 – 30 *kPa* (lower bound), 10 – 30 *kPa* (upper bound), 30 – 40 *kPa* and 50 – 60 *kPa*, respectively. Similarly, the correlation between effective stress and undrained shear strength for the FCTC was linear. The corresponding slopes were 0.21, 0.19, 0.33 and 0.41 for the assumed suction values of 20 – 30 *kPa* (lower bound), 20 - 30 *kPa* (upper bound), 30 – 40 *kPa* and 50 – 60 *kPa*, respectively. Summary of the results and literature values are presented in Table 6.4.

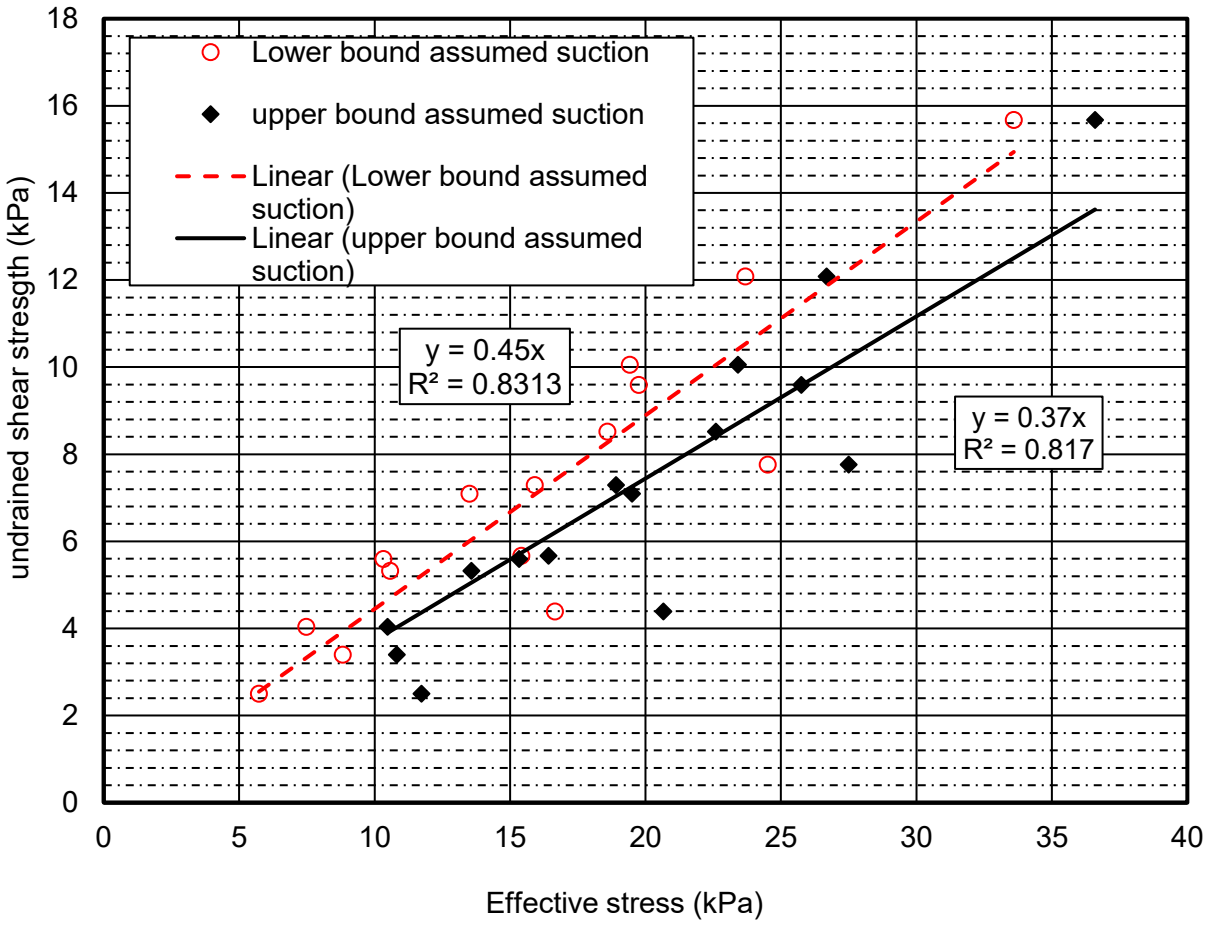

Figure 6. 28 Confining effective stress versus undrained shear strength for flocculated FFT.

The internal friction angle from the vane shear test was determined to be 20 to 33 degrees for the flocculated FFT following consolidation of the tailings using applied suction method.

The slopes from the FFT testing were compared to that of natural soils as reported in the literature (Bjerrum, 1966; Ladd, 1973; Ohara and Matsuda, 1978). However, the slope for the natural soils was smaller than the FFT. For instance, slope of 0.2 (Boston blue clay), 0.24 - 0.25 (Kaolinite clay) and 0.16 - 0.22 (Manglerud quick clay) was reported. The undrained shear strength test for the natural soils was conducted on normally consolidated state using simple shear test device.

The flocculated FFT showed reasonable linear correlation for the lower suction ranges, 10 – 40 *kPa* compared to the higher suction ranges, 50 – 60 *kPa* as shown in Figures 6.28 to Figure 6.30. As the tailings continued to dry and desiccate, wounds will be formed from continuous pre-sheared test. These wounds were not recovered (healed) as the suction values become larger. The periodical shearing might have contributed towards error measurement.

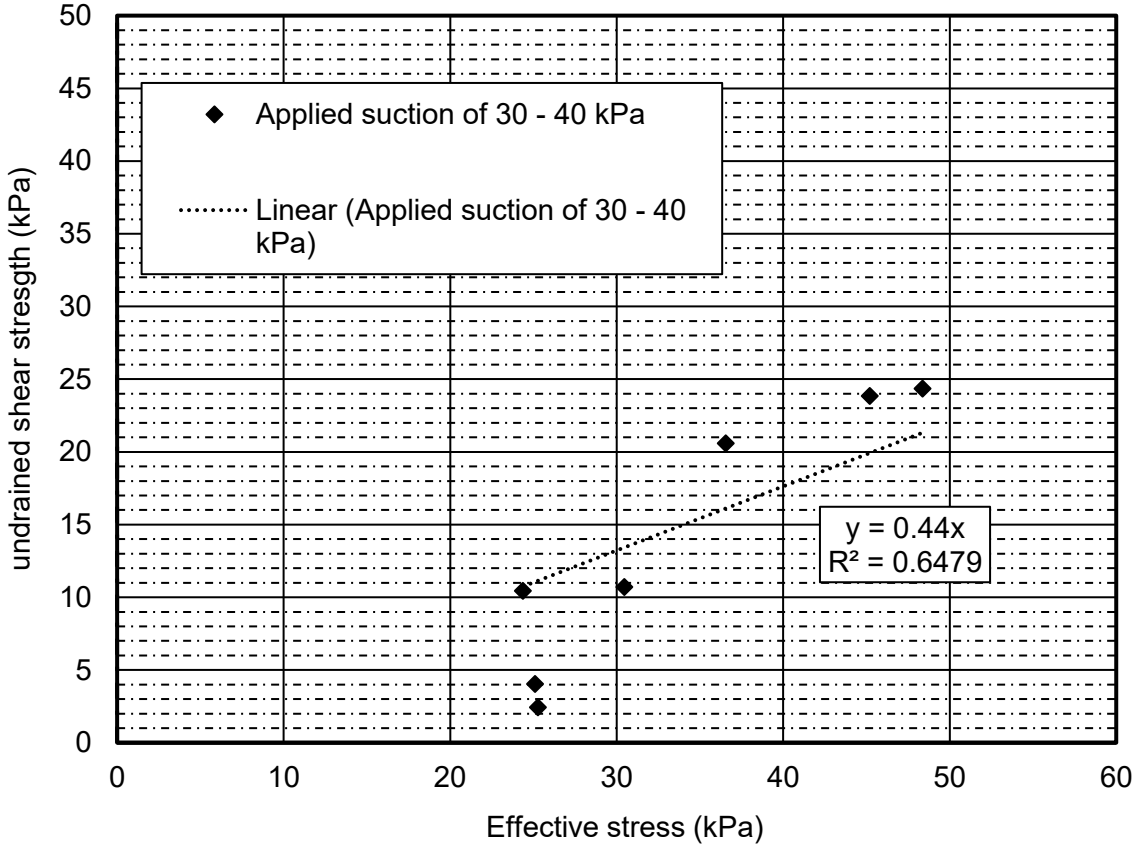

Figure 6. 29 Relationship between effective stress and undrained shear strength for flocculated FFT for the suction ranges 30 – 40 kPa.

The slope between undrained shear strength and effective stress provide the internal friction angle of the tailings. The results obtained for oil sands tailings exhibited larger internal friction angles compared to those expected from fine soils or natural clays as reported in the literature.

However, the vane device provides reasonable shear strength measurements of the material under investigation and can be used as good indicator.

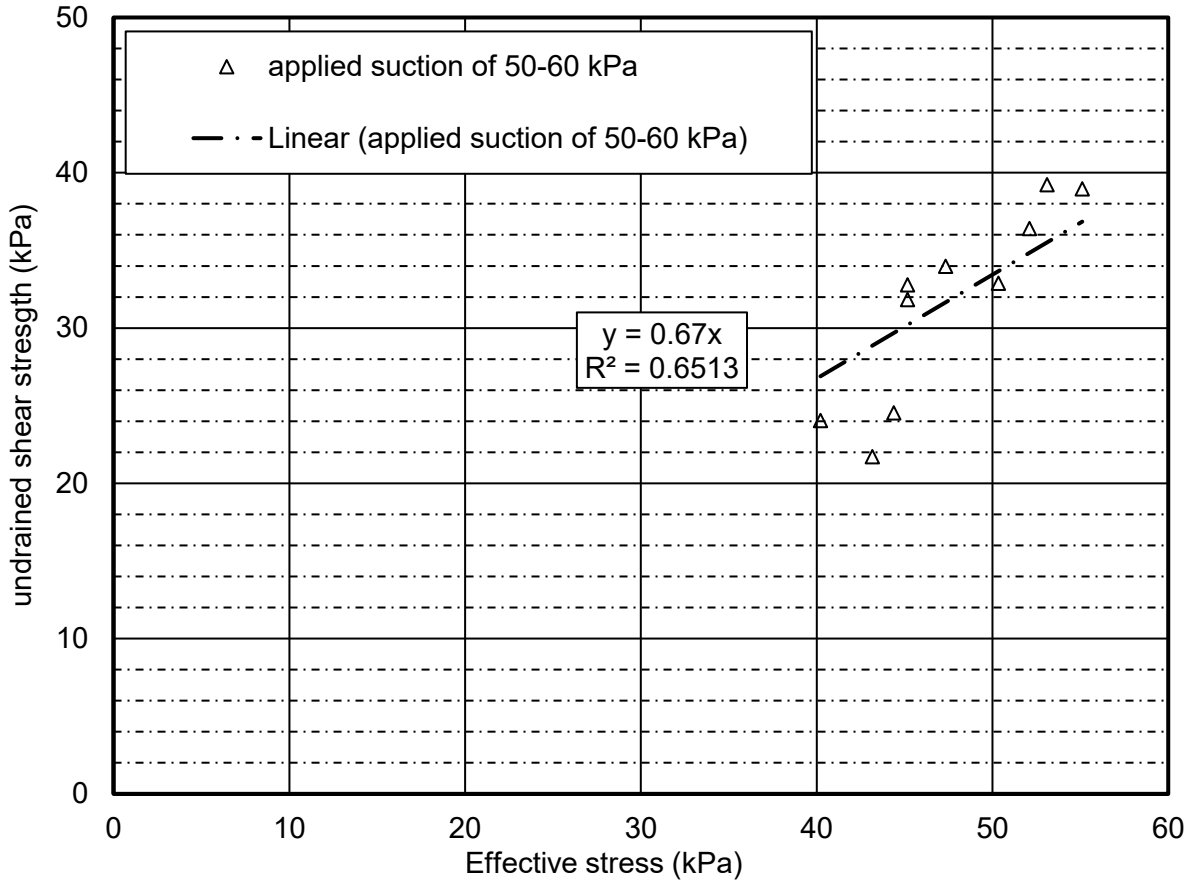

Figure 6. 30 Relationship between effective stress and undrained shear strength for flocculated FFT for the suction ranges 50 – 60 kPa.

The FCTC showed reasonable linear correlation for the most part of the 20 – 60 *kPa* suction values compared to the flocculated FFT as presented in Figures 6.31 to Figure 6.33. In addition, the FCTC shows lower slope compared to the flocculated FFT, this is due to higher fine content than the flocculated FFT. The flocculation of FFT contributed towards formation of larger aggregates of the particle.

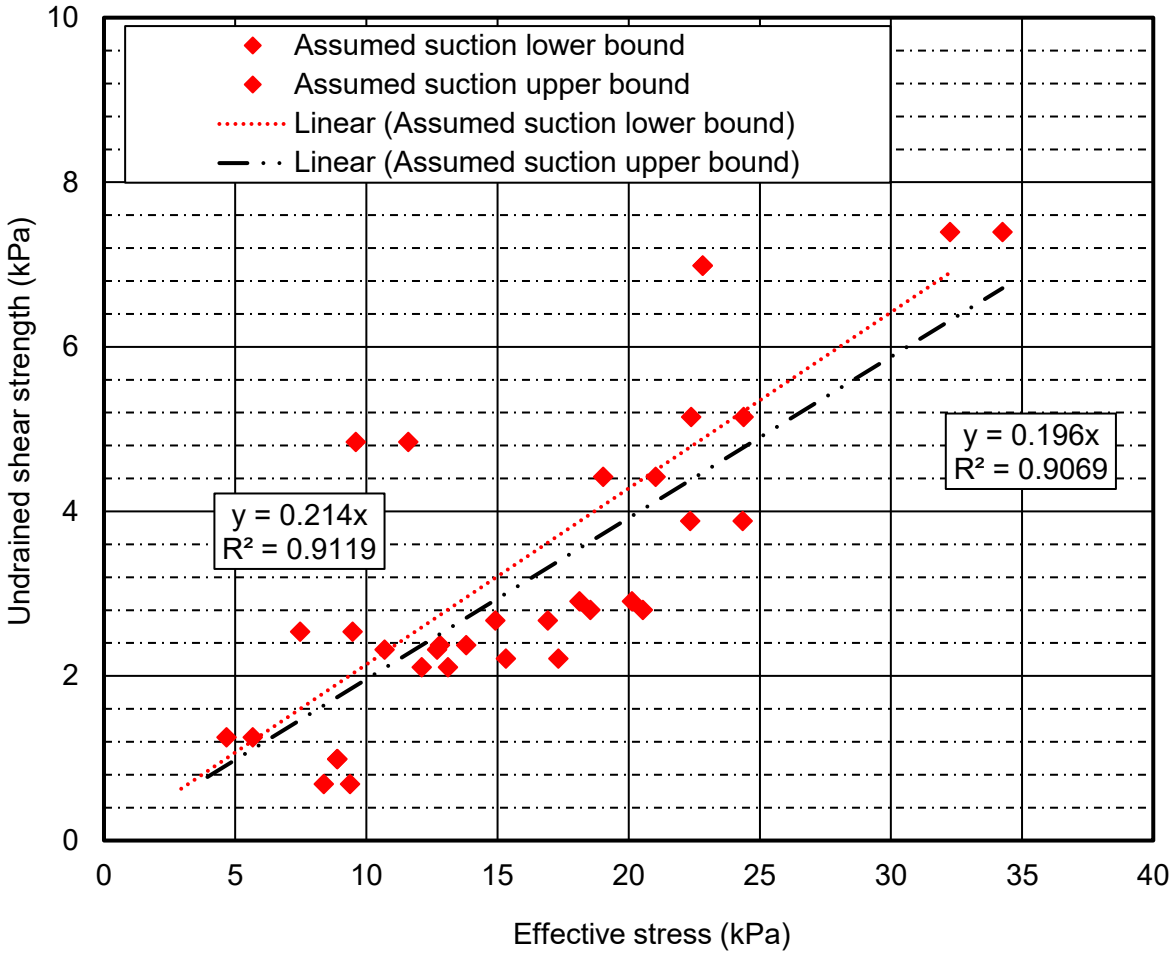

Figure 6. 31 Relationship between effective stress and undrained shear strength for the FCTC for the suction ranges 20 - 30 kPa.

The internal friction angle for the FCTC was determined to be 10 to 22 degrees following the consolidation process.

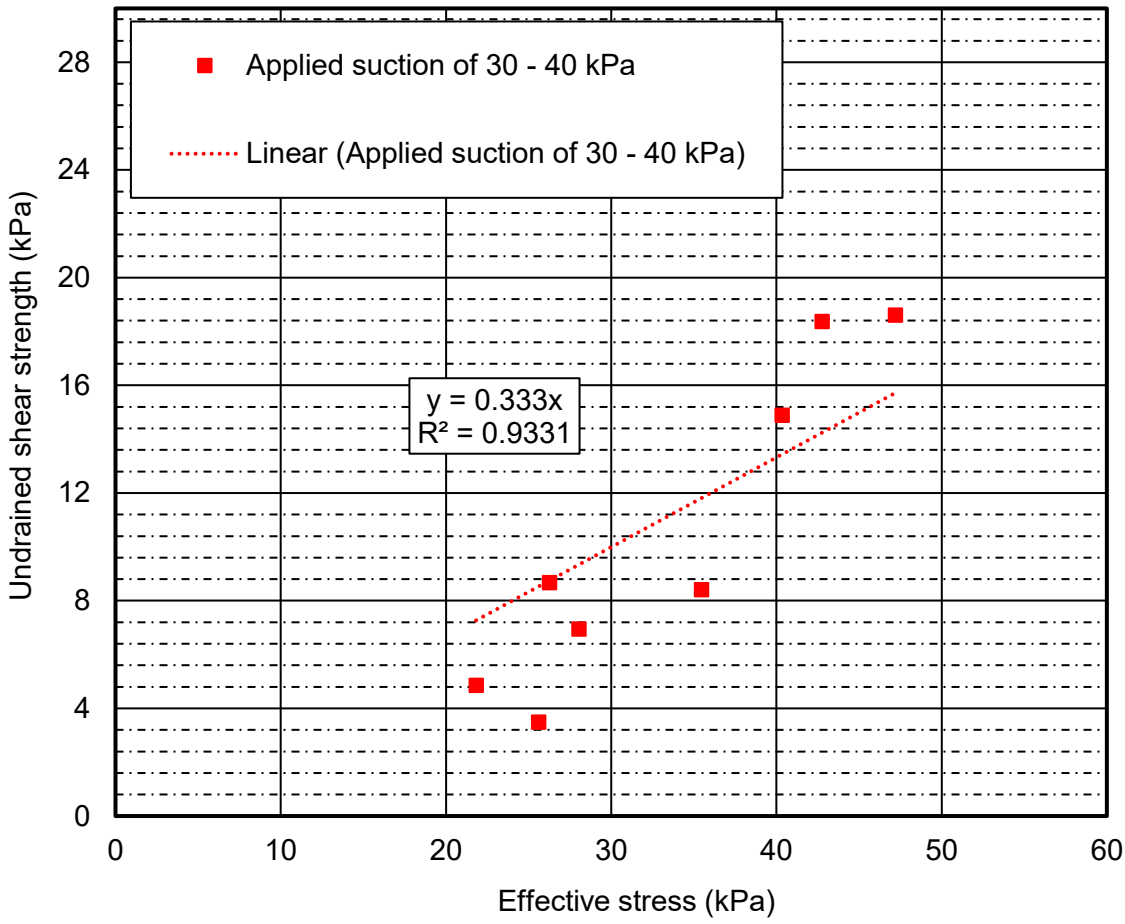

Figure 6. 32 Relationship between effective stress and undrained shear strength for the FCTC for the suction ranges 30 – 40 kPa.

Overall, the slopes between undrained shear strength and effective stress for the FFT were determined to be higher than results reported in literature. The variation between the literature and measured results from the present study can be explained as follows: i) due to the used measuring equipment (i.e., simple shear and vane shear device), ii) due to the composition of the material (i.e., natural clay versus fluid fine tailings), iii) due to the state of the sample (i.e., normally consolidated versus changing in consolidation with time), iv) not accurately measuring suction values possibly contributed towards variation and error in measurement.

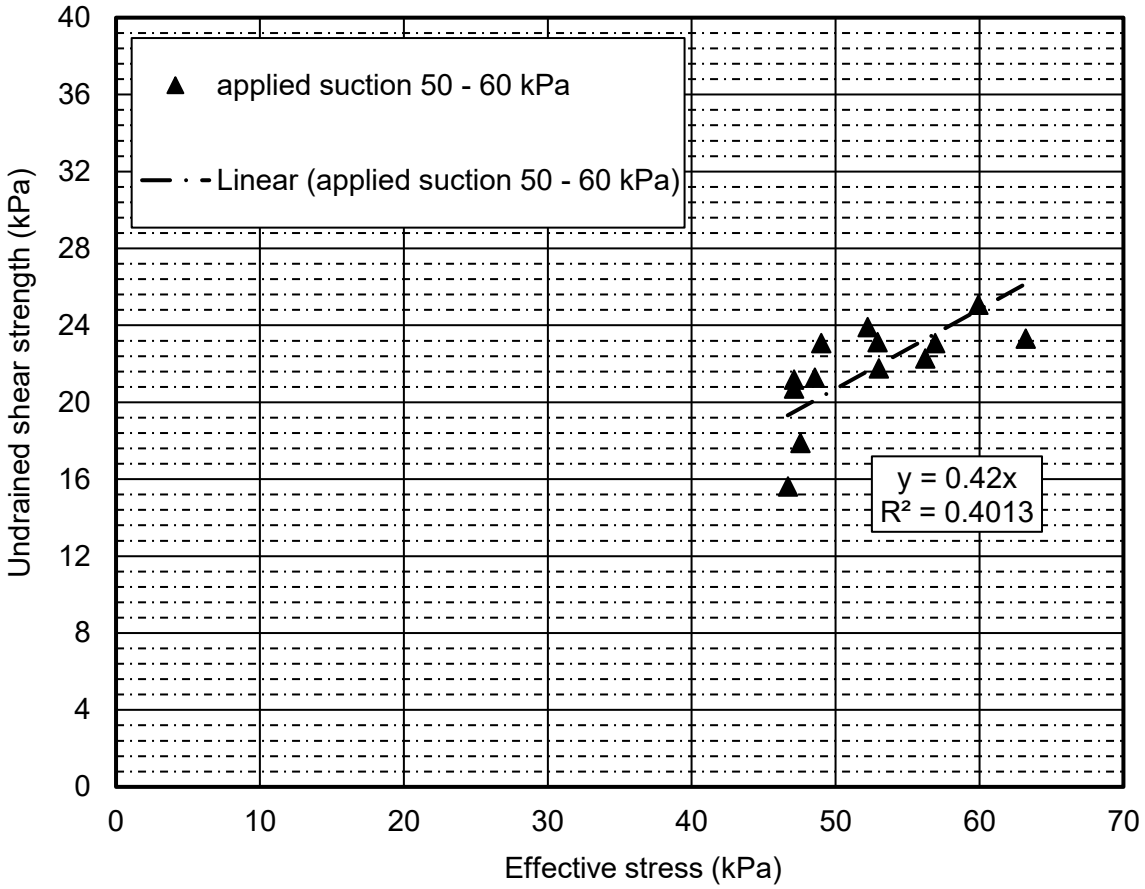

Figure 6. 33 Relationship between effective stress and undrained shear strength for the FCTC for the suction ranges 50 – 60 kPa.

6.5 Modelling

Numerical analysis was carried out to validate the measured results in the present study. An overview on the background, literature review of the numerical model is described below.

6.5.1 Background and literature review

The theory of large-strain consolidation coupled with unsaturated flow properties illustrates the consolidation behaviours for the tailings. The applied negative pore pressure and possible

evaporation near the surface of the tailings possibly allowed the formation of unsaturated zones near the tailings' surface. The literature shows the effects of evaporation in assisting the dewatering process of slurry tailings and mine reclamation processes (Daliri, et al., 2014; Fujiyasu & Fahey, 2000; Matthews et al., 2011; Simms et al., 2010; Soleimani et al., 2014; Wells, 2011).

Numerous modelling software packages which use the formulation of large-strain consolidation for unsaturated soils are described in the literature. The models use different constitutive relations to describe the material properties and various independent variables as their constitutive variables (Gibson, England, & Hussey, 1967; Lee, 1979; Yong, Siu, & Sheeran, 1983; Mcvay, Townsend, & Bloomquist, 1986; Townsend & McVay, 1990). Some of the commercially available software using large-strain formulation are Soilvision®, FSCONSOL, and CONSOL. Some models that incorporate formulation of large-strain consolidation coupled with unsaturated flow or desiccation are CONDES (Yao et al., 2002), MinTaCo (Seneviratne et al., 1996), and UNSATCON (Qi et al., 2017a; 2017b).

Some of the advantages of numerical modelling software using formulation of large-strain consolidation coupled with unsaturated flow are:

1. The unsaturated flow model is valuable in describing and understanding the soil-atmosphere interaction happening near the tailings surface. The evaporation effect reduces the potential rate of consolidation as larger total suction values develop (> 1 MPa) near the surface (De Vries, 1987; Wilson, Fredlund, & Barbour, 1997).

2. The constitutive relations are different as the degree of saturation of the tailings changes from fully saturated to partially saturated as the soil suction becomes greater than the air-entry values of the tailings under investigation.

3. The effect of the dried, desiccated, and desaturated layer on freshly placed materials above it requires proper constitutive and material property assignment due to changes in the degree of saturation that accelerate consolidation (Daliri et al., 2014; Fisseha, Bryan, & Simms, 2010).

6.5.1.1 Self-weight consolidation – stage 1

A commercially available software, SoilVision®, were considered to model the self-weight consolidation process during the present study. Two-stage modelling exercises for the flocculated FFT were carried out to validate measured results due to the self-weight consolidation exhibited (i.e., no self-weight process was observed for FCTC).

The first stage (Stage 1) was used to validate measured self-weight consolidation results using model predictions. The second stage (Stage 2) was used to validate the results obtained from the consolidation using applied suction process using recently developed model, UNSATCON, for deformation coupled unsaturated flow analysis (Qi et al., 2017a, 2017b). To date, there is no commercially available software which retains the ability to simulate the deformation process coupled with unsaturated flow behaviours. The UNSATCON model is still at its development stage, therefore, the consolidation stage due to applied suction was modelled for only flocculated FFT for validation purposes only.

6.5.1.2 Consolidation using increments of applied suction - stage 2

There are no commercially available software products that can assist in modelling the process of consolidation using increments of suction through the bottom boundary. The alternative is to conduct modelling for the transient flow using existing unsaturated/saturated flow model. However, the existing model has limitations which do not include the analysis of unsaturated flow

coupled with deformation. A newly developed model, UNSATCON, was used to verify the consolidation using incrementally applied suction results. Details of the UNSATCON model are presented below.

6.5.2 Self-weight consolidation modelling

Model setting

The self-weight consolidation (stage 1) analysis was conducted using SVFLUX-SVSOLID (consolidation) GT module of SoilVision® since the software was readily available. The material properties, initial and boundary condition used during stage 1 are used based on engineering properties obtained from the laboratory and summarized and presented in Table 6.7 below. The properties used were measured values adjusted as required to achieve convergence. The Poisson's ratio value was assumed within the acceptable range, hydraulic conductivity values was modified to achieve good agreement. Hydraulic conductivity of was adjusted from the measured (i.e., 8.64E-07 m/day) to 1.75E-07 m/day to obtain results compared to the measured total settlement. Weibull function were used for the compressibility curves to incorporate high change in volume properties of flocculated FFT.

Table 6. 7 Summary of geometry, material properties, initial and boundary conditions used during the self-weight consolidation modelling exercise for the flocculated FFT.

Geometry				
Description	**unit**	**Base reference (y-axis)**	**Thickness of material**	
Deposited tailings	m	0	0.505	
Material property				
Model type and description	Used functions	Fitting method	Parameters	
SVSOLID			*A*	0.585

	Compressibility function	Weibull function under Elasto-plastic category	*B*	-0.821
			E	-0.688
			F	-0.269
		Elastic parameters	Poisson's ratio	0.3
			Minimum stress limit (*kPa*)	0.15
SVFLUX	Saturated hydraulic conductivity	Single power function	*C* (*m/day*)	1.750E-07
			D	8.71
Initial condition				
Model type and description	Assigned parameters	unit	Type	Value
SVFLUX	Initial head	m	calculated	-
SVSOLID	initial void ratio	-	constant	4.07
Boundary condition				
Model type and description	Boundary regions	Assigned parameters	Y- direction	Value (kPa)
SVSOLID	Top	Displacement	Free	-
	Bottom		Fixed	-
SVFLUX	Top	No boundary condition (No BC)	Excess pore pressure constant	0
	Bottom	No boundary condition (No BC)	Zero flux	-
Stage setting				
Stage name	Description	Duration (days)	Total duration (days)	Increments
1st Stage	initiation	0.1	0.1	1
2nd Stage	construction	99.9	100	1

The initial model geometry (1D) for the flocculated FFT for the initial deposition stage using SVFLUX coupled SVSOLID software is presented in Figure 6.34 and Figure 6.35 for SVFLUX and SVSOLID, respectively.

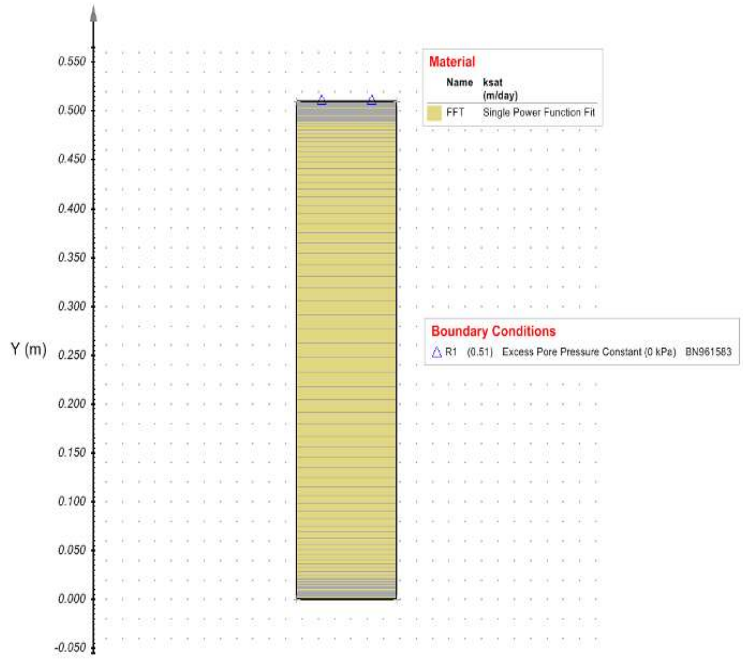

Figure 6. 34 Initial model setup using SVFLUX front view.

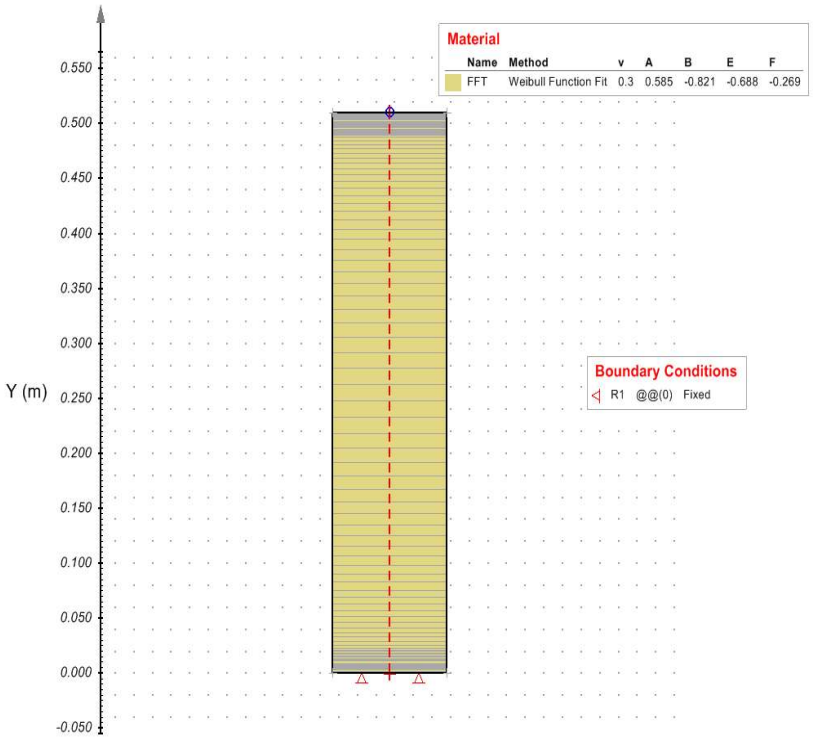

Figure 6. 35 Initial model setup using SVSOLID front view.

Model output

The output results obtained from the model are presented in this section. Figure 6.36 presents the final output results showing the final change in height and void ratio distribution for the self-weight consolidation process of the flocculated FFT. Comparison of measured results with modelled outputs are presented with the discussion below.

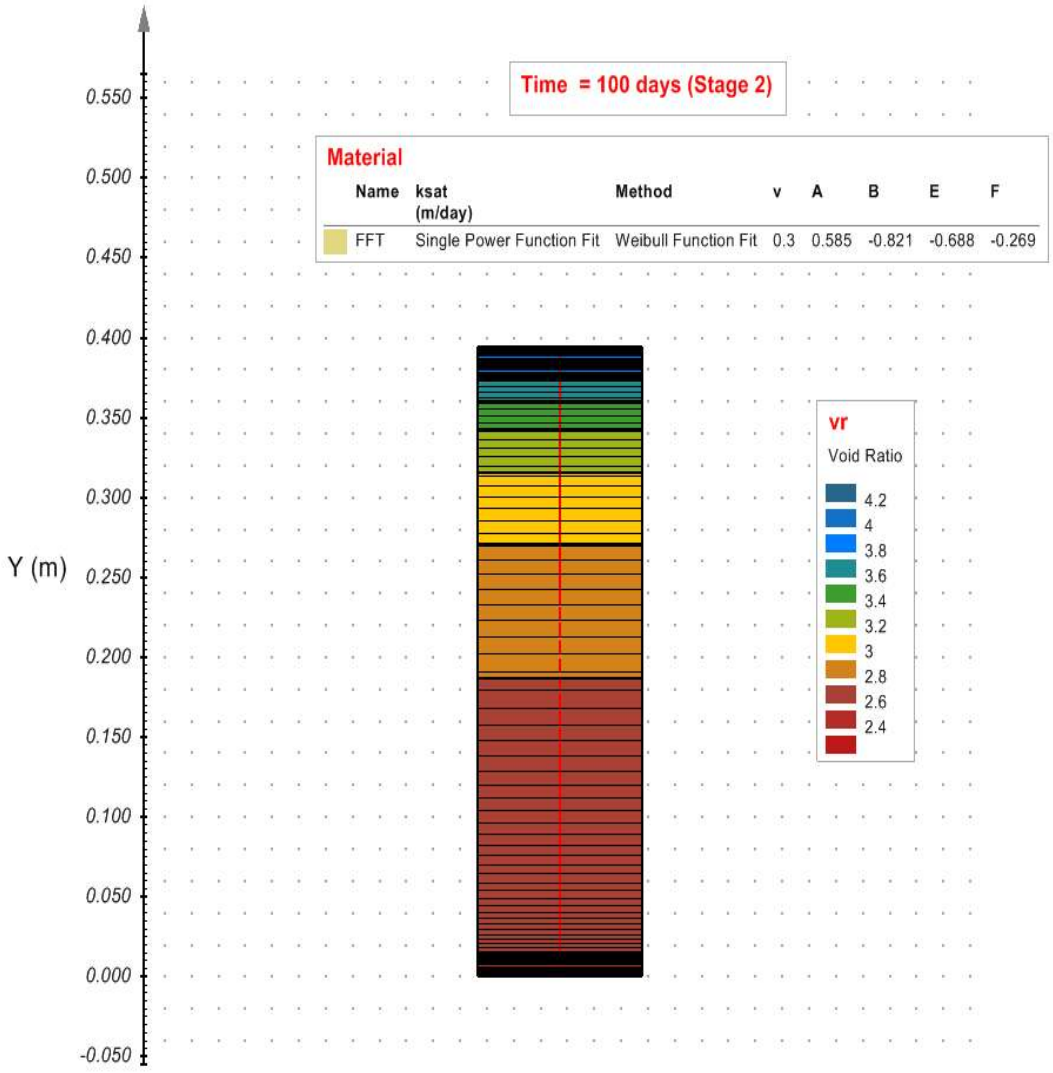

Figure 6. 36 Model output results from SVSOLID coupled SVFLUX.

Void ratio

The void ratio distribution within the flocculated FFT profile varies with depth as expected. The initial void ratio assigned was 4.07 and was uniform for the entire profile. Figure 6.36 shows output results comparison between model output and average void ratio measured. Modelled output results are presented as “Day 1” and measured values are presented as “e-avg_Day 1”. The output from the self-weight model results shows a smaller void ratio near the bottom of the column with variations along the entire material thickness, as shown in Figure 6.37.

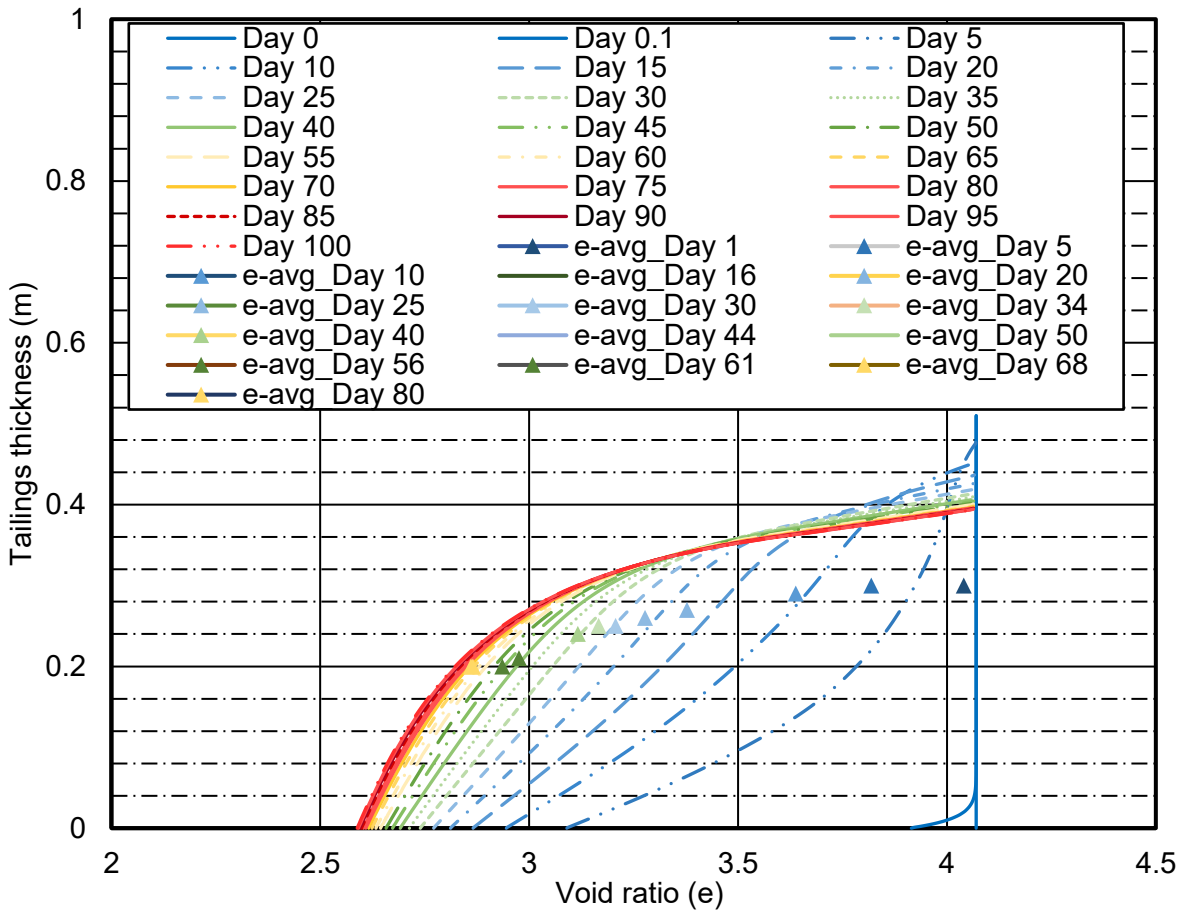

Figure 6. 37 Modeled and measured average void ratio for the flocculated FFT during stage 1.

For example, the final void ratio of 2.2 was measured at the bottom of the column by the end of the self-weight consolidation process and 4.07 was measured near the surface. Figure 6.37 presents the change in void ratio with depth and time from the measured and modelled results.

The model output was compared with the average void ratio calculated for the entire tailings column thickness. The results of the average void ratio were calculated and plotted against the average tailing thickness using single data points for a given day. The measured and predicted results were in agreement. The discrepancies were attributed to taking the average void ratio for the entire tailings thickness as opposed to the model handle.

Settlement

The modelled settlement results for the flocculated FFT are presented in Figure 6.38. These results were in reasonable agreement with measured results. The model slightly over-predicted the settlement for the first 30 days and under-predicted the settlement from day 60 until the end of the self-weight consolidation process.

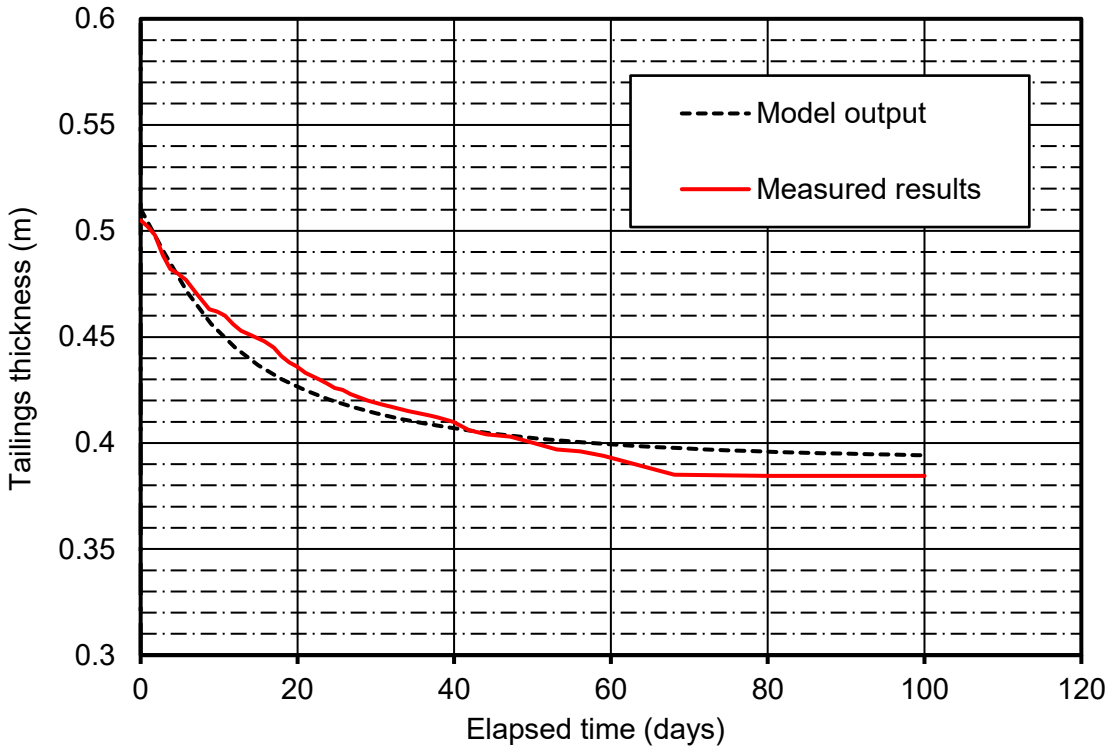

Figure 6. 38 Total vertical settlement for the flocculated FFT during the self-weight consolidation process.

In general, the model output was in agreement with the average measured settlement. It should be noted that the settlement measurements were conducted using three-point measurement and averaged methods from the surface since the tailings surface was not flat and smooth.

Excess pore pressure

The results of excess pore pressure dissipation from the model output and measurement are presented in Figure 6.39. A comparison of the modelled and measured results shows good and reasonable agreement. Pore pressure results are described as “MEpwp_Day 1” for the measured excess pore pressure and “Day 1” for the model output. Possible excitation values were

incorporated that can increase the sensitivity values of the sensor. Roughly up to +/- 5% of error can be included due to excitation and other factors.

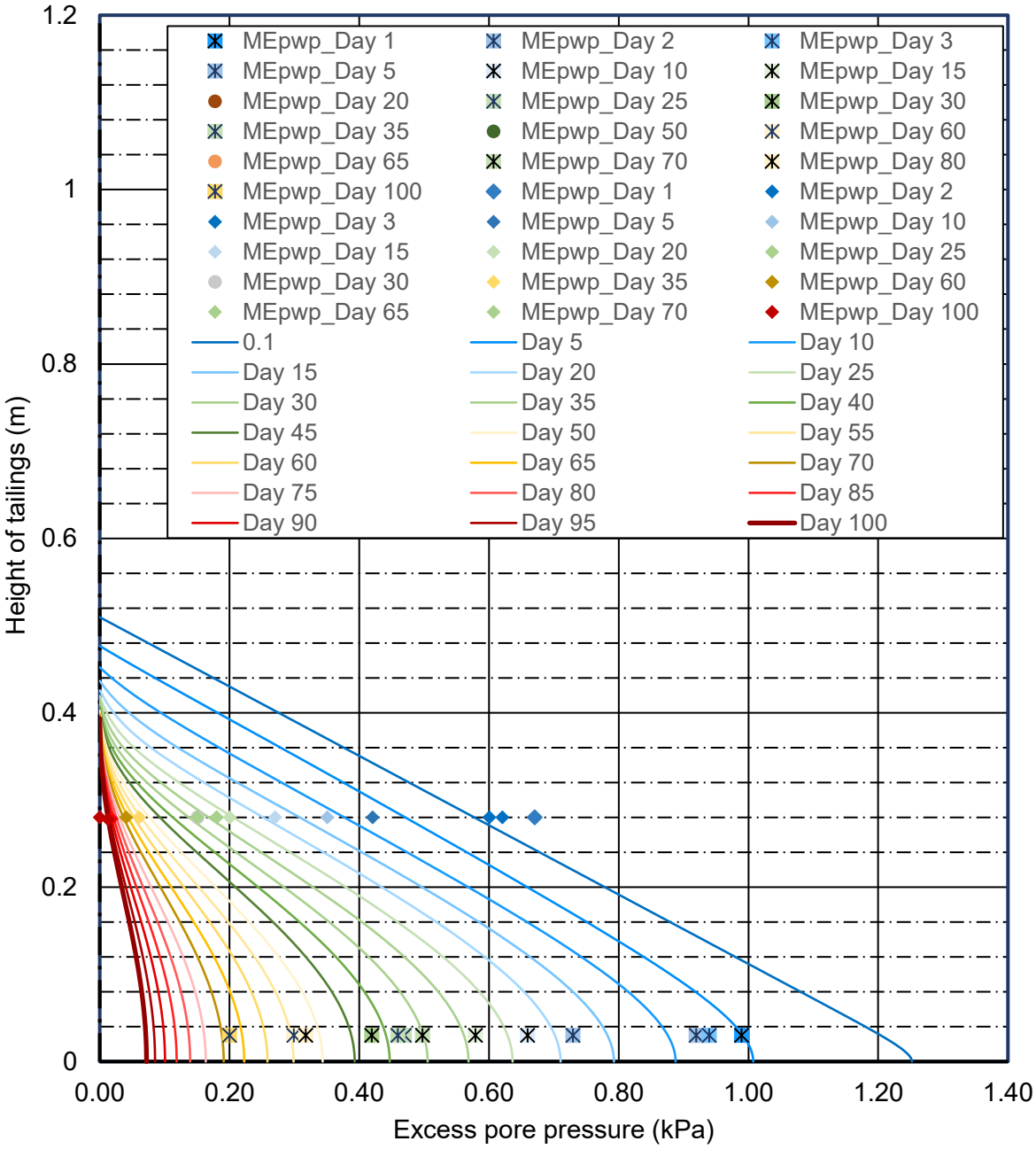

Figure 6. 39 Excess pore pressure dissipation for the flocculated FFT during the self-weight consolidation process.

The measured data points are presented with the same colour for the corresponding dissipation time presented by the model. The model and measured results are presented as line and data points in Figure 6.39 for the corresponding elevation, i.e., sensor located 3 cm and 28 cm above the column base. The same colours are used between measured and modelled excess pore pressure for the same corresponding times. Overall, a good agreement was predicted between the modelled and measured dissipation of excess pore pressure results.

Effective stress

The effective stress results calculated using the model are presented in Figure 6.40. The model output was compared with the calculated effective stress results using the change in total density presented in Chapter 5, section 5.3.

The calculated effective stress values are presented as individual data points for a given time and described in the legend as “C – Day 10 @ 28 cm” to indicate the calculated, day 10 located at 28 cm from the base of the column. The model results are given as line in the plot. The calculated effective stress results were higher than the effective stress predicted using the model. For example, the calculated effective stress was 2.6 kPa near the base of the column by the end of the self-weight consolidation period in comparison to 1.2 kPa predicted by the model. The calculated effective stress values were reasonable in agreement assuming error values of 0.4 – 1.3 kPa over time.

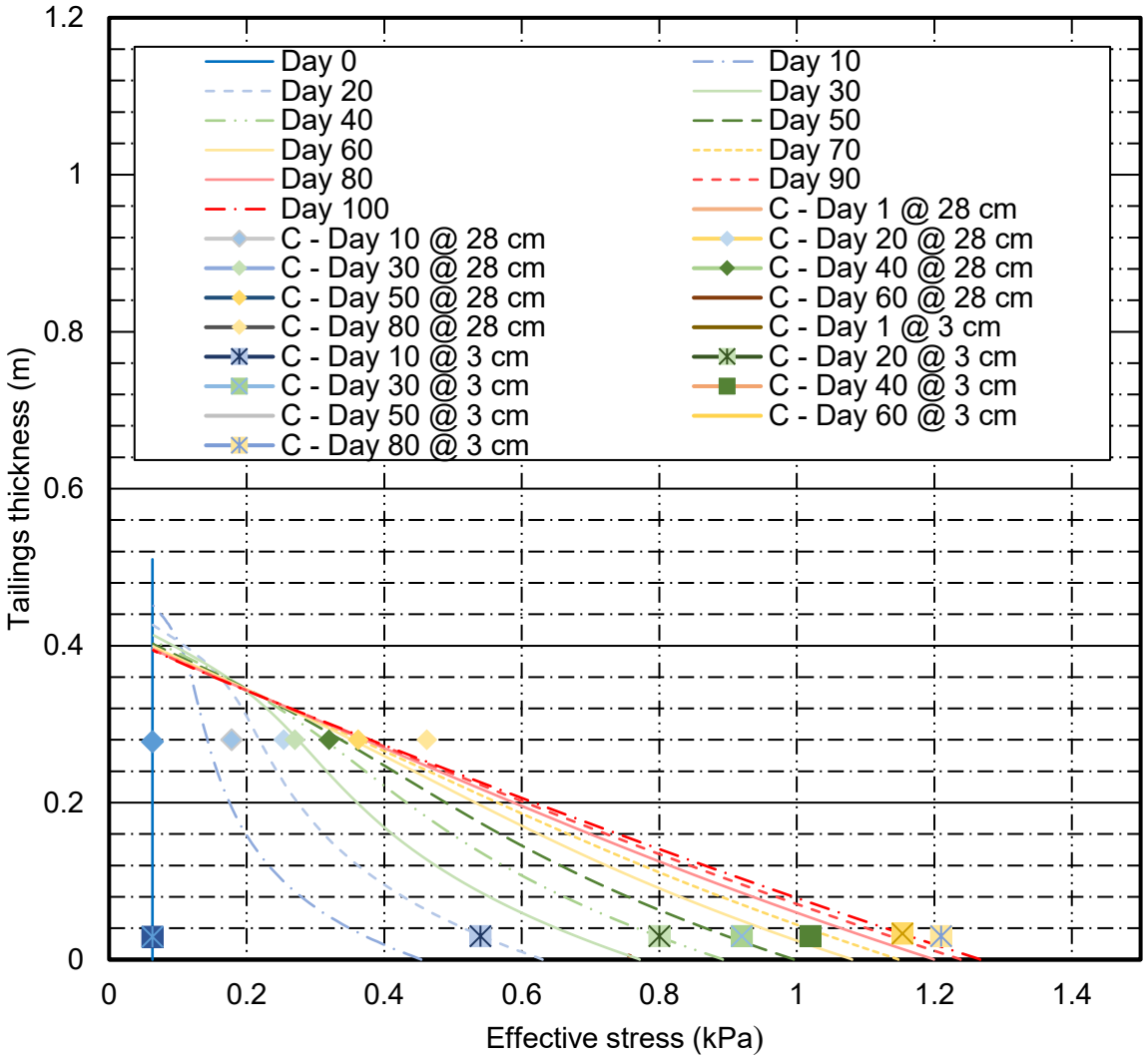

Figure 6. 40 Effective stress computed from the model output for the flocculated FFT during the self-weight consolidation process.

6.5.3 Consolidation using applied suction modelling

Model setting

UNSATCON model was used to validate the measured results during stage 2. As an example, only results for the flocculated FFT were modelled and compared with the measured results. The results displayed the change in suction distribution over time with profile.

The required parameters were determined by fitting with the empirical formula described in UNSATCON model (Qi et al., 2016, 2017a, 2017b). The parameters used from state surface model (SSM) and hydraulic conductivity functions are summarized in Table 6.8 and Table 6.9, respectively.

Table 6. 8 Summary of fitting parameters for the tailings used during the testing program.

Modified State Surface Model (SSM)								
Volume change behaviour								
Fitting parameters	**a - controls intial e**	**b - related to average slope of compression line and SWCC**	**c - curvature of compression curve**	**d - curvature of SWCC**	**f - curvature of compression curve**	**g - curvature of SWCC**	**κ**	**κ_s**
Flocculated FFT	5.3	0.85	0.06	0.006	1620	1000	0.015	0.0015
FCTC	3.0	0.5	0.005	0.0005	270	300	0.015	0.0015
Water retention behaviour								
Parameters	$C_{drying\ -\ postion\ SWCC}$		$C_{wetting}$	$\lambda_{se\ -dependence\ SWCC\ on\ e}$		$\lambda_{sr\ -\ slope\ SWCC}$	λ_{ss}	
Flocculated FFT	2.5		1.5	0.15		0.4145	0.115	
FCTC	0.5		1.5	0.15		0.334	0.108	

Table 6. 9 Summary of the parameters obtained using the power and exponential functions for the flocculated FFT and FCTC.

Permeability function parameter	**Flocculated FFT**		**FCTC**	
	Power function	**Exponential function**	**Power function**	**Exponential function**
k1	1.0E-11	8E-12	3E-10	6E-12
k2	8.7089	3.1541	4.3404	3.7686
k3	0.75	0.5	0.75	0.5

The initial and boundary conditions assigned during the modelling exercise are presented in Tables 6.10 and Table 6.11, respectively. The initial conditions were the thickness of the deposited tailings, number of depositions, initial void ratio, specific gravity, and duration of time for the model to run.

Table 6. 10. Initial condition used during the modelling exercise.

Description	Symbol	Units	Materials used	
			Flocculated FFT	FCTC
Total tailings height	*h*	*m*	0.5	0.37
Number of depositions	1	*unitless*	1	1
Initial void ratio	*e*	*unitless*	4.01	2.01
Specific gravity	G_s	*unitless*	2.22	2.58
Total run time	*t*	*days*	450	420

Table 6.11 summarizes the boundary conditions used during the modelling exercise for the flocculated FFT. The boundary condition given for the first 100 days described self-weight consolidation at the top that includes decantation. The bottom boundary condition describing incrementally applied negative water pressure (suction) was given following day 100 until the end of the experimental test (i.e., 450 days).

Table 6. 11 Boundary condition used during the modelling exercise.

Description	Stage 2	Materials used	
		Flocculated FFT	FCTC

Top boundary	No boundary condition	Decantation	N/A
Bottom boundary	Consolidation using applied suction	Incremental suction with time	

Figure 6.41 presents the increments of applied suction at the bottom boundary over time. The bottom boundary condition was specified as zero during the self-weight consolidation process. Figure 6.42 presents the graphical user interface for the UNSATCON model.

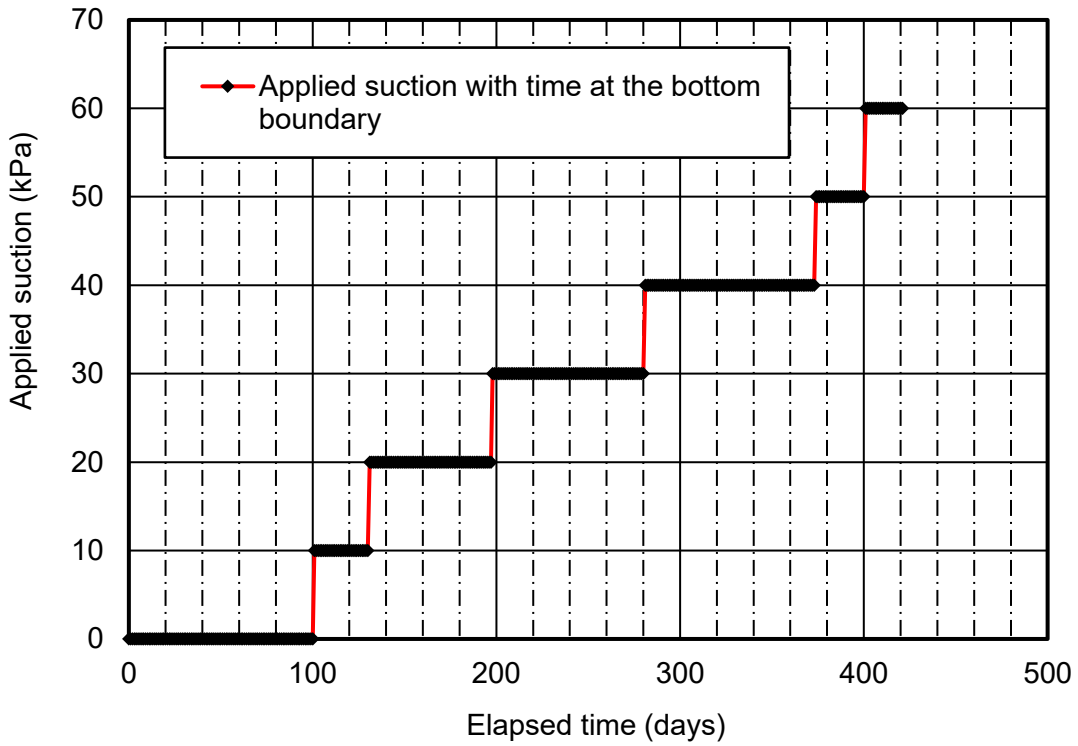

Figure 6. 41 Increments of applied suction placed at the bottom boundary during the meso-scale consolidation test.

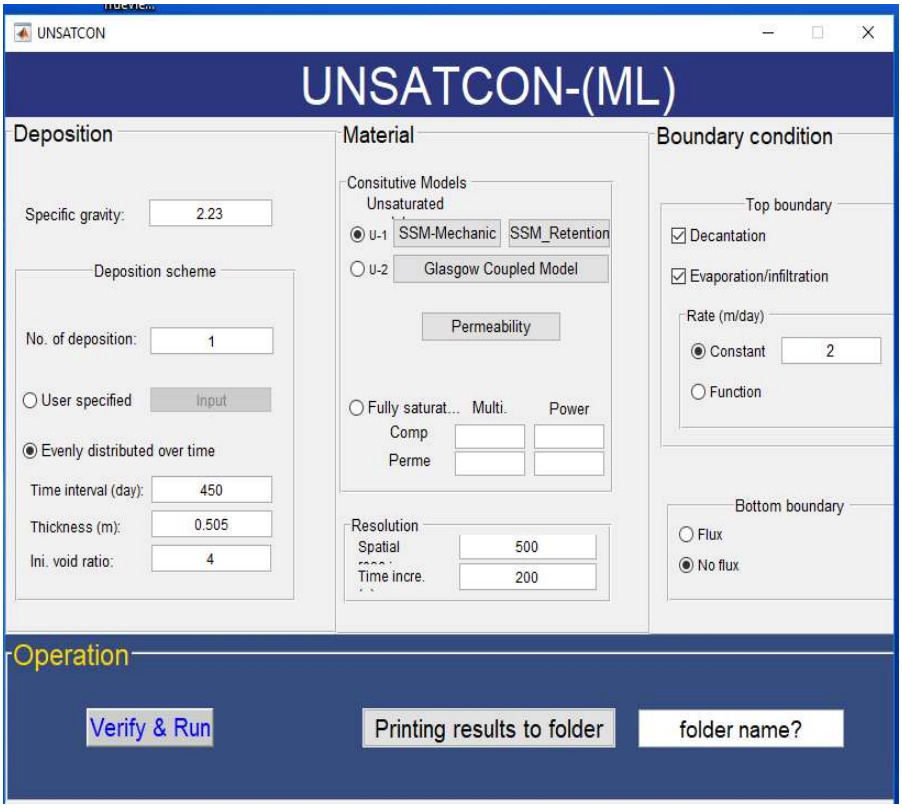

Figure 6. 42 UNSATCON model graphical user interface.

Model output

The results from the UNSATCON model was the: change in total height, gravimetric water content, solids content, void ratio, and distribution of suction with deposited tailings thickness, and are discussed in the following section.

The model requires additional calibration and refinement to achieve reasonable agreement with the measured results. The scope of this thesis does not include development of the software, refinement and calibration.

Change in total height

The measured and modelled change in total height (vertical strain) for the applied suction test are presented in Figure 6.43. The final height was 0.23 m and 0.25 m for the measured and model, respectively. Overall, reasonable, and acceptable agreement was obtained between the measured and modelled results.

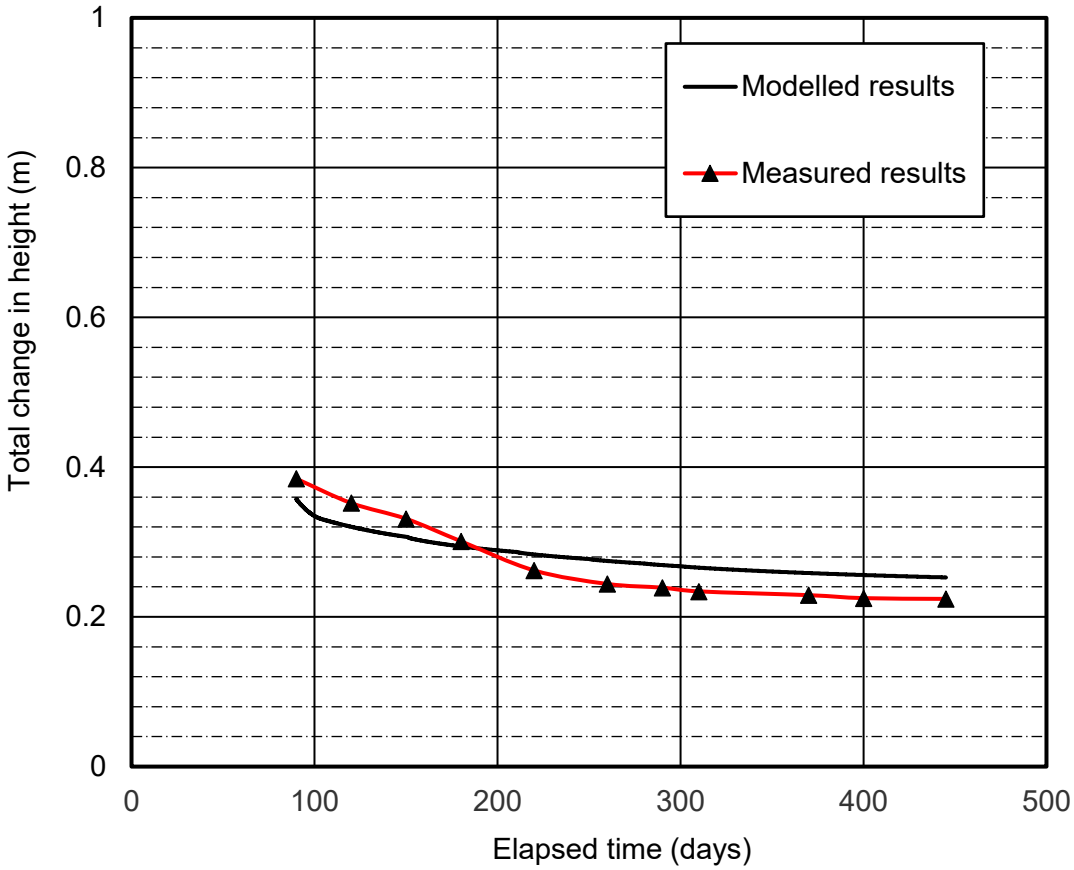

Figure 6. 43 Comparison of measured and modelled vertical strain results.

Gravimetric water content

The results of measured and modelled gravimetric water content for the applied suction test are presented in Figure 6.44. The measured gravimetric water content results were carried out once

the test was completed. Good agreement was obtained between the measured and modelled results. The final measured and modelled gravimetric water contents were 0.385 and 0.347, respectively. Overall, acceptable agreement was achieved for the flocculated FFT. The gravimetric water content calculated using the unsaturated soil properties overestimated the solids content (i.e., 0.48). Gravimetric water content was decreased three months following the completion of the test, due to effect of evaporation. The reason to include gravimetric water content results 3 months after the test completion was to show effect of evaporation while being under controlled environment (laboratory setting).

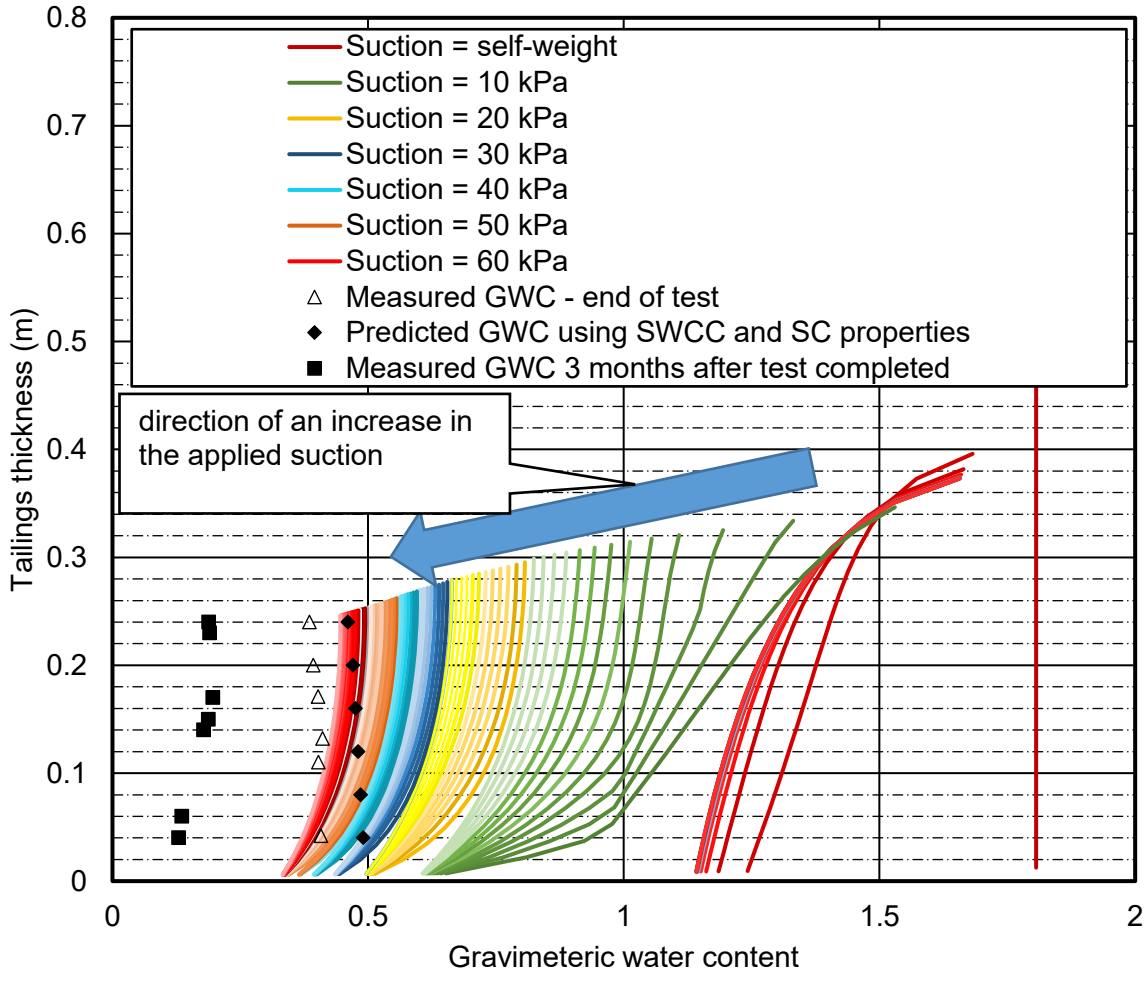

Figure 6. 44 Comparison of measured and modelled gravimetric water content results.

Solids content

The measured and modelled solids contents for the applied suction test are presented in Figure 6.41. The solids content results were calculated from the gravimetric water content; therefore, these results are related. The final solids content was an average of 72%. Overall, acceptable agreement was achieved as shown in Figure 6.45. Solids content calculated using unsaturated soils properties under predicted the results and provided an average of 68%. An increase in the solids content results observed three months after completion of the meso-scale test. There was no incremental suction was applied following completion of the test. The results assert the decrease in solids content along the profile is due to effect of evaporation.

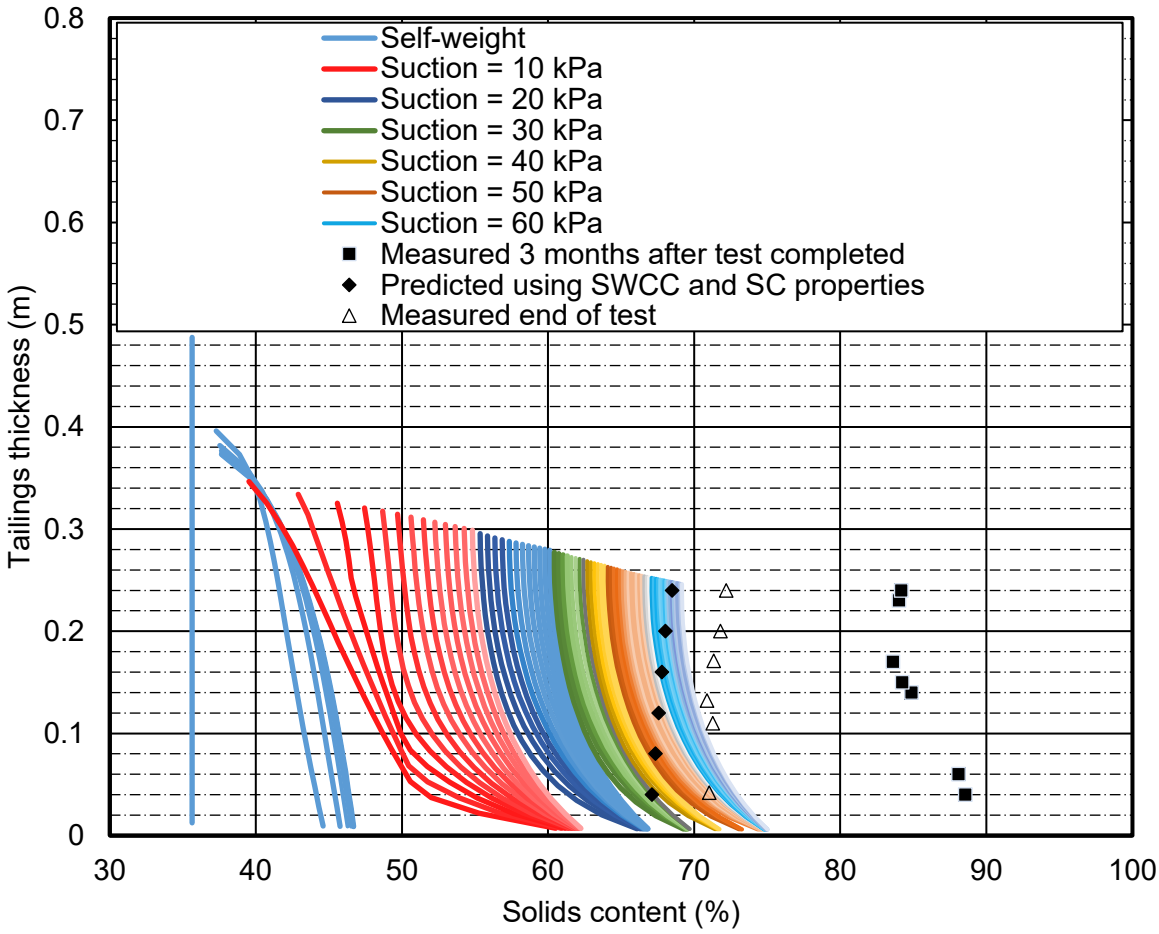

Figure 6. 45 Comparison of measured and modelled solids content results.

Void ratio

The measured and modelled void ratios are presented in Figure 6.46. The measured void ratio considered lateral deformation. The average measured void ratio for the tailings thickness is presented using a coloured “diamond mark.” The colours correspond to progression of suction line colours depicted in Figure 6.46. Averaging the void ratio shifted the void ratio values, especially when there was a larger difference between the void ratio near the surface and bottom of the tailings. The final average measured and modelled void ratios were 1.07 and 1.35, respectively. Overall, a reasonable agreement was achieved at the lower suction values. As suction values increased significant differences was observed between the calculated and modelled void ratios. Further refinement of the model is recommended to obtain more accurate results.

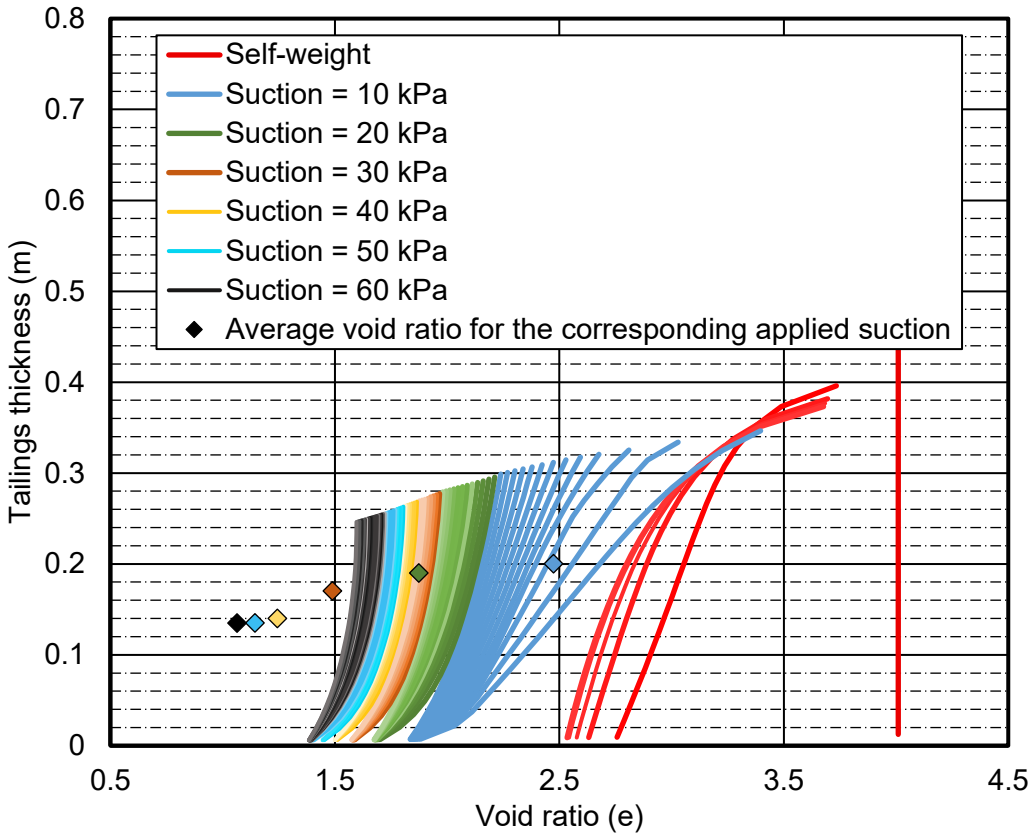

Figure 6. 46 Comparison of measured average void ratio and modelled void ratio results.

Distribution of suction

The results of the suction distribution are presented in Figure 6.47. The measured suction distribution for the tailings profile showed higher suction than applied at the base for the duration of time. On the other hand, the model results show a similar progression, which is an increase in suction compared to the previous measurement within the profile. However, the final suction results were lower than the applied suction at the bottom boundary indicating an equilibrium condition had not been reached.

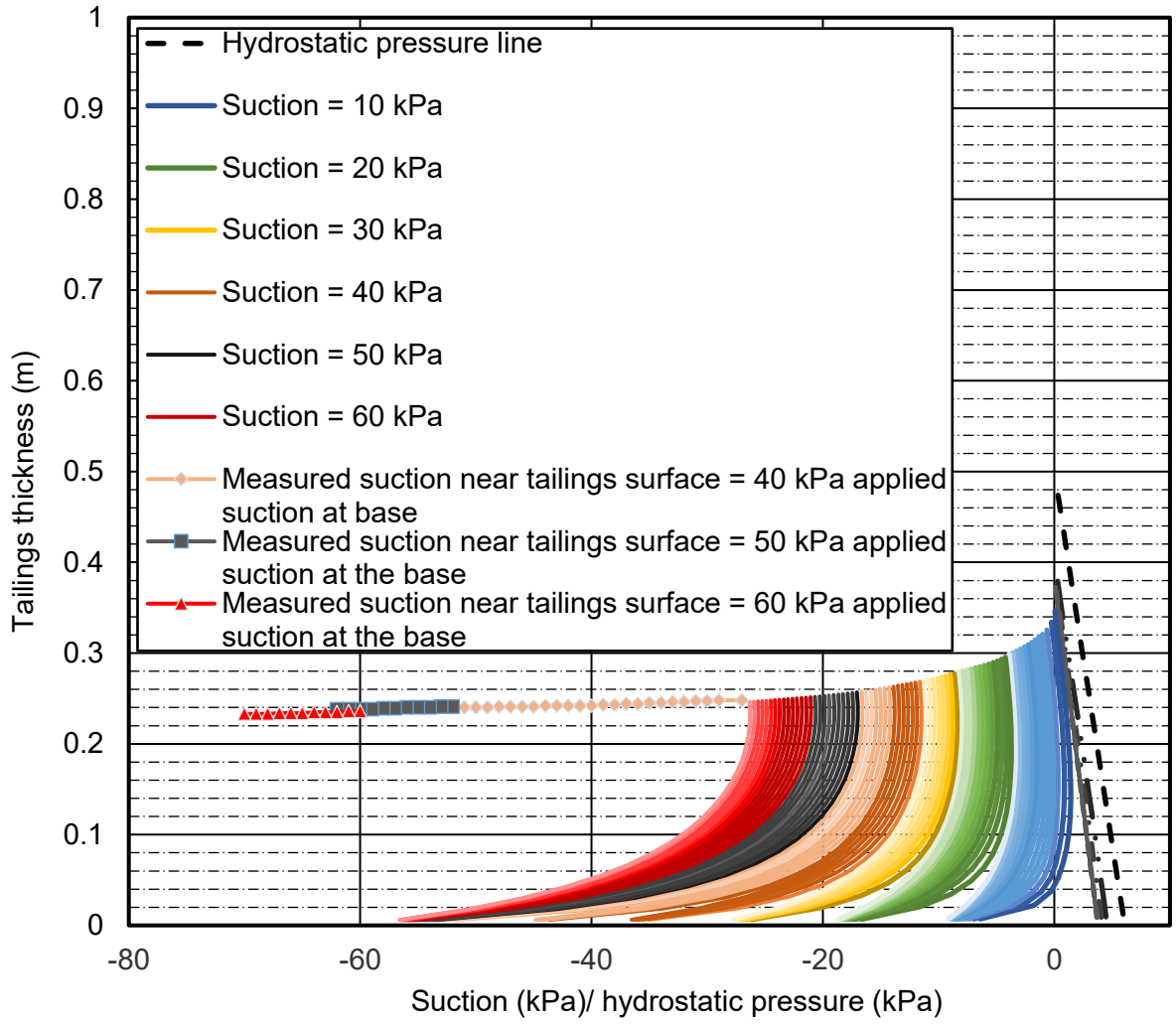

Figure 6. 47 Comparison of modelled and measured distribution of suction results.

The model results displayed the same trend with respect to developed suction over time within the tailings profile. The suction results near the tailings surface exhibited much higher suction values compared to the modelled results as shown in Figure 6.47. The results did not display an agreement due to higher suction measurements near the tailings surface. Effect of evaporation might have attributed in measuring higher suction results near the tailings surface. A calibration of the model is required to refine and correct the suction distribution results to mimic results measured results during the meso-scale laboratory test.

In conclusion, modelled results using the UNSATCON provided agreeable surface settlement compared to the measured using the meso-scale testing. The gravimetric moisture content and solids content exhibited reasonable agreement for the overall values for the given specific time, however the values displayed different trends with depth between the corresponding results of measured versus modelled.

There was no agreement for the suction results between the modelled and measured for the profiles. Therefore, further refinement and calibration of the UNSATCON model will be recommended to improve and achieve reasonable agreement using UNSATCON model. The refinement of the model was not within the scope of the thesis, and suggestion are included for the future work.

CHAPTER SEVEN: DISCUSSION

7.1 Introduction

This chapter will summarize the findings of experimental results (i.e., material characterization and meso-scale consolidation tests) and discuss the formation of a transition zone as well as its application during actual field conditions.

7.2 Findings of the present study

The findings from the present study are presented in this section.

7.2.1 Material characterization

The results of material characterization test are summarized as follows:

I. The material characterization results were compared to numerous material types reported in literature to understand the measured geotechnical index properties and flow behaviour, and to assist in the development of baseline knowledge of tailings from oil sands and base metal mines. The comparison and correlation of material properties shows repeatability of the results, and confirmation that the experiment was carried out properly. The results strengthen the case for consistency, repeatability of the material property in collected database and reassures the confidence of the user.

II. The index and engineering properties from geotechnical laboratory tests can be used to estimate the design parameters using available empirical formulations such as compressibility and hydraulic conductivity equations best-fitted using power and/or exponential functions.

These parameters are required to carry out numerical analyses. The use of geotechnical index and engineering properties for estimation are crucial since the laboratory tests are expensive and time-consuming (e.g. unsaturated soil properties).

III. The settling column test results, in the case of flocculated FFT, were used to assess the change in volume following the deposition of tailings, and for the determination of the tailings' initial hydraulic conductivity at the self-weight consolidation stage. The settling column test results assisted in the determination of the scale of the meso-scale setup by allowing for the computation of the required time to dissipate generated excess pore-water pressure from the deposited tailings based on a given thickness and drainage boundary. A slight increase in the computed effective stress was observed over time as the self-weight consolidation progressed, as expected and reported in the literature, due to the dissipation of excess pore-water pressure (Jeeravipoolvarn, 2010; Miller, 2010; Fisseha et al., 2018). The agreement between measured and predicted results from the settling column test was used to design the scaling and operation of the meso-scale test.

IV. The unsaturated soils property results (i.e., SWCC and SC) provided a baseline characterization of the deposited FFTs for the unsaturated conditions due to the atmospheric-surface boundary condition. The SWCC and SC remained essential in conducting the numerical analysis for the saturated-unsaturated flow models. As it had been stated, the change in constitutive surfaces occurred when the soil transitioned from a fully saturated state (solids and water) to a partially saturated state (solids, water, and air). Therefore, the measured unsaturated soil properties provided the basis of the tailings behaviour during the desaturation process, which occurred near the surface boundaries and was pertinent to the transition zone.

V. The consolidation results provided compressibility and hydraulic conductivity relationships for the tailings. The compressibility relationships defined the volume change (i.e., void ratio or strain) with applied total or effective stress and can be expressed using power and/or exponential functions. The relationship assisted in the approximation of the final void ratio under a given stress. The compressibility function can be used during modelling assessment to predict the long-term storage of an impoundment and expected change in total settlement. The flow behaviour of the tailings were illustrated by using the hydraulic conductivity functions. The conductivity function was used during the modelling analysis to predict the flow rate with time as a decrease in void ratio was observed. The compressibility and hydraulic conductivity properties are instrumental in predicting the long-term behaviour of the deposited tailings. These functions assist in sizing, calibrating the meso-scale column setup and determining key parameters during the design considerations.

7.2.2 Meso-scale testing

The results of the meso-scale testing include the findings from the self-weight consolidation for the flocculated FFT and consolidation using increments of applied suction for the flocculated FFT and FCTC.

7.2.2.1 Self-weight consolidation – stage 1

The following summarizes the findings from the self-weight consolidation:

I. The settling column test results were used to calibrate and validate the self-weight consolidation test results in terms of pore pressure release. In addition, the settling results were used to determine the size of the meso-scale column by considering the required time to dissipate excess pore pressure.

II. A consistent and plausible agreement was observed between measured strain (i.e., change in average void ratio) from the settling column test and meso-scale results. During the self-weight consolidation test, change in vertical strain was only recorded compared to the subsequent consolidation process (i.e., consolidation using applied suction method - stage 2), which was a change in vertical and lateral strains.

III. The dissipation of excess pore pressure during the self-weight consolidation test was consistent and in agreement with the determined projected time using methods reported by Imai (1981) based on the settling column test results. The time appropriated to dissipate excess pore pressure for the meso-scale testing was compared with that of the same material (i.e., flocculated FFT) and was threefold in volume.

IV. An increase in the calculated effective stress was observed as the self-weight consolidation progressed, as expected and reported in the literature, from the dissipation of excess pore-water pressure (Jeeravipoolvarn,2010; Miller, 2010; Fisseha et al., 2018). The agreement between measured and predicted results from the settling column test was used to validate and scaling of the meso-scale test.

V. An increase in the shear strength was observed as self-weight consolidation/settlement of the tailings continued. The increase with depth and time in the measured shear strength was correlated with the corresponding effective stress and a linear relationship was determined having slope of 0.42. The flocculated FFTs exhibited similar to properties of soft soils and soft clay foundations (Ladd, 1974).

7.2.2.2 Consolidation using applied suction – stage 2

A summary of the findings from consolidation using the applied suction stage is presented herein:

I. The process of consolidation using increments of applied suction at the bottom boundary under a stress-controlled environment (i.e., laboratory setting) forms a transient zone near the tailings surface. The methodology enables formation of transitional/interlayer zone while controlling the development of negative water pressure in the zone. This, subsequently, permits investigation and characterization of the transition zone. The characterization of the interlayer zone assists to calibrate and refine formulation of the saturated-unsaturated flow equations. The meso-scale column tests assisted in establishing the interlayer zone formation by mimicking field conditions. The development of the suction pattern along the tailings profile show good agreement compared with the conceptual field condition cases.

II. The compressibility data obtained using a multi-step loading apparatus (k_0 loading) was compared with meso-scale apparatus results, which simulated conceptual field trial of isotropic loading conditions. The results show an under-prediction of the compressibility for the flocculated FFT material using the step loading test and reasonable agreement for the FCTC. The outcome from these two testing apparatuses will assist in identifying the variation in testing methods and enable to correct variation the two methods.

III. The results confirmed the presence of a linear relationship between undrained shear strength and effective stress for both flocculated FFT and the FCTC. The correlation shows that the FFTs behaved in a similar manner as natural soils (i.e., Boston blue clay) from literature with slope of 0.25 to 0.42 for the FCTC, and 0.37 to 0.44 for the flocculated FFT. The conclusion

is that FFT or slurry tailings behave like natural soils and the adaptation of soil mechanics principles to define the constitutive equations gives good agreement with the principles.

IV. The results can be used to calibrate and further refine existing or newly developed saturated-unsaturated flow software coupled with large and small strain deformations.

7.3 Procedure to evaluate characterization of transition zone

The shear strength behaviour of soft soils (slurry tailings) and clay foundations is complex due to the nature of the soil properties, which poses a challenge for the design and stability of soil and earthwork structures. Ladd, C (1974, 1977) presented an improved design procedure to evaluate the undrained strength of clay foundations using the SHANSEP model. Impoundments full of soft and slurry tailings present significant challenges in preserving structural integrity and understanding the undrained shear behaviours' of soft tailings as the shear strength of the tailings develops over time. The changes to the undrained shear strength advances planning, scheduling and preparation of subsequent remediation works. Understanding, characterizing the materials and obtaining an accurate, reasonable assessment of the material properties can aid the development empirical formulations, advancement and refinement of numerical analysis tools (such as modelling software). The data and knowledge collected using controlled environment (standard laboratory and meso-scale characterizations results) and numerical modelling tools contributes towards stable and improved earthwork structure designs.

The findings from the present study can be used to characterize the transition zone of dried/desiccated tailings as follows:

I. The estimation of the final average void ratio corresponding to the suction developed can be correlated using the unsaturated soils properties functions (i.e., SWCC and SC) as confirmed using meso-scale testing material's characterization and comparison testing.

II. The relationship between undrained shear strength and effective stress (i.e., mainly due to suction) can be obtained from laboratory tests for a given material and provide a general understanding into the expectation from field conditions. Determining that the suction developed near the surface crust of the dried and desiccated tailings can assist in predicting the expected undrained shear strength based on the correlation developed from the laboratory tests for the given material.

III. The correlation between undrained shear strength and suction (i.e., effective stress) obtained in the laboratory can further be incorporated into a saturated-unsaturated flow model, and can be used for verification and refinement purposes by combining multiple analysis modelling considerations such as deformation (i.e., self-weight, large and small strain consolidations), and the undrained shear strength ratio. A similar concept was used to assess bearing capacity of FFT deposits with dried/desiccated surface crust using undrained shear strength functions (M. Fredlund et al., 2018). Evaluation of the granular cap placed over the treated fine tailings was also analyzed using numerical modelling trial (Greenwood et al., 2018).

IV. In general, the findings from the present study confirms the use of constitutive relationships for soft and slurry FFTs in the transition zone in relation to undrained shear strength and the adoption of principles of soil mechanics to solve practical problems. The correlation between the undrained shear strength and suction (i.e., effective stress) from the meso-scale test can be used as a guide until sufficient field characterization data are available.

7.4 Application of transition zone characterization

The advantage in characterizing the transition zone, such as estimation of its strength, plays significant role during engineering design considerations as the operation for mine waste management progressed. The need to develop simple, consistent and reliable evaluation techniques to estimate shear strength for the transition zone is key for the determination during the industry application.

The present study findings can contribute towards the development of evaluation and estimation process as attempted in the previous section. The industrial application of the findings can be illustrated conceptually as presented in Figure 7.1 and Figure 7.2.

For instance, if a decision can be made to cap or cover the dried/desiccated surface crust of tailings using coarser materials, either an upstream or centerline method of dam/dyke construction can be used to carry out remediation and reclamation work as presented in Figure 7.1. The strength of the dried/desiccated layer, its bearing capacity, type of machinery considered and the load that can supported by the dried/desiccated layer need to be evaluated and assessed prior considering essential engineering decisions. Figure 7.2 presents schematics of the machinery while pushing sand capping/coarser material over dried/desiccated layer and the orientation of undrained shear strength under consideration.

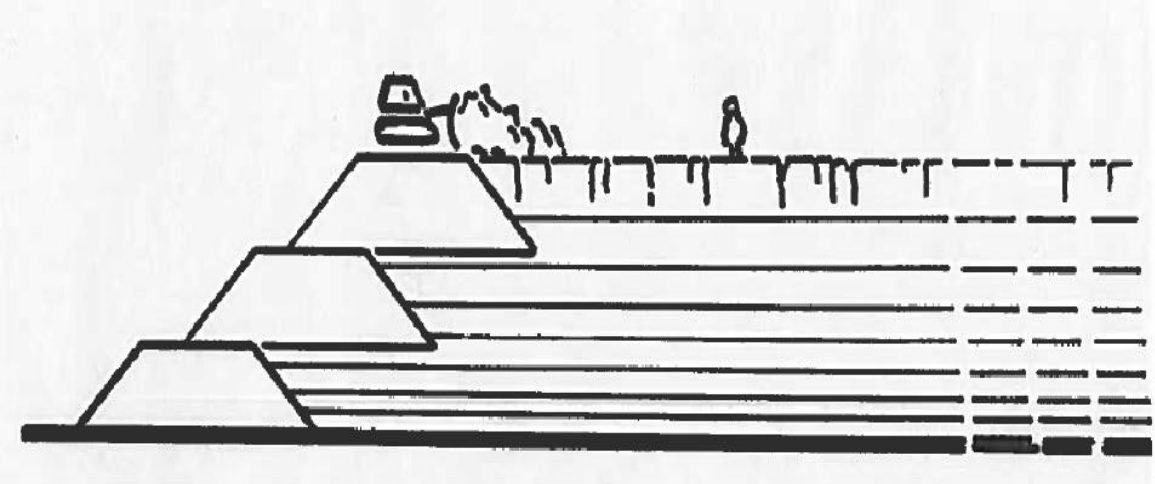

Figure 7. 1 Illustration of tailings impoundment and dried and desiccated tailings near the surface.

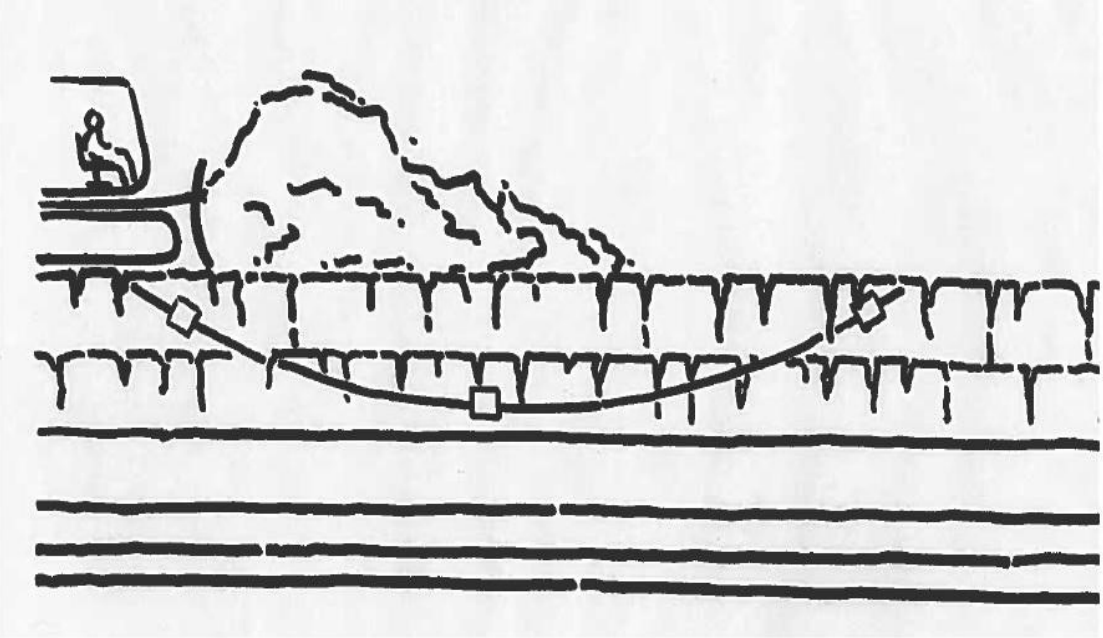

Figure 7. 2 Illustration of construction work to facilitate the next stage of tailings storage facility, remediation, and reclamation work.

CHAPTER EIGHT: CONCLUSION AND RECOMMENDATIONS

As stated in Chapter 1, the main objectives of the present study were to (i) investigate the engineering properties treated fluid find tailings, also known as, FFTs; (ii) develop a large-strain consolidation apparatus that can function using increments of applied negative water pressure in a controlled stress state; (iii) investigate the consolidation and shear strength behaviour of the tailings for saturated/unsaturated condition using the meso-scale column and vane shear measuring device; and (iv) verify the measured results using available commercial modelling tool (software).

8.1 Introduction

This chapter summarizes the existing challenges and gaps, objectives, findings of experimental results (i.e., material characterization and meso-scale consolidation tests) for the present study. Followed by modelling exercise and significant contributions achieved from the present study is presented.

8.2 Challenges and gaps

The consolidation behaviours for FFTs have been extensively studied. The constitutive relationships between compressibility and hydraulic conductivity properties have been established for FFTs (Pollock, 1988; Jeeravipoolvarn, 2010). These material properties are used to design, estimate, and analyze long-term compressibility behaviour of FFT deposits. However, little is known about the undrained shear strength of FFTs. It is important to define the relationship between undrained shear strength, effective stress and soil suction near the tailing's surface (transition zone) as consolidation progresses due to evaporation as the transition zone is being

formed/advanced (saturated/unsaturated). Familiarity with the development of shear strength for the FFTs and slurry tailings in relation to its consolidation behaviour is essential to gain insight into how the transition zone contributes towards the increase in tailings strength to support loads of cover material and machineries during reclamation work (McKenna, 2016; Ansah-Sam, 2016).

The present study assessed consolidation and shear strength behaviours of treated FFTs using increments of applied suction to investigate the transitional zone formation. The applicability of the research under field conditions is discussed in this section.

8.3 Summary and objective of the present study

It is necessary to reiterate the objectives of the present study, which are summarized below. A new column apparatus with shear strength measuring equipment has been designed and constructed to carry out laboratory tests to meet the following objectives:

I. To characterize and measure engineering properties for the FFTs in a stress-controlled environment (i.e., laboratory conditions) by using standard testing devices and meso-scale column apparatus.

II. To investigate the formation of interlayer/transition zone in the lab by using the column apparatus. The interlayer zone is situated near the surface as the state of saturation changes, in the field, due to evaporation and evapotranspiration from the surface of tailings. The column apparatus was used to consolidate placed tailings by dewatering by increments applied suction method. In doing so, the column assisted in mimicking the formation of transition/interlayer zone started at the initial state (i.e., fully saturated state).

III. To investigate the effect of scaling; to assess the use of USPFs for the estimation of engineering properties; to verify existing constitutive relationships of the tailings and to assess undrained shear strength behaviours of soft tailings (i.e., tailings behave like soft soils).

IV. To conduct numerical analysis to validate measured results by using engineering properties obtained from the standard characterization test compared to results from meso-scale column apparatus.

The research program entailed the following experimental work:

i. Developing a new column apparatus and vane shear measuring equipment to carry out the outlined laboratory tests.

ii. Conducting consolidation tests due to both self-weight and using an applied stress (i.e., suction) technique for fully saturated tailings.

iii. Carrying out undrained shear strength tests for the tailings while being consolidated as specified in part (ii).

The results from the laboratory tests provide the basis for establishing constitutive relationships with the FFTs in relation to the stress–strain state of the tailings using independent variables. The properties measured were total settlement, average void ratio, trend of negative pore pressure (i.e., suction) and undrained shear strength. These measured results can be used for the improvement, modification, and/or development of versatile numerical models that can analyze and accurately compute the saturated-unsaturated flow properties of FFTs. This is a critical first step in the development of a technology that can be used at a commercial scale.

8.4 Characterization and engineering properties of tailings

The purpose of the material characterization process was to define the geotechnical index and engineering properties, which assists to characterize and describe the tailings behaviours under various field conditions. Subsequently, knowledge of the behaviour of the materials can play a significant role during the decision-making and design stages. The engineering properties assisted in defining the materials under investigation based on established constitutive relationships using the principles of soil mechanics. Consequently, the constitutive relations are used to predict material behaviours such as volume change, coefficient of compression, shear strength gain, transient water flow analysis using numerical modelling software. In addition, the constitutive relations were used to verify the measured results from meso-scale column experiment under a stress-controlled environment and suggest modification where differences were observed. The following conclusions resulted from material characterization testing:

I. ***Geotechnical index properties*** – Characterization of the geotechnical index and engineering properties were conducted for the FFTs. The index properties were compared with tailings from both the oil sands and base metal mining industries to further understand the properties. The results were used to map the flocculated FFT and FCTC within the ternary diagram and correlate with results of treated tailings from existing data. In addition, the engineering properties of both tailings were compared for boundaries such as sedimentation/ consolidation; segregating/non-segregating; pumpable/non-pumpable; liquid/solid; and, saturation/unsaturation to establish their initial state. The tailings were compared in relation to solids content by mass and associated geotechnical index properties such as liquid, plastic, solid, and shrinkage limits.

II. ***Settling column*** – Characterization of settlement for the flocculated FFT was conducted using a standard graduated cylinder. The settling properties were used to determine the scaling of the meso-scale column, by considering excess pore pressure dissipation time. The dissipation of excess pore pressure was compared with existing empirical formulae to evaluate its accuracy.

III. ***Unsaturated soil properties*** – Characterization of unsaturated soils properties for the FFTs was conducted using the soil-water characteristic curve (SWCC) and shrinkage curve (SC) for both flocculated FFT and FCTC. The SWCC and SC results were compared with various types of tailings reported in the literature. The different types of tailings include flocculated FFTs, thickened tailings, and tailings from base metals mining (gold and copper tailings). The comparison of the measured unsaturated properties of the tailings and those reported in the literature provide a basis for how the flocculated FFT and FCTC behave when subjected to the desaturation process. A major difference was observed when comparing the SWCC for the flocculated FFT due to its high-volume change.

IV. ***Large-strain consolidation properties*** – The characterization of large-strain consolidation was conducted using a multi-stage loading apparatus. The results provided compressibility and hydraulic conductivity relationships, which were key parameters during the modelling exercise. The properties assist prediction of settlement and deformation behaviours of tailings during both self-weight and mechanical consolidation process. The compressibility and hydraulic conductivity curves were compared with existing data from other treated tailings. The measured results were in agreement with trends from existing data, providing similar properties of the oil sands tailings. The measured properties were used during the modelling simulations. The modelling and measured results provided were in agreement with the self-weight consolidation results.

The characterization and comparison of the geotechnical index and engineering properties provide the basis to understand tailings behaviour and assist the selection of empirical formulae to predict the long-term performance. These properties are instrumental during the design stage consideration.

8.5 Meso-scale column experiment

The requirement for the development of the column and experimental setup was to investigate the interlayer/transitional zone. The column assists to characterize desaturation behaviour of tailings under a controlled environment, as the tailings transitioned from fully to partially saturated state. The material within the column represents the transitional zone.

The meso-scale column testing consisted of the following components:

i) To design and develop the column apparatus, and the general setup to carry out the experiment.

ii) To characterize undrained shear strength and consolidation of FFTs.

Two different types of oil sands tailings were used for the experimental work flocculated FFT and FCTC.

Two stages of the column experiment were conducted:

i) self-weight consolidation (stage 1)

ii) consolidation using increments of applied suction (stage 2).

The measurements of undrained shear strength were conducted concurrently as the tailings continued to consolidate during stages 1 and 2.

8.5.1 Equipment developed

The design and development of the column apparatus and vane shear measuring equipment was required in order to execute the proposed research under controlled environment (conditions). These newly developed apparatuses are summarized below and presented in Chapter 4:

I. A column apparatus with a diameter of 0.3 m and height of 0.6 m. The apparatus was constructed with a high air-entry value (AEV) porous ceramic disk placed at the base. The ceramic disk with an AEV of 100 kPa was used as a membrane to control the flow of air through the base. The column was designed and used to consolidate slurry tailings using suction applied through a source supplier and desiccator to collect the water. The column was used to conduct the following tests:

    a. self-weight consolidation test was defined by the drainage boundary located at the top of tailings surface.
    b. consolidation using increments of applied suction was defined by the bottom drainage boundary.

The ceramic disk with high AEV permitted the dewatering process to progress under a controlled applied suction condition. Desaturation occurred from the tailings surface towards the bottom in a controlled manner mimicking the atmospheric-surface boundary interaction similar to the conceptual field condition. The column was used to form the interlayer/transitional zone that occurs during desaturation process.

II. The vane shear strength measuring equipment was designed and developed to characterize the undrained shear strength of materials (tailings) during

   a. self-weight consolidation stage

   b. consolidation using applied suction stage

These newly constructed equipment (devices) assisted during the research study. Tests were conducted using increments of 10 kPa suction to produce multiple, repeatable and consistent data sets.

8.5.2 Self-weight consolidation – stage 1

The process of self-weight consolidation for the flocculated FFT was investigated using the meso-scale column. The conclusions were:

In general, the self-weight consolidation process exhibited comparable pattern and an agreement to the results reported in the literature. The results from the meso-scale column confirmed the settling test results in relation to the total settlement and dissipation time for excess pore pressure. The results provide satisfactory agreement when compared to larger scale testing of similar material (Fisseha et al., 2018).

A summary of results for vertical strain, dissipation of excess pore pressure, effective stress calculation and undrained shear strength with depth are presented below.

I. ***Vertical strain*** – The measured vertical strain from the meso-scale column was compared with graduated cylinder. There was good and acceptable agreement between three of the four results from the graduated cylinder and meso-scale column tests. An initial tailings height of

0.505 m was deposited for the flocculated FFT. The total height by the end of the self-weight consolidation process was 0.384 m, a 24% change in vertical strain was observed. The strong agreement between the graduated cylinder and meso-scale column confirms repeatability and consistency of the results. In addition, it shows consistent execution of the experimental testing procedure.

There was no self-weight consolidation test for the FCTC due to high initial solids content (i.e., 52.5%), which was increased through the dewatering process using a centrifuge technique. The column test indicated that there was no considerable vertical strain measurement during the self-weight consolidation stage.

II. ***Excess pore pressure dissipation*** – The dissipation of excess pore pressure was monitored during the self-weight consolidation test. The results were compared with the expected hydrostatic pressure. Dissipation of excess pore pressure was in strong agreement with the computed hydrostatic pressure using the pore pressure measuring sensors. Dissipation process was also checked by observing change in total height as the tailing continued to settle. The remaining excess pore pressure near the column base indicated more time was required to fully dissipate the excess pressure generated.

There was no monitoring of excess pore pressure dissipation for the FCTC, since there was no self-weight consolidation test conducted.

III. ***Effective stress distribution*** – The computed effective stress values showed an increase in stress as the excess pore pressure dissipated. These results were expected from tailings with similar properties as the flocculated FFT.

IV. ***Undrained shear strength with depth –*** The experimental work showed an increase in undrained shear strength, with depth and time as the flocculated FFT underwent consolidation under its own weight. The initial undrained shear strength for the flocculated FFT was 0.77 kPa and increased to 1.4 kPa near the base of the column near the end of the self-weight consolidation process.

V. ***Undrained shear strength in relation to confining effective stress –*** The relationship between the undrained shear strength and computed effective stress for the flocculated FFT during self-weight consolidation was investigated. A linear relationship with an intercept of zero and slope of 0.42 was measured. The slope provides an internal friction angle of 23 degrees for flocculated FFT. The higher friction angle possible could be due to many factors such as the presence of excess pore pressure, the tailings were in the process of self-weight consolidation and were not reached at equilibrium, the insertion of vane b During the self-weight consolidation the It is important to recognize the shear strength test was conducted as the material continued to settle under its own self-weight. A noteworthy consideration was that flocculated FFT exhibited behaviours similar to those of natural soils reported in the literature, that is the undrained shear strength value is linearly linked to the tailings effective stress. The research findings assert that use of soil mechanics principles, available estimation, and predictive techniques to generate suitable input parameter to deal with FFTs is appropriate. Continuous research to characterize the materials and the refinement of the predictive techniques are required to achieve reasonable estimation as previously recommended in the literature (Masala, S., and Matthews, J.,2010).

8.5.3 Consolidation using incrementally applied suction – stage 2

The process of consolidation using incrementally applied suction for the flocculated FFT and FCTC was investigated. The following conclusions were drawn:

The functionality of the column apparatus in mimicking conceptual field drying/desiccation process was confirmed. A transition zone formed near the tailings surface as observed in the field trials for drying/desiccation cases. The consolidation process using increments of suction showed an increase in effective stress with increase in suction. In addition, an increase in undrained shear strength with time and depth was observed as the increase of effective stress progressed. Moreover, consolidation using increments of suction allowed comparison of the change in volumetric strain between methods using isotropic and k_0-loading conditions. In addition, the results from the meso-scale column test were compared with different predictive techniques such as using the SWCC and SC (i.e., unsaturated soils properties functions (USPF)).

I. ***Volumetric strain*** – The measured volumetric strain using the meso-scale column was compared with predictive methods using unsaturated soil properties and compressibility curve. The results show an average initial and final void ratio for the flocculated FFT was 3.2 and 1.01, respectively. The flocculated FFT show a good agreement with predictive methods using USPF, mainly for the higher suction measurements. The predictions using the compressibility curve underestimated the total volumetric strain values for the flocculated FFT.

   Similarly, the results for the average initial and final void ratio of the FCTC show 2.01 and 0.95, respectively. The predictive method using both USPF and compressibility curves overestimated the volumetric strain change for the FCTC. However, these methods can still be used to predict the final volumetric strain with reasonable acceptance.

II. ***Isotropic and k_0-loading comparison –*** The comparison between the isotropic and k_0-loading conditions was completed to verify the technique commonly used by the industry (i.e., compressibility curve from LSC test). The calculation was completed assuming a Poisson's ratio of 0.3 and modulus of elasticity due to applied suction equal to Young's modulus from LSC test. The calculated results using isotropic method shows 9% higher for the flocculated FFT and 4% higher for the FCTC compared to the k_0-loading methods. The isotropic method formulation considers applied suction effect only compared to k_0-loading condition (i.e., LSC testing method). Therefore, the LSC method overpredict the estimation of final void ratio compared to actual field condition. Appropriate correction factor should be considered as a recommendation during engineering design and modelling stages.

III. ***Suction distribution with depth and time*** – The distribution of suction within the tailings thickness over time was investigated during consolidation using increments of applied suction for both flocculated FFT and FCTC. Constant suction was applied at the bottom boundary using increments of -10 kPa up to maximum of -60 kPa for both materials. The constant applied suction was the driving force to dewater and consolidate the tailings. An advancement of suction progressed from the bottom of tailings towards the surface over time. The distribution of suction could not be constructed due to limited measurement at the tailings surface on limited time. Conceptual suction distribution was assumed based on the constant suction applied at the base of the column and a second measurement near the surface of the tailings.

A higher suction was measured at the tailings surface than at the bottom boundary. The increase in the measured suction near the tailings surface was -14 kPa for the flocculated FFT and -11 kPa for the FCTC. The increase in suction near the surface was attributed due to

evaporation. A hypothetical suction profile was reconstructed to show the transition of suction with time across the profile. The measured suction and average void ratio for the profiles were compared with USPF predictive method. The predictive method displayed satisfactory agreement. In general, effect of applied suction was analyzed in relation to change in average final void ratio. The average initial and final void ratios was determined to be 3.2 and 1.01, for the flocculated FFT, and 2.0 and 0.95, for the FCTC, with the applied suction of -60 kPa, respectively.

IV. ***Undrained shear strength with depth and time –*** The undrained shear strength was measured with depth and time during increments of applied suction stage. An increase in the undrained shear strength was observed with depth and time corresponding with the applied suction.

V. ***Undrained shear strength in relation to effective stress*** – A linear relationship between effective stress and undrained shear strength was measured with a zero intercept for both the flocculated FFT and FCTC. The slope between the effective stress and undrained shear strength was determined to be 0.44, 0.37, 0.44 and 0.66 for the flocculated FFT for the corresponding suction of upper and lower bounds of 20 - 30 kPa, 30 – 40 kPa, and 50 – 60 kPa, respectively. Similarly, the slope for the FCTC was determined to be 0.21, 0.19, 0.33, and 0.41 for the corresponding applied suction of upper and lower bounds of 20 – 30 kPa, 30 – 40 kPa, and 50 – 60 kPa, respectively. In general, the correlation between the vane shear strength and effective stress for the FFT show linear correlation as exhibited by soft and natural clays from literature (Ladd, 1974; Ladva, 1966).

The slope of vane shear strength and effective stress for the FFTs show higher internal friction angle compared to the friction angle of the natural clays. The variation the measured internal

friction angles for the FFT and natural clay was possibly due to used equipment, state of the sample, and composition of the material. However, the vane shear measurement can be used as an indicator to predict the FFT behave similar to natural soils.

These findings assert the plausible agreement in employing the constitutive equation applied to define fluid fine tailings in relation to principles of soil mechanics.

8.6 Modelling Exercise

The verification of the measured results was carried out using commercially available modelling software from *SoilVision*® Systems Ltd., known as consolidation package. The consolidation software package uses saturated-unsaturated flow model - SVFLUX coupled with stress - deformation model - SVSOLID.

Two distinct stages were used during the modelling exercise:

i) Self-weight consolidation analysis stage

ii) Transient flow analysis stage

Each modelling stage and the corresponding conclusions are presented in the section below.

8.6.1 Self-weight consolidation - stage 1

Self-weight consolidation process was verified using the modelling software packages - SVFLUX coupled SVSOLID, from *SoilVision*®. The modelled and measured results were compared using total settlement, average void ratio, dissipation of excess pore pressure, and computed effective

stress over time. The output showed plausible agreement for the overall analysis between modelled and measured results.

8.6.2 Consolidation using incrementally applied suction - stage 2

The process of consolidation using incrementally applied suction was verified using the newly developed UNSATCON model (Qi, 2016; Qi et al., 2017a, 2017b). The modelled and measured results were compared using total settlement, average void ratio, gravimetric water content, solids content and distribution of negative pore pressure (i.e., suction) over time. The output showed reasonable and acceptable agreement for the change in total height. Comparable gravimetric water content, and solids content with slightly different trend. Larger differences were observed during the average void ratio comparison. The measured and predicted suction distribution were not in agreement. The model needs to be refined and further calibrated to reproduce reasonable and acceptable results compared to the measured result.

8.7 Significant contribution

The significant contributions of this research are summarized below.

I. A column apparatus was designed and assembled to carry out proposed experimental research work under stress-controlled environment in the laboratory. The design of the apparatus mimicked the development of transition/interlayer zone in the field due to the interactions between atmosphere-surface flux boundaries for the placed tailings. The atmosphere-surface flux boundary considers principles of continuum mechanics and characterize tailings saturation state caused by changes in the water budget. Desaturation of placed tailings enables in defining and characterizing the formation of transient zone as the

saturation line constantly shifted due to the effects of evaporation and rainfall existences. Similarly, the column apparatus was designed to form transition/interlayer zone through applied increments of controlled suction at the bottom boundary. The verification of the column apparatus's functionality was completed using the meso-scale column test results such as developed suction with profile over time. The results of suction formation trend within the column testing were compared with a conceptual transition/interlayer zone formation during a field condition. For instance, the increase in negative pore pressure near the surface of the tailings tend to increase and became larger than the controlled suction applied at the bottom boundary overtime as presented in the analysis chapter 6. Therefore, the design column apparatus can be employed to replicate formation of interlayer zone and investigate further under controlled environment.

II. The effect of scaling of column apparatus's (or sizing) was verified by comparing measured governing engineering properties using the meso-scale column and standard laboratory characterization tests. The column apparatus was larger between 2 – 5 times wider than the diameter of standard device (i.e., LSC and SWCC) and between 3 – 5 times longer in height than columns used during conventional or standard testings.

III. The column apparatus validates the use of unsaturated soil property functions (USPF) estimation technique and existing constitutive equations for compressibility and conductivity properties of FFTs for the preliminary design stage. In addition, the results were confirmed through the use of commercially available software.

IV. Compressibility results obtained using the k_0-loading condition testing method were compared with the results attained using an isotropic loading condition (i.e., applied suction case). The actual field condition is idealized using an isotropic loading condition. The findings assists in

providing design considerations to account limitation exhibited in the laboratory testing and amend the limitations through implementation of correction factors using sensitivity analysis approach.

V. The shear strength was defined in relation to the confining effective stress. So far the undrained shear strength of oil sands tailings has been defined in relation to tailings solids content; however, the correlation needs to be expressed in terms an independent stress state variable rather than a material property. The shear strength and confining effective stress correlation allows the practitioners to assess, connect the if the tailings (processed materials) behave like natural soils such as clay.

VI. The process of consolidation and interlayer zone formation for FFTs similar to the field condition was simulated using recently developed saturated/unsaturated flow model coupled with deformation analysis software. The software attempted to predict the measured results using parameters obtained using standard laboratory tests. The measured results displayed limitations of the developed numerical model and anticipated being utilized for the calibration, refinement and improvement of the numerical model to attain predictions as practical as measured values. Therefore, the software can be used for future engineering design and analysis work.

8.8 Summary of Limitations

Summary of study limitations for the meso-scale column apparatus design and its application, limitations of the findings, and limitations of the numerical modelling approach considered to replicate the process of consolidation using applied suction section are presented herein:

I. The meso-scale column apparatus design can only operate to a maximum of 100 kPa applied suction (vacuum pressure) equivalent or less than atmospheric pressure (i.e., 101 kPa). The column apparatus can not be used to characterize for materials with high fines content and higher air-entry values (AEV) greater than 100 kPa. This is considered one of the limitations of the column apparatus operating using applied suction method.

II. The second limitation for the meso-scale column apparatus is its scale. The column's dimension was considered as prototype and designed to be larger. However, the scale of the meso-scale poses a challenge since it required longer time for the pore-water pressure to reach equilibrium condition.

III. The malfunction of negative pore pressure sensors during the experimental test led towards assuming suction measurements for the materials under investigation. These assumed suction values were used to calculate the effective stress distribution along the consolidated materials and correlated with vane shear strength measurements. The assumed suction values give limitations for the effective stress distribution along the profile for the initial applied suction stages.

IV. The numerical modelling assessment require further refinement to accurately predict measured results using meso-scale column apparatus. The availability of software that can operate applied suction as its boundary condition creates limitation on evaluating the modelling process rigorously.

8.9 Recommendations and Future Work

The following recommendations are suggested for future research work:

I. Additional experimental are required to closely monitor the change in negative pore pressure (i.e., suction) within the tailings by using multiple sensors to obtain precise measurement.

II. Conduct undrained shear strength test using Simple shear device for the flocculated FFT and FCTC to determine the correction factor of the measured vane shear strength.

III. More characterization for different types of tailings, such as those from base metal and FFTs form the oil sands industry, can provide a bigger database for tailings behaviour and increase the confidence of the results for a wide range of tailings.

IV. Unsaturated flow coupled deformation model is required to assess the volume change and transient flow behaviours of tailings. As, more assessment and verification can be conducted when having flexible, powerful numerical modelling tool.

References

Aas, G. 1965. A Study of the effect of vane shape and rate of strain on the measured values of in-situ shear strength of clays. *In* Proceedings of the 6th International Conference on Soil Mechanics and Foundation Engineering, Montreal, QC., 8-15 September 1965, pp. 141–145.

Abu-Hejleh, A. N., Znidarcic, D., & Barnes, B. (1996). Consolidation characteristics of phosphatic clays. Journal of Geotechnical Engineering, **122**(4): 295-301. Available from https://doi.org/10.1061/(ASCE)0733-9410(1996)122:4(295)

Alberta Energy Regulator (AER). (2018). EnerFAQs Oil Sands. Available from: https://www.aer.ca/providing-information/news-and-resources/enerfaqs-and-fact-sheets/enerfaqs-oil-sands (cited June 2016)

Airey, D. W., & Wood, D. M. (1987). An evaluation of direct simple shear tests on clay. Géotechnique, **37**(1): 25–35. http://doi:10.1680/geot.1987.37.1.25

Al-Tarhouni, M., Simms, P., & Sivathayalan, S. (2011). Cyclic behaviour of reconstituted and desiccated–rewet thickened gold tailings in simple shear. Canadian Geotechnical Journal, **48**(7): 1044–1060.doi: 10.1139/t11-022

Alonso, E. E., Olivella, S., & Pinyol, N. M. (2005). A review of Beliche Dam. Géotechnique, **55**(4): 267–285. doi: 10.1680/geot.2005.55.4.267

Alonso, E. E., Olivella, S., Soriano, A., Pinyol, N. M., & Esteban, F. (2011). Modelling the response of Lechago earth and rockfill dam. Géotechnique, **61**(5): 387–407. http://doi.10.1680/geot.SIP11.P.013

Alonso, E. E., Pinyol, N. M., & Gens, A. (2013). Compacted soil behaviour: initial state, structure and constitutive modelling. Géotechnique, **63**(6): 463–478. doi: 10.1680/geot.11. P.134

Ansah-Sam, M., Hachey, L., McKenna, G. and Mooder, B. (2016). The DBM approach for setting engineering decision criteria for an oil sand mine closure plan. *In* Proceeding of 5th International Oil Sands Tailings Conference, Lake Louise, Alberta, Canada, Dec 4-7, 2016, pp. 163-167.

Ansah-Sam, M., Thompson, A., Sheets, B., Langseth, J. (2018). Sand capping of treated tailings: insights from field trials on DDA1- centrifuge deposits. International Oil Sands Tailings Conference, Edmonton, AB, Dec 9-12.

Assouline, S., Tessier, D., & Bruand, A. (2000). Correction to “A conceptual model of the soil water retention curve” by S. Assouline, D. Tessier, and A. Braund. Water Resources Research, **36**(12), 3769. https://doi.org/10.1029/2000WR900249

Assouline, S., Tessier, D., & Bruand, A. (1998). A conceptual model of the soil water retention curve. Water Resources Research, **34**(2): 223–231. https://doi.org/10.1029/97WR03039

ASTM D422-63(2007)e2, Standard Test Method for Particle-Size Analysis of Soils (Withdrawn 2016), ASTM International, West Conshohocken, PA, 2007, www.astm.org. http://doi.org/10.1520/D0422-63R07E02

ASTM D854-14, Standard Test Methods for Specific Gravity of Soil Solids by Water Pycnometer, ASTM International, West Conshohocken, PA, 2014, www.astm.org. http://doi.org/10.1520/D0854-14

ASTM D4318-17e1, Standard Test Methods for Liquid Limit, Plastic Limit, and Plasticity Index of Soils, ASTM International, West Conshohocken, PA, 2017, www.astm.org. http://doi.org/10.1520/D4318-17E01

ASTM D2573 / D2573M-18, Standard Test Method for Field Vane Shear Test in Saturated Fine-Grained Soils, ASTM International, West Conshohocken, PA, 2018, www.astm.org. http://doi.org/10.1520/D2573_D2573M-18

ASTM D4648 / D4648M-16, Standard Test Methods for Laboratory Miniature Vane Shear Test for SaturatedFine-Grained Clayey Soil, ASTM International, West Conshohocken, PA, 2016, www.astm.org. http://doi.org/10.1520/D4648_D4648M-16

ASTM D6528-17, Standard Test Method for Consolidated Undrained Direct Simple Shear Testing of Fine Grain Soils, ASTM International, West Conshohocken, PA, 2017, www.astm.org. http://doi.org/10.1520/D6528-17

Azam, S., & Scott, J. D. (2005). Revisiting the ternary diagram for tailings characterization and management. Geotechnical News, **23**(4): 43–46. https://doi.org/10.2337/dc10-1606

Banas, L. C. 1991. Thixotropic behavior of Oil Sands tailings sludge. MSc Thesis. Department of Civil Engineering, University of Alberta. Edmonton.

Barbour, S. L. (1998). Nineteenth Canadian geotechnical colloquium: the soil-water characteristic curve: a historical perspective. Canadian Geotechnical Journal, **35**(5): 873–894. https://doi.org/10.1016/0002-8703(92)90672-I

Barr and O’Kane. (2015). Atmospheric Fines Drying (AFD) Deposition Optimization: Multi-lift versus Deep Stacking Project Progress Report, Prepared for Shell Canada Ltd.

Bartholomeeusen, G., Sills, G.C., Znidarčić, D., Van Kesteren, W., Merckelbach, L.M., Pyke, R., Carrier III, W.D., Lin, H., Penumadu, D., Winterwerp, H. and Masala, S. (2002). Sidere: numerical prediction of large-strain consolidation. Géotechnique, **52**(9): 639–648.

Baver, L. D. (1940). Soil physics. John Wiley & Sons, Inc., New York, NY.

Bayliss. P., and. Levinson, A. A. (1976). Mineralogical review of the Athabasca oil sands deposits (Lower Cretaceous, Mannville Group), Bulletin Canadian Petroleum Geology, **24**(2): 211-214.

Been, K. (1980). Stress strain behaviour of a cohesive soil deposited under water. Ph.D. thesis, Department of Engineering Science, Balliol College, The University of Oxford, Oxford, UK.

Been, K., & Sills, G. C. (1981). Self-weight consolidation of soft soils: an experimental and theoretical study. Géotechnique, **31**(4): 519–535. https://doi.org/10.1680/geot.1981.31.4.519

Beier, N., Alostaz, M., & Sego, D. (2009). Natural dewatering strategies for oil sands fine tailings. *In* Proceedings of the 13th Annual Conference on Tailings and Mine Waste, Calgary, Alta., 3-6 November 2013.

Beier, N., Wilson, G. W., Dunmola, A., Sego, D. (2013). Impact of flocculation-based dewatering on the shear strength of oil sands fine tailings. Canadian Geotechnical Journal, 50(9): 1001-1007. doi: 10.1139/cgj-2012-0262

BGC Engineering Inc. (2010). Oil sands tailings technology review. OSRIN Report 1, Oil Sands Research and Information Network (OSRIN), School of Energy and the Environment (SEE), University of Alberta, Alberta, AB. Available from https://hdl.handle.net/10402/era.17555

Biot, M. A. (1941). General theory of three-dimensional consolidation. Journal of Applied Physics, **12**(2): 155–164. doi: 10.1063/1.1712886

Bishop, A. W., & Blight, G. E. (1963). Some aspects of effective stress in saturated and partly saturated soils. Géotechnique, **13**(3): 177–197. doi: 10.1680/geot.1963.13.3.177

Bjerrum, L. (1972). Embankments on soft ground. *In* Proceedings of the Specialty Conference on Performance of Earth and Earth-supported Structures, Indiana, Lafayette. 11-14 June 1972. American Society of Civil Engineers, pp. 1–54.

Bjerrum, L. (1973). Problems of soil mechanics and construction on soft clays. *In* Proceedings of the 8th International Conference on Soil Mechanics and Foundation Engineering, Moscow. pp. 111–159.

Bjerrum, L., & Landva, A. (1966). Direct simple-shear tests on a Norwegian Quick Clay. Géotechnique, **16**(1): 1–20. https://doi.org/10.1680/geot.1966.16.1.1

Bolzon, G., Schrefler, B. A., & Zienkiewicz, O. C. (1996). Elastoplastic soil constitutive laws generalized to partially saturated states. Géotechnique, **46**(2), 279–289. https://doi.org/10.1680/geot.1996.46.2.279

Boso, M. (2005). Shear strength behaviour of a reconstituted partially saturated clayey silt, Ph.D. thesis, University of Trento, Via Calepina, Italy. Available from http://www.ing.unitn.it/dims/download/phd_boso.pdf .

Bowden, R. K. (1988). Compression behaviour and shear strength characteristics of a natural silty clay sedimented in the laboratory. Ph.D. thesis, Faculty of Engineering Science, University of Oxford, Oxford, UK. Available from https://ora.ox.ac.uk/objects/uuid:56cef40b-3e22-409f-930c-10b8e40ddfd8/download_file?safe_filename=602788983.pdf&file_format=application%2Fpdf&type_of_work=Thesis

Briggs, L. J. (1897). The mechanics of soil moisture. Government Printing Office, Washington. Available from https://www.biodiversitylibrary.org/item/94223

Bro, A. D., Stewart, J. P., & Pradel, D. (2013). Estimating undrained strength of clays from direct shear testing at fast displacement rates. *In* Proceedings of the 2013 Geo-Congress, 3-7 March 2013, San Diego, Ca. pp. 106–119. Available from https://ascelibrary.org/doi/book/10.1061/9780784412787

Bromwell, L. G., & Oxford, T. P. (1977). Waste clay dewatering and disposal. *In* Proceedings of the Conference on Geotechnical Practice for Disposal of Solids Waste Materials, Ann Arbor, Michigan: University of Michigan, pp. 541–558.

Bronswijk, J. (1991). Relation between vertical soil movement and water-content changes in cracking clays. Soil Science Society of America Journal, **55**(5): 1220–1226. doi: 10.2136/sssaj1991.03615995005500050004x

Brooks, R. H., & Corey, A. T. (1964). Hydraulic properties of porous media. Hydrology Papers 3, Colorado State University, Fort Collins, Colorado. pp. 1–27. Available from https://mountainscholar.org/bitstream/handle/10217/61288/HydrologyPapers_n3.pdf?sequence

Brutsaert, W. (1967). Some methods of calculating unsaturated permeability. Transactions of the ASAE, **10**(3): 400–0404.

Budhu, M. (1984). Non uniformities imposed by simple shear apparatus. Canadian Geotechnical Journal, **20**(2): 125–137. doi:10.1139/t84-010

Budhu, M. (2011). Soil mechanics and foundation (3rd Edition). John Wiley & Sons, Inc., Danvers, MA

Bumb, C., Murphy, C. L., & Everett, L. G. (1992). A comparison of three functional forms for representing soil moisture characteristics. Ground Water, **30**(2): 177-185.

Burdine, N. T. (1953). Relative permeability calculations from pore size distribution data. Journal of Petroleum Technology, **5**(03): 71–78. doi: 10.2118/225-G

Burger, C. A., & Shackelford, C. D. (2001a). Evaluating dual porosity of pelletized diatomaceous earth using bimodal soil-water characteristic curve functions. Canadian Geotechnical Journal, **38**(1): 53–66. doi: 10.1139/t00-084

Burger, C. A., & Shackelford, C. D. (2001b). Soil-water characteristic curves and dual porosity of sand–diatomaceous earth mixtures. Journal of Geotechnical and Geoenvironmental Engineering, **127**(9): 790–800.

Bürger, R., & Hvistendahl, K. (2001). On some upwind difference schemes for the phenomenological sedimentation-consolidation model. Journal of Engineering Mathematics, **41**(2–3): 145–166. doi: 10.1023/A:1011935232049

Cadling, L., & Odenstad, S. (1950). The vane borer: an apparatus for determining the shear strength of clay soils directly in the ground. *In* Proceedings of the Royal Swedish Geotechnical Institute, Stockholm, Sweden, pp. 1-87.

Campbell, G. S. (1974). A simple method for determining unsaturated conductivity from moisture retention data. Soil Science, **117**(6): 311–314. doi:10.1097/00010694-197406000-00001

Cargill, K. W. (1982a). Consolidation behaviour of fine-grained dredged material. Dredging Operations Technical Support. Technical Report D-83-1. National Technical Information Service, Springfield, Va.

Cargill, K. W. (1982b). Consolidation of soft layers by finite strain analysis (No. WES/MP/GL-82-3). Army Engineering Waterways Experiment Station, Vicksburg, MS Geotechnical Lab.

Cargill, K. W. (1984). Prediction of consolidation of very soft soil. Journal of Geotechnical Engineering, **110**(6): 775–795. Available from https://ascelibrary.org/doi/pdf/10.1061/%28ASCE%290733-9410%281984%29110%3A6%28775%29

Carrier, B. W. D., Bromwell, L. G., & Somogyi, F. (1983). Design capacity of slurried mineral waste ponds. Journal of Geotechnical Engineering, **109**(5), 699-716.

Carrier, W. D., and Beckman, J. F. (1984). Correlations between index tests and the properties of remoulded clays. Géotechnique, **34**(2): 211–228. doi: 10.1680/geot.1984.34.2.211

Carrier, W. D. I., & Keshian, B., J. (1979). Measurement and prediction of consolidation of dredged material. 12th Annual Dredging Seminar. Texas A & M University.

Caughill, D. L., Morgenstern, N. R., and Scott, J. D. (1993). Geotechnics of non segregating oil sand tailings. Canadian Geotechnical Journal, 30(5): 801-811.

Chalaturnyk, R.J., Scott, J.D., and Ozum, B. (2002). Management of oil sands tailings. Petroleum Science and Technology, **20**(9): 1025-1046.

Chandler, R. (1988). The in-situ measurement of the undrained shear strength of clays using the Field Vane and BT Vane Shear Strength Testing in Soils: Field and Laboratory Studies. ASTM International, 1988.

Chapuis, R. P. (2012). Predicting the saturated hydraulic conductivity of soils: a review. Bulletin of Engineering Geology and the Environment, **71**(3): 401–434. doi: 10.1007/s10064-012-0418-7

Childs, E. C., & Collis-George, N. (1950). The permeability of porous materials. Proceedings of the Royal Society A Mathematical, Physical and Engineering Sciences, **201**(1066): 392-405. Available from https://rspa.royalsocietypublishing.org/content/201/1066/392.abstract

Coe, H. S., & Clevenger, G. H. (1916). Methods for determining the capacities of slime settling tanks. Transactions American Institute of Mining Engineering, **55:** 356–385.

Concha, F., & Bustos, M. C. (1987). A modification of the Kynch theory of sedimentation. AIChE Journal, **33**(2): 312–315. doi: 10.1002/aic.690330219

Cornelis, W. M., Corluy, J., Medina, H., Hartmann, R., Van Meirvenne, M., & Ruiz, M. E. (2006). A simplified parametric model to describe the magnitude and geometry of soil shrinkage. European Journal of Soil Science, **57**(2): 258–268. doi: 10.1111/j.1365-2389.2005.00739.x

COSIA. (2018). Fluid fine tailings management methods - an analysis of impacts on mine planning, land, GHGs, costs, site water balances and recycle water chloride concentrations. Canada's Oil Sands Innovation Alliance, Calgary, AB. June 2018.

CTMC. (2012). Oil sands tailings technology development roadmap. Project report 2, Component 1 results. Alberta Innovates – Energy and Environment Solutions, AB.

Daliri, F. (2013). The influence of desiccation and stress history on monotonic and cyclic shear response of thickened gold tailings. Ph.D. thesis, Department of Civil and Environmental Engineering, Carleton University, Ottawa, ON.

Daliri, F., Kim, H., Simms, P., & Sivathayalan, S. (2014). Impact of desiccation on monotonic and cyclic shear strength of thickened gold tailings. Journal of Geotechnical and Geoenvironmental Engineering, **140**(9): 040140481- 0401404813.

Delta-T Device Ltd. (2019). User manual DL6 Data logger. https://www.delta-t.co.uk/wp-content/uploads/2017/02/DL6_Quick_Start_Guide-v1.2.pdf

De Vries, D. A. (1987). The theory of heat and moisture transfer in porous media revisited. International Journal of Heat and Mass Transfer, **30**(7): 1343–1350. doi: 10.1016/0017-9310(87)90166-9

Devenny, D. W. (2010). A screening study of oil sands tailings technologies and practices. Part A - Study Cases, 39 pages. Available from https://www.eipa.alberta.ca/media/40991/partafinaltext.pdf

Dunmola, A., Dhadli, N., Freeman, G., Kolstad, D., Fasking, T., Song, J., & Langseth, J. (2013). Geotechnical benefits of flocculation in dewatering oil sands mature fine tailings. *In* Proceedings of the 66th Canadian Geotechnical Conference and the 11th Joint CGS/IAH-CNC Groundwater Conference, 29 September - 3 October 2013. GeoMontreal, Montreal, QC, Canada.

Dunmola, A., Dhadli, N., Freeman, G., Kolstad, D., Song, J., Fasking, T., & Langseth, J. (2014). Geotechnical benefits of flocculation in dewatering oil sands mature fine tailings. *In* Proceedings of the 66th Canadian Geotechnical Conference. Regina.

Dusseault, M. B., Scafe, D. W., and Scott, J. D. (1989). Oil sands mine waste management: clay mineralogy, moisture transfer and disposal technology. AOSTR Journal of Research. **5**:303–320.

Dyvik, R., Berre, T., Lacasse, S., & Raadim, B. (1987). Comparison of truly undrained and constant volume direct simple shear tests. Géotechnique, **37**(1), 3–10. doi: 10.1680/geot.1987.37.1.3

Escario, V., & Jucâ, J. F. T. (1989). Strength and deformation of partly saturated soils. *In* Proceedings of the 12th International Conference on Soil Mechanics and Foundation Engineering, Rio de Janeiro, 2, 1989, pp. 43-46.

Estepho, B. M. (2014). Seepage induced consolidation test: characterization of mature fine tailings. Masters Thesis, University of British Columbia, Vancouver, B.C.

EUB. (2004). Alberta's Reserves 2003 and Supply/Demand Outlook 2004-2013. Statistical Series (ST) 2004-98. Available from https://www.aer.ca/documents/sts/ST98/st98-2004.pdf (cited Sep 2016).

Fair, A., (2008). Past, present, and future of tailings at Syncrude. *In* Proceedings of the International Oil Sands Tailings Conference, Edmonton, AB, December 7-10, 2008

Fair, A.E. and Beier, N.A. (2012). Invited Keynote Paper: Collaboration in Canada's Oil Sands: Fluid Fine Tailings Management. 3rd International Oil Sands Tailings Conference, Edmonton, Alberta, December 2-5, 2012. 3-12.

Farrell, D. A., & Larson, W. E. (1972). Modeling the pore structure of porous media. Water Resources Research, **8**(3), 699–706. doi: 10.1029/WR008i003p00699

Fisseha, B., Bryan, R., & Simms, P. (2010). Evaporation, Unsaturated Flow, and Salt Accumulation in Multilayer Deposits of "Paste" Gold Tailings. Journal of Geotechnical and Geoenvironmental Engineering, **136**(12), 1703–1712.

Fisseha, B., Wilson, G. W., & Fredlund, D. G. (2017a). Assessment of Large-Strain Consolidation and Shear Strength of Saturated / Unsaturated Fluid Fine Tailings, (October). 70th Canadian Geotechnical Conference and the 12th Joint CGS/IAH-CNC Groundwater Conference, Ottawa, ON. 1-4 October, 2017, GeoOttawa 2017, Ottawa.

Fisseha, B.T., Wilson, G.W., and Fredlund, D.G. (2017b). "Large-strain consolidation column with applied negative water pressures." Proceedings of the Second Pan-Am Conference on Unsaturated Soils, Dallas, TX, USA.

Fisseha, B.T., Wilson, G., & Simms, P. (2018). Assessment of self-weight consolidation of flocculated fluid fine tailings under various environmental conditions. *In* 21st International Seminar on Paste and Thickened Tailings, 2018 11-13 April, Perth (pp. 291–304). Australian Centre for Geomechanics. Available from https://papers.acg.uwa.edu.au/p/1805_23_Fisseha/#.W8f-9MTppHU.mendeley

Fitch, B. (1966a). Current theory and thickener design. Industrial & Engineering Chemistry, **58**(10): 18–28. doi: 10.1021/ie50682a006

Fitch, B. (1966b). Mechanism of Sedimentation. Industrial & Engineering Chemistry Fundamentals, **5**(1): 129–134. doi: 10.1021/i160017a023

Fitch, B. (1979). Sedimentation of flocculent suspensions: State of the art. AIChE Journal, **25**(6): 913–930. doi: 10.1002/aic.690250602

Fox, P. J., & Berles, J. D. (1997). CS2: a piecewise-linear model for large strain consolidation. International Journal for Numerical and Analytical Methods in Geomechanics, **21**(7): 453–475.

Fox, P. J., Pu, H.-F., & Berles, J. D. (2014). CS3: Large strain consolidation model for layered soils. Journal of Geotechnical and Geoenvironmental Engineering, **140**.

Fredlund, D. G., & Morgenstern, N. R. (1976). Constitutive relations for volume change in unsaturated soils. Canadian Geotechnical Journal, **13**(3): 261–276. Available from https://doi.org/10.1139/t76-029

Fredlund, D. G., & Morgenstern, N. R. (1977). Stress state variables for unsaturated soils. Journal of Geotechnical and Geoenvironmental Engineering, **103(**GT5**):** 447–466.

Fredlund, D. G., Morgenstern, N. R., & Widger, R. (1978). The shear strength of unsaturated soils. Canadian Geotechnical Journal, **15**(3): 313–321.

Fredlund, D. G., & Rahardjo, H. (1993). Soil mechanics for unsaturated soils. John Wiley and Sons Inc., Hoboken, N.J.

Fredlund, D. G., & Xing, A. (1994a). Equations for the soil-water characteristic 'curve'. Canadian Geotechnical Journal, **31**(4): 521–532.

Fredlund, D. G., Xing, A., & Huang, S. (1994b). Predicting the permeability function for unsaturated soils using the soil-water characteristic curve. Canadian Geotechnical Journal, **31**(4): 533–546.doi: 10.1139/t94-062

Fredlund, D. G., Xing, A., Fredlund, M. D., & Barbour, S. L. (1996). The relationship of the unsaturated soil shear strength to the soil-water characteristic curve. Canadian Geotechnical Journal, **33**(3): 440–448.

Fredlund, D.G., Stone, J., Stianson, J., & Sedgwick, A. (2011). Determination of water storage and permeability functions for oil sands tailings. *In* Proceedings Tailings and Mine Waste, Vancouver, B.C., 6-9 November 2011. doi: 10.14288/1.0107734

Fredlund, D. G., Rahardjo, H., & Fredlund, M. D. (2012). Unsaturated soil mechanics in engineering practice. John Wiley and Sons Inc., Hoboken, N.J.

Fredlund, D. G., & Houston, S. L. (2013a). Interpretation of soil-water characteristic curves when volume change occurs as soil suction is changed. *In* Proceedings of the First Panam International Conference on Unsaturated Soils. Available from https://soilvision.com/downloads/docs/pdf/research/Fredlund-and-Houston-Cartagena-CO.pdf

Fredlund, D. G., & Zhang, F. (2013b). Combination of shrinkage curve and soil-water characteristic curves for soils that undergo volume change as soil suction is increased. *In* Proceedings of the 18th International Conference on Soil Mechanics and Geotechnical Engineering, Paris, France, 2-6 September 2013, pp. 2–5.

Fredlund, D. G. (2017). Use of soil-water characteristic curve in the implementation of unsaturated soil mechanics. In Proceedings of the Third International Conference on Unsaturated Soils, Dallas, USA, 10-13 March 2012, pp. 1-16.

Fredlund, M. D. (2000). The role of unsaturated soil property functions in the practice of unsaturated soil mechanics. Ph.D. thesis, Department of Civil Engineering, University of Saskatchewan, Saskatoon, SK.

Fredlund, M. D., Wilson, G. W., & Fredlund, D. G. (2002). Representation and estimation of the shrinkage curve. *In* Proceedings of the Third International Conference on Unsaturated Soils, Recife, Brazil. March 2002, UNSAT. pp. 145-149.

Fredlund, M., Pham, N., Donaldson, M., Ansah-Sam, M. (2018a). Preliminary study for sand capping of treated tailings. *In* Proceedings of the International Oil Sands Tailings Conference, Edmonton, AB, 9-12 December 2018.

Fredlund, M., Pham, N., Donaldson, M., and Ansah-Sam, M. (2018b). Determining bearing capacity for sand cap placement at JackPine Mine DDA1. *In* Proceedings of the International Oil Sands Tailings Conference, Edmonton, AB, 9-12 December 2018.

Fujiyasu, Y., & Fahey, M. (2000). Experimental study of evaporation from saline tailings. Journal of Geotechnical and Geoenvironmental Engineering, **126**(1): 18–27.

Gan, J. K. M., Fredlund, D. G., & Rahardjo, H. (1988). Determination of the shear strength parameters of an unsaturated soil using the direct shear test. Canadian Geotechnical Journal, **25**(3): 500-510. doi: 10.1139/t88-055

Gardner, W. R. (1958). Some steady-state solutions of the unsaturated moisture flow equation with application to evaporation from a water table. Soil Science, **85**(4): 228-232. doi: 10.1097/00010694-195804000-00006

Geotechdata.info, Soil Young's modulus, http://geotechdata.info/parameter/soil-elastic-young-modulus.html (as of September 17.09.2013).

Gholami, M. (2014). Shear behaviour of oil sand fine tailings in simple shear and triaxial devices. M.Sc. thesis, Department of Civil and Environmental Engineering, Carleton University, Ottawa, ON.

Gibson, R. E., England, G. L., & Hussey, M. J. (1967). The Theory of one-dimensional consolidation of saturated clays: 1. finite non-linear consolidation of thin homogeneous layers. Geotechnique, **17**(3): 261–273. Available from https://www.icevirtuallibrary.com/doi/pdf/10.1680/geot.1967.17.3.261

Greenwood, J., Langseth, R., Velasquez, R., Abbasy, F., Solseng, P., (2018). Evaluation of subaqueous granular cap success conditions and failure potential on treated

fine tailings. *In* proceedings of the International Oil Sands Tailings Conference, Edmonton, AB, 9-12 December 2018.

Groenevelt, P. H., & Grant, C. D. (2004). A new model for the soil-water retention curve that solves the problem of residual water contents. European Journal of Soil Science, **55**(3): 479–485. doi: 10.1111/j.1365-2389.2004.00617.x

Gustavsson, K. (2003). Mathematical and numerical modeling of 1-D and 2-D Consolidation. Ph.D. thesis, Royal Institute of Technology, Department of Numerical Analysis and Computing Science, Stockholm, Sweden. Available from http://www.nada.kth.se/~katarina/thesis.pdf

Haines, W. B. (1923). The volume-changes associated with variations of water content in soil. The Journal of Agricultural Science, **13**(03): 296-310. doi: 10.1017/S0021859600003580

Haines, W. B. (1927). Studies in the physical properties of soils: IV. A further contribution to the theory of capillary phenomena in soil. The Journal of Agricultural Science, **17**(02), 264-290. doi: 10.1017/S0021859600018499

Hanzawa, H., Nutt, N., Lunne, T., Tang, Y. X., & Long, M. (2007). A comparative study between the NGI direct simple shear apparatus and the Mikasa direct shear apparatus, Soils and Foundations, **47**(1): 47–58. doi: 10.3208/sandf.47.47

Holdich, R. G., & Butt, G. (1997). Solid/liquid separation by sedimentation. Proceedings of the Institution of Mechanical Engineers, Part E: Journal of Process Mechanical Engineering, **211**(1), 43-52. Available from https://hdl.handle.net/2134/4517

Huerta, A., Kriegsmann, G. A.; and Krizek, R. J. (1988). Permeability and Compressibility of Slurries from Seepage-Induced Consolidation. Journal of Geotechnical Engineering, **114**(5):614. https://doi.org/10.1061/(ASCE)0733-9410(1988)114:5(614)

Hurtado, O. R. (2018). Desiccation and consolidation in centrifuge cake oil sands tailings. M.Sc thesis, Department of Civil and Environmental Engineering, Carleton University, Ottawa, ON. Available from https://curve.carleton.ca/e5cf2c70-6209-4b48-8f90-1daec6877af8

Hyndman, A., MeKenna, G., Sawatsky, L. & Vandenberg, J. (2018). Fluid Fine Tailings Processes: Disposal, Capping, and Closure Alternatives. *In* Proceeding of the 6th International Oil Sands Tailings Conference, Dec 9 – 12. Edmonton, AB.

Ignasiak, T. M., Kotlyar, L., Longstaffe, F. J., Strausz, O. P., and Montgomerry, D. S. (1983). Separation and characterization of clay from athabasca asphaltene. Fuel, **62**(3): 353–362.

Ignasiak, T.M., Zhang, Q., Kratochvil, C., Montgomery, D.S., and Strausz, O.P., (1985). Chemical and mineral characterization of the bitumen-free athabasca oil sands related to the bitumen concentration in sand tailings from the syncrude batch extraction test. AOSTRA Journal of Research, **(2)**1: 21–34.

Imai, G. (1981). Experimental studies on sedimentation mechanism and sediment formation of clay materials. Soils and Foundations, **21**(1): 7–20. doi: 10.3208/sandf1972.21.7

Innocent-Bernard, T. (2013). Evaporation, cracking, and salinity in a thickened oil sands tailings. M.Sc. thesis, Department of Civil and Environmental Engineering, Carleton University, Ottawa, ON. Available from https://curve.carleton.ca/system/files/etd/27ccfba9-f5c9-45f2-bb2f-dfbadee95b15/etd_pdf/540b6bb0dd4f83bcebf97defb46a8119/innocent-bernard-evaporationcrackingandsalinityinathickened.pdf

Inoue, T., Tan, T. S., & Lee, S. L. (1990). An investigation of shear strength of slurry clay. Soils and Foundations, **30**(4): 1–10.

Ito, T., & Matsui, T. (1975). Plastic flow mechanism of clays. *In* Proceedings of the Japan Society of Civil Engineers, 20 April 1975. Japan Society of Civil Engineers, pp. 109–123.

Jamiolkowski, M., Ladd, C., Germaine, J., & Lancellotta, R. (1985). New developments in field and lab testing of soils. *In* Proceedings of the 11th International Conference on Soil Mechanics and Foundation Engineering, San Francisco, California.

Jardine, R. J., & Hight, D. W. (1987). The behaviour and analysis of embankment on soft clays. *In* Bulletin of the public works research center, Athens, Greece. pp. 159–244.

Jeeravipoolvarn, S. (2005). Compression behaviour of thixotropic oil sands tailings. M.Sc. thesis, Department of Civil and Environmental Engineering, University of Alberta, Edmonton, AB.

Jeeravipoolvarn, S., Chalaturnyk, R. J., & Scott, J. D. (2008). Consolidation modeling of oil sands fine tailings: history matching. *In* Proceedings of 61st Canadian Geotechnical Conference, Edmonton, AB, 22–24 September. pp. 190-197

Jeeravipoolvarn, S., Chalaturnyk, R. J., & Scott, J. D. (2009a). Sedimentation-consolidation modeling with an interaction coefficient. Computers and Geotechnics, **36**(5): 751–761. Available from https://doi.org/10.1016/j.compgeo.2008.12.007

Jeeravipoolvarn, S., Scott, J. D., & Chalaturnyk, R. J. (2009b). 10 M standpipe tests on oil sands tailings: long-term experimental results and prediction. Canadian Geotechnical Journal, **46**(8): 875–888. doi: 10.1139/T09-033

Jeeravipoolvarn, S. (2010). Geotechnical behavior of In-line thickened oil sands tailings. Ph.D. thesis, Department of Civil and Environmental Engineering, University of Alberta, Edmonton, AB. doi: 10.7939/R3C04S

Jeeravipoolvarn, S., Scott, J. D., & Chalaturnyk, R. J. (2010). Composite tailings made from inline thickened oil sands tailings. *In* Proceedings of the 2nd International Oil Sands Tailings Conference, Devon, December, 2010. University of Alberta, pp. 5-8.

Kaminsky, H. A. (2008). Characterization of an Athabasca Oil Sands Ore and Process Streams. Ph.D. thesis, Department of Chemical and Materials Engineering, University of Alberta, Edmonton, AB.

Keen, B. A. (2018). The physical properties of the soil. Quarterly Journal of the Royal Meteorological Society, **58**(247): 490–491. Available from https://doi.org/10.1002/qj.49705824716

Kim, D. J., Vereecken, H., Feyen, J., Boels, D., & Bronswijk, J. J. B. (1992). On the characterization of properties of an unripe marine clay soil:I. Shrinkage processes of an unripe marine clay soil in relation to physical ripening. Soil Science, **153**(6): 471-481. Available from https://journals.lww.com/soilsci/Fulltext/1992/06000/

King, F. H. (1899). Principles and conditions of the movements of groundwater. Available from https://catalog.hathitrust.org/Record/005735536

Kjellman, W. (1951). Testing the shear strength of clay in Sweden. Geotechnique, **2**(3): 225-32.

Koppula, S. D. (1970). The consolidation of soil in two dimensions and with moving boundaries [microform] Ph.D. thesis, Department of Civil Engineering, University of Alberta, Edmonton, AB.

Kosugi, K. (1994). Three-parameter lognormal distribution model for soil water retention. Water Resources Research, **30**(4): 891–901. Available from https://doi.org/10.1029/93WR02931

Kotlyar, L.S., Sparks, B.D., and Kodama, H. (1984). Some chemical and mineralogical properties of fine solids derived from oil sands. AOSTRA Journal of Research, **1**:99–106.

Kunze, R. J., Uehara, G., & Graham, K. (1968). Factors Important in the calculation of hydraulic conductivity. Soil Science Society of America Journal, **32**(6): 760. Available from https://doi.org/10.2136/sssaj1968.03615995003200060020x

Kynch, G. J. (1952). A theory of sedimentation. Transactions of the Faraday Society, **48**(0): 166-176. doi: 10.1039/tf9524800166

Lacasse, S. M., Ladd, C. C., & Baligh, M. M. (1978). Evaluation of field vane, Dutch cone penetrometer and piezometer testing devices. *Res. Rep*.

Lacasse, S., Jamiolkowski, M., Lancellotta, R., & Lunne, T. (1981). In-situ characteristics of two Norwegian clays. *In* Proceedings of the 10th International Conference on Soil Mechanics and Foundation Engineering. **2**, pp. 7–11.

Ladd, C., & Foott, R. (1974). New design procedure for stability of soft clays. Journal of Geotechnical and Geoenvironmental Engineering,**100**(GT7): 763-786

Lahaie, R., (2008). Syncrude Canada Ltd. - New tailings concepts. *In* Proceedings of the 1st International Oil Sands Tailings Conference, Edmonton, AB., 7-10 December, 2008. pp. 1-17

Lahaie R, Sego TC, Chapman D, & Carrier WD. (2010). Development of accelerated dewatering technology for managing oil sands fine fluid tailings. *In* Proceedings of the GEO2010 Conference, Calgary, AB., 12-16 September 2010. pp. 678-685.

Laliberte, G. E. (1969). A mathematical function for describing capillary pressure-desaturation data. International Association of Scientific Hydrology Bulletin, **14**(2): 131–149. doi: 10.1080/02626666909493724

Larsson, R. (1977). Basic behavior of Scandinavian soft clays. Swedish Geotechnical Institute Report 4, Linkoping.

Lee, K. (1979). An analytical and experimental study of large strain soil consolidation. Ph.D. thesis, University of Oxford, Oxford, UK. Available from https://ora.ox.ac.uk/objects/uuid:9521ec26-f27b-46f0-8704-de5145b4d519

Lee, K., & Sills, G. C. (1981). The consolidation of a soil stratum, including self-weight effects and large strains. International Journal for Numerical and Analytical Methods in Geomechanics, **5**(4): 405–428. doi: 10.1002/nag.1610050406

Leong, E. C., & Rahardjo, H. (1997). Permeability functions for unsaturated soils. Journal Geotechnical and Geoenvironmental Engineering, **123**(12): 1118–1126.

Leroueil, S. (1996). Compressibility of clays: fundamental and practical aspects. Journal of Geotechnical Engineering, **122**(7): 534–543. Available from https://doi.org/10.1061/(ASCE)0733-9410(1996)122:7(534)

Li, H., & Williams, D. J. (1995). Numerical modeling of combined sedimentation and self-weight consolidation of an accreting coal mine tailings slurry. *In* Proceedings of Compression and Consolidation of Clayey Soils Conference, Balkema, Rotterdam, 1995, pp. 441-452.

Liu, J., & Znidarčić, D. (1991). Modeling one-dimensional compression characteristics of soils. Journal of Geotechnical Engineering, **117**(1): 162–169. Available from https://doi.org/10.1061/(ASCE)0733-9410(1991)117:1(162)

Lloret-Cabot, M., Wheeler, S. J., Pineda, J. A., Romero, E., & Sheng, D. (2018). From saturated to unsaturated conditions and vice versa. Acta Geotechnica, **13**(1): 15–37. doi: 10.1007/s11440-017-0577-6

Lofroth, H. (2008). Undrained shear strength in clay slopes – influence of stress conditions. Geotechnical Engineering. Ph.D. thesis, Department of Civil and Environmental Engineering, Division of Geo Engineering, Chalmers University of Technology, Göteborg, SE.

Luo, G., (2004). Investigation of CT beneath MFT deposition for oil sands tailings disposal. MSc thesis, University of Alberta, Civil and Environmental Engineering, Edmonton, AB.

Marinho, F. A. M. (1994). Shrinkage behaviour of some plastic soils. Ph.D. thesis, University of London, Bloomsbury, London, UK. Available from https://spiral.imperial.ac.uk/bitstream/10044/1/11381/2/Marinho-FAM-1994-PhD-Thesis.pdf

Masala, S. (1998). Numerical simulation of sedimentation and consolidation of fine tailings. M.Sc. thesis, University of Alberta, Edmonton, AB. Available from https://doi.org/10.7939/R3PN8XQ5N

Masala, S., and Matthews, J. (2010). Predicting development of undrained shear strength in soft oil sands tailings. *In* Proceedings of the 2nd International Oil Sands Tailings Conference, Devon, December, 2010. University of Alberta, pp. 31-40.

Matsui, T., & Ito, T. (1977). Flow mechanism of clay-layer system and microscopic meaning on shear parameters of soils. *In* Proceedings of the 9th ICSMFE, Special Session 9, pp. 143–152.

Matthews, J. G., Shaw, W. H., MacKinnon, M. D., & Cuddy, R. G. (2002). Development of composite tailings technology at Syncrude. International Journal of Surface Mining, Reclamation and Environment, **16**(1): 24–39. doi: 10.1076/ijsm.16.1.24.3407

Matthews, J., Dhadli, N., House, P., & Simms, P. (2011). Field trials of thin-lift deposition of amended mature fine tailings at the Muskeg River Mine in Northern Alberta. *In* Proceedings of the 14th International Seminar on Paste and Thickened Tailings, Perth, 5-7 April, 2011. Australian Centre for Geomechanics, pp. 271–280.

McKee, C. R., & Bumb, A. C. (1984). The importance of unsaturated flow parameters in designing a hazardous waste site. *In* Proceedings of the National Conference on

Hazardous Waste and Environmental Emergencies, March, 1984. Hazardous Materials Control Research Institute, Houston, Texas, pp.50-58.

McKee, C., & Bumb, A. (1987). Flow-testing coalbed methane production wells in the presence of water and gas. SPE Formation Evaluation, **2(**01): 599–608.

McKenna G, Dawson R, Hyndman A, LeSueur P & Sobkowicz J. (2012). *The Oil Sands Tailings Roadmap and Action Plan — Oil Sands Tailings State of Practice Overview*. International Oil Sands Tailings Symposium, University of Alberta Geotechnical Centre, Edmonton.

McKenna, G., Mooder, B. and Jamieson, A. (2016). Shear strength and density of oil sands fine tailings for reclamation to a boreal forest landscape. International Oil Sands Tailings Conference, Lake Louise, Alberta, December 4-7.

McRoberts, E. C., & Nixon, J. F. (1976). A theory of soil sedimentation. Canadian Geotechnical Journal, **13**(3), 294–310.

Mcvay, M., Townsend, F., & Bloomquist, D. (1986). Quiescent consolidation of phosphate waste clays. Journal of Geotechnical Engineering, **112**(11): 1033–1049. Available from https://ascelibrary.org/doi/pdf/10.1061/(ASCE)0733-9410(1986)112%3A11(1033)

Menzies, B. K., & Mailey, L. K. (1976). Some measurements of strength anisotropy in soft clays using diamond-shaped shear vanes. Geotechnique, **26**(3): 535–538.

Menzies, B. K., & Merrifield, C. M. (1980). Measurements of shear stress distribution on the edges of a shear vane blade. Geotechnique, **30**(3): 314–318.

Meter Environment © (2018). User manual for Pressure Transducer Tensiometer. Meter Group AG Munchen, version 08/2018. http://library.metergroup.com/Manuals/UMS/T5_Manual.pdf

Michaels, A. S., & Bolger, J. C. (1962). Settling rates and sediment volumes of Flocculated Kaolin Suspensions. Industrial & Engineering Chemistry Fundamentals, **1**(1): 24–33. Available from https://doi.org/10.1021/i160001a004

Mikasa, M. (1961). Settlement and treatment (Soil mechanics for river levee construction). Kansai Branch, Japanese Society of Soil Mechanics and Foundation Engineering.

Mikula, R.J., V.A. Munoz and O. Omotoso. (2009). Centrifugation options for production of dry stackable tailings in surface mined oil sands tailings management. Journal of Canadian Petroleum Technology, **48**(9): 19-23.

Miller, W. G., (2010). Comparison of geoenvironmental properties of caustic and noncaustic oil sand fine tailings. Ph.D thesis, Department of Civil and Environmental Engineering. University of Alberta, Edmonton. AB.

Mishler, R. T. (1912). Settling slimes at the Tigre Mill. Engineering and Mining Journal, **94**(4): 643–646.

Mizani, S., He, X., & Simms, P. (2013). Application of lubrication theory to modeling stack geometry of high density mine tailings. Journal of Non-Newtonian Fluid Mechanics, **198**, 59–70. Available from https://doi.org/10.1016/j.jnnfm.2013.03.002

Mizani, S. (2016). Experimental study and surface deposition modelling of amended oil sands tailings products. Ph.D thesis, Department of Environmental and Civil Engineering, Carleton University, Ottawa, ON.

Monroy, R. (2006). The influence of load and suction changes on the volumetric behaviour of compacted London Clay. Ph.D. thesis, Faculty of Engineering, Imperial College of London, University of London, Bloomsbury, London, UK.

Morgenstern, N. R., & Scott, J. D. (1995). Geotechnics of fine tailings management, Geoenvironment 2000 Report, ASCE Specialty Conference, New Orleans.

Mualem, Y. (1976). A New model for predicting the hydraulic conductivity of unsaturated porous media. Water Resources Research, **12**(3). Available from https://www.://soil.en.a.u-tokyo.ac.jp/jssp/db/pdf/106047.pdf%5Cnpapers2://publication/uuid/36CA47A0-B20A-43DD-8382-B1B80B4A1CAC

Myint, W. B. (2008). Compressibility of ultra-soft soil. Singapore: World Scientific.

Ng, C. W., & Pang, Y. W. (2000). Influence of stress state on soil-water characteristics and slope stability. Journal of Geotechnical and Geoenvironmental Engineering, **126**(2): 157–166.

Ohara, S., and Matsuda, H. (1978). Dynamic Shear Strength of Saturated Clay. Soils and Foundations. **18**(1):91-97. https://doi.org/10.3208/sandf1972.18.91

Olmedo, N., Fisseha, B.T., Wilson, G.W., Barczyk, M., Zhang, H. and Lipsett, M. (2020). “An Automated Vane Shear Test Tool for Environmental Monitoring with Unmanned Ground Vehicles.” Journal of Terramechanics **91**:53-63. June 2020. DOI: 10.1016/j.jterra.2020.05.003.

Omega Engineering Inc. (2019). General purpose pressure transmitter user manual. https://www.omega.com/en-us/sensors-and-sensing-equipment/pressure-and-strain/c/pressure-transducers.

O’Neil, S. (2002). Three-dimensional mobile bed dynamics for sediment transport modeling. Ph.D. thesis, Graduate School, The Ohio State University, Columbus, OH.

OSTC. (2012). Technical guide for fluid fine tailings management. Available from https://www.cosia.ca/uploads/documents/id7/TechGuideFluidTailingsMgmt_Aug2012.pdf

OSTC 2012 – Canada's oil sands innovation alliance 2012. Subaqueous Sand Capping of Soft Oil Sands Tailings, Evaluation, by Barr Engineering and Environmental Science Canada Ltd., Deltares, Anchor QEA, and Royal Boskalis Westminster. December 2012.

Owolagba, J., & Azam, S. (2014). Geotechnical properties of centrifuged oil sand fine tailings. Environmental Geotechnics, **2**(5): 309-316.

Pachepsky, Y. A., Shcherbakov, R. A., & Korsunskaya, L. P. (1995). Scaling of soil water retention using a fractal model. Soil Science, **159**(2): 99-104.

Pane, V., & Schiffman, R. L. (1985). A note on sedimentation and consolidation. Geotechnique, **35**(1): 69–72.

Pane, V., & Schiffman, R. L. (1997). The permeability of clay suspensions. Géotechnique, **47**(2): 273–288. Available from https://doi.org/10.1680/geot.1997.47.2.273

Parent, S.-É., Cabral, A., & Zornberg, J. G. (2007). Water retention curve and hydraulic conductivity function of highly compressible materials. Canadian Geotechnical Journal, **44**(10): 1200–1214. Available from https://doi.org/10.1139/T07-091

Pereira, J. H. F., & Fredlund, D. G. (2000). Volume change behavior of collapsible compacted gneiss soil. Geotechnical and Geoenvironmental Engineering, **126**(10): 907–916.

Perlow, M. J., & Richards, A. F. (1977). Influence of Shear Velocity on Vane Shear Strength. Journal of the Geotechnical Engineering Division, **103**(1): 19–32.

Personal communications (2016). With experienced field person from Syncrude Ltd.

Pham, H. Q., & Fredlund, D. G. (2008). Equations for the entire soil-water characteristic curve of a volume change soil. Canadian Geotechnical Journal, **45**(4): 443–453. doi: 10.1139/T07-117

Pollock, G. W. (1988). Large strain consolidation of oil sand tailings sludge. M.Sc. thesis, Department of Civil Engineering, University of Alberta, Edmonton, AB. Available from https://era.library.ualberta.ca/items/f33ace0b-23bc-4fe5-b249-4ef57eb244b0/view/46e85133-7116-47fd-b3c3-de96da455e98/ML45647.pdf

Pollock, G.W., E.C. McRoberts, G. Livingstone, G.T. McKenna, J.G. Matthews and J.D. Nelson (2000). Consolidation behaviour and modelling of oil sands composite tailings in the Syncrude CT prototype. *In* Proceedings of the International Conference on Tailings and Mine Waste '00. A Balkema Publishers. pp: 121-130.

Prevost, J. H., & Hoeg, K. (1975). Effective stress-strain-strength model for soils. Journal of Geotechnical and Geoenvironmental Engineering, **101**(GT3): 259-278.

Proskin, S. (1998). A geotechnical investigation of freeze-thaw dewatering of oil sands fine tailings. Ph.D. thesis, Department of Civil and Environmental Engineering, University of Alberta, Edmonton, AB. doi: 10.7939/R3HH6CB7C

Qi, S., Simms, P., Vanapalli, S., & Daliri, F. (2016). A large strain consolidation- unsaturated flow model for tailings analysis : mutilayers. *In* Proceedings of the 69th Annual Canadian Geotechnical Conference, Vancouver, B.C., 2-5 October 2015. Vancouver Geotechnical Society and the Canadian Geotechnical Society, Vancouver.

Qi, S., Simms, P., & Vanapalli, S.(2017a). Piecewise-linear formulation of coupled large-strain consolidation and unsaturated flow. I: Model development and implementation. Journal of Geotechnical and Geoenvironmental Engineering, **143**(7): 04017018.

Qi, S., Simms, P., Vanapalli, S., & Soleimani, S. (2017b). Piecewise-linear formulation of coupled large-strain consolidation and unsaturated flow. II: Testing and performance. Journal of Geotechnical and Geoenvironmental Engineering, **143**(7): 04017019.

Qiu, Y. (2000). Optimum deposition for sub-aerial tailings disposal. Ph.D. thesis, Faculty of Graduate Studies and Research, University of Alberta, Edmonton, AB.

Qiu, Y., & Sego, D. C. (2007). Optimum deposition for sub-aerial tailings disposal: Model applications. International Journal of Mining, Reclamation and Environment, **21**(1): 65–74. doi: 10.1080/17480930600906177

Read, P. (2014). Broad suite of practice and technology key to success in tailings management. *In* Fourth International Conference on Oil Sands Tailings, University of Alberta, Dept. of Civil & Environmental Engineering, Lake Louis, AB.

Richards, L. A. (1928). The usefulness of capillary potential to soil-moisture and plant investigations. Journal of Agriculture Research, **37:** 719-742. Available from https://pdfs.semanticscholar.org/9c59/0d108ce8a8ed643cec845f9659ceb8a5d094

Richardson, J. F., & Zaki, W. N. (1997). Sedimentation and fluidisation: Part I. Chemical Engineering Research and Design, **75**, S82-S100.

Rima, U. S. (2013). Characterization and centrifuge dewatering of oil sands fine tailings. M.Sc. thesis, Faculty of Graduate Studies and Research, University of Regina, Regina, SK.

Rima, U. S. & Beier, N. A. (2018). Effects of surficial seasonal weathering on centrifuged oil sands tailings. *In* Proceeding of 6th International Oil Sands Tailings Conference, Dec 9 - 12, Edmonton. AB.

Roscoe, K. (1953). An apparatus for the application of simple shear to soil samples. *In* Proceedings of the 3rd ICSMFE, Zurich. Vol. 1, pp. 186-191. Available from http://scholar.google.com/scholar?hl=en&btnG=Search&q=intitle:An+apparatus+for+the+application+of+simple+shear+to+soil+samples#0

Roy, M., & Leblanc, A. (1988). Factors Affecting the Measurements and Interpretation of the Vane Strength in Soft Sensitive Clays. In Vane Shear Strength Testing in Soils: Field and Laboratory Studies (pp. 117–130). ASCE.

Rozina, E., Mizani, S., Malek, M., Sanchez-Sardon, M., & Simms, P. (2015). Dewatering in a laboratory simulation of a multilayer deposit of inline flocculated mature fine tailings. *In* Proceedings of the 18th International Seminar on Paste and Thickened Tailings, Perth, WA. Australian Centre for Geomechanics. pp. 81-93

Rudman, M., Simic, K., Paterson, D. A., Strode, P., Brent, A., & Šutalo, I. D. (2008). Raking in gravity thickeners. International Journal of Mineral Processing, **86**(1– 4): 114–130. Available from https://doi.org/10.1016/j.minpro.2007.12.002

Russel, W. B., Saville, D. A., & Schowalter, W. R. (1989). Colloidal dispersions. Cambridge University Press. doi: 10.1017/CBO9780511608810

Russo, D. (1988). Determining soil hydraulic properties by parameter estimation: on the selection of a model for the hydraulic properties. Water Resources Research, **24**(3): 453–459. doi: 10.1029/WR024i003p00453

Salfate, E., Wilson, G., Wijewickreme, D., & Simms, P. (2010). Predicting void ratio in surface deposited paste tailings. *In* Proceedings of the First International Seminar on the Reduction of Risk in the Management of Tailings and Mine Waste, Perth, WA. Australian Centre for Geomechanics, pp. 473-485

Schafer, H. (2018). Freezing characteristics of Mine Waste Tailings and their relations to unsaturated soil properties. M.Sc. thesis, Department of Civil and Environmental Engineering, University of Alberta, Edmonton, AB.

Schiffman, R. L., Pane, V., & Gibson, R. E. (1984). An overview of nonlinear finite strain sedimentation and consolidation, *In* Proceedings of the ASCE Conventions. San Francisco, California, pp. 1-29.

Schofield, A., & Wroth, P. (1968). Critical state of soil mechanics. McGraw-Hill: London.

Scott, J. D., & Dusseault, M. B. (1982). Behaviour of oil sands tailings. The 33rd Annual Technical Meeting of the Petroleum Society of the Canadian Institute of Mining and Metallurgy, Calgary, Alberta.

Scott, J. D., & Cymerman, G. J. (1984). Prediction of viable tailings disposal methods, in sedimentation consolidation models: prediction and validation. *In* Proceedings of a Symposium held in conjunction with the ASCE Convention, San Francisco, October, 1984. pp. 522–544.

Scott, J., Dusseault, M., & Carrier, W. (1986). Large-scale self-weight consolidation testing. Consolidation of Soils: Testing and Evaluation. ASTM International.

Scott, K. J. (1966). Mathematical models of mechanism of thickening. Industrial and Engineering Chemistry Fundamentals, **5**(1): 109–113. Available from https://doi.org/10.1021/i160017a020

Seed, H. B., WoodWard, R. J., & Lundgren, R. (1964a). Clay Mineralogical aspects of the Atterberg limits. Journal of Soil Mechanics and Foundation Division (ASCE), **90**(SM4): 107–131.

Seed, H. B., WoodWard, R. J., & Lundgren, R. (1964b). Fundamental aspects of the Atterberg limits. Journal of Soil Mechanics and Foundation Division, **90**(SM6): 107–131.

Seneviratne, N. H., Fahey, M., Newson, T. A., & Fujiyasu, Y. (1996). Numerical modelling of consolidation and evaporation of slurried mine tailings. International Journal for Numerical and Analytical Methods in Geomechanics, **20**(9): 647–671. Available from https://doi.org/10.1002/(SICI)1096-9853(199609)20:9<647:AID-NAG844>3.3.CO;2-V

Sharifounnasab, M., & Ullrich, C. R. (1985). Rate of shear effects on vane strength. Journal of Geotechnical Engineering, **111**(1): 135–139.

Shaw, W. and Wang, N. (2005). In-line thickened tailings pilot program. Preliminary pilot results for a promising new method for thickening of high fines tailings streams.

Shell Canada Ltd., (2009a). Muskeg river mine: tailings management plan. Energy Resources Conservation Board, Calgary, AB.

Shell Canada Ltd., (2009b). Jackpine mine: tailings management plan. Energy Resources Conservation Board, Calgary, AB.

Shirato, M., Kato, H., Kobayashi, K., & Sakazaki, H. (1970). Analysis of settling of thick slurries due to consolidation. Journal of Chemical Engineering of Japan, **3**(1): 98–104. doi:10.1252/jcej.3.98

Simms, P., Grabinsky, M., & Zhan, G. (2007). Modelling evaporation of paste tailings from the Bulyanhulu mine. Canadian Geotechnical Journal, **44**(12), 1417–1432. doi: 10.1139/T07-067

Simms, P., Dunmola, A., Fisseha, B., & Bryan, R. (2010). Generic modelling of desiccation for cyclic deposition of thickened tailings to maximize density and to minimize oxidation. *In*

Proceedings of the 13th International Conference on Paste and Thickened Tailings, Perth, WA. May, 2010. Australian Centre for Geomechanics. pp. 293-301.

Sivakumar, V. (1993). A critical state framework for unsaturated soil. Ph.D. thesis, Department of Civil and Structural Engineering, University of Sheffield, UK. Available from http://etheses.whiterose.ac.uk/21744/1/262072.pdf

Slichter, C. S. (1899). Nineteenth annual report of the United States Geological Survey to the Secretary of the Interior 1897 - 1898: Part II - Papers chiefly of a theoretic nature. Annual Report. doi:10.3133/ar19_2

Slichter, C. S. (1905). Field measurements of the rate of movement of underground waters. Water Supply Paper. doi: 10.3133/wsp140

Sobkowicz, J., & Morgenstern, N. R. (2009). A geotechnical perspective on oil sands tailings. *In* Proceedings of the 13th International Conference on Tailings and Mine Waste, Banff, Alta. pp. 1-4.

SoilVision Systems Ltd. Team. (2012). SVFLUX-SVSOLID Theory and Verification Manual. SoilVision Systems Ltd.

SoilVision System Ltd. Team. (2015). Calibration of Rim Ditch Dewatering Pilot with Large-Strain Consolidation, Sedimentation, Continuous Filling, Evaporation and Thaw Strain. Report submitted to Syncrude Research Center. Edmonton, AB, Canada

Soleimani, S., Simms, P., Dunmola, A., Freeman, G., & Wilson, G. W. (2014). Desiccation and consolidation in thin-lift deposition of polymer amended mature fine tailings. *In* Proceedings of the 17th International Seminar on Paste and Thickened Tailings, Vancouver, B.C. InfoMine.

Somogyi, F. (1980). Large strain consolidation of fine grained slurries. In Presented at Canadian society for Civil Engineering. Winnipeg.

Somogyi, F., Carrier, W. D., Lawyer, J. E., & Beckman, J. F. (1984). Waste phosphatic clay disposal in mine cuts. Sedimentation consolidation models: predictions and validation. *In* Proceedings of a Symposium, New York.

Sridharan, A., & Rao, G. V. (1971). Effective Stress Theory of Shrinkage Phenomena. Canadian Geotechnical Journal, **46**(10): 1229–1235. doi:10.1139/t10-0

Stirk, G. B. (1954). Some aspects of soil shrinkage and the effect of cracking upon water entry into the soil. Australian Journal of Agricultural Research, **5**(2): 279–296. doi: 10.1071/AR9540279

Suthaker, N. N. (1995). Geotechnics of oil sand fine tailings. Ph.D. thesis, Department of Civil Engineering, University of Alberta, Edmonton, AB.

Syncrude Canada Ltd., (2008). Syncrude application for approval of the Southwest Sand Conversion Project. Energy Resources Conservation Board and Alberta Environment.

Talmage, W. P., & Fitch, E. B. (1955). Determining Thickener Unit Areas. Industrial & Engineering Chemistry, **47**(1): 38–41. doi: 10.1021/ie50541a022

Tan, S. A., Tan, T. S., Ting, L. C., Yong, K. Y., & Karunaratne, G.-P. (1988). Determination of consolidation properties for very soft clay. Geotechnical Testing Journal, **11**(4): 233–240.

Tan, T. S. (1986). Two-phase soil study: A. Finite strain consolidation; B. Centrifuge scaling considerations. Ph.D. thesis, California Institute of Technology, Pasadena, California. Available from https://thesis.library.caltech.edu/902/

Tan, T., Goh, T., Karunaratne, G., & Lee, S. (1994). Shear strength of very soft clay-sand mixtures. Geotechnical Testing Journal **17**(1): 27-34.

Tan, T. S. (1995). Sedimentation to consolidation: a geotechnical perspective. *In* Proceedings of Compression and Consolidation of Clayey Soils, Hiroshima, Japan, pp. 937-948.

Tan, T., Yong, K., Leong, E., & Lee, S. (1990). Behavior of clay slurry. Soils and Foundations, **30**(4): 105–118. doi:10.3208/sandf1972.30.4_105

Terzaghi, K. (1925). Principles of soil mechanics, IV—Settlement and consolidation of clay. Engineering News Record, **95**(3): 874–878.

Terzaghi, K. (1943). Theoretical soil mechanics. Hoboken, NJ, USA: John Wiley & Sons, Inc. doi:0.1002/9780470172766

Tiller, F. M. (1981). Revision of kynch sedimentation theory. AIChE Journal, **27**(5): 823–829. doi: 10.1002/aic.690270517

Toorman, E. A. (1996). Sedimentation and self-weight consolidation: general unifying theory. Géotechnique, **46**(1): 103–113. doi: 10.1680/geot.1996.46.1.103

Toorman, E. A. (1999). Sedimentation and self-weight consolidation: constitutive equations and numerical modelling. Geotechnique, **49**(6): 709–726. doi:10.1680/geot.1999.49.6.709

Townsend, F., & McVay, M. C. (1990). SOA: Large strain consolidation predictions. Journal of Geotechnical Engineering, **116**(2): 222–243.

van Genuchten, M. T. (1980). A closed-form equation for predicting the hydraulic conductivity of unsaturated soils 1. Soil Science Society of America Journal, **44**(5): 892-898. Available from https://hwbdocuments.env.nm.gov/Los%20Alamos%20National%20Labs/TA%2054/11569.pdf

Vanapalli, S. K., Fredlund, D. G., & Pufahl, D. E. (1996). The relationship between the soil-water characteristic curve and the unsaturated shear strength of a compacted glacial till. Geotechnical Testing Journal. doi: 10.1520/GTJ10351J

Vanapalli, S., Fredlund, D. G., Pufahl, D. E., & Clifton, A. W. (1996). Model for the prediction of shear strength with respect to soil suction. Canadian Geotechnical Journal, **33**(1): 379–392.

Vedoy, D. R. L., and Soares, J. B. P. (2015). Water-soluble polymers for oil sands tailing treatment: A Review. Canadian Journal of Chemical Engineering. **93**(5): 888-904. https://doi.org/10.1002/cjce.22129

Vu, H. Q., and Fredlund, D. G. (2006). Challenges to modelling heave in expansive soils. Canadian Geotechnical Journal, **43**(12): 1249–1272. doi:10.1139/t06-073

Watari, Y. (1984). Reclamation with clayey soils and methods of earth spreading on the surface. *In* Proceedings of Seminar on Soil Improvement and Construction Technique in Soft Ground, Singapore. Japanese Society of SMFE, pp. 103–119. Pond 1A. *In* Proceedings Tailings and Mine Waste, 9, Vancouver, BC. 6 November, 2011. Available from https://www.barbau.ca/content/long-term-situ-behaviour-oil-sands-fine-tailings-suncors-pond-1a

Wells, P. S. (2011). Long Term In-Situ Behaviour of Oil Sands Fine Tailings in Suncor's Pond 1A. *In* Proceedings of Tailings and Mine Waste 2011.

Wells, P.S. and D.A. Riley, (2007). MFT drying — case study in the use of rheological modification and dewatering of fine tailings through thin lift deposition in the oil sands of Alberta. *In* Proceedings of the 10th International Seminar on Paste and Thickened Tailings (Paste07), Perth, Australia. Australian Centre for Geomechanics, pp. 13-15.

Wilson, G. W., Fredlund, D. G., & Barbour, S. L. (1997). The effect of soil suction on evaporative fluxes from soil surfaces. Canadian Geotechnical Journal, **34**(4): 145–154. doi: 10.1162/LING_a_00021

Wilson, W. G., Kabwe, L. K., Beier, N. A., Scott, J. D. (2018). Effect of various treatments on consolidation of oil sands fluid fine tailings. Canadian Geotechnical Journal, **55**(8): 1059-1066. doi: 10.1139/cgj-2017-0268

Xu, Y., & Cymerman, G. (1999). Flocculation of fine oil sand tails. Polymers in mineral processing. *In* Proceedings of the third UBC-McGill Bi-Annual International Symposium on Fundamentals of Mineral Processing, Quebec City, QC, 22-26 August 1999. pp. 591–604.

Yao, D. T. C., de Oliveira-Filho, W. L., Cai, X. C., & Znidarcic, D. (2002). Numerical solution for consolidation and desiccation of soft soils. International Journal for Numerical and Analytical Methods in Geomechanics, **26**(2): 139–161. doi: 10.1002/nag.196

Yao, Y. (2016). Dewatering behaviour of fine oil sands tailings: an experimental study. Ph.D. thesis, Delft University of Technology, Delft, NL. Available from https://doi.org/10.4233/UUID:1AC8F35B-0738-42B4-8AE2-5A5F68941814

Yong, R. N., Siu, S. K. H., & Sheeran, D. E. (1983). On the stability and settling of suspended solids in settling ponds. Part I. Piece-wise linear consolidation analysis of sediment layer. Canadian Geotechnical Journal, **20**(4): 817–826. doi: 10.1139/t83-085

Yuan, S. and Shaw, W. (2007). Novel processes for treatment of Syncrude fine transition and marine ore tailings. Canadian Metallurgical Quarterly, **46**(3): 265-272.

Zhang, F. (2010). Soil water retention and relative permeability for full range of saturation. Pacific Northwest National Laboratory (PNNL) Richland, WA. Available from https://www.pnnl.gov/main/publications/external/technical_reports/PNNL-19800.pdf

Zhang, F. (2016). Unsaturated soil property functions for high volume change materials. Ph.D. thesis, Department of Civil and Environmental Engineering, University of Alberta, Edmonton, AB.

Zhang, F., & Fredlund, D. G. (2015). Corrigendum: examination of the estimation of relative permeability for unsaturated soils. Canadian Geotechnical Journal, **52**(12): 2077–2087. doi: 10.1139/cgj-2015-0043

Zhang, J., & Thode, R. (2012). Large-strain consolidation modelling. Saskatoon.

Zhang, L., & Chen, Q. (2005). Predicting bimodal soil-water characteristic curves. Journal of Geotechnical and Geoenvironmental Engineering, **131**(5): 666–670.

Zhang, J., & Thode, R. (2012). Large-Strain Consolidation Modelling. Ph.D. thesis, University of Saskatchewan.

Znidarcic, D., Miller, R., van Zyl, D., Fredlund, M., & Wells, S. (2011). Consolidation behaviour of oil sand fine tailings. *In* Proceedings of Tailings and Mine Waste, Banff, Alberta.

APPENDIX A: FLOCCULATED FFT

Applied suction of 10 kPa for flocculated FFT

This section presents results during the applied suction of 10 kPa.

Settlement, vertical strain and void ratio

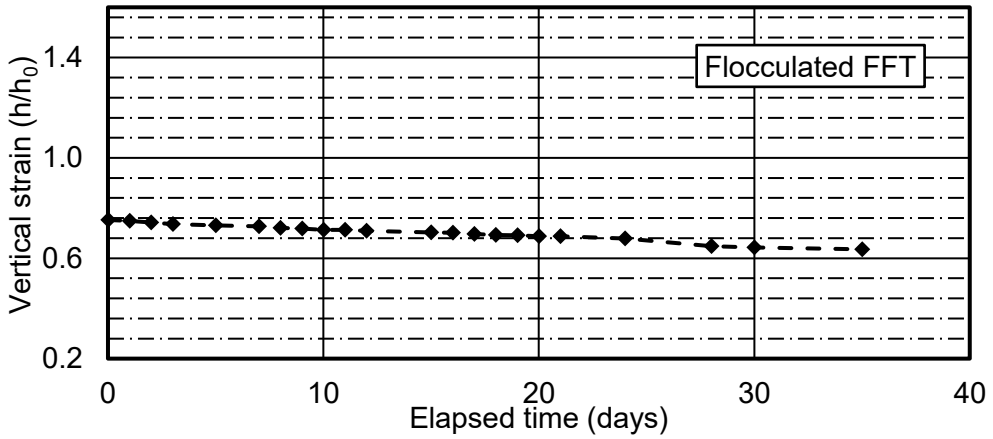

Figure A.1. Vertical strain during an applied suction of 10 kPa.

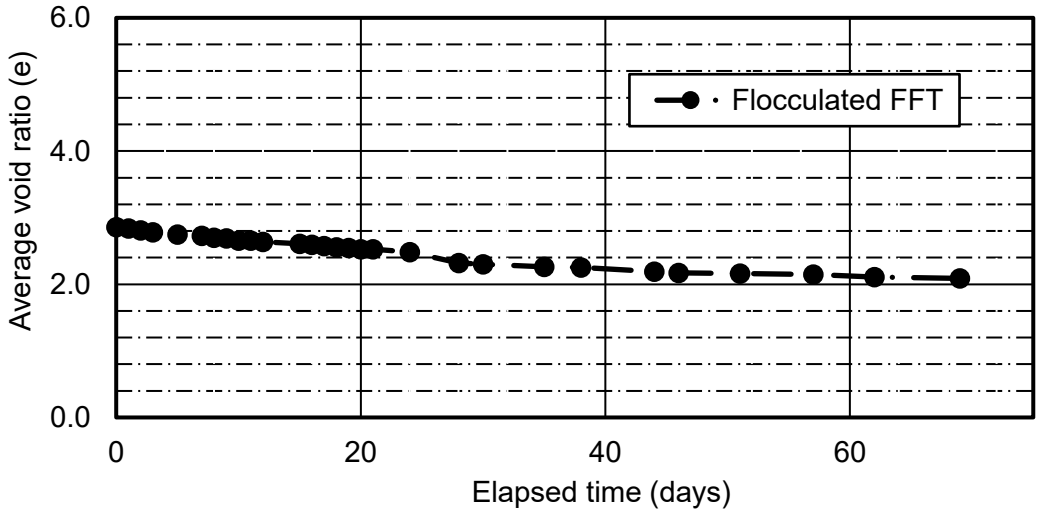

Figure A.2. Change in average void ratio during an applied suction of 10 kPa.

Pore pressure and suction distribution

The pore pressure and suction distribution results during the applied suction of 10 kPa at the bottom boundary using positive pressure transducer is presented in Figure A.3.

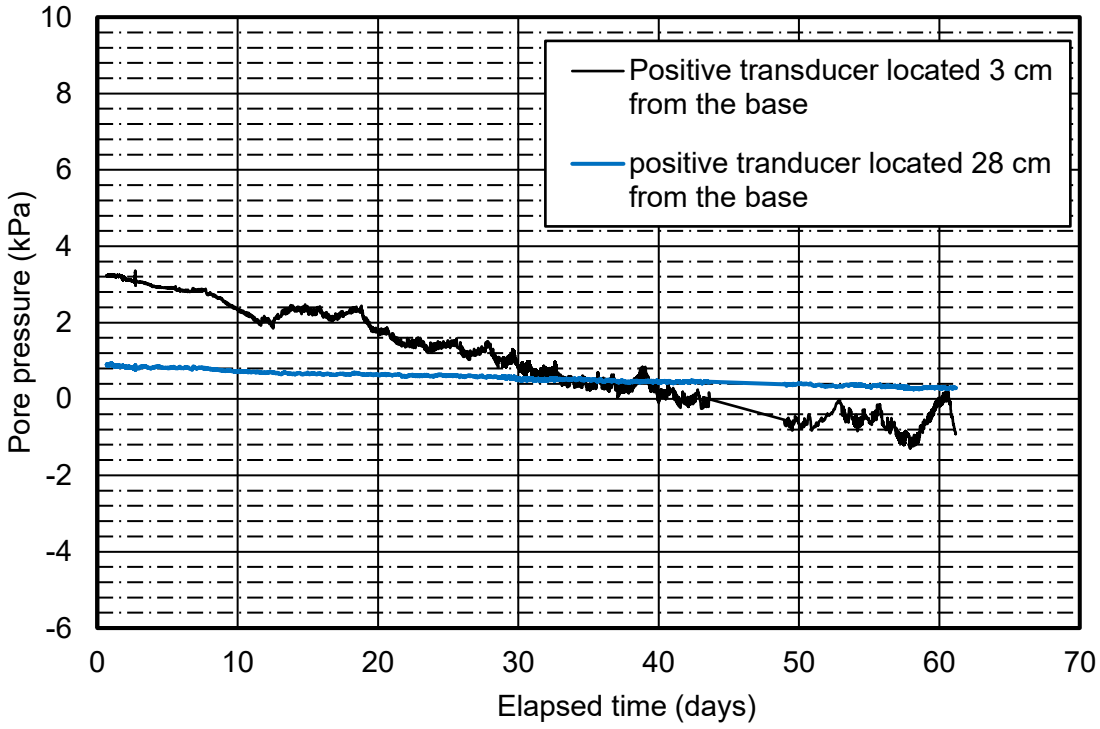

Figure A.3. Suction using positive pore pressure sensor during an applied suction of 10 kPa.

Undrained peak shear strength measurement with time and depth

The shear strength of deposited flocculated tailings was measured as the tailings consolidated using incremental applied suction. The vane shear strength versus angular deflection results are presented in A.4(a) to A.4(e).

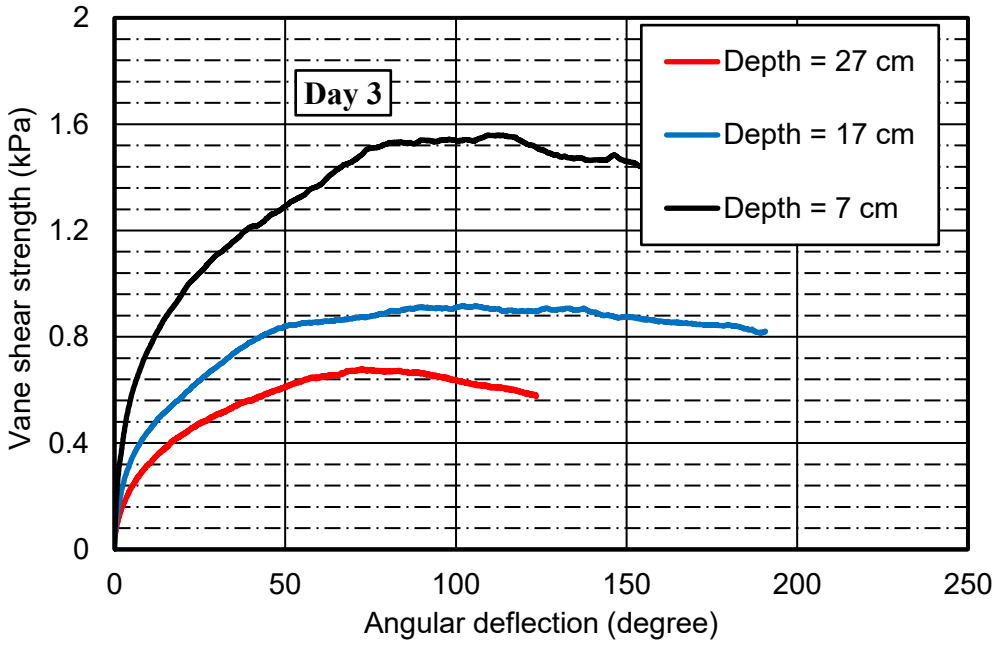

(a) Vane shear measurement by day 3

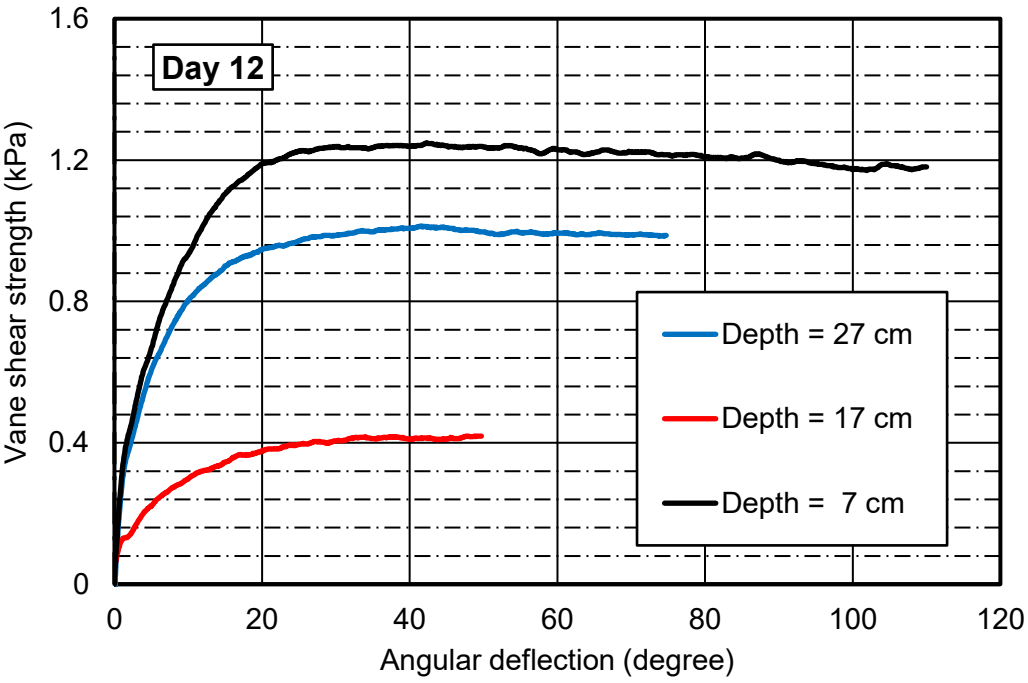

(b) Vane shear measurement by day 12

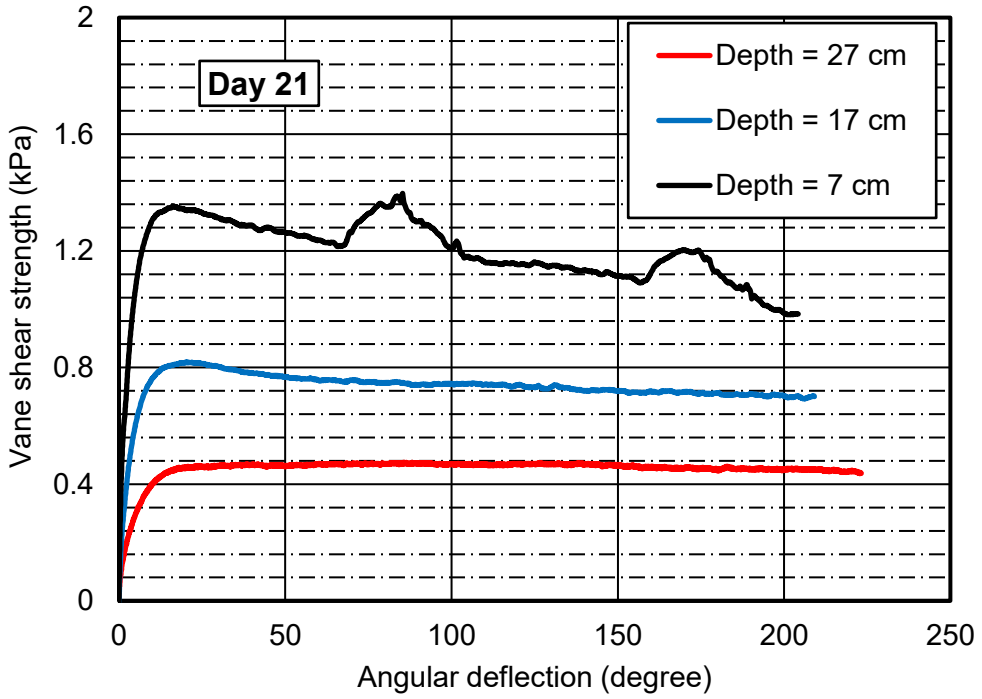

(c) Vane shear measurement by day 21

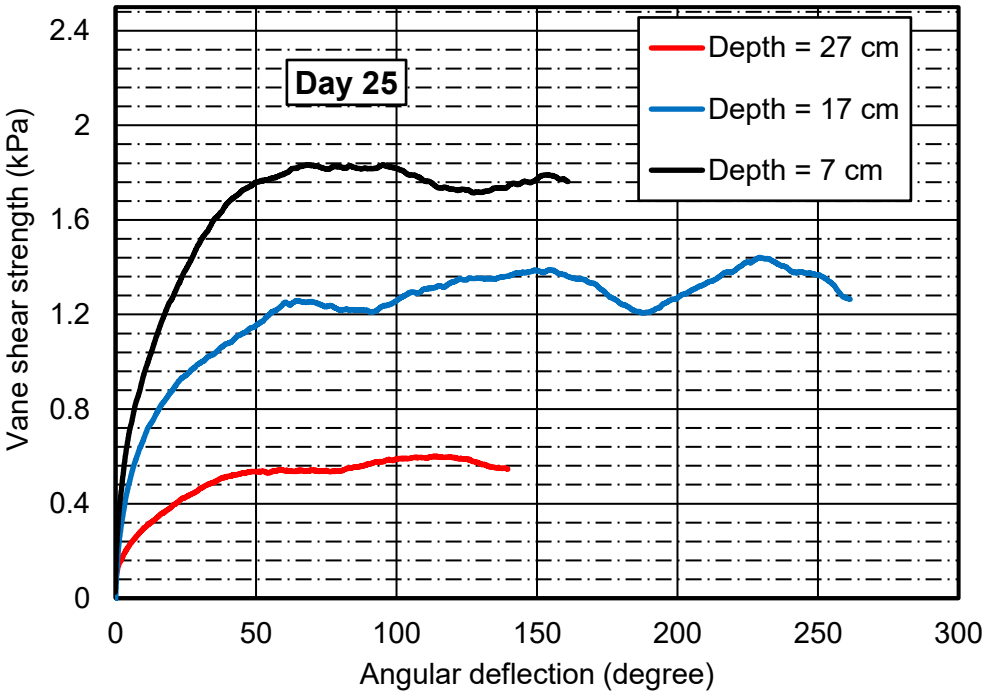

(d) Vane shear measurement by day 25

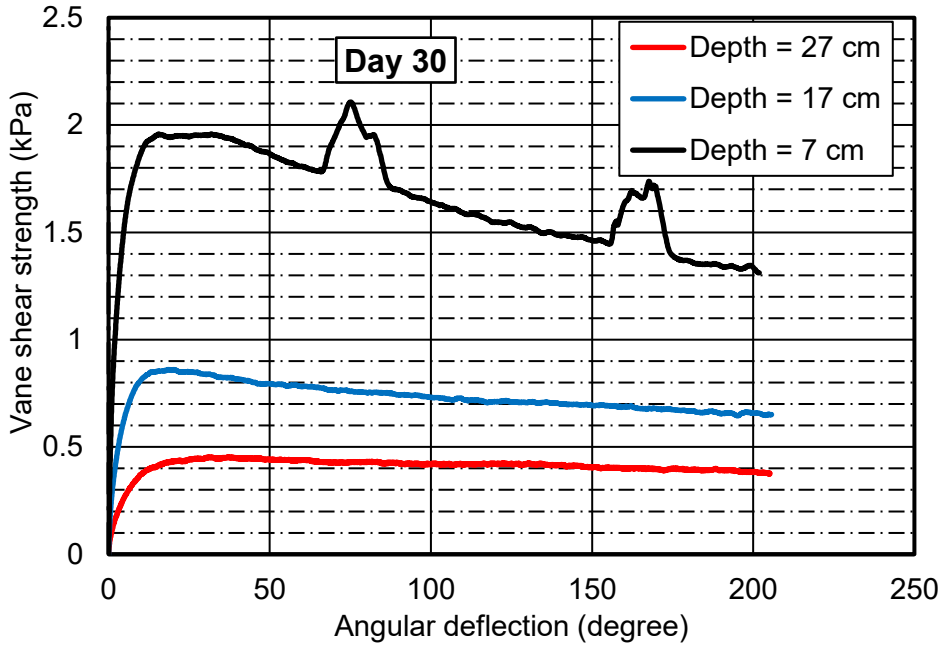

(e) Vane shear measurement by day 30

Figure A.4. Vane shear strength test during an applied suction of 10 kPa: (a) Day 3; (b) Day 12; (c) Day 21; (d) Day 25 and (d) Day 30.

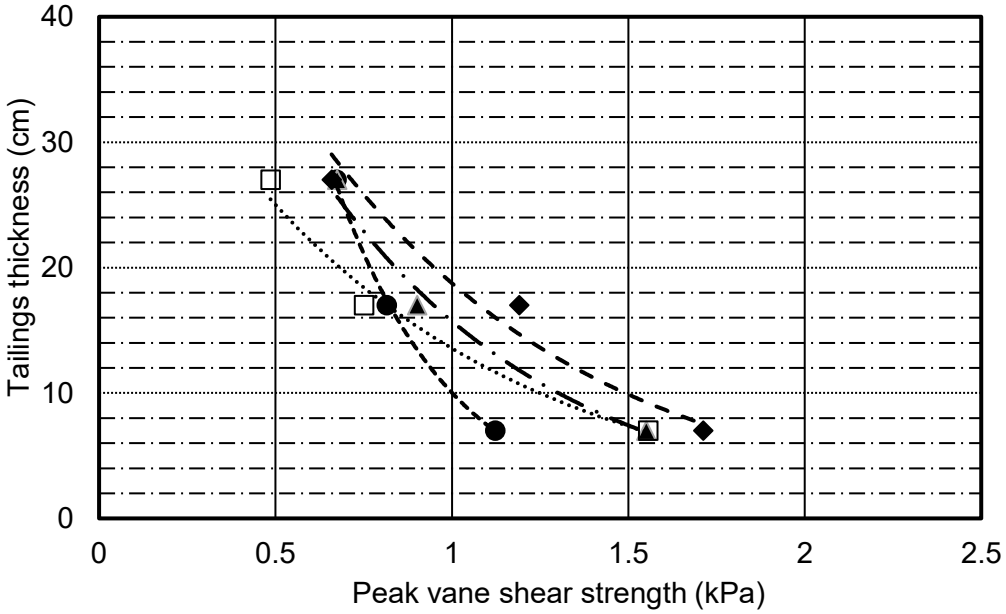

Figure A.5. Peak vane shear strength during an applied suction of 10 kPa with depth and time.

Applied suction of 30 kPa for flocculated FFT

This section presents results during the applied suction of 30 kPa.

Settlement, vertical strain and void ratio

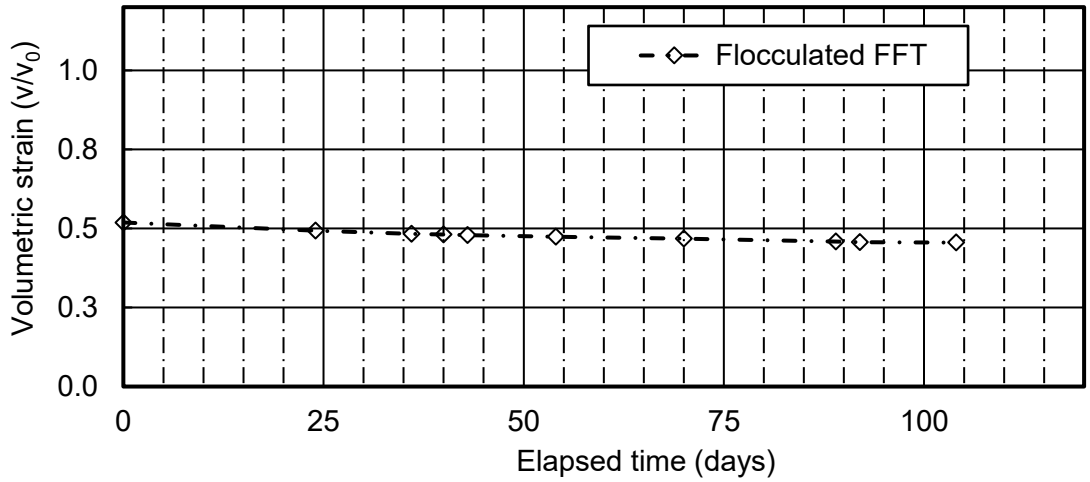

Figure A.6. Change in volumetric strain during an applied suction of 30 kPa.

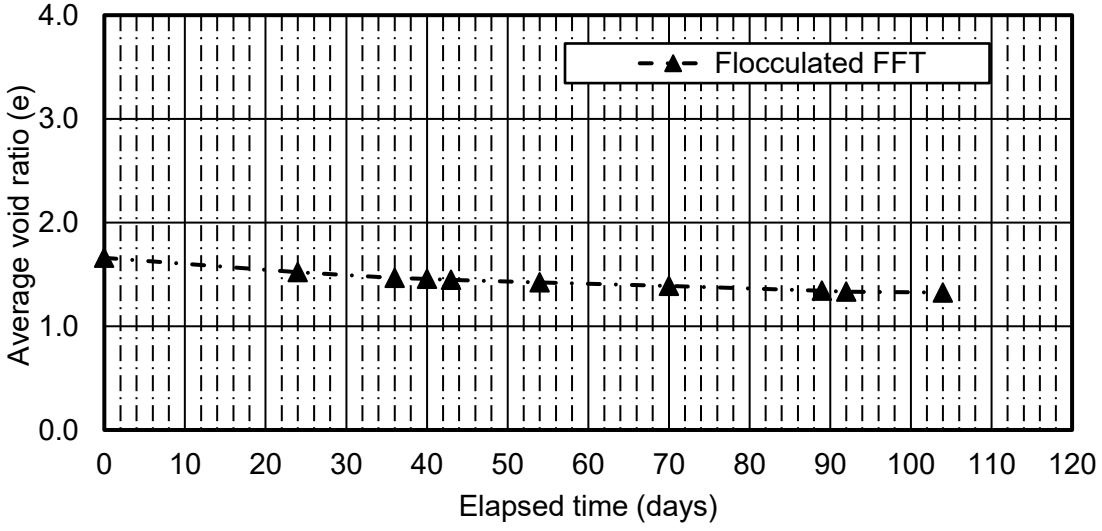

Figure A.7. Change in average void ratio during applied suction of 30 kPa.

Suction distribution

The sensor to measure negative pore pressure was not responding properly. Therefore, no suction results during the applied suction of 30 kPa.

Undrained peak shear strength measurement with time and depth

The shear strength of deposited flocculated tailings was measured as the tailings consolidated using incremental applied suction. The vane shear strength versus angular deflection results are presented in A.8(a) to A.8(d).

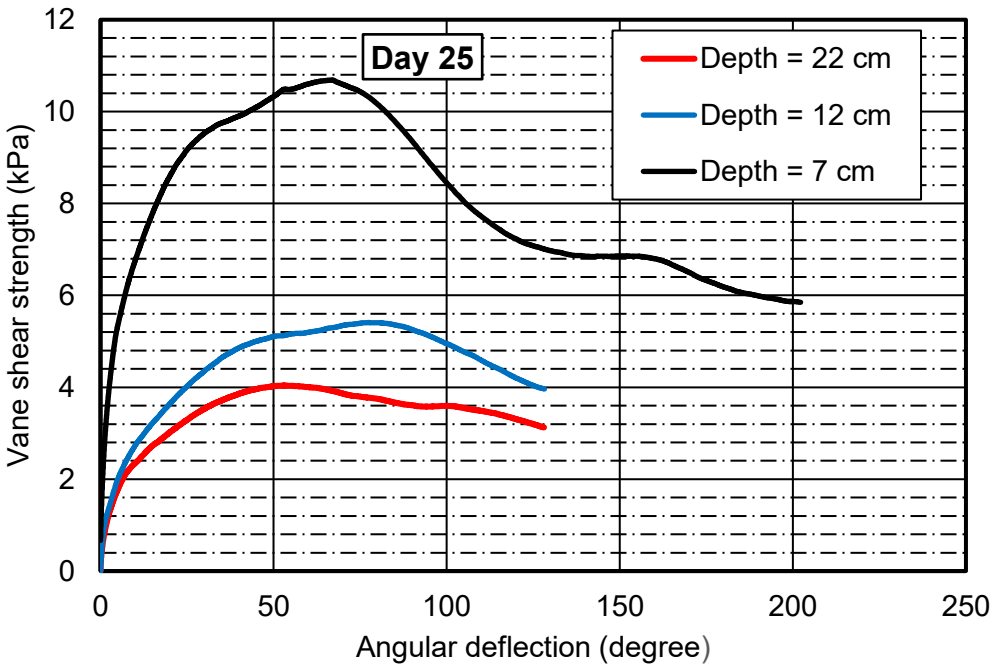

(a) Vane shear measurement by day 25

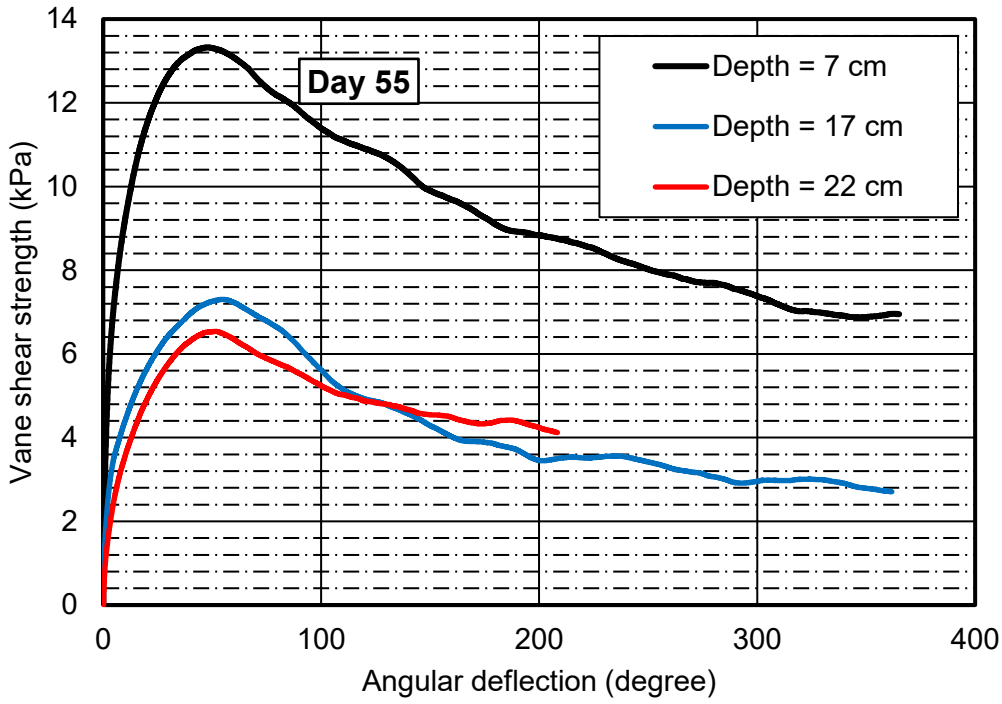

(b) Vane shear measurement by day 55

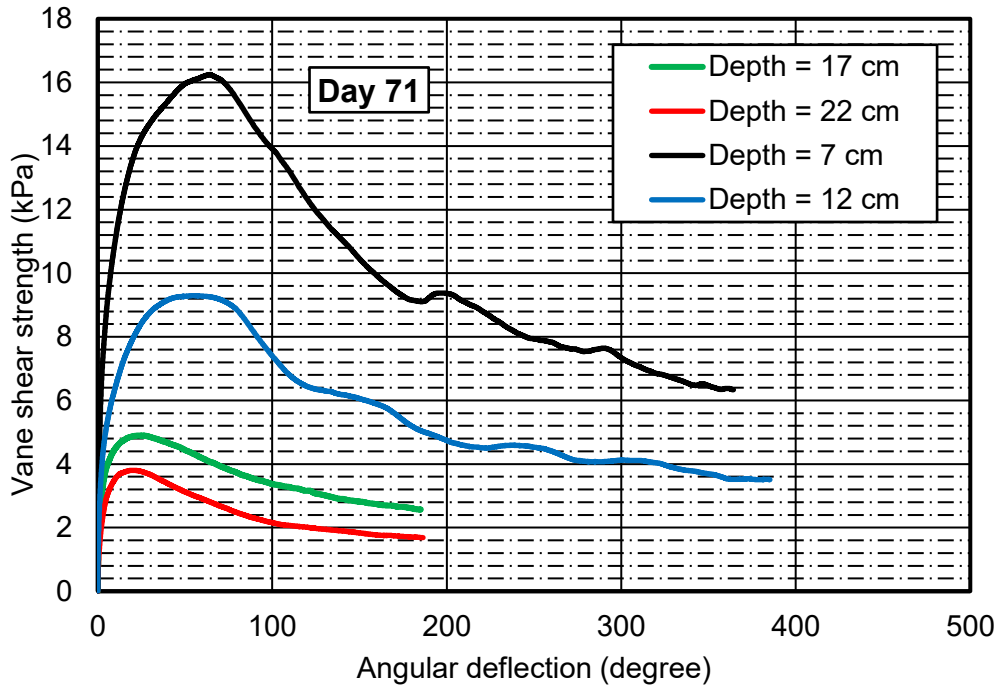

(c) Vane shear measurement by day 71

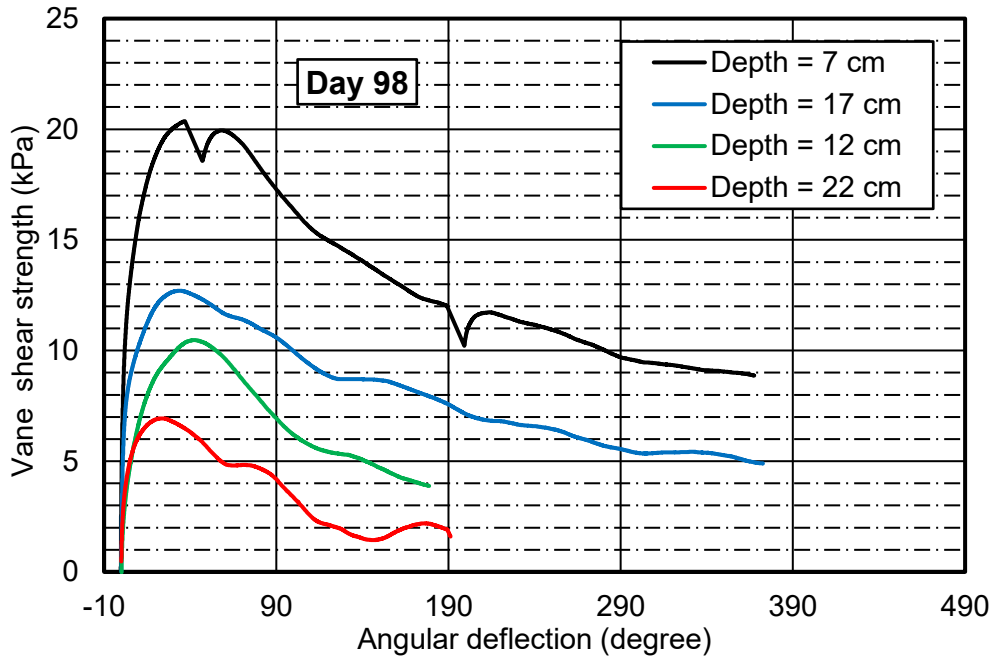

(d) Vane shear measurement by day 98

Figure A.8. Vane shear strength test during an applied suction of 30 kPa: (a) Day 25; (b) Day 55; (c) Day 71 and (d) Day 98.

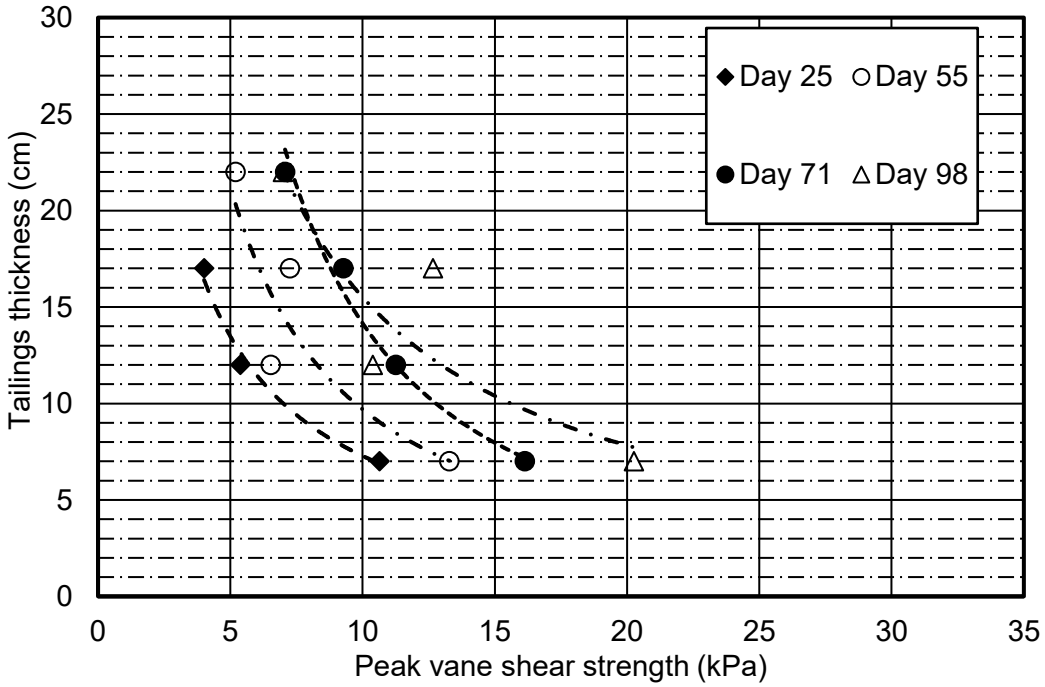

Figure A.9. Peak vane shear strength with depth and time during an applied suction of 30 kPa.

Applied suction of 40 kPa for flocculated FFT

This section presents results during the applied suction of 40 kPa.

Settlement, vertical strain and void ratio

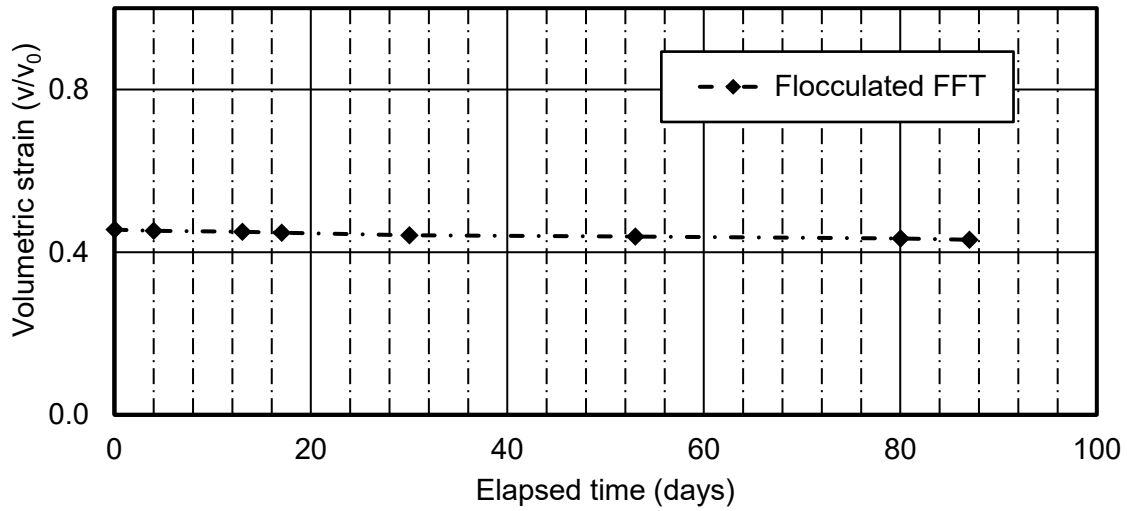

Figure A.10. Volumetric strain during an applied suction of 40 kPa.

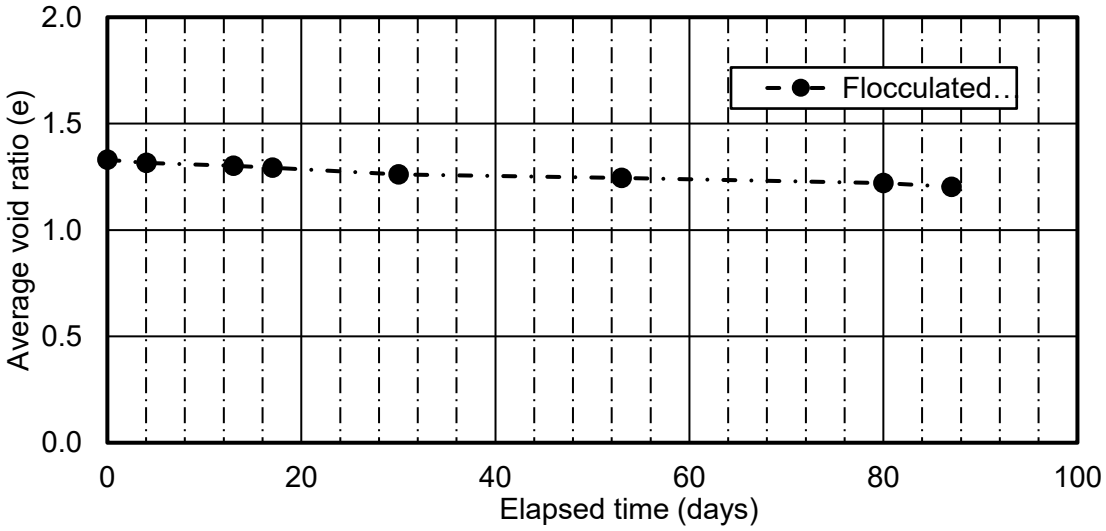

Figure A.11. Change in void ratio during an applied suction of 40 kPa.

Suction distribution

Figure A.12 presents results of suction distribution during the applied suction of 40 kPa.

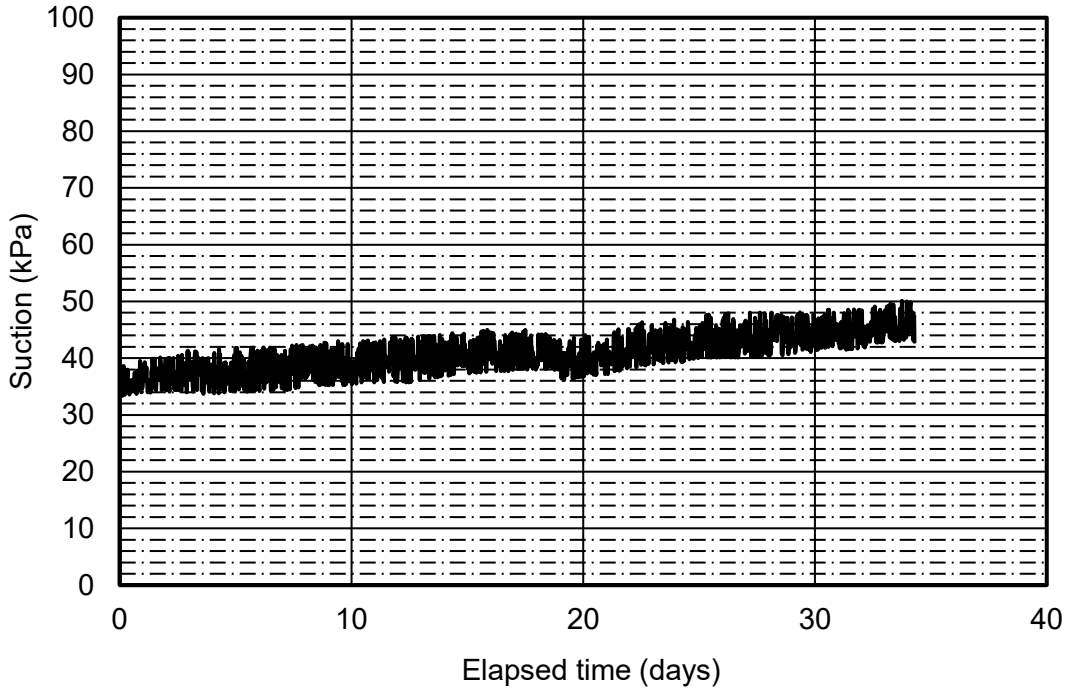

Figure A.12. Suction using the negative pore pressure sensor during applied suction of 40 kPa.

Undrained peak shear strength measurement with time and depth

The shear strength of deposited flocculated tailings was measured as the tailings consolidated using incremental applied suction. The vane shear strength versus angular deflection results are presented in A.13(a) to A.13(b).

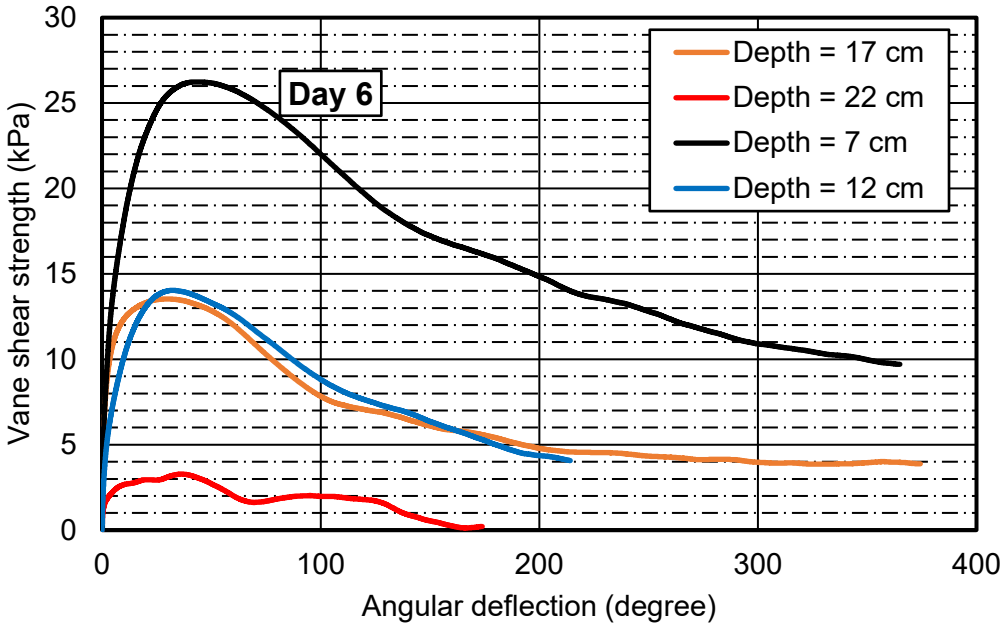

(a) Vane shear measurement by day 6

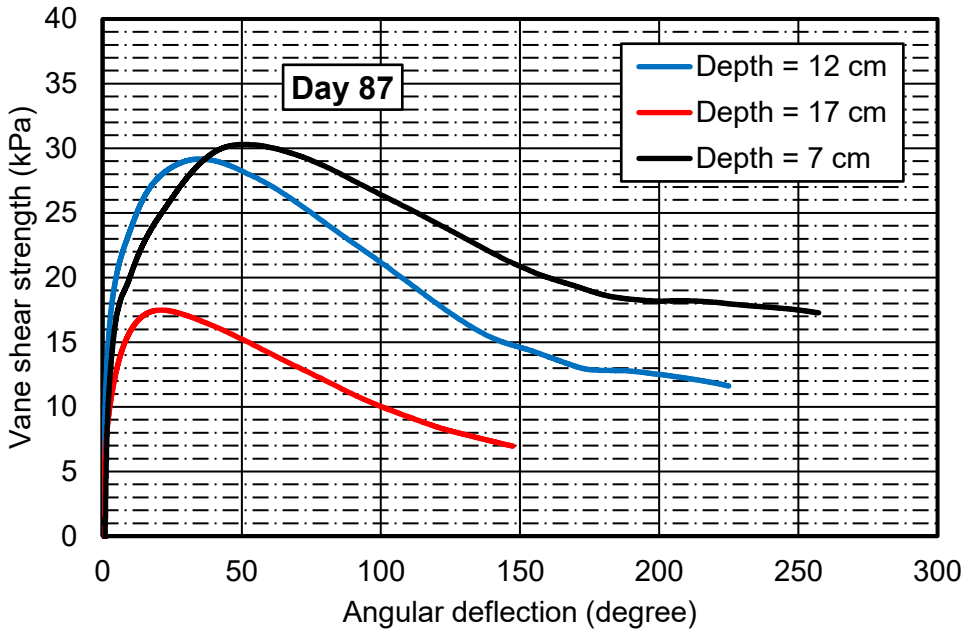

(b) Vane shear measurement by day 87

Figure A.13. Vane shear strength test during applied suction of 40 kPa: (a) Day 6 and (b) Day 87.

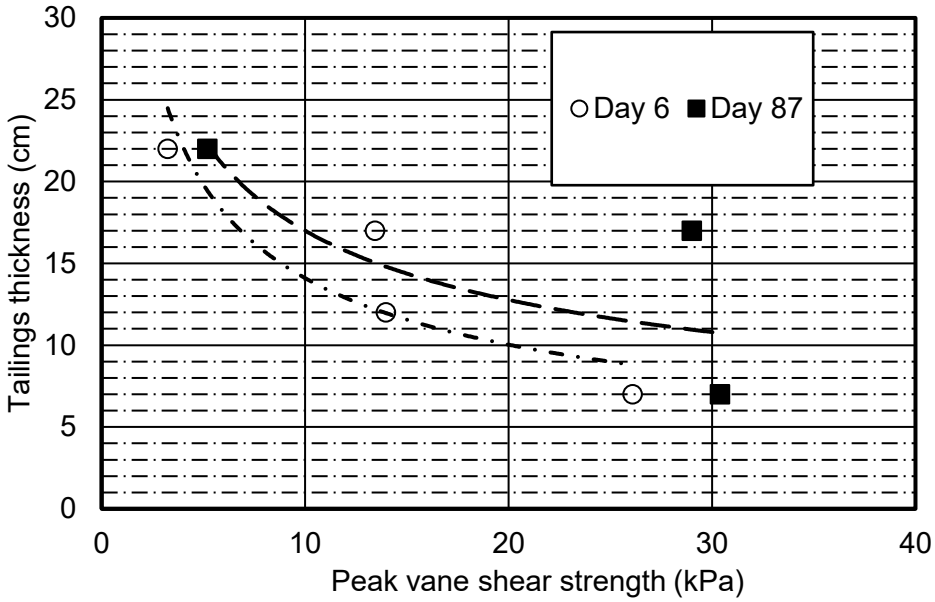

Figure A.14. Peak vane shear strength with depth and time during applied suction of 40 kPa.

Applied suction of 60 kPa for flocculated FFT

This section presents results during the applied suction of 60 kPa.

Settlement, vertical strain and void ratio

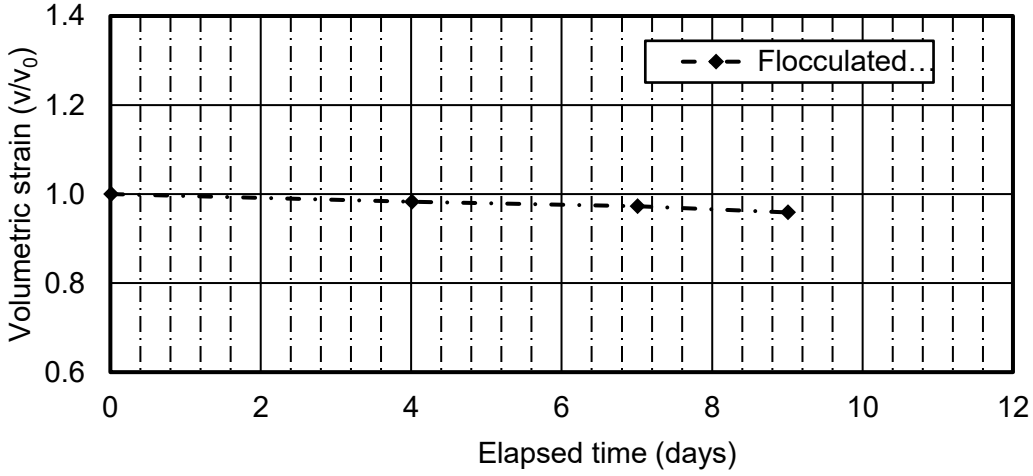

Figure A.15. Volumetric strain during applied suction of 60 kPa.

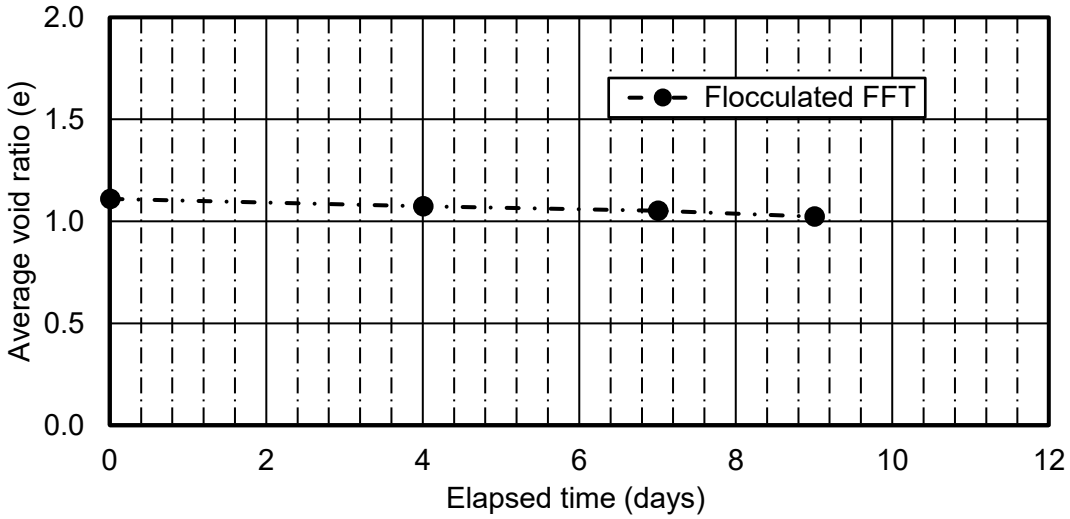

Figure A.16. Change in void ratio during an applied suction of 60 kPa.

Suction distribution

Figure A.17 presents suction results during the applied suction of 60 kPa at the bottom boundary.

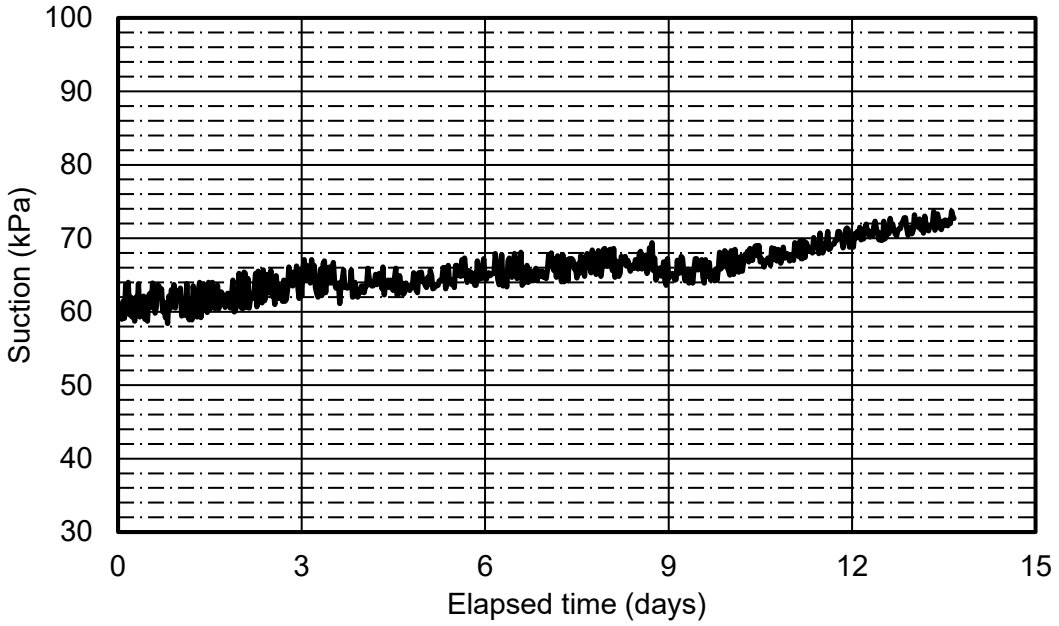

Figure A.17. Suction using the negative pore pressure sensor during applied suction of 60 kPa.

Undrained peak shear strength measurement with time and depth

The shear strength of deposited flocculated tailings was measured as the tailings consolidated using incremental applied suction. The vane shear strength versus angular deflection results are presented in A.18(a) to A.18(c).

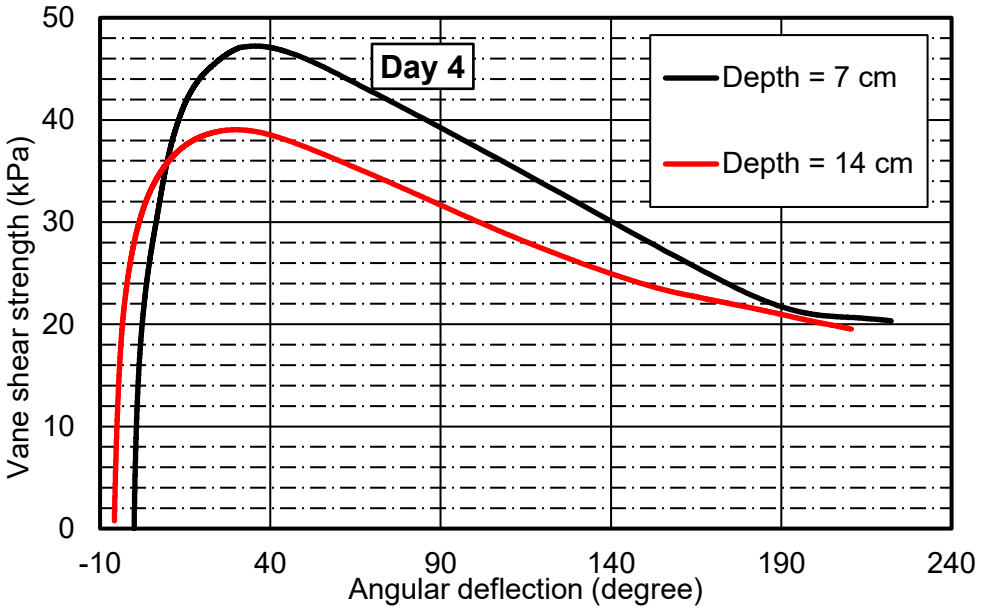

(a) Vane shear measurement by day 4

(b)

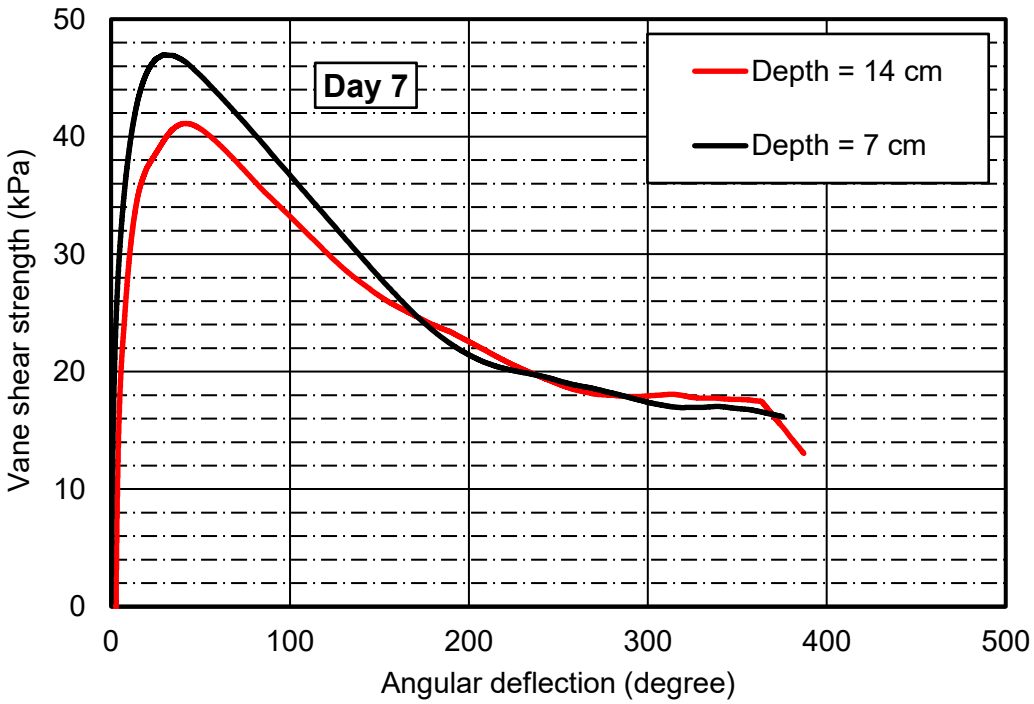

(c) Vane shear measurement by day 7

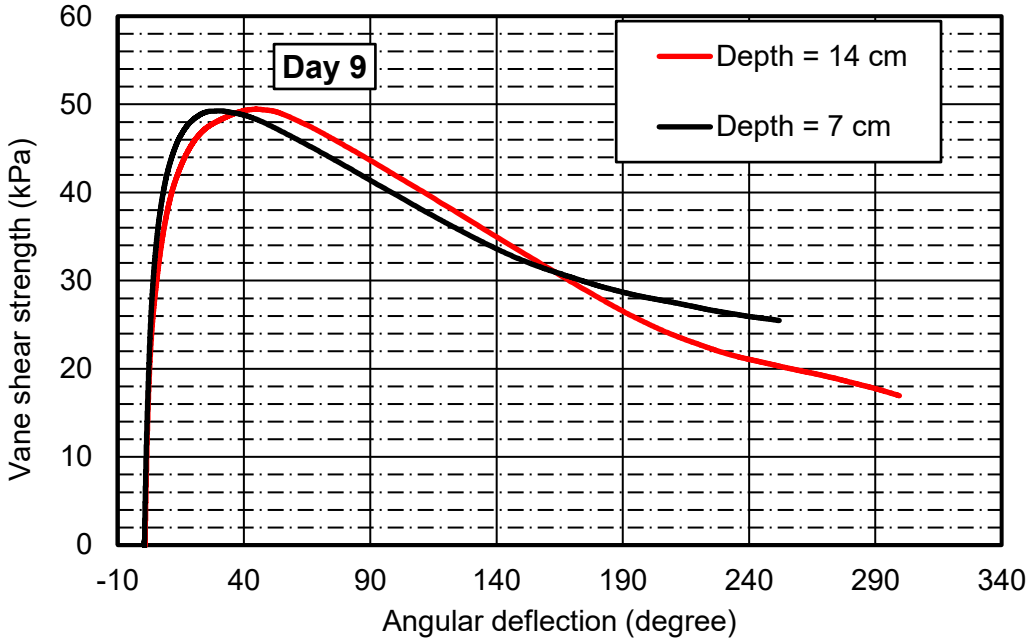

(d) Vane shear measurement by day 9

Figure A.18. Vane shear strength test during and applied suction of 60 kPa: (a) Day 4; (b) Day 7 and (c) Day 9.

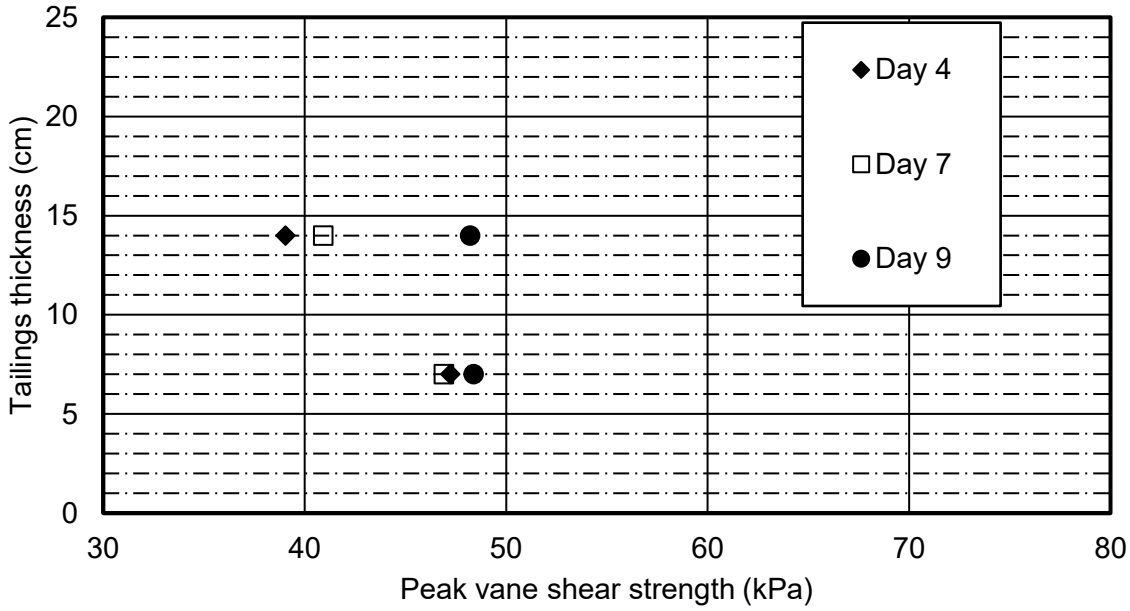

Figure A.19. Peak vane shear strength with depth and time during applied suction of 60 kPa.

APPENDIX B: Flocculated Centrifuged Tailings Cake (FCTC)

Applied suction of 30 kPa for the FCTC

This section presents results during the applied suction of 30 kPa.

Settlement, vertical strain and void ratio

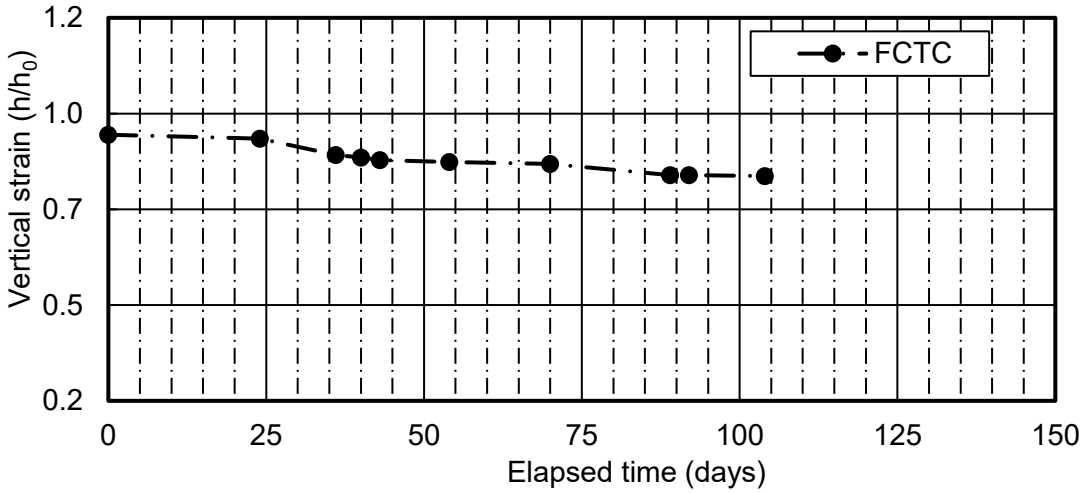

Figure B.1. Vertical strain during an applied suction of 30 kPa.

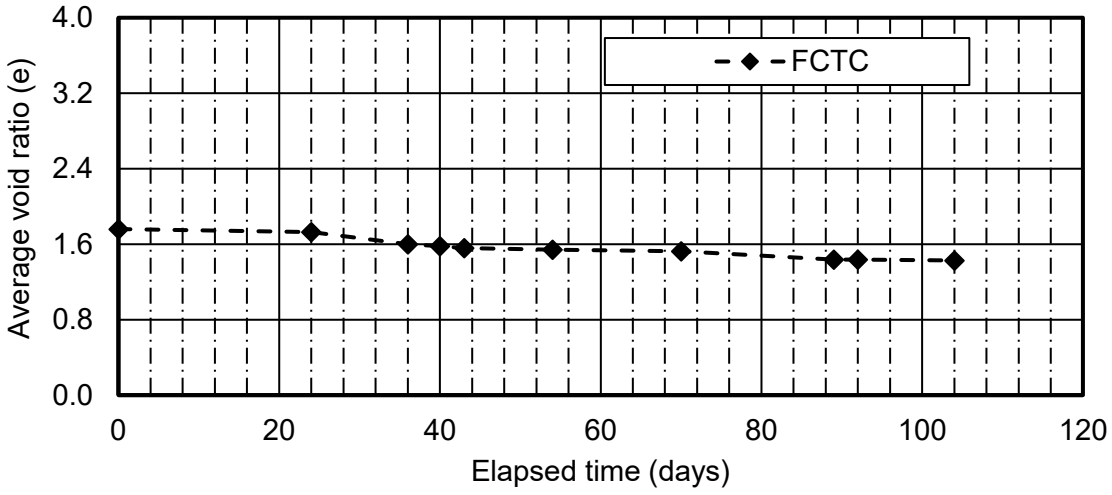

Figure B.2. Change in void ratio during an applied suction of 30 kPa.

Suction distribution

The sensor to measure negative pore water pressure was not responding. Therefore, no pore pressure distribution was measured during the applied suction of 30 kPa.

Undrained peak shear strength measurement with time and depth

The undrained peak shear strength measured with time for the FCTC during the applied suction of 30 kPa are presented in Figure B. 3(a) to B. 3(d). The peak shear strength with depth and time are presented in Figure B.4.

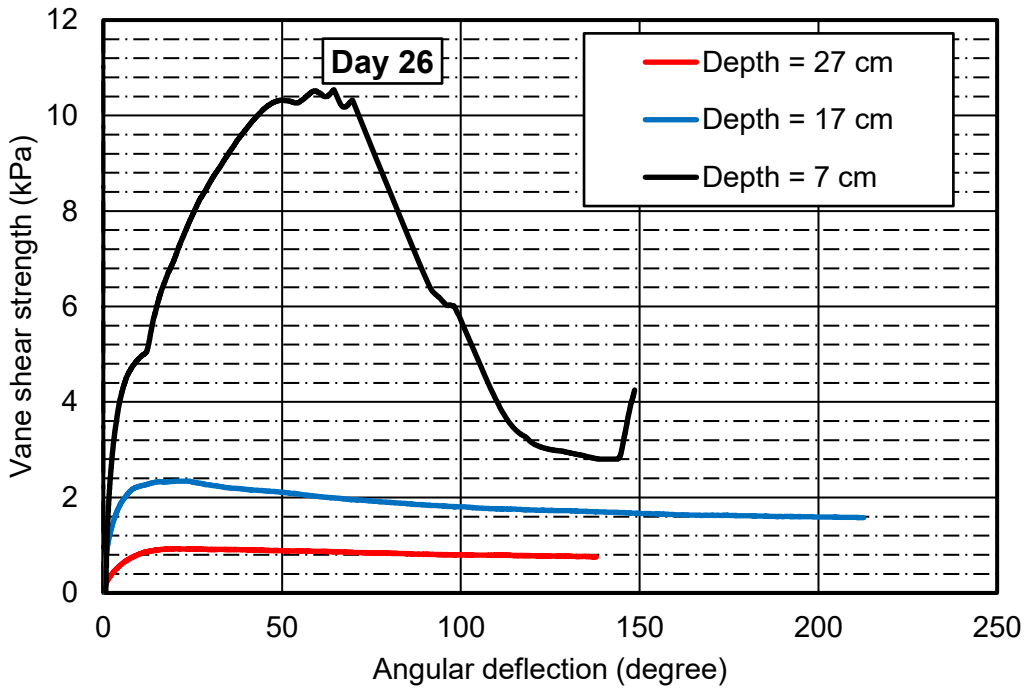

(a) Vane shear measurement by day 26

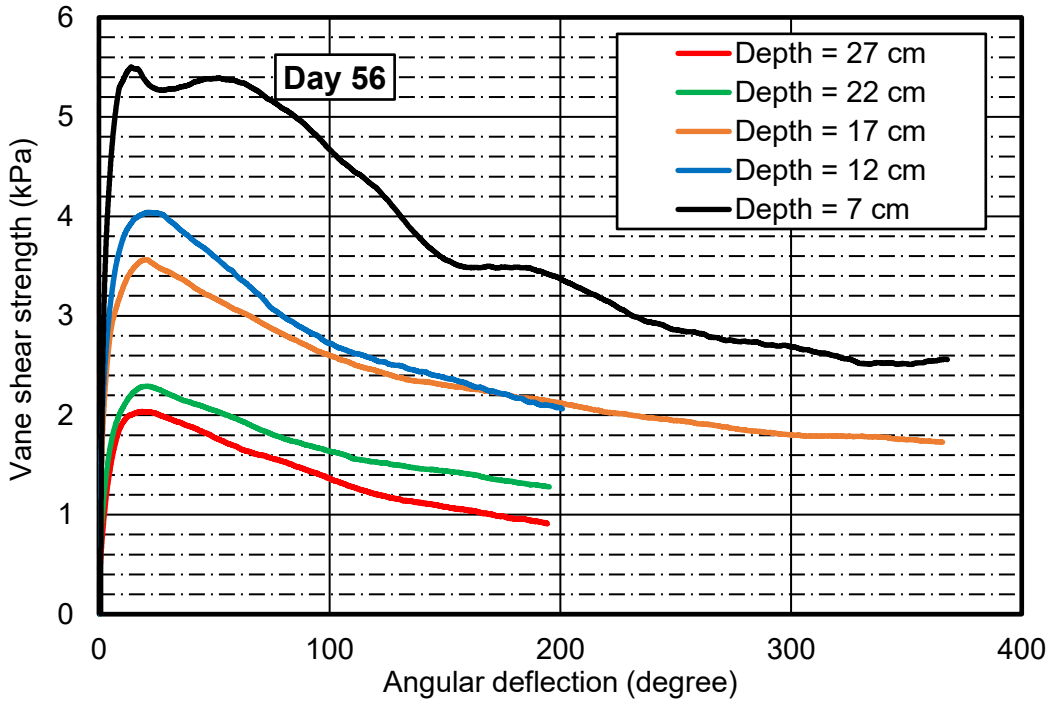

(b) Vane shear measurement by day 56

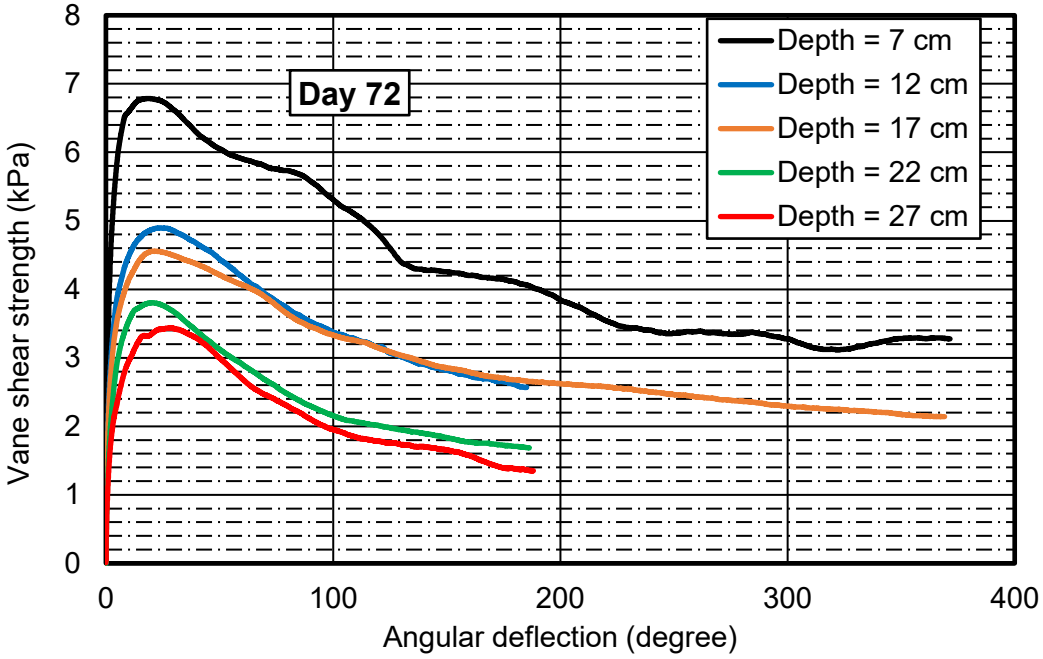

(c) Vane shear measurement by day 72

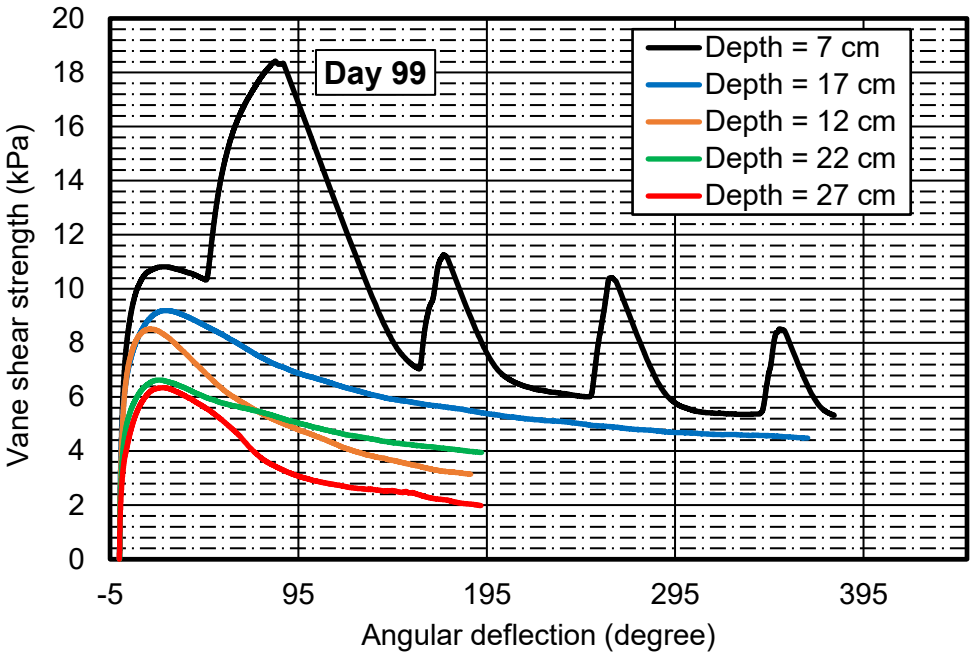

(d) Vane shear measurement by day 99

Figure B.3. Vane shear strength test during applied suction of 30 kPa: (a) Day 26; (b) Day 56; (c) Day 72 and (d) Day 99.

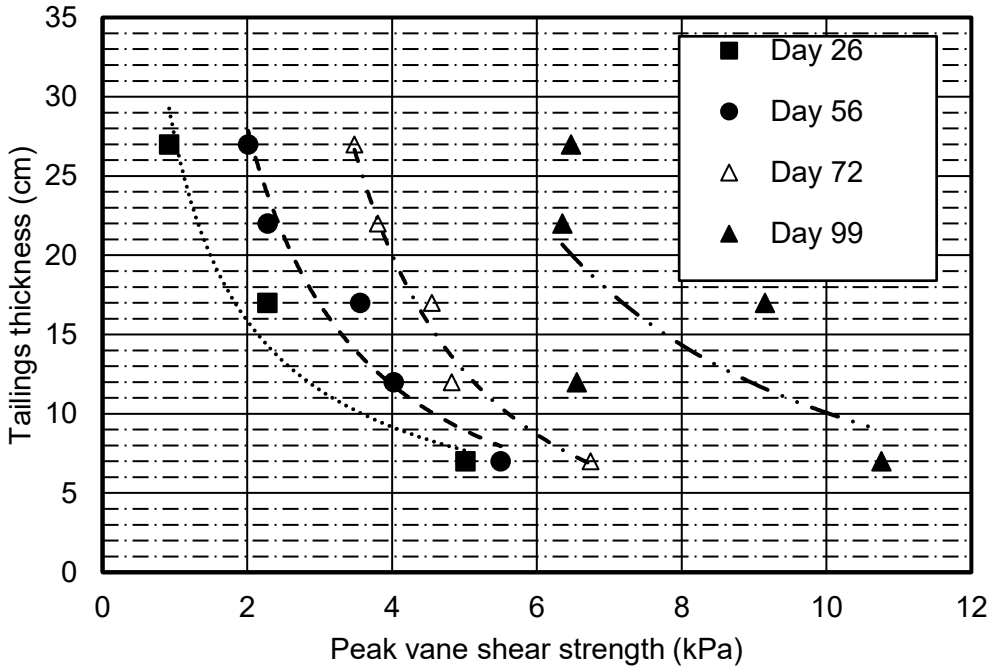

Figure B.4. Peak vane shear strength with depth and time during applied suction of 30 kPa.

Applied suction of 40 kPa for the FCTC

This section presents results during the applied suction of 40 kPa.

Settlement, vertical strain and void ratio

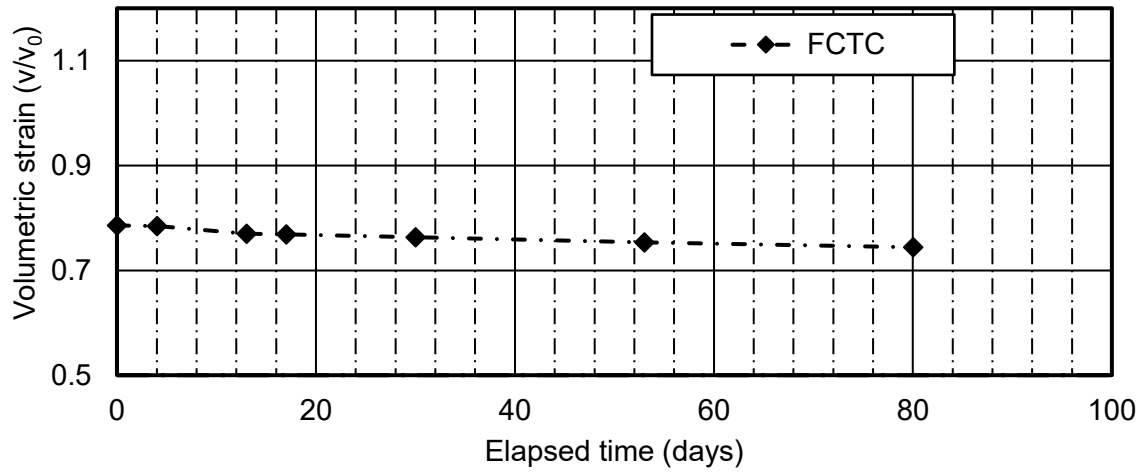

Figure B.5. Volumetric strain during applied suction of 40 kPa.

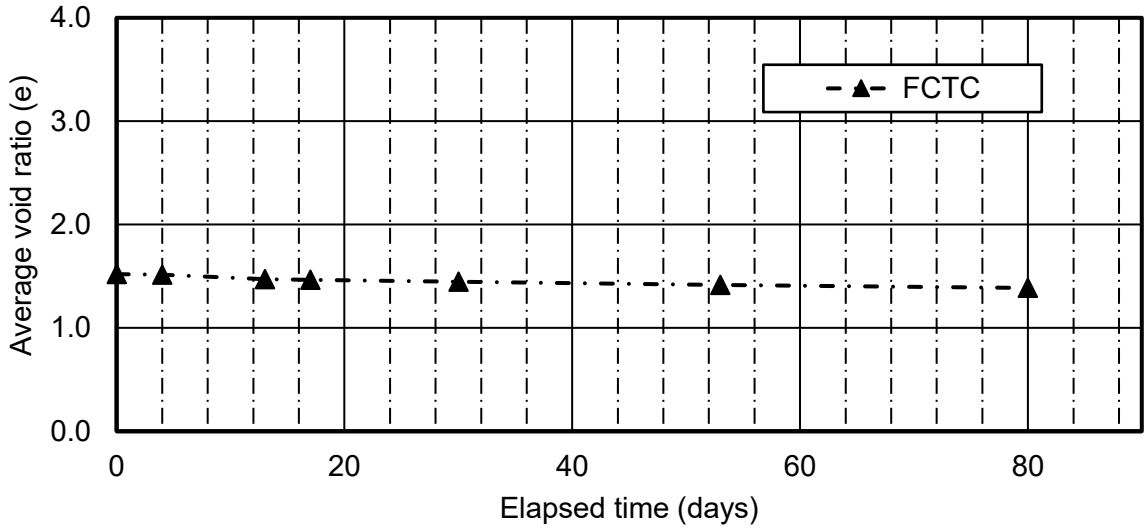

Figure B.6. Change in void ratio during applied suction of 40 kPa.

Suction distribution

Figure B.7 presents suction results during the applied suction of 40 kPa at the bottom boundary.

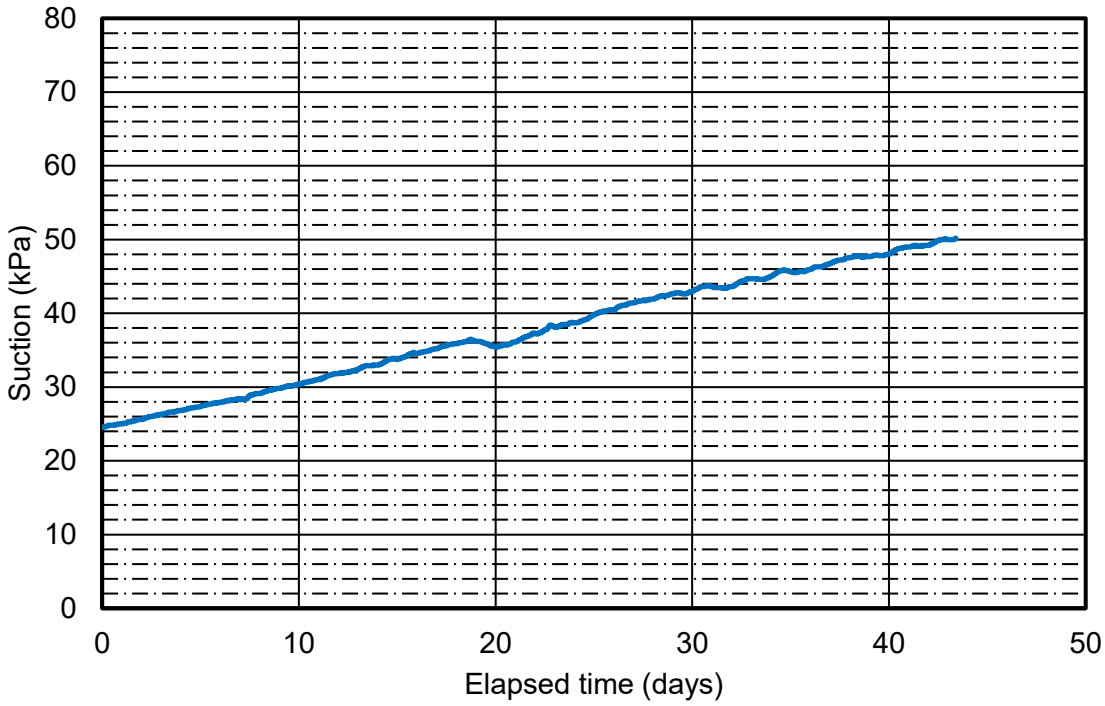

Figure B.7. Suction using the negative pore pressure sensor during an applied suction of 40 kPa.

Undrained peak shear strength measurement with time and depth

The undrained peak shear strength measured with time for the FCTC during the applied suction of 40 kPa are presented in Figure B. 8(a) to B. 8(b). The peak shear strength with depth and time are presented in Figure B.9.

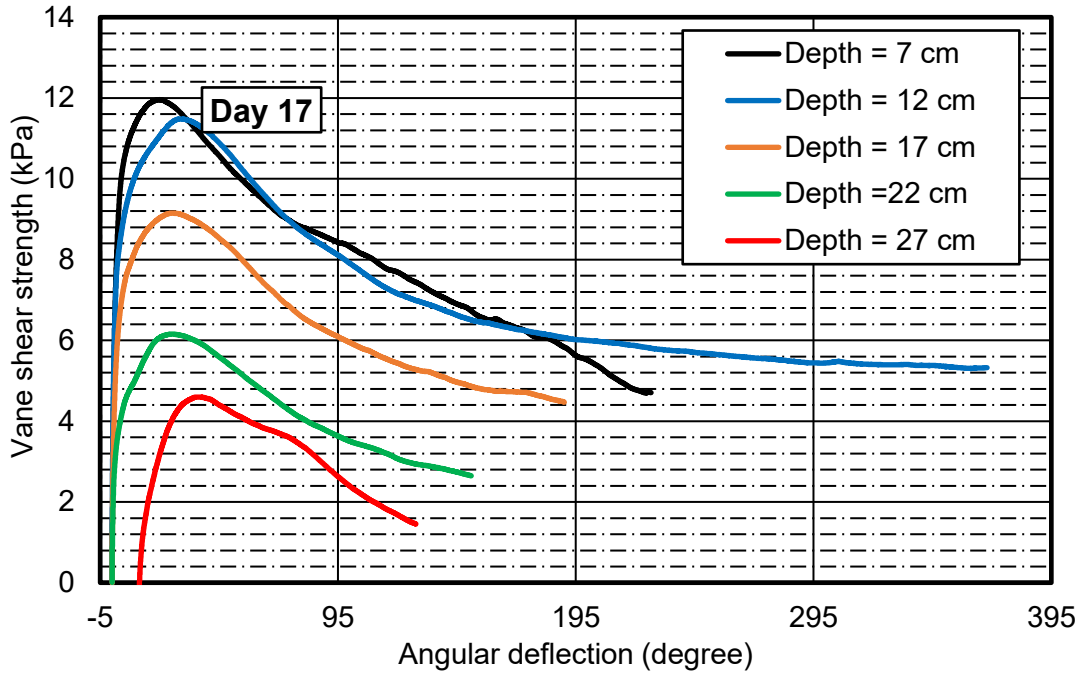

(a) Vane shear measurement by day 17

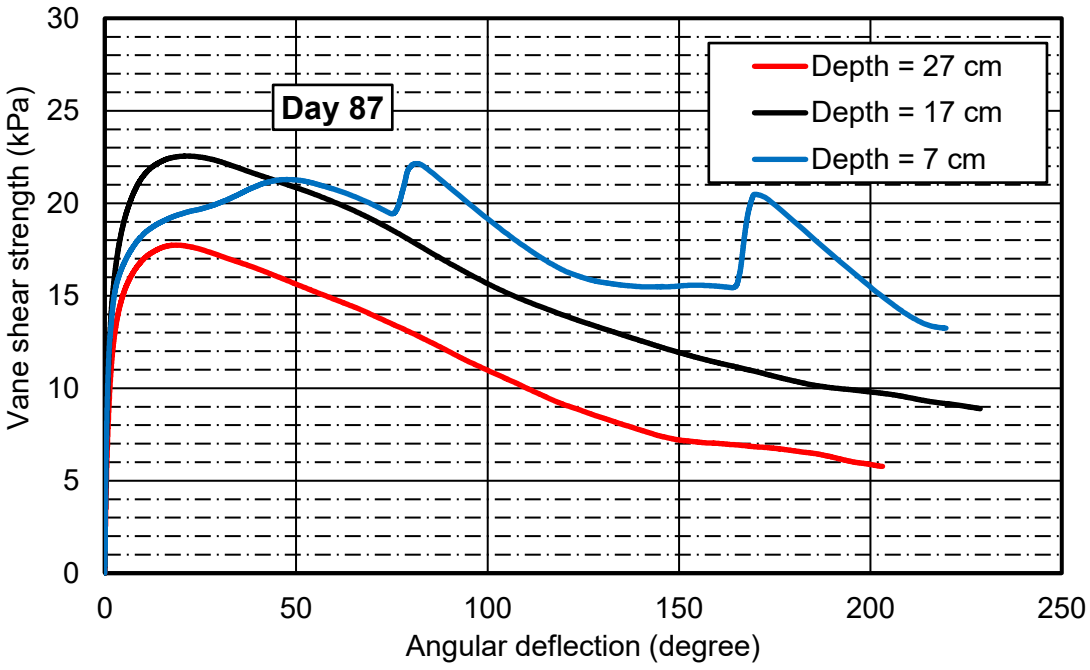

(b) Vane shear measurement by day 87

Figure B.8. Vane shear strength test for the FCTC during applied suction of 40 kPa: (a) Day 17 and (b) Day 87.

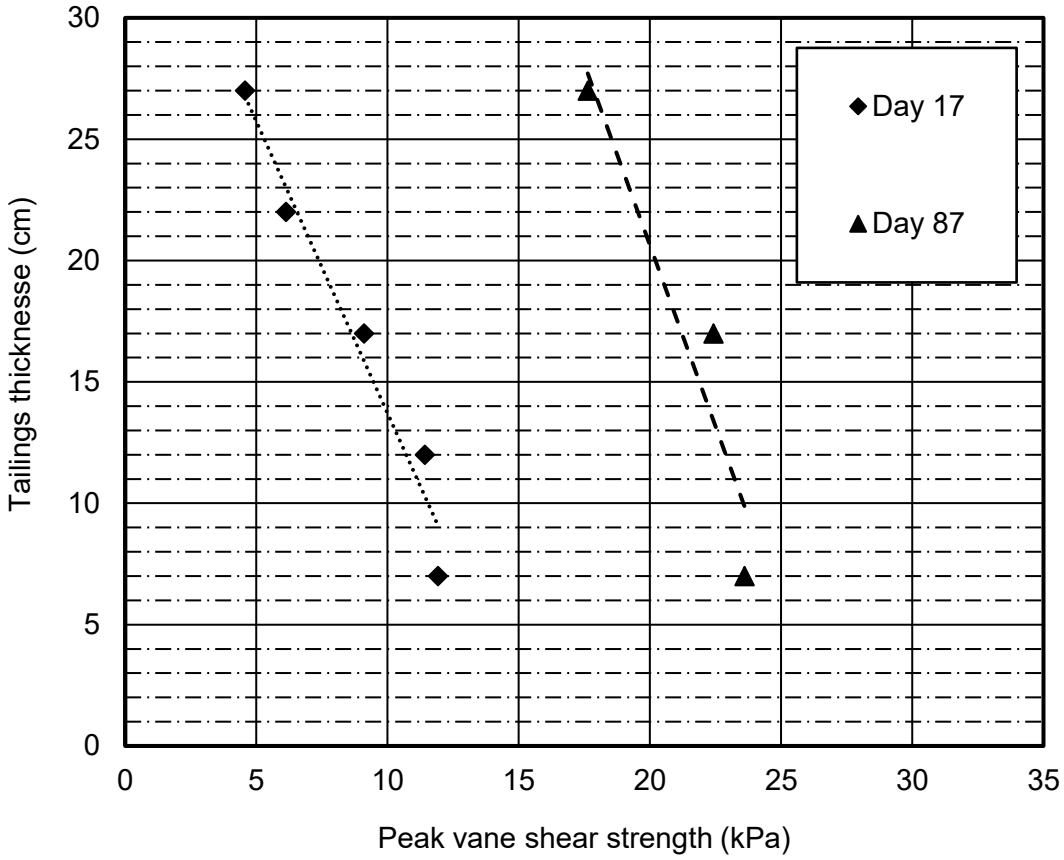

Figure B.9. Peak vane shear strength with depth and time during applied suction of 40 kPa.

Applied suction of 60 kPa for the FCTC

This section presents results during the applied suction of 60 kPa.

Settlement, vertical strain and void ratio

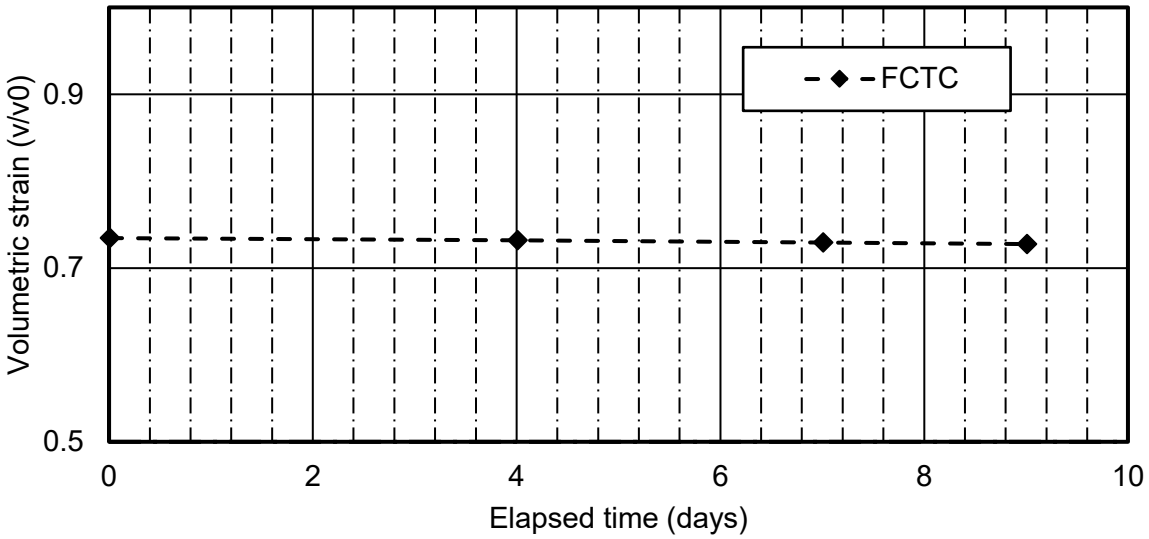

Figure B.10. Volumetric strain during applied suction of 60 kPa.

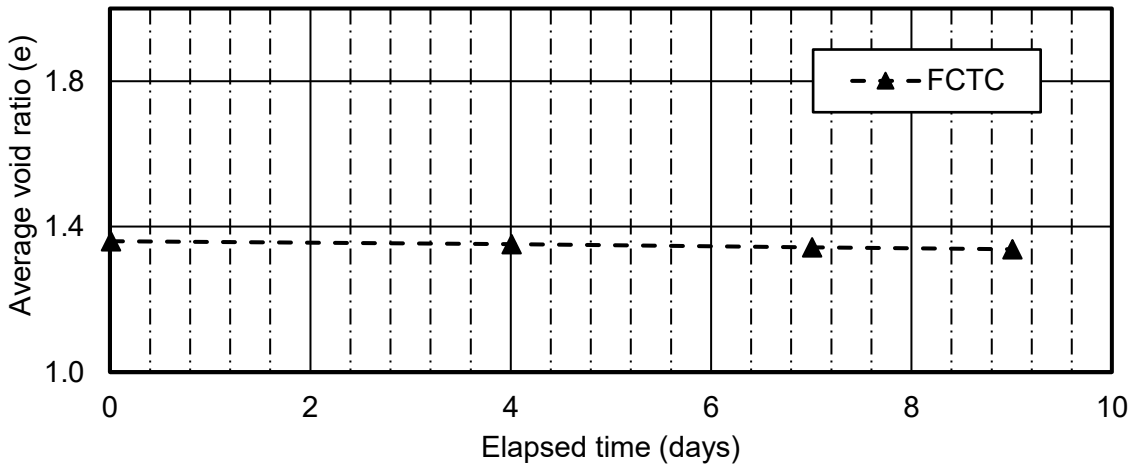

Figure B.11. Change in void ratio during applied suction of 60 kPa.

Suction distribution

Figure B. 12 presents suction results during the applied suction of 60 kPa at the bottom boundary.

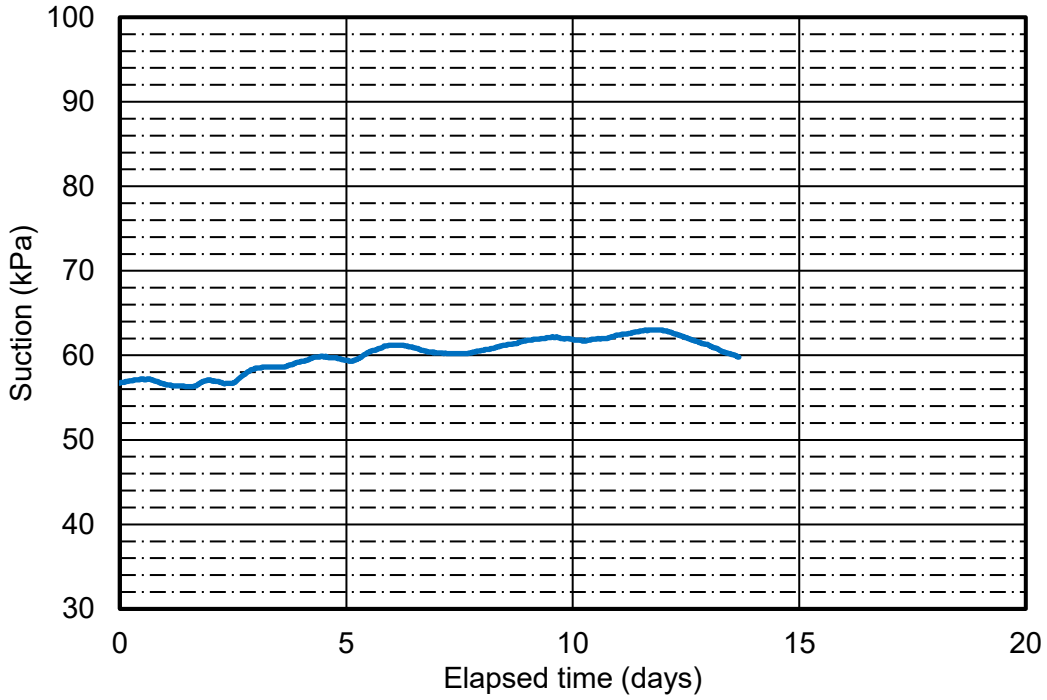

Figure B.12. Suction using the negative pore pressure sensor during applied suction of 60 kPa.

Undrained peak shear strength measurement with time and depth

The undrained peak shear strength measured with time for the FCTC during the applied suction of 60 kPa are presented in Figure B.13(a) to B.13(c). The peak shear strength with depth and time are presented in Figure B.14.

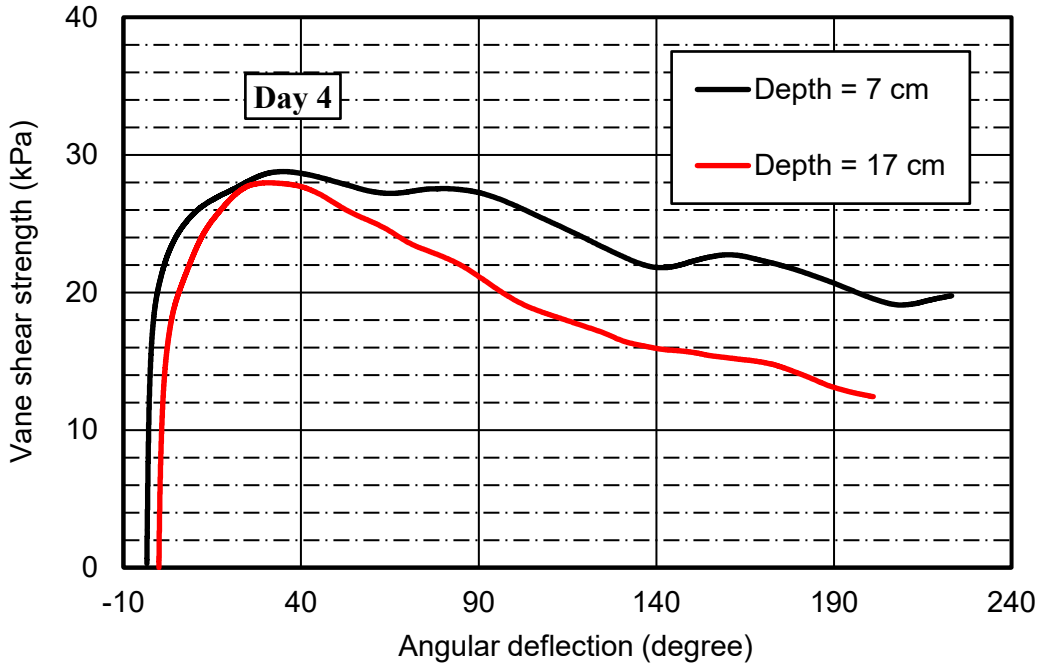

(a) Vane shear measurement by day 4

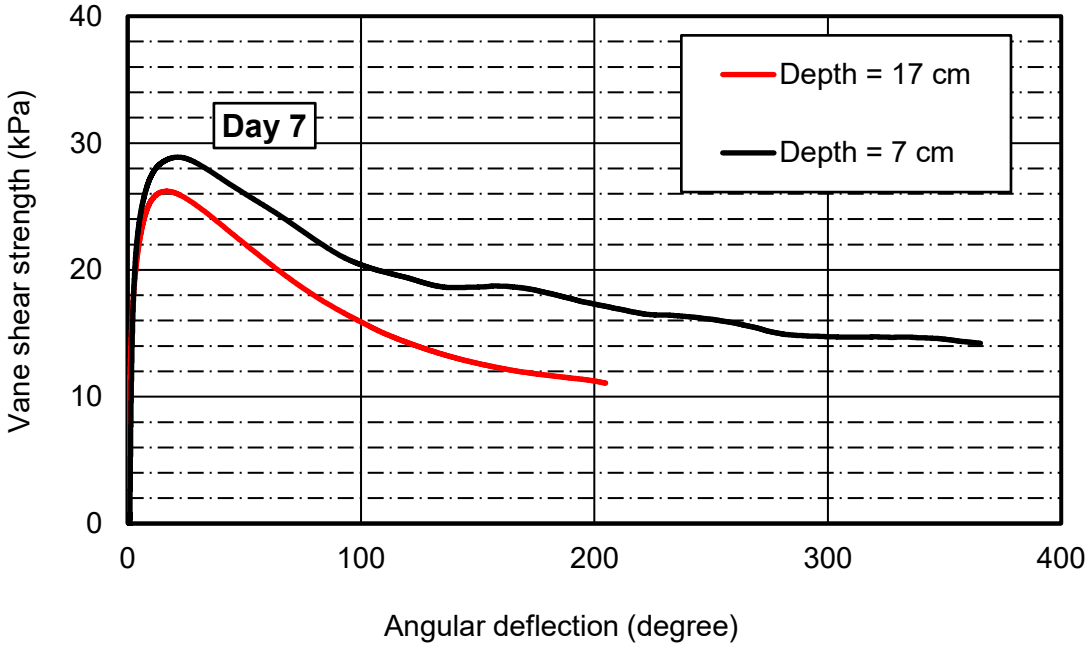

(b) Vane shear measurement by day 7

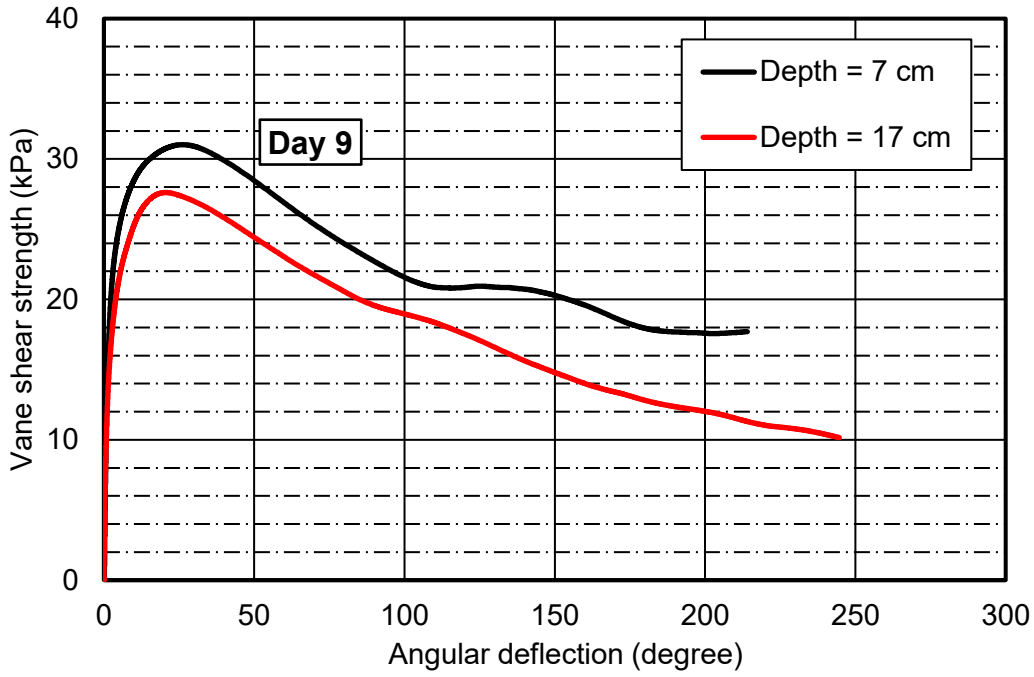

(c) Vane shear measurement by day 9

Figure B.13. Vane shear strength test during applied suction of 60 kPa: (a) Day 4; (b) Day 7; and (c) Day 9.

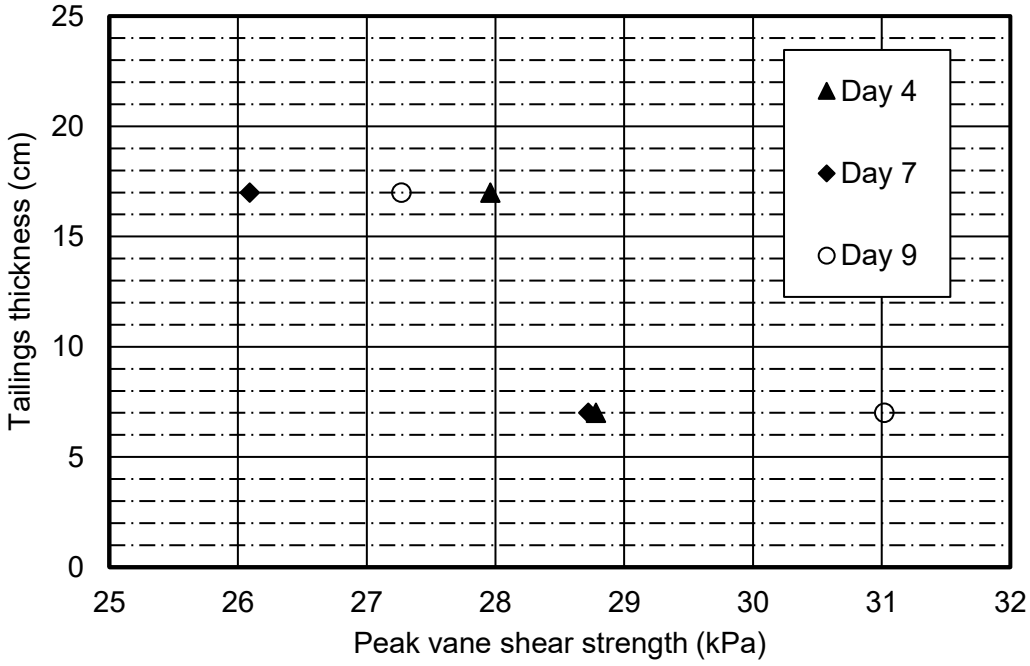

Figure B.14. Peak vane shear strength with depth and time during applied suction of 60 kPa.

APPENDIX C: POSITIVE PORE PRESSURE SENSOR CALIBRATION

Table C1 presents a summary of calibration data for the positive pressure transducers in columns 1 and 2. The calibration data were obtained using a standard calibration instrument, and the output was refined by comparing the hydrostatic pressure of a known height of water within the meso-scale column and the readout obtained prior to commencing the consolidation test. Figure C1.1 presents the correlation between the applied direct current and pore pressure.

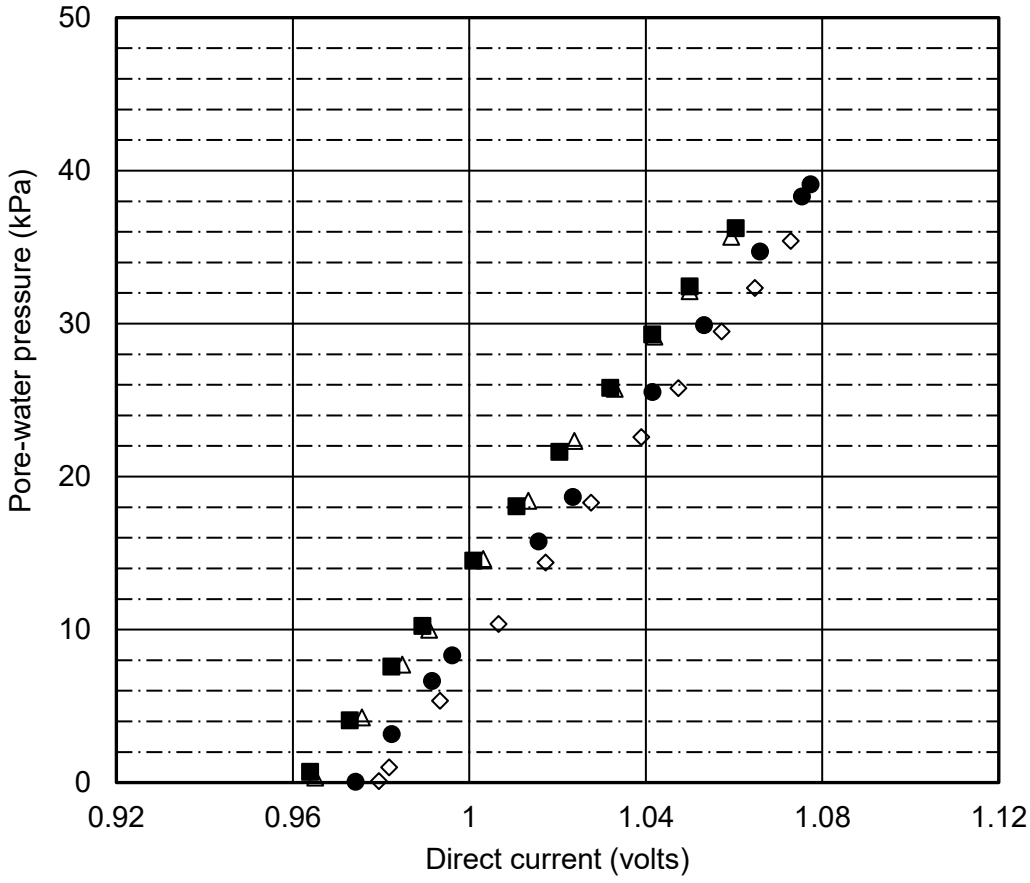

Figure C1.1 Calibration between DC and positive pore pressure sensors from Omega.

Table C1 Summary of calibration data for the positive pressure transducer used.

Transducer id							
442813		442827		442842		417991	
DC (Volts)	PWP (kPa)	DC (Volts)	PWP (kPa)	DC (Volts)	PWP (kPa)	DC (Volts)	PWP (kPa)
1.07288	35.39	1.0774	39.1	1.06041	36.23	1.05939	35.67
1.06471	32.32	1.0754	38.3	1.04997	32.43	1.04992	32.12
1.0572	29.48	1.0659	34.7	1.04145	29.29	1.04195	29.14
1.04741	25.77	1.0532	29.9	1.03198	25.8	1.03295	25.74
1.03897	22.58	1.0415	25.53	1.0204	21.62	1.02382	22.33
1.0276	18.28	1.0235	18.67	1.01069	18.05	1.0134	18.42
1.01731	14.38	1.0157	15.76	1.00092	14.51	1.00318	14.6
1.00663	10.35	0.9961	8.3	0.98938	10.23	0.99092	9.98
0.99338	5.33	0.99158	6.64	0.98233	7.58	0.98485	7.71
0.98185	0.98	0.9824	3.17	0.97294	4.06	0.97565	4.25
0.97956	0.09	0.9742	0.05	0.96394	0.69	0.96512	0.32
Calibration Equation							
Y=378.27X - 370.44		Y=378.05X - 368.24		Y=367.83X - 353.77		Y=375.10X - 361.71	
R-squared value = 1		R-squared value = 1		R-squared value = 1		R-squared value = 1	